Synthesis and optimization of pyrazolo[1,5-*a*]pyrimidine-based macrocyclic kinase inhibitors

Synthese und Strukturoptimierung von makrozyklischen Pyrazolo[1,5-*a*]pyrimidin basierten Kinaseinhibitoren

Dissertation

zur Erlangung des Doktorgrades der Naturwissenschaften

vorgelegt beim Fachbereich 14

der Johann Wolfgang Goethe-Universität Frankfurt am Main

von

Christian Georg Kurz

aus Frankfurt am Main

Frankfurt am Main 2021

D30

Christian Georg Kurz

Geboren am 03.05.1985 in Frankfurt am Main

Dekan: Prof. Dr. Clemens Glaubitz

Gutachter: Prof. Dr. Stefan Knapp

Prof. Dr. Eugen Proschak

Datum der Disputation: 25.05.2022

Table of Contents

1. Introduction

1.1 Protein kinases

Considering the top 10 leading causes of death worldwide, cancer ranks either first or second place in more than half of all countries. Estimates for 2020 were 19 million new cancer cases and 10 million cancer deaths. The decrease in mortality rates due to coronary heart disease or stroke further increases the importance of cancer as a major cause of death.[1] With the identification of the first protein kinase as an oncogene in 1978, kinases entered the field of cancer research.[2] In the following years, kinases established themselves in this field of research by finding tumor-promoting phorbol esters as hyperactivators of protein kinase C (PKC)[3], the synthesis of naphthalene sulfonamides as the first kinase inhibitors[4], and the discovery of staurosporine (**1**) as a nanomolar inhibitor of PKC.[5] With the completion of the human genome project, it was revealed that 1.7% of the human genome encodes the entirety of the human kinome with 518 kinases, illustrated in the so called kinome tree (**Figure 1**).[6,7]

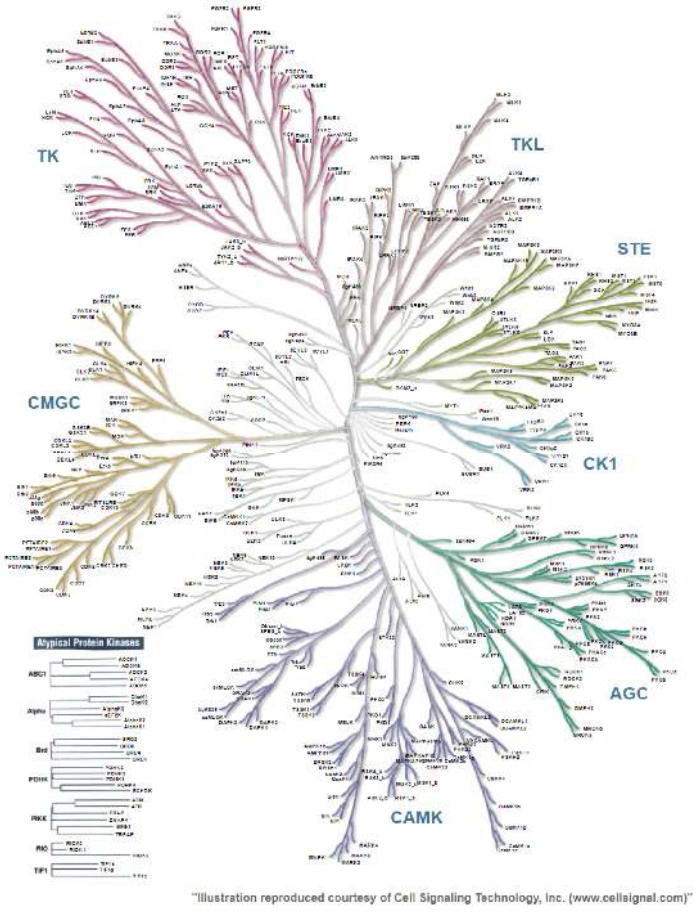

Figure 1: **Graphical representation of the human kinome in the kinome tree.** Here, the kinases, including atypical ones, are divided into six classes of serine/threonine-specific protein kinases (TKL, STE, CK1, AGC, CAMK and CMGC) and tyrosine kinases (TK).

But why are kinases so closely associated with the pathogenesis of cancer and other diseases such as autoimmune and inflammatory diseases?[8,9] This can be attributed to their critical function in cellular signaling pathways. Fischer and Krebs identified protein phosphorylation by kinases as a fundamental mechanism of protein regulation in 1955.[10] The phosphorylation state of proteins is controlled by the coordinated addition and removal of phosphates by specific kinases and phosphatases, respectively (**Figure 2**).[11] This reversible post-translational modification, like glycosylation, ubiquitination, nitrosylation, acylation and methylation, contributes to the diversity of the proteome and influences various aspects of normal and pathological physiology.[12] The abnormal oncogenic activation of kinases can be caused by various factors such as misregulated expression and/or amplification, aberrant phosphorylation, mutation, chromosomal translocation and epigenetic regulation. The resulting increased specific activity of the kinase, its overexpression or the loss of negative regulation can lead to dramatic changes in cellular processes such as proliferation, cell cycle, apoptosis, motility, growth and differentiation.[11,13]

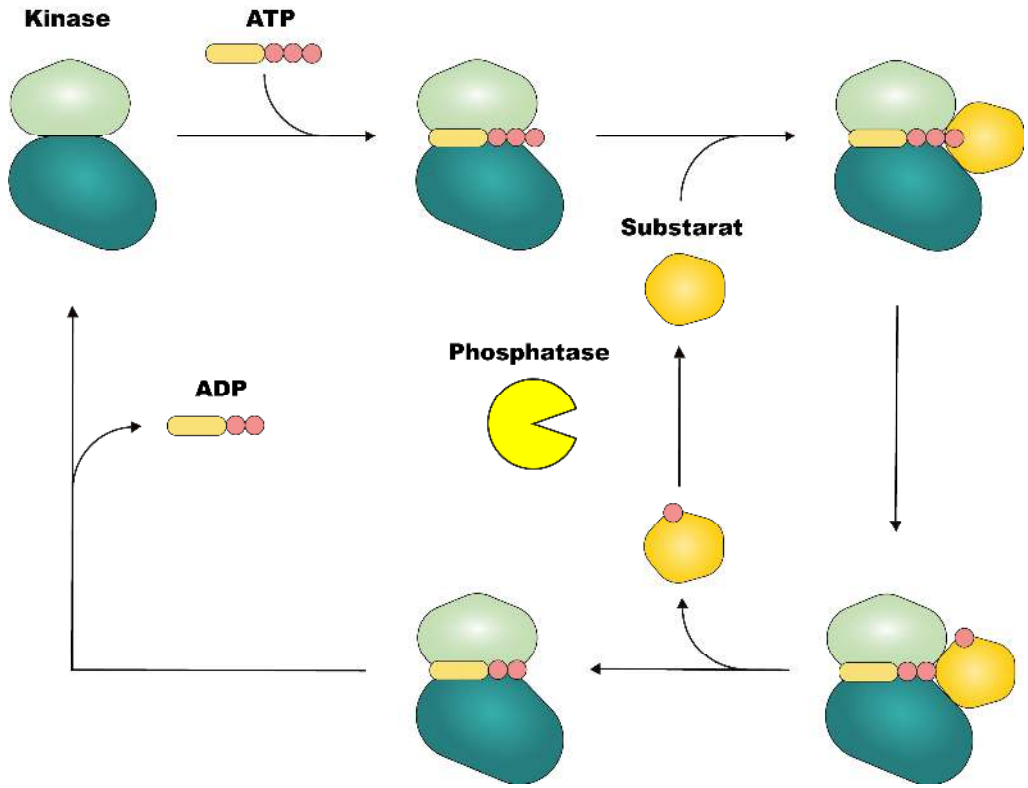

Figure 2: **Graphical representation of the catalytic cycle of phosphorylation by kinases.** First, ATP is bound in the active site, followed by the coordination of the substrate. Afterwards, the γ-phosphate of ATP is transferred to the substrate and the phosphorylated substrate is released.The final step is the release of ADP. (Modified from Ubersax et al.[14])

Modification via phosphorylation by kinases is characterized as the transfer of a γ-phosphate from adenosine triphosphate (ATP) or guanosine triphosphate (GTP) to hydroxyl groups of amino acids of different substrates. In the case of eukaryotic protein kinases (ePKs), the amino acids to be phosphorylated are mostly serine and threonine residues. However, a subset of kinases also transfers a phosphate to threonine residues. Depending on these residues, kinases are classified into serine/threonine-specific protein kinases (STPKs), tyrosine-specific protein kinases (TPKs), or tyrosine and threonine dual-specific kinases. Further subdivision was primarily based on sequence comparison of their catalytic domains.[15,16] STPKs are divided into the following six classes (**Figure 1**): TKL (tyrosine kinase like), CMGC (cyclin-dependent kinase, MAP kinase, glycogen synthase kinase, casein kinase2), AGC (protein kinase A, G, and C; PKA, PKG, PKC), CAMK (calcium/calmodulin-dependent kinase), STE (MAPK cascde families (Sterile 7/ MAP2K, Sterile 11/MAP3K and Sterile 20/MAP4K)) and CK1 (casein kinase 1). TPKs can be further divided into receptor and non-receptor TPKs.[17,18] In addition, the so-called pseudo-kinases should be emphasized with their weak to non-existent activity due to the absence of one of the important motifs in the catalytic domain. The majority of protein kinases are defined by a conserved assembly of secondary structures arranged in 12 subdomains.[19] They are folded into a bilobed structure consisting of the smaller β-stranded N-terminal lobe (N-lobe) and the larger α-helical C-terminal lobe (C-lobe) (**Figure 3**). The core catalytic structure of kinases is constituted of two lobes, which are connected via a hinge region. Substrate binding occurs at a surface groove formed by the C-lobe, while ATP binds via hydrogen bonds at the hinge region in the cleft between the two lobes.[7,20] The N-lobe, composed of 5-stranded β-sheets (β1 - β5) and an α-helix (αC), possesses a Gly-rich loop (P-loop) that contributes with its hydrophobic tip and αC to the coordination of the γ-phosphate of ATP.[21,22] The correct positioning of αC (C-helix-in) is essential for the interaction between the active site Lys of the AXK (Ala-X-Lys) motif and Glu of αC via a salt bridge and the active state of the kinase, respectively.[22,23] In contrast to the N-lobe, the C-lobe is helically dominated, with exception of four β-strands that contributes to the catalytic activity of the kinases[24]. The associated activation loop (A-loop) regulates the activity of the kinase by occluding the access of the substrate site. Phosphorylation stabilizes the active state and allows the transfer of γ-phosphate to the substrate.[18,21,25] Located at the N-terminus of the A-loop is the DFG-motif (Asp-Gly-Phe), which binds the Mg^{2+}-ion coordinating the phosphate of ATP via Asp. Via Phe, the DFG-motif interacts with αC and the HRD-motif (His-Arg-Asp) of the catalytic loop.

In the active state of the kinase, the Asp relocates from the DFG-out position to the active site (DFG-in). The HRD-motif is part of the catalytic loop, which carries most of the catalytic machinery. Responsible for the correct positioning of the P-site hydroxyl acceptor group within the substrate is the highly conserved Asp of the HRD. It is the only element which does not vary between active and inactive states.[17,21] The gatekeeper, which controls the entrance to a hydrophobic back pocket, is another structural motif of the catalytic core of kinases. In 77% of human kinases, the gatekeeper consists of large residues such as Leu, Met, or Phe and in 21% of small ones such as Thr or Val. There are no interactions with ATP, but the gatekeeper is attracting significant attention in the development of inhibitors.[17,26]

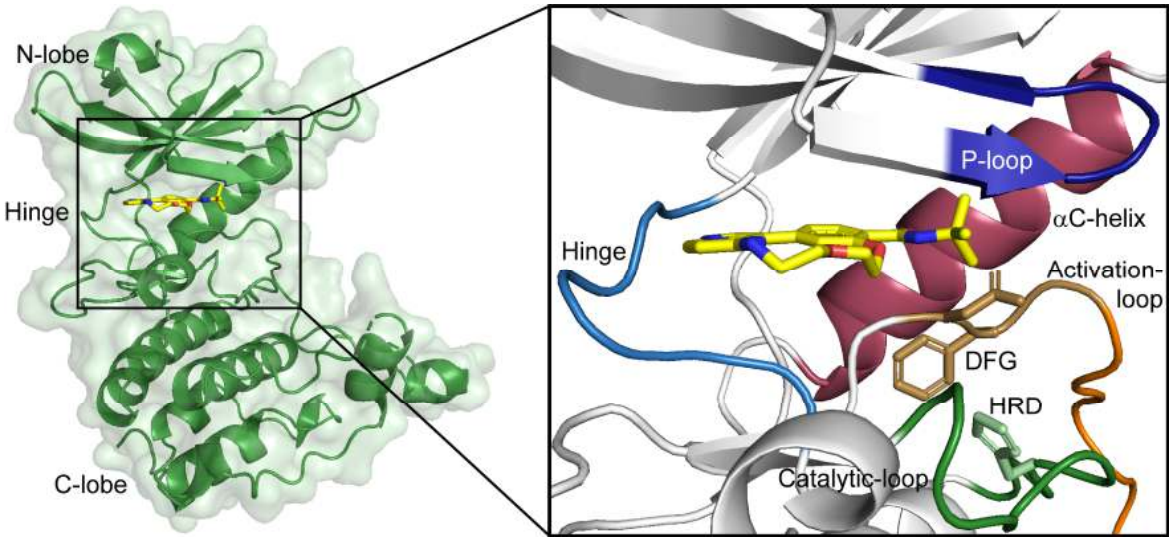

Figure 3: **Monomeric unit of the co-crystal structure of an exemplary kinase with macrocyclic inhibitor.** The N-lobe and the C-lobe are shown, which are connected by the hinge region (left). Highlighted in the cutout (right) of the active site are the hinge region (light blue), the P-loop (dark blue), the αC-helix (red), the activation loop (orange) with DFG motif (light brown), the catalytic loop (dark green) with HRD motif and the macrocyclic inhibitor (yellow).

Studies by Kornev *et al*. revealed that all kinases in the active state share a common highly conserved spatial motif, consisting of four non-consecutive hydrophobic residues.[27] These are Leu of the β4 strand and Leu of αC of the N-lobe as well as Phe of the activation loop and Tyr of the catalytic loop of the C-lobe. The ability of dynamic assembly and disassembly, due to the high mobility of the hydrophobic backbone, imparts regulatory properties over the activity of the kinase and is consequently called regulatory (R) spine.[23]

Another hydrophobic spine was also identified by Kornev *et al.*.[28] This catalytic (C) spine consists of two residues of the N-lobe, Val from β2 and Ala from the AXK motif, which are directly docked with the adenine ring of ATP. From the C-lobe, the catalytic loop docks to the adenine ring via Leu.[23]

1.2 Protein kinase inhibitors

The first step in kinase drug discovery was the ROCK inhibitor fasudil, approved in Japan in 1995 for the treatment of cerebral vasospasm.[29,30] In comparison to the nanomolar inhibition of PKC by bacteria-produced staurosporine (**1**), fasudil was not that potent.[31] More widely known and commercially successful than fasudil was the Abelson murine leukemia viral oncogene homolog (ABL) inhibitor imatinib (**3**) (Gleevec)[32], approved in 2001 for the treatment of chronic myeloid leukemia. Since that time, the number of small molecule kinase inhibitors entering clinical trials has increased dramatically. In 2019, the number of FDA-approved small molecule kinase inhibitors surpassed 50 and now exceeds 70 clinically approved inhibitors.[33] In terms of the entire human kinome, only a small number of kinases are currently targeted. Here, the focus is overwhelmingly on oncological applications.[34] The approval of the non-oncology Janus kinase (JAK) inhibitor tofacitinib for the therapy of rheumatoid arthritis was the starting point for research initiatives in the field of inflammatory diseases. The utilization of kinase inhibitors in the field of autoimmune diseases and degenerative disorders is still in its infancy.[8]

According to their binding modes, kinase inhibitors can be categorized into two classes: Covalent and non-covalent inhibitors. In most cases, covalent inhibitors consist of a binder, linker and a warhead motif and bind covalently with a nucleophilic cysteine or lysine adjacent to the ATP-binding site. Usually, irreversible binding results in a permanent blockade of the ATP site.[17,35] Noncovalent inhibitors differ fundamentally in the conformation of the binding site and the corresponding active or inactive state of the kinase. In fact, many FDA-approved kinase inhibitors target the ATP-binding pocket and are competitive with ATP.[36] This highly druggable binding cavity is located between two catalytic domains and is highly conserved and rigid in the active state within the human kinome. This fact suggests a major difficulty in selective binding of ATP-mimetic compounds.[17,34] Compared to the active state, the inactive state is dynamically and structurally diverse, suggesting the hypothesis that targeting the inactive state of kinases facilitates selective inhibition. The most prominent example of an inactive state is the DFG-out conformation.

Depending on the binding mode adopted, non-covalent inhibitors are further divided into subclasses (type I – IV). Type I inhibitors are ATP-competitive and address the rigid active state of the kinase. Analogous to ATP, 1 – 3 hydrogen bonds are formed with the hinge region and the aspartate residue of the DFG motif is extended into the active site (DFG-in conformation) (**Figure 4A**).[37] The successful design of selective type I inhibitors involves addressing unique active site features such as rare amino acids or local target-specific dynamic features flanking the hinge. The gatekeeper, for example, regulates the entrance to a hydrophobic back pocket that can be addressed in the case of small gatekeeper-residues, such as a threonine. Among others, sunitinib (**2**) (mast/stem cell growth factor receptor Kit (KIT), platelet-derived growth factor receptor (PDGFR), etc. inhibition), erlotinib (**21**) (epidermal growth factor receptor (EGFR) inhibition), dasatinib (ABL, KIT, etc. inhibition) and gefitinib (EGFR inhibition) are examples of successful FDA approval and clinical usage of type I inhibitors.[17,34–36]

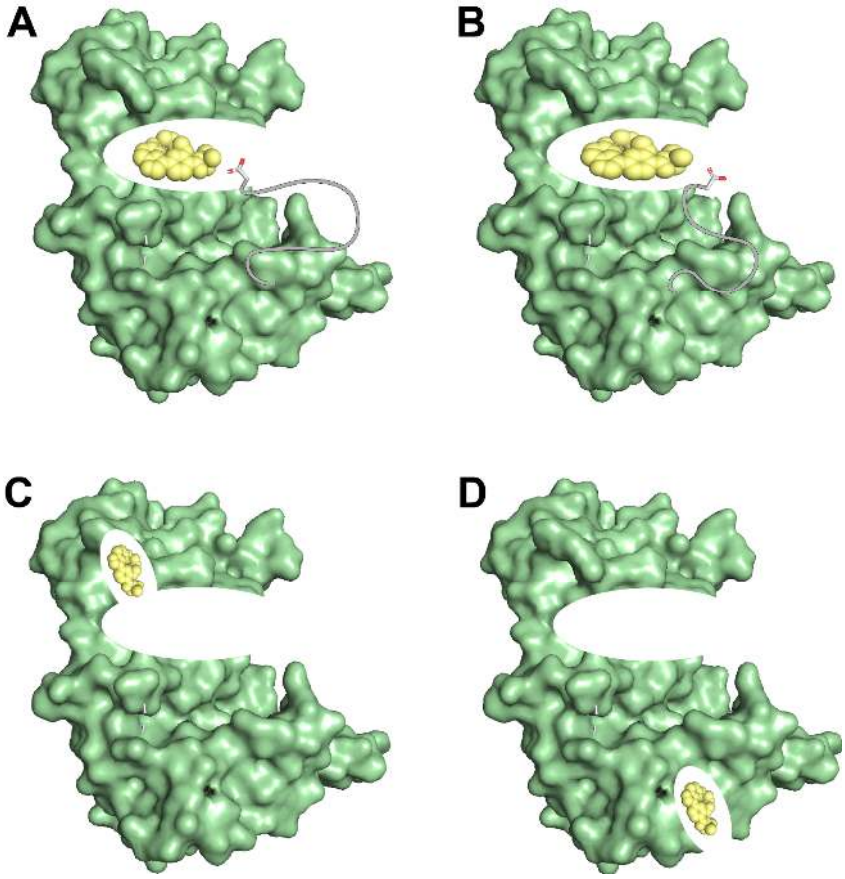

Figure 4: **Simplified illustration of four different reversible binding modes of kinase inhibitors (yellow).** **A**) Type I inhibitors coordinates in the ATP pocket in the active state of the kinase and the aspartate (gray) of the DFG motif points into the binding pocket. **B**) Type II inhibitors bind in the inactive state of the kinase and the aspartate (gray) points out of the binding pocket. **C**) Type III inhibitors address an allosteric pocket adjacent to the ATP binding pocket. **D**) Type IV inhibitors bind in an allosteric pocket remote from the ATP binding pocket. (Modified from Wu et al.[35])

Type II inhibitors bind in the inactive state of the kinase. This binding mode accompanies an approximate 180° rotation of the aspartate of the DFG motif into the DFG-out conformation (**Figure 4B**). This rearrangement results in the opening of another hydrophobic pocket that can be exploited by type II inhibitors. Contrary to expectations, studies[38] demonstrated that targeting type II conformations and the associated increased plasticity of the DFG-out conformation does not per se result in increased selectivity.[34,36] Besides DFG-out, additional kinase-specific inactive states exist, driven by conformational states of the C-helix or the A- or P-loop.[22] Imatinib (**3**) (ABL, PDGFR, KIT), sorafenib (vascular endothelial growth factor (VEGFR), PDGFR, etc.) and nilotinib (ABL, KIT, etc.) are successful examples of FDA-approved inhibitors of this class.

Type III inhibitors are non-ATP competitive and exclusively occupy an allosteric site adjacent to the ATP binding pocket (**Figure 4C**). They prevent the catalytic activity and regulatory mechanisms without affecting ATP binding. It is supposed that each kinase has some potential allosteric pockets. However, unlike type I/II inhibitors, no general screening strategy exists so far to identify type III compounds and many potent inhibitors have been discovered by chance. An example of successful development of an allosteric inhibitor is the highly selective FDA-approved MEK inhibitor trametinib (**5**) for the treatment of melanoma. The major advantage of type III inhibitors in terms of selectivity arises from the less conserved binding sites outside the ATP pocket. In contrast to the ATP site, the acceptability of allosteric pockets to various physicochemical properties is significantly higher, which may come along with additional benefits.[34,36,39]

Type IV inhibitors also target an allosteric pocket, remote to the ATP-binding pocket, or other proteins that interact with the kinas (**Figure 4D**). They prevent appropriate regulation, activation, or downstream actions of the kinase. As well as type III inhibitors, they allow exceptional selectivity due to the specificity of the allosteric binding sites in individual kinase subfamilies or mutant forms in disease. However, identification of these allosteric sites is challenging because they are not specifically defined and may be located anywhere on the kinase.[39–41] The breakpoint cluster region protein (BCR)-ABL1 inhibitor ABL001, binding allosterically in the c-ABL myristoyl pocket, is in clinical trials for the treatment of chronic myelogenous leukemia and represents the successful development of type IV inhibitors.[42]

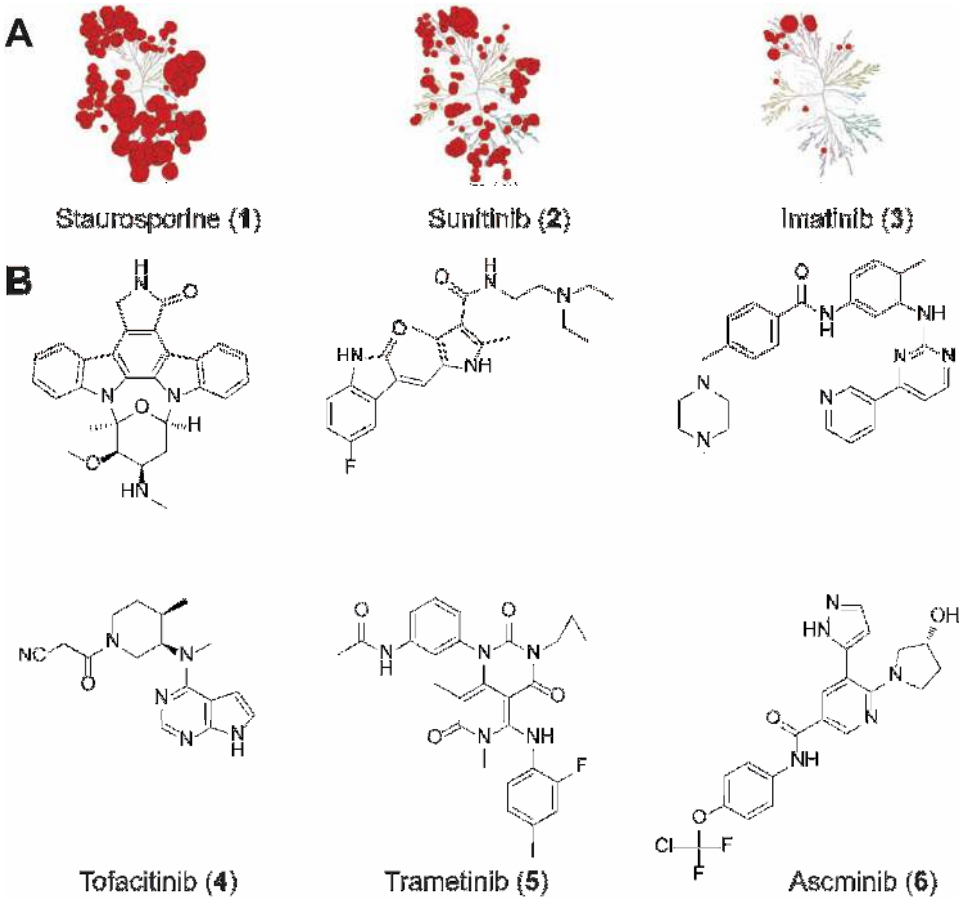

Figure 5: **Examples of FDA-approved kinase inhibitors. A**) Kinome binding maps of staurosporine (**1**), sunitinib (**2**), and imatinib (**3**) illustrating that none of the inhibitors has absolute selectivity. (Modified from Karaman et al.[43]) **B**) Pan-inhibitor staurosporine (**1**), sunitinib (**2**) (primary target VEGFR2) therapeutically indicated in gastrointestinal stromal tumor, pancreatic neuroendocrine tumor and renal cell carcinoma, imatinib (**3**) (primary target BCR-ABL) in Philadelphia chromosome-positive chronic myeloid leukemia or acute lymphoblastic leukemia, aggressive systemic mastocytosis, chronic eosinophilic leukemias, dermatofibrosarcoma protuberans, hypereosinophilic syndrome, gastrointestinal stromal tumor, myelodysplastic/myeloproliferative disease, tofacitinib (**4**) (primary target JAK3) in rheumatoid arthritis, trametinib (**5**) (primary target MEK1/2) in $BRAF^{V600E/K}$ melanoma and $BRAF^{V600E}$ non-small cell lung cancer, and asciminib (**6**) (primary target BCR-ABL1) in Philadelphia chromosome-positive chronic myeloid leukemia.[33]

The design of highly selective small-molecule inhibitors of any type is one of the major challenges in kinase drug discovery. This is emphasized by many FDA-approved kinase inhibitors that involve side effects due to off-target activities (**Figure 5A**). The rigid active state is highly conserved and can be addressed by ATP mimetics of any kind. In contrast, inactive states possess high dynamics, but are associated with the accessibility of unique binding sites. Allosteric compounds are a promising opportunity of inhibition, however, require appropriate screening methods and not every screening hit leads to successful inhibition. Besides the design or identification of selective inhibitors, the challenge is a better understanding of the cellular phenotype related to inhibition.

Consequently, in addition to side effect free therapeutics, the development of chemical tool compounds is indispensable.[34,39,44] Chemical probes should be mentioned in this context. They represent potent, selective, cell-active and broadly characterized small molecules that allow the user to ask mechanistic and phenotypic questions of the particular molecular target in biochemical, cell-based or animal studies.[45,46] However, the development of chemical probes does not contradict the field of multikinase inhibitors. As demonstrated for the type II inhibitor sorafenib, a multikinase inhibitor can also be beneficial. The combined inhibition of the MAPK pathway as well as other kinases involved in vascularization improves the efficacy of sorafinib against tumor signaling and growth.[47]

Another feasible way of achieving selectivity is the introduction of bivalent inhibitors. Therfore, an allosteric inhibitor is fused with an active site-directed inhibitor via a linker, thus increasing potency while maintaining selectivity.[48,49] The FDA-approved lorlatinib (ALK, ROS) exemplifies another promising inhibitor class focused on selectivity as a major goal: macrocycles.

1.3 Macrocyclic kinase inhibitors

Macrocyclic compounds have been of great interest in medical research for a long time. Both, natural product macrocycles and their synthetic derivatives have already found their way into clinical use. For instance, more than 100 drugs, being approved or are in the process of approval, possess a macrocyclic scaffold as bioactive component.[50] By now, macrocyclic scaffolds have become established in medicinal chemistry and are applied in the search for new drugs for many different and difficult target classes.[51] Their peculiarity is based on the occupation of a unique chemical space that cannot be covered by small molecules.[52] This feature, of cyclic frameworks consisting of twelve or more atoms with sizes up to 2000 daltons, can be attributed to a compromise of a certain degree of structural pre-organization while maintaining sufficient flexibility.[50] Macrocycles have also made their way into the field of kinase inhibitors and are still of great interest. This is exemplified by the 2018 FDA approval of the third-generation ALK/ROS1 inhibitor lorlatinib (**8**) (**Figure 6**) for the treatment of non-small cell lung carcinoma.[33,53]

From a historical perspective, there are two origins of macrocyclic drug candidates: Natural products and cyclic peptides. Natural products were used as blueprints for drugs such as erythromycin or the first FDA-approved synthetic macrocyclic kinase inhibitor temsirolimus (**7**)[54] (mTOR inhibitor) for the treatment of advanced renal cell carcinoma (**Figure 6**). Cyclic peptides provided the blueprints for drugs such as octreotide or cyclosporine.[51,55] A common assumption is that macrocycles, especially natural products or natural product analogues, violate Lipinski's rule-of-five. This rule allows, based on the physicochemical characteristics of a given drug candidate, a prediction regarding the oral activity[56]. If the molecule possesses more than 5 H-bond donors, 10 H-bond acceptors, a molecular weight higher than 500 and a calculated log P higher than 5, poor absorption or permeation is more likely.[57] Despite the large number of natural macrocycles and their synthetically derived analogs that are compliant with the rule-of-five, not all targets of interest can be addressed. This fact makes the development of synthetic macrocycles indispensable.

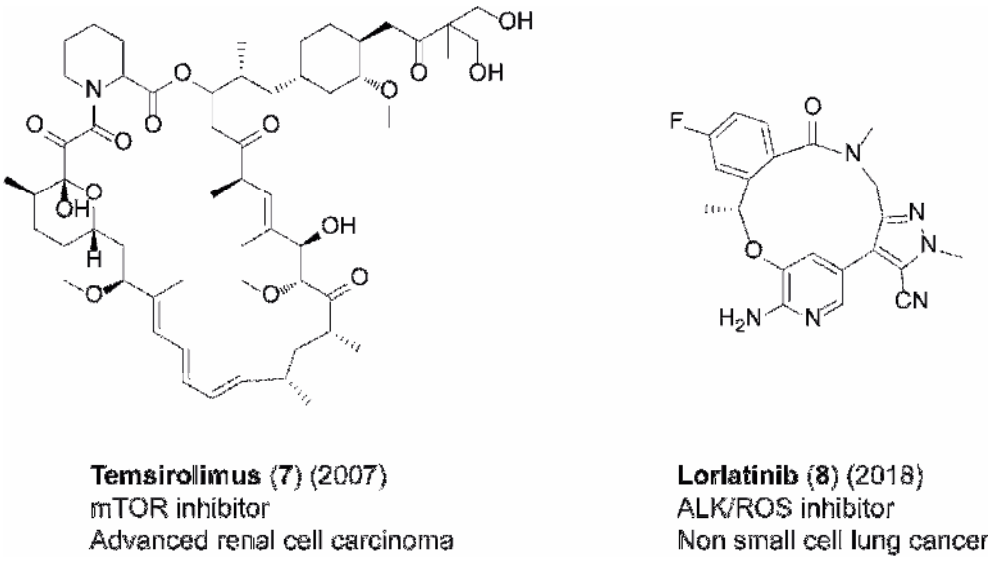

Figure 6: **FDA-approved synthetic macrocyclic kinase inhibitors.** The first approved inhibitor temsirolimus (**7**) (left) and the latest approved macrocyclic kinase inhibitor lorlatinib (**8**) (right).

Many synthetic macrocycles beeing successful in the medicinal chemistry context are not structurally related to natural products and demonstrate high target affinity and selectivity with acceptable drug-like properties.[50] Designing synthetic macrocycles can be quite challenging and therefore requires a sophisticated strategy as well as an understanding of specific ligand-target interactions. Another commonly used approach is the cyclization of a linear pharmacophore, with functionalized termini, using a linker motif (**Figure 7A**).

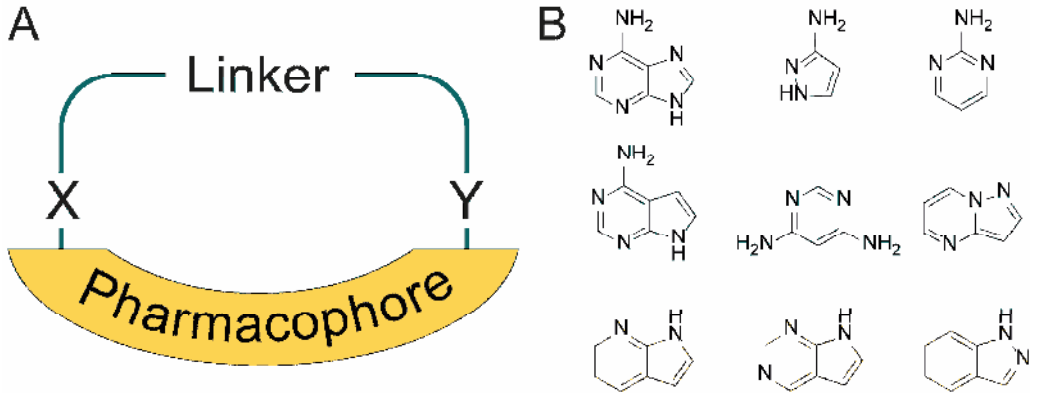

Figure 7: **Schematic architecture of a novel macrocyclic kinase inhibitor. A**) The pharmacophore, usually an ATP mimetic hinge binder scaffold, is cyclized at two positions (X, Y) via a linker motif. (Modified from Mallinson et al.[51]) **B**) Hinge binding scaffolds utilized as pharmacophore (top left to bottom right) adenine, 1H-pyrazole-3-amine, 2-aminopyridine, 7H-pyrrolo[2,3-*d*]pyrimidin-4-amine, pyrimidine-4,6-diamine, pyrazolo[1,5-*a*]pyrimidine, 1H-pyrrolo[2,3-b]pyridine, 7H-pyrrolo[2,3-*d*]pyrimidine and 1H-indazole.[58]

In the field of kinase inhibitors, an ATP-mimetic hinge binder scaffold is used as pharmacophore in most cases (**Figure 7B**). However, it should be mentioned that macrocyclization does not per se lead to the preferred bioactive conformation and studies on the favored ring size have to be performed. The utilization of unfunctionalized alkyl chains of different lengths is a favorable starting point to gain insight into the optimal size of the macrocycle. Another benefit is the direct glimpse into the effect of cyclization on potency and selectivity against a particular target. The knowledge acquired in this manner will be the foundation for further optimization.[51] Examples of successful development of macrocyclic kinase inhibitors are the ALK inhibitor **10** developed by Breslin *et al.*[59] or the ALK/ROS1 inhibitor lorlatinib (**8**) mentioned above. Based on co-crystal structures of linear ALK inhibitors, Johnson *et al.*[53] pursued a structure-based strategy for the development of the macrocyclic inhibitors. The first-generation ALK inhibitor crizotinib (**11**) adopted a U-shaped conformation and the two termini were in close proximity to each other.[60] This is also how the JAK2 and Feline McDonough sarcoma-like tyrosine kinase 3 (FLT3) inhibitor pacritinib was designed[61]. Cyclization of an acyclic ligand by a linker rigidly locked the linear molecule in a low energy bioactive conformation and subsequent structural optimizations resulted in a low nanomolar cell-active inhibitor (**Figure 8**).

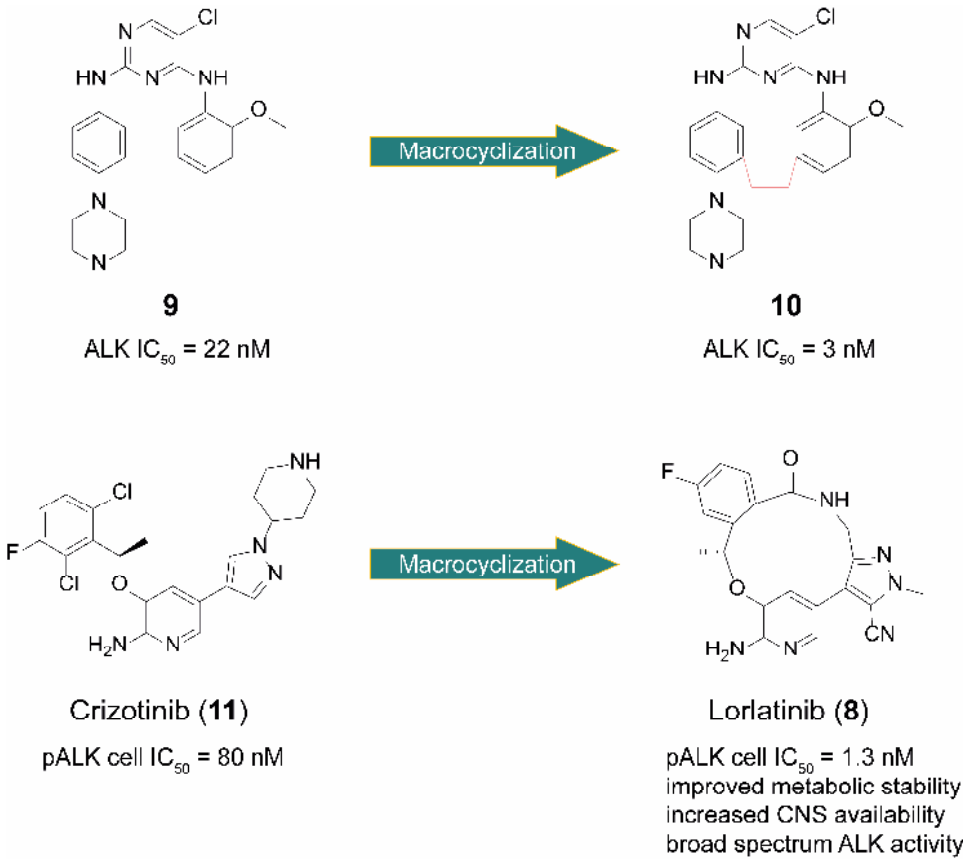

Figure 8: **Exemplary illustration of the effect of macrocyclization in terms of target affinity, physiochemical and pharmacokinetic properties.** Inhibitor **9** with already strong activity on ALK (IC_{50} = 22 nM) was present in a U-shape, which was closed by cyclization. The locked rigid bioactive conformation **10** showed significantly increased activity toward ALK (IC_{50} = 3 nM).[59] The acyclic precursor crizotinib **11** of lorlatinib (**8**) also showed a U-shape that was locked by macrocyclization and converted to the highly active and improved ALK/ROS1 inhibitor lorlatinib (**8**) by minor structural optimization.[53]

This demonstrates how conformational restriction can result in an increase in potency against the target. The cyclization is accompanied by a restricted internal bond rotation of the molecule, which results in a limitation of the number of possible conformations of the unbound molecule. However, enough flexibility remains to interact efficiently with flexible binding sites. When forming the protein-inhibitor complex, the entropic loss is significantly reduced and the affinity towards the target is increased.[50,51] In the case of lorlatinib, it has also been demonstrated how macrocyclization can improve physicochemical and pharmacological properties. The improvement of brain penetration allowed the crossing of the blood-brain barrier and the achievement of therapeutic CNS drug concentrations. In addition the metabolic stability as well as the efficiency against all known resistant ALK mutants were increased.[62,63] The effect of the length of the linker and the resulting size of the macrocycle on the inhibitor activity is demonstrated by a CHK1 inhibitor by Tao *et al.*.[64]

With increased linker length (n), the affinity of the inhibitors towards CHK1 decreases from 6 nM (n = 14) to 28 nM (n = 16). This may be due to excessive flexibility of the ring and the associated increase in entropic cost, or it may be due to steric reasons. In certain circumstances, the increase in potency may induce an increase in selectivity. A large affinity towards the target, due to specific conformation, could theoretically generate selectivity, but is not obligatory. In the course of developing multikinase inhibitors for cycline-dependent kinase (CDK), JAK2, and FLT3, William *et al.* demonstrated that structural changes in the linker can lead to altered selectivity.[65] The choice of connectivity might be important as well. This was demonstrated by Lücking *et al.* with multiple targeting of CDK and VEGF-R.[66] The fact that further structural changes lead to changes in potency and selectivity is beyond question and will not be discussed further here.

Cyclization is the critical point in the synthesis of macrocycles, which in many cases must be performed under high dilution and is still not distinguished by high yields. Since the first efforts to synthesize macrocyclic compounds, there has been a steadily growing literature on preferred cyclization methods. A well-known structural motif in natural macrocycles is the lactone and thus, macrolactonization is an attractive route for the ring-closing reaction. Exemplary is the variant of Mitsunobu *et al*. using triphenylphosphine (PPh_3) and diethyl azodicarboxylate (DEAD).[67] Established in the solid-phase peptide synthesis are coupling reagents such as (benzotriazol-1-yloxy)tripyrrolidinophosphonium hexafluorophosphate (PyBOP)[68] or 1-[bis(dimethylamino)methylene]-1H-1,2,3-triazolo-[4,5-b]pyridinium 3-oxide hexafluoro-phosphate (HATU)[69], which can be used to create so-called macrolactams. However, one of the most favored methods is the ring-closing metathesis (RCM). The carbon-carbon double bonds used, for example, in Grubbs' catalysis[70] can be introduced at any point in the synthesis, as they are not affected by most reactions conditions. Further examples that have been already successfully used in the synthesis of macrocyclic compounds are macroaldolization and palladium-catalyzed cross-coupling reactions such as the Suzuki reaction.[71,72]

1.4 Kinases in the focus of the thesis

1.4.1 Casein kinase 2

Casein kinase 2 (CK2) was discovered together with CK1 by Burnett and Kennedy in 1954 as the first protein kinases to phosphorylate casein *in vitro* (not *in vivo*).[73] The ubiquitous expressed serine/threonine kinase is highly pleiotropic and constitutively active.[74] Nevertheless, the ability to phosphorylate tyrosine is also attributed to it.[75] Over 430 CK2 phospho-sites have now been identified that are addressed using ATP and GTP as cofactors.[76,77] This vast number of putative substrates highlights CK2 as a key player of regulation in a diverse selection of cellular processes such as cell cycle progression, apoptosis and transcription.[78,79] A possible explanation for the involvement in diverse pathways (**Figure 9**) is the ubiquitous distribution from the cell nucleus to the plasma membrane and the possibility to interact with different substrates.[80]

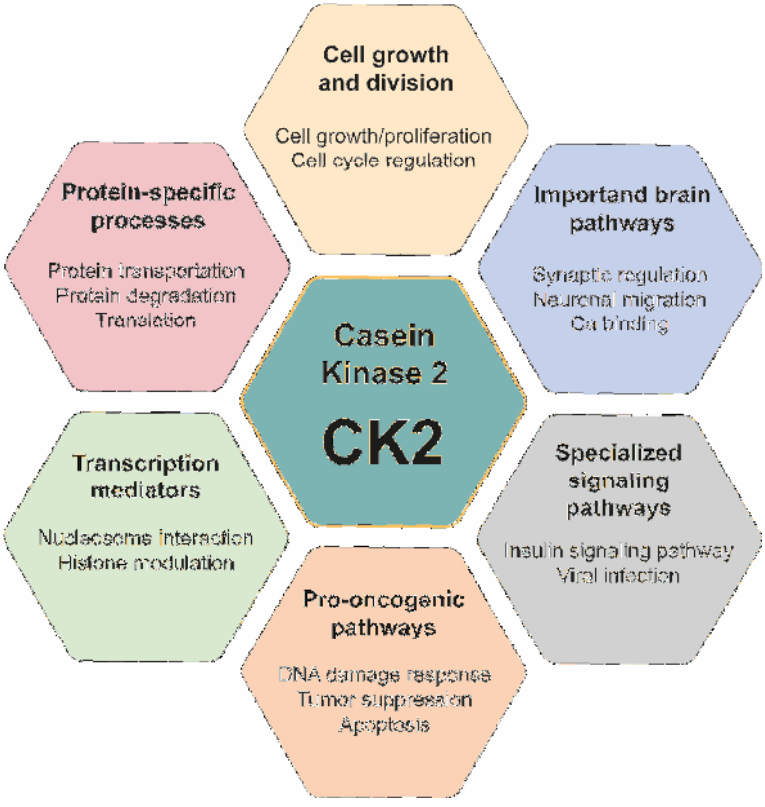

Figure 9: **Illustrated summary of most common CK2 mediated pathways with corresponding examples.**[81]

Structural studies revealed that the holoenzyme CK2 appears to exist as an $\alpha_2\beta_2$ heterotetrameric complex (**Figure 10**) in eukaryotic organisms. It is composed of two isoenzymic forms of the catalytic subunit (CK2α and/or CK2α'), which are also catalytically active alone as a subunit[82], and two regulatory subunits (CK2β).[83] The sequence similarity of the CK2α isoforms is 75%, with the main differences being found in the C-terminal domain.[84] Unlike many other kinases, CK2 is always in its active state. The A-loop does not need to be phosphorylated to promote maximum activity. It is frozen in an open, and thus active, conformation and the activity of the kinase is regulated by stable interaction of the N-terminal tail and the kinase domain as well as the activation segment, respectively.[85,86] The CK2β subunits contribute to the stability of the tetrameric complex. The N-terminal domain is responsible for the interaction with a second CK2β subunit and the C-terminal domain for the complex formation with the CK2α subunits and their regulation.[87] The regulatory subunits form, via zinc finger domains, a dimer that links the catalytic subunits.[88] Across the extended C-terminal tail of CK2β, each catalytic subunit interacts with both regulatory chains. The formation of the holoenzyme significantly increases the activity of CK2 compared to CK2α/α'.[84] Due to constitutive activity, CK2 regulation is not mediated by phosphorylation, but rather by expression level and localization.

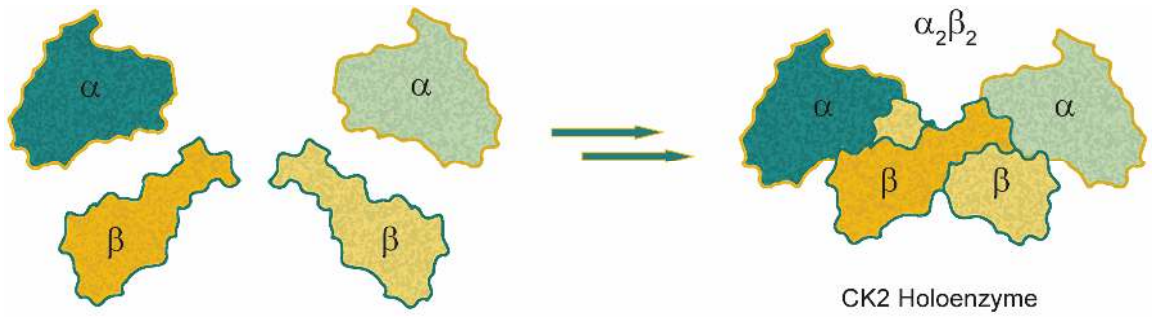

Figure 10: **Schematic formation of the symmetric CK2 holoenzyme.** The holoenzyme consists of two α catalytic (green) and two β regulatory (yellow) subunits. (Modified from Lolli et al.[89])

A vast landscape of studies demonstrated that CK2 and its dysregulation are implicated in many different human pathologies such as cardiovascular diseases, inflammation, neurodegeneration, vascular, muscle diseases, virus and parasite infections as well as various types of cancer.[90] In tumors, such as in breast, lung, colon and prostate cancer, CK2 activity is invariably more increased in the nuclear compartment than in corresponding normal tissues/cells.[78,91]

The increased CK2 activity appears to create a cellular milieu favorable for cancer progression and is referred to as addiction. In contrast to other oncogenic kinases, no mutation has been detected for CK2 that gives rise to tumor formation. However, since CK2 is involved in almost all essential tumor-promoting signal transduction pathways, these are enhanced by upregulated CK2 activity due to overexpression. Particular attention has been paid to the role of CK2 in the suppression of apoptosis and cell survival, as cancer cells exhibit not only dysregulated growth but also dysregulated cell death.[92,93] The engagement of the caspase pathway is an example of how CK2 is correlated with apoptosis. The consensus recognition motif for cleavage by caspases and phosphorylation by CK2 are strikingly similar. Several studies demonstrated that caspase substrates, such as the BH3 interacting omain death agonist (Bid), could be phosphorylated by CK2 in proximity to the caspase cleavage site. This results in blocking their degradation and consequently the formation of the cleavage products that promote apoptotic progression.[78,94–96] CK2 is also involved in another pathway of regulation for cell survival in cancer: DNA damage response and DNA repair pathways. Proteins such as mediator of DNA damage checkpoint protein 1 (MDC1), DNA repair protein RAD51 and treacle ribosome biogenesis factor 1 (TCOF1) require phosphorylation by CK2 to interact with the forkhead-associated domain (FHA) domain of the nibrin (NBN) component of the MRN (double-strand break repair protein meiotic recombination 11; RAD50; NBN) complex. This plays an important role in the initial processing of DNA damage repair.[78,97,98] Both, the correlation with apoptosis and DNA damage repair are involved in antitumor drug resistance in addition to the reduction of intracellular drug concentration by drug efflux or drug metabolism.[99]

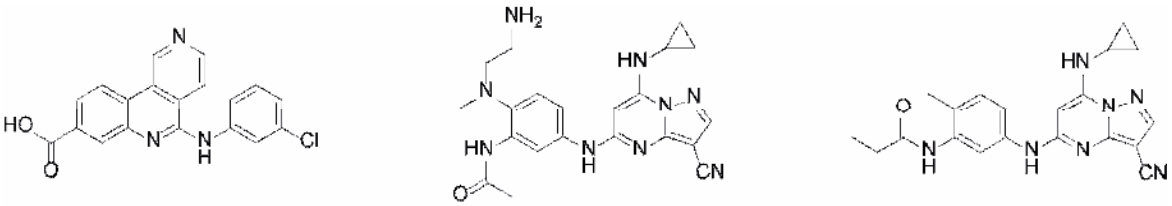

Figure 11: **Representative inhibitors of CK2.** Silmitasertib (**12**): An FDA-approved drug against advanced cholangiocarcinoma; AstraZeneca CK2 (**13**): A highly potent pyrazolo[1,5-*a*]pyrimidine-based inhibitor, but associated with off-target effects; SGC-CK2-1 (**14**): A highly selective chemical probe compound.

In the field of small molecule inhibitors, many attempts have been made to address CK2.[81,82,100–105] Some highlight compounds are shown in **Figure 11** above. The role of CK2 as a therapeutic target was highlighted by the granting of orphan drug status by the FDA for the promising inhibitor silmitasertib (**12**) (CX-4945), in the treatment of advanced cholangiocarcinoma.[106] Downregulation of CK2 results in reduction of cancer cell viability and induction of apoptosis.[107] Inhibition of CK2 by silmitasertib (**12**) is based on ATP competitive binding to both isoforms of the catalytic subunits (CK2α and CK2α') in a low nanomolar range (IC_{50} = 1 nM). However, the putative selectivity was disproved by the identification of a significant number of off-targets. In a screen against 238 kinases, potent inhibition of death-associated protein kinase 3 (DAPK3) (17 nM), FLT3 (35 nM), TANK-binding kinase 1 (TBK1) (35 nM), cell division cycle kinase-like kinase 3 (CLK3) (41 nM), homeodomain-interacting protein kinase 3 (HIPK3) (45 nM), proto-oncogene serine/threonine-protein kinase Pim-1 (PIM1) (46 nM), and CDK1 (56 nM) was detected.[108,109] AstraZeneca developed a pyrazolo[1,5-*a*]pyrimidine-based inhibitor (CK2α IC_{50} < 3 nM), but it is also associated with significant off-target activity on, for example, dual-specificity tyrosine regulated kinases (DYRK), DAPKs, and HIPKs in the nanomolar range.[110] For studying CK2, the highly selective chemical probe SGC-CK2-1 (**14**) (CK2α IC_{50} = 4.2 nM, CK2α´ IC_{50} = 2.3 nM) based on the AstraZeneca one, was introduced by Wells *et al*..[81]

1.4.2 Death-associated protein kinase-related apoptosis-inducing protein kinase 1

Serine/threonine kinase (STK17A), also known as death-associated protein kinase-related apoptosis-inducing protein kinase 1 (DRAK1)[111], belongs to the family of death-associated protein kinases (DAPKs), which is assigned to the group of CAMKs. The origin of DAPKs is found in the isolation of DAPK1 from a screen for genes whose proteins are responsible for interferon-y-induced death in HeLa cells. Further investigation revealed the closely related DAPK2 and DAPK3 with highly conserved kinase domain (83% and 80% identity with DAPK1). As the name implies, DAPK1 is regulatory involved in both caspase-dependent and independent cell death. Besides apoptosis, this most studied kinase of the small family is also involved in the regulation of other cellular processes such as autophagy and many more.[112] The two other family members, the more distantly related DRAK1 and DRAK2, sharing 48% and 51% identity at the amino acid level compared to DAPK1.[113]

While the N-terminal catalytic kinase domains share high similarity, the C-terminal regulatory domains of DAPKs differ substantially[114], resulting from different stimuli as triggers for induced cell death in a context dependent way. In comparison with DAPK1-3, DRAK1 and DRAK2 are significantly understudied. They are part of the so-called dark kinome and there is a lack of knowledge about their role in cell signaling. Sanjo *et al.* described morphological changes characteristic of apoptosis in NIH3T3 cells induced by overexpression of these two ubiquitously expressed kinase. The DRAK1 gene, located on chromosome 7, encodes the 46-kDa kinase DARK1, which consists of 414 residues.[115]

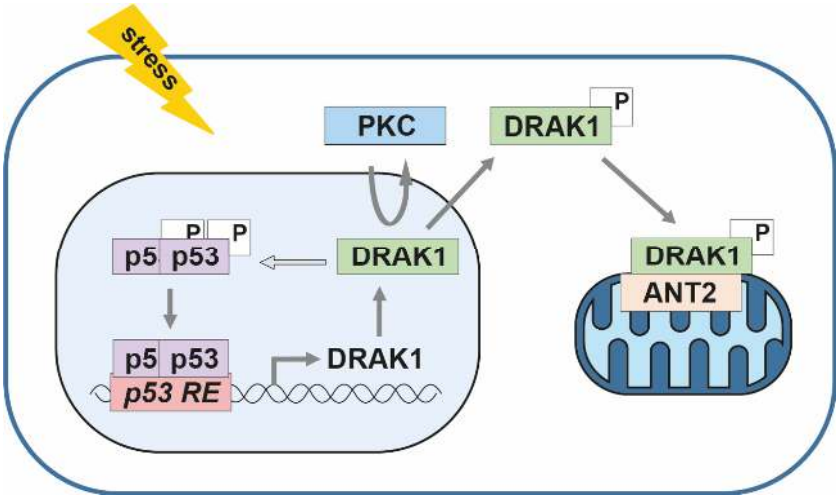

Figure 12: **Proposed model of the DRAK1 signaling pathway.** Possible translocalization of DRAK1 outside the nucleus (light blue) into the cytosol (white) and interaction with ANT2 in the mitochendria (dark blue; right). Upregulation of DRAK1 by cellular stress and DRAK1 as a direct target gene of the tumor suppressor p53 in testicular cancer cells (left). p53 RE, p53-responsive element. (Modified from Oue et al.[116])

In studies by Mao *et al.*[117], DRAK1 was identified as a direct target gene of the tumor suppressor p53 in testicular cancer cells. p53 directly binds to an upstream element in the DRAK1 gene and induces expression (**Figure 12**). DRAK1 is upregulated by the DNA-damage agent cisplatin and overexpression of DRAK1 results in an increase in reactive oxygen species (ROS). In this manner, DRAK1 regulates cell survival, apoptosis and ROS accumulation in testicular cancer cells. DRAK1 is mainly localized in the nucleus of various cancer cells where interaction with p53 occurs.[115] However, Oue *et al.*[116] postulate a possible translocalization of DRAK1, initiated via phosphorylation by PKC, from the nucleus to the cytosol, including mitochondria; as well as a positive regulation of p53 transcriptional activity in U2OS cells (**Figure 12**).

In the mitochondria, DRAK1 interacts with the anti-apoptotic oncoprotein adenine nucleotide translocase 2 (ANT2). Thus, DRAK1 may also be involved in pro-death activity in a regulatory manner. The oncogenic activity of cytoplasmic DRAK1 in head and neck squamous carcinoma (HNSCC) was studied by Park *et al.*.[118] DRAK1 binds to the C-terminal Mad Homology 2 (MH2) domain of small mothers against decapentaplegic 3 (Smad3) and blocks the formation of the Smad3/4 complex in the cytoplasm. This effects the inhibition of the transforming growth factor b (TGF-b) downstream pathway. In this manner, DRAK1 regulates TGF-b1-induced transcriptional activity and expression of the tumor suppression gene p21WAF1/Cip1 and promotes tumorigenesis of HNSCC cells.

In addition to HNSCC, DARK1 is also overexpressed in a grade-dependent manner in various gliomas compared to normal brain tissue.[112,119] The highest expression levels were found in glioblastoma multiforme (GBM) and are associated with a significant survival disadvantage among patients with glioma.[120] GBM is the most common and aggressive malignant primary brain tumor and an important cause of morbidity and mortality.[121] Mao *et al.* demonstrated that DRAK1 knockdown results in a significant alteration of cell shape associated with decreased proliferation, clonogenicity, migration, invasion and anchorage independent colony formation.[120] The capacity of DRAK1 as a downstream effector of EGFR, which is amplified and mutated in a large subset of patients[122], and phosphoinositide 3 kinases (PI3K) signaling pathway was revealed by Chen *et al.*. It is hypothesized that DRAK1 potentiates EGFR signaling and thus enhances myosin regulatory light chain (MRLC) activation. Through the associated effect on the human aniline analog ANLN, mitosis and cytokinesis are regulated in gliomas.[123]

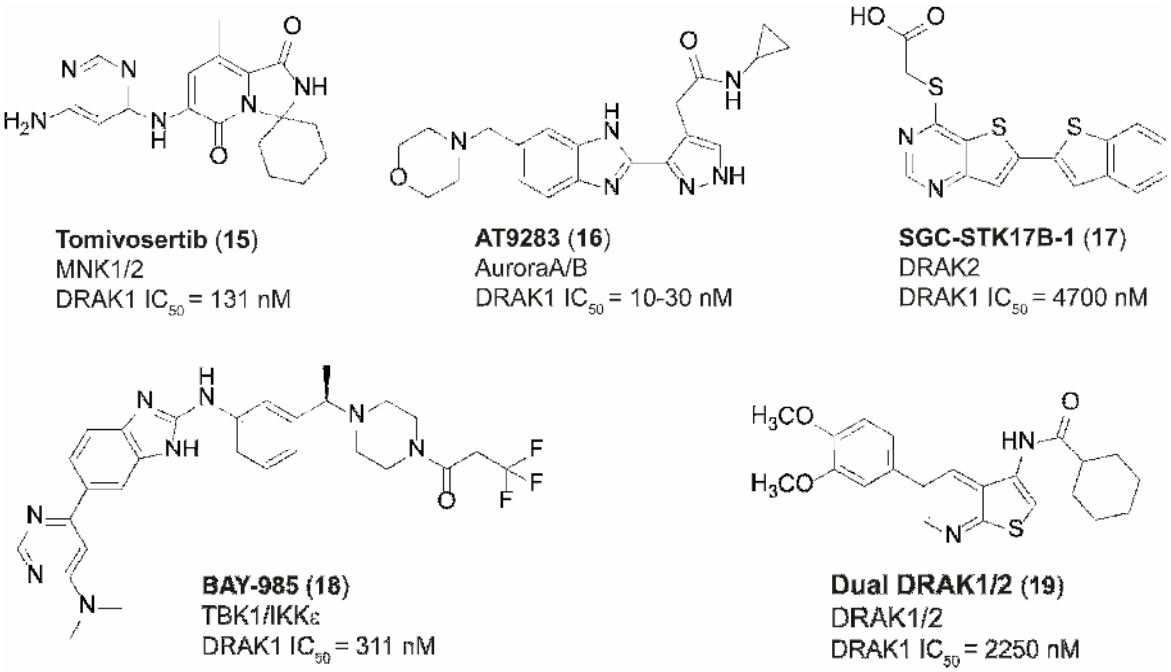

Figure 13: **Kinase inhibitors with inhibitory activity an DRAK1.** Tomivosertib (**15**), AT9283 (**16**), SGC-STK17B-1 (**17**) and BAY-985 (**18**) addressing DRAK1 as an off-target. However, a dual DRAK1 and DRAK2 inhibitor (**19)** is available. Up to now, no exclusive DRAK1 inhibitors are known.

To date the number of DRAK1 inhibitors is negligible and no selective inhibitor is available. Examples are shown in **Figure 13**. In almost all the cases, DRAK1 have been identified as an off-target as in the case of the highly potent MNK1/2 inhibitor tomivosertib (**15**) (eFT508) (IC_{50} = 2.4 nM and 1 nM), which also inhibits DRAK1 (IC_{50} = 131 nM).[124] Other examples are the Aurora A/B inhibitor AT9283 (**16**) (AurA/B IC_{50} = 3 nM; DRAK1 IC_{50} = 10 – 30 nM) and the TBK1/ inhibitor of nuclear factor kappa-B kinase subunit epsilon (IKKε) inhibitor BAY-985 (**18**) (TBK1/IKKε IC_{50} = 2/30 nM (low/high ATP) and 2 nM; DRAK1 IC_{50} = 311 nM).[125,126] Recently Picado *et al*. have developed a chemical probe (**17**) for DRAK2 (IC_{50} = 34 nM) with good isoform selectivity and low micromolar activity on DRAK1 (IC_{50} = 4700 nM).[119] Since 2014, a dual DRAK1 and DRAK2 inhibitor (**19**) by Gao *et al.* is available as a potential starting point for chemical probes, however, no follow-up studies have been reported.[127]

1.4.3 AP-2-associated protein kinase

AP-2-associated protein kinase (AAK1) is a serine-threonine kinase of the highly diverse Numb-associated kinase (NAK) family. It is named after the *Drosphila* protein NAK, which is associated with the protein numb homolog Numb and involved in asymmetric cell division. Besides AAK1, members of this family are BMP-2-inducible kinase (BIKE/BMP2K), cyclin G-associated kinase (GAK) and myristoylated and palmitoylated serine/threonine kinase 1 (STK16/MPSK1). Within the kinase domains, there is approximately 30% familial sequence similarity. AAK1 and BIKE are the most closely related and show an overall sequence similarity of 50% and more than 70% in the kinase domain. This is particularly evident in the strong interaction with the same inhibitors, such as baricitinib (**20**) (AAK1 K_D = 17; BIKE K_D = 40). Concerning cellular functions, the NAK family is related to a broad spectrum such as receptor-mediated endocytosis, Notch pathway modulation, osteoblast differentiation and dendrite morphogenesis.[128]

AAK1 is a key player in clathrin-mediated endocytosis, which is a crucial process in vesicular trafficking. In this process, a wide range of cargo molecules is transported from cell surface to the interior. Clustering of endocytic coat proteins from the cytosol in the inner leaflet of the plasma membrane is the initial step. With further recruitment of other coat proteins from the cytosolic pool, protein coat assembly proceeds. Cargo molecules are concentrated at the coated region of the membrane. After cargo recruitment, the plasma membrane, promoted by the assembling coat, is bent and clathrin-coated pits (CCPs) are formed. So called scission proteins achieve the separation of the clathrin-coated vesicles. The shaping of the membrane is promoted by the cooperation of actin polymerization with the coat and scission proteins. In the final step, the cargo-filled vesicle is released by uncoating and the endocytotic protein machinery is disassembled.[129]

Besides clathrin, the adapter protein (AP) 2 complex, composed of four subunits (α, β2, μ2 and σ2), is essential for clathrin-dependent endocytosis[130]. The two major subunits α and β2 are responsible for binding to the plasma membrane, clathrin and other accessory proteins. The middle subunit μ2 interacts with the tyrosine-based sorting signal YXXΦ (Y: tyrosine, X: any amino acid, Φ: amino acid with bulky hydrophobic side chain) in the cytoplasmic tail of cargo molecules and appears to be the recognition of endocytic cargo. The small σ subunit is involved in the recognition of dileucine-based sorting motifs.[131]

AAK1 and GAK phosphorylate the μ2 subunit of the AP-2 complex, resulting in a conformational change and exposure of the binding site of the tyrosine-based YXXΦ internalization motif[130,132,133], which is located at the cytoplasmic tail of some receptors and mediates cargo recruitment to clathrin-coated vesicles (CCV).[134] By increasing the activity of AAK1 through interaction with assembled clathrin, cargo uptake can be enhanced in CCPs.[132] Also phosphorylated by AAK1/GAK is the AP-1 complex, which is involved in the formation of CCVs as well. Unlike AP-2, AP-1-containing CCVs are formed in the trans-Golgi network (TGN) and facilitate the transport of cargo from the TGN to endosomes.[135] AAK1/GAK regulate clathrin-mediated endocytosis through additional pathways. Alternative sorting adapters, such as peripheral membrane-associated Numb, may collaborate with AP-2.[136] Numb, which is phosphorylated by AAK1, has an amino-terminal phosphotyrosine-binding domain (PTB) for binding its cargos. Via an aspartic acid-proline-phenylalanine motif (DPF), Numb mediates a conserved interaction with the α subunit of AP-2 and promote receptor recruitment into CCPs. Further interactions may occur with EPS15 (regulation of endocytosis and vesicle transport) and EHD1/5 (membrane receptor recycling).[131,137,138]

Neveu *et al*. demonstrated that phosphorylation of AP-2 plays a key role in the life cycle of hepatitis C virus (HCV). The HCV core (capsid) protein has a YXXΦ motif which is bound by AP-2. Utilizing this mechanism, the virus is able to hijack endocytic functions for its assembly.[139] A model also proposed by Neveu *et al*. suggests an important function of AAK1 and GAK in the entry of HCV. This is based on the critical role of EGFR in HCV entry and the involvement of AAK1 and GAK in EGFR internalization and recycling. After phosphorylation of AP-2 (μ2 subunit) by AAK1/GAK and Numb by AAK1, they collaborate with other endocytic factors. This enhances endocytosis as well as recycling of EGFR and potentionally an additional HCV coreceptor.[140] Bekerman *et al*. revealed the activity of AP-1, regulated by AAK1 and GAK, in HCV release. While AP-2 cotraffics with HCV entry and assembly, AP-1 cotraffics with HCV upon release.[141] The involvement of AAK1 and GAK in clathrin-mediated endocytosis and the involvement in viral entry, assembly, and release, respectively, are schematically illustrated in **Figure 14**.

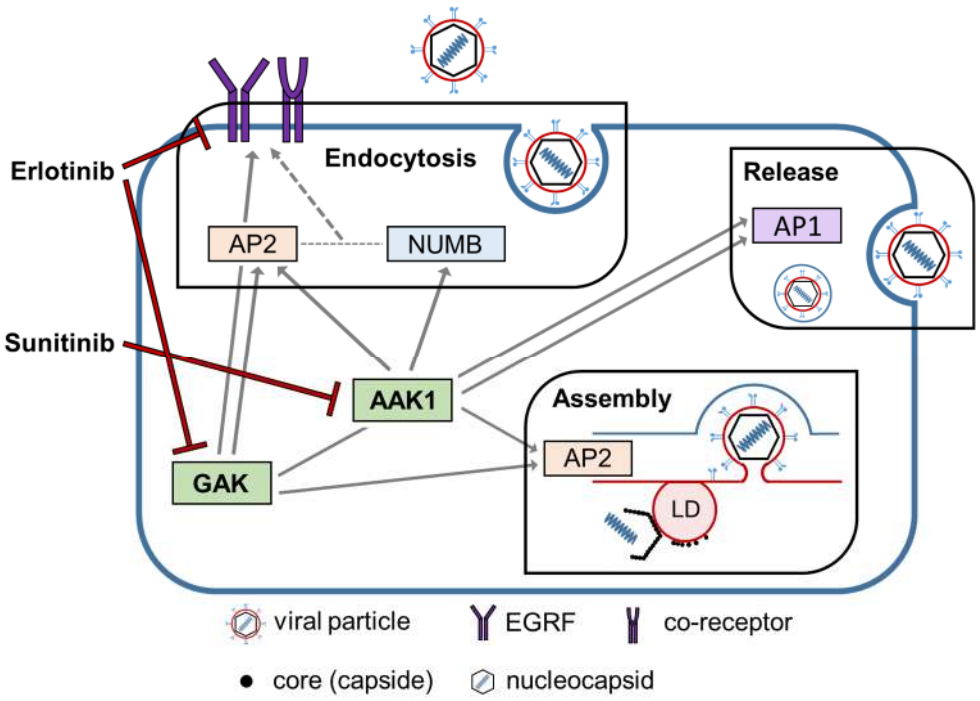

Figure 14: **Proposed model of AAK1 and GAK as drug target in the viral live cycle of HCV.** Both kinases phosphorylate the AP-1/2 complexes and AAK1 phosphorylates Numb as well. Collaboration of these complexes with other endocytotic factors enhances endocytosis, assembly, and release. In the case of endocytosis, recycling of EGFR and potential HCV coreceptors is also promoted. Collaboration of these complexes with other endocytotic factors enhances endocytosis, assembly, and release. In the case of endocytosis, recycling of EGFR and potential HCV coreceptors is also promoted. Sunitinib (**2**) inhibits AAK1 and erlotinib (**21**) inhibits GAK and EGFR and disrupt these temporally distinct steps of the viral life cycle. (Modified from Neveu et al.[140])

The regulation of AP-1 and AP-2 by AAK1 and GAK can be applied to other RNA viruses. For example, the anti-cancer drugs sunitinib (**2**) (AAK1 IC_{50} = 33 nM) and erlotinib (**21**) (GAK IC_{50} = 40 nM) show potent antiviral activity against dengue virus (DENV) and Ebola virus (EBOV) *in vitro* and *in vivo*.[141,142] However, AAK1 is also related to other diseases and is targeted in neurological diseases such as schizophrenia, Parkinson's disease, neuropathic pain, bipolar disorders and Alzheimer's disease.[143–145] Some literature has pointed to a possible involvement of AAK1 in the SARS-CoV-2 life cycle as well.[146–149]

A screen of 144 clinically used kinase inhibitors in a thermal shift assay by Sorrell *et al.* showed surprisingly high affinities of many of the drugs toward AAK1 and other NAK kinases. Interestingly, many of these kinase inhibitors have been reported in literature to be highly selective. One possible reason could be the absence of the NAK kinases in commercial selectivity panels.[128]

The receptor tyrosine kinase (RTK) inhibitor sunitinib (**2**) (AAK1 IC_{50} = 33 nM), for the treatment of advanced renal cell carcinoma and gastrointestinal stromal tumors[150], and the JAK1/2 inhibitor baricitinib (**20**) (AAK1 IC_{50} = 17 nM), indicated against rheumatoid arthritis[151] and in combination with remdesivir against COVID-19[152], are given as examples (**Figure 15**). Kostich *et al*. presented the highly potent (AAK1 IC_{50} = 3.3 nM) and selective inhibitor LP-935509 (**22**) with off-target activity within the NAK family (BIKE IC_{50} = 14 nM, GAK IC_{50} = 320) as an approach to treat neuropathic pain.[143] For studying AAK1 and GAK, a 3-acylaminoindazole based selective chemical probe, dual inhibiting AAK1 (IC_{50} = 233 nM) and GAK (IC_{50} = 1.48 µM), was presented by Wells *et al*..[153]

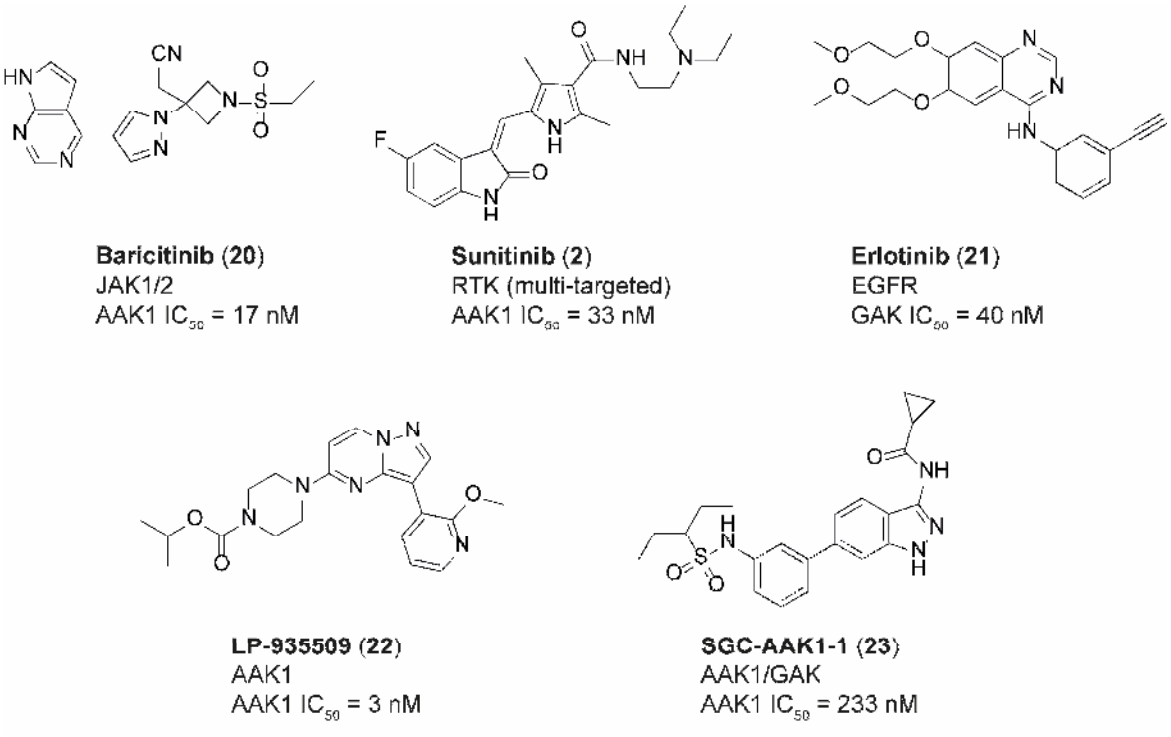

Figure 15: **Representative kinase inhibitors with AAK1 or GAK activity.** Sunitinib (**2**) and baricitinib (**20**) with strong off-target activity on AAK1 and the EGFR inhibitor erlotinib (**21**) with GAK activity. Both sunitinib (**2**) and erlotinib (**20**) showed antiviral effects in experiments with HCV as described above. The compounds LP-935509 (**22**) and SGC-AAK1-1 (**23**) represent AAK1 inhibitors with high, but not exclusive, selectivity.

2. Objectives

Being involved in many critical functions in cellular signaling pathways, kinases are key players in a large diversity of diseases, especially in oncology. Their activity is characterized by phosphorylation of a downstream signaling event and is catalyzed by ATP binding in a highly conserved active site. The development of highly selective ATP-mimetic inhibitors is challenging due to the highly conserved binding pocket. Locking the bioactive conformation of acyclic inhibitors by macrocyclization provides an opportunity to improve their shape complementarity. The formation of a 12 or more atoms ring system with conformational restriction might reduce the entropic cost during binding, presumably resulting in increased affinity toward the target protein. Macrocyclic kinase inhibitors are usually composed of a hinge binding motif, for example a pyrazolo[1,5-*a*]pyrimidine, which is cyclized via a linker. Compound ODS2004070 (**37**), which was part of structure-activity relationship (SAR) studies for the development of an FLT3 inhibitor, is also based on this structural motif known from the literature.[154] This kinase inhibitor revealed strong activity against a large number of target proteins, making it an ideal starting point for the development of highly selective and potent inhibitors. A schematic illustration of the aims of the thesis is shown in **Figure 16**.

Consequently, the aims of this thesis are:

- **Synthesis of macrocyclic kinase inhibitors based on ODS2004070 (37).**
- **Identification of potential target proteins.**
- **Target-specific structure-activity relationship (SAR) studies.**
- **Structural optimization of promising compounds.**
- **Characterization of most promising compounds regarding their selectivity, potency and potential biological activity.**

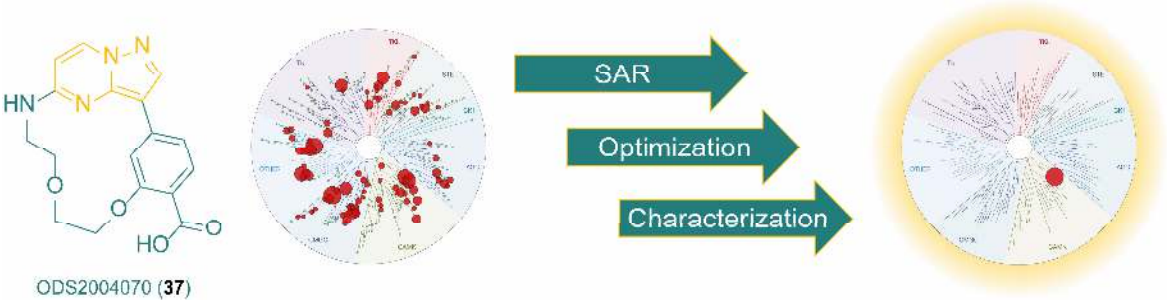

Figure 16: **Aims of this thesis schematically illustrated.** Starting from the unselective pyrazolo[1,5-*a*]-pyrimidine-based macrocyclic compound ODS2004070 (**37**), SAR studies should be performed and, by structural optimization, highly selective kinase inhibitors are to be synthesized and characterized.

3. Results and discussion

3.1 Organic synthesis

The macrocyclic scaffold **37** was generated in a twelve-step synthesis route, which can be seen in **Scheme 1** below. It can be divided into three sections (**A** – **C**). The synthesis of the dual protected pyrazolo[1,5-*a*]pyrimidine hinge binder motif with polyethylene glycol (PEG) linker **28** (**A**), the synthesis of the pinacolborane ester **32** (**B**), and the fusion of the two building blocks followed by ring closure followed by deprotection (**C**). As a starting point for the synthesis of **37**, a protocol out of literature[154] was used and modified.

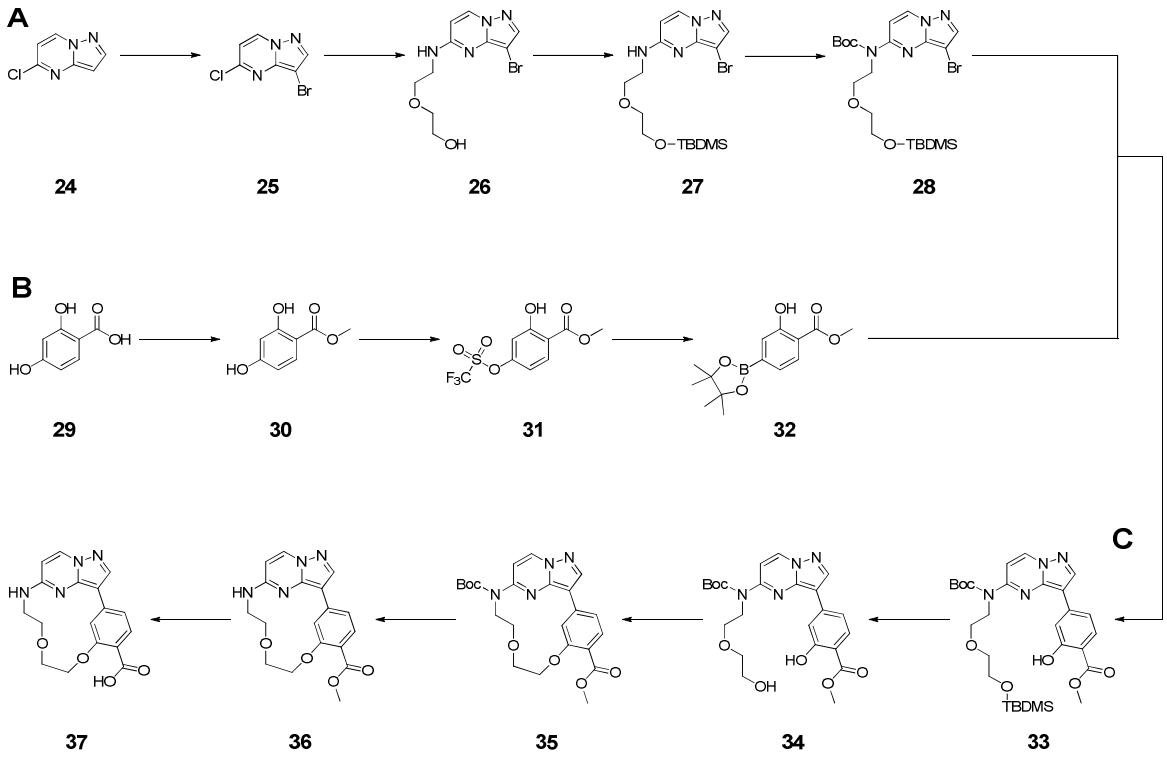

Scheme 1: **Synthesis overview of the macrocyclic scaffold 37, divided into three sections. A**) Synthesis of dual protected hinge binder with linker **28**. **B**) Synthesis of the pinacol borane ester **32**. **C**) Fusion of the building blocks **28** and **32** followed by ring closure and deprotection towards **37**.

The derivatization of the macrocyclic scaffold **37** could be realized at different sites by various methods (**Scheme 2**). Amines were introduced at the carboxylic acid via amide coupling (**A**) to give the compounds **61** – **73** (**Scheme 11** and **Scheme 12**) and **107** – **121** (**Scheme 17**, **Scheme 18** and **Scheme 19**). Alternatively, different amines could be introduced via the Curtius reaction (**B**), also at the carboxylic acid, forming the corresponding urea derivatives **85** – **92** (**Scheme 14** and **Scheme 15**). Another modification of interest is the introduction of different residues at the secondary amine between hinge binder and linker motif. Due to the deactivation of the amine by the adjacent heteroaromatic system with a nitrogen in *para* position, a synthesis strategy using triphosgene was established (**C**). The primary amines, introduced by this synthetic pathway, were linked to the macrocyclic scaffold **37** via urea or carbamate to give the compounds **151** – **156** (**Scheme 23**) as well as **167** and **168** (**Scheme 25**).

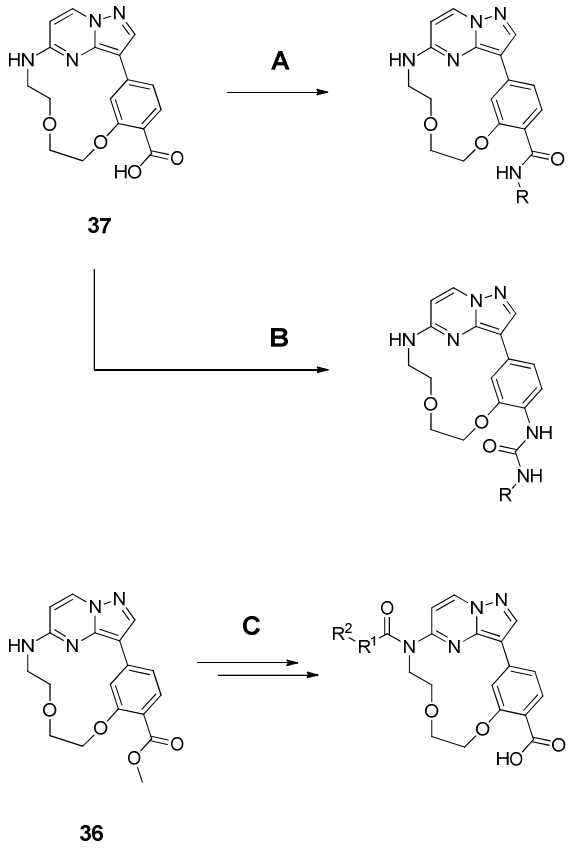

Scheme 2: **Derivatization of the macrocyclic scaffold 37. A**) Amide coupling, **B**) Curtius reaction or **C**) reaction with triphosgene (urea and carbamate derivatives).

The exchange of the linker motif represents another possibility for variation of the macrocyclic scaffold **37** and is illustrated in the following **Scheme 3**. The synthesis proceeded following the route shown in **Scheme 1**, but differs in the choice of the linker motif in section **A**. Thus, the macrocyclic scaffolds **38** and **39** could be obtained. These were also modified via amide coupling at the carboxylic acid and compounds **138** – **143** (**Scheme 21** and **Scheme 22**) were obtained.

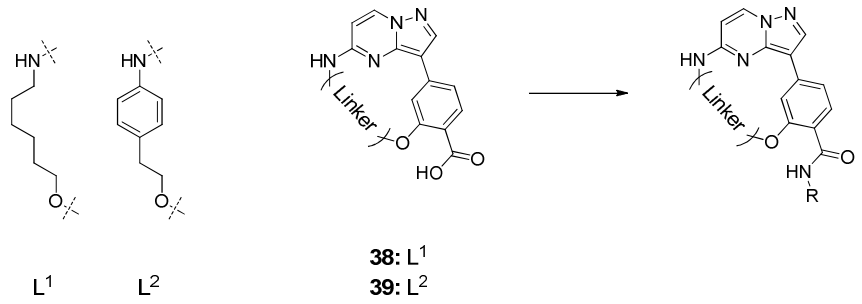

Scheme 3: Variation of the linker motif and derivatization of 38 and 39. The linker motif of **37** was substituted by an six-membered aliphatic (L^1) or an aromatic (L^2) linker motif and the resulting macrocycles **38** and **39** were derivatized at the carboxylic acid by amide coupling.

3.1.1 Synthesis of *tert*-butyl *N*-{3-bromopyrazolo[1,5-*a*]pyrimidin-5-yl}-*N*-(2-{2-[(*tert*-butyldimethylsilyl)oxy]ethoxy}ethyl)carbamate (28).

The synthesis of the dual protected pyrazolo[1,5-*a*]pyrimidine hinge binder motif was carried out in four steps (see **Scheme 4**). In the initial step the 5-chloropyrazolo [1,5-*a*]pyrimidine (**24**) was brominated with *N*-bromosuccinimide (NBS). The reaction was almost quantitative (96% yield). In the second step, the linker was introduced via a nucleophilic aromatic substitution. Therefore, **25** was reacted with 2-(2-aminoethoxy)-ethanol, using *N,N*-diisopropylethylamine (DIPEA), with a yield of 81%. The protection of the hydroxy group was carried out, also under basic conditions, using *tert*-butyldimethylsilyl chloride (TBDMSCl) with a yield of 75%. The secondary amine of **27** was finally protected as *tert*-butyl carbamate (Boc) under basic conditions and usage of 4-(dimethylamino)pyridine (4-DMAP). The turnover rate of **27** to **28** was quantitative (95% yield) and the overall yield of building block **28** was in a good range of 55%.

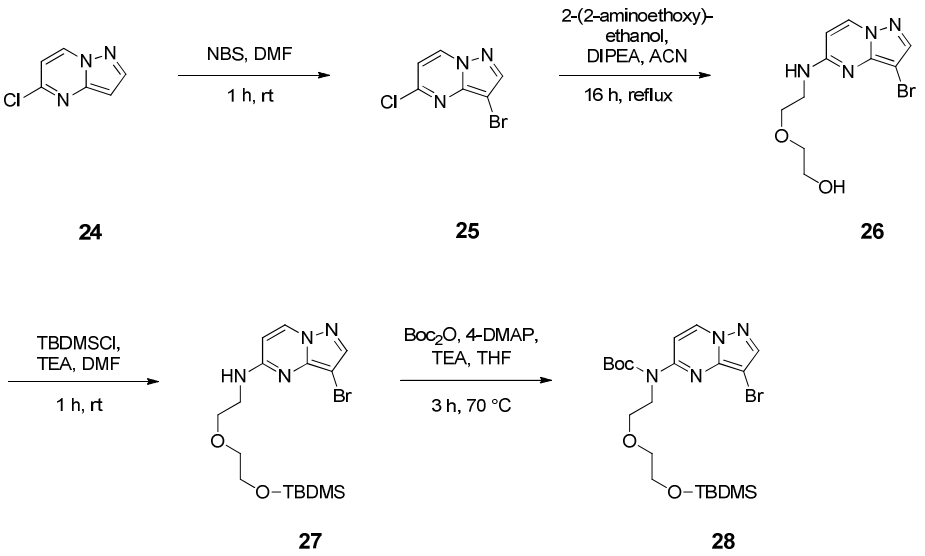

Scheme 4: **Synthesis of dual protected pyrazolo[1,5-*a*]pyrimidine hinge binder motif 28.** First, **24** was brominated, the linker motif was introduced to **25** by nucleophilic substitution, the hydroxy group of **26** was protected as silyl ether and the secondary amine of **27** was Boc protected.

3.1.2 Synthesis of methyl 2-hydroxy-4(4,4,5,5-tetramethyl-1,3,2-dioxaborolan-2-yl)benzoate (32).

For the preparation of the pinacol borane ester **32**, a three-step synthetic route was pursued (see **Scheme 5**). To protect the carboxylic acid of 2,4-dihydroxybenzoic acid **29**, it was esterified in methanol (MeOH) under acidic conditions. The methyl ester **30** was obtained with a manageable yield of 46%.

Removal of water by separation, in order to balance the equilibrium on the product side, did not significantly increase the turnover rate. In the second step, the hydroxyl group in para position to the methyl ester was activated by triflation. For this purpose, **30** was reacted, under basic conditions and catalyzed by 4-DMAP, with trifluoromethanesulfonic anhydride (Tf_2O). The yield was almost quantitative (91%).

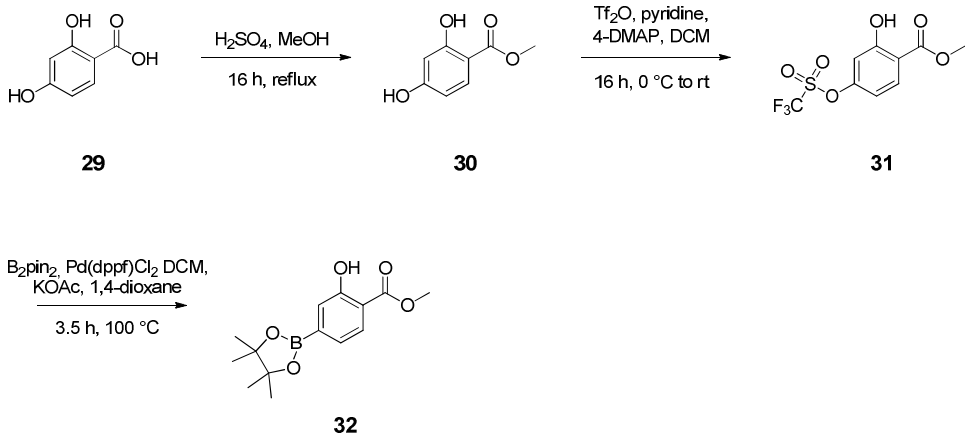

Scheme 5: **Synthesis of the pinacol borane ester 32**. First, **29** was esterified, the hydroxy group of **30** was triflated and **31** converted into the pinacol boronic ester **32**.

The obtained corresponding triflate **31** was converted to the pinacol boronic ester **32** in a Miyaura borylation. The turnover rate of this reaction was 81%. The slightly reduced overall yield of the synthesis of building block **32** of 34% is related to the esterification but was accepted due to economic factors. The reaction was carried out using bis(pinacolato)-diborone (B_2pin_2), [1,1′-bis(diphenylphosphino)ferrocene]dichloro-palladium(II) complex with dichloromethane ($Pd(dppf)Cl_2 \cdot DCM$) and potassium acetate (KOAc) in 1,4-dioxane. The general mechanism of the Miyaura reaction is shown in **Scheme 6**. It is a palladium-catalyzed cross-coupling of aryl halides or aryl triflates with bis(pinacolato)diborone.

The catalytic cycle is initiated by the oxidative addition of the aryl triflate **41** to the palladium catalyst **40**. With cleavage of the triflate anion, an acetate anion coordinates to the palladium complex **42**. The addition of the pinacol boronic ester to complex **43** in trans position to the aryl group, takes place with cleavage of the acetate anion. This step is called transmetalation. In the subsequent step, *cis*/*trans* isomerization takes place in complex **44**. Finally, the desired pinacol boronic ester **46** is cleaved from complex **45** under reductive elimination and the catalyst complex **40** is regenerated again.[155,156]

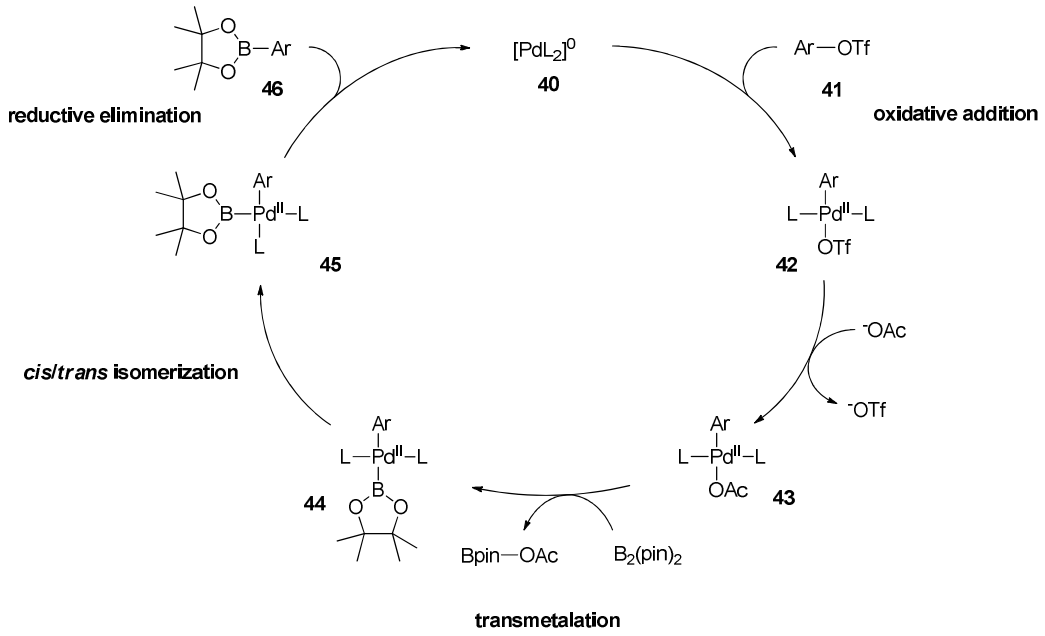

Scheme 6: **General catalytic cycle of the Miyaura borylation using aryl triflate and B_2pin_2.**

3.1.3 Synthesis of 7,10-dioxa-13,17,18,21-tetraazatetracyclo[12.5.2.1²,⁶.0¹⁷,²⁰]-docosa-1(20),2,4,6(22),14(21),15,18-heptaene-5-carboxylic acid (37).

In the synthesis of the macrocyclic pyrazolo[1,5-*a*]pyrimidine-based scaffold **37**, the two building blocks **28** and **32** were linked and the ring was closed. This rout consists of five synthetic steps which are subdivided in linkage and ring closure (**Scheme 7**) and deprotection (**Scheme 10**). To investigate potential effects of macrocyclization compared to the corresponding acyclic compounds, **46** and **47** were also synthesized (**Scheme 7**). First step was the fusion of building blocks **28** and **32** via Suzuki cross-coupling.

For this purpose, tris(dibenzylideneacetone)dipalladium(0) ($Pd_2dba)_3$), 2-dicyclohexyl-phosphino-2′,4′,6′-triisopropylbiphenyl (XPhos) and potassium phosphate (K_3PO_4) in 1,4-dioxane and water were used. The reaction was carried out with very good yields up to 91%. The general mechanism can be seen in **Scheme 8**.

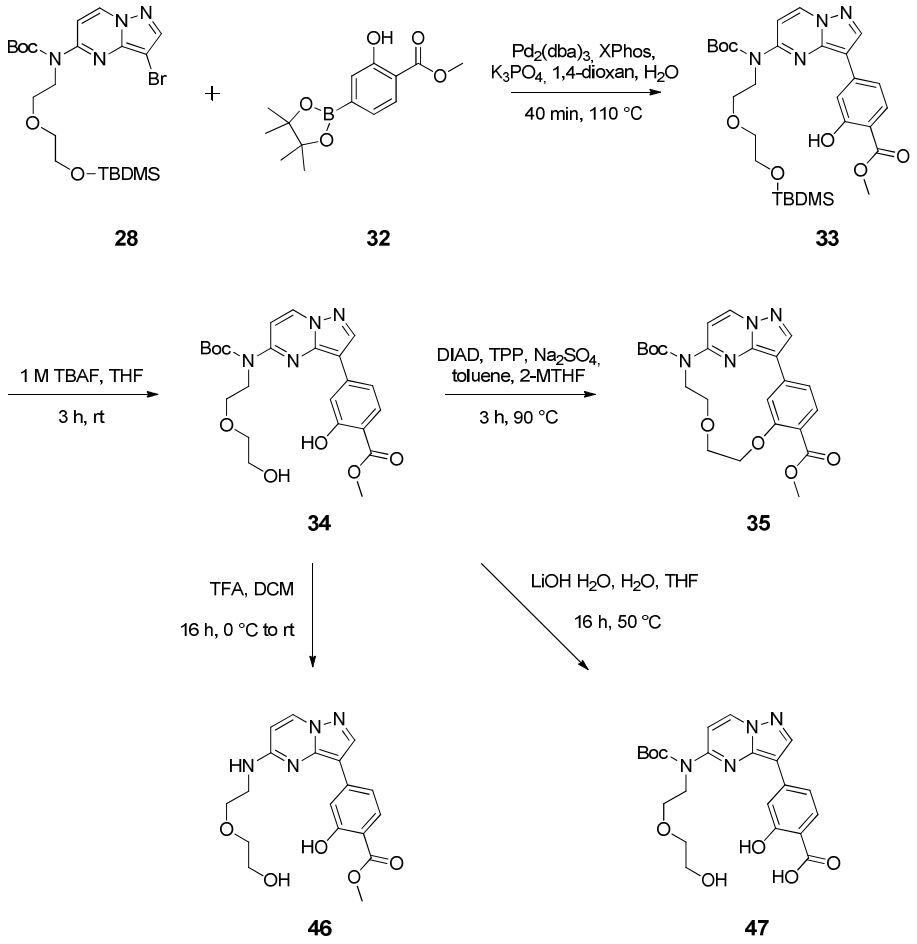

Scheme 7: **Synthesis of macrocyclic compound 35 and acyclic compounds 34, 46 and 47.** First, **28** and **32** were fused by Suzuki cross-coupling, the silyl ether of **33** was cleaved and **35** was obtained by macrocyclization of **34** via Mitsunobu reaction. **46** was obtained by cleavage of the Boc protecting group and **47** by ester cleavage.

The Suzuki coupling is a palladium-catalyzed cross-coupling reaction between organoboronic acids and halides under basic conditions. In the initial step, the halogen compound **49** is bound to the Pd^0 complex **48** via an oxidative addition. Coordination of a base to the catalyst complex **50** is accompanied by cleavage of the halide ion. The polar bond, formed between palladium and oxygen in **51**, enhances the transmetalation that proceeds in the next step. Here, the activated organoboronic acid **52** binds to the catalytic complex **51** under cleavage of the base.

In the final step of the catalysis cycle, the product **54** is cleaved from the complex **53** under reductive elimination and the catalyst is regenerated [157–159].

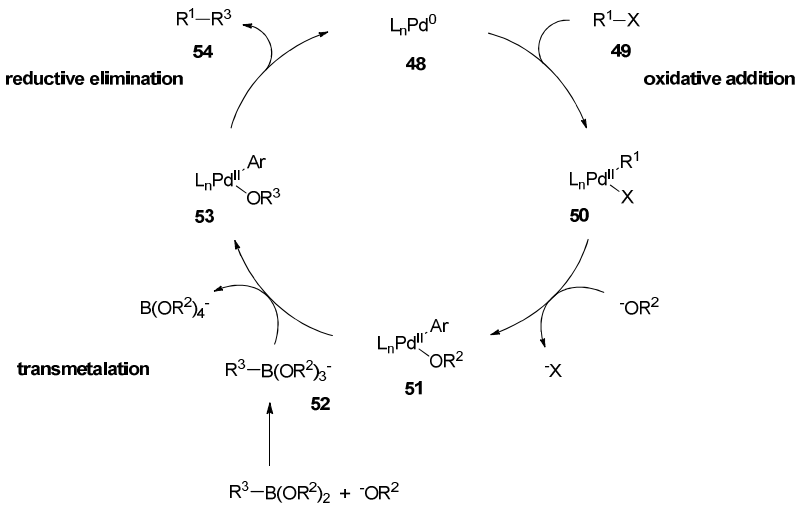

Scheme 8: **General mechanism of a Suzuki cross-coupling reaction between organoboronic acid and halide.**

In the second step, the silyl protecting group was cleaved from **33** to enable ring closure. For deprotection, 1 M tetrabutylammonium fluoride (TBAF) solution was used and **34** was obtained in a yield of 85%. Ring closure to form the macrocyclic compound **35** was done by Mitsunobu reaction using triphenylphosphine (TPP) and diisopropyl azodicarboxylate (DIAD) in toluene and 2-methyltetrahydrofuran (2-MTHF). To avoid intermolecular side reaction, the reaction was carried out under very high dilution (0.0037 M) and sodium sulfate (Na_2SO_4) was added as a desiccant. The yield was very good with 87%. However, significant upscaling effects were observed at a batch size larger than 500 mg and the yields were decreased. The general mechanism of the conversion of two alcohols to an ether is shown in **Scheme 9**. The acidity of one of the alcohols, such as a phenol or a carboxylic acid, is required for this reaction. In the first step, the nitrogen of DIAD (**55**) is nucleophilically attacked by TPP. The resulting betaine intermediate **56** deprotonates the first alcohol. In the next step, the second alcohol binds to the phosphonium ion (**57**), followed by reduction of DIAD to the hydrazine derivative (**59**) and oxidation of the phosphorus. This results in the cleavage of the alcohol triphenylphosphonium ion (**58**). The final step consists of the nucleophilic substitution attack of the alkoxide on **60** to give the desired ether **61**. The formation of the strong phosphorus oxygen bond in the triphenylphosphine oxide is considered to be the driving force of the reaction.[160–162]

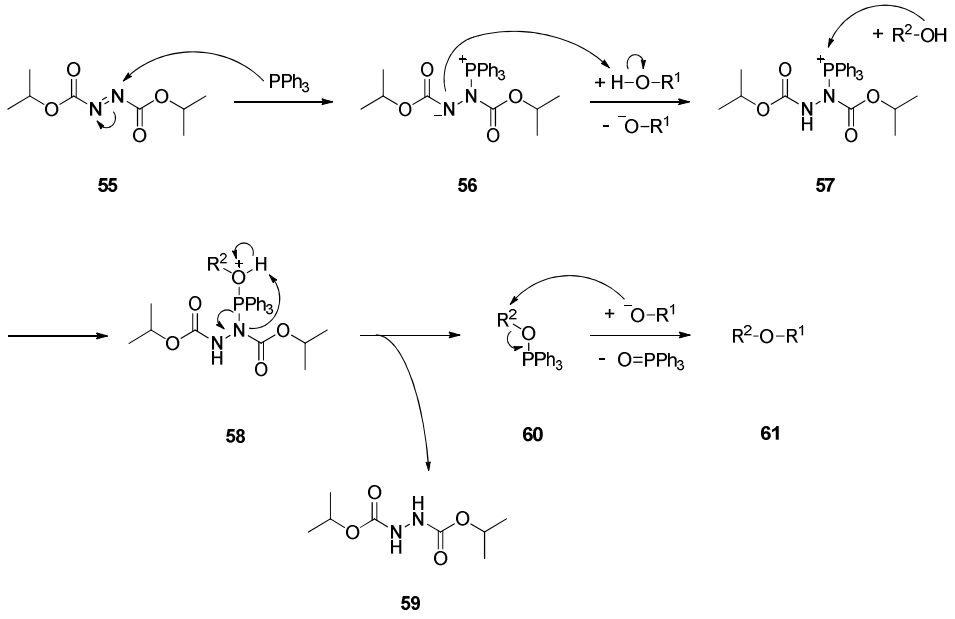

Scheme 9: **General mechanism of the Mitsunobu reaction of two alcohols using DIAD and TPP.**

The acyclic compound **34** was partially deprotected. Addition of trifluoroacetic acid (TFA) resulted in the cleavage of the Boc group and **46** was obtained in 85% yield. Reaction of **34** with lithium hydroxide monohydrate (LiOH · H_2O) led to cleavage of the methyl ester. The low yield of 42% can be related to the Boc group, which was also partially cleaved. To circumvent this problem, different reaction conditions were established to synthesize the cyclic compound **47**. The methyl ester, while retaining the Boc group, was selectively hydrolyzed with trimethyltin hydroxide (Me_3SnOH) under microwave radiation in dichloroethane (DCE)[163]. The yield could be increased to 54%. The very mild basic character of trimethyltin hydroxide may be an explanation of the incomplete turnover rate. The final steps in the synthetic rout to macrocyclic scaffold **37** consisted of the cleavage of the protecting groups from **35** and are illustrated in **Scheme 10**. Reaction with TFA in dichloromethane (DCM) resulted in cleavage of the Boc group, yielding **36** with a turnover rate of 84%. In the subsequent step, the methyl ester was hydrolyzed almost quantitatively (94%) using LiOH · H_2O to give **37**. The overall yield of macrocyclic scaffold **37** was quite high, yielding 18% over 12 steps.

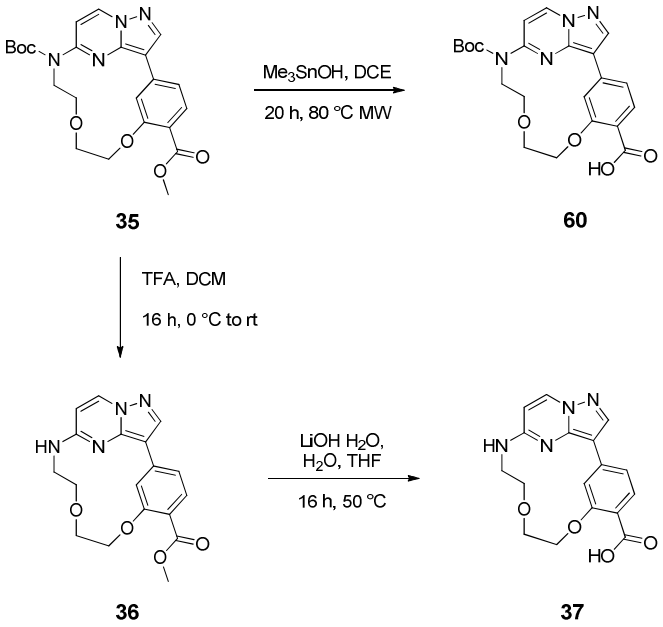

Scheme 10: **Synthesis of macrocyclic compounds 36, 37 and 60.** The ester of 35 was cleaved to obtain **60**. Deprotecting of the secondary amine of **35** resulted in **36**, followed by ester cleavage to obtain **37**.

3.1.4 Synthesis of benzylamide-based derivatives.

To synthesize the single and dual substituted benzylamide-based derivatives **61** – **73**, the carboxylic acid of the macrocyclic scaffold **37** was modified via amide coupling (**Scheme 11** and **Scheme 12**). For this step, the coupling reagent (1-[bis(dimethylamino)methylene]-1*H*-1,2,3-triazolo[4,5-*b*]pyridinium 3-oxide hexafluorophosphate (HATU) was used. The reactions were carried out under basic conditions with DIPEA in dimethylformamide (DMF).

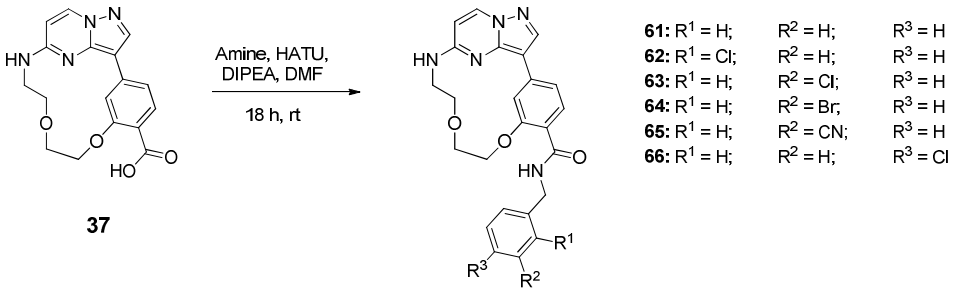

Scheme 11. **Synthesis of single substituted benzylamide-based derivatives (61 – 66).** The derivatives were obtained by amide coupling of the carboxylic acid of **37** with the corresponding amine.

In these reactions, a primary amine was combined with a carboxylic acid using the coupling reagent to form a secondary amide. Derivatizations with single and dual substituted benzyl amines were performed under identical reaction conditions. The yields ranged from 53 to 97%.

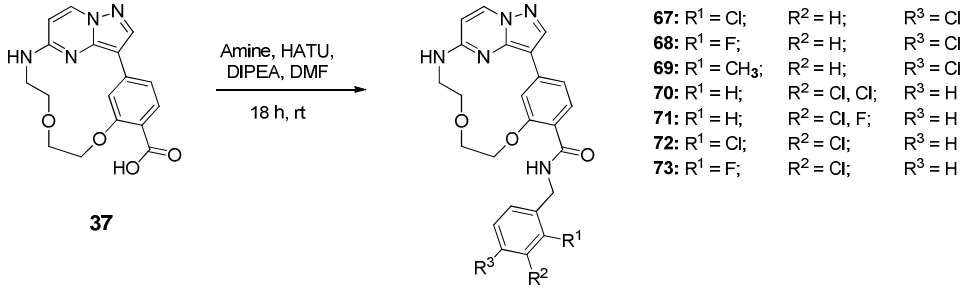

Scheme 12: **Synthesis of dual substituted benzylamide-based derivatives (67 – 73).** The derivatives were obtained by amide coupling of the carboxylic acid of **37** with the corresponding amine.

The general mechanism of the derivatization reactions can be seen in **Scheme 13**. In the initial step, the deprotonated carboxylic acid **74** nucleophilically attacks HATU (**75**). Cleavage of **76** gives the unstable O-acyl(tetramethyl)isouronium salt **78** and the 1-hydroxy-7-azabenzotriazole (HOAt) anion **77** attacks **78**. Compound **79** decomposes to give tetramethylurea **80** and the activated OAt ester **81**. The ester is nucleophilically attacked by the amine and the decomposition of **82** results in the formation of HOAt (**83**) and the desired amide **84**.[164–166]

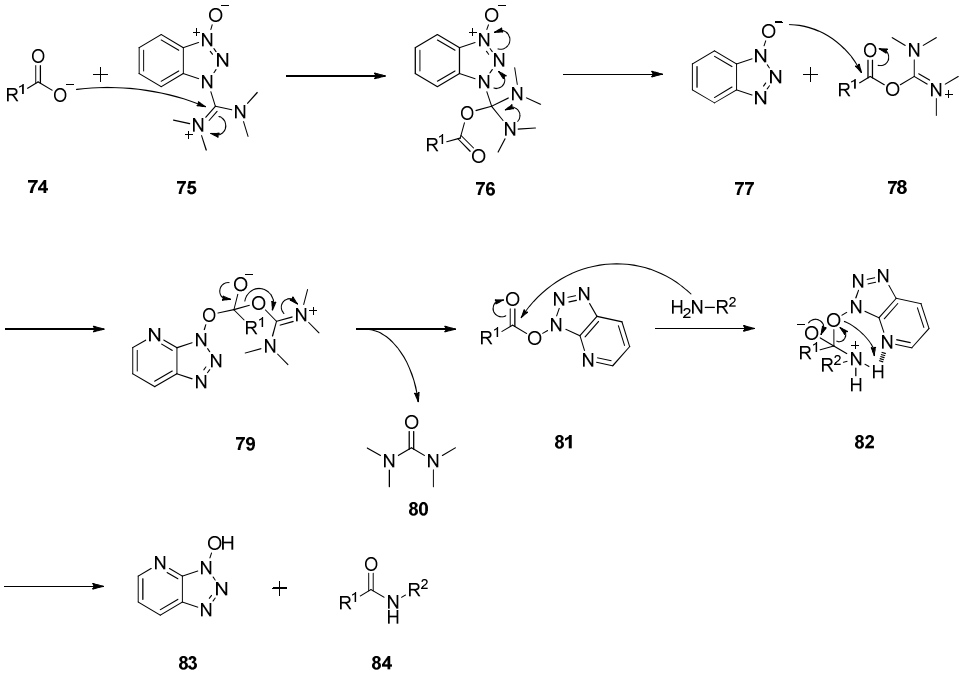

Scheme 13: **General mechanism of the amide coupling using HATU under basic conditions.**

3.1.5 Synthesis of benzylurea-based and heterocyclic urea derivatives.

Another strategy for the introduction of different residues at the carboxylic acid of **37**, was the Curtius reaction. Within this reaction, various primary amines were coupled to the carboxylic acid as corresponding urea. Using the azide source diphenylphosphoryl azide (DPPA) and triethylamine (TEA) in acetonitrile (ACN), compounds **85** – **92** were obtained (**Scheme 14** and **Scheme 15**). The general reaction mechanism is shown in **Scheme 16**. The yields of these syntheses varied from 19 to 37%.

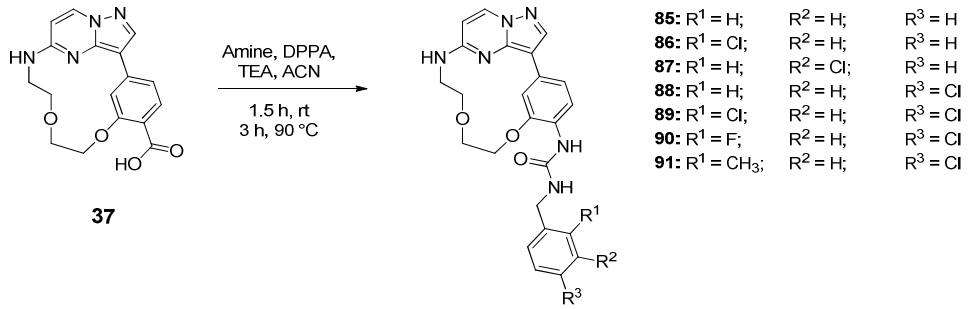

Scheme 14: **Synthesis of the benzylurea-based derivates (85 – 91).** The derivatives were obtained by Curtius reaction of the carboxylic acid of **37** with the corresponding amine.

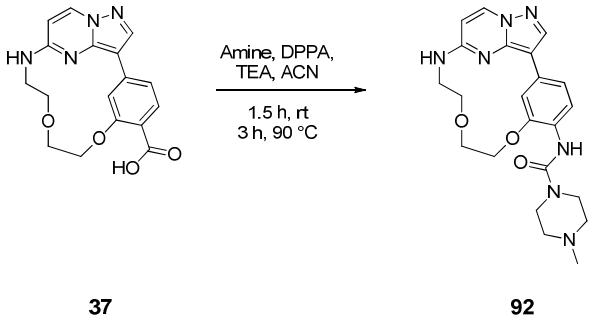

Scheme 15: **Synthesis of the heterocyclic urea derivative 92.** The derivatives were obtained by Curtius reaction of the carboxylic acid of **37** with the corresponding amine.

The nucleophilic attack of the deprotonated carboxylic acid **93** at the phosphorus of DPPA (**94**) constitutes the first step of the Curtius reaction. By cleavage of the azide ion **97** from intermediate **95**, the acyl phosphate **96** is formed. This is attacked *in situ* by the azide ion **97** and intermediate **98** is formed. In the next step, formation of the acyl azide **100/101** and intermediate **99** occurs under cleavage of **98**. With the addition of heat, the acyl azide **101** is converted to the corresponding isocyanate **104**.

This rearrangement proceeds with the elimination of elemental nitrogen **102** via the acyl nitrene **103**. In the final step, the amine **105** attacks the carbon of the isocyanate **104** and the corresponding urea **106** is formed.[167,168]

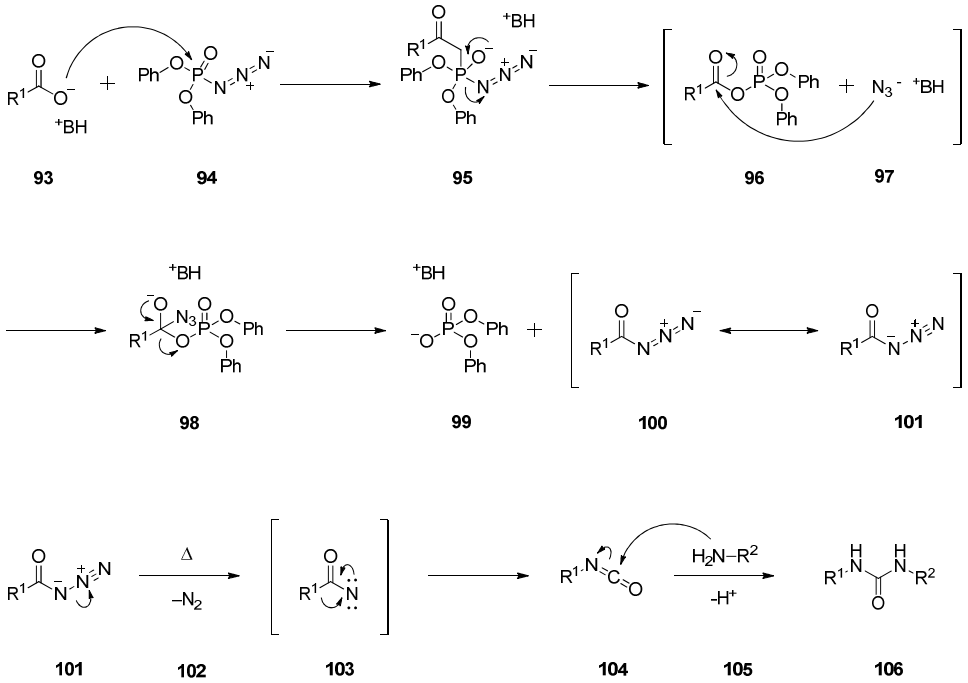

Scheme 16: **General mechanism of the Curtius reaction using DPPA and TEA.**

3.1.6 Synthesis of phenylethan- and naphtylmethyl/ethylamide based derivatives.

The macrocyclic compounds **107** – **111** (**Scheme 17**) were obtained via amide coupling of macrocyclic scaffold **37** with the corresponding amine using HATU and DIPEA in DMF. Conditions and mechanism of the reaction are identical to those used for the synthesis of compounds **61** – **73** (chapter 3.1.4). The yields of the derivatizations ranged from 63 to 83%. They are comparable to those of the benzylamide-based compounds **61** – **73**.

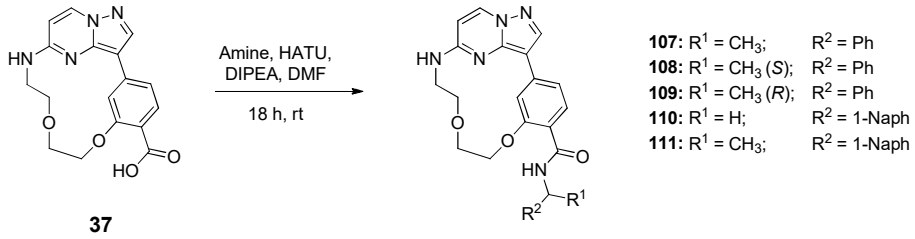

Scheme 17: **Synthesis of the phenylethan- and naphtylmethyl/ethylamide-based derivatives (107 – 110).** The derivatives were obtained by amide coupling of the carboxylic acid of **37** with the corresponding amine.

3.1.7 Synthesis of heterocyclic amide derivatives.

The macrocyclic amide derivatives **112** – **118** (**Scheme 18**) were also synthesized using the coupling reagent HATU under basic conditions (see chapter 3.1.4). In this case, heteroaromatic and heterocyclic amines were introduced to **37**. The turnover rate of these reactions ranged from 71 to 90%.

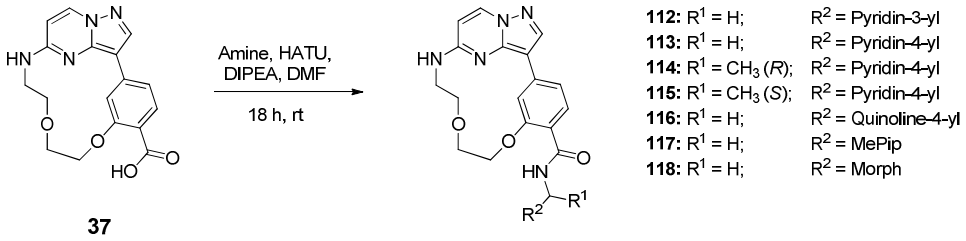

Scheme 18: **Synthesis of the heterocyclic amide derivatives (112 – 118).** The derivatives were obtained by amide coupling of the carboxylic acid of **37** with the corresponding amine.

3.1.8 Synthesis of small amide derivatives.

The macrocyclic compounds **119** – **121** were synthesized using small amines (**Scheme 19**). Therefore, they were coupled to the macrocyclic scaffold **37** using HATU and DIPEA in DMF as amide (chapter 3.1.4). The yields of these reactions ranged from 42 to 67%.

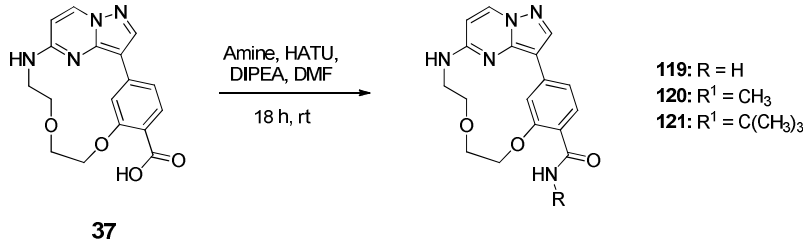

Scheme 19: **Synthesis of the small amide derivatives (119 – 121).** The derivatives were obtained by amide coupling of the carboxylic acid of **37** with the corresponding amine.

3.1.9 Synthesis of macrocyclic compounds with six-membered alkyl and aromatic linker motifs.

The synthesis of the macrocyclic scaffolds with six-membered alkyl linker **38** and with aromatic linker **39** were carried out under reaction conditions as described in the synthesis of **37** (**Scheme 4**). The bromination of the 5-chloropyrazolo[1,5-*a*]pyrimidine (**24**) with NBS was identical. In the next step (**a**), the linkers were introduced as 6-aminohexan-1-ol or 2-(4-aminophenyl)ethanol via nucleophilic substitution at the aromatic. The yields were 63% for **122** and 66% for **123**. Subsequently, the hydroxyl group of the linker was protected as silyl ether with TBDMSCl (**b**) under quantitative conversion (99% **124** and 96% **125**). In the next step, the secondary amine was Boc-protected (**c**), also with very good yields of 95% for **126** and 90% for **128**.

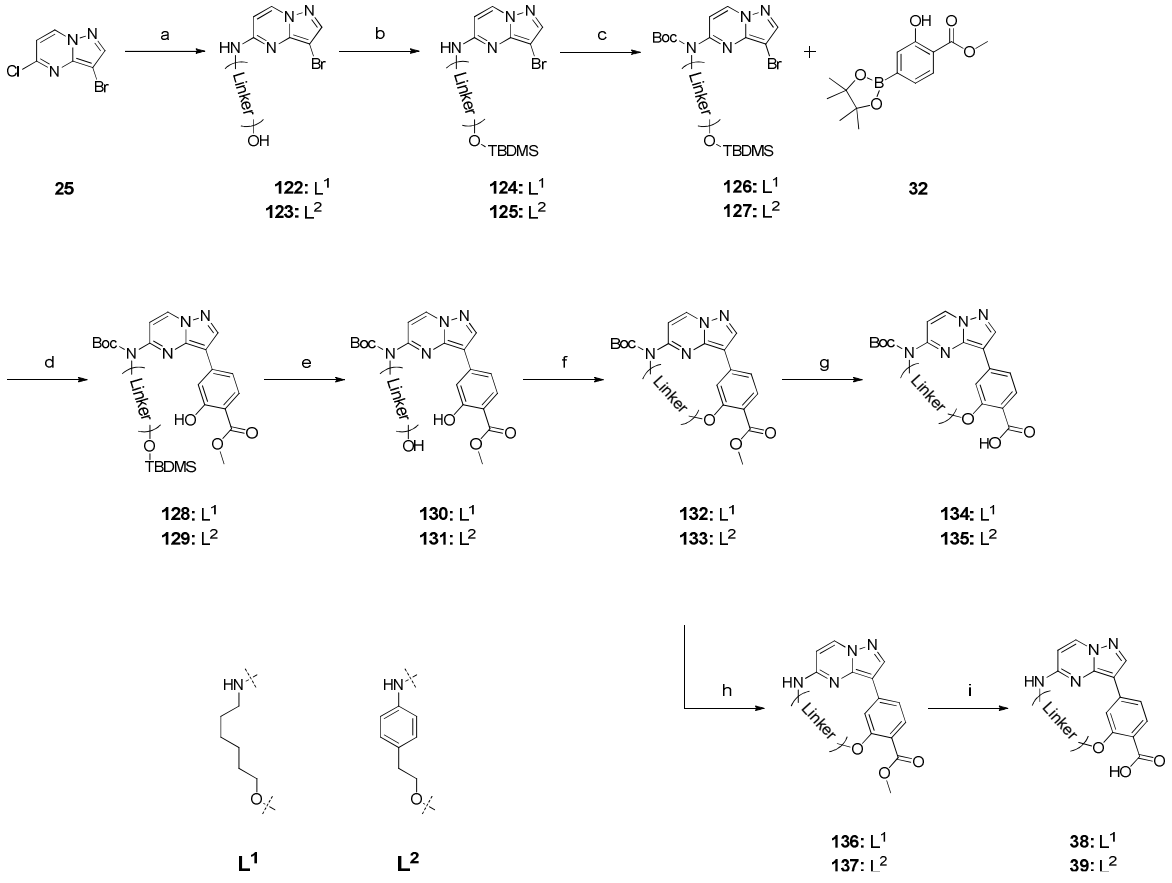

Scheme 20: **Synthesis overview of macrocyclic scaffolds 38 and 39.** Instead of the PEG linker motif of **37**, a six-membered aliphatic linker motif (L^1) was used to synthesize **38** and an aromatic one (L^2) in the synthesis of **39**.

The *tert*-butyl (3-bromopyrazolo[1,5-*a*]pyrimidin-5-yl)(6-((*tert*-butyldimethylsilyl)oxy)-hexyl) carbamate (**126**) and the *tert*-butyl (3-bromopyrazolo[1, 5-*a*]pyrimidin-5-yl)(4-(2-((*tert*-butyldimethylsilyl)oxy)ethyl)phenyl)carbamate (**127**) were linked to the pinacol borane ester **9** via a Suzuki cross-coupling (**d**). The yields were slightly lower than those of **33**, but still in a quite good range of 83% for **128** and 80% for **129**. Before ring closure, the silyl protecting groups were cleaved with 1 M TBAF (**e**). Again, good yields of 91% for **130** and 83% for **131** were obtained. Cyclization (**f**) was carried out via Mitsunobu reaction with DIAD and TPP. The yield of **132** was 90%, while **133** was only obtained at 46%. This can be attributed to steric hindrance by the benzene group in linker $\mathbf{L^2}$. The protectiong groups of the macrocyclic compounds were removed in the subsequent steps. Compounds **134** and **135** were obtained by ester hydrolysis (**g**) of **132** and **133** with LiOH · H_2O with yields of 47% for **134** and 75% for **135**, respectively. The cleavage of Boc group (**h**) from **132** and **133** was performed by addition of TFA with yields of 74% for **136** and 77% for **137**. Finally, the macrocyclic scaffolds **38** and **39** were obtained by the cleavage of the methyl esters with LiOH · H_2O (**i**). The conversion rate of the reactions was 63% for **38** and 87% for **39**.

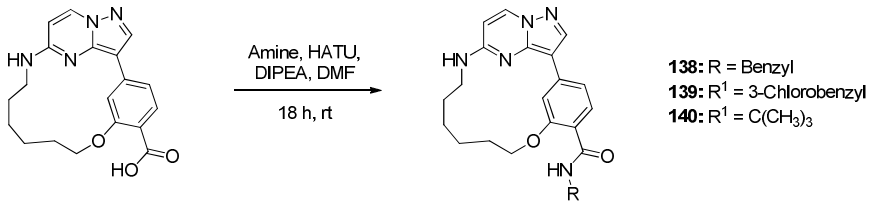

38

Scheme 21: **Synthesis of macrocyclic derivatives with six-membered alkyl linker (138 – 140).** The derivatives were obtained by amide coupling of the carboxylic acid of **38** with the corresponding amine.

The introduction of various residues at the macrocyclic scaffold **38** (**Scheme 21**) was carried out by amide coupling at the carboxylic acid, as described in chapter 3.1.4. The coupling reagent HATU and DIPEA as base with DMF as solvent were used for these reactions under identical conditions. In this manner, the benzylamide-based derivatives **138** and **139** as well as the small amide derivative **140** were obtained. The yields were in a quite good range between 77 and 83%.

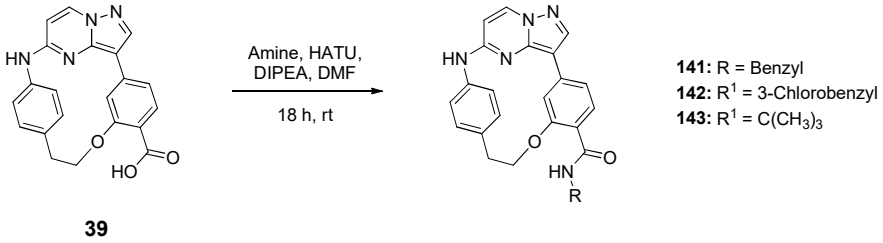

39

Scheme 22: **Synthesis of macrocyclic derivatives with aromatic linker motif (141 – 143).** The derivatives were obtained by amide coupling of the carboxylic acid of **39** with the corresponding amine.

The derivatization of **39** was also done via amide coupling at the carboxylic acid and is shown in **Scheme 22**. After reaction with the coupling reagent HATU, DIPEA in DMF and the corresponding amine, the benzylamine-based compounds **141** and **142** as wells as the small amide compound **143** were obtained. The yields were comparable to those of **138** – **140** and ranged from 75 to 79%.

3.1.10 Synthesis of urea- and carbamate-based derivatives.

The synthesis of the urea-based derivatives **151** – **166** was performed by using bis(trichloromethyl) carbonate (BTC; triphosgene), TEA and the corresponding amine in DCM.[169] Under these conditions, the amines were introduced at the secondary amine of the macrocyclic scaffold as urea (**Scheme 23**). However, since triphosgene also reacts with carboxylic acids[170], derivatization was carried out with the macrocyclic methyl ester **36**. The ester motif of the obtained compounds **144** – **150** was hydrolyzed subsequently. The cleavage of the ester was carried out with Me_3SnOH, since this base proved to be particularly suitable while retaining a residue on the secondary amine (see synthesis of **60** chapter 3.1.3). The general mechanism of the derivatization reaction can be seen in **Scheme 24**. The yields of the introduction of urea varied between 53 and 81%. The ester hydrolysis could be carried out with yields ranging from 31 to 50%. Reasons for the moderate yields can be seen in the mild but selective conditions of this reaction.

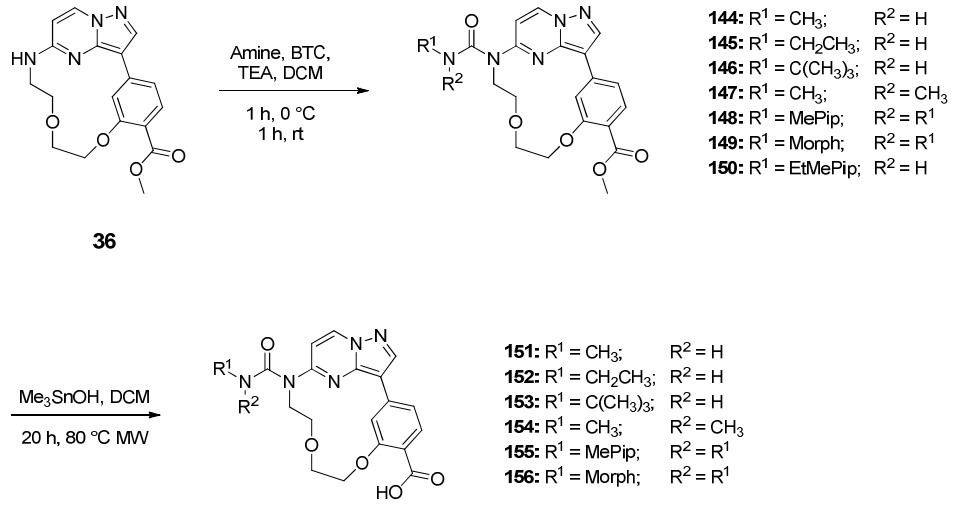

Scheme 23: **Synthesis of the macrocyclic urea-based derivates (144 – 156).** Derivatives **144** – **150** with methyl ester were obtained by reaction of **36** with triphosgene (BTC) and the corresponding amine. Subsequently, the esters were cleaved and derivatives **151** – **156** were obtained.

The first step in the formation of the urea motif with triphosgene is the nucleophilic attack of the deprotonated amine **157** on triphosgene (**158**). The by-product of the addition-elimination reaction is carbonyl dichloride (phosgene) (**162**) as well as a chloride ion, which together with the protonated base forms the corresponding HCl salt **159**. Deprotonation of **160** again leads to the formation of another **162** as well as **159**, but also to the isocyanate **161**. Meanwhile, the phosgene formed as an intermediate is nucleophilically attacked by further deprotonated amine **157**, and further **159** and **161** are formed. The following nucleophilic attack of the second also deprotonated amine **164** on the carbon of isocyanate **161** gives the desired urea **165**. The reaction mechanism reveals that it was essential to add the second amine after the isocyanate was fully formed and to use an excess of base. Otherwise, the second amine might link to each other. An insufficient amount of base prevents the complete formation of the isocyanate. It was also important to precisely maintain the temperature ranges. Excessive cooling during isocyanate formation slows down the reaction and the second amine added afterwards also forms isocyanate. This has drastic effects on the yield. A slight shortage of triphosgene had a positive effect.[169,171]

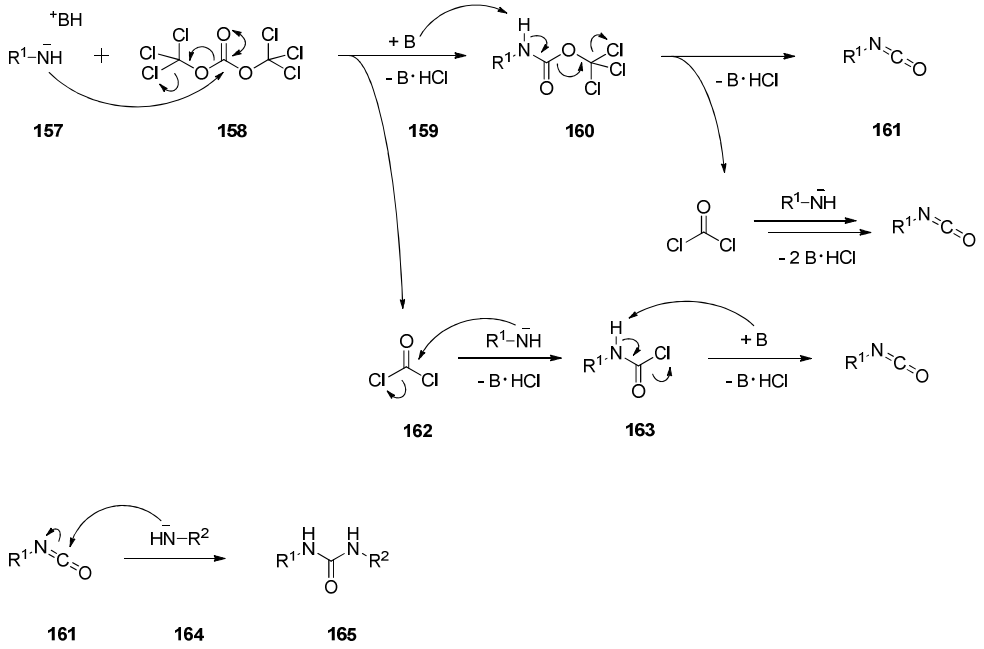

Scheme 24: **General mechanism of linking two amines via urea in a reaction with triphosgene under basic conditions.**

If the reaction is not performed with two amines and with one amine and one alcohol instead, the corresponding carbamate is formed.[172] The usage of more reactive sodium alcoholates instead of alcohol was a chance to improve the reaction process. Under reaction conditions already described above for urea synthesis, carbamates **165** and **166** could be introduced to the macrocyclic methyl ester **36** (**Scheme 25**). The yields varied between 65 and 84%. Hydrolysis of the esters with Me_3SnOH gave compounds **167** and **168** in yields ranging from 21 – 28%.

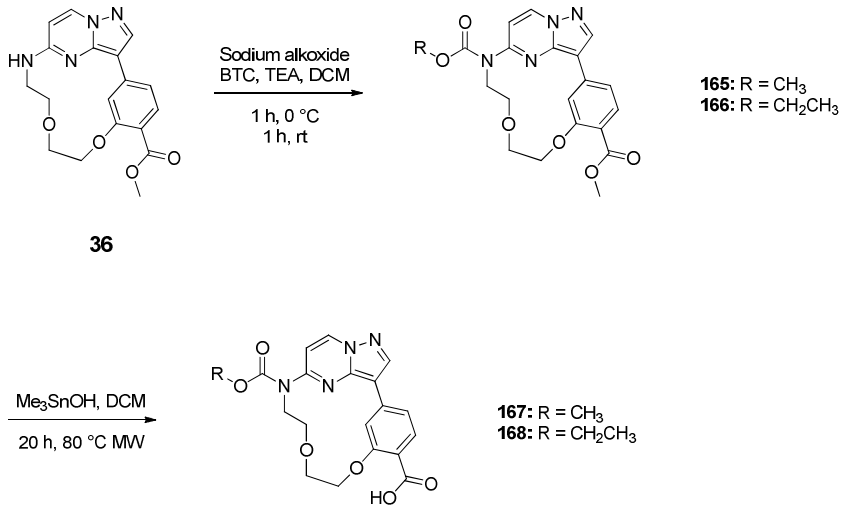

Scheme 25: **Synthesis of the macrocyclic carbamate-based derivates (165 – 168).** Derivatives **165** – **166** with methyl ester were obtained by reaction of **36** with triphosgene and the corresponding sodium alkoxide. Subsequently, the esters were cleaved and derivatives **167** – **168** were obtained.

3.2 Optimization of pyrazolo[1,5-*a*]pyrimidines lead to the identification of a highly selective CK2 inhibitor

3.2.1 Differential scanning fluorimetry

The first *in vitro* characterization of compounds **34** – **37**, **46** – **47**, **60**, **61** and **169** – **177** towards their selectivity was realized by differential scanning fluorimetry (DSF). This assay is a robust and sensitive method to determine protein-ligand interactions. It is suitable for rapid selectivity screening without prior knowledge of the activity or substrate of the protein of interest. The assay is based on the protein folding state and the thermal stabilization of a native protein by binding of a ligand. The unfolding of the protein is determined in a temperature range of 25 – 95°C using the dye SYPRO^{TM} Orange. During unfolding, the dye interacts with hydrophobic parts of the protein and an increase in fluorescence, in dependence of temperature, is measurable. After complete unfolding and fluorescence maximum, aggregation of the protein causes dissociation of the dye and a decrease in fluorescence. The turning point of the resulting curve is defined as the melting point (T_m) of the protein. Due to binding of a small molecule inhibitor, a stabilization of the protein and consequently a shift of the melting point, compared to the native protein, may occur. This T_m-shift (ΔT_m) allows conclusions to be drawn about protein-inhibitor affinity.[173,174] The compounds were screened against a panel of 48 kinases, which also included some of the known off-targets (CLKs, DAPK, DYRK, PIM) of CK2. Also included were kinases responsible for cell proliferation. **Table 1** lists the T_m-shifts, which were obtained by these experiments. It could be observed that some of the compounds have a clear preference towards CK2α and CK2α´. Herein, particularly high ΔT_m values on CK2 were obtained for the acyclic compound **47**, with a Boc group at the secondary amine at 5-position of the pyrazolo[1,5-*a*]pyrimidine, the corresponding macrocycle **60**, and the macrocyclic scaffold **37** without Boc group. However, cleavage of the Boc group of **37** was followed by a decrease in affinity for CK2. The common structural element of these compounds is the carboxylic acid. Variation at this position, in both the cyclic and acyclic compounds, such as the introduction of a methyl ester (**35**) or the removal of the carboxylic acid (**175**) also resulted in a sharp decrease in ΔT_m. Nevertheless, substitution with a nitrile group (**173**) still showed activity on CK2, but slightly decreased compared to **47**. Thus, both the Boc group and the carboxylic acid were shown to be essential for potent binding to CK2.

Regarding selectivity on CK2 within the panel, compounds **60** (4 kinases $\Delta T_m > 5$) and **47** (6 kinases $\Delta T_m > 5$) also showed quite promising results. Removal of the Boc group, however, worsened the selectivity of the macrocyclic scaffold **37** (15 kinases $\Delta T_m > 5$) and AAK1 and GAK were identified as main off-targets ($\Delta T_m > 9$) of **37**.

Table 1: Structure-activity relationship of acyclic and macrocyclic compounds (34 – 37, 46 – 47, 60, 61 and 169 – 177). In a DSF assay the compounds were screend against a pannel of 48 kinases and the results are highlighted with a heat map. It ranges from no stabilization (white) to the highest stabilization (dark green) of the kinase by the compounds. Staurosporine (**1**) was used as a reference. The trend of stabilization ($\Delta T_m > 5$) is shown with green triangles (increase), yellow minus signs (steady), and red triangles (decrease). The bottom row shows the number of kinases with an affinity of $\Delta T_m > 5$.

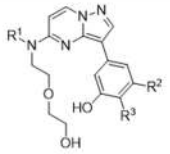

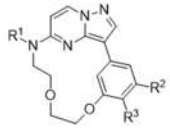

R^1	Boc	Boc	Boc	Boc	H	Boc	Boc	Boc	Boc	Boc	Boc	H	H	$COCH_3$	$COCHMe_2$	H	
R^2	H	H	CN	H	H	H	H	H	CN	H	H	H	H	H	H	H	
R^3	COOMe	CN	H	H	COOMe	COOH	COOMe	CN	H	H	COOH	COOMe	COOH	COOMe	COOMe	$CONHBn$	
Compound	**34**	**169**	**170**	**172**	**46**	**47**	**35**	**173**	**174**	**175**	**60**	**36**	**37**	**176**	**177**	**61**	**Staurosporine**
AAK1	2.3	3.6	2.1	n.d.	3.8	3.2	1.7	n.d.	n.d.	n.d.	3.9	7.9	9.3	4.1	3.2	n.d.	14.6
AurB	0.6	1.9	1.1	n.d.	1.6	-2.8	0.8	n.d.	n.d.	n.d.	-1.6	1.0	2.1	1.7	1.0	n.d.	14.9
BMX	1.0	-0.3	-0.3	n.d.	0.5	0.3	0.5	n.d.	n.d.	n.d.	0.5	0.9	0.1	0.1	0.1	n.d.	7.0
BRAF	0.3	7.2	5.3	n.d.	-0.5	2.5	0.0	n.d.	n.d.	n.d.	2.8	1.8	1.0	0.6	0.5	n.d.	0.8
CaMK1g	-0.7	-0.1	-0.4	n.d.	-0.7	-0.2	-0.3	n.d.	n.d.	n.d.	-0.3	-0.5	0.0	-0.5	0.0	n.d.	10.7
CaMKK2	0.8	4.7	0.5	1.6	3.0	5.5	1.6	6.7	0.9	2.5	6.0	5.0	8.7	2.5	1.9	7.2	21.8
CASK	-0.3	0.3	-0.3	n.d.	-0.4	-0.1	0.0	n.d.	n.d.	n.d.	0.3	0.2	0.1	-0.1	-0.1	n.d.	5.2
CDK2	0.0	1.7	0.0	0.9	0.7	2.6	0.0	2.1	-0.2	0.5	2.4	5.3	7.0	1.7	0.6	1.5	15.7
CHK2	0.9	0.5	0.5	0.6	0.8	1.1	0.7	0.4	0.4	0.4	0.8	2.4	4.3	0.6	0.4	5.9	18.3
CK1d	0.3	0.6	0.6	n.d.	0.2	1.3	0.3	n.d.	n.d.	n.d.	1.6	0.7	2.5	0.5	0.4	n.d.	3.3
CK2α	0.1	7.4	2.2	2.2	0.4	15.1	0.4	3.8	0.4	0.3	11.7	2.3	10.6	0.8	1.5	0.8	4.4
CK2α´	0.8	7.6	3.4	2.1	1.2	15.7	1.6	4.4	1.0	0.7	11.8	3.5	11.3	1.7	2.4	2.7	4.4
CLK1	1.4	2.6	1.0	1.2	3.9	2.9	0.9	2.8	0.1	0.6	1.5	6.3	7.1	2.9	1.4	6.5	12.0
DAPK1	0.2	0.5	1.0	0.7	0.8	4.9	0.2	0.9	1.0	0.1	2.0	1.1	3.1	0.0	0.2	1.3	9.1
DAPK3	0.5	1.6	3.0	2.0	2.6	11.6	-0.2	1.4	1.0	0.1	6.2	3.2	8.7	0.5	0.3	5.9	16.9
DRAK2	1.1	1.4	0.6	1.0	3.1	1.9	1.4	0.8	-0.1	0.2	1.2	3.9	0.7	2.6	1.5	2.1	12.4
DYRK1A	-1.1	0.0	-1.0	0.6	0.5	1.7	-1.0	0.6	-0.7	-0.3	-0.1	0.2	0.6	-1.1	-1.2	-1.1	6.5
EphA2	0.3	0.2	0.5	n.d.	0.2	0.0	0.3	n.d.	n.d.	n.d.	0.2	0.7	0.7	0.3	0.4	n.d.	7.3
ERK1	-0.3	n.d.	n.d.	n.d.	-0.3	0.0	0.6	n.d.	n.d.	n.d.	1.0	-0.7	0.8	-0.1	-0.6	n.d.	n.d.
ERK2	-0.4	0.8	-0.6	n.d.	0.5	0.5	-0.5	n.d.	n.d.	n.d.	1.0	1.5	-0.2	-0.4	0.0	n.d.	2.0
ERK3	0.5	n.d.	n.d.	n.d.	0.9	-0.1	-0.2	n.d.	n.d.	n.d.	-0.3	1.2	0.5	0.1	0.4	n.d.	n.d.
FER	0.0	n.d.	n.d.	n.d.	0.4	0.8	0.1	n.d.	n.d.	n.d.	0.5	0.3	-0.7	-1.3	0.2	n.d.	n.d.
FES	-0.6	-0.1	-0.7	-0.6	-0.7	-0.4	-0.5	-0.5	-0.6	-0.8	-0.4	0.1	0.0	-0.4	-0.5	-0.4	7.3
FGFR2	-0.1	0.4	1.3	1.0	1.1	0.6	-0.1	0.0	0.2	0.2	0.1	1.8	1.6	0.5	0.0	5.2	8.7
FLT1	0.3	1.2	4.6	2.9	1.8	2.3	0.4	1.5	1.6	1.1	1.2	3.4	3.5	1.6	0.8	3.9	13.5
GAK	1.3	3.1	3.3	2.5	3.9	4.6	1.2	3.5	2.1	1.0	4.5	6.0	9.1	3.6	3.7	7.0	10.4
GPRK5	-0.2	0.0	-0.1	n.d.	0.0	0.7	-0.2	n.d.	n.d.	n.d.	0.0	0.8	0.8	0.1	0.2	n.d.	7.5
Haspin	0.4	2.2	1.0	n.d.	1.4	1.0	0.6	n.d.	n.d.	n.d.	0.9	3.4	2.9	1.9	1.0	n.d.	8.9
JNK1	0.4	0.0	-0.3	n.d.	0.1	0.9	0.1	n.d.	n.d.	n.d.	-0.2	0.4	0.3	0.4	0.5	n.d.	7.7
JNK2	-0.3	0.5	0.2	0.0	0.7	0.6	0.0	0.3	-0.1	0.0	0.3	1.1	0.3	0.2	0.2	-0.1	4.2
LOK	-0.3	0.3	2.0	n.d.	0.0	2.3	-0.2	n.d.	n.d.	n.d.	0.8	3.4	6.0	1.1	1.2	n.d.	21.3
MAP2K2	1.6	n.d.	n.d.	n.d.	7.6	4.6	4.2	n.d.	n.d.	n.d.	2.5	6.4	7.6	6.1	7.3	n.d.	n.d.
MAP2K4	-0.1	1.7	0.6	1.0	2.3	1.6	0.5	1.1	0.3	1.1	2.0	3.7	6.5	1.6	1.6	5.4	10.1
MAP2K6	-0.1	0.4	-0.1	0.2	0.6	0.6	0.4	0.2	0.2	0.0	0.4	1.5	1.2	0.9	0.4	1.8	11.5
MAP2K7	-0.4	n.d.	n.d.	n.d.	0.1	0.2	0.0	n.d.	n.d.	n.d.	0.4	0.4	1.8	-0.6	0.2	n.d.	n.d.
MAP3K5	0.1	0.7	0.4	0.1	0.7	2.4	0.5	3.4	0.3	0.2	1.6	3.6	5.0	0.5	0.4	5.1	17.5
MELK	2.8	4.1	1.8	2.5	4.6	1.1	1.6	3.7	1.1	0.8	0.1	6.6	5.0	3.4	3.2	6.9	17.8
MER	-0.5	-0.2	0.1	n.d.	-0.3	0.8	-0.6	n.d.	n.d.	n.d.	-0.2	-0.5	0.0	-0.3	0.1	n.d.	5.2
MSK1_b	0.3	2.5	3.3	2.5	1.1	6.0	-0.3	1.9	0.0	0.7	2.5	2.8	6.2	0.4	0.2	2.6	16.4
MST2	0.3	0.6	1.0	n.d.	1.1	0.2	0.5	n.d.	n.d.	n.d.	0.3	5.5	3.2	2.3	0.7	n.d.	13.4
MYT1	0.9	n.d.	n.d.	n.d.	0.5	-0.9	-0.7	n.d.	n.d.	n.d.	1.1	-0.8	-1.0	0.8	0.9	n.d.	n.d.
p38a	-0.5	0.0	-0.7	-0.4	0.1	0.0	-0.5	-0.5	-0.3	-0.5	0.0	0.1	0.3	-0.1	-0.2	-0.7	1.3
PAK1	-0.4	-0.2	0.2	1.6	0.7	-1.4	-0.8	0.2	-0.5	-0.4	-0.9	-1.7	-1.5	-0.6	-0.5	0.9	8.7
PAK4	1.2	2.5	1.6	n.d.	1.1	1.1	1.3	n.d.	n.d.	n.d.	0.8	0.9	1.3	1.3	1.7	n.d.	12.2
PBK	-0.4	0.1	-0.4	-0.4	0.1	0.3	-0.5	-0.1	-0.2	-0.4	0.2	0.4	0.7	0.2	-0.2	0.9	7.8
PDHK4	-0.1	n.d.	n.d.	n.d.	0.4	0.0	-0.7	n.d.	n.d.	n.d.	-0.9	0.1	-0.4	0.3	-0.2	n.d.	n.d.
PHKG2	0.2	1.1	-0.1	n.d.	0.6	0.7	0.2	n.d.	n.d.	n.d.	0.4	5.0	5.8	1.6	0.4	n.d.	21.2
PIM1	-1.1	-0.3	-0.2	n.d.	-0.9	4.3	-0.3	n.d.	n.d.	n.d.	0.3	0.5	2.4	0.2	-0.3	n.d.	11.9
PIM3	1.4	n.d.	n.d.	n.d.	2.8	5.7	1.0	n.d.	n.d.	n.d.	4.0	3.8	4.8	1.6	2.5	n.d.	n.d.
PKG2	-0.8	n.d.	n.d.	n.d.	0.8	-0.9	0.2	n.d.	n.d.	n.d.	-0.5	0.6	-0.1	2.3	1.9	n.d.	n.d.
PLK4	0.2	1.0	2.0	1.5	1.9	4.4	0.2	1.3	0.5	0.4	3.6	4.5	7.0	1.8	1.0	7.1	20.0
RSK1_b	0.1	0.1	0.9	n.d.	-0.1	0.1	0.1	n.d.	n.d.	n.d.	1.8	2.0	2.8	0.4	0.1	n.d.	3.2
STLK3	-0.6	0.5	1.0	-0.1	0.7	0.0	-0.1	0.5	0.1	-0.1	-0.1	1.9	1.7	0.1	-0.1	2.2	11.1
TTK	-0.5	-0.1	-0.5	n.d.	0.2	1.6	0.5	n.d.	n.d.	n.d.	1.0	2.2	-1.1	2.3	0.7	n.d.	9.0
ULK3	1.0	1.7	1.8	2.5	3.4	1.5	2.6	2.4	0.6	2.1	1.8	8.8	5.3	6.5	4.4	6.9	19.7
WNK1	0.5	0.3	0.3	0.1	0.2	0.4	0.5	0.5	0.5	0.3	0.2	0.3	0.3	0.2	0.5	0.4	1.3
Stabilization of CK2	▼	▲	▼	▼	▼	▲	▼	▼	▼	▼	▲	▼	▲	▼	▼	▼	
Selectivity X/56 Kinases	**0**	**3**	**1**	**0**	**1**	**6**	**0**	**1**	**0**	**0**	**4**	**8**	**15**	**2**	**1**	**11**	

3.2.2 Co-crystal structures

The crystal structures of **37** and **47** confirmed the assumption that the pyrazolo[1,5-*a*]pyrimidine binds ATP competitively. As can be seen in **Figure 17**, this involves interaction with the hinge via the backbone nitrogen of residue V116. Also verified were the findings from the DSF assay regarding the importance of the carboxylic acid toward the back pocket. A network of polar interactions could explain the total loss of inhibitory properties by introduction of the methyl ester. This network was formed by conserved CK2 back pocket residues such as a salt bridge with the VIAK (Val-Ile-Aln-Lys) motif lysine K68, a water mediated hydrogen bond to the conserved αC glutamate (E81) and a hydrogen bond to the backbone nitrogen of D175. This nitrogen is part of the degenerate DFG (DWG; Asp-Trp-Gly) motif, which is exclusive to the two isoforms of CK2 within the human kinome. A further interaction occurred between the carbonyl group of the Boc group of **47** and the hinge region. A hydrogen bond with side-chain nitrogen N118 was formed, which might be considered, together with the interactions of the carboxylic acid, as an explanation for the high affinity in the DSF assay. Due to the very similar orientation of the pyrazolo[1,5-*a*]pyrimidine ring system and the attached 3-phenyl ring system in **47** and **60**, conclusions could be drawn about the similar bioactive binding modes and the similar selectivity profiles. (*Experiments were performed by Dr. Andreas Krämer*)

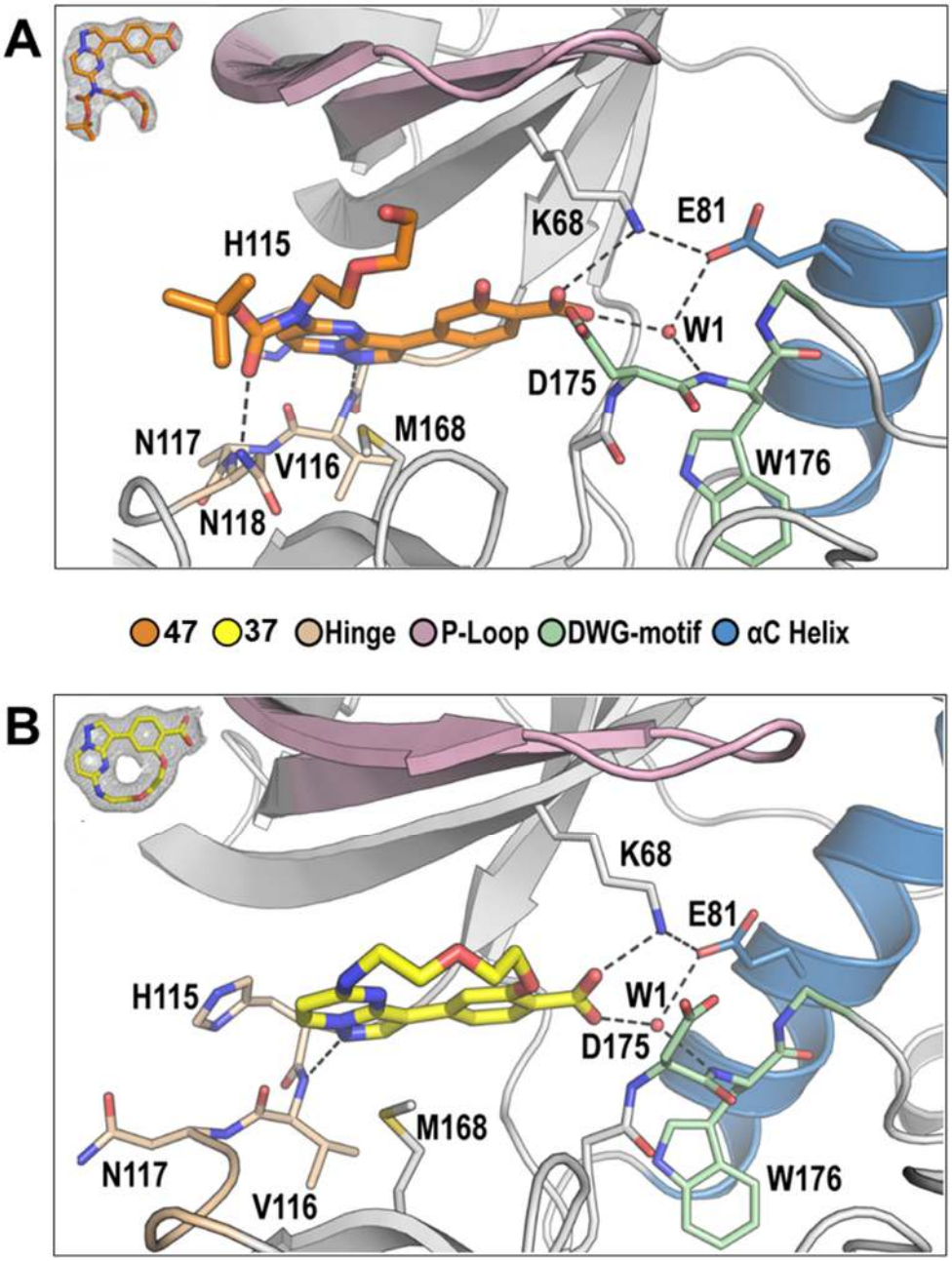

Figure 17: **Binding mode of acyclic 47 (A) and macrocyclic 37 (B) in complex with CK2 in stick representaion. 47** (PDB: 6YUM) in orange and **37** (PDB: 6YUL) in yellow. Water molecules are illustrated as red spheres and structural motifs of intrest are highlited in colour (see legend). Black dashed lines represent potential hydrogen bonds. The ligands are identifiable as ATP competitive (type I) inhibitors which are bound to the hinge region of CK2. The approximate binding modes of **47** and **37** are comparable. Between the carboxylate anion of the ligands and the cationic ammonium sidechain of K68 a salt bridge is formed and a water mediated bridge to E81. Via the carboxyl group of the Boc group, harbourd at the acyclic **47**, an additional hydrogen bond to the side chain N118 can be formed. This can be seen as an explanation for a higher affinity observed for compounds possessing this functional group. The electron density of each compound is shown in the insert on the upper left corner of figure A and B.

3.2.3 Isothermal titration calorimetry

As mentioned above, the entropic cost of macrocycles of binding should be low, due to their conformational restriction. Compared to acyclic compounds, the number of possible conformations is limited.[51] To investigate this assumption with regard to compounds **47** and **60**, the thermodynamic binding properties were studied by isothermal titration calorimetry (ITC). In a sample cell, a series of small volumes of highly concentrated inhibitor solution was titrated into protein solution. The heat absorbed or released during binding of the inhibitor is detected as heat flow between a sample cell and a reference cell. This allows to determine the dissociation constant K_D, the reaction stoichiometry n, the free binding energy ΔG, the entropy ΔS and the enthalpy ΔH.[175] The curves obtained in these experiments can be seen in **Figure 18**. The data showed that both, the macrocyclic and acyclic compound are highly potent. **47** has a K_D value of 12 nM and **60** has a K_D value of 82 nM. These findings are consistent with the DSF data. The enthalpic and entropic contributions to binding differ minimally. Due to the similar binding modes of the compounds, this was to be expected. The binding of the two compounds was driven by a very favorable change in binding enthalpy and counteracted by the entropy ($T\Delta S$). This indicates that the co-planar orientation of the ring systems of the acyclic compound is preferential. However, cyclization leads to less interaction with the kinase domain, and therefore favoring **47** as a potent inhibitor of CK2α1. (*Experiments were performed by Dr. Andreas Krämer*)

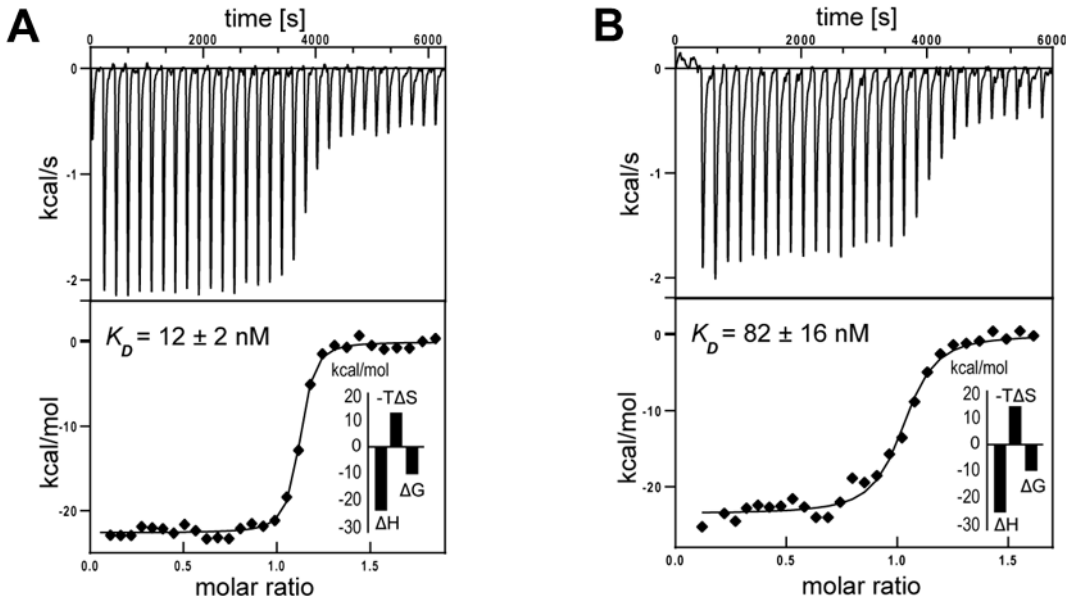

Figure 18: **Isothermal titration calorimetry of 47 (A) and 60 (B).** The experiments revealed two-digit nanomolar binding affinities towards CK2. Small variations in the overall Gibbs free energy, the entalpic and entropic contribution of binding is detectable.

3.2.4 KINOME*scan*® assay

Considering the promising selectivity within the DSF panel, **47** and **60** should be tested against a larger screening panel. Particularly suitable for determining selectivity over large parts of the human kinome is the KINOME*scan*® assay from Eurofins (formerly DiscoverX). This active site-directed competition binding assay allows quantification of the selectivity of compounds, based on the Selectivity Score (S-Score) calculated by the ratio of kinase hits at a set cut off by the total number of tested kinases. A value of 35% displacement (35%Ctrl) was used as potency threshold resulting in S_{35} = (number of non-mutant kinases with %Ctrl <35)/(number of non-mutant kinases tested) More specifically, all hits of non-mutant kinases with %Ctrl < 35 were considered and thus the S_{35} value was determined.[176] The *scan*MAX panel, which was used for this assay platform, provides 469 kinases (80% of the human kinome) including disease relevant mutants. The selectivity data for **47** and **60** at a screening concentration of 1 µM are shown graphically in **Figure 19**. In accordance with the DSF data, macrocyclic compound **60** showed good selectivity with S_{35} = 0.07. With S_{35} = 0.02, the acyclic compound **47** showed a significantly better selectivity within the panel. Nevertheless, there is a possible false posivitve rate of 1% in the KINOME*scan*® platform, which necessitated further verification of the results. Some of the potential hits were already been screened in the DSF panel and did not show any activity. This suggested that p21-activated kinase 1 (PAK1), PIM3, DAPK2, and GAK were false positive hits for **60**. This was also the case for DYRK1A for **47**. Not addressing very similar isoforms of hits also indicates a false positive result. This was observed for INSR and PAK2 for **60**. There remained some off-targets for the macrocyclic compound. Notwithstanding low activities on DAPK3, DYRK1A, and HIPK1, the acyclic **47** showed excellent selectivity over the two CK2 isoforms in KINOME*scan*®.

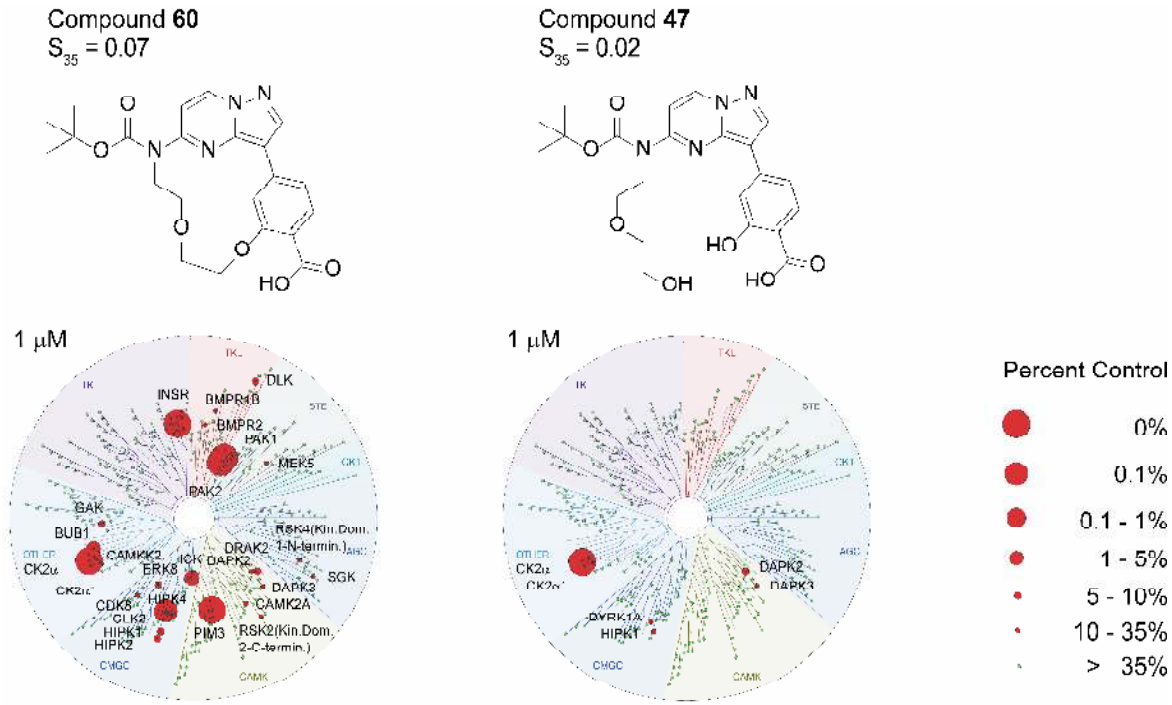

Figure 19: **Selectivity screening of macrocyclic 60 and acyclic 47.** Selectivity was determined in the KINOMEscan® assay by Eurofins (formerly DiscoverX) against 469 kinases of the *scan*MAX pannel. Screening was performed at a concentration of 1 µM and targeted kinases are highlited by red circles.

3.2.5 NanoBRET™ target engagement assay

Investigation of the cellular activity of compounds **60** and **47** was the next step after the promising kinome-wide selectivity data and nanomolar *in vitro* potency. For this purpose, the NanoBRET™ target engagement assay was utilized, which uses proximity-based bioluminescent resonance energy transfer (BRET) technology. The advantage of this cellular tracer displacement assay is the quantitative analysis of binding of compounds under physiological ATP concentration to full-length kinases. For this purpose, the target of interest was coupled to a 19-kDa luciferase (NanoLuc®), transiently transfected and expressed in HEK293T cells. By binding of a cell-permeable fluorescent energy transfer probe (tracer) to the tagged protein, a BRET signal is detectable. The competitive displacement of the tracer by an inhibitor leads to a dose-dependent decrease in energy transfer and thereby in a detectable BRET signal. In this way, the half maximum inhibitory concentration (IC_{50}) of the inhibitor can be determined.[177,178] The potency of **60** and **47** as well as the unselective macrocyclic scaffold **37** were investigated and silmitasertib (**12**) was used as positive control. The inhibitory activities were lower than the binding affinities obtained in the ITC experiments.

This effect was detectable in former experiments when moving to the cellular system, but not significantly higher than a factor of 10. IC_{50} values ranged from 1.5 µM to 7.5 µM for **60** and **47** on CK2α and CK2α´, respectively. The corresponding curves are shown in **Figure 20** top. **37** showed lower potency with IC_{50} values of 5.7 µM and 16.2 µM. These values were consistent with DSF data. Silmitasertib (**12**) showed IC_{50} values in a range of 100 nM to 500 nM for the CK2 isoforms, matching those known from the literature.[179] To evaluate the phenomenon of lowered cellular potency, the focus was placed on the carboxylic acid of the tested compounds. Correlations with the high intracellular ATP concentration or problems regarding cell permeability both were possible.

Brear *et al*. Reported a pro-drug method for masking carboxylic acids as methyl esters to regain potency against CK2.[180] In a repeated NanoBRET™ experiment with the corresponding methyl esters **34**, **35**, and **36**, no inhibition of CK2 was observed. This suggests that the ester could not be cleaved during a 2 hours incubation period. Further experiments were performed, now using permeabilized cells by addition of digitonin.[177] These results should allow conclusions about possible problems concerning cell penetration. The most potent compound **47** showed similar potency as silmitasertib (**12**) with IC_{50} values of 8 nM against CK2α and 38 nM against CK2α´. The curves of these NanoBRET™ experiments are shown in **Figure 20** below. The data were again consistent with those of the DSF and ITC experiments. In conclusion, it can be said that the first series of pyrazolo[1,5-*a*]pyrimidine compounds is highly selective and highly potent *in vitro*. However, the poor cell penetration of **47** and **60** leads to low micromolar inhibition. (*Experiments were performed by Dr. Benedict-Tilman Berger*)

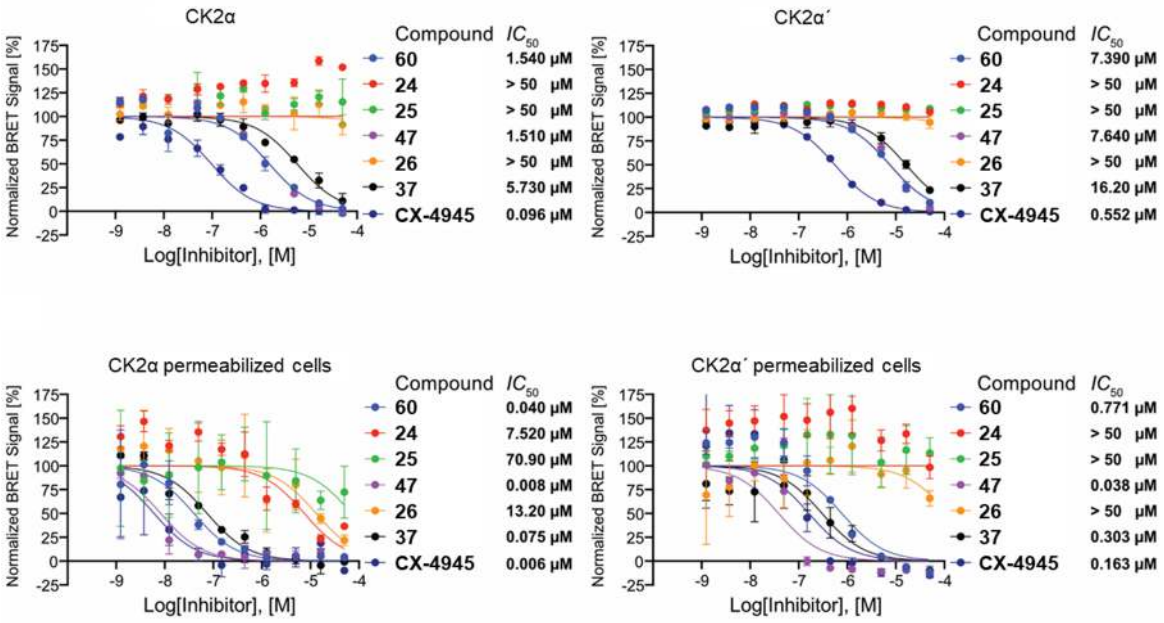

Figure 20: **Cellular potencies of differnet pyrazolo[1,5-*a*]pyrimidines on CK2α1/CK2α2.** Cellular activity was determined with NanoBRET™ experiments in HEK293T cells (top). Cellular activity of differnet pyrazolo[1,5-*a*]pyrimidines on CK2α1/CK2α2 determined by NanoBRET™ in permeabilized HEK293T cells (bottom). Silmitasertib (**12**) was used as a reference. Corresponding IC_{50} values can be found in the legend.

3.2.6 Growth inhibition of cancer cells (NCI-60 Panel)

In cancer cell biology, CK2 has a key role due to its crucial function in cell growth, cell death and cell survival.[181,182] Using CK2 inhibitors such as silmitasertib (**12**) or inactive mutants of the catalytic subunit α of CK2, antiproliferative or anti-angiogenic effects have been demonstrated.[108,183] To investigate possible effects in cancer cell lines, the selective and potent compound **47** was screened against the NCI-60 cancer cell panel. This is the panel of the National Cancer Institute (NCI). The results of the one-dose assay at an inhibitor concentration of 10 µM are shown in **Figure 21**. The values are shown relative to the no-drug control. No cell toxic effect for **47** was detected in all 60 cell lines. However, in several cell lines, such as in SNB-19 and U251 (glioblastoma), minor anti-proliferative effects were seen. A possible explanation is the high selectivity of **47** compared to silmitasertib (**12**), which addresses several off-targets that are important for cell proliferation and survival. Another reason for the low anti-proliferative effects may be due to the poor cell penetration of **47**. Further cell-based studies are needed to precisely validate the role of CK2 in cancer cell survival. Also important is the potential use of CK2 inhibitors for cancer patients. Nevertheless, in all cases the use of selective inhibitors is indispensable.

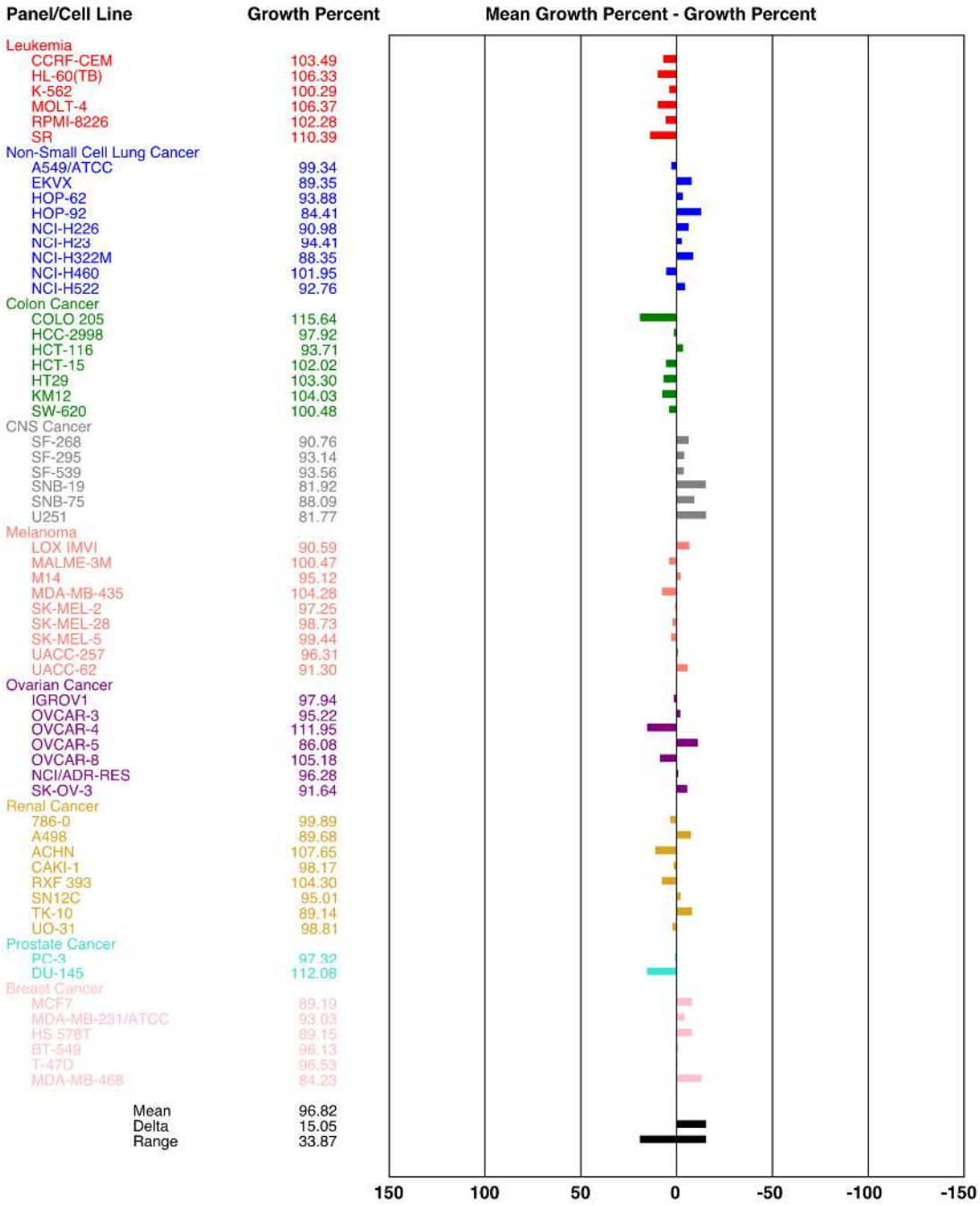

Figure 21: **Growth inhibition of cancer cell lines treated with 47.** 60 differnet cancer cell lines (NCI-60 panel) from the national cancer institute were treated with **47** and growth inhibition was detected. Hence, a single-dose assay at a concentration of 10 µM was performed and the results were presented relative to the no drug control.

3.3 Illuminating the dark: Highly selective inhibition of DRAK1 with pyrazolo[1,5-*a*]pyrimidine-based macrocycles

3.3.1 Differential scanning fluorimetry

For the first *in vitro* characterization of the synthesized compounds **61**, **67** – **73** and **107** – **121**, a DSF assay was performed using a panel of 44 kinases. A theoretical description of this method can be found in chapter 3.2.1. The results can be seen in **Table 2** below. The dual substituted benzylamide derivatives **67** – **73** with chlorine, fluorine, or methyl group as well as the unsubstituted benzylamide **61** resulted in similar stabilization of DRAK1. An exception was the *ortho/meta* chloro-substituted compound **72** with a significantly lower Tm-shift (ΔT_m = 6.2). However, the panel-wide selectivity of **72** was relatively good and DRAK1 was addressed exclusively with $\Delta T_m > 5$. The substitution of chlorine with fluorine in *ortho* position improved affinity of **73** compared to **72**, but with a drop of selectivity. The *ortho/para* and *meta/meta* substituted compounds **67** – **71** showed similar affinity towards DRAK1 (ΔT_m = 9 – 11) and selectivity (4 - 6/44 kinases with $\Delta T_m > 5$), except of **71** (dual *meta* chlorine/fluorine) with a drop of selectivity. With a high T_m-shift on DRAK1, it stabilizes 11 other kinases with $\Delta T_m > 5$. The phenylethane- and naphtylmethyl/ethylamide-based compounds (**107** – **111**) revealed diverse activities and selectivities. The introduction of a methyl group at the alkyl carbon of the benzylamide, as racemate **107** and as *R* stereoisomer **109**, resulted in some of the highest stabilizations (ΔT_m > 12) of DRAK1 within the SAR. Nevertheless, selectivity was negatively affected (> 10/44 kinases with $\Delta T_m > 5$). The *S* stereoisomer **108**, on the other hand, showed moderate values. There was also a significant increase in affinity (ΔT_m > 12) for compounds **112 – 116** of the heteroaromatic series. Substitution of the phenyl of **61** by a pyridine (**113**) also led to a significant improvement in selectivity. Both stereoisomers **114** and **115** only showed activities on 4 other kinases with ΔT_m > 5 beside DRAK1. The introduction of larger aromatic residues such as naphthyl (**110**, **111**) or quinoline (**116**) was less tolerated. Thus, a trend emerged that large asymmetric residues, as well as the *ortho/para* chloro-substituted **72**, lead to a drop of affinity. The heteroaromatic derivatives **117** and **118** showed a dramatic decrease in binding affinity towards DRAK1 and mostly all other kinases in the panel. This drop in affinity toward the kinase panel, including DRAK1, makes **117** and **118** potential candidates for a negative control compound.

The small amidic residues of compounds **119 – 121** significantly increased the binding affinity of the macrocycle with T_m-shifts between 10 and 13 degrees. However, the primery amide **119** showed similar low selectivity due to its similarity to the macrocyclic core structure **37**. The methylamide **120** showed a comparative trend. In contrast, the *tert*-butylamide **121** convinced with an excellent selectivity within the panel (3/44 kinases with $\Delta T_m > 5$). Within the panel, the NAK kinases AAK1, BIKE and GAK were identified as possible off-targets for almost all compounds. Interestingly, none of the compounds revealed DRAK2 activities. Against DAPK3, the other DAPK kinase in the panel, none of the compounds showed a significant affinity.

Table 2: Structure-activity relationship of macrocyclic pyrazolo[1,5-*a*]pyrimidines 61, 67 – 73 and 107 – 121. In a DSF assay the compounds were screend against a pannel of 44 kinases and the results are highlighted with a heat map. It ranges from no stabilization (white) to the highest stabilization (dark green) of the kinase by the compounds. Staurosporine (**1**) was used as a reference. The trend of stabilization of DRAK1 compared to **61** is illustrated with green triangles (increase), yellow minus signs (steady), and red triangles (decrease). The bottom row shows the number of kinases with an affinity of $\Delta T_m > 5$.

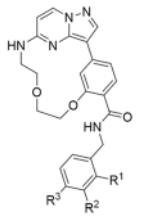

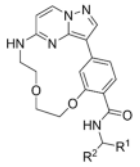

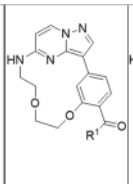

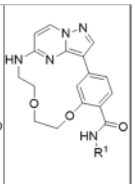

R^1 =	H	Cl	F	CH_3	H	H	Cl	F	H	CH_3	CH_3 *S*	CH_3 *R*	CH_3	H	H	CH_3 *R*	CH_3 *S*	H	MePip	Morph	H	CH_3	*t*-butyl
R^2 =	H	H	H	H	Cl, Cl	Cl, F	Cl	Cl	1-Naph	Ph	Ph	Ph	1-Naph	Pyr-3yl	Pyr-4yl	Pyr-4yl	Pyr-4yl	Quin-4yl	-	-	-	-	-
R^3 =	H	Cl	Cl	Cl	H	H	H	H	-	-	-	-	-	-	-	-	-	-	-	-	-	-	-
Compound	**61**	**67**	**68**	**69**	**70**	**71**	**72**	**73**	**110**	**107**	**108**	**109**	**111**	**112**	**113**	**114**	**115**	**116**	**117**	**118**	**119**	**120**	**121**	**positive control**
AAK1	7.5	6.5	4.7	7.3	8.4	9.3	4.9	8.5	8.2	6.2	6.8	9.6	5.2	8.2	7.1	7.2	7.1	8.1	3.2	3.9	12.9	9.0	5.6	14.0
ABL1	2.0	-0.8	0.0	-0.4	3.4	5.7	1.5	3.0	2.1	3.7	1.5	4.6	2.1	4.7	6.1	2.5	2.5	1.3	0.0	0.7	9.0	2.8	0.7	7.7
AKT3	0.1	1.3	0.6	1.5	0.4	0.9	-0.1	0.5	-0.1	-0.2	-1.0	2.5	0.2	0.0	-0.1	-0.7	-0.3	-0.4	-0.1	0.0	0.4	0.1	0.1	5.9
AurB	8.8	2.8	5.6	5.5	1.6	n.d.	n.d.	1.7	1.7		5.2	9.3	4.7	0.5	0.6	6.1	5.9	6.0	1.5	1.7	7.3	5.3	0.4	14.1
BIKE	11.0	9.4	12.2	9.7	10.7	9.5	0.2	11.4	9.5	6.2	8.8	9.8	5.8	12.6	12.5	11.1	11.1	12.0	5.3	6.3	15.8	12.0	8.0	16.7
BMX	0.0	0.0	0.5	1.1	1.0	1.0	-0.1	0.7	0.4	0.4	0.7	1.2	0.6	0.3	0.2	0.3	0.5	0.2	-0.2	0.3	-0.3	-1.8	0.2	6.7
BRAF	1.2	0.4	0.8	0.9	0.6	0.3	0.1	0.0	0.1	0.1	1.7	1.7	1.5	1.0	0.8	1.5	1.4	1.3	0.4	0.9	1.7	0.6	0.3	0.4
CaMK1g	0.2	-0.2	1.7	2.4	n.d.	2.1	1.0	2.5	0.4	0.4	1.8	1.8	2.5	0.6	0.9	-0.3	0.3	1.0	-0.6	-0.1	0.2	-0.6	0.1	20.3
CaMK2b	6.0	3.3	2.0	4.5	4.2	5.7	0.8	5.1	2.0	5.4	2.2	7.2	1.8	5.2	4.8	4.1	4.4	2.8	1.4	1.6	12.5	6.5	2.7	23.2
CASK	-0.1	0.1	0.0	0.0	n.d.	1.2		0.4		0.3	-0.1	-0.4	0.4	0.2	-0.3	-0.7	-0.5	-0.4	-0.2	0.3	1.3	-0.1	-1.1	4.3
CDK2	1.4	2.4	2.7	1.3	2.2	1.7	0.8	2.8	2.1	1.1	0.8	1.9	1.0	0.3	0.4	0.0	-0.1	0.6	0.0	2.5	7.8	1.8	1.0	14.3
CHK2	2.7	3.2	2.7	1.7	4.7	4.1	1.3	3.3	3.3	5.7	2.0	7.0	3.2	2.7	3.5	2.6	2.2	1.2	0.0	0.1	7.7	2.6	0.4	15.1
CK1d	1.6	0.3	0.6	1.1	0.8	1.3	0.5	0.9	0.8	1.8	0.8	2.7	0.8	1.2	3.2	2.4	2.3	1.5	0.0	0.3	8.4	4.1	1.0	1.1
CK2α	1.6	1.4	2.1	2.1	-1.2	0.4	-2.1	3.5	0.1	-0.9	1.2	0.8	0.3	-0.2	0.9	1.1	1.1	1.7	0.2	1.1	11.2	5.5	0.8	2.8
CK2α'	4.9	1.3	2.7	1.7	1.6	3.2	0.7	6.3	2.9	1.9	0.1	1.3	0.0	3.2	3.7	0.2	0.1	1.2	0.9	2.5	11.0	6.6	2.3	2.7
DAPK3	4.1	1.9	2.8	2.9	4.9	6.2	2.5	5.7	3.2	3.7	0.2	3.6	0.4	3.8	5.4	3.0	3.6	0.7	-0.3	0.4	11.2	6.4	3.1	14.3
DRAK1	9.3	10.2	9.0	11.1	9.8	10.7	6.2	8.8	8.5	12.1	9.6	12.8	7.3	9.9	10.4	12.1	12.3	7.2	2.1	3.0	13.3	10.5	11.3	12.5
DRAK2	-0.1	2.5	2.5	n.d.	3.4	0.8	-0.6	1.6	0.8	0.1	2.3	1.6	2.5	1.3	2.0	1.4	1.3	2.3	0.1	-0.5	1.9	2.3	1.6	10.1
DYRK1A	0.6	-0.4	-0.1	1.7	1.9	3.7	1.2	3.0	0.0	0.8	0.7	1.9	1.3	1.2	1.6	-0.2	-0.3	1.5	-0.7	0.2	3.7	1.5	-0.1	5.4
EphA2	0.5	0.1	0.1	0.2	0.6	0.8	0.6	0.7	0.4	0.6	0.6	1.1	0.7	0.3	1.1	1.2	1.2	0.6	0.0	0.3	2.5	1.3	0.5	6.7
ERK2	3.7	0.4	0.9	1.3	1.4	0.9	0.9	0.6	1.0	0.5	0.6	6.0	2.0	0.5	1.3	2.8	2.5	0.9	0.4	0.4	2.4	1.1	0.4	1.5
FES	0.0	0.0	0.4	0.6	0.2	0.4	0.3	0.4	0.0	0.2	0.5	0.7	0.2	0.2	0.3	0.1	0.3	0.2	-0.2	0.1	1.5	0.7	0.2	6.6
FGFR2	4.8	4.3	5.6	5.6	4.7	5.1	1.9	4.2	4.1	5.0	2.5	5.7	3.7	3.0	3.8	3.3	3.4	1.6	1.2	0.8	5.1	2.1	1.1	8.3
GAK	6.0	5.9	7.4	7.5	n.d.	7.1	3.8	6.8	5.8	5.7	3.5	7.5	4.5	4.7	5.0	4.6	4.6	4.1	1.2	2.1	9.9	6.8	4.1	8.0
GPRK5	1.5	-0.3	-0.1	0.0	1.2	1.9	0.5	1.0	1.0	1.8	n.d.	n.d.	n.d.	2.2	1.9	n.d.	n.d.	n.d.	0.1	-0.3	2.0	0.9	0.2	7.3
GSK3B	2.4	1.6	1.3	2.5	2.4	n.d.	n.d.	3.0	1.3	5.1	1.7	6.1	0.7	3.1	3.8	3.5	3.1	2.1	0.3	0.4	8.6	5.3	0.5	10.0
Haspin	5.8	0.2	1.3	1.5	3.0	5.3	0.7	2.6	1.7	3.5	1.5	4.9	1.5	4.2	5.9	3.4	3.4	3.8	0.5	0.6	8.1	6.7	1.2	7.6
JNK1	1.5	0.0	0.8	2.0	2.8	2.4	0.9	2.9	1.5	3.2	1.6	3.5	2.2	1.7	2.1	2.5	2.4	1.5	0.3	0.8	1.9	1.3	1.6	6.0
JNK2	0.3	0.6	0.5	0.9	1.4	0.4	0.1	0.4	0.9	1.0	0.6	2.1	1.3	0.3	0.5	1.1	1.1	0.7	0.1	0.2	0.8	0.5	0.6	2.8
LOK	5.0	-1.7	1.8	4.5	4.7	7.2	1.2	5.9	5.0	6.0	3.3	7.6	4.0	5.5	5.4	4.6	4.0	2.5	1.3	0.2	n.a.	n.a.	1.8	21.6
MAP2K1	1.2	0.3	0.8	0.6	0.4	1.8	0.7	1.3	0.4	1.0	0.6	1.5	1.1	0.0	0.2	0.3	0.2	0.3	1.0	1.0	0.3	0.0	-0.7	2.7
MAP2K6	1.5	1.2	1.3	1.8	2.5	2.0	1.1	1.8	1.6	3.2	3.9	3.0	2.6	1.2	1.4	1.2	1.3	1.3	0.3	0.2	3.1	1.8	0.8	11.4
MER	0.6	0.1	0.1	0.0	1.5	2.7	0.6	1.8	0.6	0.8	0.2	0.6	0.9	-0.4	0.0	-0.3	-0.3	-0.3	0.1	0.0	3.1	0.7	0.3	5.2
MSK1_b	3.2	3.3	3.9	3.0	3.9	2.2	0.6	3.1	1.3	1.6	2.0	2.7	2.2	0.3	0.0	0.7	0.7	-0.1	0.1	0.2	7.9	2.3	1.2	12.9
MST2	4.2	0.8	2.4	4.7	n.d.	5.7	2.2	5.7	3.7	4.9	4.5	6.7	3.7	3.3	3.8	4.2	3.9	2.8	0.7	1.0	4.8	3.8	2.0	9.9
NDR2	-0.1	0.3	0.6	1.8	3.9	4.9	2.0	3.6	2.4	4.7	1.3	6.2	3.4	2.2	2.3	2.9	3.1	1.8	-0.1	0.1	-0.1	-0.1	0.0	10.3
PAK4	0.8	-0.3	0.3	0.7	2.7	2.0	1.5	1.5	1.1	1.6	1.9	1.6	1.5	0.5	0.4	0.4	0.3	1.1	-0.1	0.5	3.2	0.3	1.0	21.2
PHKG2	0.5	0.0	0.6	1.0	n.d.	n.d.	2.3	5.0	0.3	4.4	1.8	1.3	1.3	3.8	5.3	0.4	0.5	1.0	0.0	0.6	8.9	2.1	0.8	21.2
PIM1	2.3	-0.1	-2.4	-0.2	3.2	4.3	1.7	3.6	2.2	5.4	3.5	7.4	2.7	4.4	4.3	4.3	3.8	2.0	0.4	0.8	12.2	8.8	1.2	11.3
RSK1_b	0.9	0.4	0.7	0.8	0.1	-0.4	1.7	-0.5	-0.2	-0.5	0.5	-0.2	0.4	0.1	-0.3	0.1	0.3	0.3	0.3	0.1	-0.5	-0.6	-0.4	0.0
STLK3	5.3	4.1	3.4	3.0	0.8	0.3	-0.9	0.3	1.0	0.4	-0.4	1.7	0.7	0.0	0.3	1.2	1.5	0.7	2.7	0.7	5.3	5.6	0.2	7.5
TTK	1.5	1.0	1.8	3.0	3.1	2.9	-0.2	2.3	1.9	1.8	0.1	1.3	-0.3	1.2	0.4	0.2	1.4	-0.3	0.6	0.4	1.7	1.2	1.6	7.9
ULK3	5.0	2.8	3.9	4.8	6.3	7.6	1.9	5.6	4.5	6.6	6.6	7.5	7.5	4.7	7.7	7.5	7.5	7.5	0.5	1.0	8.5	6.5	4.5	17.8
VRK1	0.3	0.9	0.9	1.8	1.2	1.6	-0.1	1.1	0.9	0.9	0.5	1.6	1.3	0.5	0.7	0.2	0.4	0.4	0.0	0.1	3.4	1.9	0.3	2.5
Stabilization of DRAK1		▲		▲		▲	▼			▲		▲	▼		▲	▲	▲	▼	▼	▼	▲	▲	▲	
Selectivity X/44 Kinases	8	4	5	6	4	12	1	10	4	10	5	15	4	5	9	5	5	5	1	1	21	14	3	

3.3.2 KINOME*scan*® assay

To validate the findings regarding selectivity from the DSF assay, the lead structure **61** as well as the most promising compounds **107**, **115** and **121** were screened in the KINOME*scan*® assay. A theoretical description of this method can be found in chapter 3.2.4. Also screened against the 468 kinases of the *scan*MAX panel was the macrocyclic scaffold **37**. The compounds were screened at concentrations of 0.1 µM and 1 µM, respectively. The data obtained are shown graphically in **Figure 22**. As suspected, the macrocyclic scaffold **37** was hardly conspicuous for selectivity with S_{35} = 0.26 at 1 µM, but the introduction of the benzylamide **61** significantly increased the S-Score to S_{35} = 0.03 at 100 nM and S_{35} = 0.09 at 1 µM. For compound **107**, the selectivity was further improved due to the added methyl group at the alkyl carbon of the benzylamide. With S_{35} = 0.02 at 100 nM and S_{35} = 0.05 at 1 µM, the S-score could be almost halved. For compound **115**, the aromatic system of the benzylamide motif was replaced by a heteroaromatic pyridine. Surprisingly, this variation had a dramatic effect on the selectivity. With S_{35} = 0.18 at 1 µM, the S-score was close to that of the unselective macrocyclic scaffold **37**. The selectivity of the *tert*-butyl derivative **121**, which was already promising in the DSF panel, was confirmed in the *scan*MAX panel and increased more than twofold compared to **107**. The S-score for **107** was S_{35} = 0.005 at 100 nM and S_{35} = 0.02 at 1 µM. At both screening concentrations, **121** revealed high activities on both CK2 isoforms. Nevertheless, the CK2 isoforms had already been validated in the DSF assay and no significant affinity has been detected. Thus, it was reasonable to suspect that these were false positives, but this should be revalidated *in cellulo*. The NAK kinases BIKE and GAK as well as DRAK2 would be potential off-targets at a screening concentration of 1 µM. DRAK2 could also be identified, by the undetectable affinity towards **121** in the DSF assay, as a false positive result.

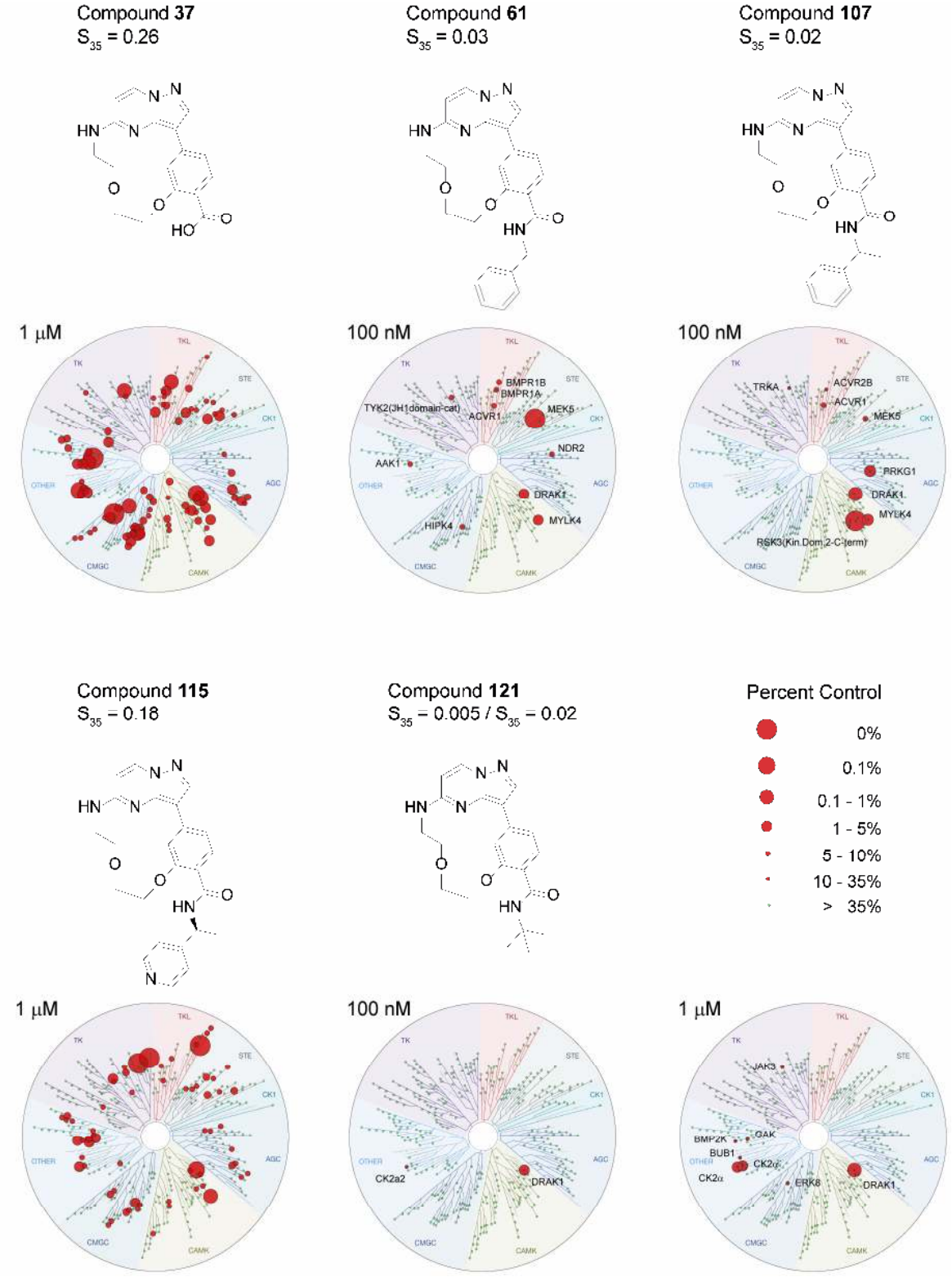

Figure 22: **Selectivity screening of 37, 61, 107, 115 and 121.** Selectivity was determined in the KINOMEscan® assay by Eurofins (formerly DiscoverX) against 469 kinases of the scanMAX pannel. Screening was performed at a concentration of 100 nM and/or 1 µM and targeted kinases are highlited by red circles.

3.3.3 Isothermal titration calorimetry and ^{33}PanQinase^{TM} assay.

ITC experiments were performed to quantify the affinity of the compounds towards DRAK1. A theoretical description of this method can be found in chapter 3.2.3. For this purpose, the promising compound **121** as well as **115**, which showed the highest stabilization of DRAK1 with also high selectivity in the DSF assay, were investigated. The results are shown in **Figure 23** below. As expected, both compounds were highly potent with K_D values of 21 nM (**121**) and 9 nM (**115**). The enthalpic and entropic contributions to binding of **121** and **115** differed only slightly. (*Experiments were performed by Franziska Preuß*)

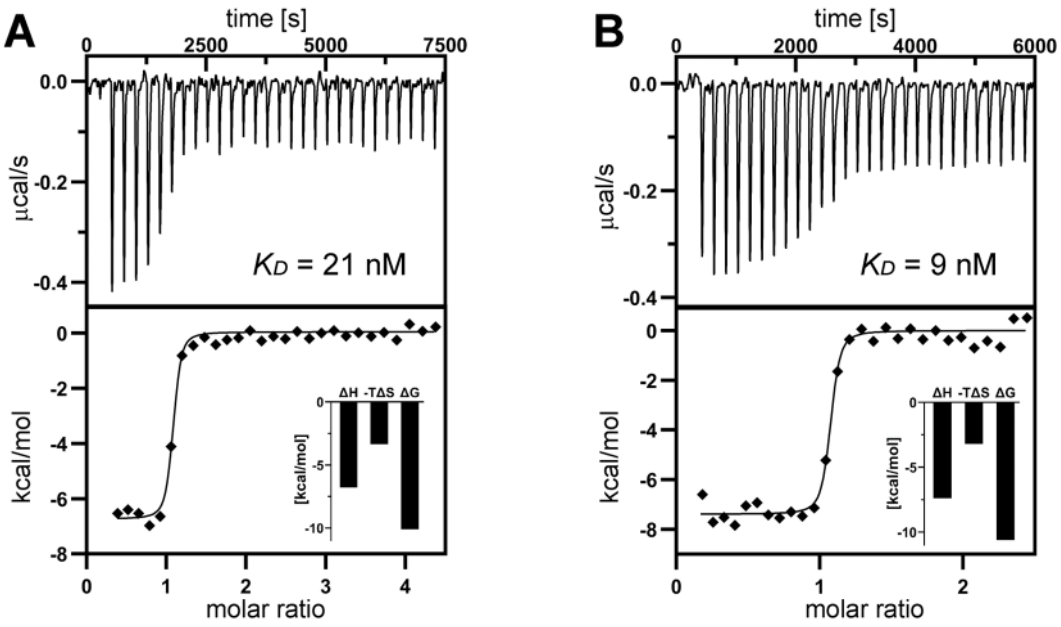

Figure 23: **Isothermal titration calorimetry of 121 (A) and 115 (B).** The experiments reveals low nanomolar binding affinity towards DRAK1. There are no significant deviations in the overall Gibbs free energy, the entalpic and entropic contribution of binding.

To confirm these results, compounds **61**, **107**, **115**, and **121** were tested in ProQinase's ^{33}PanQinase^{TM} assay. This is a scintillation proximity assay (SPS) in well plate format. In this radiometric activity assay, a ^{33}P-labled phosphate of ATP is transferred from the kinase to a kinase substrate. The wells of the FlashPlates® used for the reaction are coated with a polyester-based scintillator for detection. The results of this assay, together with those of ITC, are shown in **Table 3**. The trend already observed in DSF regarding the affinities of the compounds was confirmed. With an IC_{50} = 155 nM, **61** has the lowest potency on DRAK1, followed by **121** with IC_{50} = 49 nM.

Compounds **107** (IC_{50} = 31 nM) and **115** (IC_{50} = 15 nM) were close together and just like **121** (IC_{50} = 49 nM) in the very good two-digit nanomolar range. Regarding the possible off-target activity of **121** on CK2, some low activities were revealed but was negligible. The potency of **121** on CK2α was IC_{50} = 950 nM and on CK2α´ IC_{50} = 380 nM.

Table 3: **Binding affinities of macrozyclic pyrazolo[1,5-*a*]pyrimidines towards DRAK1.** Promising compounds were examined by ITC and in ^{33}PanQinase™ assay (ProQinase). Potential off-target activity of **121** against CK2 was determined in ^{33}PanQinase™ assay as well.

Compound	ITC K_D	^{33}PanQinase™ IC_{50}		
	DRAK1	DRAK1	CK2α	CK2α´
61	-	155 nM	-	-
107	-	31 nM	-	-
115	9 nM	15 nM	-	-
121	21 nM	49 nM	950 nM	380 nM

3.3.4 NanoBRET™ target engagement assay

The promising kinome-wide selectivity profiles of **121** and **107**, as well as the low two-digit nanomolar potency of the compounds, made a determination of cellular activity inevitable. Also to be assayed in the cellular system were the affinities of **121** towards the potential off-targets, revealed in KINOME*scan*®. For this purpose, several NanoBRET™ experiments were performed. A theoretical description of this method can be found in chapter 3.2.5. Compounds **61**, **107**, **115** and **121** were tested against DRAK1 using staurosporine (**1**) as positive control. Also examined were the negative control candidates **117** and **118**. Obtained data are shown graphically in **Figure 24**. The IC_{50} values of **61** and **121** were in a close range with 171 nM and 181 nM, respectively. **107** and **115** with IC_{50} values of 71 nM and 70 nM were also close to each other. As already suspected from DSF results, no significant *in cellulo* activity on DRAK1 was detectable for **117** and **118** with IC_{50} values >50 µM and they were appropriate as negative control compounds. Staurosporine (**1**) showed IC_{50} = 52 nM, which correlated with published *in vitro* data (IC_{50} = 17 nM).[184] Apart from the slightly weaker potency of **121**, the correlation of affinity data from the different experiments toward DRAK1 was again confirmed. An overall view can be seen in **Table 12** chapter 4.2.

Validation of the potency of **121** against potential off-targets CK2α, CK2α´, GAK, BIKE and DRAK2 was done by NanoBRET™ experiments as well (**Figure 24**). The IC_{50} values were in the low micromolar range between 8 µM and 39 µM and were more than 40-fold higher than the DRAK1 activity (IC_{50} = 181 nM) of **121**. Thus, it was confirmed that **121** is a highly selective and highly potent inhibitor on DRAK1. (*Experiments were performed by Lena Berger*)

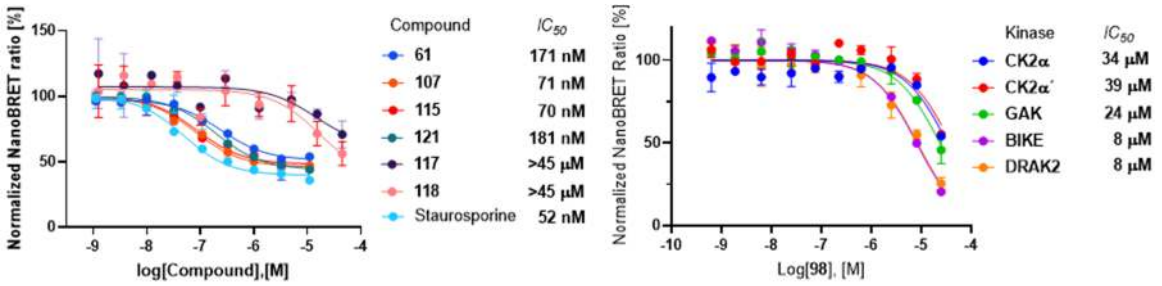

Figure 24: **Cellular potencies of 61, 107, 115, 121, 117 and 118 on DRAK1 and of 121 on potential off-targets (CK2α, CK2α´, GAK,BIKE and DRAK2).** IC_{50} values determined with NanoBRET™ experiments in HEK293T cells can be seen in the figure legend.

3.3.5 Co-crystal structures

The co-crystal structures of DRAK1 in complex with **61** and **121** revealed that they represent canonical type I inhibitors and an excellent form complementarity of **121** with the active sites. The ATP-mimetic interaction with the hinge occurred between the pyrazole nitrogen and the backbone nitrogen of alanine A141 in both compounds (**Figure 25**). As well as the benzylamide residue of **61**, the *tert*-butylamide residue of **98** also pointed into a spacious unoccupied back pocket (**Figure 26B**). Another interaction was observed between the carbonyl oxygen and the catalytic lysine K90 in the β3 strand. The absence of this interaction may be seen as the reason for the lower affinity of urea derivatives **85** and **89** – **91** toward DRAK1. The alignment of the co-crystal structures uncovered an interesting structural feature and a difference in binding modes of **61** and **98**, respectively (**Figure 26A**). It suggested that the alternation from the large benzylamide residue (**61**) to the smaller *tert*-butylamide (**121**) allowed a deeper penetration of the active site toward the hinge. This resulted in tighter binding of **121** via the carbonyl oxygen with the catalytic lysine K90. This is demonstrated by the varying distances of 1.3 Å for **121** and 2.8 Å for **61**.

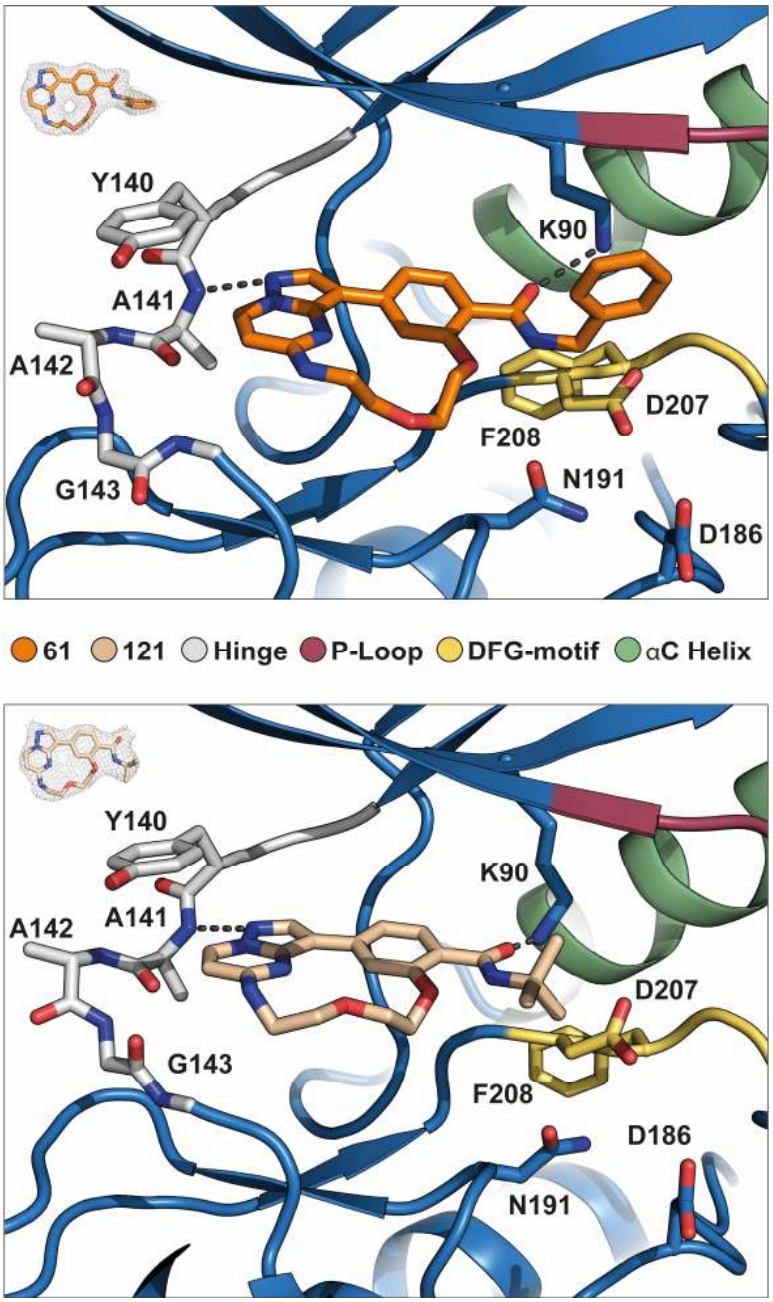

Figure 25: **Binding modes of 61 and 121 in complex with DRAK1 in stick representaion.** Pyrazolo[1,5-*a*] pyrimidine-based macrocycles **61** (orange) and **121** (beige) are identifiable as ATP competetive (type I) inhibitors, which are bound to the hinge by formation of hydrogen bond (dashed line) at the backbone nitrogen A141. An aditional hydrogen bond was formed between the side chain amine of the catalytic lysine K90 and the carbonyl oxygen of the amide in both cases. Structural motifes of interest are highlited in a colour code (see legend). The electron density of each compound is shown in the insert on the upper left corners.

Another conformational detail was a slight displacement of the P-loop for **61** with the bulky benzylamide motif (**Figure 26C**). However, the deeper binding was enabled by a conformational rearrangement in the hinge region. Strikingly, in the binding mode of **61**, glycine G143 in the linker region adjacent to the hinge was significantly twisted compared with the binding mode of **121** (**Figure 25**).

Such a flexible hinge region is rather rare but possible and has been reported for the highly selective p38 inhibitor skepinone-L.[185,186] However, a completely fliped glycine as for skepinone-L did not happened in the binding mode of **121**. This could indicate a certain degree of flexibility within the back pocket. (*Experiments were performed by Franziska Preuß and Dr. Sebastian Mathea*)

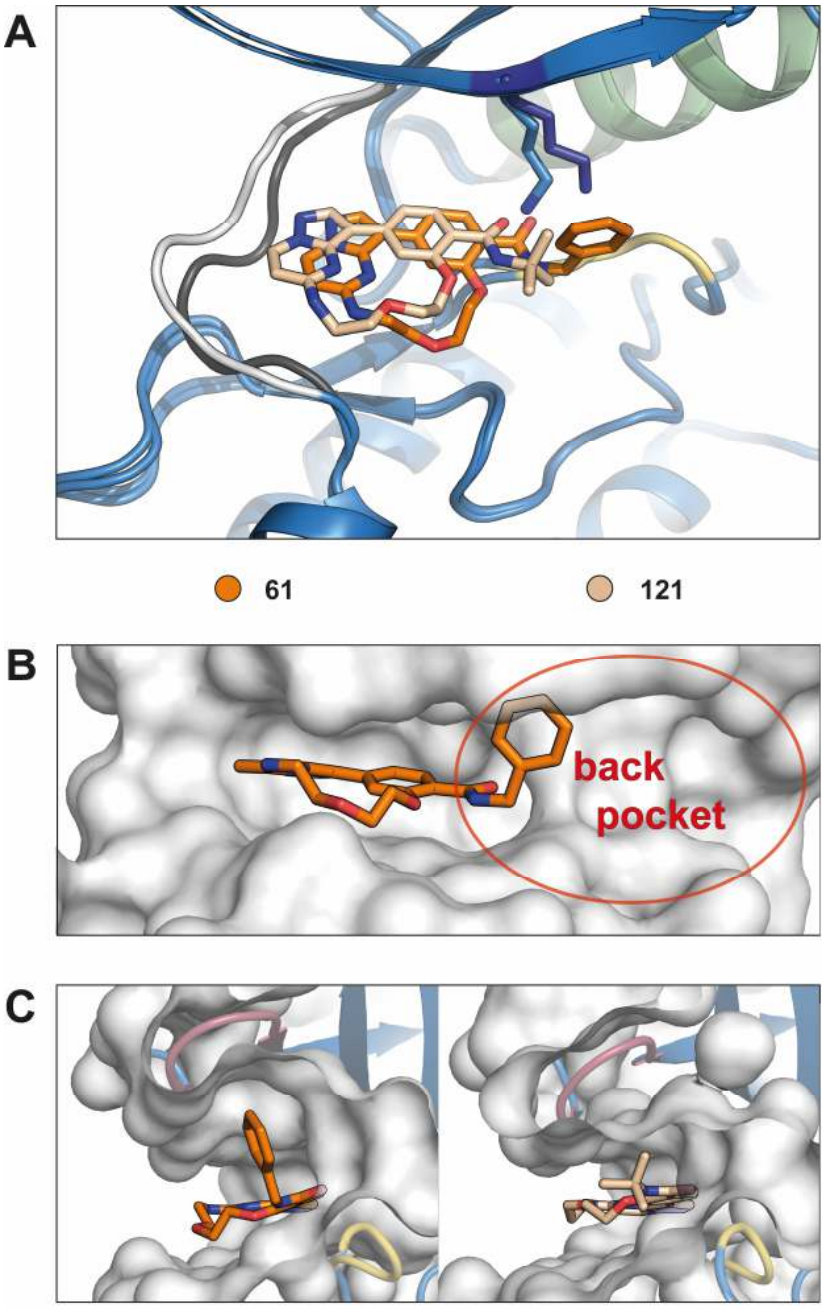

Figure 26: **Binding modes of 61 and 121 in complex with DRAK1 in stick representaion. A**) Alignment of **61** and **121**, **B**) highlited benzyl amide residue of **61** which extends into a spacious back pocket (surface representation), **C**) view into the catalytic pocket (surface representation) with bounded ligands **61** and **121** from direction of the back pocket. The alignment of the binding modes demonstrated that **61** binds slightly deeper in the catalytic pocket, resulting in a slight deformation of the hinge. In **C**, the comparison of **61** and **121** reveals that there is a slight displacement of the P-loop when **61** is bound.

3.3.6 Cellular effects

Since compound **121** has been identified as highly selective and potent inhibitor, the next step was to study its activity towards glioma cells. First, the effect of pyrazolo[1,5-*a*]pyrimidines in general cell viability was evaluated in three different cell lines: human embryonic kidney cells (HEK293T), osteosarcoma cells (U2OS), and non-transformed human lung fibroblasts (MRC-9). In a multiplex high-content assay, employing a confocal microscope (CQ1, Yokogawa), cells were treated with fluorescent dyes to detect apoptosis (Alexa Fluor 680 conjugate), Nuclei/DNA (Hoechst33342), mitochondria function (Mitotracker red) and microtubule shape (BioTracker™ 488 Green Microtubule Cytoskeleton Dye). In addition to the highly selective **121**, the highly potent **115** and the dual chlorinated compounds **67** and **72** were also screened at two different concentrations (1 μM and 10 μM). Fluorescence and cell shape were determined before and 18 h as well as 36 h after compound exposure. Staurosporine (**1**) was used as positive control at 10 μM and error bars were determined using two technical duplicates. At lower concentration of 1 μM, no significant cytotoxic effects were observed for any of the compounds at all time points in each cell line (**Figure 27A**). However, higher concentration of 10 μM caused a significant decrease in the number of healthy cells. Thus, a noticeable cytotoxic effect was observed for **67** and **72** after 18 h and 36 h. The treatment with **115** and **121** at 10 μM, however, resulted in a minor decreased healthy cell count in all three cell lines.

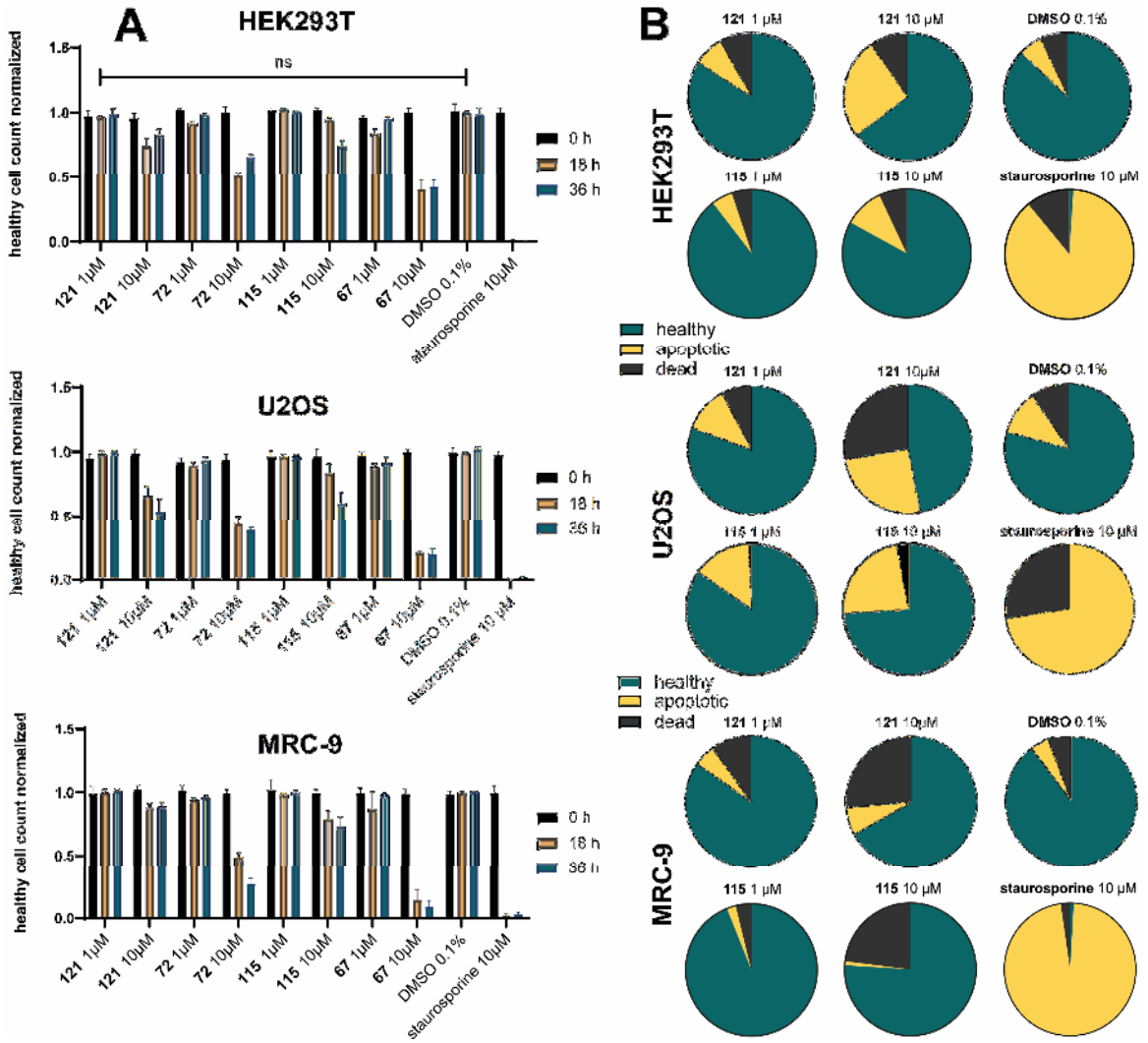

Figure 27: **Live cell high content screen of HEK293T, U2OS and MRC-9 cells. A**) Healthy cell count before as well as after 18 h and 36 h after treatment with **67**, **72**, **115** and **121** at concentrations of 1µM and 10 µM. Staurosporine (**1**) was used as reference and cell count was normelized to healthy cells exposed to DMSO 0.1%. **B**) Fraction of healthy (green), apoptotic (yellow) and dead cells (black) after 18 h of 1 µM and 10 µM compound exposure (**121**, **115** and staurosporine (**1**)) compared to 0.1% DMSO control.

The distributions of healthy, apoptotic, and dead cells were determined for **115** and **121** after 18 h. The results are shown graphically in **Figure 27B** and no significant difference in the distributions of healthy versus dying cells at 1 µM compared to 0.1% DMSO control was detectable for compounds **115** and **121**. A slight increase of apoptotic rate for **115** and **121** in HEK293T cells at a concentration of 10 µM was observed. In the U2OS cell line, the rate of dead and apoptotic cells increased noticeably at higher concentration, whereas in the MRC-9 line, there were more dead cells detected than apoptotic ones.

Figure 28 shows the bright field confocal images of the three cell lines, treated with fluorescent dyes to detect apoptosis (Alexa Fluor 680 conjugate), Nuclei/DNA (Hoechst33342), mitochondria function (Mitotracker red) and microtubule shape observed (BioTracker™ 488 Green Microtubule Cytoskeleton Dye), 18 h after treatment with **121**.

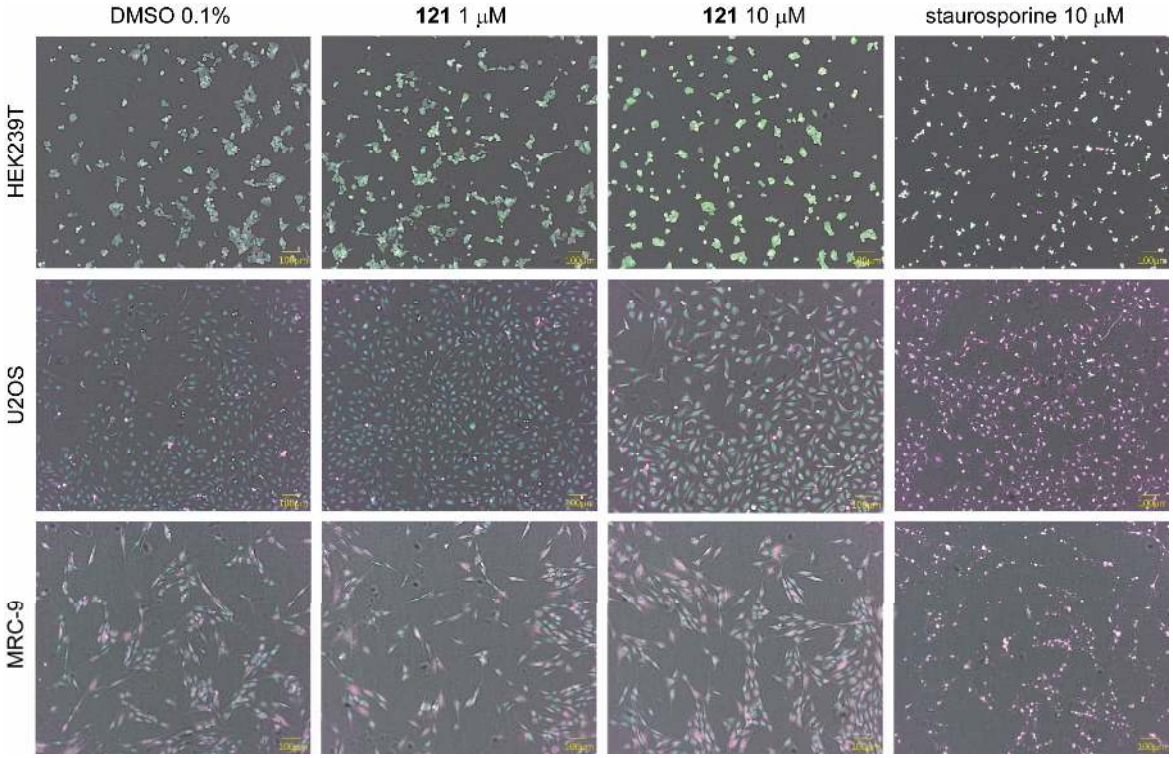

Figure 28: **Brightfield confocal images of satined cells.** Cells (HEK293T, U2OS and MRC-9) were analyzed after 18 h of 1μM and 10 μM exposure of **121** (blue: DNA/nuclei, green: microtubule, red: mitochondria, magenta: Annexin V apoptosis marker). Staurosporine (**1**) and DMSO 0.1% were used as references.

Referring to these data, it can be concluded that the investigated compounds **115** and **121** did not show a general cytotoxicity at 1 μM. At this concentration, the cytotoxic effect was at DMSO level and only a slightly increase was detected at 10 μM. (*Experiments were performed by Amelie Tjaden*)

As mentioned above, studies by Mao *et al*. had revealed the high overexpression of DRAK1 in gliomas. In knockdown experiments, a significant change in cell shape was observed in the absence of DRAK1, which was associated with a decrease in proliferation, clonogenicity or migration.[120] Based on these findings regarding DRAK1 as a potential target against glioma, the macrocyclic inhibitors were evaluated in a cell viability assay towards their activity in glioma cells.

Cell lines LN-229, D-247MG, T98G, and LN18 were treated with **115** and **121** at a concentration range of 0 – 20 µM in a dose dependent manner and analyzed after 1 day and 7 days. Both LN-229 and D-247MG showed the highest expression levels in the previous analysis of their expression patterns (**Figure 29**). Both were significantly above that of cell line U-87MG, being used and reported as high expressing glioma cell line.[120] Consequently, these cell lines should have an increased sensitivity towards DRAK1 inhibition. The other cell lines T98G and LN18 showed lower expression levels and thus should be less sensitive.

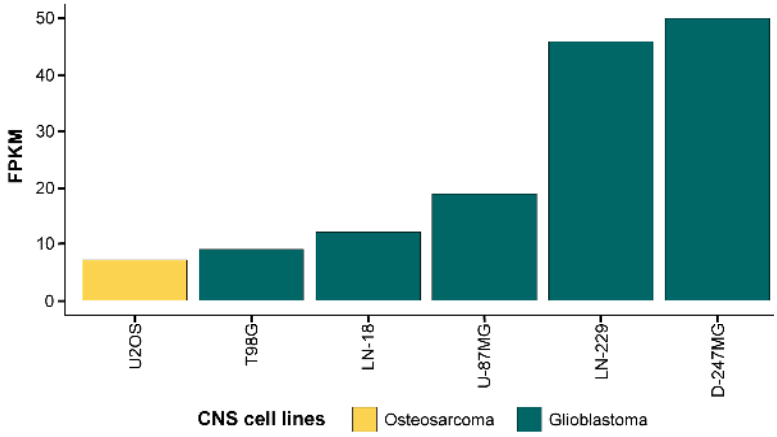

Figure 29: **Normalized DRAK1 gene expression in central nervous system (CNS) cell lines.** Expression in six different CNS cell lines (osteosarcoma (yellow): U2OS; glioblastoma (green): T98G, LN-18, U-87MG, LN-229 and D-247MG) was determined by RNA-seq. FPKM: Fragments Per Kilobase per Million.

Surprisingly, the half-maximal effective concentration (EC_{50}) values of **121** (9 – 11 µM), determined after seven days with resazurin, did not indicate a significant effect by inhibition of DRAK1 (**Figure 30**). In D-247MG cells, the activity towards DRAK1 was slightly lower (EC_{50} = 2.75 µM), which could be attributed to the high expression level of DARK1. Treatment of the cells with **115** yielded EC_{50} values between 1 µM and 2 µM (**Figure 30**). These were lower than those of **121**, but there was a noticeable discrepancy with the low nanomolar activity of the compounds in the NanoBRET™ assay with 70 nM and 181 nM, respectively. Against expectations, no cellular phenotype was observed in the high-expressing LN-229 and D-247MG cells that could be matched with the observations by Mao *et al.*. Only minor morphological changes were detected in low-expressing T98G cells at concentration of 12.5 µM. The surviving cells were larger, flatter, more elongated, and appeared more differentiated, neuron-like (**Figure 31**).

However, this effect was more pronounced for **115** and visible in DMSO-treated cells to a small extent as well. Nevertheless, based on the selectivity profile of **115** from KINOME*scan*® assay, it was feasible that morphological changes of the cells were due to off-target effects. (*Experiments were performed by Dr. Martin Cusack and Dr. Dr. Tobias Weiss university of Zurich*)

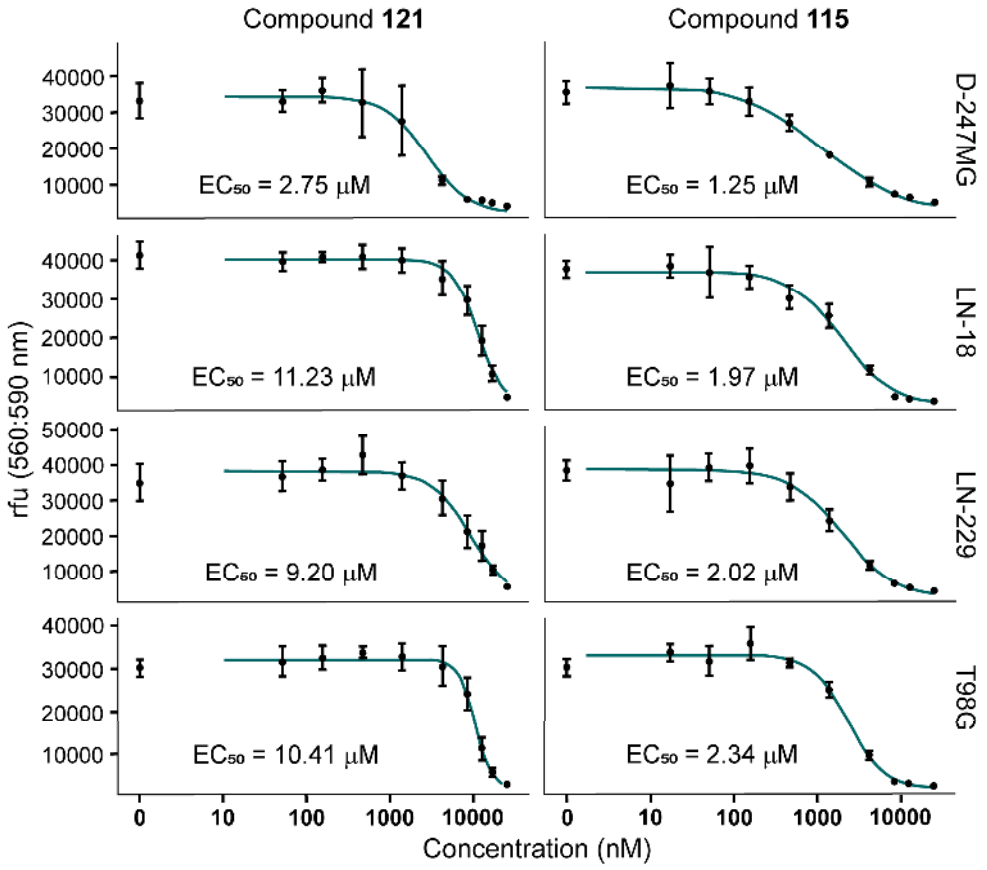

Figure 30: **Glioma cell viability assay.** Dose-response curves of **115** and **121** in D-247MG, LN-18, LN229 and T98G glioblastoma cell lines. Cell viability was determined in a resazurin reduction assay at a concentration range of 0 – 20 µM over seven days and mean fluorescence was plotted ± SD, n = 6. The corresponding EC_{50} values are shown below the curves.

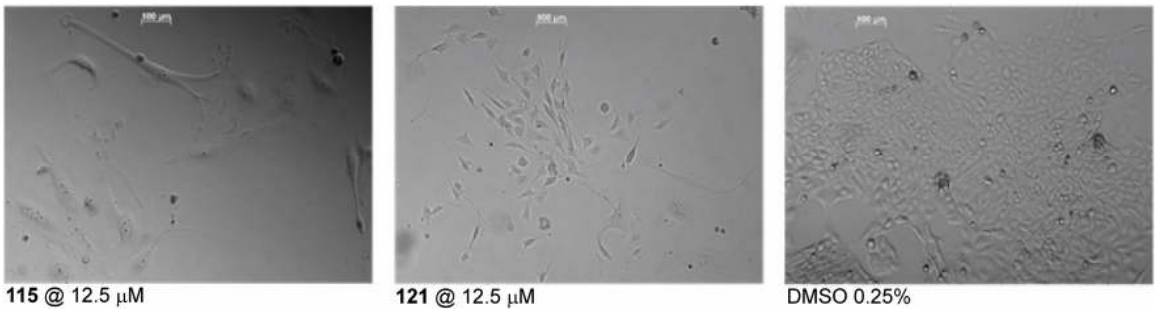

Figure 31: Brightfield microscopy image of T98G cells. Cells were analyzed 5 days after exposure to 12.5 µM **115** and **121** with DMSO 0.25% as a reference.

3.4 Raiders of the antiviral effect: Pyrazolo[1,5-*a*]pyrimidine-based macrocyclic inhibitors of AAK1

3.4.1 Differential scanning fluorimetry

Compounds **61** – **73** (single/dual substituted benzylamides), **85** – **92** (benzylureas), **117** and **118** (heterocyclic benzylamides), **144** – **156** (urea-based derivatives), **165** – **168** (carbamate-based derivatives), **132** – **143** (alkyl/aromatic linker derivatives) as well as **38** and **39** (alkyl/aromatic linker scaffolds) were screened concerning their binding affinities *in vitro* in the DSF assay against 44 kinases as described in chapter 3.2.1. **Table 4** shows the results of the singel and dual substituted benzylamide derivatives. The benzylamide lead structure **61** showed good stabilization of AAK1 ($\Delta T_m = 7.5$), but also high binding affinities towards the other NAK kinases BIKE and GAK as well as aurora kinase B (AurB) and DRAK1. *Ortho* substitution with chlorine (**62**) resulted in an overall drop of affinity, whereas chlorine substitution in *meta* position (**63**) resulted in an increased affinity on both AAK1 ($\Delta T_m = 8.1$) and the off-targets mentioned above. Variation of the substituent in meta position (bromine **64** and nitrile **65**) resulted in an increase of T_m-shifts on AAK1 ($\Delta T_m \geq 9$), while a decrease was observed on BIKE and AurB. A slight increase was observed on DRAK1 and GAK. The nitrile-substituted compound **65** showed the best results in terms of selectivity (7 kinases with $\Delta T_m > 5$) as well as stabilization of AAK1 ($\Delta T_m = 9.1$). The para substitution with chlorine (**66**) was highly tolerated by the off-target kinases. Among the dual substituted compounds **67** – **73** BIKE, GAK and DRAK1 were also highly stabilized. The *ortho/para* substituted compounds **67** and **68** showed a decrease in stabilization of AAK1 ($\Delta T_m < 7$). However, compound **70** with chlorine in both *meta* positions of the phenyl ring was significantly more tolerated ($\Delta T_m = 8.4$) and showed no significant affinity toward AurB. Within the panel, good selectivity was evident and besides the NAK kinases, only unc-51-like kinase 3 (ULK3) was stabilized with $\Delta T_m > 5$. Substitution of chlorine by a smaller fluorine (**71**) resulted in a further increased stabilization of AAK1 ($\Delta T_m = 9.3$) and a simultaneous loss of selectivity (12 kinases with $\Delta T_m > 5$). The *ortho/meta* chlorinated compound **72** showed a huge decrease in affinity within the panel. Replacement of ortho chlorine with fluorine (**73**) was significantly more tolerated, but stabilized all NAK kinases and again a loss of selectivity was observed (10 kinases $\Delta T_m > 5$). There was a clear trend towards preference of AAK1 over *meta* (mono or dual) substituted benzylamide derivatives. Substitution in *ortho* and or *para* position was significantly less tolerated, then dual substitution in *ortho* and *meta* position.

Table 4: **Structure-activity relationship of macrocyclic pyrazolo[1,5-*a*]pyrimidines 61 – 73.** In a DSF assay the compounds were screend against a pannel of 44 kinases and the results are highlighted with a heat map. It ranges from no stabilization (white) to the highest stabilization (dark green) of the kinase by the compounds. Staurosporine (**1**) was used as a reference. The trend of stabilization of AAK1 compared to **38** is illustrated with green triangles (increase), yellow minus signs (steady), and red triangles (decrease). The bottom row shows the number of kinases with an affinity of $\Delta T_m > 5$.

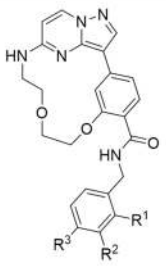

R^1	H	Cl	H	H	H	H	Cl	F	CH_3	H	H	Cl	F	
R^2	H	H	Cl	Br	CN	H	H	H	H	Cl, Cl	F, Cl	Cl	Cl	
R^3	H	H	H	H	H	Cl	Cl	Cl	Cl	H	H	H	H	
Compound	**61**	**62**	**63**	**64**	**65**	**66**	**67**	**68**	**69**	**70**	**71**	**72**	**73**	**Stauro-sporine**
AAK1	7.5	6.5	8.1	9.0	9.1	9.2	6.5	4.7	7.3	8.4	9.3	4.9	8.5	14.0
ABL1	2.0	3.2	2.2	4.3	4.5	1.2	-0.8	0.0	-0.4	3.4	5.7	1.5	3.0	7.7
AKT3	0.1	0.5	0.3	0.3	0.1	0.9	1.3	0.6	1.5	0.4	0.9	-0.1	0.5	5.9
AurB	8.8	6.1	8.7	1.4	n.d.	8.0	2.8	5.6	5.5	1.6	n.d.	n.d.	1.7	14.1
BIKE	11.0	8.1	12.4	10.0	7.7	12.1	9.4	12.2	9.7	10.7	9.5	0.2	11.4	16.7
BMX	0.0	0.0	0.5	0.3	0.7	1.1	0.0	0.5	1.1	1.0	1.0	-0.1	0.7	6.7
BRAF	1.2	0.6	0.9	0.0	1.2	1.0	0.4	0.8	0.9	0.6	0.3	0.1	0.0	0.4
CaMK1g	0.2	0.4	1.2	1.0	1.6	2.1	-0.2	1.7	2.4	n.d.	2.1	1.0	2.5	20.3
CaMK2b	6.0	3.9	8.3	4.9	5.3	5.8	3.3	2.0	4.5	4.2	5.7	0.8	5.1	23.2
CASK	-0.1	-0.1	0.2	1.0	0.7	0.7	0.1	0.0	0.0	n.d.	1.2	n.d.	0.4	4.3
CDK2	1.4	1.6	0.7	0.9	0.8	2.9	2.4	2.7	1.3	2.2	1.7	0.8	2.8	14.3
CHK2	2.7	0.4	1.5	2.8	4.0	4.2	3.2	2.7	1.7	4.7	4.1	1.3	3.3	15.1
CK1d	1.6	0.4	0.5	0.9	1.5	1.3	0.3	0.6	1.1	0.8	1.3	0.5	0.9	1.1
CK2α	1.6	2.3	3.1	0.8	0.8	2.5	1.4	2.1	2.1	-1.2	0.4	-2.1	3.5	2.8
CK2α´	4.9	1.7	2.9	2.8	3.6	3.0	1.3	2.7	1.7	1.6	3.2	0.7	6.3	2.7
DAPK3	4.1	4.4	6.9	6.9	6.5	3.1	1.9	2.8	2.9	4.9	6.2	2.5	5.7	14.3
DRAK1	9.3	8.7	7.8	9.1	9.8	7.9	10.2	9.0	11.1	9.8	10.7	6.2	8.8	12.5
DRAK2	-0.1	-0.6	-0.5	0.5	-0.4	3.3	2.5	2.5	n.d.	3.4	0.8	-0.6	1.6	10.1
DYRK1A	0.6	-0.6	1.1	1.2	1.4	1.2	-0.4	-0.1	1.7	1.9	3.7	1.2	3.0	5.4
EphA2	0.5	0.1	0.3	0.7	0.7	1.1	0.1	0.1	0.2	0.6	0.8	0.6	0.7	6.7
ERK2	3.7	0.8	1.5	0.9	0.8	2.8	0.4	0.9	1.3	1.4	0.9	0.9	0.6	1.5
FES	0.0	-0.1	0.2	0.3	0.2	0.5	0.0	0.4	0.6	0.2	0.4	0.3	0.4	6.6
FGFR2	4.8	2.5	3.1	6.1	3.1	7.0	4.3	5.6	5.6	4.7	5.1	1.9	4.2	8.3
GAK	6.0	3.0	6.9	6.5	7.6	6.9	5.9	7.4	7.5	n.d.	7.1	3.8	6.8	8.0
GPRK5	1.5	-0.2	-0.2	2.1	1.3	1.5	-0.3	-0.1	0.0	1.2	1.9	0.5	1.0	7.3
GSK3B	2.4	0.3	0.6	3.9	3.7	2.2	1.6	1.3	2.5	2.4	n.d.	n.d.	3.0	10.0
Haspin	5.8	1.0	2.0	4.0	4.5	3.6	0.2	1.3	1.5	3.0	5.3	0.7	2.6	7.6
JNK1	1.5	0.3	1.0	3.0	2.1	1.6	0.0	0.8	2.0	2.8	2.4	0.9	2.9	6.0
JNK2	0.3	0.1	0.0	0.0	0.6	0.8	0.6	0.5	0.9	1.4	0.4	0.1	0.4	2.8
LOK	5.0	-0.6	2.0	6.3	4.7	7.2	-1.7	1.8	4.5	4.7	7.2	1.2	5.9	21.6
MAP2K1	1.2	0.6	1.1	1.5	0.6	2.2	0.3	0.8	0.6	0.4	1.8	0.7	1.3	2.7
MAP2K6	1.5	1.1	1.8	1.4	1.3	1.8	1.2	1.3	1.8	2.5	2.0	1.1	1.8	11.4
MER	0.6	0.0	0.2	1.4	1.1	0.8	0.1	0.1	0.0	1.5	2.7	0.6	1.8	5.2
MSK1_b	3.2	0.1	4.2	2.7	0.7	2.4	3.3	3.9	3.0	3.9	2.2	0.6	3.1	12.9
MST2	4.2	2.3	2.7	4.6	4.1	4.1	0.8	2.4	4.7	n.d.	5.7	2.2	5.7	9.9
NDR2	-0.1	0.0	0.2	3.8	3.9	1.3	0.3	0.6	1.8	3.9	4.9	2.0	3.6	10.3
PAK4	0.8	-0.2	0.5	0.8	0.8	1.5	-0.3	0.3	0.7	2.7	2.0	1.5	1.5	21.2
PHKG2	0.5	0.3	0.6	4.2	5.0	0.7	0.0	0.6	1.0	n.d.	n.d.	2.3	5.0	21.2
PIM1	2.3	3.4	3.1	4.0	3.8	-3.6	-0.1	-2.4	-0.2	3.2	4.3	1.7	3.6	11.3
RSK1_b	0.9	0.5	0.4	-0.9	0.0	0.7	0.4	0.7	0.8	0.1	-0.4	1.7	-0.5	0.0
STLK3	5.3	3.0	-1.3	0.0	0.8	1.6	4.1	3.4	3.0	0.8	0.3	-0.9	0.3	7.5
TTK	1.5	1.2	2.6	2.8	2.2	3.0	1.0	1.8	3.0	3.1	2.9	-0.2	2.3	7.9
ULK3	5.0	3.0	3.7	7.5	7.3	4.6	2.8	3.9	4.8	6.3	7.6	1.9	5.6	17.8
VRK1	0.3	0.1	0.1	1.1	1.2	1.1	0.9	0.9	1.8	1.2	1.6	-0.1	1.1	2.5
Stabilization of AAK1		▼	▲	▲	▲	▲	▼	▼		▲	▲	▼	▲	
Selectivity X/44 Kinases	**8**	**4**	**7**	**8**	**7**	**8**	**4**	**5**	**6**	**4**	**12**	**1**	**10**	

The single and dual substituted benzylurea derivatives **85** – **92** were also characterized in the DSF assay (**Table 5**). Some binding affinities towards AAK1 were observed, but with T_m-shifts less than 5 degrees, these were significantly lower than those of the mono and dual substituted benzylamide derivatives ($\Delta T_m = 5 – 9$). However, the affinity towards BIKE and GAK remained almost invariant for all urea derivatives. DRAK1 was no longer highly stabilized. Some of the compounds showed increased stabilization of lymphocyte-oriented kinase (LOK), especially **91** ($\Delta T_m = 11.1$). However, this was negligible compared to staurosporine (**1**) ($\Delta T_m = 21.6$).

Table 6 shows the data from the DSF assay of the urea- and carbamate-based compounds **144** – **156** and **165** – **168**. The introduction of urea derivatives at the secondary amine at 5-position of the pyrazoly[1,5-*a*]pyrimidine resulted in a dramatic loss of binding affinity against AAK1 ($\Delta T_m < 5$), compared to the lead structure **61** ($\Delta T_m = 7.5$). This was observed to the same extent for the methyl esters **144** – **150** as well as for the carboxylic acids **151** – **156**. With increasing steric demand of the urea residues from **144** to **150**, a slight decrease in the stabilization of AAK1 was observed. This trend, within the series, was observed for the carboxylic acids **151** – **156** in the same manner. The T_m-shifts of the carbamates **165** – **168** were also below 5 degrees. However, the affinity of the compounds towards BIKE was preserved, while GAK and AurB were significantly less stabilized. As the steric demand of the urea residues increased, the affinity of the compounds toward DRAK1 also decreased. However, **150** was an exception, which could be related to its alkyl elongation motif. Due to the hydrolysis of the ester, the binding affinity of the compounds **151** – **156** towards the two CK2 isoforms was dramatically increased ($\Delta T_m = 8 - 13$). This was to be expected since the carboxylic acid motif is essential for binding to CK2 as described in chapter 3.2.1.

Table 5: **Structure-activity relationship of macrocyclic pyrazolo[1,5-*a*]pyrimidines 85 – 92.** In a DSF assay the compounds were screend against a pannel of 44 kinases and the results are highlighted with a heat map. It ranges from no stabilization (white) to the highest stabilization (dark green) of the kinase by the compounds. Compound **61** and Staurosporine (**1**) were used as references. The trend of stabilization of AAK1 compared to **61** is illustrated with green triangles (increase), yellow minus signs (steady), and red triangles (decrease). The bottom row shows the number of kinases with an affinity of $\Delta T_m > 5$.

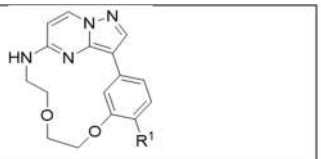

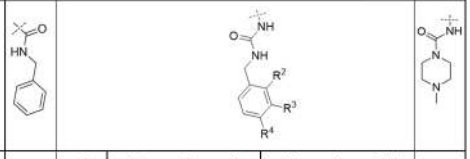

R^2	-	H	Cl	H	H	Cl	F	CH_3	-	
R^3	-	H	H	Cl	H	H	H	H	-	
R^4	-	H	H	H	Cl	Cl	Cl	Cl	-	
Compound	**61**	**85**	**86**	**87**	**88**	**89**	**90**	**91**	**92**	**Stauro-sporine**
AAK1	7.5	4.1	6.8	5.2	6.1	3.9	5.2	5.4	6.2	14.0
ABL1	2.0	2.7	0.3	-1.5	-1.0	-0.8	-1.0	-0.6	0.5	7.7
AKT3	0.1	0.0	0.3	0.3	0.3	0.5	0.2	0.4	-0.2	5.9
AurB	8.8	4.5	5.3	7.2	6.6	5.0	7.0	4.5	1.5	14.1
BIKE	11.0	10.8	9.5	9.6	10.7	7.8	10.2	8.0	10.9	16.7
BMX	0.0	0.9	1.1	1.5	1.5	0.9	1.1	1.2	0.0	6.7
BRAF	1.2	0.8	0.4	0.3	0.4	0.4	0.5	0.5	0.4	0.4
CaMK1g	0.2	0.3	-0.1	0.2	0.4	0.8	0.6	1.5	0.2	20.3
CaMK2b	6.0	3.1	2.8	4.9	2.2	2.2	2.4	1.2	2.7	23.2
CASK	-0.1	0.5	1.9	1.1	1.0	1.2	1.5	1.5	0.1	4.3
CDK2	1.4	3.4	3.7	4.2	6.2	3.7	5.0	3.4	0.8	14.3
CHK2	2.7	5.0	7.1	4.8	5.0	4.6	4.7	6.1	0.4	15.1
CK1d	1.6	0.3	0.3	0.7	0.7	0.4	0.4	0.9	0.2	1.1
CK2α	1.6	1.1	1.2	1.7	2.0	1.5	1.7	1.3	0.5	2.8
CK2α´	4.9	3.1	2.0	2.3	2.4	1.0	1.5	1.2	1.2	2.7
DAPK3	4.1	1.9	-0.2	1.4	1.0	0.8	0.8	0.2	0.8	14.3
DRAK1	9.3	6.2	4.6	7.2	3.9	3.7	3.2	3.0	2.6	12.5
DRAK2	-0.1	1.4	2.9	3.3	2.5	2.9	3.5	3.8	0.1	10.1
DYRK1A	0.6	0.2	-0.7	-0.8	-1.2	-0.2	-0.9	1.8	-0.5	5.4
EphA2	0.5	0.3	0.4	0.7	0.6	0.3	0.4	0.5	0.1	6.7
ERK2	3.7	0.3	1.0	1.1	0.8	0.6	0.7	0.6	0.1	1.5
FES	0.0	0.4	0.3	0.6	0.6	0.5	0.6	1.2	0.0	6.6
FGFR2	4.8	4.4	2.9	3.9	4.3	2.5	3.3	2.5	1.5	8.3
GAK	6.0	5.4	6.4	5.9	6.5	6.5	6.5	6.6	4.0	8.0
GPRK5	1.5	-0.3	-0.1	0.1	-0.3	0.7	-0.2	0.2	-0.2	7.3
GSK3B	2.4	0.6	0.6	0.5	0.5	0.1	0.3	-0.3	0.6	10.0
Haspin	5.8	1.1	0.3	0.8	0.6	0.3	0.4	0.8	0.7	7.6
JNK1	1.5	0.1	1.9	0.4	0.2	0.8	0.5	1.3	1.0	6.0
JNK2	0.3	0.6	1.0	1.1	1.1	1.1	1.1	1.0	0.2	2.8
LOK	5.0	4.6	8.5	8.0	7.3	5.2	6.3	11.1	2.3	21.6
MAP2K1	1.2	0.3	1.8	1.3	1.3	1.5	1.9	1.4	1.3	2.7
MAP2K6	1.5	1.0	0.8	0.8	0.8	0.6	0.8	0.6	0.2	11.4
MER	0.6	1.0	1.1	0.8	1.1	0.5	0.8	0.9	0.1	5.2
MSK1_b	3.2	0.4	1.6	1.8	2.4	2.8	3.2	1.1	0.7	12.9
MST2	4.2	3.6	4.3	4.4	4.3	3.3	4.2	4.8	0.7	9.9
NDR2	-0.1	-0.1	0.7	0.8	0.8	1.2	1.3	0.9	-0.1	10.3
PAK4	0.8	0.3	0.5	0.3	0.2	0.4	0.2	1.2	-0.1	21.2
PHKG2	0.5	1.1	1.4	1.2	1.2	0.9	1.2	0.9	0.4	21.2
PIM1	2.3	2.1	3.9	-0.3	-1.4	-0.1	-0.3	-0.1	0.9	11.3
RSK1_b	0.9	1.1	1.6	1.1	1.2	0.6	1.1	0.8	0.3	0.0
STLK3	5.3	3.8	0.5	4.2	4.9	5.0	4.2	3.5	2.2	7.5
TTK	1.5	1.9	2.5	1.6	1.6	1.5	1.5	2.3	0.9	7.9
ULK3	5.0	5.2	5.4	5.8	5.9	5.0	6.2	4.1	2.6	17.8
VRK1	0.3	0.1	0.1	0.1	0.1	0.8	0.5	1.4	0.2	2.5
Stabilization of AAK1		▼	▼	▼	▼	▼	▼	▼	▼	
Selectivity X/44 Kinases	**8**	**4**	**7**	**7**	**7**	**3**	**6**	**5**	**2**	

Table 6: **Structure-activity relationship of macrocyclic pyrazolo[1,5-*a*]pyrimidines 144 – 156 and 165 – 168.** In a DSF assay the compounds were screend against a pannel of 44 kinases and the results are highlighted with a heat map. It ranges from no stabilization (white) to the highest stabilization (dark green) of the kinase by the compounds. Compound **61** and Staurosporine (**1**) were used as references. The trend of stabilization of AAK1 compared to 38 is illustrated with green triangles (increase), yellow minus signs (steady), and red triangles (decrease). The bottom row shows the number of kinases with an affinity of $\Delta T_m > 5$.

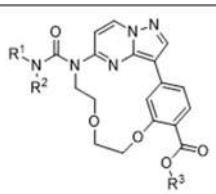

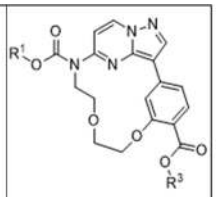

R^1		Me	Et	*t*-Bu	Et	Me-pip	Morph	$C_7H_{17}N_3$	Me	Et	*t*-Bu	Et	Me-pip	Morph	Me	Et	Me	Et	
R^2		H	H	H	Et	Me-pip	Morph	H	H	H	H	Et	Me-pip	Morph	-	-	-	-	
R^3		Me	Me	Me	Me	Me	Me	Me	H	H	H	H	H	H	Me	Me	H	H	
Compound	**61**	**144**	**145**	**146**	**147**	**148**	**149**	**150**	**151**	**152**	**153**	**154**	**155**	**156**	**165**	**166**	**167**	**168**	**Stauro-sporine**
AAK1	7.5	4.2	4.1	3.0	2.8	2.9	3.0	3.8	4.7	4.9	4.2	3.1	2.9	2.8	2.6	1.7	4.1	3.4	14.5
ABL1	2.0	0.0	0.9	-0.1	0.2	0.1	0.3	-0.2	0.1	0.1	-0.2	1.3	0.0	0.8	0.1	-0.1	0.0	0.8	10.9
AKT3	0.1	-0.1	0.0	-0.2	0.0	0.0	0.0	0.0	-0.3	0.0	0.6	0.1	0.0	-0.2	0.0	-0.1	-0.1	0.1	6.3
AurB	8.8	0.6	-0.9	-0.1	1.2	1.2	0.3	1.4	-0.4	-0.2	-1.3	-1.5	0.1	-0.7	1.0	0.8	-0.2	-1.1	8.9
BIKE	11.0	8.2	8.1	6.2	7.0	7.7	7.9	7.4	8.7	8.9	8.2	8.3	8.1	8.1	5.8	2.8	8.4	7.4	17.4
BMX	0.0	0.3	0.8	0.2	0.4	0.3	0.4	0.2	0.0	0.2	-0.2	0.5	0.1	0.0	0.4	0.2	0.3	0.5	6.5
BRAF	1.2	2.8	1.9	0.5	1.8	0.8	0.8	1.5	0.6	0.7	0.2	1.0	0.5	0.6	1.1	1.0	1.7	1.7	0.4
CaMK1g	0.2	-0.9	-0.6	-1.3	-1.3	-1.4	-1.1	-1.3	-1.2	-0.5	-1.3	-0.8	-1.3	-0.8	-1.1	-1.2	-1.2	-0.8	9.5
CaMK2b	6.0	2.5	2.0	1.1	0.8	0.3	0.1	1.9	7.4	6.8	3.6	1.9	0.9	1.0	3.1	2.3	9.4	8.3	24.3
CASK	-0.1	0.0	0.8	0.6	0.6	0.6	0.8	0.4	0.7	0.1	0.9	0.7	0.6	0.5	0.7	0.4	1.1	1.1	4.0
CDK2	1.4	1.2	0.7	0.2	0.6	-0.1	0.3	0.6	2.5	1.8	0.8	1.4	0.1	0.5	1.1	0.3	3.1	2.3	14.8
CHK2	2.7	0.4	0.1	0.2	0.2	0.0	-0.1	0.3	1.2	1.0	0.3	0.4	0.1	-0.1	0.4	0.1	1.4	1.1	16.3
CK1d	1.6	0.5	1.0	0.8	0.3	0.2	0.3	0.6	1.3	1.7	1.2	1.3	0.7	0.3	0.4	0.2	1.6	1.3	1.1
CK2α	1.6	2.6	2.7	2.8	1.2	0.8	0.9	1.2	11.4	11.7	11.5	8.9	7.4	7.5	2.8	2.1	12.2	12.0	3.1
CK2α´	4.9	3.8	4.6	4.8	2.9	2.4	2.5	3.3	12.6	12.4	13.1	10.4	9.3	9.3	4.4	3.7	13.5	13.2	4.6
DAPK3	4.1	1.2	1.3	0.6	0.0	0.3	0.2	1.6	7.1	6.9	6.0	4.0	3.3	3.1	1.0	0.4	7.9	6.6	17.7
DRAK1	9.3	7.2	6.8	4.3	2.0	1.5	1.0	8.2	6.1	5.4	4.6	2.4	2.7	2.2	5.8	4.0	4.6	3.3	13.6
DRAK2	-0.1	3.1	3.6	2.7	1.4	2.1	1.6	1.7	0.7	1.1	0.1	0.9	0.0	0.4	2.5	0.6	0.6	0.0	10.5
DYRK1A	0.6	0.3	1.1	0.0	0.1	0.1	0.2	0.3	0.6	0.8	0.2	1.0	0.2	0.2	-0.2	-0.1	1.0	0.9	6.6
EphA2	0.5	0.2	0.3	0.1	0.2	0.1	0.2	0.1	0.0	0.2	0.2	0.4	0.1	-0.1	-0.3	0.1	0.3	0.4	6.6
ERK2	3.7	-0.2	0.0	-0.2	0.0	0.0	0.1	-0.1	-0.3	-0.2	-0.1	0.0	0.0	-0.3	0.1	-0.1	0.0	0.2	1.1
FES	0.0	0.0	0.1	0.0	-0.2	0.0	0.1	0.0	-0.2	0.1	-0.1	0.0	0.1	-0.2	-0.4	0.0	0.1	0.1	6.5
FGFR2	4.8	0.1	0.1	-0.2	1.5	0.1	0.3	0.0	0.1	0.2	0.1	0.8	0.1	0.3	0.1	-0.1	0.2	0.1	7.5
GAK	6.0	3.0	3.1	1.8	2.8	0.6	1.1	2.2	5.7	5.8	5.5	2.2	2.1	2.0	3.4	1.6	5.5	4.9	8.7
GPRK5	1.5	0.0	0.1	0.0	0.1	-0.1	0.1	0.0	0.0	0.2	0.0	0.0	0.0	0.0	0.0	-0.1	0.5	0.2	6.9
GSK3B	2.4	3.4	2.9	1.9	3.6	1.6	1.9	1.6	5.1	4.6	3.1	4.6	1.2	1.6	2.2	1.1	4.4	4.1	9.4
Haspin	5.8	2.1	1.9	1.1	1.8	1.3	0.9	2.0	1.0	0.9	0.5	0.8	0.3	0.2	2.0	1.2	1.2	1.1	8.6
JNK1	1.5	0.5	1.2	0.5	0.6	0.1	0.3	0.5	0.4	0.4	0.1	0.5	0.3	0.2	0.7	-0.2	0.3	0.1	7.0
JNK2	0.3	0.3	0.6	0.1	0.4	0.3	0.4	0.1	0.2	0.1	0.0	0.3	0.2	0.1	0.6	-0.1	0.2	0.2	3.3
LOK	5.0	n.d.	2.8	1.3	1.3	1.5	1.8	1.9	5.6	4.8	4.0	3.2	2.9	2.9	1.3	0.8	4.0	3.8	23.7
MAP2K1	1.2	-0.2	-7.5	-0.2	-7.5	-7.2	-8.3	-0.2	0.0	0.1	-0.3	-7.5	-7.1	0.1	-8.4	0.0	-6.8	-7.5	1.5
MAP2K6	1.5	0.5	-6.1	0.0	-5.9	-5.4	-5.9	0.1	0.3	0.3	-0.2	-5.8	-5.4	0.0	-5.8	-0.1	-4.8	-5.9	11.4
MER	0.6	-0.1	0.2	-0.1	-0.1	0.0	0.2	0.0	0.1	0.2	0.0	0.4	0.1	-0.1	0.1	-0.1	0.3	0.4	6.1
MSK1_b	3.2	0.5	0.6	0.2	0.7	0.2	0.4	0.3	1.9	1.5	0.9	1.3	0.6	0.7	0.3	0.2	2.7	2.0	2.9
MST2	4.2	1.7	1.6	0.6	0.5	0.2	0.2	0.8	0.6	0.5	0.0	0.2	0.0	-0.1	1.4	0.4	0.7	0.5	13.2
NDR2	-0.1	0.9	0.8	0.1	0.4	0.5	0.3	0.4	0.2	0.3	0.1	0.2	-0.1	-0.1	0.6	0.3	0.3	0.4	10.7
PAK4	0.8	0.2	0.6	0.4	0.9	1.0	0.8	0.2	0.4	0.3	0.4	0.6	0.7	0.5	0.7	0.2	0.9	1.0	12.7
PHKG2	0.5	1.6	1.4	0.5	0.5	0.4	0.3	1.6	2.4	1.9	0.7	0.5	0.5	0.2	1.2	0.7	2.8	1.8	21.1
PIM1	2.3	1.7	2.3	0.7	1.7	1.3	n.d.	2.5	2.4	2.1	1.1	3.1	1.4	1.3	1.3	0.9	2.8	1.9	13.1
RSK1_b	0.9	0.5	0.6	0.2	0.7	0.2	0.4	0.3	1.9	1.5	0.9	1.3	0.6	0.7	0.3	0.2	2.7	2.0	2.9
STLK3	5.3	-0.1	0.0	-0.1	0.2	-0.2	-0.1	0.2	0.2	-0.1	0.0	-0.2	-0.1	0.0	-0.1	-0.2	0.1	-0.1	9.0
TTK	1.5	3.2	2.9	1.9	1.1	1.0	1.2	0.7	0.3	0.0	-0.1	0.1	0.0	-0.1	1.7	0.3	0.5	-0.2	9.2
ULK3	5.0	6.3	6.5	3.8	4.4	2.2	2.6	3.6	2.5	2.7	1.6	1.2	0.4	0.5	5.5	1.8	3.2	2.3	18.0
VRK1	0.3	0.0	0.1	-0.3	0.0	0.0	0.1	-0.3	0.3	0.3	0.1	1.1	0.1	0.5	0.1	-0.2	0.7	0.4	2.8
Stabilization of AAK1		▬	▼	▼	▼	▼	▼	▼	▼	▼	▼	▼	▼	▼	▼	▼	▼	▼	
Selectivity X/44 Kinases	**8**	**3**	**3**	**1**	**1**	**1**	**1**	**2**	**9**	**7**	**5**	**3**	**3**	**3**	**3**	**0**	**6**	**5**	

The macrocyclic compounds with alkyl and aromatic linker motif **132** – **143**, **38** and **39** were also characterized in the DSF assay. Data are shown in **Table 7**. Compounds **132** and **133** with Boc group and methyl ester did not show significant stabilization within the panel. Without the methyl ester, increased binding affinity ($\Delta T_m > 5$) was observed for **134** and **135** toward BIKE, calcium/calmodulin-dependent protein kinase 2 subunit β (CaMK2b), CDK2, CK2, DAPK3, glycogen synthase kinase 3 β (GSK3B), and for **135** at PAK4. Compounds **136** and **114** with methyl ester but without Boc group showed a decrease in T_m-shifts. However, a significant increase was detectable for **136** at BIKE and for **137** at mammalian STE20-like kinase 2 (MST2) and ULK3. The macrocyclic core structures **38** and **39** showed the lowest selectivity within the panel, as expected because of their structural similarity with **137** (>10 kinases with $\Delta T_m > 5$). The alkyl linker of **38** was significantly better tolerated by AAK1 than the aromatic linker motif of **39**. The introduction of the benzylamide increased the affinity toward AAK1 for **138** and **141**. In direct comparison to the lead structure **61** ($\Delta T_m = 7.5$), **138** ($\Delta T_m = 7.5$) showed a similar T_m-shift, whereas **141** ($\Delta T_m = 6.3$) was lower. Interestingly, the affinity of **138** toward the potential off-targets AurB, BIKE, and DRAK1 was lower than that of the lead structure **61**. The introduction of the *meta*-chlorinated benzylamide derivatives **139** and **142** led to a decrease in binding affinity ($\Delta T_m < 5$) towards AAK1 and thus to a degradation compared to **63** with PEG linker ($\Delta T_m = 8.1$). However, for **142**, T_m-shifts in fibroblast growth factor receptor 2 (FGFR2) ($\Delta T_m = 8.4$) and sterile-20-like kinase 3 (STLK3) ($\Delta T_m = 7.5$) were very high. The *tert*-butyl derivatives **140** and **143** did not show significant improvement in binding affinity and selectivity in the panel compared with **121**. In conclusion, the introduction of the aromatic linker motif resulted in a loss of binding affinity toward AAK1. Compared to the lead structure **61**, the benzylamide derivative **138** with alkyl linker showed a consistent affinity towards AAK1, but a significant drop in affinity ≥2 degrees towards the main off-targets AurB, BIKE and DRAK1.

Table 7: **Structure-activity relationship of macrocyclic pyrazolo[1,5-*a*]pyrimidines 132 – 143 and 38 – 39.** In a DSF assay the compounds were screend against a pannel of 44 kinases and the results are highlighted with a heat map. It ranges from no stabilization (white) to the highest stabilization (dark green) of the kinase by the compounds. Compounds **61**, **63** and **121** as well as Staurosporine (**1**) were used as references. The trend of stabilization of AAK1 compared to **61** is illustrated with green triangles (increase), yellow minus signs (steady), and red triangles (decrease). The bottom row shows the number of kinases with an affinity of $\Delta T_m > 5$.

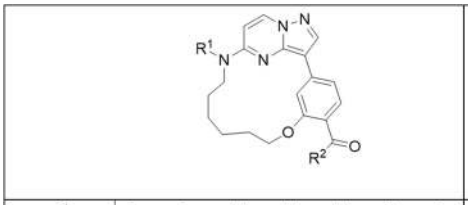

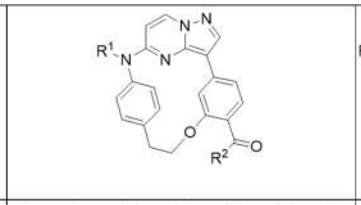

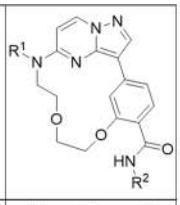

R^1 / R^2	Boc / OCH_3	Boc / OH	H / OCH_3	H / OH	H / 	H / 	H / 	Boc / OCH_3	Boc / OH	H / OCH_3	H / OH	H / 	H / 	H / 	H / 	H / 	H / 
Compound	**132**	**134**	**136**	**38**	**138**	**139**	**140**	**133**	**135**	**137**	**39**	**141**	**142**	**143**	**61**	**63**	**121**	**Stauro-sporine**
AAK1	0.6	3.2	6.3	7.4	7.5	4.4	5.3	0.4	1.5	3.1	1.9	6.3	4.8	2.3	7.5	8.1	5.6	14.0
ABL1	0.6	0.3	4.9	4.0	1.6	0.9	0.9	0.4	1.8	1.9	3.3	2.9	2.0	1.0	2.0	2.2	0.7	7.7
AKT3	-0.1	-0.7	-0.2	0.0	0.6	0.3	0.4	0.2	-0.5	0.0	0.2	1.1	0.5	0.1	0.1	0.3	0.1	5.9
AurB	0.0	-0.6	3.1	4.1	3.6	2.3	-0.6	0.1	1.5	3.0	3.0	1.3	2.0	-0.9	8.8	8.7	0.4	14.1
BIKE	1.5	6.5	10.4	11.0	8.5	5.0	7.1	1.2	4.8	5.4	5.0	6.3	4.5	3.2	11.0	12.4	8.0	16.7
BMX	0.2	0.3	0.7	1.2	1.8	1.4	2.2	-2.6	-0.1	1.7	0.9	2.1	1.8	1.2	0.0	0.5	0.2	6.7
BRAF	-0.1	4.5	-0.2	2.9	0.2	0.2	0.3	0.1	1.7	0.2	0.5	0.4	0.5	0.2	1.2	0.9	0.3	0.4
CaMK1g	-0.8	-1.1	-0.2	0.8	-1.3	1.2	0.5	-1.2	-0.4	-0.1	0.7	1.8	2.4	0.7	0.2	1.2	0.1	20.3
CaMK2b	0.7	10.8	6.3	13.4	4.9	4.5	4.4	n.d.	9.0	6.6	11.2	5.2	3.7	2.3	6.0	8.3	2.7	23.2
CASK	1.0	1.9	0.3	-0.3	1.0	1.3	0.3	-1.0	-0.7	1.1	-0.4	0.4	-1.1	0.1	-0.1	0.2	-1.1	4.3
CDK2	0.0	5.2	5.3	8.1	2.3	2.6	1.3	0.3	5.2	5.5	7.0	4.8	2.5	1.4	1.4	0.7	1.0	14.3
CHK2	-0.2	0.6	1.9	4.0	3.0	0.4	0.9	0.0	0.4	3.1	3.3	5.5	2.6	1.3	2.7	1.5	0.4	15.1
CK1d	0.1	2.2	0.1	2.8	0.2	0.0	0.4	0.1	1.4	0.4	1.5	0.6	0.2	0.3	1.6	0.5	1.0	1.1
CK2α	1.1	12.6	1.8	0.4	2.3	1.4	0.6	0.6	-0.1	2.5	0.2	1.4	1.6	1.6	1.6	3.1	0.8	2.8
CK2α´	2.3	13.2	2.6	11.7	2.4	1.6	1.3	0.4	10.3	4.5	10.5	2.2	1.6	0.8	4.9	2.9	2.3	2.7
DAPK3	0.0	8.5	3.9	9.2	2.8	3.0	1.9	-1.0	6.7	4.0	8.0	2.6	1.8	1.4	4.1	6.9	3.1	14.3
DRAK1	0.1	3.2	4.5	8.7	7.4	4.7	8.6	0.5	3.7	4.4	10.5	4.0	3.4	7.8	9.3	7.8	11.3	12.5
DRAK2	0.5	0.3	4.7	0.3	2.4	0.8	2.5	0.2	-0.2	3.3	-0.7	2.1	3.8	1.9	-0.1	-0.5	1.6	10.1
DYRK1A	0.2	2.2	1.9	5.2	2.7	4.0	3.6	-1.6	2.9	1.6	4.1	3.1	5.8	1.9	0.6	1.1	-0.1	5.4
EphA2	0.2	-0.1	0.2	1.0	1.0	0.8	0.7	-0.1	0.5	1.0	1.3	0.5	1.2	0.8	0.5	0.3	0.5	6.7
ERK2	0.0	-0.1	0.1	0.5	1.1	0.6	0.5	0.3	0.1	0.0	0.4	0.9	3.3	0.3	3.7	1.5	0.4	1.5
FES	0.0	-0.3	1.5	0.5	1.1	0.6	0.5	0.1	-0.2	0.9	0.5	1.8	0.5	0.8	0.0	0.2	0.2	6.6
FGFR2	-0.3	0.1	2.6	3.4	5.8	2.3	2.4	0.3	1.2	3.4	2.1	7.7	8.4	2.4	4.8	3.1	1.1	8.3
GAK	0.4	4.5	6.5	9.0	5.9	3.5	3.8	0.2	3.6	4.0	4.7	4.5	3.9	1.8	6.0	6.9	4.1	8.0
GPRK5	-0.2	0.2	0.6	2.1	0.9	0.9	0.6	0.3	0.7	1.5	1.7	1.3	1.5	0.7	1.5	-0.2	0.2	7.3
GSK3B	1.0	6.0	2.4	3.2	0.6	0.1	0.6	2.9	8.1	2.6	3.7	4.2	0.7	0.8	2.4	0.6	0.5	10.0
Haspin	0.5	1.3	4.1	4.5	2.0	1.0	0.8	0.6	2.1	5.1	5.0	2.2	2.6	1.9	5.8	2.0	1.2	7.6
JNK1	0.3	0.3	1.4	0.9	1.9	2.0	1.4	-0.7	0.1	1.8	0.5	1.5	2.2	1.4	1.5	1.0	1.6	6.0
JNK2	0.2	0.1	1.5	0.6	0.7	-0.2	0.9	-0.4	-0.1	1.6	0.2	1.5	0.9	0.9	0.3	0.0	0.6	2.8
LOK	0.3	2.9	5.5	8.2	7.9	3.3	4.5	n.d.	4.3	4.2	8.8	4.8	5.5	3.1	5.0	2.0	1.8	21.6
MAP2K1	-7.0	-8.3	0.2	-0.6	-0.7	-0.5	-1.4	-0.1	-1.2	-7.5	-0.9	1.6	-0.9	-1.6	1.2	1.1	-0.7	2.7
MAP2K6	-5.7	-5.7	1.4	2.0	1.0	1.0	0.7	0.5	1.8	-5.2	2.0	2.9	2.1	1.2	1.5	1.8	0.8	11.4
MER	0.2	-0.1	0.5	1.1	-0.2	-0.1	1.0	0.0	1.0	1.3	1.3	1.4	1.6	0.7	0.6	0.2	0.3	5.2
MSK1_b	0.4	1.7	n.d.	6.8	3.8	4.8	3.4	0.1	3.0	0.8	3.3	3.2	3.3	1.3	3.2	4.2	1.2	12.9
MST2	-0.1	0.2	6.1	4.9	2.7	1.7	1.4	0.5	1.2	8.1	7.7	7.1	3.5	3.6	4.2	2.7	2.0	9.9
NDR2	0.1	0.1	3.0	0.0	0.0	0.2	0.9	-0.4	-0.4	1.6	0.0	0.6	1.3	0.5	-0.1	0.2	0.0	10.3
PAK4	0.2	1.4	0.2	9.8	1.0	-0.2	0.1	0.0	8.0	2.0	8.1	-0.4	0.1	0.0	0.8	0.5	1.0	21.2
PHKG2	0.1	0.8	4.2	4.7	1.5	1.8	1.2	-0.1	1.7	4.2	5.7	1.4	1.8	1.1	0.5	0.6	0.8	21.2
PIM1	0.0	3.0	3.6	4.4	3.7	2.4	0.8	0.2	2.4	4.5	2.7	2.9	1.3	2.5	2.3	3.1	1.2	11.3
RSK1_b	0.4	1.7	-0.5	0.2	0.3	0.0	0.7	-0.8	-0.3	0.8	0.0	0.4	0.1	0.1	0.9	0.4	-0.4	0.0
STLK3	-0.2	-0.4	2.3	4.9	2.5	3.7	3.3	3.1	0.7	2.6	5.0	3.1	7.5	2.5	5.3	-1.3	0.2	7.5
TTK	0.1	0.0	3.7	0.6	1.2	0.5	1.7	-0.3	0.3	2.8	-0.9	0.4	1.8	1.3	1.5	2.6	1.6	7.9
ULK3	0.8	3.0	0.3	6.0	4.0	0.7	3.2	2.8	4.6	9.7	7.0	8.3	6.4	3.7	5.0	3.7	4.5	17.8
VRK1	-0.1	3.8	0.0	5.1	0.3	0.1	0.4	0.3	4.2	0.3	3.7	0.9	1.0	0.1	0.3	0.1	0.3	2.5
Stabilization of AAK1	▼	▼	▼	–	–	▼	▼	▼	▼	▼	▼	▼	▼	▼	–	▲	▼	
Selectivity X/44 Kinases	0	6	7	14	6	0	3	0	6	5	10	7	5	1	8	7	3	

3.4.2 Binding displacement assay

To get deeper insights into the binding affinities of the compounds towards the NAK kinases (AAK1, BIKE, GAK), STK2 and LOK, a binding displacement assay was performed. This assay utilizes Time-Resolved Fluorescence Energy Transfer (TR-FRET) technology in a 16-point dose dependent format. The kinase of interest, tagged with a FRET donor ATP competitively binds a fluorescent energy transfer probe (tracer). By displacing the tracer, the decrease in FRET signal could be detected. Thus, the IC_{50} values and using the Cheng-Prusoff equation, considering the concentration as well as the previously determined K_D values of the tracer, the inhibitory constants (K_i values) were determined[187,188]. The IC_{50} and K_i values of compounds **61** – **63**, **66** – **69**, **85** – **92**, **117** and **118** are listed in **Table 8**. Staurosporine (**1**) was used as a positive control. The lead structure **61** revealed very high affinities towards all NAK kinases with very low IC_{50} values between 4.4 nM and 19 nM and K_i values between 2 nM and 10 nM. The *meta* chlorinated benzylamide derivative **63** showed comparable significant inhibitory effects with IC_{50} values between 4 nM and 12 nM and K_i values between 1.9 nM and 6.3 nM. The *ortho* and *para* substituted compounds **62** and **66** were also in the low two-digit nanomolar range for AAK1, but with a drop of potency on BIKE and GAK by a factor of five. From the series of dual substituted compounds, **68** with *ortho* fluorine and *para* chlorine revealed the highest affinity towards NAK kinases, with a slight preference for AAK1 (IC_{50} = 25 nM, K_i = 12 nM). The IC_{50} values of the benzylureas **85** – **92** and the heteroaromatic amides **117** and **118** ranged from 0.1 µM to 1.1 µM (K_i = 0.04 – 1.5 µM). An exception was the methylpiperazine urea **92** with IC_{50} = 49 nM and K_i = 21 nM on BIKE. No significant activity was found on STK2 and LOK. From the binding replacement assay, a clear preference of AAK1 towards the benzylamide **61** or the *meta* chlorinated derivative **63** with low one-digit nanomolar potencies of 4.4 nM and 4.0 nM could be identified. Also, for the dual substituted **68** with fluorine in ortho and chlorine in para position which showed a potency of 25 nM. (*Experiments were performed by James Bennett and Dr. Fiona Sorrell*)

Table 8: ***In vitro* potency determined in a binding displacement assay.** Different benzylamine and benzylurea derivatives were investigated towards their activity on AAK1, BIKE, GAK, STK2 and LOK.

Compound	AAK1		BIKE		GAK		STK2		LOK	
	IC_{50} [µM]	Ki [µM]	IC_{50} [µM]	Ki [µM]	IC_{50} [µM]	Ki [µM]	IC_{50} [µM]	Ki [µM]	IC_{50} [µM]	Ki [µM]
61	0.0044	0.002	0.015	0.0066	0.019	0.01	0.82	0.45	0.22	0.10
62	0.021	0.0096	0.11	0.047	0.082	0.044	37.54	20.54	n.d.	n.d.
63	0.004	0.0019	0.0100	0.0058	0.012	0.0063	2.94	1.36	0.71	0.33
66	0.03	0.014	0.1600	0.07	0.12	0.067	1.12	0.61	0.43	0.20
67	0.14	0.066	0.59	0.26	0.50	0.27	19.50	10.67	11.83	5.48
68	0.025	0.012	0.06	0.026	0.073	0.04	n.d.	n.d.	1.75	0.81
69	0.11	0.053	0.60	0.26	0.35	0.19	n.d.	n.d.	n.d.	n.d.
85	0.097	0.045	0.066	0.029	0.16	0.085	0.99	n.d.	0.50	0.23
86	0.094	0.043	0.095	0.041	0.087	0.047	0.30	0.16	0.21	0.10
87	0.27	0.13	0.20	0.089	0.20	0.11	1.06	0.58	0.46	0.21
88	0.76	0.35	0.56	0.24	0.35	0.19	4.52	2.47	2.34	1.09
89	1.08	0.50	1.03	0.45	0.37	0.20	1.06	0.58	0.71	n.d.
90	0.18	0.082	0.1400	0.061	0.18	0.094	0.67	0.36	0.31	0.14
91	0.29	0.13	0.26	0.11	0.13	0.068	0.43	0.23	0.24	0.11
92	0.086	0.04	0.0490	0.021	0.26	0.14	1.69	0.93	1.13	0.53
117	0.93	0.43	0.4600	0.20	2.18	1.51	6.15	3.36	2.32	n.d.
118	0.61	0.28	0.3500	0.15	1.24	0.66	11.83	6.47	2.32	n.d.
Staurosporine	0.0028	0.0013	0.0032	0.0014	0.014	0.0075	0.00044	0.00024	0.00024	0.00011

3.4.3 KINOME*scan*® assay

Considering the favorable potencies in the low nanomolar range of compounds **61** and **63**, their selectivity within the kinome-wide *scan*MAX panel should be investigated in the KINOME*scan*® assay. A theoretical description of this method can be found in chapter 3.2.4. The results are shown graphically in **Figure 32**. The *meta* dual substituted **70** was also screened against the 469 kinases of the *scan*MAX panel at a concentration of 100 nM. The lead structure **61** showed good selectivity with S_{35} = 0.03. Due to the introduction of a chlorine in *meta* position of the benzylamide **63**, there was a decline of selectivity to S_{35} = 0.04 compared to **61** (S_{35} = 0.03). In contrast, the dual substitution in *meta* position (**70**) showed a significant increase with S_{35} = 0.02. To verify these results, **61** and **70** were screened again with a concentration of 1 µM. In this run, the less potent compounds **66** and **92** were also examined, since they had also shown good selectivity profiles (≤ 8 kinases with $\Delta T_m > 5$) within the smaller DSF panel. Compound **66**, chlorinated in para position, revealed the weakest selectivity profile with S_{35} = 0.14. **61** and **70** were both below **66** with S_{35} = 0.09. The methylpiperazine urea **92** showed the best selectivity profile with S_{35} = 0.08.

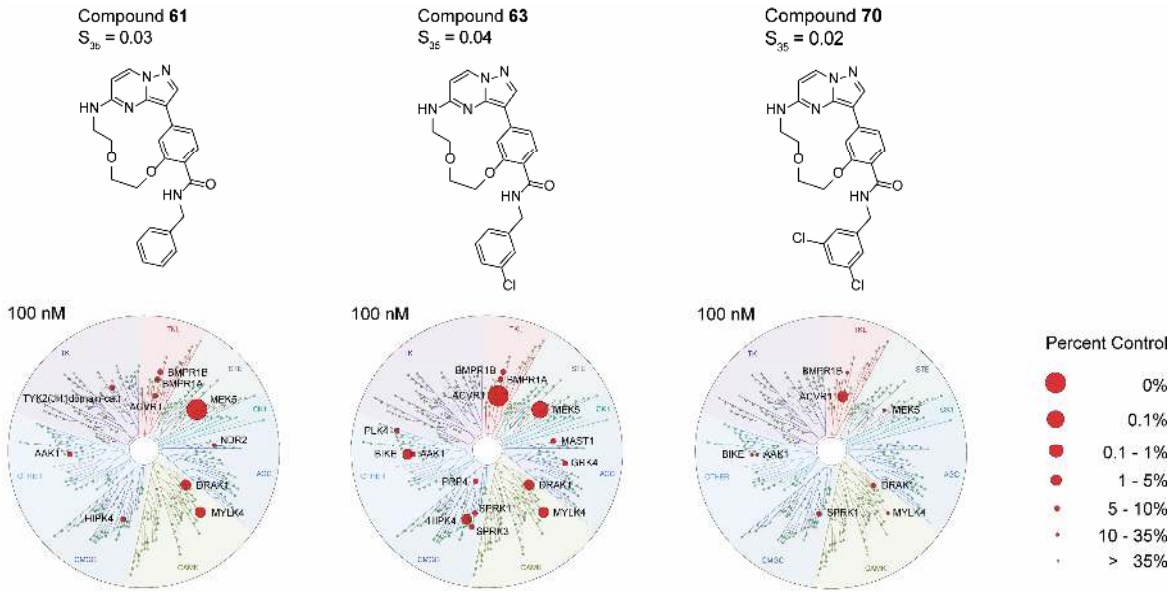

Figure 32: **Selectivity screening of 61, 63 and 70.** Selectivity was determined in the KINOMEscan® assay by Eurofins (formerly DiscoverX) against 469 kinases of the *scan*MAX pannel. Screening was performed at a concentration of 100 nM and targeted kinases are highlited by red circles.

3.4.4 NanoBRET™ target engagement assay

Validation of the promising low nanomolar *in vitro* potencies from the binding replacement assay and the determination of cellular activity were performed in NanoBRET™ experiments. A theoretical description of this method can be found in chapter 3.2.5. Also, to be investigated were the activities of **61** on BIKE and STK10. The data obtained for compounds **61** – **63**, **66** – **69**, **85** – **92**, **117** and **118** are shown graphically in **Figure 33** and the corresponding IC_{50} values in **Table 9**, compared to the *in vitro* potencies determined in the binding replacement assay. Compounds **61** and **63** were also highly potent on AAK1 *in cellulo* with IC_{50} values of 38 nM and 32 nM, respectively. The other single chlorinated compounds **62** and **66** were slightly above **61** with 156 nM and 94 nM. The dual halogenated **68** with *ortho* fluorine and *para* chlorine also showed low three-digit nanomolar potency (IC_{50} = 121 nM). This fact confirmed the trend observed in the binding displacement assay. The benzylurea derivatives **85** – **92** and the heteroaromatic derivatives **117** and **118** did not show strong activitie for AAK1 in cell. However, considering the higher IC_{50} values in the range of 0.3 - 1.1 µM in the binding replacement assay, this was to be expected. In the case of the methylpiperazine urea **92**, there was a significant discrepancy between binding replacement assay (IC_{50} = 86 nM) and NanoBRET™ (IC_{50} = 668 nM). A possible reason might be seen in the poor cell penetration of the large urea motif.

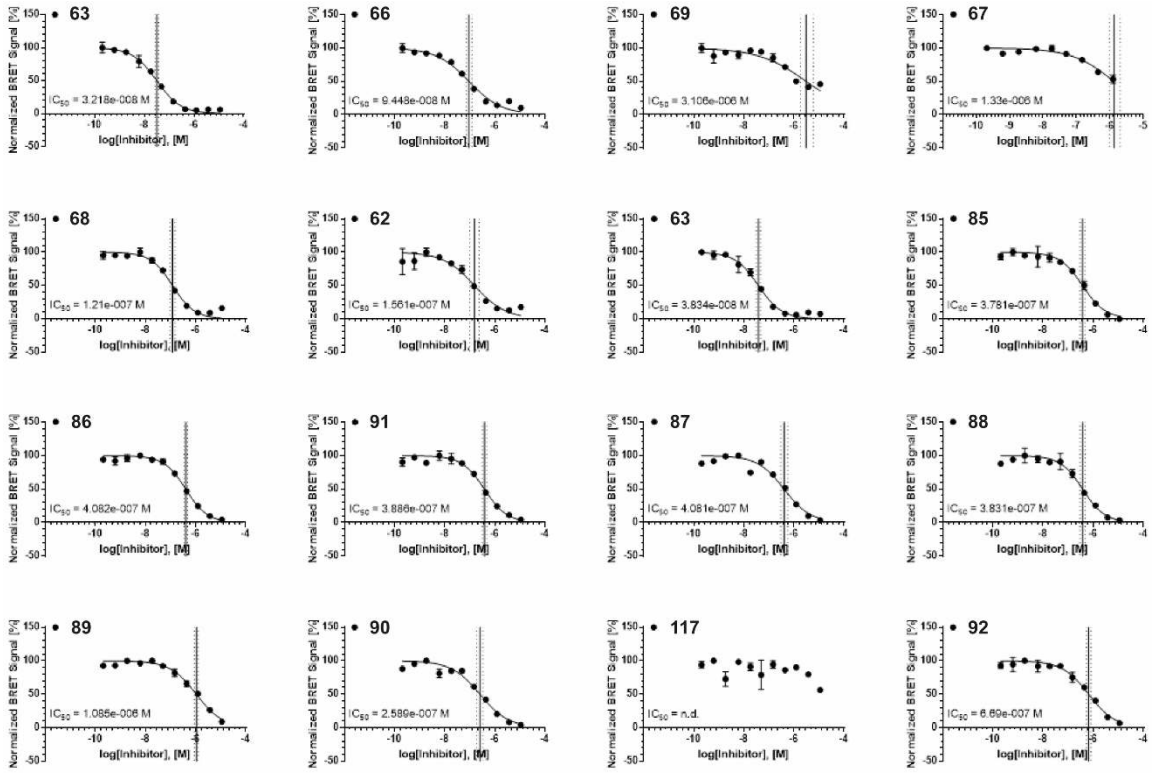

Figure 33: **Cellular potencies of differnet benzylamine and benzylurea derivatives on AAK1.** IC_{50} values of **61** – **63**, **66** – **69**, **85** – **92**, **117** and **118**, determined with NanoBRET™ experiments in HEK293T cells, are written under the corresponding curves.

Table 9: ***In cellulo* versus *in vitro* potencies on AAK1.** Comparison of cellular potencies determined by NanoBRET™ with *in vitro* potencies from the binding displacement assay of differnet benzylamine and benzylurea derivatives on AAK1.

Compound	AAK1 *IC 50* [μM]	
	NanoBRET™	Binding displacement
61	0.0384	0.0044
62	0.156	0.021
63	0.0322	0.004
66	0.0944	0.03
67	1.33	0.14
68	0.121	0.025
69	3.10	0.11
85	0.378	0.097
86	0.408	0.094
87	0.408	0.27
88	0.383	0.76
89	1.09	1.08
90	0.259	0.18
91	0.388	0.29
92	0.668	0.086
117	n.d.	0.93
118	n.d.	0.61

In the binding displacement assay, the lead structure **61** revealed significant affinity towards BIKE (IC_{50} = 15 nM) and LOK (IC_{50} = 220 nM) in addition to AAK1. To validate these possible off-target activities, another NanoBRET™ experiment was performed and the inhibitory activities on BIKE and LOK were determined in cell (**Figure 34**). Here, low cellular activities of **61** on BIKE with 3.1 µM and LOK with 6.7 µM were observed. Compared to AAK1 (IC_{50} = 38 nM), this was a >100-fold drop in potency and consequently a clear selectivity of **61** on AAK1 over BIKE and LOK. (*Experiments were performed by Dr. Benedict-Tilman Berger*)

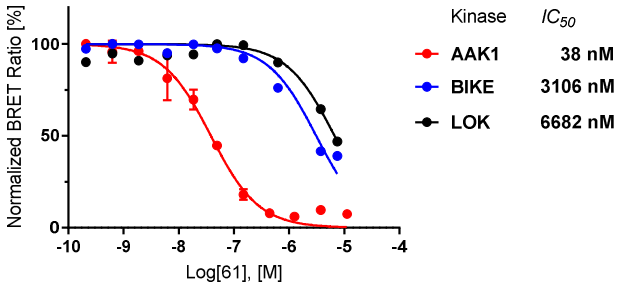

Figure 34: **Cellular potencies of 61 on AAK1 and on potential off-targets (BIKE and LOK).** IC_{50} values, determined with NanoBRET™ experiments in HEK293T cells, can be seen in the figure legend.

3.4.5 Co-crystal structure

The co-crystal structure of AAK1 in complex with **61** revealed that the pyrazolo[1,5-*a*]pyrimidine-based macrocycle binds ATP competitively, as described previously for DRAK1 (chapter 3.3.5). **Figure 35** illustrates the interaction of pyrazolo[1,5-*a*]pyrimidine with the hinge region occurring between the backbone nitrogen of cysteine C129 and the pyrazole of **61**. The DFG motif was clearly located in the in position and was not displaced by binding. This confirmed the assumption that **61** is a canonical type I inhibitor of AAK1. An additional interaction occurred between the catalytical lysine K74 of the β3-strand and the carbonyl oxygen of **61**. Regarding the shape of the macrocyclic scaffold, a roughly flat shape was observed, like the binding modes in CK2 and DRAK1 (chapter 3.2.2 and 3.3.5). Disruption of this planarity and possible effects on binding were investigated by introducing an aromatic ring system into the linker motif.

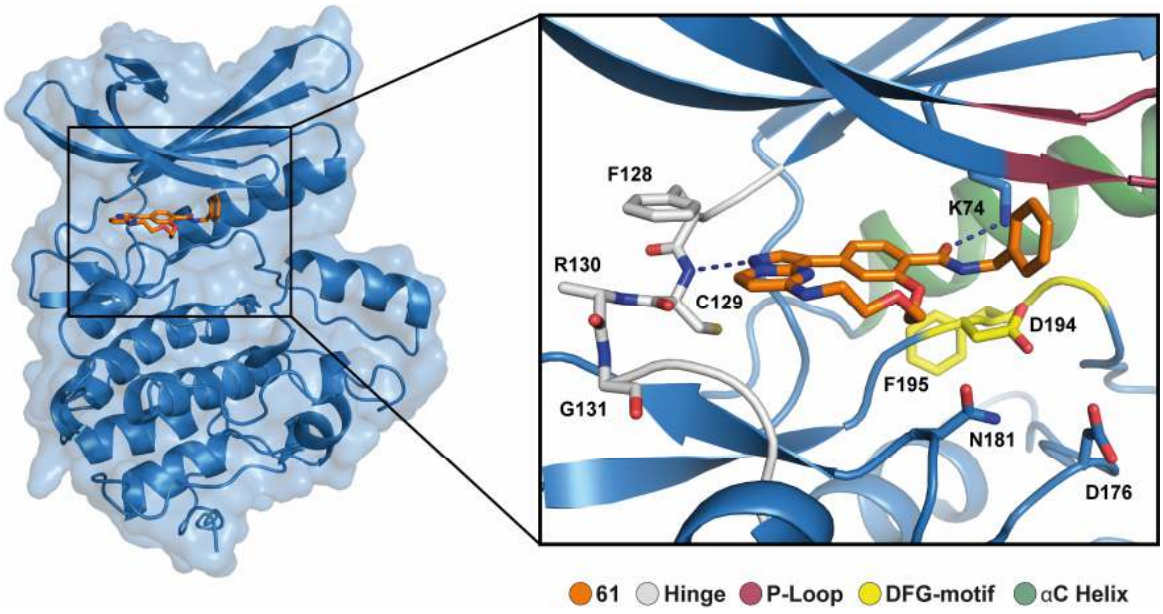

Figure 35: **Binding mode of 61 in complex with AAK1 in stick representaion.** Pyrazolo[1,5-*a*]pyrimidine-based macrocycle **61** (orange) was identifiable as ATP competetive (type I) inhibitor, which was bound to the hinge by formation of hydrogen bond (dashed line) at the backbone nitrogen C129. An aditional hydrogen bond was formed between the side chain amine of the catalytic lysine K74 and the carbonyl oxygen of the amide in both cases. Structural motifes of interest are highlited in a colour code (see legend).

Interestingly, the co-crystal structure of AAK1 in complex with **61** demonstrated a similar characteristic with the one of DRAK1: A voluminous unoccupied back pocket (**Figure 36**). It opens behind the benzylamide motif, which extends into it a bit. This pocket should be addressed with space-occupying residues such as substituted benzylamides, benzylureas, and heterocycles. The co-crystal structure provided another opportunity for derivatization. Adjacent to the hinge region, the solvent exposed region opens up (**Figure 36**). This region should be explored by the introduction of urea and carbamate motifs of variable size, linked to the secondary amine between hinge binder and linker motif (position 10). (*Experiments were performed by Dr. Sebastian Mathea*)

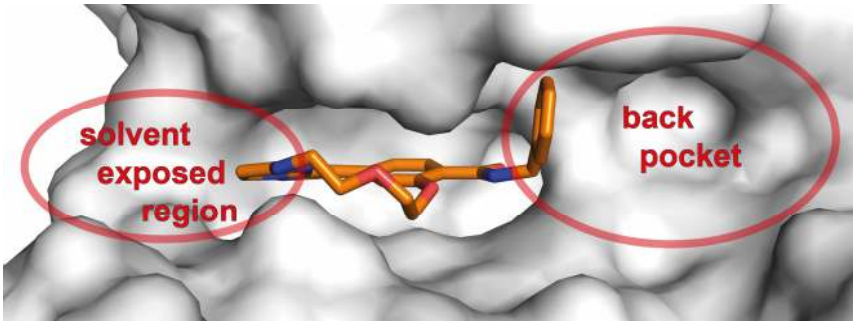

Figure 36: **View inside the catalytic pocket of AAK1 in complex with 61.** Highlighted spacious back pocket, with the benzylamide residue as well as solvent exposed region. The spacious back pocket, with the benzylamide residue pointing into it, and the solvent exposed region are highlighted.

3.4.6 Immunoprecipitation of AP2 complex

With **61** and **63** found to be low nanomolar inhibitors of AAK1 *in cellulo*, the next step was to investigate the compounds in a cell biological context. Conner and Schmid demonstrated that AAK1 plays an important role in receptor-mediated endocytosis. AAK1 binds to clathrin and regulates the µ2 subunit of adaptor protein 2 (AP2).[130] The inhibition of the AP2 complex by **61** was investigated in an immunoprecipitation experiment. This is a method for separating proteins from cell lysate using a specific antibody. This antibody immobilized on agarose beads (sedimentable matrix) via protein A/G binds the corresponding antigen. The method is also appropriate for the isolation of protein complexes (co-immunoprecipitation). Samples were separated by SDS-PAGE or western blot analysis.[189,190] For immunoprecipitation of the AP2 complex inhibited with **61**, retinal pigment epithelium (RPE) cells were incubated for 2 hours and the in total immunoprecipitated AP2 complex was analyzed by western blots. Antibodies anti-AP2α for control cells and anti-AP2µ-pT156 (monoclonal) for inhibitor-treated cells were utilized. The highly potent NAK inhibitor LP-935509 (**22**) (AAK1 IC_{50} = 3.3 nM)[143] was used as a positive control. **Figure 37** shows two independent biological replicates at a concentration of 2 µM for **61** and **63** and 10 µM for the positive control. Treatment with LP-935509 (**22**) at 10 µM showed 63% inhibition of the AP2 complex. In cells incubated with **61**, at lower concentrations of 2 µM, an almost identical inhibition of 60% was detected. The inhibition rate of **63** at 2 µM was slightly lower than that of **61** at 42%. (*Experiments were performed by Zuzana Kadlecova university of Cambidge*)

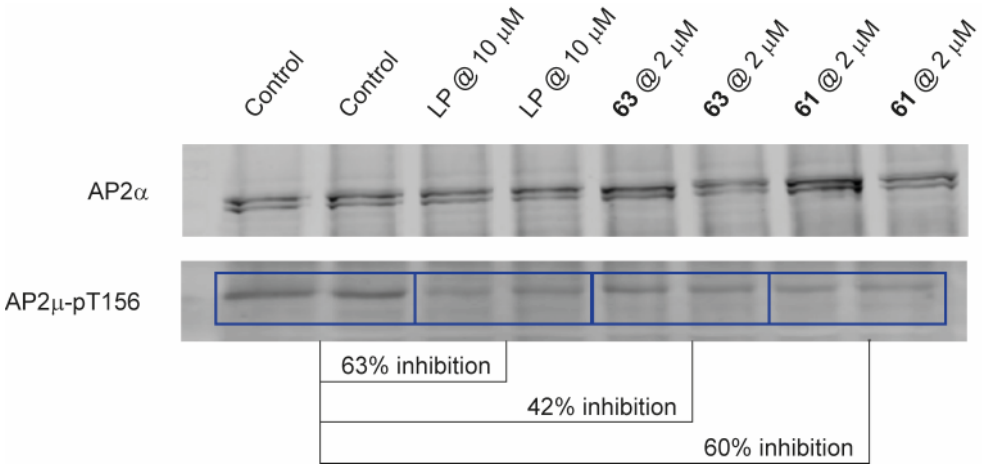

Figure 37: **Immunoprecipitation of the AP2 complex with inhibition of AAK1 by 63 and 61.** RPE cells were incubated for 2 h (inhibitor concentration of 2 µM), the AP2 complex was immmunorecipitated in total and analyzed by western blots. The highly potent AAK1 inhibitor LP-935509 (**22**) was used as a reference at 10 µM.

3.4.7 Anti SARS-CoV-2 effect of AAK1 inhibition

In the immunoprecipitation assay, **61** proved to be a promising way to inhibit the AP2 complex (60% inhibition at 2 µM). Neveu *et al*. demonstrated that regulation of the AP2 complex by inhibiting AAK1 and GAK blocked HCV assembly and viral entry.[139,140] Other antiviral effects by inhibiting AAK1 are known for multiple unrelated RNA viruses such as EBOV and DENV.[141,142] In affinity-purification mass spectrometry (AP-MS) experiments, Gordon *et al.* identified 332 high-confidence protein-protein interactions between the severe acute respiratory syndrome coronavirus type 2 (SARS-CoV-2) and human proteins.[191] Among these was the interaction of the SARS-CoV-2 protein NSP10 with AP2. Relying on these findings, it was obvious to investigate the highly potent compounds **61** and **63** regarding their antiviral activities. For this purpose, a colorimetric MTT assay, using 3-(4,5-dimethylthiazol-2-yl)-2,5-diphenyltetrazolium bromide as a dye, was performed with SARS-CoV-2 infected Caco2 cells. Also examined were the AAK1 inhibitors sunitinib (**2**)[140], LP-935509 (**22**)[143] and SGC-AAK1-1 (**23**)[153], the EGFR and GAK inhibitor erlotinib (**21**)[140] and the GAK selective SGC-GAK-1[192]. The antiviral drug remdesivir[193] was used as positive control and **117** and DMSO, respectively, as negative control. Incubation of cells with the inhibitors (0.01 – 10 µM) was done together with infection in triplicates. The measurement was carried out 48 h after infection. The results are shown graphically in **Figure 38**. Interestingly, none of the inhibitors, except for remdesivir, showed a significant positive effect on cell viability.

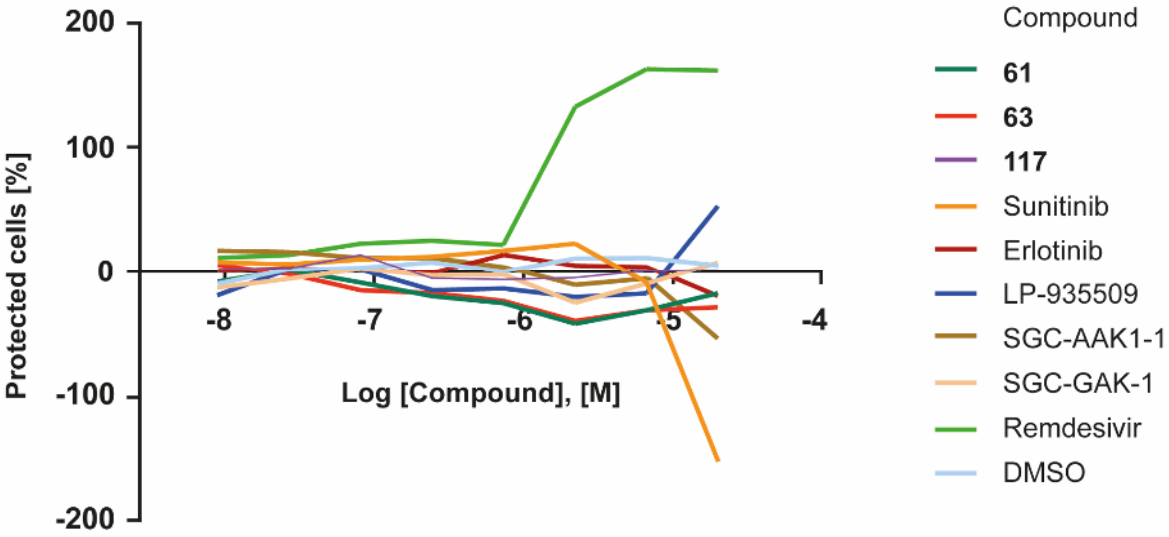

Figure 38: **Investigation of the anti SARS-CoV-2 effect of 61 and 63.** An MTT assay was performed with Caco2 cells under simultaneous incubation (0.01 - 10 µM) and infection. The analysis was performed after 24 h. The AAK1 and GAK inhibitors sunitinib (**2**), LP-935509142 (**22**), SGC-AAK1-1 (**23**), erlotinib (**21**) and SGC-GAK-1 were also examined. Remdesivir was used as reference and **117** as well as DMSO as negative controls.

To quantify the cell entry, real-time PCR (qPCR) experiments were performed with SARS-CoV-2 infected Caco2 cells. Incubation with **61** and the other AAK1 and GAK inhibitors, already used in the previous experiments, at concentrations of 0.04 – 10 µM was done simultaneously with infection and RNA was harvested after 3 hours. The associated numbers of cycles required for the fluorescence signal to exceed the threshold (Ct values; cycle threshold) are listed in **Table 10**. Compared with the DMSO blank, the Ct values were almost identical. Since the Ct value is inversely proportional to the amount of target nucleic acid, the low values indicate high viral load in the samples. This suggested that none of the inhibitors had a significant effect on viral entry or SARS-CoV-2 assembly in Caco2 cells. It was suggested that SARS-CoV-2 virus entry did not involve the AP-2 pathway.

Table 10: **Cell entry of SARS-CoV-2 viruses into Caco2 cells.** Ct values were determined by qPCR to investigate the viral cell entry. Cells were treated with **61**, LP-935509 (**22**), SGC-GAK-1, SGC-AAK1 (**23**), erlotinib (**21**), and sunitinib (**2**). **117** and DMSO were used as negative controls.

	Ct values					
Inhibitor [µM]	0.04	0.12	0.37	1.11	3.33	10.00
61	27.81	27.10	27.22	27.07	27.08	27.34
117	27.18	27.29	27.50	27.12	27.66	27.06
LP-935509	26.80	27.13	27.07	27.89	26.83	27.02
SGC-GAK-1	26.57	26.65	26.55	26.31	26.16	26.32
SGC-AAK1-1	26.92	26.86	26.72	26.82	26.83	27.17
Erlotinib	27.04	26.73	26.92	26.74	26.47	26.54
Sunitinib	26.30	26.18	26.25	26.19	26.23	27.56
DMSO	27.59	27.61	27.23	27.12	27.09	27.39

Another protein-protein interaction identified in the AP-MS experiments of Gordon *et al.* was that between SARS-CoV-2 protein N and CK2α′[191]. Therefore, the CK2 inhibitors **47**, **60**, silmitasertib (**12**)[194] and SGC-CK2-1 (**14**)[81] were examined in a crystal violet assay using Caco2 cells (**Figure 39**). Nafamostat[195] was used as positive control. Again, there was no positive effect on cell viability by the CK2 inhibitors.

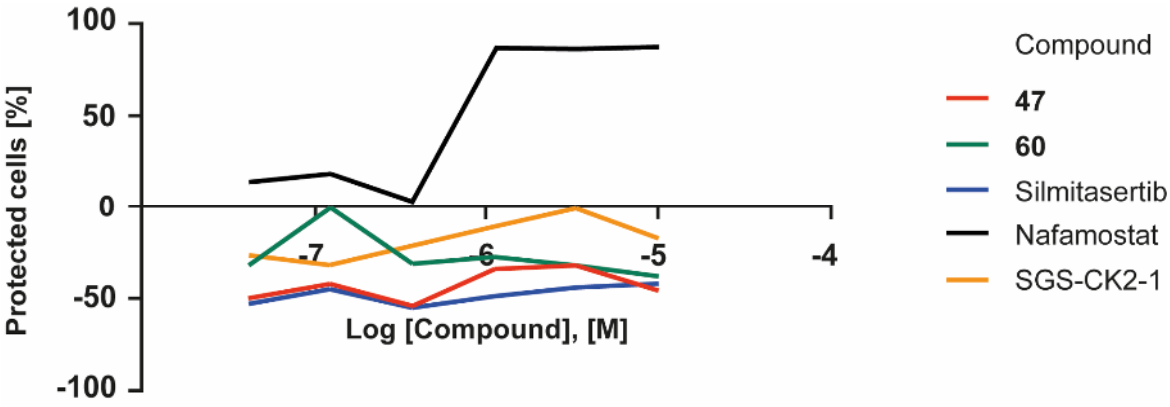

Figure 39: **Investigation of the anti SARS-CoV-2 effect of CK2 inhibitors 47 and 60.** An MTT assay was performed with Caco2 cells under simultaneous incubation (0.01 - 10 µM) and infection. The analysis was performed after 24 h. The CK2 inhibitors silmitasertib (**12**) and SGC-CK2-1 (**14**) were also examined. Nafamostat was used as a reference.

To validate the results from the experiments in Caco2 cells and to exclude cell-specific effects, another crystal violet experiment was performed with Vero cells. Infection, however, was done with SARS-CoV-1 virus. AAK1 and GAK inhibitors **61**, sunitinib (**2**), erlotinib (**21**), LP-935509 (**22**), SGC-AAK1-1 (**23**) and SGC-GAK-1 as well as CK2 inhibitors **47**, **60**, silmitasertib (**12**) and SGC-CK2-1 (**14**) including nafamostat were examined for their antiviral effect. The data obtained are shown graphically in **Figure 40**. The results were comparable to those of the previous experiments and no significant antiviral effect of the inhibitors used were visible in Vero cells.

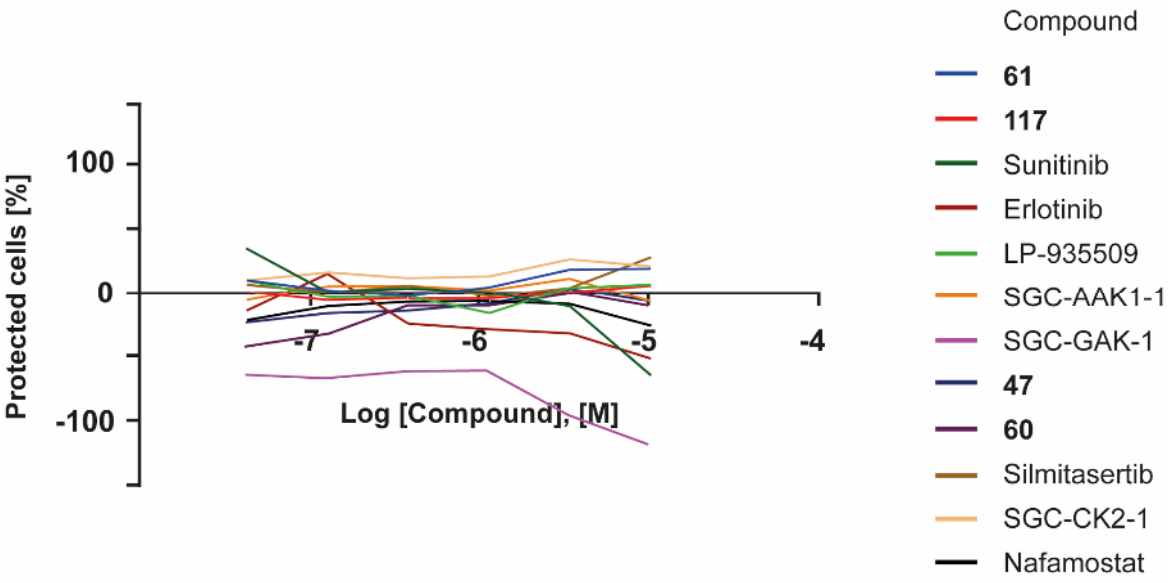

Figure 40: **Investigation of the anti SARS-CoV-1 effect of AAK1 (61) and CK2 (47 and 60) inhibitors.** Crystal violet experiments were performed with Vero cells under simultaneous incubation (0.01 - 10 µM) and infection. The AAK1 and GAK inhibitors sunitinib (**2**), LP-935509142 (**22**), SGC-AAK1-1 (**23**), erlotinib (**21**) and SGC-GAK-1 as well as the CK2 inhibitors silmitasertib (**12**) and SGC-CK2 (**14**) were also examined. Nafamostad was used as reference and **117** as an AAK1 negative control.

Hoffmann *et al.*[196] demonstrated that SARS-CoV-2 utilizes the SARS-CoV receptor angiotensin-converting enzyme 2 (ACE2) for cell entry and the responsibility of serine protease transmembrane protease serine subtype 2 (TMPRSS2) for spike protein priming. Since the compounds we tested had no proven inhibitory activity on ACE2 or TMPRSS2, this might be a feasible explanation for the lack of antiviral activity in the experiments. (*Experiments were performed by Dr. Tuna Toptan Grabmair university hospital Frankfurt*)

4. Summary and conclusion

In 2001, imatinib (**3**), the first small-molecule kinase inhibitor, was approved for clinical applications. Since that time, the number of kinase inhibitors in clinical trials has increased rapidly. Being involved in crucial functions in cellular signaling pathways, kinases are one of the most important drug target families in various human diseases. The most prominent application of kinase inhibitors is oncology. However, there are other diseases such as autoimmune and inflammatory diseases where kinase inhibitors are used as therapeutic agents. Prevention of post-translational modifications by phosphorylation and thus regulation of downstream signaling events is the target of kinase inhibitors. The catalytic activity of kinases is dependent on ATP, which is localized in a highly conserved binding pocket. This active site is located between two catalytically active lobes and is known as hinge region. Due to this high conservation, the development of highly selective ATP-mimetic inhibitors is quite challenging. The typical shape of ATP mimetics is flat and the hydrophobic molecules usually have a large number of rotatable single bonds. To circumvent the problem of partial lack of selectivity arising from this flexibility, a bioactive conformation of the inhibitor can be locked by macrocyclization. Typically, an ATP-mimetic pharmacophore is preorganized by a linker in a macrocycle of 12 or more atoms. As a consequence of the conformational restriction, the entropic cost of binding might be reduced, resulting in increased affinity towards the kinase. Nevertheless, macrocycles have enough flexibility to interact with dynamic binding sites and are not completely rigid. However, the potential of macrocyclization is beyond modulating selectivity and potency of inhibitors. Variation in physicochemical and pharmacokinetic properties, such as solubility, lipophilicity, metabolic stability, and bioactivity, for example, represents another benefit.

4.1 CK2 inhibition by macrocyclic pyrazolo[1,5-*a*]pyrimidines

A prominent example of serine/threonine kinases is the pleiotropic and constitutively active casein kinase 2 (CK2). The number of more than 430 identified phosphorylation sites of CK2 illustrates its important role in the regulation of various cellular processes such as cell cycle progression, apoptosis or transcription.[76–79] Dysregulation of CK2 is frequently associated with the pathology of diseases such as cancer, making CK2 a promising target of clinical investigation.[92,93] The most advanced CK2 inhibitor with application in clinical trials is silmitasertib (**12**), however, it also targets various other kinases.[106] Thus, the search for a selective inhibitor of CK2 is closely linked to the study of the role of CK2 in cancer and other diseases as well as its normal physiology.

Within the CK2 project it was possible to develop the highly selective and potent inhibitors **47** and **60** for CK2 by specific modifications on **37**. Previously, pyrazolo[1,5-*a*]pyrimidines were known more as inhibitors for PIM1, RET, JAK1, ALK2/3 or RIPK2.[197–202] However, in this work it has been demonstrated that small structural changes, such as macrocyclization, can have significant effects on selectivity and potency. Compounds **47** and **60** showed comparable *in vitro* potency with silmitasertib (**12**), which is used as an agent for clinical trials. In the cellular system, their inhibitory activity is slightly lower, although still in the low micromolar range. In the DSF assay, the compounds also showed very high T_m-shifts and first indications of their high selectivity. These selectivity data were validated by the kinome-wide KINOME*scan*® assay with excellent selectivity scores of S_{35} = 0.02 (**47**) and S_{35} = 0.07 (**60**) at a screening concentration of 1 µM. In Comparison with known CK2 inhibitors such as silmitasertib (**12**), TBB[203], or emodin[204], **47** and **60** exceeded their selectivity. **Table 11** presents an overview of the consistent data acquired from these different assay systems.

Table 11: **Summary of binding affinities towards CK2.** Binding affinities of the promising compounds **47** and **60** against the CK2 isoforms from various assay platforms (DSF, ITC, and NanoBRET™) as well as the selectivity score determined in the KINOMEscan® assay. Compared to the macrocyclic scaffold **37**, all compounds showed an improved affinity towards CK2 in the DSF assay. The potencies in vitro are in a fantastic range of low two-digit and high two-digit nanomolar. The cellular affinities, revealed by NanoBRET™, are in a comparable range and have been improved as well.

Compound	DSF T_m-shift		ITC K_D	NanoBRET™ IC_{50}		KINOMEscan® S_{35}
	CK2a1	CK2a2	CK2a1	CK2α	CK2α´	1 µM
37	10.6	11.3	-	5.73 µM	16.20 µM	0.26
47	11.8	15.7	12 nM	1.51 µM	7.64 µM	0.02
60	11.7	15.1	82 nM	1.54 µM	7.39 µM	0.07

CK2 is considered a worthwhile target in the treatment of cancer. This is due to its involvement in cell growth, cell death and cell survival. In various cancers such as basal cell carcinoma (NCT03897036), breast cancer (NCT00891280), cholangiocarcinoma (NCT02128282), medulloblastoma (NCT03904862), multiple myeloma (NCT01199718) or kidney cancer (NCT03571438), the CK2 inhibitor silmitasertib (**12**) has been used in clinical trials. However, it can be hypothesized that the antiproliferative effect of silmitasertib (**12**) is due to addressing off-targets, as there is no exclusive CK2 selectivity.[108] Examples of such off-targets are CDK1[205,206], PIM1[207], HIPK3[208,209], TBK1[210], or FLT3[211,212]. There are known selective CK2 inhibitors such as GO289[213], CAM4066[180] or SGC-CK2-1 (**14**)[81]. Nevertheless, the potency of CAM4066 is weak, GO289 has not been extensively characterized with respect to its selectivity and SGC-CK2-1 (**14**) was published just recently. This reveals the importance of compound **47** for future functional studies. Another interesting aspect for further work is the optimization of cell penetration. A possible starting point might be the modification of the carboxylic acid.

4.2 DRAK1 inhibition by macrocyclic pyrazolo[1,5-*a*]pyrimidines

Serine/threonine kinase 17A (STK17A) or death-associated protein kinase-related apoptosis-inducing protein kinase 1 (DRAK1) belongs to the family of DAPKs. Among others, DRAK1 is part of the so-called dark kinome and its cellular function and involvement in pathophysiological processes is quite understudied. However, DRAK1 has been reported to be overexpressed in various forms of brain tumors in the central nervous system (glioma).[112,119] Further research is limited by an inherent lack of selective DRAK1 inhibitors.

During the DRAK1 project, minor modifications of the macrocyclic scaffold **37**, which was also used as a precursor for the CK2 inhibitors **47** and **60**, shifted the selectivity towards DRAK1. In the initial steps, the kinome-wide selectivity profile was significantly improved by introducing space-filling groups at the carboxylic acid, towards the back pocket. Further structural optimization of these derivatives resulted in the highly potent DRAK1 inhibitors **107** and **115** with IC_{50} values of 31 nM and 15 nM, respectively. However, these still did not show the desired selectivity in the KINOME*scan*® (S_{35} = 0.05 and 0.18 at 1 µM). Switching from benzylamide-based derivatives to small amides represented a breakthrough.

Compound **121**, containing a *tert*-butylamide residue, impressed with an *in vitro* potency of 49 nM and a very high selectivity in the KINOME*scan*® with S_{35} = 0.005 (100 nM) and S_{35} = 0.02 (1 µM). Within the DAPK family, DRAK1 was exclusively addressed. Validation of potential off-targets *in cellulo* revealed a 30-fold lower affinity than to DRAK1 with IC_{50} = 181 nM. **Table 12** summarizes these data. Studies of the co-crystal structure of DRAK1 in complex with **121** confirmed the hypothesis of a type I inhibitor binding to the hinge region via the pyrazolo[1,5-*a*]pyrimidine. In this case, the *tert*-butylamide pointed toward the back pocket.

Table 12: **Summary of binding affinities towards DRAK1.** Binding affinities of the promising compounds **61**, **107**, **115**, **117** – **118** and **121** against DRAK1 from various assay platforms (DSF, ITC, ^{33}PanQinase™ and NanoBRET™) as well as the selectivity score determined in the KINOMEscan® assay. The affinities against the potential off-targets CK2α and CK2α´ were also determined, but no significant off-target effects were observed. Compared to the macrocyclic scaffold **37**, all compounds showed an improved affinity towards DRAK1 in the DSF assay. The potencies in vitro are in a fantastic range of low one-digit and low two-digit nanomolar. The cellular affinities, revealed by NanoBRETTM, are in a comparable range of high two-digit and low three-digit nanomolar. Compared to **37**, the selectivity profile was also dramatically improved and the highly selective DRAK1 inhibitor **121** was identified.

Compound	DSF T_m-shift			ITC K_D	^{33}PanQinase™ IC_{50}			NanoBRET™ IC_{50}			KINOMEscan® S_{35}
	DRAK1	CK2α	CK2α	STK17A	DRAK1	CK2α	CK2α´	DRAK1	CK2α	CK2α´	100 nM / 1 µM
37	7.9	10.6	11.3	-	-	-	-	-	-	-	- / 0.26
61	9.3	1.7	4.9	-	155 nM	-	-	171 nM	-	-	0.03 / 0.09
107	12.1	-0.9	1.9	-	31 nM	-	-	71 nM	-	-	0.02 / 0.05
115	12.3	1.2	0.1	9 nM	15 nM	-	-	70 nM	-	-	- / 0.18
117	2.1	0.2	0.9	-	-	-	-	>45 µM	-	-	-
118	3.0	1.1	2.5	-	-	-	-	>45 µM	-	-	-
121	11.3	0.8	2.3	21 nM	49 nM	950 nM	380 nM	181 nM	34 µM	39 µM	0.005 / 0.02

Follow-up determination of cytotoxicity in three different cell lines did not show any effects at a concentration of 1 µM and only minor effects above 10 µM. Previous experiments by Mao *et al*. demonstrated that knockout of DRAK1 in glioblastoma cell lines resulted in dramatic alteration in cell shape[120]. This effect was associated with decreased proliferation, clonogenicity, migration, invasion and anchorage independent colony formation. The studies regarding the association of DRAK1 inhibition and glioma cell survival revealed unexpected results. The low micromolar EC_{50} values determined in various GBM cells did not correlate with the promising low nanomolar IC_{50} values observed in the NanoBRET™ experiments. However, in D-247MG cells with the highest DRAK1 expression level, the EC_{50} value of **121** was 2.75 µM.

By observing the cell morphology, a minor change in low expressing T98G cells could be detected only at concentrations of 12.5 µM. The other cell lines did not show any significant phenotype. The stronger effect of the more potent inhibitor **115** (EC_{50} < 3 µM) might be related to off-target effects, due to its lower selectivity in the KINOME*scan*® (S_{35} = 0.18 at 1 µM). Given these surprising insights, it is evident that further systematic investigation of the essentiality of DRAK1 in glioblastoma cell lines is necessary to clarify the role of DRAK1 in glioma and to define the potential for prospective therapeutic application of selective DRAK1 inhibition.

4.3 AAK1 inhibition by macrocyclic pyrazolo[1,5-*a*]pyrimidines

The serine/threonine kinase AP-2-associated protein kinase 1 (AAK1) from the NAK family, which consists of AAK1, BIKE and GAK, has been identified as a potential therapeutic target for many diseases such as neuropathic pain, schizophrenia and parkinson´s disease[143–145]. By regulating the clathrine-mediated endocytosis, AAK1 is involved in the intracellular trafficking of multiple unrelated RNA and DNA viruses as well, such as HCV, DENV or EBOV[129,139,141,142]. As many of these viral infections still lack an adequate therapy, AAK1 seems to be a worthwhile target. The approved but quite unselective anticancer kinase drugs sunitinib (**2**) and erlotinib (**21**), which inhibits AAK1 and GAK, have demonstrated antiviral activity[141,142]. Also reported was a possible association with the SARS-CoV-2 virus, which strongly increased the interest in new selective AAK1 inhibitors[146–149].

The development of the selective and highly potent AAK1 inhibitors **61** and **62** was based on the macrocyclic scaffold **37**, which already has been utilized in the DRAK1 project. By introducing different benzylamidic residues, the kinome-wide selectivity was modulated and focused on AAK1. Thus, a shift from S_{35} = 0.26 (**37** at 1 µM) to S_{35} = 0.09 (**61** and **70** at 1 µM) was achieved in the KINOME*scan*® assay. **63** revealed slightly lower selectivity at 100 nM (S_{35} = 0.04) compared to **61** (S_{35} = 0.03). Further investigation regarding the affinity of the compounds towards the NAK kinases in a binding displacement assay revealed **61** and **63** as highly potent inhibitors of AAK1 with IC_{50} values of 4 nM. Off-target validation was performed in NanoBRET™ experiments. Here, both **61** and **63** showed high potencies against AAK1 *in cellulo* with IC_{50} values 38 nM and 32 nM, respectively.

The affinity of **61** towards BIKE was very low with 3 µM, but towards GAK it could not be excluded. However, as expected, **61** showed significant affinity for DRAK1 (IC_{50} = 171 nM). A summary of these data from various assay platforms can be seen in **Table 13**.

Table 13: **Summary of binding affinities towards AAK1.** Binding affinities of the promising compounds **61**, **63** and **70** against AAK1 from various assay platforms (DSF, binding displacement assay, and NanoBRET™) as well as the selectivity score determined in the KINOMEscan® assay. Despite the avoidable decrease in the DSF assay compared to the macrocyclic scaffold **37**, **61** and **63** showed marvelous activities towards AAK1 in vitro as well as in cellulo in a low one-digit to low two-digit nanomolar range. Compared to the macrocyclic scaffold **37**, all compounds showed an improved selectivity profile illustrated by the S-score determined in the KINOMEscan® assay.

Compound	DSF T_m-shift			Binding-displacement IC_{50}			NanoBRET™ IC_{50}				KINOMEscan® S_{35}
	AAK1	BIKE	DRAK1	AAK1	BIKE	GAK	AAK1	BIKE	LOK	STK17A	100 nM / 1 µM
37	9.3	-	-	-	-	-	-	-	-	-	- / 0.26
61	7.5	11.0	9.3	4 nM	15 nM	19 nM	38 nM	3 µM	7 µM	171 nM	0.03 / 0.09
63	8.1	12.4	7.8	4 nM	10 nM	12 nM	32 nM	-	-	-	0.04 / -
70	8.4	10.7	9.8	-	-	-	-	-	-	-	0.02 / 0.09

Analysis of the co-crystal structure of AAK1 confirmed **61** as a type I inhibitor with hinge interaction via the pyrazolo[1,5-*a*]pyrimidine motif. Based on these findings, further efforts were made to increase selectivity. Structural optimizations were directed toward the back pocket with bulky residues and toward the solvent exposed region with small ureas. The effect of the variation of the linker motif towards the selectivity profile was also investigated. Thus, the dual chloro-substituted benzylamide derivative **70** attracted attention with a high selectivity for AAK1 as evident in the S-scores of 0.02 (100 nM) 0.09 (1 µM). Experiments by Conner and Schmid demonstrated a critical involvement of AAK1 in receptor-mediated endocytosis, where the AP2 complex was regulated by AAK1 binding to clathrin.[130] In immunoprecipitation experiments, regarding the AP2 complex, **61** exceeded the highly potent NAK inhibitor LP-935509 (**22**), which was used as positive control. **63** showed almost identical very good results. Based on these findings and the potential interaction of the AP2 complex and the SARS-CoV-2 protein NSP10 identified by Gordon *et al.*[191], the antiviral effect of the highly potent and selective compounds **61** and **63** by AAK1 inhibition was investigated. Surprisingly, no positive effect on cell entry or infection progression was observed *in cellulo*. However, this could be explained by the later findings of Hoffmann *et al*. regarding the dependence of cell entry and spike protein priming of SARS-CoV-2 virus on ACE2 and TMPRSS2.[196]

4.4 Overall conclusion and perspectives

The keystone of this thesis was the macrocyclic pyrazolo[1,5-*a*]pyrimidine-based kinase inhibitor ODS2004070 (**14**). It was part of the development of an FLT3 inhibitor and was patented by Oncodesign.[154] In a kinome-wide screening of macrocyclic kinase inhibitors in the ^{33}PanQinase™ assay against 366 kinases, **37** was screened among others. Here, high affinities towards a large number of differnet kinases were detected. However, approximately 130 kinases were inhibited with >60%, making **37** a compound with an unacceptable selectivity profile. Given these properties, the unselective macrocyclic scaffold **37** was predestined as lead structure for the design of potent and selective kinase inhibitors.

In the course of this thesis, the pyrazolo[1,5-*a*]pyrimidine-based hinge binding motif, known from the literature and already used in PIM1, RET, JAK1, ALK2/3, and RIPK2 inhibitors, remained invariant.[197–201,214] Apart from a small series of derivatives to study the effect of varying the linker, the macrocyclic scaffold **37** was conserved.

Structural optimizations, to focus selectivity on the kinase of interest, were performed on the secondary amine between hinge binder and linker as well as via the carboxylic acid of the benzyl group. This is shown in a graphical summary in **Figure 41** below.

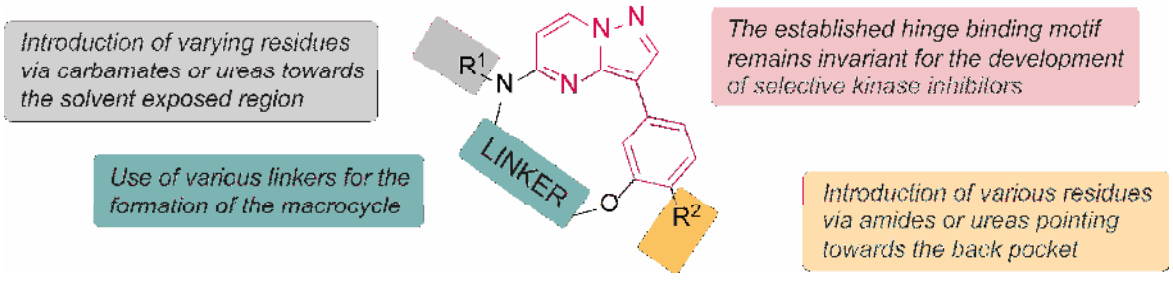

Figure 41: **Graphical summary of structural modifications, employed 37 as starting point, within structure-activity relationship studies as a part of this thesis.**

Initial specific modifications resulted in the synthesis of the highly potent and highly selective CK2 inhibitors **47** and **60** (**Figure 42**). An interesting aspect for further work is the optimization of cell penetration. A possible starting point for this is the modification of the carboxylic acid.

Rescreening of compounds from the CK2 series in the DSF assay revealed potential targets for further projects. These included the NAK family kinases AAK1, BIKE, and GAK, as well as DRAK1 from the DAPK family. Further structural variations on the carboxylic acid function of **37**, while preserving the macrocyclic core structure, led to the highly selective and highly potent DRAK1 inhibitor **121** ()**Figure 42**. Having an *in vitro* potency below 100 nM, exclusive selectivity within the DAPK family, 30 fold lower affinity towards off-targets, cellular activity < 1 µM as well as an available negative control compound (**117** or **118**), **121** fulfills the requirements to become a Structural Genomics Consortium (SGC) chemical probe.[46] This can be employed in further studies in glioblastoma cell lines on the role of DRAK1 in glioma and help to elucidate the biological role of DRAK1. Also of interest would be studies of the interaction between DRAK1 and the tumor suppressor p53, as described by Mao *et al.*[117], and the effects on cell survival, apoptosis, and ROS accumulation in testicular cancer cells. Further applications of the DRAK1 chemical probe would be investigations regarding the role of DRAK1 in HNSCC (Park *et al.*[118]) as well as the translocalization of DRAK1 and the resulting interaction with the anti-apoptotic oncoprotein ANT2 or p53 in U2OS cells (Oue *et al.*[116]).

Since NAK kinases also represented a worthwhile target in a rescreen of the CK2 compounds, the NAK kinases were focused on in further structure-activity relationship studies. This yielded the highly potent and quite selective AAK1 inhibitors **61** and **63** (**Figure 42**). They possess a good selectivity profile but did not show exclusive inhibition of AAK1. Here, in addition to further refinement of the selectivity profile, lies potential for worthwhile future research. Both compounds revealed excellent inhibitory activity against the AP2 complex, which is regulated by AAK1. This regulation by AAK1 and GAK as well was identified by Neveu *et al*. as a key role in both viral assembly and entry of HCV.[139,140] Consequently, a mandatory target for future studies would be to evaluate the antiviral activity of **61** and **63** in HCV. Bekerman and Verdonck demonstrated the potential use of AAK1 inhibitors against multiple RNA viruses such as EBOV and DENV.[141,142] The screening panel for antiviral activ macrocyclic AAK1 inhibitors should therefore be expanded to include other unrelated RNA viruses in addition to HCV. Because of its role in the regulation of the AP2 complex and thus its critical role in endocytosis and viral assembly, GAK is also a potential target for antiviral inhibitors. Both, **61** and **63** exhibited strong affinity for GAK in various *in vitro* assays. Herein resides the possibility of developing a dual inhibitor for AAK1 and GAK. Further validation of this affinity towards GAK would be the first step on this path.

As a result of the structural optimizations, other possible targets for selective inhibition by compounds based on the macrocyclic scaffold **37** have been identified. For example, some of the of the benzylurea derivatives, such as **85** or **92** demonstrated an interesting combination of high affinity and selectivity toward BIKE and GAK. Additionally, the rather high affinity of **91** on LOK would be of interest as a starting point for further research.

Based on the promising selectivity profile of **70**, determined in the DSF panel as well as in the KINOME*scan*® assay (S_{35} = 0.02 at 100 nM and 0.09 at 1 µM), further characterization and structural optimization is a desirable goal for future work. The series of derivatives addressing the solvent exposed region also showed activity, albeit attenuated, on BIKE and DRAK1. Here, a fusion with highlight compounds from previous series would be possible to create, for example, a selective pyrazolo[1,5-*a*]pyrimidine-based BIKE inhibitor or to increase potency of DRAK1 inhibitor **121** even further.

Variation of the linker motif on a small scale showed that this also represents a possibility for modulating the selectivity profile. In the case of **61**, for example, AAK1 completely tolerated the switch to the aliphatic linker in **138**, whereas DRAK1 showed a significant drop of activity (**Table 7**).

In contrast, the introduction of the aromatic linker system in **141** was not well tolerated by either AAK1 or DRAK1. Interestingly, affinities towards other kinases were observed that had not been stabilized by either **61** (PEG linker) or **138** (aliphatic linker) in the DSF assay. Thus, FGFR2, MST2, and ULK3 came to the fore. This clearly showed that the variation of the linker motif and the introduction of other linkers, such as those with amino functions, non-aromatic ring systems, or even heterocycles are projects with great potential for future research. Also feasible would be the introduction of other linker motifs by varying the ring closure procedure. Here, the employment of Grubbs catalysts, known from olefin metathesis, or also the so-called click chemistry could be mentioned. In this way, linkers with an unsaturated character or with a triazole function could be generated.

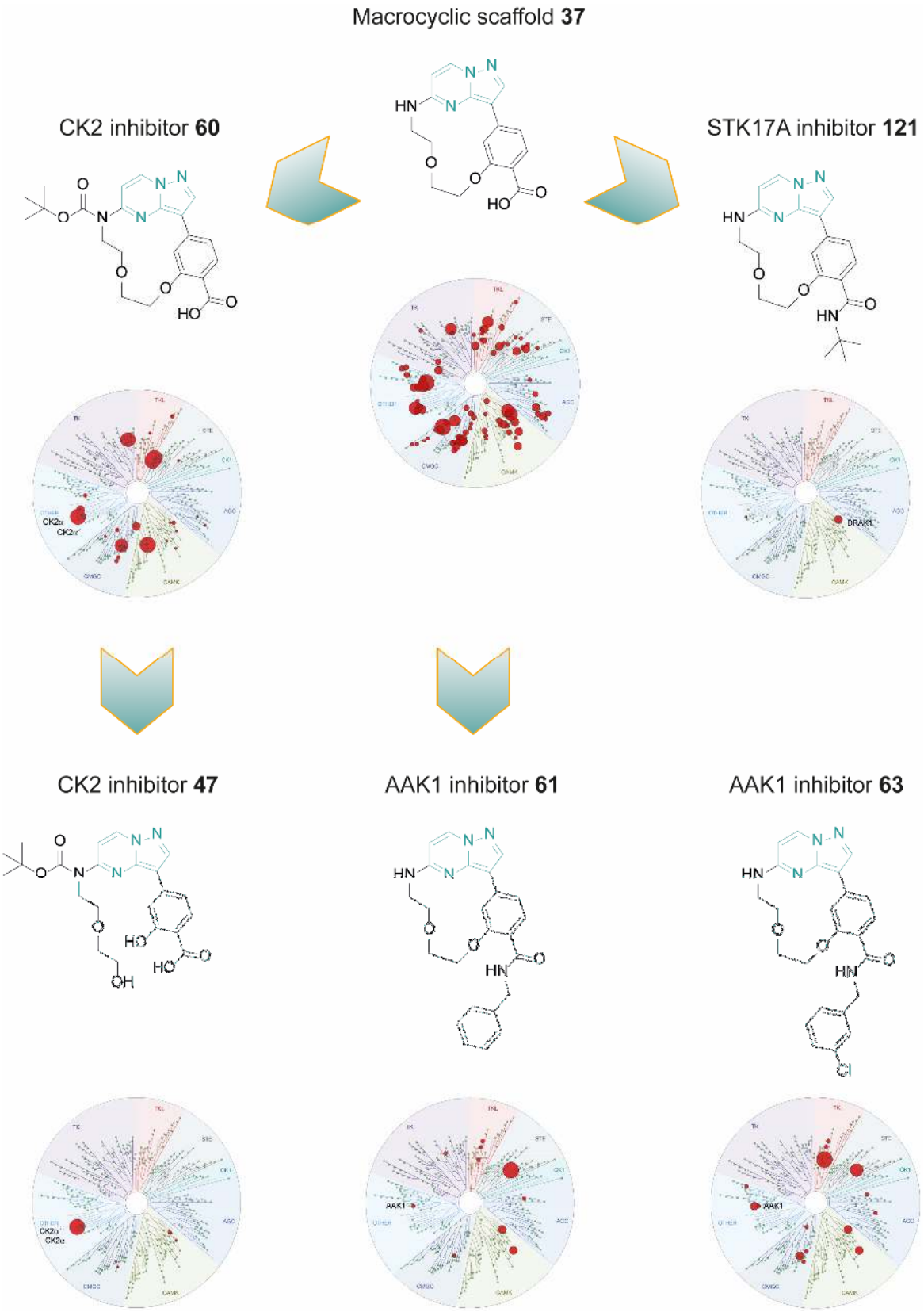

Figure 42: **Schematic review of the highly potent and selective kinase inhibitors synthesised and characterized in this thesis.** Based on the pyrazolo[1,5-*a*]pyrimidine-based macrocyclic scaffold **37**, a diverse set of SAR studies were performed, promising compounds were optimized and characterized in various assay platforms. In this manner, the CK2 inhibitors **60** and **47**, the DRAK1 inhibitor **121**, and the AAK1 inhibitors **61** and **63** were obtained.

To finally sum up, this thesis has succeeded in developing and characterizing highly potent and selective kinase inhibitors for CK2, DRAK1 and AAK1 based on a strongly unselective macrocyclic scaffold. Studies of multiple structure-activity relationships revealed that it is feasible to vary kinome-wide selectivity and to focus the inhibitory activity on a single kinase by minor structural modifications of the macrocyclic scaffold **37 (Figure 42).** The success of this thesis is not only reflected by the synthesis of these new macrocyclic kinase inhibitors. It also provides new starting points for future projects to develop highly potent and selective compounds as potential chemical probe for application in scientific research.

5. Deutsche Zusammenfassung und Ausblick

Im Jahr 2001 wurde mit Imatinib (**3**) der erste niedermolekularer Kinaseinhibitor für klinische Anwendungen zugelassen. Seither ist die Zahl der Kinaseinhibitoren in klinischen Studien rasant gestiegen. Die Beteiligung an Schlüsselfunktionen in zellulären Signalwegen macht Kinasen zu einem vielversprechenden Ansatzpunkt in der Wirkstoffentwicklung bei verschiedenen menschlichen Krankheiten.[18,34,215,216] Das prominenteste Einsatzgebiet von Kinaseinhibitoren ist die Onkologie. Mittlerweile sind jedoch auch andere Krankheiten bekannt, wie zum Beispiel Autoimmun- und Entzündungskrankheiten, bei denen sie als bereits zugelassene Wirkstoffe zum Einsatz kommen.[8] Die Prävention von post-translationalen Modifikationen durch Phosphorylierung und somit die Regulierung des nachgeschalteten Signalwegs ist das Ziel von Kinaseinhibitoren. Die katalytische Aktivität von Kinasen ist abhängig von ATP, welches in einer hochkonservierten Bindetasche lokalisiert wird. Dieses aktive Zentrum verbindet zwei katalytisch aktive Bereiche (englisch *lobes*) und wird als Gelenk-Region (englisch *hinge*) bezeichnet. Abhängig von der Aminosäure, die durch eine Kinase phosphoryliert wird, werden diese klassifiziert in Serin/Threonin, Tyrosin oder Tyrosin und Threonin dual spezifische Kinasen.[17,18] Bedingt durch die hohe Konservierung des aktiven Zentrums stellt die Entwicklung von hoch selektiven ATP-mimetischen Inhibitoren eine Herausforderung dar[34,44]. Die typische Erscheinungsform von ATP-Mimetika ist flach und die oft hydrophoben Moleküle weisen meist eine große Zahl an frei rotierbaren Bindungen auf. Um das aus dieser Flexibilität hervorgehende Problem der teils mangelnden Selektivität zu umgehen, kann eine bioaktive Konformation des Inhibitors durch Zyklisierung fixiert werden.

Typischerweise wird hierzu ein ATP-mimetisches Pharmakophor durch einen Linker in einem zwölf oder mehr Atome großen Makrozyklus vororganisiert.[55] Als Konsequenz dieser konformationellen Einschränkung können die entropischen Kosten während des Bindens reduziert werden und folglich zu einer gesteigerten Affinität gegenüber der Kinase führen.[50] Dennoch besitzen Makrozyklen genug Flexibilität, um mit dynamischen Bindungsstellen zu interagieren und sind nicht völlig versteift.[61] Die Möglichkeiten der Makrozyklisierung gehen jedoch über die Modulierung von Selektivität und Potenz der Inhibitoren hinaus. So stellt die Variation der physikochemischen und pharmakokinetischen Eigenschaften, wie zum Beispiel der Löslichkeit, Lipophilie, metabolische Stabilität und Bioaktivität, einen weiteren Benefit dar.[51]

Der Grundstein dieser Arbeit war der makrozyklische Pyrazolo[1,5-*a*]pyrimidin basierte Kinaseinhibitor ODS2004070 (**37**).[154] Er war Teil der Entwicklung eines FLT3 Inhibitors und wurde von der Firma Oncodesign patentiert. Im Rahmen eines kinomweiten Screenings von makrozyklischen Kinaseinhibitoren im ^{33}PanQinase™ Assay von ProQinase gegen 366 Kinasen, wurde **37** ebenfalls untersucht. So konnte eine hohe Affinität zu vielen verschiedenen Kinasen detektiert werden. Allerdings wurden ungefähr 130 Kinasen mit >60% inhibiert, was **37** zu einer Verbindung mit einem nicht besonders starken Selektivitätsprofil machte. Bedingt durch diese Eigenschaften war das makrozyklische Grundgerüst **37** jedoch als Leitstruktur für das Design von potenten und selektiven Kinaseinhibitoren prädestiniert.

Im Rahmen dieser Arbeit blieb das literaturbekannte und bereits in PIM1, RET, JAK1, ALK2/3 und RIPK2 Inhibitoren verwendete Pyrazolo[1,5-*a*]pyrimidin basierte *hinge* Bindemotiv unverändert.[197–202] Abgesehen von einer kleinen Serie an Derivaten zur Untersuchung der Auswirkung der Variation des Linkers, blieb auch das gesamte makrozyklische Grundgerüst **37** erhalten. Strukturelle Optimierungen zur Fokussierung der Selektivität wurden am sekundären Amin zwischen *hinge* Bindemotiv und Linker sowie über die Carbonsäure der Benzylgruppe durchgeführt.

Ein Beispiel für eine Serin/Threonin Kinase ist die pleiotropisch und konstitutiv aktive Casein Kinase 2 (CK2). Eine Anzahl von mehr als 430 identifizierten Phosphorylierungsstellen von CK2 verdeutlicht die regulatorische Beteiligung an verschiedenen zellulären Prozessen wie dem Verlauf des Zellzyklus, der Apoptose oder der Transkription.[76–79] Die Fehlregulation von CK2 wird häufig mit der Pathologie von Krankheiten wie zum Beispiel Krebs assoziiert, was CK2 zu einem vielversprechenden Ziel klinischer Untersuchungen macht.[92,93] Der am weitesten fortgeschrittene CK2 Inhibitor mit Anwendung in klinischen Studien ist Silmitasertib (**12**), der jedoch auch verschiedene andere Kinasen adressiert.[106] Somit ist die Suche nach einem selektiven Inhibitor von CK2 eng verknüpft mit der Untersuchung der Rolle von CK2 in Krebs und anderen Krankheiten. Im Rahmen des CK2-Projekts war es möglich, durch spezifische Modifikationen an **37**, die hoch selektiven und potenten CK2-Inhibitoren **47** und **60** zu entwickeln. Ebenfalls gezeigt wurde, dass kleine strukturelle Veränderungen, wie z.B. Makrozyklisierung, einen signifikanten Effekt auf Selektivität und Potenz des Inhibitors haben können. Die Verbindungen **47** und **60** zeigten vergleichbare *in vitro* Affinitäten gegenüber CK2 wie das in klinischen Studien eingesetzte Silmitasertib (**12**). Im zellulären Kontext lag ihre inhibitorische Aktivität zwar hinter der von Silmitasertib (**12**), jedoch immer noch im niedrigen mikromolaren Bereich. Neben den hohen T_m-Verschiebungen im DSF Assay waren hier erste Anzeichen auf eine potenziell hohe Selektivität zu erkennen. Die Validierung dieser ersten Selektivitätsdaten wurden im kinomweiten KINOME*scan*® Assay von Eurofins (früher DiscoverX) durchgeführt und lieferte vielversprechende Werte von S_{35} = 0.02 (**47**) und S_{35} = 0.07 (**60**) bei einer Screeningkonzentration von 1 µM. Im direkten Verglichen mit anderen bekannten CK2 Inhibitoren wie Silmitasertib (**12**), TBB[203] oder Emodin[204], wurden deren Selektivität deutlich übertroffen. Da CK2 an Prozessen wie dem Zellwachstum, Zelltod und Zellüberleben involviert ist, wird es als lohnendes Ziel bei der Behandlung von Krebs angesehen. In klinischen Studien zu verschiedenen Krebsarten wie dem Basalzellkarzinom (NCT03897036), Brustkrebs (NCT00891280), Gallenblasen-karzinom (NCT02128282), Medulloblastom (NCT03904862), multiplem Myelom (NCT01199718) Nierenkrebs (NCT03571438) wird Silmitasertib (**12**) eingesetzt. Es lässt sich jedoch die Hypothese aufstellen, dass der antiproliferative Effekt von Silmitasertib (**12**) nicht auf die Inhibierung von CK2, sondern, aus Mangel an Selektivität, auf die Adressierung von anderen Kinasen zurückzuführen ist.[108] Als Beispiele für solche möglichen Nebenziele seien CDK1[205,206], PIM1[207], HIPK3[208,209], TBK1[210], und FLT3[211,212] genannt.

Es existieren zwar selektive CK2 Inhibitoren wie GO289[213], CAM4066[180] oder SGC-CK2-1 (**14**)[81], allerdings überzeugt GO289 nicht durch hohe inhibitorische Aktivität, CAM4066 wurde nicht explizit auf seine Selektivität hin charakterisiert und SGC-CK2-1 (**14**) wurde erst vor kurzem publiziert. Dies zeigt dennoch, wie wichtig potente und vor allem selektive Verbindungen wie **47** für zukünftige funktionelle Studien sind. Ein weiterer interessanter Aspekt für zukünftige Arbeiten ist die Optimierung der Zellpenetration. Ein möglicher Ausgangspunkt ist in der Modifikation der freien Carbonsäure zu sehen.

Die Serin/Threonin Kinase 17A (STK17A) oder auch *death-associated protein kinase-related apoptosis-inducing protein kinase 1* (DRAK1) gehört zur Familie der DAPKs. Zusammen mit anderen Kinasen gehört sie zu dem so genannten dunklen Kinom und bis heute ist nicht viel über zelluläre Funktionen und die Beteiligung an pathophysiologischen Prozessen bekannt. Berichtet wurde jedoch eine Überexpression in verschiedenen Formen von Hirntumoren des zentralen Nervensystems (Gliom).[112,119] Erschwert wird die weitere Erforschung mitunter durch einen inhärenten Mangel an selektiven DRAK1 Inhibitoren. Startpunkt für das DRAK1 Projekt war das makrozyklische Gerüst **37,** welches auch als Grundlage für die CK2-Inhibitoren **47** und **60** diente. Geringfügige Modifikationen ermöglichten die Modulation der Selektivität und eine Verschiebung hin zu DRAK1. In ersten Schritten wurde das kinomweite Selektivitätsprofil durch die Einführung von raumfüllenden Gruppen an der Carbonsäure in Richtung der hinteren Bindetasche deutlich verbessert. Weitere strukturelle Optimierungen dieser Derivate führte zu den hoch potenten DRAK1-Inhibitoren **107** und **115** mit IC_{50}-Werten von 31 nM bzw. 15 nM. Diese zeigten jedoch noch nicht die gewünschte exklusive Selektivität im KINOME*scan*® Assay (S_{35} = 0.05 und0.18 bei 1 µM). Mit dem Wechsel von Benzylamid basierten Derivaten zu kleinen Amiden gelang jedoch der Durchbruch. Verbindung **121**, die eine *tert*-Butylamidfunktion enthält, beeindruckte mit einer *in vitro* Potenz von 49 nM und einer sehr hohen Selektivität im KINOME*scan*® mit S_{35} = 0.005 bei 100 nM und S_{35} = 0.02 bei 1 µM. Innerhalb der DAPK Familie bestand eine exklusive Affinität gegenüber DRAK1. Die Validierung anderer ebenfalls adressierter Kinasen *in cellulo* ergab eine 30-fach geringere Affinität im Vergleich zu DRAK1 mit IC_{50} = 181 nM. Untersuchungen der Co-Kristallstruktur von DRAK1 im Komplex mit **121** bestätigte die Hypothese eines Typ-I Inhibitors, der über das Pyrazolo[1,5-*a*]pyrimidin Motiv an die *hinge* Region bindet. Das *tert*-Butylamid war in Richtung der hinteren Bindetasche lokalisiert. Die anschließende Bestimmung der Zytotoxizität in drei verschiedenen Zelllinien zeigte bei einer Konzentration von 1 µM keine Effekte und nur geringe oberhalb von 10 µM.

Frühere Experimente von Mao *et al*. zeigten, dass der Knockout von DRAK1 zu einer dramatischen Veränderung der Zellform führte.[120] Dieser Effekt wurde mit einer verminderten Proliferation, Klonogenität, Migration, Invasion und verankerungs-unabhängigen Koloniebildung in Verbindung gesetzt. Untersuchungen zum Zusammenhang zwischen der Hemmung von DRAK1 und dem Überleben von Gliomzellen zeigten jedoch unerwartete Ergebnisse. Die in verschiedenen Gliomzellen ermittelten niedrigen mikromolaren EC_{50}-Werte korrelierten nicht mit den vielversprechenden niedrigen nanomolaren IC_{50}-Werten, die in NanoBRET™ Experimenten zu beobachten waren. In D-247MG-Zellen, mit dem höchsten DRAK1 Expressionsniveau der verwendeten Zellen, lag der EC_{50}-Wert von **121** bei 2.75 µM. Bezüglich der Zellmorphologie konnte lediglich eine geringfügige Veränderung in den niedrig exprimierenden T98G-Zellen bei einer Konzentration von 12.5 µM beobachtet werden. Die anderen Zelllinien wiesen keinen signifikanten Phänotyp auf. Die erhöhte Wirkung des potenteren Inhibitors **115** (EC_{50} < 3 µM) könnte aufgrund seiner weniger gut ausgeprägten Selektivität (S_{35} = 0.18 bei 1 µM), auf die Aktivität gegenüber anderen Kinasen zurückzuführen sein. Angesichts dieser überraschenden Erkenntnisse sind weitere systematische Untersuchungen der Aktivität von DRAK1 in Glioblastom-Zelllinien unumgänglich, um die Rolle von DRAK1 im Gliom zu beleuchten und somit die Grundlage für eine mögliche zukünftige therapeutische Anwendung zu schaffen.

Die Serin/Threonin Kinase AP-2-assoziierte Protein Kinase 1 (AAK1) aus der NAK Familie, bestehend aus AAK1, BIKE und GAK, wurde als potenzielles therapeutisches Ziel für viele verschieden Krankheiten wie z.B. neuropathische Schmerzen, Schizophrenie und Parkinson identifiziert.[143–145] Durch die Regulierung der Clathrin-mediierten Endozytose ist AAK1 an intrazellulären Bewegungen verschiedener nicht zusammenhängenden RNS- und DNS-Viren, wie beispielsweise HCV, DENV oder EBOV, beteiligt.[129,139,141,142] Da es bei vielen viralen Infektionen an adäquaten Therapiemöglichkeiten mangelt, ist AAK1 von Interesse für die Forschung. Die zugelassenen, jedoch nicht hoch selektiven AAK1 und GAK inhibierenden Krebstherapeutika Sunitinib (**2**) und Erlotinib (**21**), zeigten antivirale Aktivität.[141,142] Ebenfalls berichtet wurde eine mögliche Assoziation mit dem SARS-CoV-2 Virus, was das Interesse an neuen selektiven AAK1 Inhibitoren verstärkte.[146–149] Die Entwicklung der hochpotenten und selektiven AAK1-Inhibitoren **61** und **63** basierte ebenfalls auf dem makrozyklischen Grundgerüst **37**, das bereits im CK2- und DRAK1-Projekt verwendet wurde. Durch die Einführung verschiedener benzylamidischer Reste wurde die kinomweite Selektivität moduliert und auf AAK1 fokussiert.

So wurde im KINOME*scan*® Assay eine Verbesserung von S_{35} = 0.26 (**37** bei 1 µM) auf S_{35} = 0.09 (**61** und **70** bei 1 µM) erreicht. Weitere Untersuchungen zur Affinität der Verbindungen gegenüber den anderen NAK-Kinasen in einem Verdrängungs-Assay bestätigten **61** und **63** als hochpotente Inhibitoren von AAK1 mit IC_{50}-Werten von 4 nM. Die Validierung der identifizierten Nebenziele erfolgte in NanoBRET™ Experimenten. Hier zeigten sowohl **61** als auch **63** hohe inhibitorische Aktivitäten gegenüber AAK1 *in cellulo* mit IC_{50}-Werten von 38 nM bzw. 32 nM. Die Aktivität von **61** gegenüber BIKE war mit 3 µM sehr gering, gegenüber GAK konnte sie jedoch nicht ausgeschlossen werden. Wie erwartet zeigte **61** jedoch eine signifikante Aktivität auf DRAK1 (IC_{50} = 171 nM). Die Analyse der Co-Kristallstruktur von AAK1 im Komplex mit **61** bestätigte die Vermutungen, dass es sich bei **61** um einen Typ-I Inhibitor mit Interaktion zur *hinge* Region über das Pyrazolo[1,5-*a*]pyrimidin Motiv handelte. Basierend auf diesen Erkenntnissen wurden weitere Anstrengungen unternommen, um die Selektivität zu erhöhen. Strukturelle Optimierungen fokussierten sich mit sperrigen Resten auf die hintere Bindetasche und mit kleinen Harnstoffen auf die lösungsmittelexponierte Region. Auch die Auswirkung der Variation des Linker Motivs auf das Selektivitätsprofil wurde untersucht. So fiel das zweifach chlorsubstituierte Benzylamid Derivat **70** mit einer signifikanten Aktivität auf AAK1 und hoher Selektivität auf, die sich im KINOME*scan*® Assay mit Werten von 0.02 bei 100 nM und 0.09 bei 1 µM widerspiegelte. Experimente von Conner und Schmid zeigten eine essenzielle Beteiligung von AAK1 an der Rezeptor-vermittelten Endozytose, wobei der AP2-Komplex durch die Bindung von AAK1 an Clathrin reguliert wurde.[130] In Immunpräzipitationsexperimenten unter Inhibierung des AP2 Komplexes übertraf **61** den hochpotenten NAK-Inhibitor LP-935509 (**22**), der als Positivkontrolle verwendet wurde. Verbindung **63** zeigte fast identische, sehr gute Ergebnisse. Basierend auf diesen Daten und der von Gordon *et al*. identifizierten möglichen Interaktion des AP2-Komplexes mit dem SARS-CoV-2-Protein NSP10[191], wurde die antivirale Wirkung der hochpotenten und selektiven Verbindungen **61** und **63** durch AAK1-Inhibition untersucht. Überraschenderweise wurde *in cellulo* kein Effekt auf den Zelleintritt oder den Infektionsfortschritt beobachtet. Dies könnte jedoch mit den späteren Erkenntnissen von Hoffmann *et al*. über die Abhängigkeit des Zelleintritts und des Spike-Protein-Primings des SARS-CoV-2-Virus von ACE2 und TMPRSS2 erklärt werden.[196]

Die Regulation des AP2 Komplexes, bedingt durch AAK1 und GAK Inhibierung, und die daraus resultierende Blockierung der viralen Assemblierung und des Eintritts wurde von Neveu *et al*. für HCV berichtet.[139,140] Ein lohnendes Ziel für zukünftige Untersuchungen wäre folglich die Evaluierung der antiviralen Aktivität von **61** und **63** bei HCV. Bekerman und Verdonck zeigten die Einsatzmöglichkeit von AAK1 Inhibitoren bei weiteren RNA Viren wie EBOV und DENV.[141,142] Das Testspektrum für die makrozyklischen AAK1 Inhibitoren bezüglich antiviraler Aktivität sollte folglich, neben HCV, um weitere RNS Viren erweitert werden.

Aus den strukturellen Optimierungen sind weitere mögliche Ziele für die selektive Inhibierung durch Verbindungen, basierend auf dem makrozyklischen Grundgerüst **37**, hervorgegangen. So zeigten manche der Benzylharnstoff-Derivate wie **85** oder **92** eine interessante Kombination aus hoher Affinität und Selektivität gegenüber BIKE und GAK. Ebenfalls weiter zu verfolgen wäre die vergleichsweise hohe Affinität von **91** gegenüber LOK.

Die Vervollständigung der Charakterisierung von Verbindung **70**, sowie deren weitere strukturelle Optimierung, könnte aufgrund des vielversprechenden Selektivitätsprofil sowohl im verwendeten DSF Panel als auch im KINOME*scan*® Assay (S_{35} = 0.02 bei 100 nM und 0.09 bei 1 μM) ebenfalls ein Ziel für zukünftige Arbeiten darstellen. Die Serie der Derivate mit Adressierung der lösungsmittelzugewandten Region zeigte ebenfalls eine, wenn auch abgeschwächte, Affinität zu BIKE und DRAK1. Hier wäre eine Fusion mit Verbindungen aus vorangegangen Serien möglich um zum Beispiel einen selektiven Pyrazolo[1,5-*a*]pyrimidin basierten BIKE Inhibitor zu entwickeln oder die Potenz des DRAK1 Inhibitors **121** weiter zu steigern.

Die Variation der Linker Motive im kleinen Rahmen zeigte, dass auch diese ein möglicher Ansatzpunkt zur Modifikation des Selektivitätsprofils darstellt. Beispielsweise im Fall von Verbindung **61** tolerierte AAK1 den Wechsel zum aliphatischen Linker **138**, während die Affinität gegenüber DRAK1 einen deutlichen Einbruch verzeichnete.

Die Einführung des aromatischen Linkersystems **141** hingegen wurde weder von AAK1 noch von DRAK1 besonders gut toleriert. Interessanterweise tauchten jedoch andere Kinasen im Fokus auf, die weder von **61** (PEG Linker) noch von **138** (aliphatischer Linker) im DSF stabilisiert wurden. So traten FGFR2, MST2 und ULK3 in den Vordergrund.

Dies zeigt deutlich, dass die Variation des Linker Motivs und die Einführung weiterer Linker, wie zum Beispiel mit Aminofunktionen, nichtaromatischen Ringsystemen oder auch Heterozyklen ein Projekt mit Zukunftsaussicht ist. Ebenso möglich wäre die Einführung andere Linker Motive durch die Variation des Ringschlussverfahrens. Hier sei die Verwendung von Grubbs Katalysatoren, bekannt aus der Olefinmetathese, oder auch die so genannte Click Chemie genannt. Auf diese Weise ließen sich Linker mit ungesättigtem Charakter oder auch mit einer Triazol Funktion generieren.

Zusammenfassend lässt sich sagen, dass es im Rahmen dieser Arbeit gelungen ist, ausgehend von einem höchst unselektiven makrozyklischen Grundgerüst, hochpotente und selektive Kinaseinhibitoren für CK2, DRAK1 und AAK1 zu entwickeln und zu charakterisieren. Im Zuge von Untersuchungen verschiedener Struktur-Wirkungsbeziehungen wurde gezeigt, dass es durch geringfügige strukturelle Modifikationen am makrozyklischen Grundgerüst **37** möglich ist, die kinomweite Selektivität zu variieren und auf eine Kinase zu fokussieren (**Figure 42**). Diese Arbeit brachte nicht nur die erwähnten Inhibitoren hervor, sondern bildet auch die Grundlage für weitere Projekte zur Entwicklung von hoch potenten und selektiven Verbindungen als potenzielle chemische Werkzeuge für den Einsatz in der Forschung.

6. Experimental procedures

6.1 Organic synthesis

All commercial chemicals and reagents were obtained from Fluorochem, Merck, TCI, abcr or Apollo Scientific. Unless otherwise indicated, the purity was ≥ 95%. The solvents used in analytical grade were obtained from Fisher Scientific, Merck and VWR Chemicals and all dry solvents, with AcroSeal septum, from Acros Organics. All performed thin layer chromatography (TLC) was done with silica gel on aluminum foils (60 Å pore diameter) obtained from Macherey-Nagel and visualized with ultraviolet light (λ = 254 and 365 nm). The purification via flash chromatography was performed with a Interchim (Montluçon, F) puriFlash® XS 420+ equipped with a multi-wavelength UV-DAD (200 – 400 nm) detector using Interchim PF-30SIHP and PF-50SIHP normal phase columns and PF-30C18HP reversed phase (C_{18}) columns. The nuclear magnetic resonance spectroscopy (NMR) was performed with spectrometers from Bruker (Karlsruhe, Germany) with 126, 151, 250, 400, 500 and 600 MHz. The spectra were recorded in deuterated dimethyl sulfoxide (DMSO-d6) or deuterated chloroform ($CDCl_3$-*d*) and the solvent signal was used as a reference (2.50 ppm or 7.26 ppm). Coupling constants (*J*) were reported in hertz (Hz) and multiplicities were designated as followed. s (singlet), d (doublet), dd (double doublet), t (triplet), q (quartet) and m (multiplet). Mass spectrometric analysis was done with an electrospray ionization device (VG Platform II) from Fisons Instruments (Glasgow, UK). For MALDI-HRMS a MALDI LTQ Orbitrap XL system from Thermo Scientific (Waltham, MA, USA) was used. Purity of the synthesized compounds was determined with: (I) Agilent Technologies (Santa Clara, CA, USA) 1260 Infinity II device with a 1260 MWD detector (G7165A; 254 nm, 280 nm) and a LC/MSD device (G6125B, ESI pos. 100-1000) using an Agilent Technologies Eclipse XDB-C18 5 µm 4.6 x 250 mm reversed phase (C_{18}) column. As mobile phase Milli-Q water (A) and acetonitrile (B) + 0.1% TFA were used with a flowrate of 1 mL/min. The gradient was running over 19 min starting with 98% A and 2% B, going down on 2% A and 98% B and finishing at 98% A and 2% B. (II) Agilent Technologies (Santa Clara, CA, USA) 1260 Infinity II device with a 1260 DAD HS detector (G7117C; 254 nm, 280 nm, 210 nm) and a LC/MSD device (G6125B, ESI pos. 100-1000) using an Agilent Technologies Poroshell 12 EC-C18 2.7 µm 3 x 150 mm reversed phase (C_{18}) column. As mobile phase Milli-Q water (A) and acetonitrile (B) + 0.1% TFA were used with a flowrate of 0.5 mL/min.

The gradient was running over 8 min starting with 98% A and 2% B, going down on 2% A and 98% B and finishing at 98% A and 2% B. (III) Shimadzu (Duisburg, Germany) LC-20AD HPLC equipped with a Shimadzu LCMS-2020 detector (254 nm, 280 nm) using a Phenomenex LTD (Aschaffenburg, Germany) Luna 10 µm 21.2 x 250 mm reversed phase (C_{18}) column. As mobile phase Milli-Q water (A) and acetonitrile (B) + 0.1% formic acid were used with a flowrate of 1 mL/min. The gradient was running over 25 min starting with 95% A and 5% B, going down on 10% A and 90% B and finishing at 95% A and 5% B. The purity of all synthesized final compounds was 95% or higher.

6.1.1 Synthesis of 3-bromo-5-chloropyrazolo [1,5-*a*]pyrimidine (25).

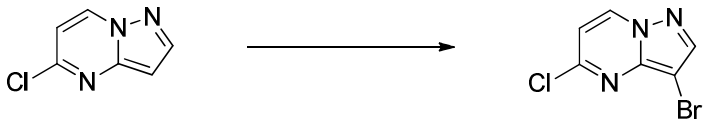

24 **25**

5-Chloropyrazolo [1,5-*a*]pyrimidine (**24**) (20.00 g, 1.0 eq, 130.23 mmol) was suspended in dimethylformamide (250 mL) and *N*-bromosuccinimide (25.50 g, 1.1 eq, 143.26 mmol) was added in small portions while stirring. Alter 1 h at room temperature, the reaction was quenched with water (300 mL). The precipitation was vacuum filtered and washed with water. After drying, the bright yellow solid was the desired compound (28.90 g, 96%).

^{1}H NMR (250 MHz, DMSO-d_6): δ 9.21 (d, J = 7.3 Hz, 1H, HetH), 8.43 (s, 1H, HetH), 7.22 (d, J = 7.3 Hz, 1H, HetH) ppm.

6.1.2 Synthesis of 2-[2-({3-bromopyrazolo[1,5-*a*]pyrimidine-5-yl}amino)ethoxy] ethan-1-ol (26).

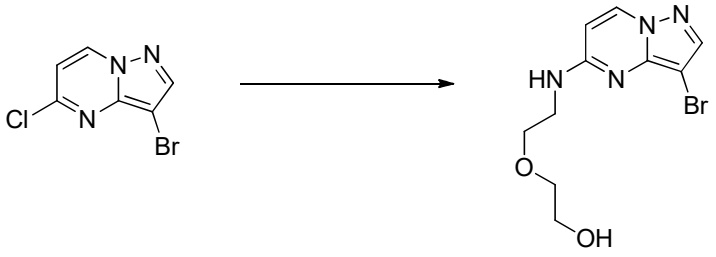

25 **26**

A solution of 3-bromo-5-chloropyrazolo [1,5-*a*]pyrimidine (**25**) (28.90 g, 1.0 eq, 124.32 mmol), 2-(2-aminoethoxy)ethanol (7.46 g, 1.1 eq, 136.75 mmol) and *N,N*-diisopropylethylamine (10.01 g, 1.2 eq, 149.18 mmol) in acetonitrile (380 mL) was stirred under reflux for 16 h. Next step was the evaporation of the solvent in vacuo. The residue was taken up in ethyl acetate and washed with water and brine. After drying over $MgSO_4$ the solvent was evaporated under reduced pressure and the crude product was purified with silica gel column chromatography with a mobile phase of petroleum ether and tetrahydrofuran (ratio gradually ranging from 3:1 to 0:1). The title compound was obtained as a white solid (30.32 g, 81%).

^{1}H NMR (250 MHz, DMSO-d_6): δ 8.45 (d, J = 7.5 Hz, 1H Het*H*), 7.87 (s, 1H, Het*H*), 7.70 (t, J = 5.0 Hz, 1H, N*H*), 6.34 (d, J = 7.6 Hz, 1H, Het*H*), 4.57 (s, 1H, O*H*), 3.66 – 3.45 (m, 8H, CH_2) ppm.

6.1.3 Synthesis of 3-bromo-5-(8,8,9,9-tetramethyl-4,7-dioxa-1-aza-8-siladecan-1-yl)pyrazolo-[1,5-*a*]pyrimidine (27).

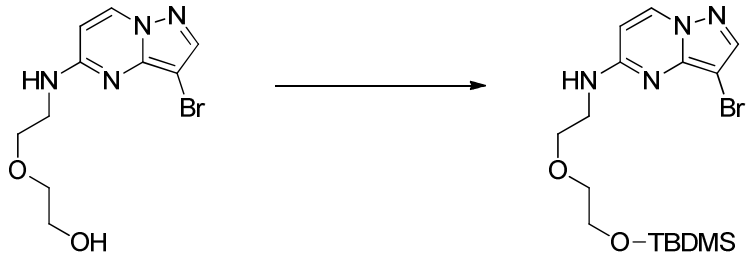

26 **27**

2-[2-({3-Bromopyrazolo[1,5-*a*]pyrimidine-5-yl}amino)ethoxy]ethan-1-ol (**26**) (30.30 g, 1.0 eq, 100.62 mmol) and triethylamine (20.36 g, 2.0 eq, 201.24 mmol) are dissolved in dry dimethylformamide (280 mL). While stirring, *tert*-butyldimethylsilyl chloride (22.75 g, 1.5 eq, 150.93 mmol) was added in small portions. After 1 h at room temperature the solvent was removed under reduced pressure and the residue was dissolved in water. The aqueous layer was extracted with ethyl acetate, the organic layer washed with brine and dried over $MgSO_4$. The solvent was removed under reduced pressure and further purification was carried out by a silica gel column chromatography with a mobile phase of *n*-hexane an ethyl acetate (ratio of 1:1). The title compound was obtained as a white solid (31.40 g, 75%).

^{1}H NMR (250 MHz, DMSO-d_6): δ 8.44 (d, J = 7.6 Hz, 1H, Het*H*), 7.86 (s, 1H, Het*H*), 7.70 (t, J = 5.4 Hz, 1H, N*H*), 6.33 (d, J = 7.6 Hz, 1H, Het*H*), 3.74 – 3.67 (m, 2H, CH_2), 3.64 – 3.48 (m, 6H, CH_2), 0.83 (s, 9H, (CH_3)$_3$), 0.02 (s, 6H, Si(CH_3)$_2$) ppm.

6.1.4 Synthesis of *tert*-butyl *N*-{3-bromopyrazolo[1,5-*a*]pyrimidin-5-yl}-*N*-(2-{2-[(*tert*-butyl-dimethylsilyl)oxy]ethoxy}ethyl)carbamate (28).

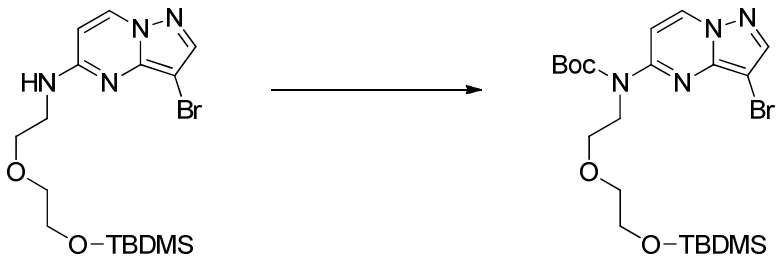

27 **28**

Triethylamine (8.54 g, 1.2 eq, 84.44 mmol) was added to a solution of 3-bromo-5-(8,8,9,9-tetramethyl-4,7-dioxa-1-aza-8-siladecan-1-yl)pyrazolo[1,5-*a*]pyrimidine (**27**) (29.23 g, 1.0 eq, 70.37 mmol), di-*tert*-butyldicarbonate (38.39 g, 2.50 eq, 175.91 mmol) and 4-(dimethylamino)pyridine (171.93 g, 0.02 eq, 1.41 mmol) in tetrahydrofuran (260 mL). The reaction mixture was heated to reflux for 3 h and afterwards, the solvent was evaporated. The residue was taken up in ethyl acetate and washed with water and brine. After drying over $MgSO_4$ the organic layer was removed under reduced pressure. Further purification was done with silica gel column chromatography with a mobile phase of *n*-hexane an ethyl acetate (ratio gradually ranging from 1:0 to 0:1). The desired compound was yielded as a yellowish oil (34.50 g, 95%).

^{1}H NMR (250 MHz, DMSO-d_6): δ 8.95 (d, J = 7.8 Hz, 1H, Het*H*), 8.24 (s, 1H, Het*H*), 7.42 (d, J = 7.8 Hz, 1H, Het*H*), 4.18 (t, J = 6.1 Hz, 2H, CH_2), 3.69 (t, J = 6.0f Hz, 2H, CH_2), 3.61 – 3.55 (m, 2H, CH_2), 3.50 – 3.44 (m, 2H, CH_2), 1.51 (s, 9H, (CH_3)$_3$), 0.79 (s, 9H, (CH_3)$_3$), -0.06 (s, 6H, Si(CH_3)$_2$) ppm.

6.1.5 Synthesis of methyl 2,4-dihydroxybenzoate (30).

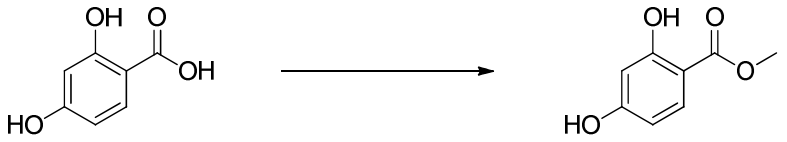

29 **30**

A solution of 2,4-dihydroxybenzoic acid (**29**) (20.00 g, 1.0 eq, 129.77 mmol) in dry methanol (300 mL) and concentrated sulfuric acid (2.6 mL) was stirred under reflux for 16 h. After reaction completion, the solvent was removed under reduced pressure and the residue was taken up with ethyl acetate. The organic layer was washed with brine, dried over $MgSO_4$ and evaporated in vacuo. Further purification was done with silica gel column chromatography with a mobile phase of dichloromethane and methanol (ratio of 20:1). The desired compound was obtained as a white solid (10.13 g, 46%).

^{1}H NMR (250 MHz, DMSO-d_6): δ 10.70 (s, 1H, O*H*), 10.45 (s, 1H, O*H*), 7.64 (d, J = 8.7 Hz, Ph*H*), 6.37 (dd, J = 8.7, 2.4 Hz, 1H, Ph*H*), 6.29 (d, J = 2.3 Hz, 1H, Ph*H*), 3.84 (s, 3H, OCH_3) ppm.

6.1.6 Synthesis of methyl 2-hydroxy-4-(trifluoromethansulfonyloxy)benzoate (31).

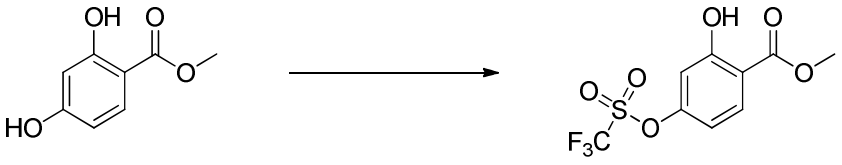

30 **31**

Methyl-2,4-dihydroxybenzoate (**30**) (10.13 g, 1.0 eq, 60.26 mmol), pyridine (4.86 g, 1.0 eq, 60.26 mmol) and 4-(dimethylamino)-pyridine (0.29 g, 0.04 eq, 2.41 mmol) were dissolved in dry methylene chloride (150 mL) under argon atmosphere. The solution was cooled to 0 °C and 1 M trifluoromethanesulfonic anhydride in methylene chloride (60 mL, 1.0 eq, 60.26 mmol) was added dropwise. The reaction was allowed to stir for 16 h at room temperature and was quenched with 10% hydrochloric acid (25 mL). The aqueous layer was extracted with ethyl acetate and the organic layer was dried over $MgSO_4$ and evaporated in vacuo.

The crude product was purified with silica gel column chromatography with a mobile phase of *n*-hexane and ethyl acetate (ratio gradually ranging from 1:0 to 30:1). The white solid obtained is the title compound (16.46 g, 91%).

^{1}H NMR (250 MHz, DMSO-d_6): δ 10.89 (s, 1H, O*H*), 7.92 (d, J = 8.7 Hz, 1H, Ph*H*), 7.13 (d, J = 2.5 Hz, 1H, Ph*H*), 7.05 (dd, J = 8.8, 2.5 Hz, 1H, Ph*H*), 3.88 (s, 3H, OCH_3) ppm.

6.1.7 Synthesis of methyl 2-hydroxy-4(4,4,5,5-tetramethyl-1,3,2-dioxaborolan-2-yl)benzoate (32).

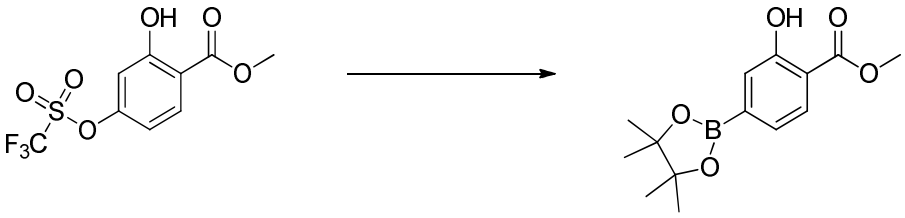

31 **32**

To a solution of methyl-2-hydroxy-4-(((trifluoromethyl)sulfonyl)oxy)benzoate (**31**) (16.46 g, 1.0 eq, 54.83 mmol) in dry 1,4-dioxane (250 mL), bis(pinacolato)diboron (20.89 g, 1.5 eq, 82.25 mmol), potassium acetate (16.14 g, 3.0 eq, 164.49 mmol) and Pd(dppf)Cl_2·DCM (2.24 g, 0.05 eq, 2.74 mmol) were added. The reaction solution was flushed with argon for 10 min and stirred at 100 °C for 3.5 h. Subsequently the reaction was diluted with ethyl acetate and water and the layers were separated. The organic layer was washed with brine and dried over $MgSO_4$. After removal of the solvent under reduced pressure, the crude product was purified with silica gel column chromatography with a mobile phase of *n*-hexane and ethyl acetate (ratio gradually ranging from 1:0 to 30:1). The title compound was obtained as a white solid (12.46 g, 82%).

^{1}H NMR (250 MHz, DMSO-d_6): δ 10.35 (s, 1H, O*H*), 7.76 (d, J = 7.8 Hz, 1H, Ph*H*), 7.21 – 7.18 (m, 2H, Ph*H*), 3.88 (s, 3H, OCH_3), 1.30 (s, 12H, CH_3) ppm.

6.1.8 Synthesis of methyl 4-(5-((*tert*-butoxycarbonyl)(2-(2-((*tert*-butyldimethylsilyl)oxy)-ethoxy)ethyl)amino)pyrazolo[1,5-*a*]pyrimidin-3-yl)-2-hydroxybenzoate (33).

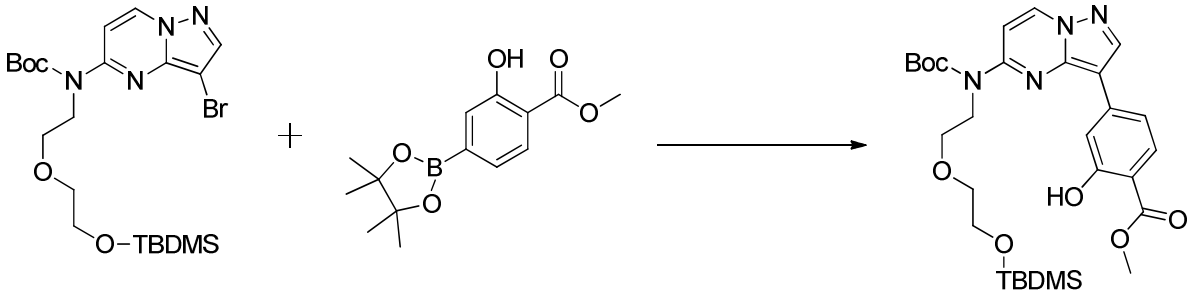

28 **32** **33**

tert-Butyl *N*-{3-bromopyrazolo[1,5-*a*]pyrimidin-5-yl}-*N*-(2-{2-[(tert-butyldimethylsilyl)-oxy]ethoxy}ethyl)carbamate (**28**) (4.63 g, 1.0 eq, 8.99 mmol) and methyl 2-hydroxy-4(4,4,5,5-tetramethyl-1,3,2-dioxaborolan-2-yl)benzoate (**32**) (5.00 g, 2.0 eq 17.98 mmol) were suspended together with $Pd_2(dba)_3$ (823 mg, 0.1 eq, 0.90 mmol), XPhos (429 mg, 0.1 eq, 0.90 mmol) and potassium phosphate (7.63 g, 4.0 eq, 35.96 mmol) in 1,4-dioxane (50 mL) and water (20 mL). The reaction was running for 40 min at 110 °C. After diluting with ethyl acetate layers were separated, the organic one was washed with water and brine and dried over $MgSO_4$. The solvent was evaporated in vacuo. Purification was performed by flash silica gel column chromatography with a mobile phase of *n*-hexane an ethyl acetate (ratio gradually ranging from 1:0 to 0:1). The white solid obtained was the desired compound (4.85 g, 91%).

^{1}H NMR (250 MHz, DMSO-d_6): δ 10.62 (s, 1H, OH), 8.99 (d, J = 7.8 Hz, 1H, Het*H*), 8.74 (s, 1H, Het*H*), 7.79 (d, *J* = 8.2 Hz, 1H, Ph*H*), 7.71 – 7.66 (m, 2H, Ph*H*), 7.49 (d, *J* = 7.8 Hz, 1H, Het*H*), 4.23 (t, *J* = 6.2 Hz, 2H, CH_2), 3.90 (s, 3H, OCH_3), 3.77 (t, *J* = 6.2 Hz, 2H, CH_2), 3.61 (t, *J* = 5.2 Hz, 2H, CH_2), 3.48 (t, *J* = 5.0 Hz, 2H, CH_2), 1.53 (s, 9H, (CH_3)$_3$), 0.76 (s, 9H, (CH_3)$_3$), -0.08 (s, 6H, Si(CH_3)$_2$) ppm.

6.1.9 Synthesis of methyl 4-(5-{[(*tert*-butoxy)carbonyl][2-(2-hydroxyethoxy)-ethyl]amino}-pyrazolo[1,5-*a*]pyrimidin-3-yl)-2-hydroxybenzoate (34).

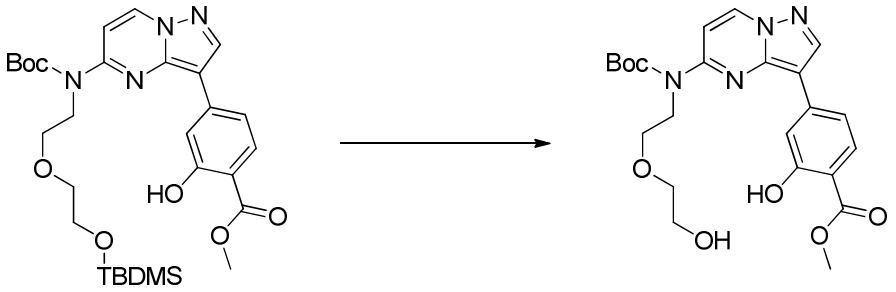

33 **34**

To a solution of methyl 4-(5-((*tert*-butoxycarbonyl)(2-(2-((*tert*-butyldimethylsilyl)oxy)-ethoxy)ethyl)amino)pyrazolo[1,5-*a*]pyrimidin-3-yl)-2-hydroxybenzoate (**33**) (4.13 g, 1.0 eq, 7.04 mmol) in tetrahydrofuran (60 mL) was added a 1 M tetrabutylammonium fluoride solution (10.6 mL, 10.56 mmol) in tetrahydrofuran. The reaction stirred at room temperature. After 3 h the solvent was removed under reduced pressure. Subsequently the residue was taken up with ethyl acetate, washed with water and brine and the solvent was evaporated again. Further purification was done with flash silica gel column chromatography with a mobile phase of *n*-hexane an ethyl acetate (ratio gradually ranging from 1:0 to 0:1). The title compound was yielded as white solid (2.81 g, 85%).

^{1}H NMR (500 MHz, DMSO-d_6): δ 10.62 (s, 1H, O*H*), 8.99 (d, J = 7.8 Hz, 1H, Het*H*), 8.75 (s, 1H, Het*H*), 7.81 (d, J = 8.3 Hz, 1H, Ph*H*), 7.71 – 7.68 (m, 2H, Ph*H*), 7.49 (d, J = 7.8 Hz, 1H, Het*H*), 4.52 (t, J = 5.1 Hz, 1H, O*H*), 4.22 (t, J = 6.3 Hz, 2H, CH_2), 3.91 (s, 3H, OCH_3), 3.77 (t, J = 6.3 Hz, 2H, CH_2), 3.48 – 3.42 (m, 4H, CH_2), 1.53 (s, 9H, (CH_3)$_3$) ppm.

^{13}C NMR (126 MHz, DMSO-d_6): δ 169.44, 160.83, 153.83, 152.82, 143.78, 143.09, 139.79, 136.58, 130.15, 116.35, 112.68, 109.33, 106.19, 104.73, 82.53, 72.24, 67.98, 60.21, 52.34, 45.82, 27.64 ppm.

MS (ESI+) *m/z:* 473.04 $[M + H]^+$.

HRMS *m/z:* $[M + H]^+$ calcd for $C_{23}H_{29}N_4O_7$, 473.20308; found 473.20216.

HPLC (III): t_R = 16.063, purity ≥ 95%.

6.1.10 Synthesis of 9-(*tert*-butyl) 2^4-methyl (1^3Z,1^4E)-3,6-dioxa-9-aza-1(3,5)-pyrazolo[1,5-*a*]pyrimidina-2(1,3)-benzenacyclononaphane-2^4,9-dicarboxylate (35).

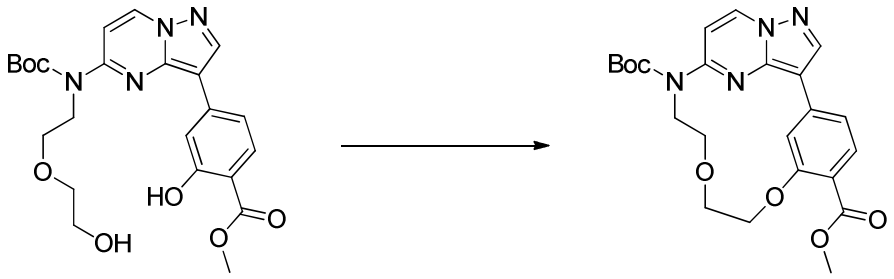

34 **35**

A suspension of triphenylphosphine (832 mg, 3.0 eq 3.17 mmol) and sodium sulfate in dry toluene (240 mL) was added dropwise with a solution of diisopropyl azodicarboxylate (642 mg, 3.0 eq, 3.17 mmol) in dry toluene (75 mL). Afterwards methyl 4-(5-{[(*tert*-butoxy)carbonyl][2-(2-hydroxyethoxy)ethyl]amino}pyrazolo[1,5-*a*]pyrimidin-3-yl)-2-hydroxybenzoate (**34**) (500 mg, 1.0 eq, 1.06 mmol) was dissolved in 2-methyltetrahydrofuran (50 mL) and this solution was added dropwise. Reaction took place over 3 h at 90 °C under argon atmosphere. Sodium sulfate was separated by filtration and the solvent was evaporated in vacuo. Purification was achieved by silica gel column chromatography with a mobile phase of *n*-hexane an ethyl acetate (ratio gradually ranging from 9:1 to 0:1). The yellowish solid obtained was the title compound (417 mg, 87%).

^{1}H NMR (500 MHz, DMSO-d_6): δ 9.01 (d, J = 7.8 Hz, 1H, Het*H*), 8.75 (d, J = 1.2 Hz, 1H, Ph*H*), 8.71 (s, 1H, Het*H*), 7.69 (d, J = 8.1 Hz, 1H, Ph*H*), 7.55 (d, J = 7.8 Hz, 1H, Het*H*), 7.43 (dd, J = 8.1, 1.4 Hz, 1H, Ph*H*), 4.39 (t, J = 6.0 Hz, 2H, CH_2), 4.09 (t, J = 6.6 Hz, 2H, CH_2), 3.92 (t, J = 6.6 Hz, 2H, CH_2), 3.88 (t, J = 6.0 Hz, 2H, CH_2), 3.78 (s, 3H, OCH_3), 1.54 (s, 9H, (CH_3)$_3$) ppm.

^{13}C NMR (126 MHz, DMSO-d_6): δ 165.78, 158.86, 153.40, 152.43, 143.08, 142.97, 137.60, 136.52, 131.23, 116.61, 112.64, 106.34, 104.16, 82.78, 67.51, 66.80, 66.57, 51.69, 46.57, 27.66 ppm.

MS (ESI+) *m/z:* 455.03 $[M + H]^+$.
HRMS *m/z:* $[M + H]^+$ calcd for $C_{23}H_{27}N_4O_6$, 455.19251; found 455.19082.
HPLC (III): t_R = 16.694, purity ≥ 95%.

6.1.11 Synthesis of methyl 2-hydroxy-4-(5-{[2-(2-hydroxyethoxy)ethyl]amino} pyrazolo[1,5-*a*]pyrimidin-3-yl)benzoate (46).

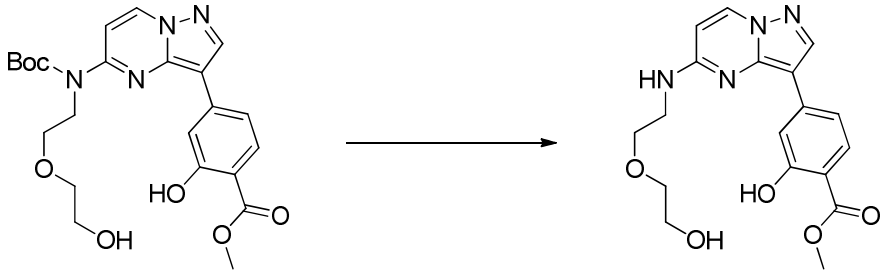

34 **46**

Methyl 4-(5-{[(*tert*-butoxy)carbonyl][2-(2-hydroxyethoxy)ethyl]amino}pyrazolo[1,5-*a*]-pyrimidin-3-yl)-2-hydroxybenzoate (**34**) (75 mg, 0.16 mmol) was suspended in methylene chloride (2.5 mL) and trifluoroacetic acid (0.75 mg, 6.50 mmol) was added slowly at 0 °C. After stirring for 16 h at room temperature the solvent was evaporated under vacuum. The crude product was purified by silica gel column chromatography with a mobile phase of *n*-hexane and ethyl acetate (ratio gradually ranging from 1:0 to 0:1). The white solid obtained was the desired compound (50 mg, 85%).

^{1}H NMR (500 MHz, DMSO-d_6): δ 10.62 (s, 1H, COO*H*), 8.52 (d, J = 7.6 Hz, 1H, Het*H*), 8.44 (s, 1H, Het*H*), 7.88 (t, J = 5.3 Hz, 1H, N*H*), 7.78 – 7.75 (m, 2H, Ph*H*), 7.66 (dd, J = 8.4, 1.6 Hz, 1H, Ph*H*), 6.39 (d, J = 7.6 Hz, 1H, Het*H*), 3.89 (s, 3H, OCH_3), 3.72 – 3.49 (m, 9H, (CH_2), O*H*) ppm.

^{13}C NMR (126 MHz, DMSO-d_6): δ 169.63, 160.93, 157.89, 156.33, 145.58, 142.43, 141.34, 135.58, 129.88, 115.81, 111.74, 108.03, 103.05, 100.52, 72.25, 68.41, 60.23, 52.25, 40.51 ppm.

MS (ESI+) *m/z:* 372.96 $[M + H]^+$.

HRMS *m/z:* $[M + H]^+$ calcd for $C_{18}H_{21}N_4O_5$, 373.15065; found 373.15150.

HPLC (III): t_R = 12.941, purity ≥ 95%.

6.1.12 Synthesis of 4-(5-((*tert*-butoxycarbonyl)(2-(2-hydroxyethoxy)ethyl)amino)-pyrazolo[1,5-*a*]pyrimidin-3-yl)-2-hydroxybenzoic acid (47).

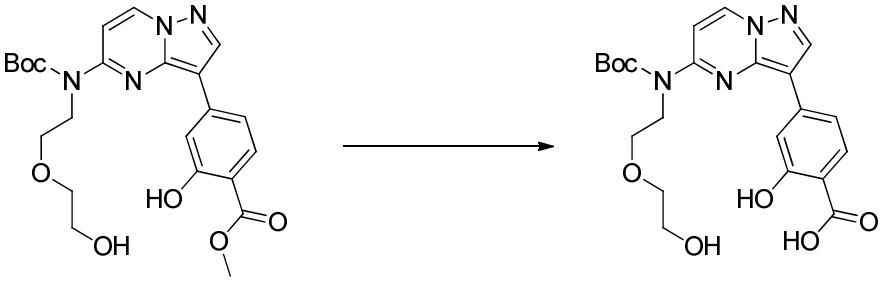

34 **47**

A solution of lithium hydroxide monohydrate (31 mg, 0.74 mmol) in water (1 mL) was added to a solution of methyl 4-(5-{[(*tert*-butoxy)carbonyl][2-(2-hydroxyethoxy)ethyl]-amino}pyrazolo[1,5-*a*]pyrimidin-3-yl)-2-hydroxybenzoate (**34**) (70 mg, 0.15 mmol) in tetrahydrofuran (5 mL) and it was stirred for 16 h at 50 °C. The solvent was removed in vacuo and the residue was taken up with water. Afterwards the solution was acidified with 1N HCl and it was extracted with ethyl acetate. The organic layers were dried over $MgSO_4$ and the solvent was evaporated. The crude product was purified by flash silica gel column chromatography with a mobile phase of petroleum ether and tetrahydrofuran with the addition of 1% acetic acid (ratio gradually ranging from 1:1 to 0:1). The white solid (29 mg, 42%) was the title compound.

^{1}H NMR (500 MHz, DMSO-d_6): δ 11.40 (s, 1H, COO*H*), 9.00 (d, J = 7.7 Hz, 1H, Het*H*), 8.76 (s, 1H, Het*H*), 7.80 (d, J = 8.2 Hz, 1H, Ph*H*), 7.69 – 7.66 (m, 2H, Ph*H*), 7.49 (d, J = 7.7 Hz, 1H, Het*H*), 4.54 (s, 1H, O*H*), 4.22 (t, J = 6.4 Hz, 2H, CH_2), 3.78 (t, J = 6.4 Hz, 2H, CH_2), 3.49 – 3.43 (m, 4H, CH_2), 1.53 (s, 9H, (CH_3)$_3$) ppm.

^{13}C NMR (126 MHz, DMSO-d_6): δ 171.90, 161.71, 153.79, 152.83, 143.79, 143.04, 139.53, 136.58, 130.51, 116.07, 112.49, 106.40, 104.75, 82.54, 72.27, 67.98, 60.23, 45.83, 31.16, 29.83, 27.67 ppm.

MS (ESI+) *m/z:* 458.98 $[M + H]^+$.

HRMS *m/z:* $[M + H]^+$ calcd for $C_{22}H_{27}N_4O_7$, 459.18743; found 459.18597.

HPLC (III): t_R = 14.984, purity ≥ 95%.

6.1.13 Synthesis of (1^3Z,1^4E)-9-(*tert*-butoxycarbonyl)-3,6-dioxa-9-aza-1(3,5)-pyrazolo[1,5-*a*]-pyrimidina-2(1,3)-benzenacyclononaphane-2^4-carboxylic acid (60).

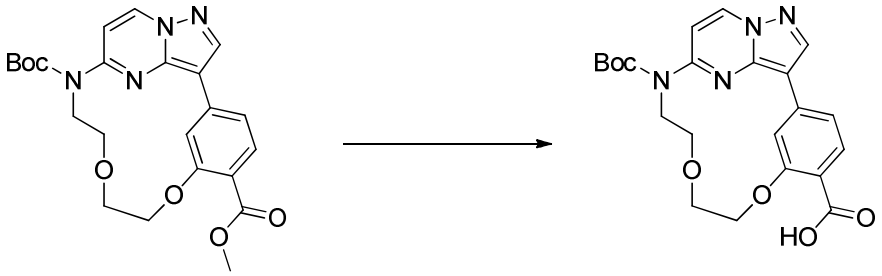

35 **60**

9-(*tert*-Butyl) 2^4-methyl (1^3Z,1^4E)-3,6-dioxa-9-aza-1(3,5)-pyrazolo[1,5-*a*]pyrimidina-2(1,3)-benzenacyclononaphane-2^4,9-dicarboxylate (**35**) (150 mg, 1.0 eq, 0.33 mmol) and trimethyltin hydroxide (358 mg, 6.0 eq, 1.98 mmol) were solved in dichloroethane (12 mL) and the reaction mixture was stirred for 10 h under microwave radiation at 80 °C. After reaction control (TLC), trimethyltin hydroxide (179 mg, 3.0 eq, 0.99 mmol) was added and it was stirred for 10 h at 80 °C under microwave radiation. This process was repeated one more time. Subsequently, the solvent was removed under reduced pressure and the residue was taken up in ethyl acetate. It was washed with 1 M HCl, the organic phase was washed with brine, dried over $MgSO_4$ and the solvent was removed in vacuo. Purification was done by flash silica gel column chromatography with a mobile phase of *n*-hexane and ethyl acetate with the addition of1% acetic acid (ratio gradually ranging from 1:0 to 0:1). The title compound was obtained as a white solid (79 mg, 54%).

^{1}H NMR (500 MHz, DMSO-d_6): δ 12.35 (s, 1H, COO*H*), 9.01 (d, J = 7.8 Hz, 1H, Het*H*), 8.75 (d, J = 1.5 Hz, 1H, Het*H*), 8.72 (s, 1H, Ph*H*), 7.70 (d, J = 8.1 Hz, 1H, Ph*H*), 7.55 (d, J = 7.8 Hz, 1H, Het*H*), 7.42 (dd, J = 8.1, 1.5 Hz, 1H, Ph*H*), 4.40 (t, J = 6.0 Hz, 2H, CH_2), 4.10 (t, J = 6.6 Hz, 2H, CH_2), 3.93 (t, J = 6.6 Hz, 2H, CH_2), 3.89 (t, J = 6.0 Hz, 2H, CH_2), 1.54 (s, 9H, (CH_3)$_3$) ppm.
^{13}C NMR (126 MHz, DMSO-d_6): δ 166.83, 158.82, 153.36, 152.45, 143.03, 142.93, 137.23, 136.50, 131.42, 117.64, 116.61, 112.61, 106.46, 104.15, 82.77, 67.51, 66.86, 66.58, 46.60, 27.67 ppm.

MS (ESI+) *m/z:* 441.00 $[M + H]^+$.
HRMS *m/z:* $[M + H]^+$ calcd for $C_{22}H_{25}N_4O_6$, 441.17686; found 441.17510.
HPLC (III): t_R = 15.136, purity ≥ 95%.

6.1.14 Synthesis of methyl (1^3Z,1^4E)-3,6-dioxa-9-aza-1(3,5)-pyrazolo[1,5-*a*]-pyrimidina-2(1,3)-benzenacyclononaphane-2^4-carboxylate (36).

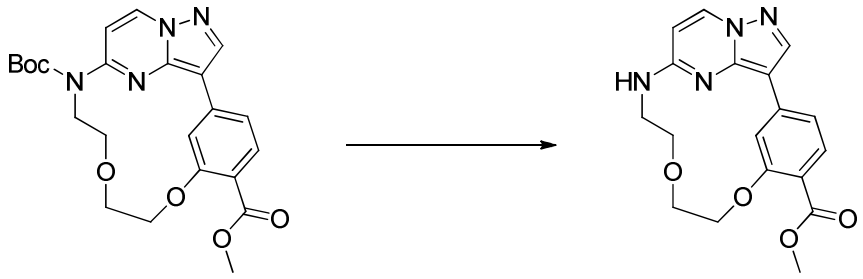

35 **36**

To a 0 °C cooled solution of 9-(*tert*-butyl) 2^4-methyl (1^3Z,1^4E)-3,6-dioxa-9-aza-1(3,5)-pyrazolo[1,5-*a*]pyrimidina-2(1,3)-benzenacyclononaphane-2^4,9-dicarboxylate (**35**) (1.05 g, 1.0 eq, 2.31 mmol) in dry methylene chloride (40 mL), trifluoroacetic acid (8.3 mL g, 47.0 eq, 108.59 mmol) was added dropwise and it was stirred for 16 h at room temperature. Afterwards the solvent was removed under reduced pressure and the residue was taken up in ethyl acetate. The organic phase was washed with saturated potassium carbonate solution and the aqueous phase was extracted with ethyl acetate. The combined organic phases were washed with brine was added to the stirring solution. Subsequently, the solution was filtrated and the solvent was removed again. The residue was taken up with ethyl acetate and it was washed with water and brine and dried over $MgSO_4$. After removal of the organic solvent under vacuum purification was done by flash column chromatography with a mobile phase of ethyl acetate (isocratic ratio). The title compound was yielded as a white solid (0.69 g, 84%).

^{1}H NMR (500 MHz, DMSO-d_6): δ 8.83 (d, J = 1.5 Hz, 1H, Het*H*), 8.57 (d, J = 7.6 Hz, 1H, Het*H*), 8.39 (s, 1H, Ph*H*), 7.94 (t, J = 5.4 Hz, 1H, N*H*), 7.70 (d, J = 8.1 Hz, 1H, Ph*H*), 7.29 (dd, J = 8.1, 1.4 Hz, 1H, Ph*H*), 6.34 (d, J = 7.6 Hz, 1H, Het*H*), 4.37 (t, J = 7.9 Hz, 2H, CH_2), 4.00 – 3.97 (m, 2H, CH_2), 3.89 – 3.86 (m, 2H, CH_2), 3.76 (s, 3H, OCH_3), 3.56 – 3.50 (m, 2H, CH_2) ppm.

^{13}C NMR (126 MHz, DMSO-d_6): δ 165.66, 158.08, 156.18, 145.33, 141.81, 139.04, 135.82, 131.61, 115.64, 114.82, 110.45, 103.40, 100.21, 65.35, 65.27, 51.57 ppm.

MS (ESI+) *m/z:* 354.96 $[M + H]^+$.
HRMS *m/z:* $[M + H]^+$ calcd for $C_{18}H_{19}N_4O_4$, 355.14008; found 355.14078.
HPLC (III): t_R = 12.868, purity ≥ 95%.

6.1.15 Synthesis of (1^3Z,1^4E)-3,6-dioxa-9-aza-1(3,5)-pyrazolo[1,5-*a*]pyrimidina-2(1,3)-benzenacyclononaphane-2^4-carboxylic acid (37).

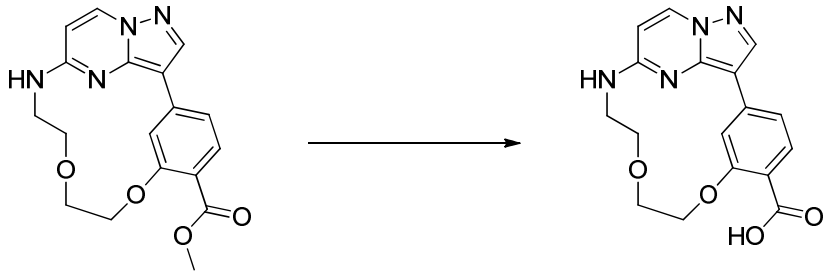

36 **37**

In tetrahydrofuran (10 mL) methyl (1^3Z,1^4E)-3,6-dioxa-9-aza-1(3,5)-pyrazolo[1,5-*a*]-pyrimidina-2(1,3)-benzenacyclononaphane-2^4-carboxylate (**36**) (150 mg, 10.0 eq, 0.42 mmol) and lithium hydroxide monohydrate (89 mg, 2.12 mmol) were dissolved and water (2 mL) was added. The reaction mix was stirred at 50 °C for 16 h. After that, the solvent was removed under reduced pressure and the residue was taken up in water. By adding 10% hydrochloric acid pH 1 was set and the precipitated solid was filtrated. Washing with water and drying of the filtrate resulted in the white solid tile compound (135 mg, 94%).

^{1}H NMR (500 MHz, DMSO-d_6): δ 12.24 (bs, 1H, COO*H*), 8.81 (s, 1H, Het*H*), 8.57 (d, J = 7.6 Hz, 1H, Het*H*), 8.38 (s, 1H, Ph*H*), 7.93 (t, J = 5.4 Hz, 1H, N*H*), 7.70 (d, J = 8.1 Hz, Ph*H*), 7.27 (dd, J = 8.1, 1.4 Hz, 1H, Ph*H*), 6.34 (d, J = 7.6 Hz, 1H, Het*H*), 4.38 (t, J = 7.1 Hz, 2H, CH_2), 3.99 (t, J = 7.5 Hz, 2H, CH_2), 3.89 – 3.86 (m, 2H, CH_2), 3.56 – 3.50 (m, 2H, CH_2) ppm.

^{13}C NMR (126 MHz, DMSO-d_6): δ 166.70, 158.07, 156.14, 145.27, 141.76, 138.69, 135.80, 131.82, 115.79, 115.61, 110.39, 103.50, 100.18, 65.31, 65.22, 63.89, 59.77 ppm.

MS (ESI+) *m/z:* 340.93 $[M + H]^+$.

HRMS *m/z:* $[M + H]^+$ calcd for $C_{17}H_{17}N_4O_4$, 341.12443; found 341.12573.

HPLC (III): t_R = 11.407, purity ≥ 95%.

6.1.16 Synthesis of (1^3Z,1^4E)-*N*-benzyl-3,6-dioxa-9-aza-1(3,5)-pyrazolo[1,5-*a*]-pyrimidina-2(1,3)-benzenacyclononaphane-2^4-carboxamide (61).

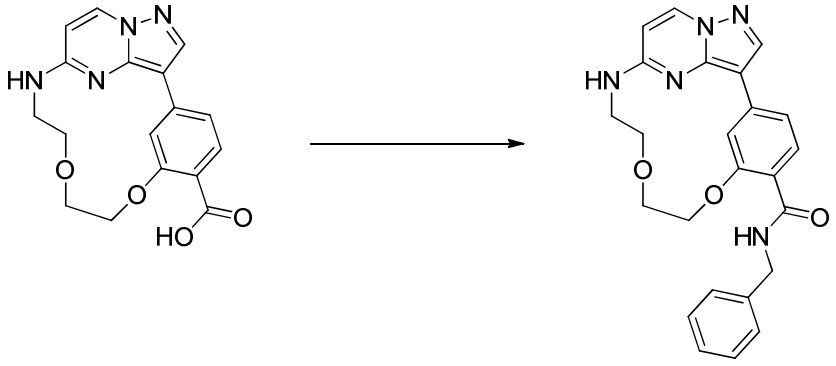

37 **61**

(1^3Z,1^4E)-3,6-dioxa-9-aza-1(3,5)-pyrazolo[1,5-*a*]pyrimidina-2(1,3)-benzenacyclononaphane-2^4-carboxylic acid (**37**) (35 mg, 1.0 eq, 0.09 mmol) was dissolved in dry dimethylformamide (5 mL) and dry *N,N*-diisopropylethylamine (29 mg, 2.4 eq, 0.22 mmol) as well as (1-[bis(dimethylamino)methylene]-1H-1,2,3-triazolo[4,5-*b*]pyridinium 3-oxide hexafluoro-phosphate (41 mg, 1.2 eq, 0.11 mmol) were added. The mixture was stirred for 1 h at room temperature under argon atmosphere. Afterwards benzylamine (12 mg, 1.2 eq, 0.11 mmol) was added and the mixture was stirred at room temperature for 18 h. After quenching with water and acidification with 1 N HCl, the precipitate was separated by vacuum filtration. The desired product was obtained as a white solid (33 mg, 75%).

^{1}H NMR (500 MHz, DMSO-d_6): δ 8.82 (d, J = 1.5 Hz, 1H, Ph*H*), 8.64 (t, J = 6.1 Hz, 1H, N*H*), 8.57 (d, J = 7.6 Hz, 1H, Het*H*), 8.38 (s, 1H, Het*H*), 7.91 (t, J = 5.4 Hz, 1H, N*H*), 7.83 (d, J = 8.1 Hz, 1H, Ph*H*), 7.33 (d, J = 4.5 Hz, 5H, Ph*H*), 7.27 – 7.19 (m, 1H, Ph*H*), 6.34 (d, J = 7.6 Hz, 1H, Het*H*), 4.52 (d, J = 6.1 Hz, 2H, CH_2), 4.50 – 4.43 (m, 2H, CH_2), 4.04 (dd, J = 9.1, 6.3 Hz, 2H, CH_2), 3.89 (dd, J = 9.2, 6.0 Hz, 2H, CH_2), 3.54 (q, J = 7.2, 6.8 Hz, 2H, CH_2) (ppm).

^{13}C NMR (126 MHz, DMSO-d_6): δ 164.69, 156.50, 156.10, 145.20, 141.66, 140.00, 137.64, 135.80, 131.11, 128.26, 127.02, 126.58, 117.92, 116.20, 110.02, 103.57, 100.15, 65.46, 65.36, 64.03 (ppm).

MS (ESI+) *m/z:* 429.95 $[M + H]^+$.
HRMS *m/z:* $[M + H]^+$ calcd for $C_{24}H_{23}N_5O_3$, 430.18737; found 430.18729.
HPLC (I): t_R = 13.843, purity ≥ 95%.

6.1.17 Synthesis of (1^3Z,1^4E)-*N*-(2-chlorobenzyl)-3,6-dioxa-9-aza-1(3,5)-pyrazolo-[1,5-*a*]pyrimidina-2(1,3)-benzenacyclononaphane-2^4-carboxamide (62).

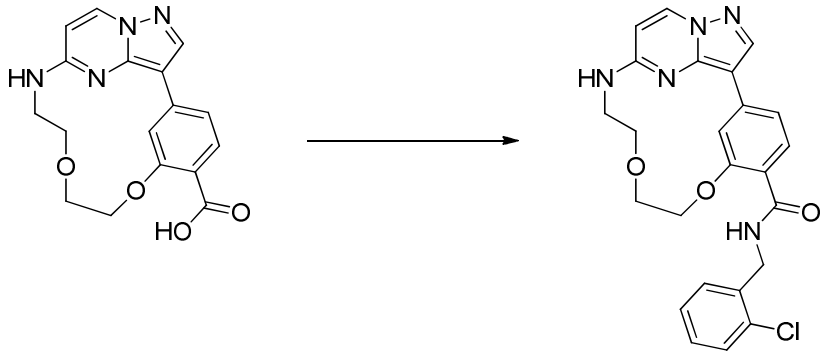

37 **62**

The title compound was synthesized according to the procedure of **61** using (2-chlorophenyl)methanamine (23 mg, 1.2 eq, 0.16 mmol). The desired product was obtained as a white solid (65 mg, 95%).

^{1}H NMR (500 MHz, DMSO-d_6): δ 8.84 (d, J = 1.5 Hz, 1H, Ph*H*), 8.72 (t, J = 6.1 Hz, 1H, N*H*), 8.57 (d, J = 7.6 Hz, 1H, Het*H*), 8.39 (s, 1H, Het*H*), 7.92 (t, J = 5.4 Hz, 1H, N*H*), 7.84 (d, J = 8.1 Hz, 1H, Ph*H*), 7.46 (dd, J = 7.8, 1.4 Hz, 1H, Ph*H*), 7.39 – 7.25 (m, 4H, Ph*H*), 6.34 (d, J = 7.6 Hz, 1H, Het*H*), 4.57 (d, J = 6.1 Hz, 2H, CH_2), 4.54 – 4.45 (m, 2H, CH_2), 4.12 – 4.00 (m, 2H, CH_2), 3.89 (m, 2H, CH_2), 3.54 (m, 2H, CH_2) (ppm).

^{13}C NMR (126 MHz, DMSO-d_6): δ 164.78, 162.32, 156.62, 156.12, 145.24, 141.68, 137.87, 136.75, 135.81, 131.84, 131.13, 129.08, 128.47, 128.43, 127.21, 117.55, 116.27, 110.10, 103.55, 100.17, 65.58, 65.41, 64.11, 40.69 (ppm).

MS (ESI+) *m/z:* 463.95 $[M + H]^+$.

HRMS *m/z:* $[M + H]^+$ calcd for $C_{24}H_{22}ClN_5O_3$, 464.14839; found 464.14780.

HPLC (I): t_R = 14.851, purity ≥ 95%.

6.1.18 Synthesis of (1^3Z,1^4E)-*N*-(3-chlorobenzyl)-3,6-dioxa-9-aza-1(3,5)-pyrazolo-[1,5-*a*]pyrimidina-2(1,3)-benzenacyclononaphane-2^4-carboxamide (63).

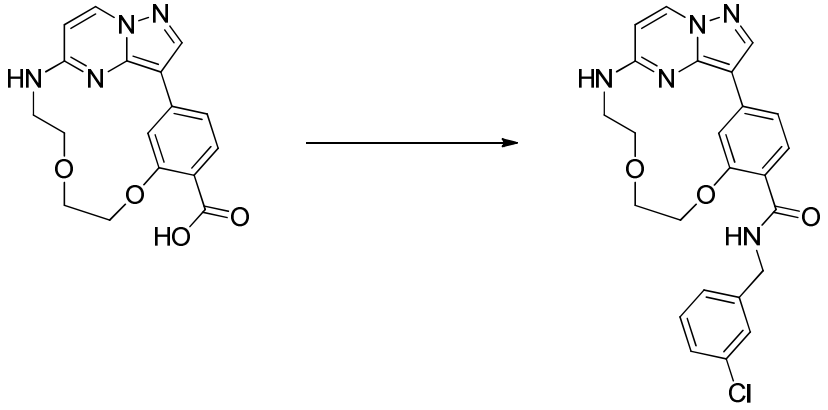

37 **63**

The title compound was synthesized according to the procedure of **61** using (3-chlorophenyl)methanamine (23 mg, 1.2 eq, 0.16 mmol). The desired product was obtained as a white solid (64 mg, 94%).

^{1}H NMR (500 MHz, DMSO-d_6): δ 8.83 (d, J = 1.5 Hz, 1H, Ph*H*), 8.71 (t, J = 6.2 Hz, 1H, N*H*), 8.57 (d, J = 7.6 Hz, 1H Het*H*), 8.38 (s, 1H, Het*H*), 7.91 (t, J = 5.4 Hz, 1H, N*H*), 7.80 (d, J = 8.1 Hz, 1H, Ph*H*), 7.43 – 7.25 (m, 5H, Ph*H*), 6.34 (d, J = 7.6 Hz, 1H, Het*H*), 4.54 – 4.43 (m, 4H, CH_2), 4.10 – 4.00 (m, 2H, CH_2), 3.95 – 3.84 (m, 2H, CH_2), 3.61 – 3.48 (m, 2H, CH_2) (ppm).

^{13}C NMR (126 MHz, DMSO-d_6): δ 164.89, 156.45, 156.10, 145.21, 142.76, 141.66, 137.67, 135.81, 132.92, 131.00, 130.15, 126.85, 126.50, 125.75, 117.96, 116.19, 110.00, 103.57, 100.15, 65.41, 64.03, 42.10 (ppm).

MS (ESI+) *m/z:* 464.00 $[M + H]^+$.

HRMS *m/z:* $[M + H]^+$ calcd for $C_{24}H_{22}ClN_5O_3$, 464.14839; found 464.14759.

HPLC (I): t_R = 14.783, purity ≥ 95%.

6.1.19 Synthesis of (1³*Z*,1⁴*E*)-*N*-(3-bromobenzyl)-3,6-dioxa-9-aza-1(3,5)-pyrazolo-[1,5-*a*]pyrimidina-2(1,3)-benzenacyclononaphane-2⁴-carboxamide (64).

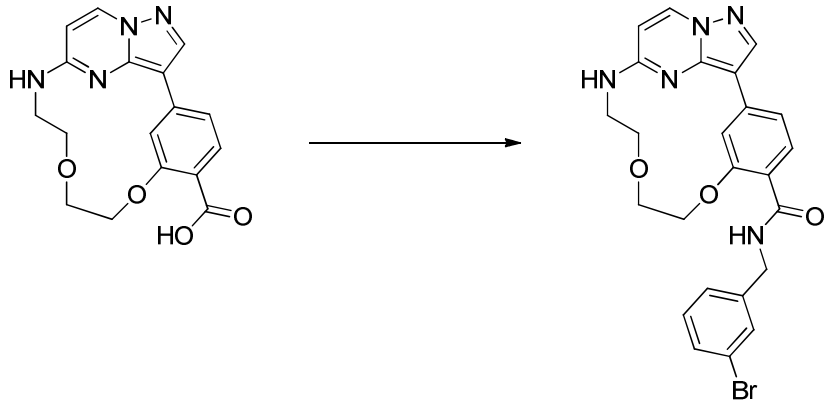

37 **64**

The title compound was synthesized according to the procedure of **61** using (3-chlorophenyl)methanamine (26 mg, 1.2 eq, 0.14 mmol). The desired product was obtained as a white solid (48 mg, 80%).

^{1}H NMR (500 MHz, DMSO-*d*$_6$): δ 8.83 (d, *J* = 1.5 Hz, 1H, Ph*H*), 8.70 (t, *J* = 6.2 Hz, 1H, N*H*), 8.56 (d, *J* = 7.6 Hz, 1H, Het*H*), 8.37 (s, 1H, Het*H*), 7.90 (t, *J* = 5.4 Hz, 1H, N*H*), 7.79 (d, *J* = 8.1 Hz, 1H, Ph*H*), 7.53 (t, *J* = 1.8 Hz, 1H, Ph*H*), 7.43 (dt, *J* = 7.6, 1.7 Hz, 1H, Ph*H*), 7.35 – 7.27 (m, 3H, Ph*H*), 6.34 (d, *J* = 7.6 Hz, 1H, Het*H*), 4.52 – 4.48 (m, 4H, C*H*$_2$), 4.09 – 4.01 (m, 2H, C*H*$_2$), 3.93 – 3.84 (m, 2H, C*H*$_2$), 3.56 – 3.51 (m, 2H, C*H*$_2$) (ppm).

^{13}C NMR (126 MHz, DMSO-*d*$_6$): δ 164.97, 156.48, 156.13, 145.24, 143.03, 141.67, 137.69, 135.80, 131.01, 130.48, 129.76, 129.42, 126.19, 121.62, 118.03, 116.23, 110.06, 103.60, 100.19, 65.51, 65.45, 64.15, 42.09, 35.82 (ppm).

MS (ESI+) *m/z:* 510.20 $[M + H]^+$.

HRMS *m/z:* $[M + H]^+$ calcd for $C_{24}H_{23}BrN_5O_3$, 508.09788; found 508.09719.

HPLC (I): t_R = 13.925, purity ≥ 95%.

6.1.20 Synthesis of (1^3Z,1^4E)-*N*-(3-cyanobenzyl)-3,6-dioxa-9-aza-1(3,5)-pyrazolo-[1,5-*a*]pyrimidina-2(1,3)-benzenacyclononaphane-2^4-carboxamide (65).

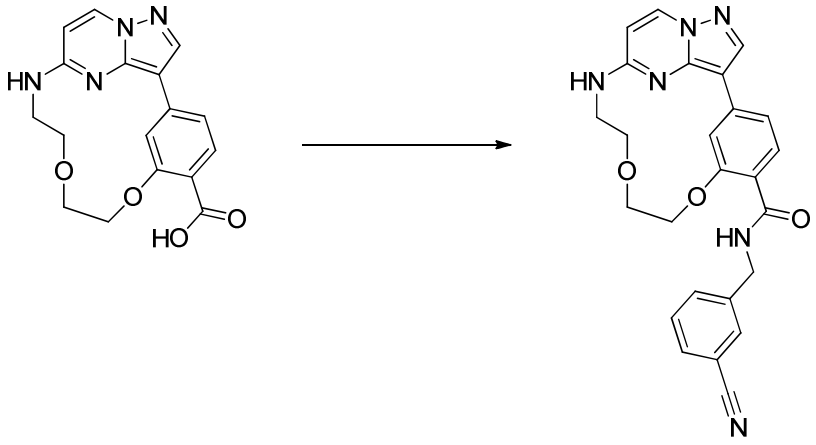

37 **65**

The title compound was synthesized according to the procedure of **61** using (3-chlorophenyl)methanamine (18 mg, 1.2 eq, 0.14 mmol). The desired product was obtained as a white solid (38 mg, 71%).

^{1}H NMR (500 MHz, DMSO-d_6): δ 8.83 (d, J = 1.5 Hz, 1H, Ph*H*), 8.75 (t, J = 6.2 Hz, 1H, N*H*), 8.55 (d, J = 7.6 Hz, 1H, Het*H*), 8.37 (s, 1H, Het*H*), 7.90 (t, J = 5.4 Hz, 1H, N*H*), 7.80 (d, J = 8.1 Hz, 1H, Ph*H*), 7.77 – 7.75 (m, 1H, Ph*H*), 7.69 (td, J = 16.0, 8.0, 1.5 Hz, 2H, Ph*H*), 7.55 (t, J = 7.7 Hz, 1H, N*H*), 7.32 (dd, J = 8.1, 1.4 Hz, 1H, Ph*H*), 6.34 (d, J = 7.6 Hz, 1H, Het*H*), 4.55 (d, J = 6.2 Hz, 2H, CH_2), 4.52 – 4.47 (m, 2H, CH_2), 4.08 – 4.01 (m, 2H, CH_2), 3.91 – 3.85 (m, 2H, CH_2), 3.56 – 3.51 (m, 2H, CH_2) (ppm).

^{13}C NMR (126 MHz, DMSO-d_6): δ 165.07, 156.54, 156.13, 145.24, 141.87, 141.66, 137.76, 135.79, 132.11, 131.02, 130.61, 130.43, 129.56, 118.96, 117.88, 116.22, 111.17, 111.16, 110.05, 103.59, 100.19, 65.53, 65.45, 64.14, 42.08 (ppm).

MS (ESI+) *m/z:* 455.20 $[M + H]^+$.

HRMS *m/z:* $[M + H]^+$ calcd for $C_{25}H_{23}N_6O_3$, 455.18262; found 455.18168.

HPLC (I): t_R = 12.938, purity ≥ 95%.

6.1.21 Synthesis of (1^3*Z*,1^4*E*)-*N*-(4-chlorobenzyl)-3,6-dioxa-9-aza-1(3,5)-pyrazolo-[1,5-*a*]pyrimidina-2(1,3)-benzenacyclononaphane-2^4-carboxamide (66).

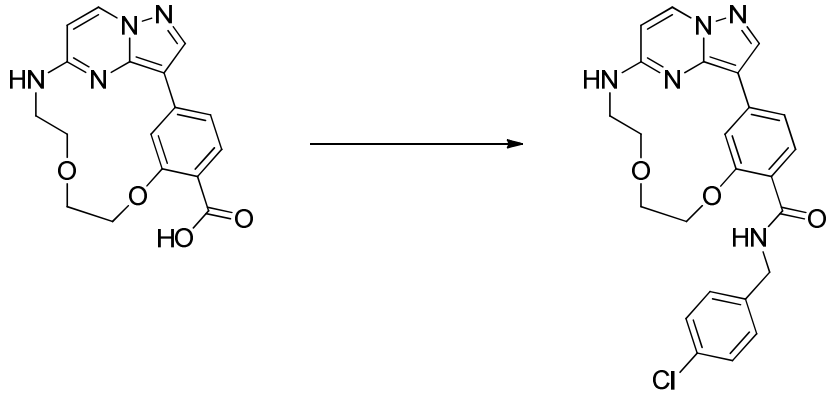

37 **66**

The title compound was synthesized according to the procedure of **61** using (4-chlorophenyl)methanamine (23 mg, 1.2 eq, 0.16 mmol). The desired product was obtained as a white solid (66 mg, 97%).

^{1}H NMR (500 MHz, DMSO-d_6): δ 8.82 (d, J = 1.5 Hz, 1H, Ph*H*), 8.69 (t, J = 6.2 Hz, 1H, N*H*), 8.56 (d, J = 7.6 Hz, 1H, Het*H*), 8.37 (s, 1H, Het*H*), 7.93 (t, J = 5.4 Hz, 1H, N*H*), 7.82 (d, J = 8.1 Hz, 1H, Ph*H*), 7.41 – 7.28 (m, 5H, Ph*H*), 6.34 (d, J = 7.6 Hz, 1H, Het*H*), 4.55 – 4.43 (m, 4H, CH_2), 4.07 – 4.00 (m, 2H, CH_2), 3.94 – 3.84 (m, 2H, CH_2), 3.59 – 3.49 (m, 2H, CH_2) (ppm).

^{13}C NMR (126 MHz, DMSO-d_6): δ 164.80, 156.54, 156.12, 145.23, 141.68, 139.15, 137.73, 135.80, 131.12, 131.10, 130.91, 128.97, 128.64, 128.21, 117.80, 116.20, 110.02, 103.58, 100.18, 65.46, 65.38, 64.04, 42.03 (ppm).

MS (ESI+) *m/z:* 463.97 $[M + H]^+$.

HRMS *m/z:* $[M + H]^+$ calcd for $C_{24}H_{22}ClN_5O_3$, 464.14839; found 464.14798.

HPLC (I): t_R = 14.814, purity ≥ 95%.

6.1.22 Synthesis of (1^3*Z*,1^4*E*)-*N*-(2,4-dichlorobenzyl)-3,6-dioxa-9-aza-1(3,5)-pyrazolo[1,5-*a*]pyrimidina-2(1,3)-benzenacyclononaphane-2^4-carboxamide (67).

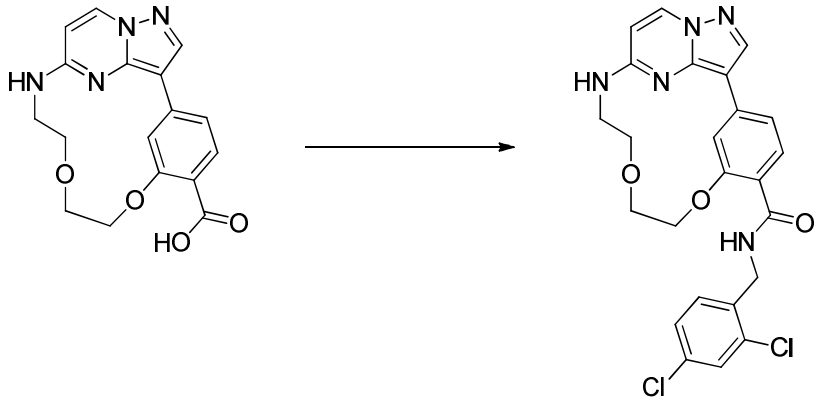

37 **67**

The title compound was synthesized according to the procedure of **61** using 2,4-dichlorobenzylamine (28 mg, 1.2 eq, 0.16 mmol). The desired product was obtained as a white solid (53 mg, 72%).

^{1}H NMR (500 MHz, DMSO-*d*$_6$): δ 8.84 (d, *J* = 1.4 Hz, 1H, Ph*H*), 8.74 (t, *J* = 6.1 Hz, 1H, N*H*), 8.57 (d, *J* = 7.6 Hz, 1H, Het*H*), 8.39 (s, 1H, Het*H*), 7.92 (t, *J* = 5.4 Hz, 1H, N*H*), 7.82 (d, *J* = 8.1 Hz, 1H, Ph*H*), 7.63 (d, *J* = 2.2 Hz, 1H, Ph*H*), 7.44 (dd, *J* = 8.4, 2.2 Hz, 1H, Ph*H*), 7.36 (d, *J* = 8.4 Hz, 1H, Ph*H*), 7.33 (dd, *J* = 8.2, 1.4 Hz, 1H, Ph*H*), 6.34 (d, *J* = 7.6 Hz, 1H, Het*H*), 4.54 (d, *J* = 6.1 Hz, 2H, C*H*$_2$), 4.52 – 4.47 (m, 2H, C*H*$_2$), 4.12 – 3.99 (m, 2H, C*H*$_2$), 3.94 – 3.84 (m, 2H, C*H*$_2$), 3.61 – 3.48 (m, 2H, C*H*$_2$) (ppm).

^{13}C NMR (126 MHz, DMSO-*d*$_6$): δ 164.86, 156.63, 156.13, 145.25, 141.70, 137.92, 136.07, 135.82, 132.68, 131.95, 131.11, 129.84, 128.51, 127.38, 117.46, 116.26, 110.08, 103.55, 100.17, 65.55, 65.40, 64.09 (ppm).

MS (ESI+) *m/z:* 598.01 $[M + H]^+$.

HRMS *m/z:* $[M + H]^+$ calcd for $C_{24}H_{23}Cl_2N_5O_3$, 499.11278; found 499.11153.

HPLC (I): t_R = 16.058, purity ≥ 95%.

6.1.23 Synthesis of (1^3Z,1^4E)-*N*-(4-chloro-2-fluorobenzyl)-3,6-dioxa-9-aza-1(3,5)-pyrazolo[1,5-*a*]pyrimidina-2(1,3)-benzenacyclononaphane-2^4-carboxamide (68).

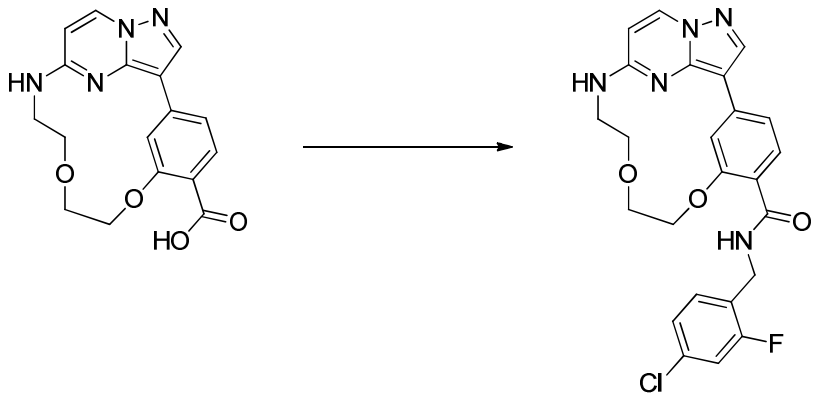

37 **68**

The title compound was synthesized according to the procedure of **61** using (4-chloro-2-fluorophenyl)methanamine (25 mg, 1.2 eq, 0.16 mmol). The desired product was obtained as a white solid (53 mg, 75%).

^{1}H NMR (500 MHz, DMSO-d_6): δ 8.83 (d, J = 1.5 Hz, 1H, Ph*H*), 8.68 (t, J = 6.1 Hz, 1H, N*H*), 8.57 (d, J = 7.6 Hz, 1H, Het*H*), 8.38 (s, 1H, Het*H*), 7.92 (t, J = 5.4 Hz, 1H, N*H*), 7.81 (d, J = 8.1 Hz, 1H, Ph*H*), 7.41 (dd, J = 10.1, 2.1 Hz, 1H, Ph*H*), 7.37 (t, J = 8.3 Hz, 1H, Ph*H*), 7.32 (dd, J = 8.1, 1.4 Hz, 1H, Ph*H*), 7.28 (dd, J = 8.3, 2.0 Hz, 1H, Ph*H*), 6.34 (d, J = 7.6 Hz, 1H, Het*H*), 4.55 – 4.44 (m, 4H, CH_2), 4.12 – 3.98 (m, 2H, CH_2), 3.96 – 3.83 (m, 2H, CH_2), 3.60 – 3.49 (m, 2H, CH_2) (ppm).

^{13}C NMR (126 MHz, DMSO-d_6): δ 164.89, 160.75, 158.78, 156.59, 156.12, 145.24, 141.69, 137.86, 135.81, 131.94, 131.09, 130.39, 126.03, 124.62, 117.56, 116.22, 115.74, 115.54, 110.04, 103.55, 100.17, 65.49, 65.38, 64.05 (ppm). MS (ESI+) *m/z:* 482.10 $[M + H]^+$.

MS (ESI+) *m/z:* 482.05 $[M + H]^+$.

HRMS *m/z:* $[M + H]^+$ calcd for $C_{24}H_{21}ClFN_5O_3$, 482.13897; found 482.13833.

HPLC (I): t_R = 15.182, purity ≥ 95%.

6.1.24 Synthesis of (1^3Z,1^4E)-*N*-(4-chloro-2-methylbenzyl)-3,6-dioxa-9-aza-1(3,5)-pyrazolo[1,5-*a*]pyrimidina-2(1,3)-benzenacyclononaphane-2^4-carboxamide (69).

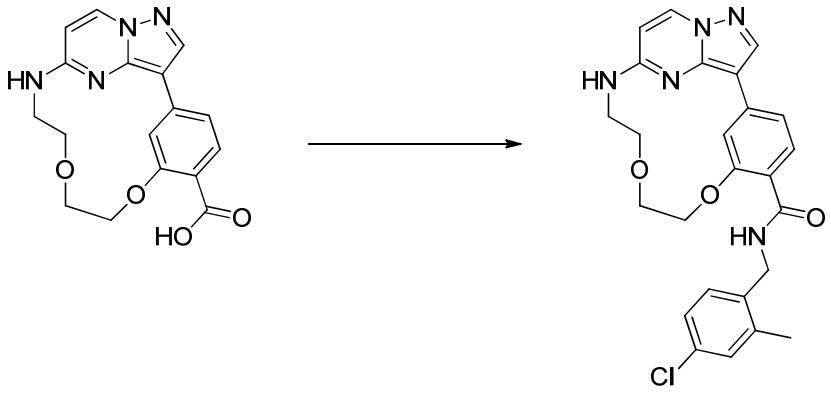

37 **69**

The title compound was synthesized according to the procedure of **61** using (4-chloro-2-methylphenyl)methanamine (25 mg, 1.2 eq, 0.16 mmol). The desired product was obtained as a white solid (57 mg, 81%).

^{1}H NMR (500 MHz, DMSO-d_6): δ 8.82 (d, J = 1.5 Hz, 1H, Ph*H*), 8.62 – 8.54 (m, 2H, N*H*, Het*H*), 8.38 (s, 1H, Het*H*), 7.91 (t, J = 5.4 Hz, 1H, N*H*), 7.80 (d, J = 8.1 Hz, 1H, Ph*H*), 7.32 (dd, J = 8.1, 1.4 Hz, 1H, Ph*H*), 7.28 – 7.20 (m, 3H, Ph*H*), 6.34 (d, J = 7.5 Hz, 1H, Het*H*), 4.52 – 4.42 (m, 4H, CH_2), 4.09 – 4.00 (m, 2H, CH_2), 3.94 – 3.84 (m, 2H, CH_2), 3.59 – 3.49 (m, 2H, CH_2), 2.33 (s, 3H, CH_3) (ppm).

^{13}C NMR (126 MHz, DMSO-d_6): δ 164.74, 156.47, 156.09, 145.22, 145.20, 141.67, 137.75, 137.66, 136.71, 135.81, 131.02, 130.80, 129.33, 128.62, 125.58, 117.96, 116.22, 110.05, 103.58, 100.16, 65.49, 65.38, 64.05, 18.41 (ppm).

MS (ESI+) *m/z:* 478.09 $[M + H]^+$.

HRMS *m/z:* $[M + H]^+$ calcd for $C_{25}H_{24}ClN_5O_3$, 478.16404; found 478.16341.

HPLC (I): t_R = 15.436, purity ≥ 95%.

6.1.25 Synthesis of (1^3*Z*,1^4*E*)-*N*-(3,5-dichlorobenzyl)-3,6-dioxa-9-aza-1(3,5)-pyrazolo[1,5-*a*]pyrimidina-2(1,3)-benzenacyclononaphane-2^4-carboxamide (70).

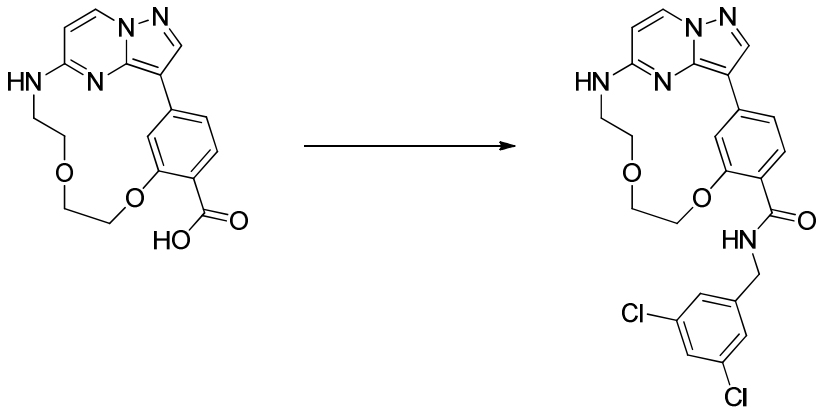

37 **70**

The title compound was synthesized according to the procedure of **61** using (3,5-dichlorophenyl)methanamine (22 mg, 1.2 eq, 0.12 mmol). The desired product was obtained as a white solid (39 mg, 76%).

^{1}H NMR (500 MHz, DMSO-d_6): δ 8.83 (d, J = 1.5 Hz, 1H, Ph*H*), 8.73 (t, J = 6.2 Hz, 1H, N*H*), 8.56 (d, J = 7.6 Hz, 1H, Het*H*), 8.37 (s, 1H, Het*H*), 7.90 (t, J = 5.4 Hz, 1H, N*H*), 7.77 (d, J = 8.0 Hz, 1H, Ph*H*), 7.47 (t, J = 2.0 Hz, 1H, Ph*H*), 7.39 (d, J = 1.9 Hz, 2H, Ph*H*), 7.32 (dd, J = 8.1, 1.4 Hz, 1H, Ph*H*), 6.34 (d, J = 7.6 Hz, 1H, Het*H*), 4.56 – 4.43 (m, 4H, CH_2), 4.10 – 4.00 (m, 2H, CH_2), 3.95 – 3.83 (m, 2H, CH_2), 3.60 – 3.49 (m, 2H, CH_2) (ppm).

^{13}C NMR (126 MHz, DMSO-d_6): δ 165.06, 156.41, 156.08, 145.20, 144.64, 141.62, 137.71, 135.76, 133.83, 130.89, 126.16, 125.85, 117.93, 116.18, 110.00, 103.54, 100.13, 65.43, 65.40, 64.09, 41.80 (ppm).

MS (ESI+) *m/z:* 498.20 $[M + H]^+$.

HRMS *m/z:* $[M + H]^+$ calcd for $C_{24}H_{22}Cl_2N_5O_3$, 498.10942; found 498.10905.

HPLC (I): t_R = 14.624, purity ≥ 95%.

6.1.26 Synthesis of (1^3Z,1^4E)-*N*-(3-chloro-5-fluorobenzyl)-3,6-dioxa-9-aza-1(3,5)-pyrazolo[1,5-*a*]pyrimidina-2(1,3)-benzenacyclononaphane-2^4-carboxamide (71).

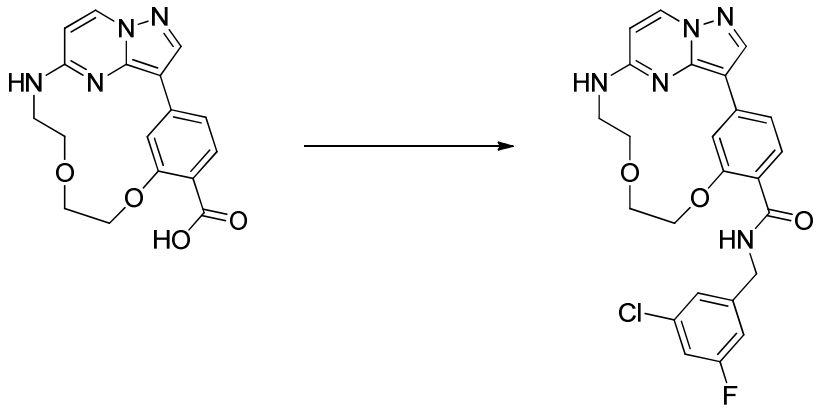

37 **71**

The title compound was synthesized according to the procedure of **61** using (3-chloro-5-fluorophenyl)methanamine (23 mg, 1.2 eq, 0.14 mmol). The desired product was obtained as a white solid (30 mg, 53%).

^{1}H NMR (500 MHz, DMSO-d_6): δ 8.83 (d, J = 1.5 Hz, 1H, Ph*H*), 8.74 (t, J = 6.2 Hz, 1H, N*H*), 8.55 (d, J = 7.5 Hz, 1H, Het*H*), 8.37 (s, 1H, Het*H*), 7.90 (t, J = 5.4 Hz, 1H, N*H*), 7.78 (d, J = 8.1 Hz, 1H, Ph*H*), 7.32 (dd, J = 8.2, 1.4 Hz, 1H, Ph*H*), 7.28 (dt, J = 8.6, 2.2 Hz, 1H, Ph*H*), 7.26 – 7.25 (m, 1H, Ph*H*), 7.18 – 7.13 (m, 1H, Ph*H*), 6.34 (d, J = 7.6 Hz, 1H, Het*H*), 4.52 – 4.47 (m, 4H, CH_2), 4.09 – 4.00 (m, 2H, CH_2), 3.93 – 3.84 (m, 2H, CH_2), 3.56 – 3.51 (m, 2H, CH_2) (ppm).

^{13}C NMR (126 MHz, DMSO-d_6): δ 165.55, 163.59, 161.63, 156.94, 156.57, 145.68, 145.47, 145.40, 142.09, 138.22, 136.22, 134.20, 134.11, 131.43, 123.65, 123.63, 118.32, 116.67, 114.63, 114.43, 113.39, 113.21, 110.50, 104.02, 100.63, 65.95, 65.90, 64.59, 42.42 (ppm).

MS (ESI+) *m/z:* 482.20 $[M + H]^+$.

HRMS *m/z:* $[M + H]^+$ calcd for $C_{24}H_{22}ClFN_5O_3$, 482.13897; found 482.13835.

HPLC (I): t_R = 14.031, purity ≥ 95%.

6.1.27 Synthesis of (1^3Z,1^4E)-*N*-(2,3-dichlorobenzyl)-3,6-dioxa-9-aza-1(3,5)-pyrazolo[1,5-*a*]pyrimidina-2(1,3)-benzenacyclononaphane-2^4-carboxamide (72).

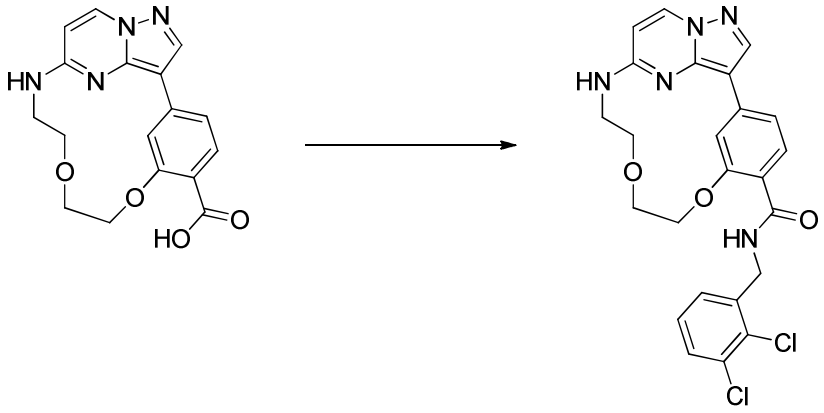

37 **72**

The title compound was synthesized according to the procedure of **61** using (2,3-dichlorophenyl)methanamine (25 mg, 1.2 eq, 0.14 mmol). The desired product was obtained as a white solid (46 mg, 79%).

^{1}H NMR (500 MHz, DMSO-d_6): δ 8.85 (d, J = 1.5 Hz, 1H, Ph*H*), 8.77 (t, J = 6.1 Hz, 1H, N*H*), 8.57 (d, J = 7.6 Hz, 1H, Het*H*), 8.38 (s, 1H, Het*H*), 7.91 (t, J = 5.4 Hz, 1H, N*H*), 7.83 (d, J = 8.1 Hz, 1H, Ph*H*), 7.55 (dd, J = 7.8, 1.8 Hz, 1H, Ph*H*), 7.40 – 7.30 (m, 3H, Ph*H*), 6.34 (d, J = 7.6 Hz, 1H, Het*H*), 4.60 (d, J = 6.1 Hz, 2H, CH_2), 4.53 – 4.48 (m, 2H, CH_2), 4.10 – 4.01 (m, 2H, CH_2), 3.93 – 3.86 (m, 2H, CH_2), 3.58 – 3.51 (m, 2H, CH_2) (ppm).

^{13}C NMR (126 MHz, DMSO-d_6): δ 164.84, 156.63, 156.10, 145.22, 141.65, 139.56, 137.91, 135.77, 131.57, 131.08, 129.66, 128.75, 128.09, 126.94, 117.44, 116.24, 110.09, 103.52, 100.15, 65.61, 65.44, 64.17, 41.39 (ppm).

MS (ESI+) *m/z:* 498.10 $[M + H]^+$.

HRMS *m/z:* $[M + H]^+$ calcd for $C_{24}H_{22}Cl_2N_5O_3$, 498.10942; found 498.10862.

HPLC (II): t_R = 9.533, purity ≥ 95%.

6.1.28 Synthesis of (1^3Z,1^4E)-*N*-(3-chloro-2-fluorobenzyl)-3,6-dioxa-9-aza-1(3,5)-pyrazolo[1,5-*a*]pyrimidina-2(1,3)-benzenacyclononaphane-2^4-carboxamide (73).

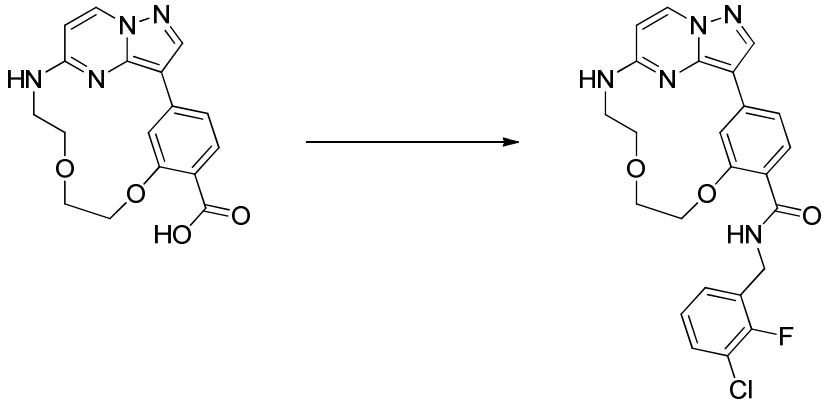

37 **73**

The title compound was synthesized according to the procedure of **61** using (3-chloro-2-fluorophenyl)methanamine (23 mg, 1.2 eq, 0.14 mmol). The desired product was obtained as a slightly yellow solid (38 mg, 67%).

^{1}H NMR (500 MHz, DMSO-d_6): δ 8.83 (d, J = 1.5 Hz, 1H, Ph*H*), 8.71 (t, J = 6.0 Hz, 1H, N*H*), 8.55 (d, J = 7.5 Hz, 1H, Het*H*), 8.37 (s, 1H, Het*H*), 7.90 (t, J = 4.9 Hz, 1H, N*H*), 7.81 (d, J = 8.1 Hz, 1H, Ph*H*), 7.46 (td, J = 7.6, 1.7 Hz, 1H, Ph*H*), 7.36 – 7.29 (m, 2H, Ph*H*), 7.23 – 7.17 (m, 1H, Ph*H*), 6.34 (d, J = 7.6 Hz, 1H, Het*H*), 4.57 (d, J = 6.0 Hz, 2H), 4.52 – 4.46 (m, 2H, CH_2), 4.07 – 4.01 (m, 2H, CH_2), 3.90 – 3.87 (m, 2H, CH_2), 3.54 – 3.52 (m, 2H, CH_2) (ppm).

^{13}C NMR (126 MHz, DMSO-d_6): δ 165.38, 157.07, 156.58, 145.69, 142.10, 138.33, 136.22, 131.55, 129.33, 129.27, 129.21, 128.38, 128.35, 125.70, 125.65, 125.62, 117.98, 116.69, 110.55, 104.01, 100.64, 66.05, 64.61, 37.05 (ppm).

MS (ESI+) *m/z:* 482.20 $[M + H]^+$.

HRMS *m/z:* $[M + H]^+$ calcd for $C_{24}H_{22}ClFN_5O_3$, 482.13897; found 482.13837.

HPLC (I): t_R = 13.927, purity ≥ 95%.

6.1.29 Synthesis of 1-((1^3*Z*,1^4*E*)-3,6-dioxa-9-aza-1(3,5)-pyrazolo[1,5-*a*]-pyrimidina-2(1,3)-benzenacyclononaphane-2^4-yl)-3-benzylurea (85).

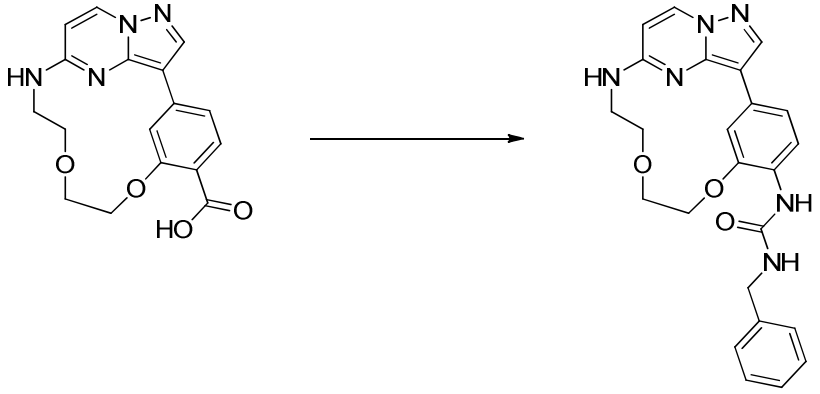

37 **85**

7(1^3*Z*,1^4*E*)-3,6-dioxa-9-aza-1(3,5)-pyrazolo[1,5-*a*]pyrimidina-2(1,3)-benzenacyclononaphane-2^4-carboxylic acid (50 mg, 1.0 eq, 0.13 mmol) (**37**) was dissolved in dry acetonitrile (10 mL) and triethylamine (27 mg, 2.0 eq, 0.26 mmol) as well as diphenylphosphoryl azide (47 mg, 1.3 eq, 0.17 mmol) were added. The mixture was stirred for 1.5 h at room temperature under argon atmosphere. Afterwards it was stirred under reflux for 1.5 h and benzylamine (21 mg, 1.5 eq, 0.20 mmol) was added. After another 1.5 h stirred under reflux, the solvent was removed under reduced pressure and the residue was taken up with ethyl acetate. It was washed with water and brine and the organic phase was dried over $MgSO_4$. After removement of the solvent in vacuo, the crude product was purified by flash reversed phase silica gel column chromatography with a mobile phase of acetonitrile and water (ratio gradually ranging from 1:9 to 1:2). The desired product was obtained as a white solid (23 mg, 35%).

^{1}H NMR (500 MHz, DMSO-d_6): δ 8.67 (d, J = 1.9 Hz, 1H, Ph*H*), 8.51 (d = 7.6 Hz, 1H, Het*H*), 8.24 (s, 1H, Het*H*), 8.04 (d, J = 8.3 Hz, 1H, Ph*H*), 7.95 (s, 1H, N*H*), 7.76 (t, J = 5.4 Hz, 1H, N*H*), 7.37 – 7.28 (m, 4H, Ph*H*), 7.27 – 7.21 (m, 2H, N*H*, Ph*H*), 7.12 (dd, J = 8.4, 1.8 Hz, 1H, Ph*H*), 6.28 (d, J = 7.6 Hz, 1H, Het*H*), 4.39 – 4.33 (m, 2H, CH_2), 4.29 (d, J = 5.1 Hz, 2H, CH_2), 4.03 – 3.96 (m, 2H, CH_2), 3.91 – 3.84 (m, 2H, CH_2), 3.56 – 3.48 (m, 2H, CH_2) (ppm).

^{13}C NMR (126 MHz, DMSO-d_6): δ 155.41, 155.17, 145.98, 144.19, 140.80, 140.29, 135.63, 128.36, 127.18, 126.77, 126.42, 126.13, 124.97, 118.42, 116.05, 109.62, 104.38, 99.70, 65.13, 64.99, 63.75, 42.75 (ppm).

MS (ESI+) *m/z:* 445.20 $[M + H]^+$.

HRMS *m/z:* $[M + H]^+$ calcd for $C_{24}H_{24}N_6O_3$, 445.19827; found 445.19666.

HPLC (I): t_R = 13.270, purity ≥ 95%.

6.1.30 Synthesis of 1-((1^3*Z*,1^4*E*)-3,6-dioxa-9-aza-1(3,5)-pyrazolo[1,5-*a*]-pyrimidina-2(1,3)-benzenacyclononaphane-2^4-yl)-3-(2-chlorobenzyl)urea (86).

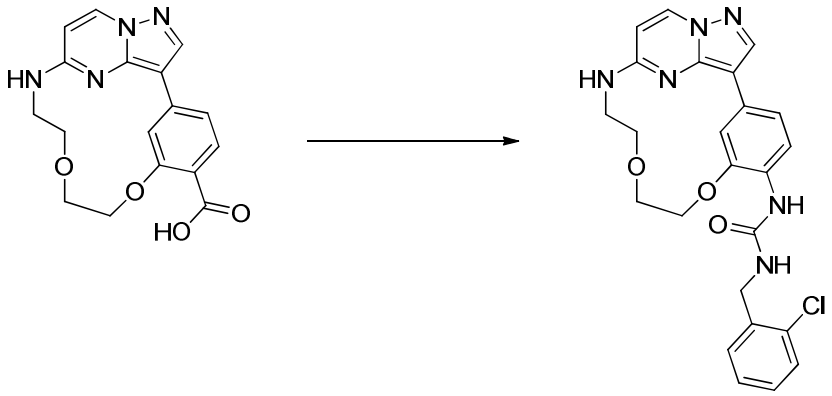

37 **86**

The synthesis of the title compound was carried out according to the procedure of **85** using (2-chlorophenyl)methanamine (28 mg, 1.5 eq, 0.20 mmol). Purification was done by flash reversed phase silica gel column chromatography with a mobile phase of acetonitrile and water (ratio gradually ranging from 1:9 to 1:2). The desired product was obtained as a white solid (20 mg, 28%).

^{1}H NMR (250 MHz, DMSO-*d*$_6$): δ 8.69 (d, *J* = 1.8 Hz, 1H, Ph*H*), 8.51 (d, *J* = 7.6 Hz, 1H, Het*H*), 8.23 (s, 1H, Het*H*), 8.06 (s, 1H, N*H*), 8.03 (d, *J* = 8.3 Hz, 1H, Ph*H*), 7.75 (t, *J* = 5.2 Hz, 1H, N*H*), 7.49 – 7.23 (m, 5H, N*H*, Ph*H*), 7.12 (d, *J* = 8.3 Hz, 1H, Ph*H*), 6.28 (d, *J* = 7.6 Hz, 1H, Het*H*), 4.46 – 4.28 (m, 4H, C*H*$_2$), 4.11 – 3.94 (m, 2H, C*H*$_2$), 3.94 – 3.80 (m, 2H, C*H*$_2$), 3.62 – 3.52 (m, 2H, C*H*$_2$) (ppm).

^{13}C NMR (126 MHz, DMSO-*d*$_6$): δ 155.41, 155.10, 146.05, 144.21, 140.80, 137.33, 135.62, 132.14, 129.15, 129.11, 128.66, 127.28, 126.55, 126.01, 118.46, 116.04, 109.63, 104.36, 99.71, 65.13, 65.01, 63.76, 40.73 (ppm).

MS (ESI+) *m/z:* 479.10 $[M + H]^+$.

HRMS *m/z:* $[M + H]^+$ calcd for $C_{24}H_{23}ClN_6O_3$, 479.15929; found 479.15793.

HPLC (I): t_R = 14.035, purity ≥ 95%.

6.1.31 Synthesis of 1-((1^3*Z*,1^4*E*)-3,6-dioxa-9-aza-1(3,5)-pyrazolo[1,5-*a*]-pyrimidina-2(1,3)-benzenacyclononaphane-2^4-yl)-3-(3-chlorobenzyl)urea (87).

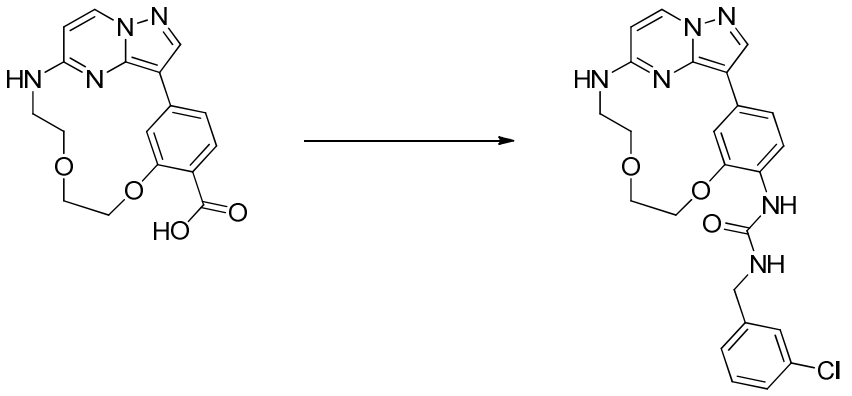

37 **87**

The synthesis of the title compound was carried out according to the procedure of **85** using (3-chlorophenyl)methanamine (47 mg, 1.5 eq, 0.17 mmol). Purification was done by flash reversed phase silica gel column chromatography with a mobile phase of acetonitrile and water (ratio gradually ranging from 1:9 to 1:2). The desired product was obtained as a white solid (21 mg, 30%).

^{1}H NMR (250 MHz, DMSO-d_6): δ 8.68 (d, J = 1.8 Hz, 1H, Ph*H*), 8.51 (d, J = 7.6 Hz, 1H, Het*H*), 8.24 (s, 1H, Het*H*), 8.02 (d, J = 8.4 Hz, 1H, Ph*H*), 7.98 (s, 1H, N*H*), 7.76 (t, J = 5.4 Hz, 1H, N*H*), 7.40 – 7.25 (m, 5H, N*H*, Ph*H*), 7.12 (dd, J = 8.3, 1.7 Hz, 1H, Ph*H*), 6.28 (d, J = 7.6 Hz, 1H, Het*H*), 4.42 – 4.33 (m, 2H, CH_2), 4.30 (d, J = 5.9 Hz, 2H, CH_2), 4.05 – 3.94 (m, 2H, CH_2), 3.93 – 3.83 (m, 2H, CH_2), 3.58 – 3.46 (m, 2H, CH_2) (ppm).

^{13}C NMR (126 MHz, DMSO-d_6): δ 55.42, 155.20, 146.10, 144.21, 143.12, 140.81, 135.62, 133.01, 130.26, 126.86, 126.67, 126.62, 125.96, 125.81, 118.56, 116.05, 109.64, 104.36, 99.71, 65.13, 65.00, 63.75, 42.19 (ppm).

MS (ESI+) *m/z:* 479.14 $[M + H]^+$.

HRMS *m/z:* [M rad] calcd for $C_{24}H_{23}ClN_6O_3$, 478.15147; found 478.14963.

HPLC (I): t_R = 14.043, purity ≥ 95%.

6.1.32 Synthesis of 1-((1^3*Z*,1^4*E*)-3,6-dioxa-9-aza-1(3,5)-pyrazolo[1,5-*a*]-pyrimidina-2(1,3)-benzenacyclononaphane-2^4-yl)-3-(4-chlorobenzyl)urea (88).

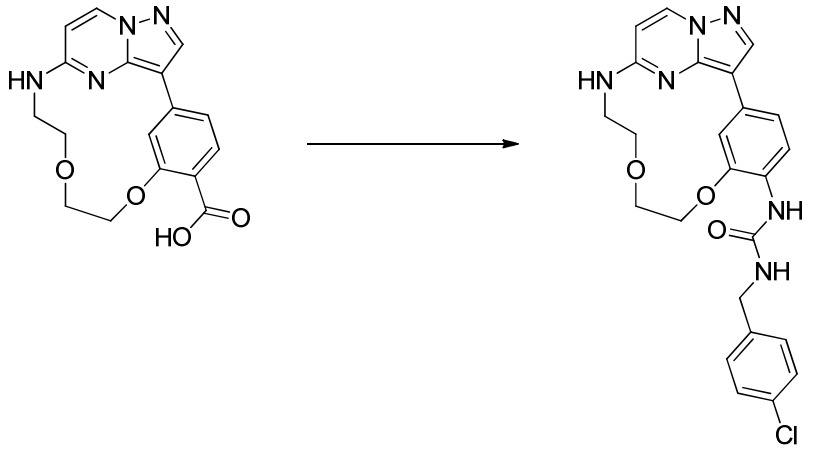

37 **88**

The synthesis of the title compound was carried out according to the procedure of **85** using (4-chlorophenyl)methanamine (47 mg, 1.5 eq, 0.17 mmol). Purification was done by flash reversed phase silica gel column chromatography with a mobile phase of acetonitrile and water (ratio gradually ranging from 1:9 to 1:2). The desired product was obtained as a white solid (13 mg, 19%).

^{1}H NMR (600 MHz, DMSO-d_6): δ 8.68 (s, 1H, Ph*H*), 8.50 (d, J = 7.6 Hz, 1H, Het*H*), 8.24 (s, 1H, Het*H*), 8.03 (d, J = 8.3 Hz, 1H, Ph*H*), 7.95 (s, 1H, N*H*), 7.75 (t, J = 5.3 Hz, 1H, N*H*), 7.48 – 7.22 (m, 5H, N*H*, Ph*H*), 7.12 (d, J = 8.4 Hz, 1H, Ph*H*), 6.28 (d, J = 7.5 Hz, 1H, Het*H*), 4.45 – 4.22 (m, 4H, CH_2), 4.07 – 3.81 (m, 4H, CH_2), 3.59 – 3.46 (m, 2H, CH_2) (ppm).

^{13}C NMR (151 MHz, DMSO-d_6): δ 155.38, 155.14, 146.07, 139.43, 135.54, 131.20, 128.98, 128.94, 128.90, 128.21, 126.54, 126.00, 121.82, 118.50, 115.99, 109.67, 104.35, 99.66, 65.24, 65.07, 63.88, 42.03 (ppm).

MS (ESI+) *m/z:* 479.14 $[M + H]^+$.

HRMS *m/z:* $[M + H]^+$ calcd for $C_{24}H_{23}ClN_6O_3$, 479.15929; found 479.15805.

HPLC (I): t_R = 14.072, purity ≥ 95%.

6.1.33 Synthesis of 1-((1^3*Z*,1^4*E*)-3,6-dioxa-9-aza-1(3,5)-pyrazolo[1,5-*a*]-pyrimidina-2(1,3)-benzenacyclononaphane-2^4-yl)-3-(2,4-dichlorobenzyl)-urea (89).

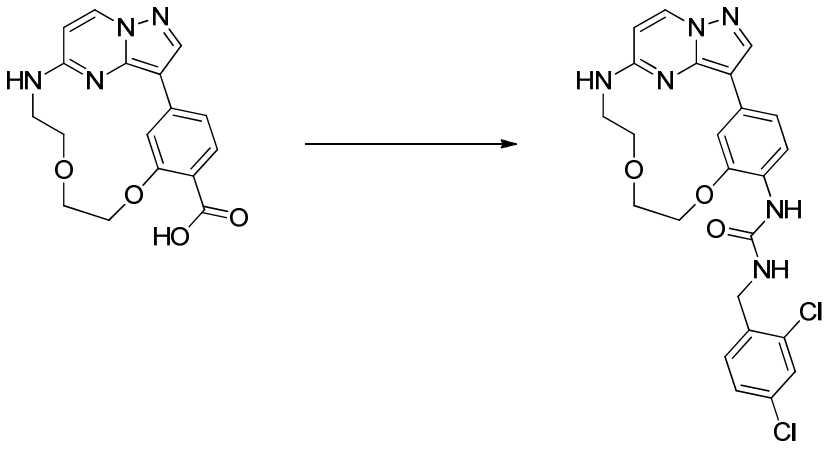

37 **89**

The synthesis of the title compound was carried out according to the procedure of **85** using 2,4-dichlorobenzylamine (35 mg, 1.5 eq, 0.20 mmol). Purification was done by flash reversed phase silica gel column chromatography with a mobile phase of acetonitrile and water (ratio gradually ranging from 1:9 to 1:2). The desired product was obtained as a white solid (20 mg, 27%).

^{1}H NMR (600 MHz, DMSO-*d*$_6$): δ 8.69 (d, *J* = 1.9 Hz, 1H, Ph*H*), 8.51 (d, *J* = 7.6 Hz, 1H, Het*H*), 8.23 (s, 1H, Het*H*), 8.06 (s, 1H, N*H*), 8.01 (d, *J* = 8.2 Hz, 1H, Ph*H*), 7.75 (t, *J* = 5.3 Hz, 1H, N*H*), 7.61 (d, *J* = 2.0 Hz, 1H, Ph*H*), 7.45 (dd, *J* = 8.3, 2.0 Hz, 1H, Ph*H*), 7.42 (d, *J* = 8.5 Hz, 1H, Ph*H*), 7.33 – 7.29 (m, 1H, N*H*), 7.11 (dd, *J* = 8.4, 1.8 Hz, 1H, Ph*H*), 6.28 (d, *J* = 7.6 Hz, 1H, Het*H*), 4.40 – 4.35 (m, 2H, C*H*$_2$), 4.34 (d, *J* = 5.8 Hz, 2H, C*H*$_2$), 4.02 – 3.96 (m, 2H, C*H*$_2$), 3.91 – 3.85 (m, 2H, C*H*$_2$), 3.55 – 3.48 (m, 2H, C*H*$_2$) (ppm).

^{13}C NMR (151 MHz, DMSO-*d*$_6$): δ 155.38, 155.04, 146.12, 144.18, 140.73, 136.59, 135.54, 132.94, 132.12, 130.34, 128.52, 127.34, 126.63, 125.88, 118.51, 115.98, 109.68, 106.48, 104.30, 99.66, 65.26, 65.10, 63.91, 40.27 (ppm).

MS (ESI+) *m/z:* 513.08 $[M + H]^+$.

HRMS *m/z:* $[M + H]^+$ calcd for $C_{24}H_{22}Cl_2N_6O_3$, 514.12368; found 514.10914.

HPLC (I): t_R = 15.028, purity ≥ 95%.

6.1.34 Synthesis of 1-((1^3*Z*,1^4*E*)-3,6-dioxa-9-aza-1(3,5)-pyrazolo[1,5-*a*]-pyrimidina-2(1,3)-benzenacyclononaphane-2^4-yl)-3-(2,4-dichloro-benzyl)urea (90).

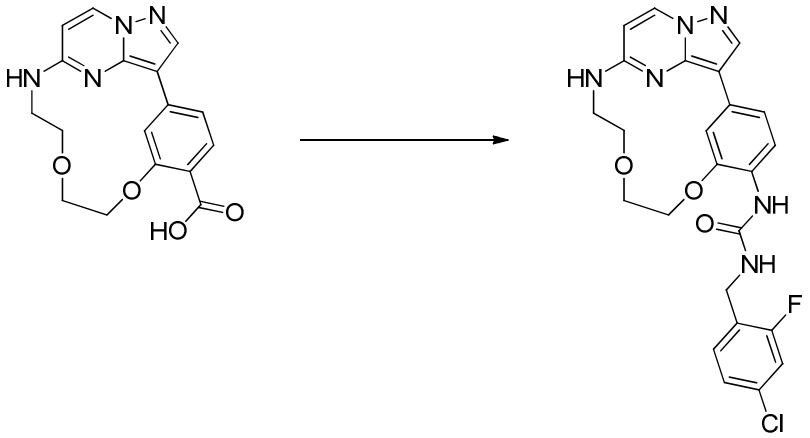

37 **90**

The synthesis of the title compound was carried out according to the procedure of **85** using (4-chloro-2-fluorophenyl)methanamine (32 mg, 1.5 eq, 0.17 mmol). Purification was done by flash reversed phase silica gel column chromatography with a mobile phase of acetonitrile and water (ratio gradually ranging from 1:9 to 1:2). The desired product was obtained as a white solid (23 mg, 32%).

^{1}H NMR (600 MHz, DMSO-*d*$_6$): δ 8.68 (d, *J* = 1.9 Hz, 1H, Ph*H*), 8.50 (d, *J* = 7.5 Hz, 1H, Het*H*), 8.23 (s, 1H, Het*H*), 8.04 – 7.97 (m, 2H, N*H*, Ph*H*), 7.76 (t, *J* = 5.4 Hz, 1H, N*H*), 7.44 – 7.37 (m, 2H, Ph*H*), 7.32 – 7.25 (m, 2H, N*H,* Ph*H*), 7.11 (dd, *J* = 8.3, 1.8 Hz, 1H, Ph*H*), 6.28 (d, *J* = 7.6 Hz, 1H, Het*H*), 4.40 – 4.34 (m, 2H, C*H*$_2$), 4.31 (d, *J* = 5.8 Hz, 2H, C*H*$_2$), 4.03 – 3.95 (m, 2H, C*H*$_2$), 3.92 – 3.82 (m, 2H, C*H*$_2$), 3.56 – 3.47 (m, 2H, C*H*$_2$) (ppm).

^{13}C NMR (151 MHz, DMSO-*d*$_6$): δ 155.38, 155.04, 146.08, 144.17, 140.72, 135.54, 130.78, 126.61, 126.34, 126.24, 125.90, 124.56, 118.50, 115.98, 115.77, 115.60, 109.68, 104.30, 99.66, 65.24, 65.07, 63.88, 36.28 (ppm).

MS (ESI+) *m/z:* 497.11 $[M + H]^+$.

HRMS *m/z:* $[M + H]^+$ calcd for $C_{24}H_{22}ClFN_6O_3$, 497.14816; found 497.14987.

HPLC (I): t_R = 14.367, purity ≥ 95%.

6.1.35 Synthesis of 1-((1³*Z*,1⁴*E*)-3,6-dioxa-9-aza-1(3,5)-pyrazolo[1,5-*a*]-pyrimidina-2(1,3)-benzenacyclononaphane-2⁴-yl)-3-(4-chloro-2-methyl-benzyl)urea (91).

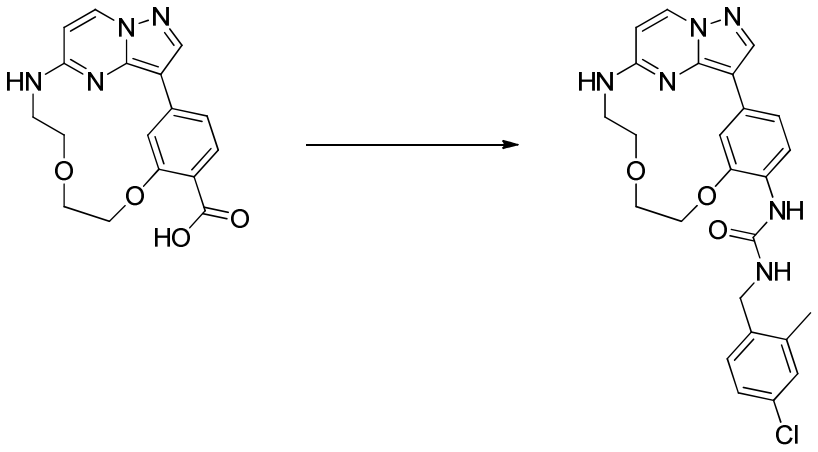

37 **91**

The synthesis of the title compound was carried out according to the procedure of **85** using (4-chloro-2-methylphenyl)methanamine (31 mg, 1.5 eq, 0.20 mmol). Purification was done by flash reversed phase silica gel column chromatography with a mobile phase of acetonitrile and water (ratio gradually ranging from 1:9 to 1:2). The desired product was obtained as a white solid (20 mg, 28%).

^{1}H NMR (500 MHz, DMSO-d_6): δ 8.67 (d, J = 1.9 Hz, 1H, Ph*H*), 8.51 (d, J = 7.6 Hz, 1H, Het*H*), 8.23 (s, 1H, Het*H*), 8.03 (d, J = 8.3 Hz, 1H, Ph*H*), 7.96 (s, 1H, N*H*), 7.76 (t, J = 5.3 Hz, 1H, N*H*), 7.28 – 7.22 (m, 3H, Ph*H*), 7.15 (t, J = 5.7 Hz, 1H, N*H*), 7.12 (dd, J = 8.4, 1.7 Hz, 1H, Ph*H*), 6.27 (d, J = 7.6 Hz, 1H, Het*H*), 4.43 – 4.32 (m, 2H, CH_2), 4.25 (d, J = 5.6 Hz, 2H, CH_2), 4.05 – 3.95 (m, 2H, CH_2), 3.94 – 3.83 (m, 2H, CH_2), 3.56 – 3.46 (m, 2H, CH_2), 2.30 (s, 3H, CH_3) (ppm).

^{13}C NMR (126 MHz, DMSO-d_6): δ 155.41, 155.04, 145.96, 144.20, 140.81, 138.13, 137.10, 135.64, 131.10, 129.47, 129.18, 126.45, 126.09, 125.62, 118.34, 116.05, 109.62, 104.37, 99.70, 65.12, 65.00, 63.75, 18.33 (ppm).

MS (ESI+) *m/z:* 493.17 $[M + H]^+$.

HRMS *m/z:* $[M + H]^+$ calcd for $C_{25}H_{25}ClN_6O_3$, 493.17494; found 493.17324.

HPLC (I): t_R = 14.631, purity ≥ 95%.

6.1.36 Synthesis of *N*-((1^3*Z*,1^4*E*)-3,6-dioxa-9-aza-1(3,5)-pyrazolo[1,5-*a*]-pyrimidina-2(1,3)-benzenacyclononaphane-2^4-yl)-4-methylpiperazine-1-carboxamide (92).

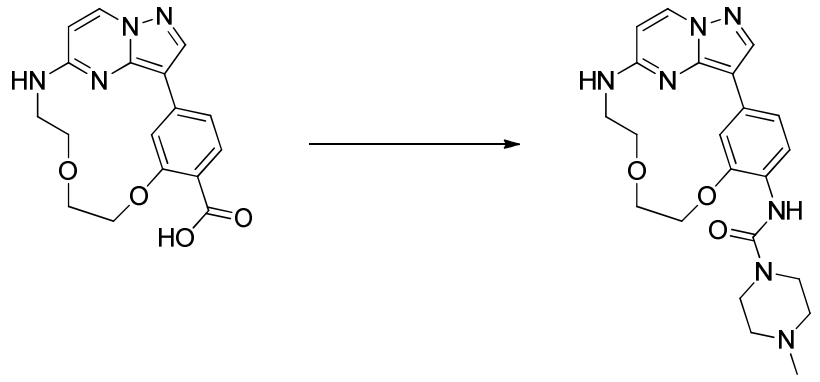

37 **92**

The synthesis of the title compound was carried out according to the procedure of **85** using 1-methylpiperazine (20 mg, 1.5 eq, 0.20 mmol). Purification was done by flash reversed phase silica gel column chromatography with a mobile phase of acetonitrile and water (ratio gradually ranging from 1:9 to 1:2). The desired product was obtained as a brownish solid (24 mg, 37%).

^{1}H NMR (500 MHz, DMSO-*d*$_6$): δ 8.69 (d, *J* = 1.9 Hz, 1H, Ph*H*), 8.52 (d, *J* = 7.6 Hz, 1H, Het*H*), 8.26 (s, 1H, Het*H*), 7.78 (t, *J* = 5.4 Hz, 1H, N*H*), 7.57 (s, 1H, N*H*), 7.56 (d, *J* = 8.2 Hz, 1H, Ph*H*), 7.14 (dd, *J* = 8.2, 1.8 Hz, 1H, Ph*H*), 6.28 (d, *J* = 7.6 Hz, 1H, Het*H*), 4.38 – 4.30 (m, 2H, C*H*$_2$), 4.04 – 3.94 (m, 2H, C*H*$_2$), 3.92 – 3.81 (m, 2H, C*H*$_2$), 3.57 – 3.47 (m, 2H, C*H*$_2$), 3.40 (t, *J* = 4.6 Hz, 4H, C*H*$_2$), 2.31 (t, *J* = 5.0 Hz, 4H, C*H*$_2$), 2.19 (s, 3H, C*H*$_3$) (ppm).

^{13}C NMR (126 MHz, DMSO-*d*$_6$): δ 155.53, 155.04, 149.15, 144.39, 140.96, 135.65, 135.52, 128.80, 125.03, 123.12, 115.79, 109.85, 104.27, 99.79, 65.16, 65.06, 63.86, 54.45, 45.78, 45.70, 43.58 (ppm).

MS (ESI+) *m/z:* 438.13 $[M + H]^+$.

HRMS *m/z:* [M rad] calcd for $C_{22}H_{27}N_7O_3$, 437.21699; found 437.21768.

HPLC (I): t_R = 8.250, purity ≥ 95%.

6.1.37 Synthesis of (1^3Z,1^4E)-*N*-(1-phenylethyl)-3,6-dioxa-9-aza-1(3,5)-pyrazolo[1,5-*a*]pyrimidina-2(1,3)-benzenacyclononaphane-2^4-carboxamide (107).

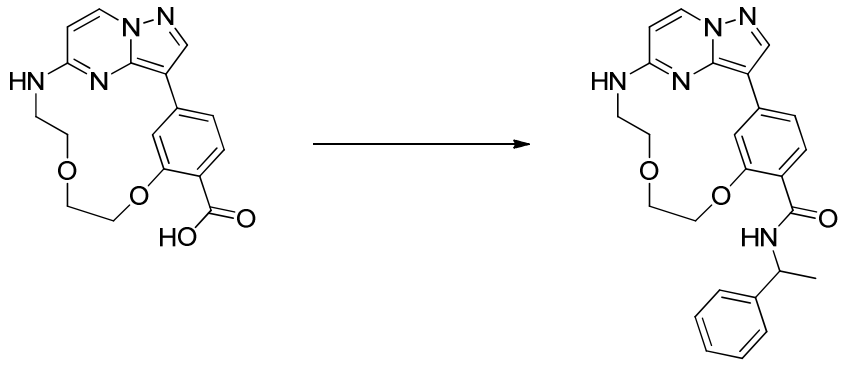

37 **107**

The title compound was synthesized according to the procedure of **61** using 1-phenylethanamine (*rac*) (17 mg, 1.2 eq, 0.14 mmol). The desired product was obtained as a white solid (38 mg, 72%).

^{1}H NMR (500 MHz, DMSO-d_6): δ 8.83 (d, J = 1.5 Hz, 1H, Ph*H*), 8.55 (d, J = 7.5 Hz, 1H, Het*H*), 8.38 (d, J = 8.0 Hz, 1H, N*H*), 8.37 (s, 1H, Het*H*), 7.90 (t, J = 5.4 Hz, 1H, N*H*), 7.74 (d, J = 8.1 Hz, 1H, Ph*H*), 7.41 – 7.30 (m, 5H, Ph*H*), 7.25 – 7.21 (m, 1H, Ph*H*), 6.34 (d, J = 7.6 Hz, 1H, Het*H*), 5.18 – 5.10 (m, 1H, C*H*), 4.52 – 4.44 (m, 2H, CH_2), 4.08 – 4.00 (m, 2H, CH_2), 3.94 – 3.85 (m, 2H, CH_2), 3.57 – 3.52 (m, 2H, CH_2), 1.47 (d, J = 7.0 Hz, 3H, CH_3) (ppm).

^{13}C NMR (126 MHz, DMSO-d_6): δ 163.91, 156.46, 156.12, 145.22, 144.81, 141.65, 137.56, 135.80, 130.84, 128.39, 126.69, 125.97, 125.94, 118.36, 116.32, 110.30, 103.59, 100.19, 65.89, 65.56, 64.32, 48.44, 35.83, 22.84 (ppm).

MS (ESI+) *m/z:* 444.20 $[M + H]^+$.

HRMS *m/z:* $[M + H]^+$ calcd for $C_{25}H_{26}N_5O_3$, 444.20302; found 444.20375.

HPLC (I): t_R = 13.596, purity ≥ 95%.

6.1.38 Synthesis of (1^3Z,1^4E)-*N*-((*S*)-1-phenylethyl)-3,6-dioxa-9-aza-1(3,5)-pyrazolo[1,5-*a*]pyrimidina-2(1,3)-benzenacyclononaphane-2^4-carboxamide (108).

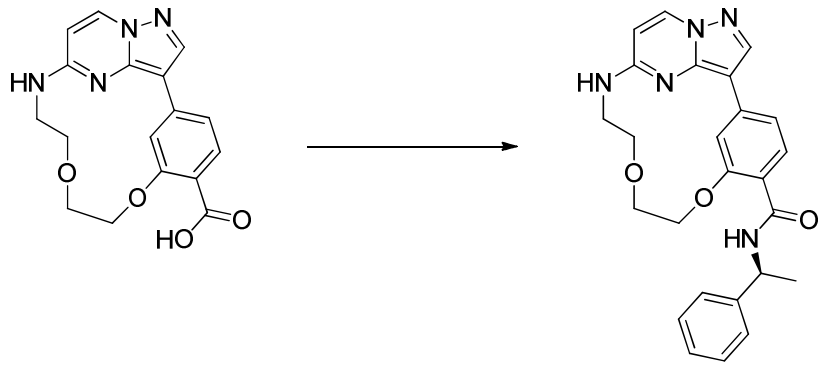

37 **108**

The title compound was synthesized according to the procedure of **61** using (*S*)-1-phenylethanamine (13 mg, 1.2 eq, 0.11 mmol). Purification was done by flash silica gel column chromatography with a mobile phase of ethyl acetate and ethanol with the addition of 1% acetic acid (ratio gradually ranging from 1:0 to 1:1). The obtained slightly yellow solid (32 mg, 82%) was the title compound.

^{1}H NMR (500 MHz, DMSO-d_6): δ 8.84 (s, 1H, Ph*H*), 8.56 (d, J = 7.5 Hz, 1H, Het*H*), 8.41 – 8.34 (m, 2H, Het*H*, N*H*), 7.91 (t, J = 5.4 Hz, 1H, N*H*), 7.75 (d, J = 8.0 Hz, 1H, Ph*H*), 7.41 – 7.30 (m, 5H, Ph*H*), 7.26 – 7.21 (m, 1H), 6.34 (d, J = 7.6 Hz, 1H, Het*H*), 5.14 (p, J = 7.1 Hz, 1H, C*H*), 4.56 – 4.42 (m, 2H, CH_2), 4.05 (t, J = 7.5 Hz, 2H, CH_2), 3.95 – 3.85 (m, 2H, CH_2), 3.59 – 3.51 (m, 2H, CH_2), 1.47 (d, J = 7.0 Hz, 3H, CH_3) (ppm).

^{13}C NMR (126 MHz, DMSO-d_6): δ 164.31, 156.89, 156.55, 145.66, 145.26, 142.09, 137.99, 136.24, 131.27, 128.82, 127.11, 126.40, 118.81, 116.74, 110.72, 104.02, 100.61, 66.28, 65.96, 64.72, 48.86, 23.28 (ppm).

MS (ESI+) *m/z:* 444.10 $[M + H]^+$.

HRMS *m/z:* $[M + Na]^+$ calcd for $C_{25}H_{25}N_5NaO_3$, 466.18496; found 466.18413.

HPLC (II): t_R = 8.938, purity ≥ 95%.

6.1.39 Synthesis of (1^3Z,1^4E)-*N*-((*R*)-1-phenylethyl)-3,6-dioxa-9-aza-1(3,5)-pyrazolo[1,5-*a*]pyrimidina-2(1,3)-benzenacyclononaphane-2^4-carboxamide (109).

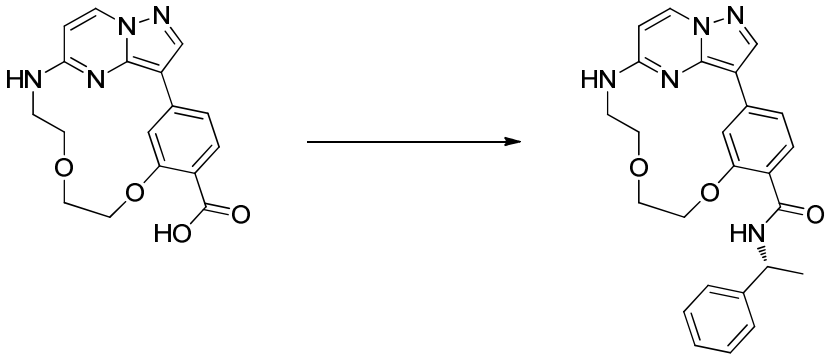

37 **109**

The title compound was synthesized according to the procedure of **61** using (*R*)-1-phenylethanamine (11 mg, 1.2 eq, 0.09 mmol). Purification was done by flash reversed phase silica gel column chromatography with a mobile phase of ethyl acetonitrile and water (ratio gradually ranging from 1:9 to 1:0. The title compound was obtained as a white solid (27 mg, 83%).

^{1}H NMR (500 MHz, DMSO-d_6): δ 8.84 (d, J = 1.5 Hz, 1H, Ph*H*), 8.56 (d, J = 7.6 Hz, 1H, Het*H*), 8.41 – 8.35 (m, 2H, Het*H*, N*H*), 7.91 (t, J = 5.4 Hz, 1H, N*H*), 7.75 (d, J = 8.0 Hz, 1H, Ph*H*), 7.42 – 7.38 (m, 2H, Ph*H*), 7.37 – 7.30 (m, 3H, Ph*H*), 7.26 – 7.21 (m, 1H, Ph*H*), 6.34 (d, J = 7.6 Hz, 1H, Het*H*), 5.14 (p, J = 7.1 Hz, 1H, C*H*), 4.54 – 4.44 (m, 2H, CH_2), 4.11 – 3.99 (m, 2H, CH_2), 3.95 – 3.84 (m, 2H, CH_2), 3.60 – 3.49 (m, 2H, CH_2), 1.47 (d, J = 7.0 Hz, 3H, CH_3) (ppm).

^{13}C NMR (126 MHz, DMSO-d_6): δ 163.82, 156.40, 156.06, 145.16, 144.78, 141.60, 137.50, 135.75, 130.78, 128.33, 126.62, 125.92, 118.32, 116.25, 110.23, 103.54, 100.12, 65.80, 65.47, 64.23, 48.37, 22.80 (ppm).

MS (ESI+) *m/z:* 444.10 $[M + H]^+$.

HRMS *m/z:* $[M + H]^+$ calcd for $C_{25}H_{26}N_5O_3$, 444.20302; found 444.20273.

HPLC (II): t_R = 8.939, purity ≥ 95%.

6.1.40 Synthesis of (1³*Z*,1⁴*E*)-*N*-(naphthalen-1-ylmethyl)-3,6-dioxa-9-aza-1(3,5)-pyrazolo[1,5-*a*]pyrimidina-2(1,3)-benzenacyclononaphane-2⁴-carboxamide (110).

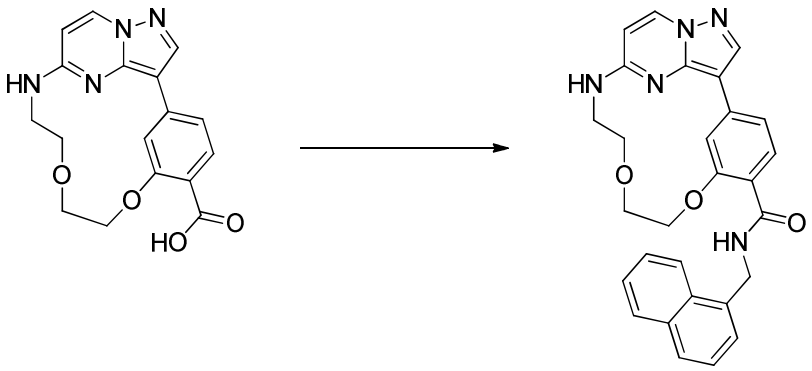

37 **110**

The title compound was synthesized according to the procedure of **61** using naphthalen-1-ylmethanamine (19 mg, 1.2 eq, 0.12 mmol). The desired product was obtained as a white solid (31 mg, 63%).

^{1}H NMR (500 MHz, DMSO-*d*$_6$): δ 8.82 (d, *J* = 1.5 Hz, 1H, Ph*H*), 8.68 (t, *J* = 6.0 Hz, 1H, N*H*), 8.56 (d, *J* = 7.6 Hz, 1H, Het*H*), 8.37 (s, 1H, Het*H*), 8.22 (dd, *J* = 8.4, 1.1 Hz, 1H, Ph*H*), 7.99 – 7.94 (m, 1H, Ph*H*), 7.91 (t, *J* = 5.4 Hz, 1H, N*H*), 7.86 – 7.81 (m, 2H, Ph*H*), 7.62 – 7.53 (m, 2H, Ph*H*), 7.52 – 7.46 (m, 2H, Ph*H*), 7.33 (dd, *J* = 8.1, 1.4 Hz, 1H, Ph*H*), 6.34 (d, *J* = 7.6 Hz, 1H, Het*H*), 4.98 (d, *J* = 5.9 Hz, 2H, C*H*$_2$), 4.50 – 4.36 (m, 2H, C*H*$_2$), 4.07 – 3.96 (m, 2H, C*H*$_2$), 3.93 – 3.81 (m, 2H, C*H*$_2$), 3.62 – 3.45 (m, 2H, C*H*$_2$) (ppm).

^{13}C NMR (126 MHz, DMSO-*d*$_6$): δ 164.64, 156.46, 156.07, 145.18, 141.61, 137.62, 135.75, 134.94, 133.29, 131.00, 130.75, 128.54, 127.27, 126.15, 125.74, 125.48, 124.77, 123.40, 118.03, 116.21, 110.10, 103.54, 100.12, 65.57, 65.41, 64.12, 40.68 (ppm).

MS (ESI+) *m/z:* 480.15 $[M + H]^+$.

HRMS *m/z:* $[M + H]^+$ calcd for $C_{28}H_{26}N_5O_3$, 480.20302; found 480.20349.

HPLC (II): t_R = 9.264, purity ≥ 95%.

6.1.41 Synthesis of (1^3Z,1^4E)-*N*-(1-(naphthalen-1-yl)ethyl)-3,6-dioxa-9-aza-1(3,5)-pyrazolo[1,5-*a*]pyrimidina-2(1,3)-benzenacyclononaphane-2^4-carboxamide (111).

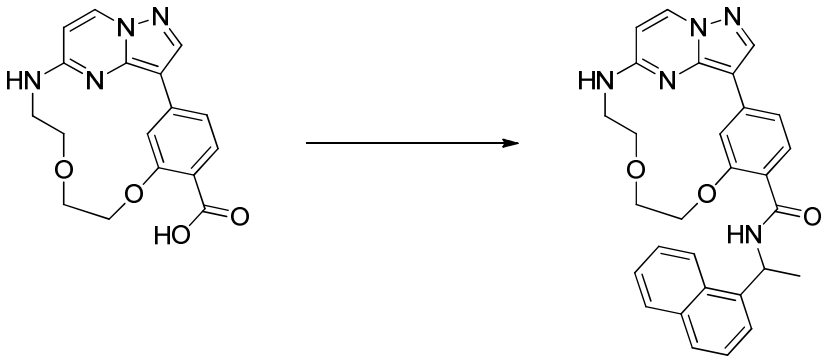

37 **111**

The title compound was synthesized according to the procedure of **61** using 1-(naphthalen-1-yl)ethanamine (*rac*) (18 mg, 1.2 eq, 0.11 mmol). The desired product was obtained as a white solid (33 mg, 76%).

^{1}H NMR (500 MHz, DMSO-d_6): δ 8.83 (d, J = 1.5 Hz, 1H, Ph*H*), 8.60 – 8.52 (m, 2H, Het*H*, N*H*), 8.36 (s, 1H, Het*H*), 8.23 (d, J = 8.4 Hz, 1H, Ph*H*), 7.96 (dd, J = 8.2, 1.4 Hz, 1H) , Ph*H*, 7.90 (t, J = 5.4 Hz, 1H, N*H*), 7.83 (d, J = 8.1 Hz, 1H, Ph*H*), 7.73 (d, J = 8.0 Hz, 1H, Ph*H*), 7.65 – 7.48 (m, 4H, Ph*H*), 7.31 (dd, J = 8.1, 1.4 Hz, 1H, Ph*H*), 6.33 (d, J = 7.6 Hz, 1H, Het*H*), 5.93 (p, J = 7.1 Hz, 1H, C*H*), 4.51 – 4.38 (m, 2H, CH_2), 4.09 – 3.96 (m, 2H, CH_2), 3.93 – 3.83 (m, 2H, CH_2), 3.59 – 3.49 (m, 2H, CH_2), 1.61 (d, J = 6.9 Hz, 3H, CH_3) (ppm).

^{13}C NMR (126 MHz, DMSO-d_6): δ 163.94, 156.44, 156.10, 145.21, 141.63, 140.50, 137.53, 135.78, 133.48, 130.75, 130.23, 128.75, 127.28, 126.19, 125.64, 123.22, 122.59, 118.49, 116.30, 110.29, 103.59, 100.17, 65.84, 65.53, 64.28, 45.03, 22.12 (ppm).

MS (ESI+) *m/z:* 494.05 $[M + H]^+$.

HRMS *m/z:* $[M + Na]^+$ calcd for $C_{29}H_{27}N_5NaO_3$, 516.20061; found 516.20013.

HPLC (II): t_R = 9.589, purity ≥ 95%.

6.1.42 Synthesis of (1³*Z*,1⁴*E*)-*N*-(pyridin-3-ylmethyl)-3,6-dioxa-9-aza-1(3,5)-pyrazolo[1,5-*a*]pyrimidina-2(1,3)-benzenacyclononaphane-2⁴-carboxamide (112).

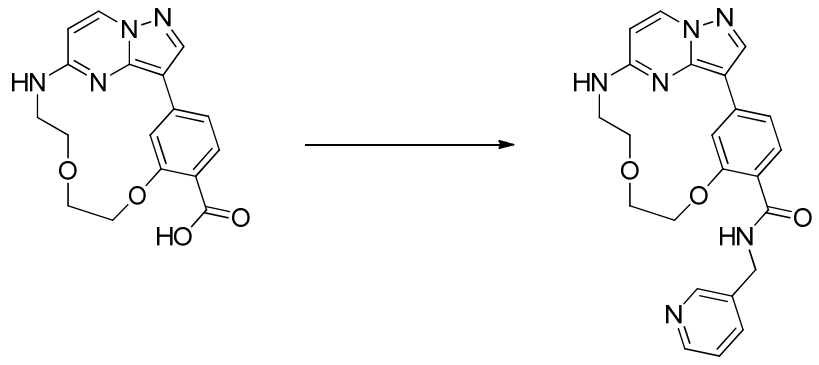

37 **112**

The title compound was synthesized according to the procedure of **61** using pyridin-3-ylmethanamine (15 mg, 1.2 eq, 0.14 mmol). The desired product was obtained as a white solid (40 mg, 79%).

^{1}H NMR (500 MHz, DMSO-d_6): δ 8.82 (d, J = 1.5 Hz, 1H, Ph*H*), 8.73 (t, J = 6.1 Hz, 1H, N*H*), 8.56 – 8.54 (m, 2H, Het*H*), 8.47 – 8.42 (m, 1H, Het*H*), 8.37 (s, 1H, Het*H*), 7.90 (t, J = 5.4 Hz, 1H, N*H*), 7.82 (d, J = 8.1 Hz, 1H, Ph*H*), 7.73 (dt, J = 7.9, 2.0 Hz, 1H, Het*H*), 7.36 (dd, J = 7.9, 4.8 Hz, 1H, Ph*H*), 7.31 (dd, J = 8.1, 1.4 Hz, 1H, Het*H*), 6.33 (d, J = 7.6 Hz, 1H, Het*H*), 4.53 (d, J = 6.1 Hz, 2H, CH_2), 4.50 – 4.44 (m, 2H, CH_2), 4.08 – 3.99 (m, 2H, CH_2), 3.92 – 3.83 (m, 2H, CH_2), 3.53 (q, J = 6.7 Hz, 2H, CH_2) (ppm).

^{13}C NMR (126 MHz, DMSO-d_6): δ 164.91, 156.56, 156.11, 148.70, 147.85, 145.23, 141.66, 137.77, 135.78, 135.57, 135.02, 131.10, 123.50, 117.72, 116.20, 110.04, 103.57, 100.17, 65.51, 65.44, 64.11, 40.44 (ppm).

MS (ESI+) *m/z:* 431.20 $[M + H]^+$.

HRMS *m/z:* $[M + H]^+$ calcd for $C_{23}H_{23}N_6O_3$, 431.18262; found 431.18114.

HPLC (I): t_R = 11.177, purity ≥ 95%.

6.1.43 Synthesis of (1^3Z,1^4E)-*N*-(pyridin-4-ylmethyl)-3,6-dioxa-9-aza-1(3,5)-pyrazolo[1,5-*a*]pyrimidina-2(1,3)-benzenacyclononaphane-2^4-carboxamide (113).

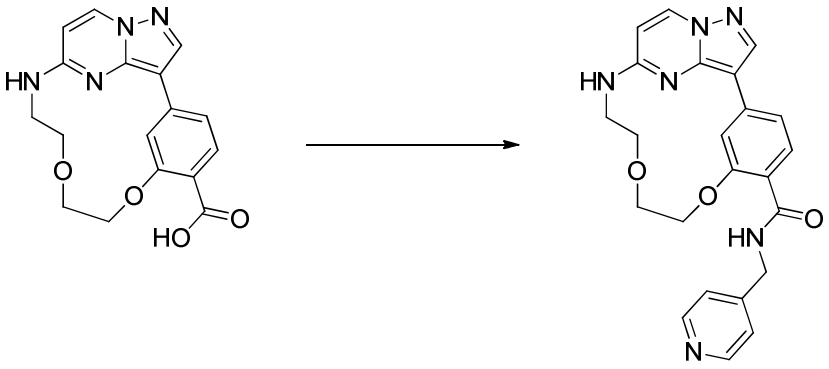

37 **113**

The title compound was synthesized according to the procedure of **61** using pyridin-4-ylmethanamine (15 mg, 1.2 eq, 0.14 mmol). The desired product was obtained as a white solid (42 mg, 83%).

^{1}H NMR (500 MHz, DMSO-d_6): δ 8.84 (d, J = 1.5 Hz, 1H, Ph*H*), 8.74 (t, J = 6.1 Hz, 1H, N*H*), 8.56 (d, J = 7.6 Hz, 1H, Het*H*), 8.53 – 8.47 (m, 2H, Het*H*), 8.38 (s, 1H, Het*H*), 7.91 (t, J = 5.4 Hz, 1H, N*H*), 7.82 (d, J = 8.1 Hz, 1H, Ph*H*), 7.35 – 7.28 (m, 3H, Het*H*, Ph*H*), 6.34 (d, J = 7.6 Hz, 1H, Het*H*), 4.57 – 4.46 (m, 4H, CH_2), 4.09 – 4.02 (m, 2H, CH_2), 3.93 – 3.86 (m, 2H, CH_2), 3.59 – 3.50 (m, 2H, CH_2) (ppm).

^{13}C NMR (126 MHz, DMSO-d_6): δ 164.96, 156.57, 156.09, 149.43, 149.07, 145.20, 141.63, 137.78, 135.76, 131.08, 122.00, 117.64, 116.17, 110.02, 103.54, 100.14, 65.48, 65.40, 64.08, 41.83 (ppm).

MS (ESI+) *m/z:* 431.20 $[M + H]^+$.

HRMS *m/z:* $[M + H]^+$ calcd for $C_{23}H_{23}N_6O_3$, 431.18262; found 431.18294.

HPLC (I): t_R = 11.404, purity ≥ 95%.

6.1.44 Synthesis of (1^3Z,1^4E)-*N*-((*R*)-1-(pyridin-4-yl)ethyl)-3,6-dioxa-9-aza-1(3,5)-pyrazolo[1,5-*a*]pyrimidina-2(1,3)-benzenacyclononaphane-2^4-carboxamide (114).

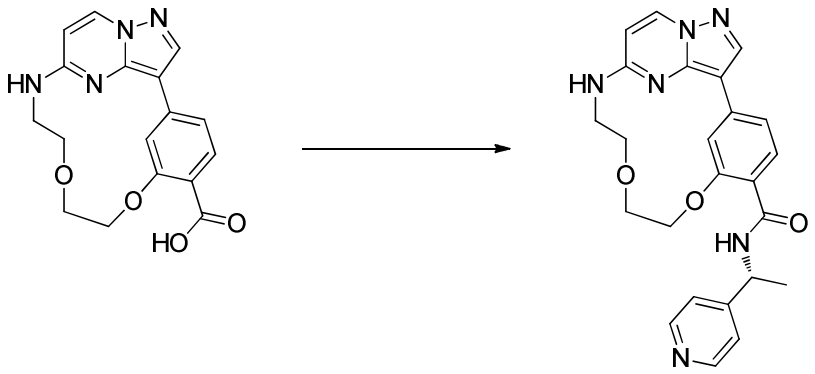

37 **114**

The title compound was synthesized according to the procedure of **61** using (*R*)-1-(pyridin-4-yl)ethanamine (13 mg, 1.2 eq, 0.11 mmol). The crude product was purified by flash silica gel column chromatography with a mobile phase of ethyl acetate and ethanol with the addition of 1% acetic acid (ratio gradually ranging from 1:0 to 0:1). The title compound was obtained as a dark yellow solid (34 mg, 87%).

^{1}H NMR (500 MHz, DMSO-d_6): δ 8.84 (d, J = 1.5 Hz, 1H, Ph*H*), 8.56 (d, J = 7.5 Hz, 1H, Het*H*), 8.54 – 8.50 (m, 2H, Het*H*), 8.44 (d, J = 7.6 Hz, 1H, N*H*), 8.37 (s, 1H, Het*H*), 7.92 (t, J = 5.4 Hz, 1H, N*H*), 7.71 (d, J = 8.0 Hz, 1H, Ph*H*), 7.41 – 7.36 (m, 2H, Het*H*), 7.31 (dd, J = 8.1, 1.3 Hz, 1H, Ph*H*), 6.34 (d, J = 7.6 Hz, 1H, Het*H*), 5.12 (p, J = 7.1 Hz, 1H, C*H*), 4.56 – 4.45 (m, 2H, CH_2), 4.11 – 4.02 (m, 2H, CH_2), 3.94 – 3.85 (m, 2H, CH_2), 3.59 – 3.48 (m, 2H, CH_2), 1.48 (d, J = 7.1 Hz, 3H, CH_3) (ppm).

^{13}C NMR (126 MHz, DMSO-d_6): δ 164.31, 156.40, 156.08, 153.53, 149.60, 145.18, 141.60, 135.75, 130.69, 121.24, 118.30, 116.20, 110.18, 103.54, 100.13, 65.73, 65.46, 64.20, 47.73, 21.84 (ppm).

MS (ESI+) *m/z:* 445.10 $[M + H]^+$.

HRMS *m/z:* $[M + Na]^+$ calcd for $C_{24}H_{24}N_6NaO_3$, 467.18021; found 467.17882.

HPLC (II): t_R = 6.782, purity ≥ 95%.

6.1.45 Synthesis of (1^3Z,1^4E)-*N*-((*S*)-1-(pyridin-4-yl)ethyl)-3,6-dioxa-9-aza-1(3,5)-pyrazolo[1,5-*a*]pyrimidina-2(1,3)-benzenacyclononaphane-2^4-carboxamide (115).

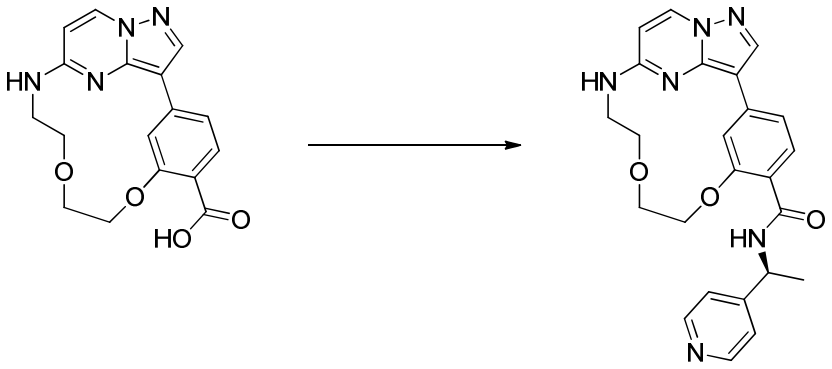

37 **115**

The title compound was synthesized according to the procedure of **61** using (*S*)-1-(pyridin-4-yl)ethanamine (13 mg, 1.2 eq, 0.11 mmol). Purification was done by flash silica gel column chromatography with a mobile phase of ethyl acetate and ethanol with the addition of 1% acetic acid (ratio gradually ranging from 1:0 to 0:1). The slightly yellow solid (32 mg, 82%) was the desired product.

^{1}H NMR (500 MHz, DMSO-d_6): δ 8.84 (d, J = 1.5 Hz, 1H, Ph*H*), 8.56 (d, J = 7.6 Hz, 1H, Het*H*), 8.54 – 8.50 (m, 2H, Het*H*), 8.44 (d, J = 7.7 Hz, 1H, N*H*), 8.37 (s, 1H, Het*H*), 7.92 (t, J = 5.4 Hz, 1H, N*H*), 7.71 (d, J = 8.1 Hz, 1H, Ph*H*), 7.41 – 7.37 (m, 2H, Het*H*), 7.31 (dd, J = 8.0, 1.4 Hz, 1H, Ph*H*), 6.34 (d, J = 7.6 Hz, 1H, Het*H*), 5.12 (p, J = 7.1 Hz, 1H, C*H*), 4.56 – 4.45 (m, 2H, CH_2), 4.14 – 4.02 (m, 2H, CH_2), 3.95 – 3.85 (m, 2H, CH_2), 3.61 – 3.49 (m, 2H, CH_2), 1.48 (d, J = 7.0 Hz, 3H, CH_3) (ppm).

^{13}C NMR (126 MHz, DMSO-d_6): δ 164.31, 156.40, 156.08, 153.52, 149.60, 145.18, 141.60, 137.57, 135.75, 130.69, 121.24, 118.30, 116.20, 110.18, 103.54, 100.13, 65.73, 65.46, 64.20, 47.73, 21.84 (ppm).

MS (ESI+) *m/z:* 445.15 $[M + H]^+$.

HRMS *m/z:* $[M + H]^+$ calcd for $C_{24}H_{25}N_6O_3$, 445.19827; found 445.19843.

HPLC (II): t_R = 6.788, purity ≥ 95%.

6.1.46 Synthesis of (1³*Z*,1⁴*E*)-*N*-(quinolin-4-ylmethyl)-3,6-dioxa-9-aza-1(3,5)-pyrazolo[1,5-*a*]pyrimidina-2(1,3)-benzenacyclononaphane-2⁴-carboxamide (116).

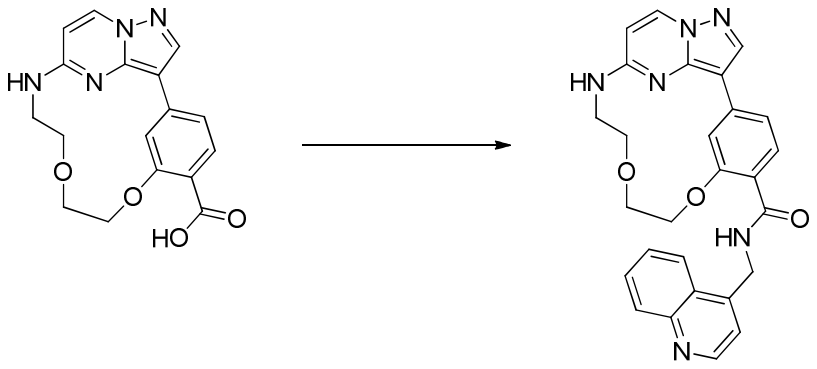

37 **116**

The title compound was synthesized according to the procedure of **61** using quinolin-4-ylmethanamine (21 mg, 1.2 eq, 0.11 mmol). The desired product was obtained as a slightly yellow solid (30 mg, 71%).

^{1}H NMR (500 MHz, DMSO-d_6): δ 8.89 (d, J = 4.5 Hz, 1H, Het*H*), 8.86 – 8.81 (m, 2H, N*H*, Ph*H*), 8.57 (d, J = 7.5 Hz, 1H, Het*H*), 8.39 (s, 1H, Het*H*), 8.31 (dd, J = 8.4, 1.4 Hz, 1H, Het*H*), 8.08 (dd, J = 8.4, 1.3 Hz, 1H, Het*H*), 7.91 (t, J = 5.4 Hz, 1H, N*H*), 7.85 – 7.81 (m, 2H, Het*H*, Ph*H*), 7.74 – 7.69 (m, 1H, Het*H*), 7.47 (d, J = 4.6 Hz, 1H, Het*H*), 7.34 (dd, J = 8.1, 1.4 Hz, 1H, Ph*H*), 6.35 (d, J = 7.6 Hz, 1H, Het*H*), 5.05 (d, J = 5.9 Hz, 2H, CH_2), 4.56 – 4.46 (m, 2H, CH_2), 4.09 – 4.03 (m, 2H, CH_2), 3.93 – 3.87 (m, 2H, CH_2), 3.59 – 3.52 (m, 2H, CH_2) (ppm).

^{13}C NMR (126 MHz, DMSO-d_6): δ 165.03, 156.57, 156.10, 145.22, 141.64, 137.81, 135.78, 131.04, 126.84, 125.99, 123.69, 118.84, 117.75, 116.21, 110.08, 103.55, 100.15, 65.53, 65.43, 64.12 (ppm).

MS (ESI+) *m/z:* 481.15 $[M + H]^+$.

HRMS *m/z:* $[M + Na]^+$ calcd for $C_{27}H_{24}N_6NaO_3$, 503.18021; found 503.17904.

HPLC (II): t_R = 7.067, purity ≥ 95%.

6.1.47 Synthesis of ((1^3*Z*,1^4*E*)-3,6-dioxa-9-aza-1(3,5)-pyrazolo[1,5-*a*]pyrimidina-2(1,3)-benzena-cyclononaphane-2^4-yl)(4-methylpiperazin-1-yl)methanone (117).

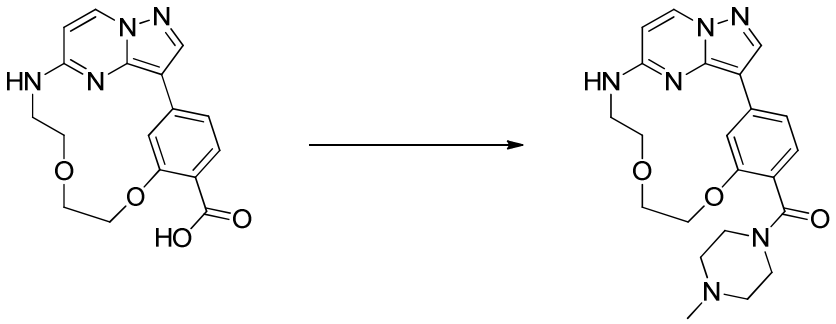

37 **117**

The title compound was synthesized according to the procedure of **61** using 1-methylpiperazine (16 mg, 1.2 eq, 0.16 mmol). Purification was done by flash silica gel column chromatography with a mobile phase of dichloromethane and methanol (isocratic ratio 93:7). The desired product was obtained as a white solid (55 mg, 89%).

^{1}H NMR (250 MHz, DMSO-d_6): δ 8.72 (d, J = 1.3 Hz, 1H, Ph*H*), 8.54 (d, J = 7.6 Hz, 1H, Het*H*), 8.33 (s, 1H, Het*H*), 7.86 (t, J = 5.2 Hz, 1H, N*H*), 7.25 (dd, J = 7.8, 1.2 Hz, 1H, Ph*H*), 7.13 (d, J = 7.8 Hz, 1H, Ph*H*), 6.32 (d, J = 7.6 Hz, 1H, Het*H*), 4.42 – 4.25 (m, 2H, CH_2), 4.08 – 3.77 (m, 4H, CH_2), 3.67 – 3.47 (m, 4H, CH_2), 3.23 – 3.11 (m, 2H, CH_2), 2.45 – 2.17 (m, 7H, CH_2, CH_3) (ppm).

^{13}C NMR (151 MHz, DMSO-d_6): δ 166.49, 155.83, 153.71, 144.93, 141.27, 135.64, 135.42, 128.13, 121.38, 116.14, 109.61, 103.72, 99.98, 65.27, 64.70, 63.83, 61.98, 55.99, 54.67, 54.19, 46.04, 45.42 (ppm).

MS (ESI+) *m/z:* 423.40 $[M + H]^+$.

HRMS *m/z:* $[M + Na]^+$ calcd for $C_{22}H_{26}N_6O_3$, 425.19586; found 445.19612.

HPLC (I): t_R = 8.139, purity ≥ 95%.

6.1.48 Synthesis of ((1³*Z*,1⁴*E*)-3,6-dioxa-9-aza-1(3,5)-pyrazolo[1,5-*a*]pyrimidina-2(1,3)-benzena-cyclononaphane-2⁴-yl)(morpholino)methanone (118).

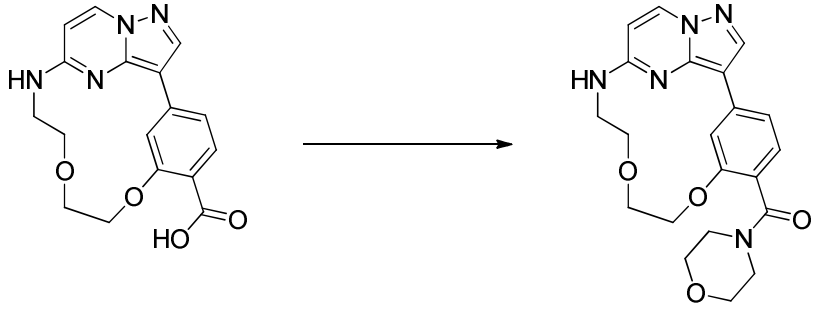

37 **118**

The title compound was synthesized according to the procedure of **61** using morpholine (14 mg, 1.2 eq, 0.16 mmol). The desired product was obtained as a white solid (54 mg, 90%).

^{1}H NMR (500 MHz, DMSO-d_6): δ 8.73 (d, J = 1.4 Hz, 1H, Ph*H*), 8.55 (d, J = 7.5 Hz, 1H, Het*H*), 8.33 (s, 1H, Het*H*), 7.87 (t, J = 5.4 Hz, 1H, N*H*), 7.26 (dd, J = 7.8, 1.3 Hz, 1H, Ph*H*), 7.17 (d, J = 7.8 Hz, 1H, Ph*H*), 6.32 (d, J = 7.6 Hz, 1H, Het*H*), 4.42 – 4.27 (m, 2H, CH_2), 4.07 – 3.79 (m, 4H, CH_2), 3.69 – 3.57 (m, 4H, CH_2), 3.57 – 3.44 (m, 4H, CH_2), 3.23 – 3.11 (m, 2H, CH_2) (ppm).

^{13}C NMR (126 MHz, DMSO-d_6): δ 166.62, 155.89, 153.72, 144.98, 141.40, 135.75, 135.60, 128.39, 121.01, 116.25, 109.52, 103.74, 100.04, 66.37, 66.10, 65.11, 64.59, 63.65, 48.61, 46.91, 41.67 (ppm).

MS (ESI+) *m/z:* 410.00 $[M + H]^+$.

HRMS *m/z:* $[M + H]^+$ calcd for $C_{21}H_{23}N_5O_4$, 410.18228; found 410.18262.

HPLC (I): t_R = 11.067, purity ≥ 95%.

6.1.49 Synthesis of (1^3Z,1^4E)-*N*,*N*-dimethyl-3,6-dioxa-9-aza-1(3,5)-pyrazolo[1,5-*a*]pyrimidina-2(1,3)-benzenacyclononaphane-2^4-carboxamide (119).

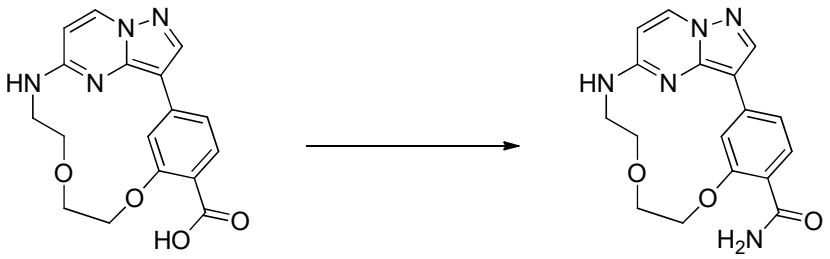

37 **119**

The title compound was synthesized according to the procedure of **61** using ammonia 2 M in ethanol (88 µL, 1.2 eq, 0.18 mmol). Purification was done by flash silica gel column chromatography with a mobile phase of *n*-hexane and ethyl acetate (ratio gradually ranging from 1:0 to 9:1). The title compound was obtained as a white solid (23 mg, 42%).

^{1}H NMR (500 MHz, DMSO-d_6): δ 8.80 (d, J = 1.5 Hz, 1H, Ph*H*), 8.56 (d, J = 7.6 Hz, 1H, Het*H*), 8.37 (s, 1H, Het*H*), 7.90 (t, J = 5.5 Hz, 1H, N*H*), 7.86 (d, J = 8.1 Hz, 1H, Ph*H*), 7.58 (s, 1H, N*H*), 7.42 (s, 1H, N*H*), 7.31 (dd, J = 8.1, 1.4 Hz, 1H, Ph*H*), 6.33 (d, J = 7.6 Hz, 1H, Het*H*), 4.54 – 4.40 (m, 2H, CH_2), 4.07 – 3.99 (m, 2H, CH_2), 3.93 – 3.83 (m, 2H, CH_2), 3.61 – 3.48 (m, 2H, CH_2) (ppm).

^{13}C NMR (126 MHz, DMSO-d_6): δ 165.81, 156.71, 156.07, 145.17, 141.63, 137.82, 135.76, 131.34, 117.70, 116.06, 109.88, 103.55, 100.12, 65.31, 63.95 (ppm).

MS (ESI+) *m/z:* 340.20 $[M + H]^+$.

HRMS *m/z:* $[M + H]^+$ calcd for $C_{17}H_{18}N_5O_3$, 340.14042; found 340.14063.

HPLC (I): t_R = 9.218, purity ≥ 95%.

6.1.50 Synthesis of (1^3*Z*,1^4*E*)-*N*-methyl-3,6-dioxa-9-aza-1(3,5)-pyrazolo[1,5-*a*]-pyrimidina-2(1,3)-benzenacyclononaphane-2^4-carboxamide (120).

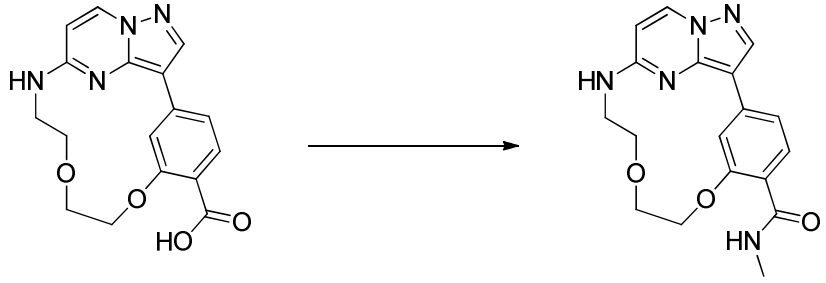

37 **120**

The title compound was synthesized according to the procedure of **61** using methylamine 33% in ethanol (22 μL, 1.2 eq, 0.18 mmol). The desired product was obtained as a white solid (30 mg, 58%).

^{1}H NMR (500 MHz, DMSO-d_6): δ 8.79 (d, J = 1.5 Hz, 1H, Ph*H*), 8.56 (d, J = 7.5 Hz, 1H, Het*H*), 8.36 (s, 1H, Het*H*), 8.07 (q, J = 4.6 Hz, 1H, N*H*), 7.89 (t, J = 5.4 Hz, 1H, N*H*), 7.83 (d, J = 8.1 Hz, 1H, Ph*H*), 7.30 (dd, J = 8.1, 1.5 Hz, 1H, Ph*H*), 6.33 (d, J = 7.6 Hz, 1H, Het*H*), 4.51 – 4.42 (m, 2H, CH_2), 4.06 – 4.00 (m, 2H, CH_2), 3.92 – 3.85 (m, 2H, CH_2), 3.58 – 3.49 (m, 2H, CH_2), 2.81 (d, J = 4.7 Hz, 3H, CH_3) (ppm).

^{13}C NMR (126 MHz, DMSO-d_6): δ 164.96, 156.34, 156.04, 145.14, 141.60, 137.41, 135.75, 131.00, 117.94, 116.06, 109.84, 103.55, 100.11, 65.32, 65.25, 63.91, 26.34 (ppm).

MS (ESI+) *m/z:* 354.20 $[M + H]^+$.

HRMS *m/z:* $[M + H]^+$ calcd for $C_{18}H_{19}N_5O_3$, 354.15607; found 354.15544.

HPLC (I): t_R = 9.411, purity ≥ 95%.

6.1.51 Synthesis of (1^3Z,1^4E)-*N*-(*tert*-butyl)-3,6-dioxa-9-aza-1(3,5)-pyrazolo[1,5-*a*]-pyrimidina-2(1,3)-benzenacyclononaphane-2^4-carboxamide (121).

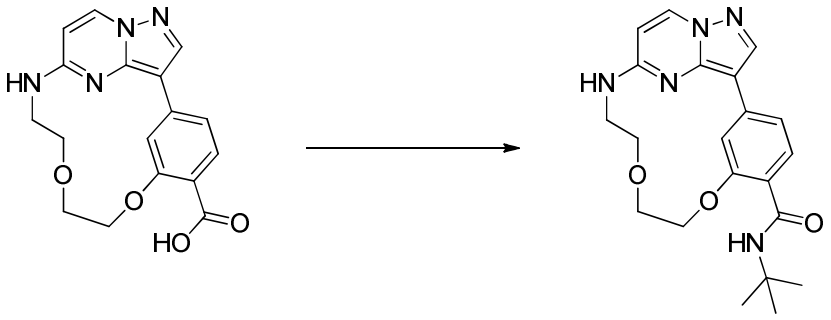

37 **121**

The title compound was synthesized according to the procedure of **61** using 2-methylpropan-2-amine (12 mg, 1.2 eq, 0.16 mmol). The desired product was obtained as a beige solid (39 mg, 67%).

^{1}H NMR (500 MHz, DMSO-d_6): δ 8.82 (d, J = 1.5 Hz, 1H, Ph*H*), 8.56 (d, J = 7.6 Hz, 1H, Het*H*), 8.37 (s, 1H, Het*H*), 7.90 (t, J = 5.4 Hz, 1H, N*H*), 7.86 – 7.81 (m, 2H, N*H*, Ph*H*), 7.32 (dd, J = 8.1, 1.4 Hz, 1H, Ph*H*), 6.33 (d, J = 7.6 Hz, 1H, Het*H*), 4.52 – 4.41 (m, 2H, CH_2), 4.08 – 3.98 (m, 2H, CH_2), 3.93 – 3.83 (m, 2H, CH_2), 3.60 – 3.49 (m, 2H, CH_2), 1.38 (s, 9H, C(CH_3)$_3$) (ppm).

^{13}C NMR (126 MHz, DMSO-d_6): δ 163.43, 156.29, 156.05, 145.13, 141.60, 137.44, 135.74, 130.81, 118.65, 116.34, 110.26, 103.48, 100.09, 65.97, 65.48, 64.27, 50.22, 28.67 (ppm).

MS (ESI+) *m/z:* 396.20 $[M + H]^+$.

HRMS *m/z:* $[M + H]^+$ calcd for $C_{21}H_{26}N_5O_3$, 396.20302; found 396.20288.

HPLC (I): t_R = 14.615, purity ≥ 95%.

6.1.52 Synthesis of *tert*-butyl (2-(2-((*tert*-butyldimethylsilyl)oxy)ethoxy)ethyl)(3-(3-hydroxy-phenyl)pyrazolo[1,5-*a*]pyrimidin-5-yl)carbamate (171).

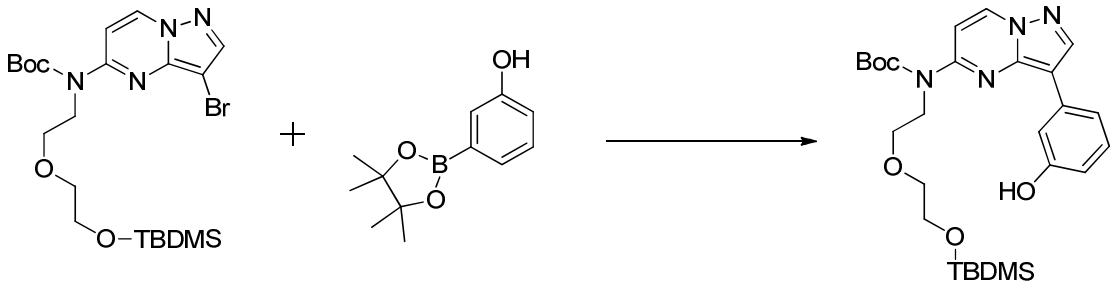

28 **171**

The title compound was synthesized according to the procedure of **33** using 3-(4,4,5,5-tetramethyl-1,3,2-dioxaborolan-2-yl)phenol (0.50 g, 2.0 eq, 2.27 mmol). Purification was done by flash silica gel column chromatography with a mobile phase of *n*-hexane and ethyl acetate (ratio gradually ranging from 1:0 to 0:1). The desired product was obtained as yellowish solid (690 mg, 86%).

^{1}H NMR (500 MHz, DMSO-d_6): δ 9.33 (s, 1H, O*H*), 8.94 (d, J = 7.7 Hz, 1H, Het*H*), 8.54 (s, 1H, Het*H*), 7.48 (dt, J = 7.7, 1.2 Hz, 1H, Ph*H*), 7.44 (t, J = 2.0 Hz, 1H, Ph*H*), 7.37 (d, J = 7.7 Hz, 1H, Het*H*), 7.18 (t, J = 7.9 Hz, 1H, Ph*H*), 6.63 (ddd, J = 8.0, 2.4, 1.0 Hz, 1H, Ph*H*), 4.22 (t, J = 6.2 Hz, 2H, CH_2), 3.74 (t, J = 6.2 Hz, 2H, CH_2), 3.58 (dd, J = 5.7, 4.4 Hz, 2H, CH_2), 3.46 (dd, J = 5.7, 4.4 Hz, 2H, CH_2), 1.52 (s, 9H, (CH_3)$_3$), 0.77 (s, 9H, (CH_3)$_3$), -0.07 (s, 6H, Si(CH_3)$_2$) ppm.

6.1.53 Synthesis of *tert*-butyl (2-(2-hydroxyethoxy)ethyl)(3-(3-hydroxyphenyl)-pyrazolo[1,5-*a*]-pyrimidin-5-yl)carbamate (172).

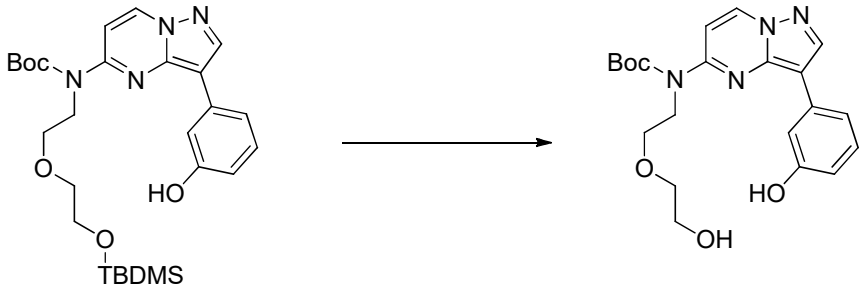

171 **172**

The title compound was synthesized according to the procedure of **34** using *tert*-butyl (2-(2-((*tert*-butyldimethylsilyl)oxy)ethoxy)ethyl)(3-(3-hydroxyphenyl)pyrazolo[1,5-*a*]-pyrimidin-5-yl)carbamate (**171**) (260 mg, 1.0 eq, 0.49 mmol).

The crude product was purified by flash silica gel column chromatography with a mobile phase of *n*-hexane and ethyl acetate (ratio gradually ranging from 9:1 to 1:1). The title compound was yielded as yellow solid (180 mg, 88%).

^{1}H NMR (500 MHz, DMSO-d_6): δ 9.35 (s, 1H, O*H*), 8.94 (d, J = 7.7 Hz, 1H, Het*H*), 8.55 (s, 1H, Het*H*), 7.52 – 7.46 (m, 1H, Ph*H*), 7.45 (t, J = 2.0 Hz, 1H, Ph*H*), 7.39 (d, J = 7.8 Hz, 1H, Het*H*), 7.19 (t, J = 7.9 Hz, 1H, Ph*H*), 6.64 (dd, J = 8.0, 2.5 Hz, 1H, Ph*H*), 4.52 (t, J = 5.2 Hz, 1H, O*H*), 4.21 (t, J = 6.3 Hz, 2H, CH_2), 3.74 (t, J = 6.3 Hz, 2H, CH_2), 3.50 – 3.38 (m, 4H, CH_2), 1.52 (s, 9H, (CH_3)$_3$) ppm.

^{13}C NMR (126 MHz, DMSO-d_6): δ 157.57, 153.06, 152.89, 142.93, 142.23, 136.17, 133.21, 129.51, 116.26, 112.84, 112.27, 107.85, 104.63, 82.26, 72.20, 68.04, 60.22, 45.74, 27.68 ppm.

MS (ESI+) *m/z:* 414.95 $[M + H]^+$.

HRMS *m/z:* $[M + H]^+$ calcd for $C_{21}H_{27}N_4O_5$, 415.19760; found 415.19744.

HPLC (III): t_R = 13.631, purity ≥ 95%.

6.1.54 Synthesis of *tert*-butyl (1^3*Z*,1^4*E*)-3,6-dioxa-9-aza-1(3,5)-pyrazolo[1,5-*a*]-pyrimidina-2(1,3)-benzenacyclononaphane-9-carboxylate (175).

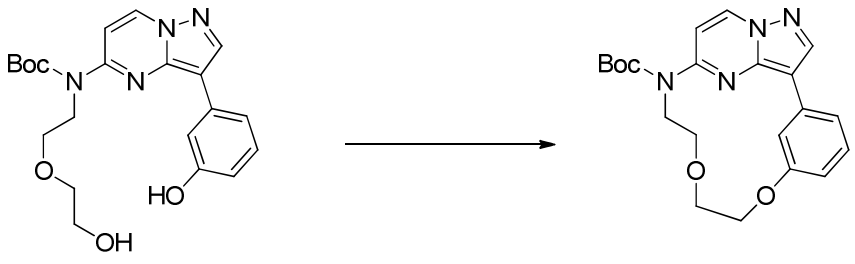

172 **175**

The title compound was synthesized according to the procedure of **35** using *tert*-butyl (2-(2-hydroxyethoxy)ethyl)(3-(3-hydroxyphenyl)pyrazolo[1,5-*a*]pyrimidin-5-yl)carbamate (**172**) (90 mg, 1.0 eq, 0.22 mmol). Purification was done by flash silica gel column chromatography with a mobile phase of *n*-hexane and ethyl acetate (ratio gradually ranging from 1:0 to 2:1). The obtained bright yellow solid (51 mg, 59%) was the title compound.

^{1}H NMR (500 MHz, DMSO-d_6): δ 8.97 (d, J = 7.8 Hz, 1H, Het*H*), 8.67 – 8.57 (m, 2H, Het*H*, Ph*H*), 7.51 (d, J = 7.8 Hz, 1H, Het*H*), 7.33 (d, J = 7.6 Hz, 1H Ph*H*), 7.25 (t, J = 7.9 Hz, 1H, Ph*H*), 6.69 (dd, J = 8.3, 2.7 Hz, 1H, Ph*H*), 4.31 (t, J = 6.3 Hz, 2H, CH_2), 4.08 (t, J = 6.9 Hz, 2H, CH_2), 3.92 (t, J = 6.9 Hz, 2H, CH_2), 3.87 (t, J = 6.3 Hz, 2H, CH_2), 1.54 (s, 9H, (CH_3)$_3$) ppm.

^{13}C NMR (126 MHz, DMSO-d_6): δ 158.94, 152.70, 152.46, 142.43, 136.29, 133.32, 129.38, 116.92, 114.41, 110.88, 107.29, 103.62, 82.64, 66.15, 65.84, 46.18, 27.66 ppm.

MS (ESI+) *m/z:* 397.00 $[M + H]^+$.

HRMS *m/z:* $[M + H]^+$ calcd for $C_{21}H_{25}N_4O_4$, 397.18703; found 397.18689.

HPLC (III): t_R = 17.929, purity ≥ 95%.

6.1.55 Synthesis of 6-((3-bromopyrazolo[1,5-*a*]pyrimidin-5-yl)amino)hexan-1-ol (122).

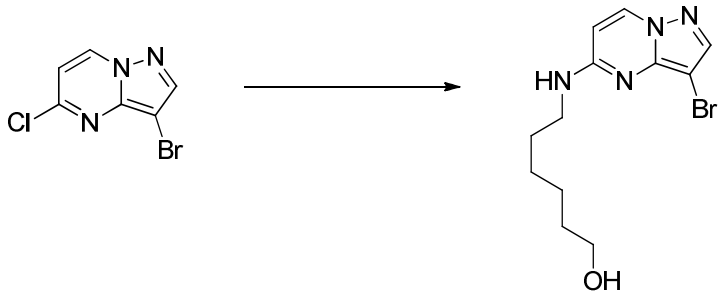

25 **122**

The title compound was synthesized according to the procedure of **26** using 6-aminohexan-1-ol (277 mg, 1.1 eq, 2.37 mmol).

Purification was done by flash silica gel column chromatography with a mobile phase of dichloromethane and methanol (ratio gradually ranging from 1:0 to 9:1). The slightly yellow solid (420 mg, 63%) was the title compound.

^{1}H NMR (250 MHz, DMSO-d_6): δ 8.42 (d, J = 7.4 Hz, 1H, Het*H*), 7.85 (s, 1H, Het*H*), 7.62 (t, J = 5.3 Hz, 1H, N*H*), 6.28 (d, J = 7.6 Hz, 1H, Het*H*), 4.32 (t, J = 5.1 Hz, 1H O*H*), 3.44 – 3.32 (m, 4H, CH_2), 1.65 – 1.50 (m, 2H, CH_2), 1.49 – 1.26 (m, 6H, CH_2) (ppm).

6.1.56 Synthesis of 3-bromo-*N*-(6-((*tert*-butyldimethylsilyl)oxy)hexyl)pyrazolo-[1,5-*a*]-pyrimidin-5-amine (124).

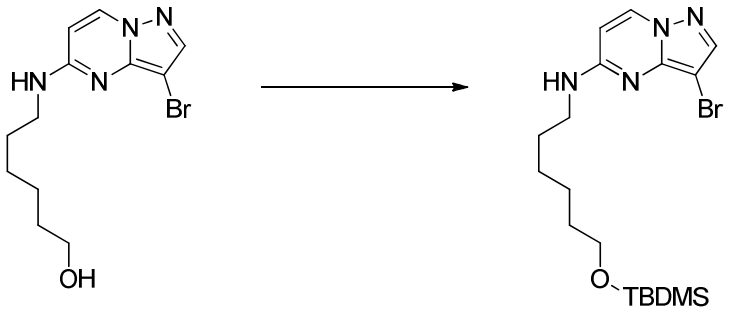

122 **124**

The title compound was synthesized according to the procedure of **27** using 6-((3-bromopyrazolo[1,5-*a*]pyrimidin-5-yl)amino)hexan-1-ol (**122**) (420 mg, 1.0 eq, 1.34 mmol). The desired product was obtained as slightly yellow solid (565 mg, 99%).

^{1}H NMR (250 MHz, $CDCl_3$-*d*): δ 8.17 (d, J = 7.5 Hz, 1H, Het*H*), 7.80 (s, 1H, Het*H*), 6.06 (d, J = 7.6 Hz, 1H, Het*H*), 5.34 (bs, 1H, N*H*), 3.61 (t, J = 6.3 Hz, 2H, CH_2), 3.46 (q, J = 6.6 Hz, 2H, CH_2), 1.73 – 1.36 (m, 8H, CH_2), 0.92 – 0.86 (m, 9H, C(CH_3)$_3$), 0.04 (s, 6H, Si(CH_3)$_2$) (ppm).

6.1.57 Synthesis of *tert*-butyl (3-bromopyrazolo[1,5-*a*]pyrimidin-5-yl)(6-((*tert*-butyldimethylsilyl)oxy)hexyl)carbamate (126).

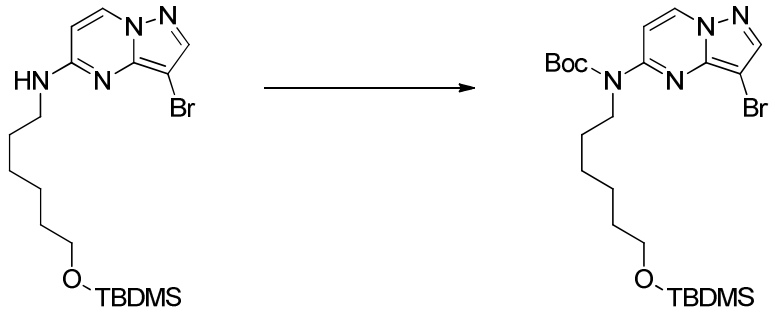

124 **126**

The title compound was synthesized according to the procedure of **28** using 3-bromo-*N*-(6-((*tert*-butyldimethylsilyl)oxy)hexyl)pyrazolo[1,5-*a*]pyrimidin-5-amine (**124**) (565 mg, 1.0 eq, 1.32 mmol). The desired product was obtained as brownish thick high viscous oil (663 mg, 95%).

^{1}H NMR (250 MHz, DMSO-d_6): δ 8.94 (d, J = 7.8 Hz, 1H, Het*H*), 8.23 (s, 1H, Het*H*), 7.48 (d, J = 7.8 Hz, 1H, Het*H*), 4.02 – 3.92 (m, 2H, CH_2), 3.55 (t, J = 6.1 Hz, 2H, CH_2), 1.75 – 1.60 (m, 2H, CH_2), 1.51 (s, 9H, C(CH_3)$_3$), 1.48 – 1.40 (m, 2H, CH_2), 1.37 – 1.27 (m, 4H, CH_2), 0.83 (s, 9H, C(CH_3)$_3$), -0.01 (s, 6H, Si(CH_3)$_2$) (ppm).

6.1.58 Synthesis of methyl 4-(5-((*tert*-butoxycarbonyl)(6-((*tert*-butyldimethylsilyl)-oxy)hexyl)-amino)pyrazolo[1,5-*a*]pyrimidin-3-yl)-2-hydroxybenzoate (128).

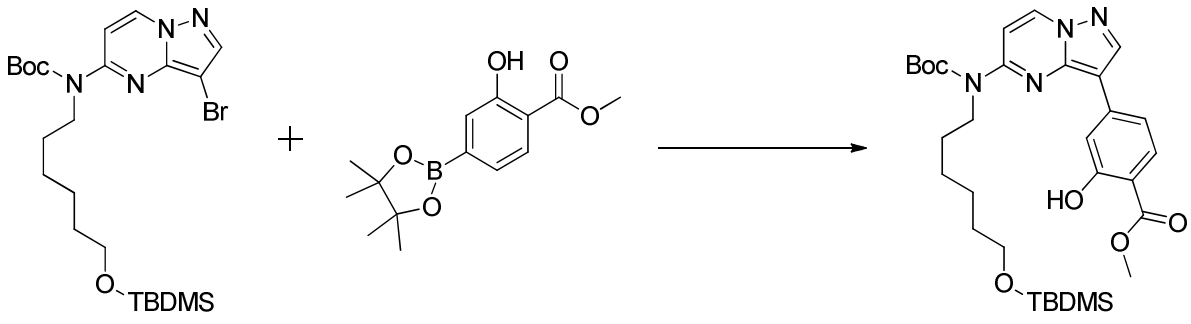

126 **32** **128**

The title compound was synthesized according to the procedure of **33** using *tert*-butyl (3-bromopyrazolo[1,5-*a*]pyrimidin-5-yl)(6-((*tert*-butyldimethylsilyl)oxy)hexyl)carbamate (**126**) (427 mg, 1.0 eq, 0.81 mmol). Purification was done by flash silica gel column chromatography with a mobile phase of *n*-hexane and ethyl acetate (ratio gradually ranging from 1:0 to 0:1). The desired product was obtained as yellow solid (401 mg, 83%).

^{1}H NMR (250 MHz, $CDCl_3$-*d*): δ 10.76 (s, 1H, O*H*), 8.46 (d, *J* = 7.9 Hz, 1H, Het*H*), 8.38 (s, 1H, Het*H*), 7.83 (d, *J* = 8.4 Hz, 1H, Ph*H*), 7.72 (s, 1H, Ph*H*), 7.70 (d, *J* = 5.9 Hz, 1H, Het*H*), 7.55 (dd, *J* = 8.4, 1.7 Hz, 1H, Ph*H*), 4.14 – 4.08 (m, 2H, CH_2), 3.95 (s, 3H, OCH_3), 3.60 (t, *J* = 6.4 Hz, 2H, CH_2), 1.89 – 1.77 (m, 2H, CH_2), 1.58 (s, 9H, C(CH_3)$_3$), 1.56 – 1.39 (m, 6H, CH_2), 0.87 (s, 9H, C(CH_3)$_3$), 0.02 (s, 6H, Si(CH_3)$_2$) (ppm).

6.1.59 Synthesis of methyl 4-(5-((*tert*-butoxycarbonyl)(6-hydroxyhexyl)amino)-pyrazolo[1,5-*a*]-pyrimidin-3-yl)-2-hydroxybenzoate (130).

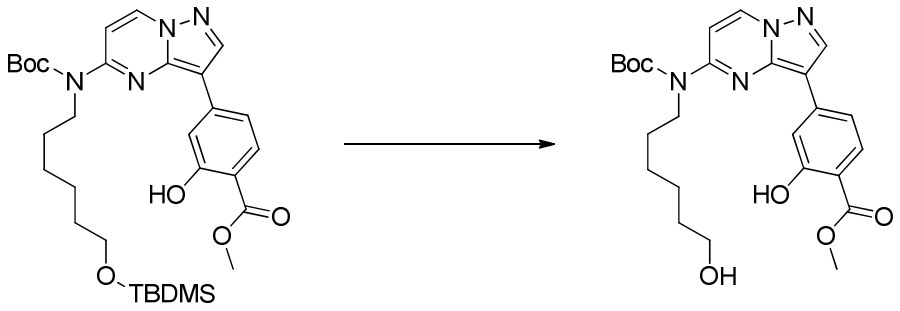

128 **130**

The title compound was synthesized according to the procedure of **34** using methyl 4-(5-((*tert*-butoxycarbonyl)(6-((*tert*-butyldimethylsilyl)oxy)hexyl)amino)pyrazolo[1,5-*a*]-pyrimidin-3-yl)-2-hydroxybenzoate (**128**) (400 mg, 1.0 eq, 0.67 mmol).

The crude product was purified by flash silica gel column chromatography with a mobile phase of *n*-hexane and ethyl acetate (ratio gradually ranging from 9:1 to 1:1). The title compound was yielded as yellow solid (296 mg, 91%).

^{1}H NMR (250 MHz, $CDCl_3$-*d*): δ 10.78 (s, 1H, O*H*), 8.47 (d, *J* = 7.9 Hz, 1H, Het*H*), 8.38 (s, 1H, Het*H*), 7.83 (d, *J* = 8.4 Hz, 1H, Ph*H*), 7.75 (d, *J* = 1.7 Hz, 1H, Ph*H*), 7.70 (d, *J* = 7.9 Hz, 1H, Het*H*), 7.51 (dd, *J* = 8.4, 1.7 Hz, 1H, Ph*H*), 4.19 – 4.06 (m, 2H, CH_2), 3.95 (s, 3H, OCH_3), 3.65 (t, *J* = 6.3 Hz, 2H, CH_2), 1.94 – 1.77 (m, 2H, CH_2), 1.67 – 1.60 (m, 2H, CH_2), 1.58 (s, 9H, C(CH_3)$_3$), 1.57 – 1.34 (m, 6H, CH_2) (ppm).

6.1.60 Synthesis of 10-(*tert*-butyl) 24-methyl (1^3Z,1^4E)-3-oxa-10-aza-1(3,5)-pyrazolo[1,5-*a*]pyrimidina-2(1,3)-benzenacyclodecaphane-2^4,1^0-dicarboxylate (132).

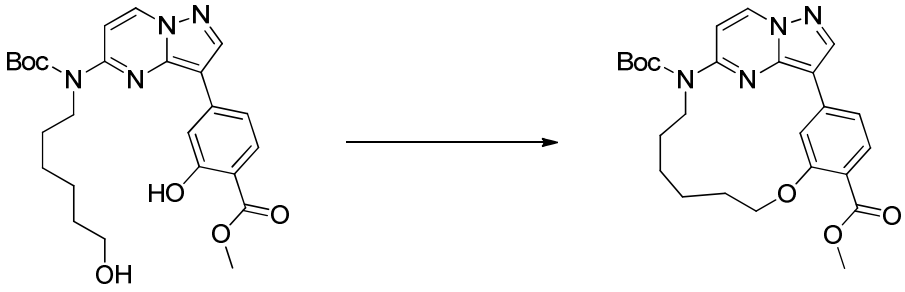

130 **132**

The title compound was synthesized according to the procedure of **35** using methyl 4-(5-((*tert*-butoxycarbonyl)(6-hydroxyhexyl)amino)pyrazolo[1,5-*a*]pyrimidin-3-yl)-2-hydroxy-benzoate (**130**) (290 mg, 1.0 eq, 0.60 mmol). Purification was done by flash silica gel column chromatography with a mobile phase of *n*-hexane and ethyl acetate (ratio gradually ranging from 1:0 to 3:2). The obtained yellow solid (252 mg, 90%) was the title compound.

^{1}H NMR (500 MHz, DMSO-d_6): δ 8.98 – 8.90 (m, 1H, Het*H*), 8.72 – 8.66 (m, 1H, Het*H*), 8.00 – 7.93 (m, 1H, Ph*H*), 7.71 – 7.66 (m, 1H, Ph*H*), 7.52 – 7.46 (m, 1H, Het*H*), 7.46 – 7.41 (m, 1H, Ph*H*), 4.24 – 4.14 (m, 2H, CH_2), 3.90 – 3.82 (m, 2H, CH_2), 3.78 (s, 3H, OCH_3), 1.91 – 1.75 (m, 4H, CH_2), 1.52 (s, 9H, C(CH_3)$_3$), 1.48 (s, 4H, CH_2) (ppm).

^{13}C NMR (126 MHz, DMSO-d_6): δ 165.84, 158.04, 154.02, 152.62, 143.76, 142.80, 137.61, 136.29, 131.52, 117.27, 116.94, 110.86, 106.52, 104.31, 82.33, 68.35, 51.65, 46.83, 27.65, 24.33, 24.02, 23.56, 21.42 (ppm).

MS (ESI+) *m/z:* 466.60 $[M + H]^+$.

HRMS *m/z:* $[M + Na]^+$ calcd for $C_{25}H_{30}N_4O_5Na$, 489.21084; found 489.21036.

HPLC (I): t_R = 19.128, purity ≥ 95%.

6.1.61 Synthesis of (1^3Z,1^4E)-10-(*tert*-butoxycarbonyl)-3-oxa-10-aza-1(3,5)-pyrazolo[1,5-*a*]pyrimidina-2(1,3)-benzenacyclodecaphane-2^4-carboxylic acid (134).

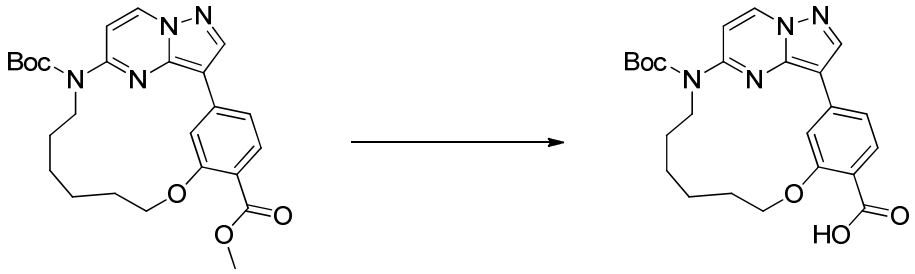

132 **134**

The title compound was synthesized according to the procedure of **37** using **132** (35 mg, 1.0 eq, 0.08 mmol). The crude product was purified by flash silica gel column chromatography with a mobile phase of *n*-hexane and ethyl acetate with the addition of 1% acetic acid (ratio gradually ranging from 7:3 to 0:1). The desired product was obtained as a yellow solid (16 mg, 47%).

^{1}H NMR (500 MHz, DMSO-d_6): δ 12.33 (s, 1H, COO*H*), 8.96 (d, J = 7.8 Hz, 1H, Het*H*), 8.69 (s, 1H, Het*H*), 7.97 (d, J = 1.5 Hz, 1H, Ph*H*), 7.69 (d, J = 8.1 Hz, 1H, Ph*H*), 7.49 (d, J = 7.8 Hz, 1H, Het*H*), 7.43 (dd, J = 8.2, 1.5 Hz, 1H, Ph*H*), 4.27 – 4.16 (m, 2H, CH_2), 3.95 – 3.83 (m, 2H, CH_2), 1.94 – 1.78 (m, 4H, CH_2), 1.53 (s, 9H, , C(CH_3)$_3$), 1.51 – 1.47 (m, 4H, CH_2) (ppm).

^{13}C NMR (126 MHz, DMSO-d_6): δ 167.12, 157.83, 153.97, 152.66, 143.71, 142.73, 136.92, 136.28, 131.57, 117.02, 111.01, 106.72, 104.32, 82.33, 68.43, 46.89, 27.66, 24.42, 24.14, 23.65, 21.52 (ppm).

MS (ESI+) *m/z:* 352.40 [M - Boc]$^+$.

HRMS *m/z:* [M + Na]$^+$ calcd for $C_{24}H_{28}N_4O_5Na$, 475.19519; found 475.19443.

HPLC (I): t_R = 17.637, purity ≥ 95%.

6.1.62 Synthesis of methyl (1^3Z,1^4E)-3-oxa-10-aza-1(3,5)-pyrazolo[1,5-*a*]-pyrimidina-2(1,3)-benzenacyclodecaphane-2^4-carboxylate (136).

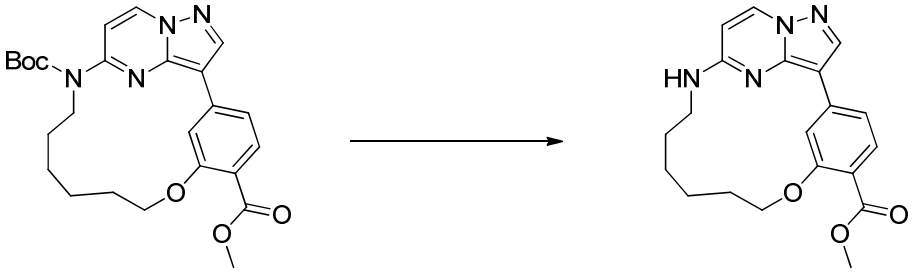

132 **136**

The title compound was synthesized according to the procedure of **36** using **132** (200 mg, 1.0 eq, 0.43 mmol). Purification was done by flash silica gel column chromatography with a mobile phase of *n*-hexane and ethyl acetate (ratio gradually ranging from 1:4 to 0:1). The title compound was yielded as a white solid (117 mg, 74%).

^{1}H NMR (500 MHz, DMSO-d_6): δ 8.48 (d, J = 7.5 Hz, 1H, Het*H*), 8.42 (s, 1H, Het*H*), 8.35 (d, J = 1.5 Hz, 1H, Ph*H*), 7.98 (t, J = 5.9 Hz, 1H, N*H*), 7.66 (d, J = 8.2 Hz, 1H, Ph*H*), 7.34 (dd, J = 8.3, 1.4 Hz, 1H, Ph*H*), 6.28 (d, J = 7.6 Hz, 1H, Het*H*), 4.25 – 4.16 (m, 2H, CH_2), 3.76 (s, 3H, OCH_3), 3.35 – 3.30 (m, 2H, CH_2) 1.96 – 1.85 (m, 2H, CH_2), 1.85 – 1.73 (m, 2H, CH_2), 1.56 – 1.41 (m, 4H, CH_2) (ppm).

^{13}C NMR (126 MHz, DMSO-d_6): δ 165.88, 158.31, 156.22, 145.38, 142.17, 139.16, 135.44, 131.47, 115.45, 115.32, 109.78, 103.14, 100.57, 68.48, 51.49, 24.03, 23.80, 23.11, 21.42 (ppm).

MS (ESI+) *m/z:* 366.40 $[M + H]^+$.

HRMS *m/z:* $[M + Na]^+$ calcd for $C_{20}H_{22}N_4O_3Na$, 389.15841; found 389.15814.

HPLC (I): t_R = 15.499, purity ≥ 95%.

6.1.63 Synthesis of (1^3Z,1^4E)-3-oxa-10-aza-1(3,5)-pyrazolo[1,5-*a*]pyrimidina-2(1,3)-benzena-cyclodecaphane-2^4-carboxylic acid (38).

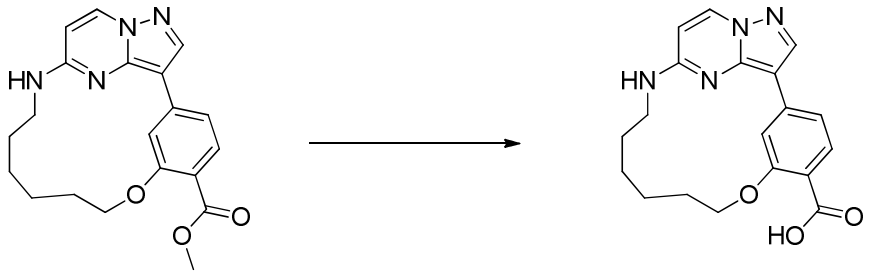

136 **38**

The title compound was synthesized according to the procedure of **37** using **136** (100 mg, 1.0 eq, 0.27 mmol). The desired product was obtained as a white solid (61 mg, 63%).

^{1}H NMR (500 MHz, DMSO-d_6): δ 12.15 (s, 1H, COO*H*), 8.48 (d, J = 7.6 Hz, 1H, Het*H*), 8.42 (s, 1H, Het*H*), 8.34 (s, 1H, Ph*H*), 7.98 (t, J = 5.8 Hz, 1H, N*H*), 7.67 (d, J = 8.2 Hz, 1H, Ph*H*), 7.34 (d, J = 8.2 Hz, 1H, Ph*H*), 6.28 (d, J = 7.6 Hz, 1H, Het*H*), 4.30 – 4.15 (m, 2H, CH_2), 1.99 – 1.86 (m, 2H, CH_2), 1.85 – 1.74 (m, 2H, CH_2), 1.58 – 1.40 (m, 4H, CH_2) (ppm).

^{13}C NMR (126 MHz, DMSO-d_6): δ 166.87, 158.24, 156.20, 145.33, 142.15, 138.89, 135.45, 131.72, 116.19, 115.53, 109.75, 103.22, 100.56, 68.53, 24.06, 23.84, 23.14, 21.46 (ppm).

MS (ESI+) *m/z:* 353.10 $[M + H]^+$.

HRMS *m/z:* $[M + Na]^+$ calcd for $C_{19}H_{20}N_4O_3Na$, 375.14276; found 375.14249.

HPLC (I): t_R = 8.494, purity ≥ 95%.

6.1.64 Synthesis of (1^3Z,1^4E)-N-benzyl-3-oxa-10-aza-1(3,5)-pyrazolo[1,5-*a*]-pyrimidina-2(1,3)-benzenacyclodecaphane-2^4-carboxamide (138).

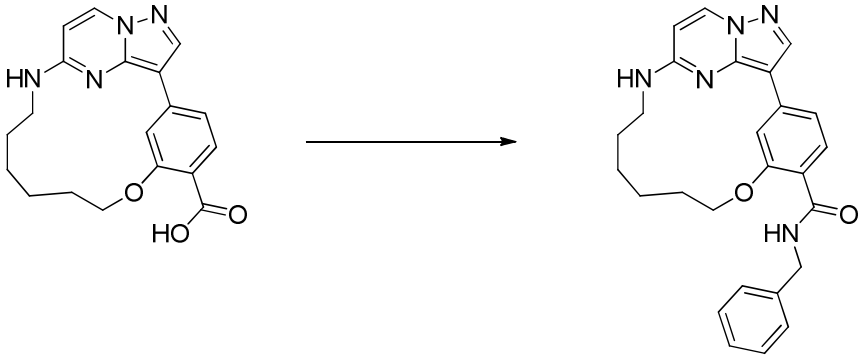

38 **138**

The title compound was synthesized according to the procedure of **61** using **38** (50 mg, 1.0 eq, 0.14 mmol) and benzylamine (16 mg, 1.1 eq, 0.15 mmol). The desired product was obtained as a white solid (48 mg, 80%).

^{1}H NMR (500 MHz, DMSO-d_6): δ 8.65 (t, J = 6.1 Hz, 1H, N*H*), 8.48 (d, J = 7.6 Hz, 1H, Het*H*), 8.42 (s, 1H, Het*H*), 8.35 (d, J = 1.5 Hz, 1H, Ph*H*), 7.99 – 7.93 (m, 2H, N*H*, Ph*H*), 7.82 (d, J = 8.2 Hz, 1H, Ph*H*), 7.38 (dd, J = 8.3, 1.4 Hz, 1H, Ph*H*), 7.34 – 7.32 (m, 4H, Ph*H*), 6.27 (d, J = 7.6 Hz, 1H, Het*H*), 4.52 (d, J = 6.1 Hz, 2H, CH_2), 4.38 – 4.29 (m, 2H), 3.39 – 3.32 (m, 2H, CH_2), 2.04 – 1.94 (m, 2H, CH_2), 1.86 – 1.77 (m, 2H, CH_2), 1.56 – 1.42 (m, 4H, CH_2) (ppm).

^{13}C NMR (126 MHz, DMSO-d_6): δ 164.90, 162.30, 156.63, 156.15, 145.21, 142.06, 140.02, 137.87, 135.43, 131.14, 128.24, 127.02, 126.56, 118.04, 115.90, 108.63, 103.31, 100.52, 68.29, 42.56, 35.76, 30.76, 23.93, 23.64, 22.96, 21.23 (ppm).

MS (ESI+) *m/z:* 442.20 $[M + H]^+$.

HRMS *m/z:* $[M + H]^+$ calcd for $C_{26}H_{28}N_5O_2$, 442.22375; found 442.22343.

HPLC (I): t_R = 16.052, purity ≥ 95%.

6.1.65 Synthesis of (1^3Z,1^4E)-*N*-(3-chlorobenzyl)-3-oxa-10-aza-1(3,5)-pyrazolo-[1,5-*a*]pyrimidina-2(1,3)-benzenacyclodecaphane-2^4-carboxamide (139).

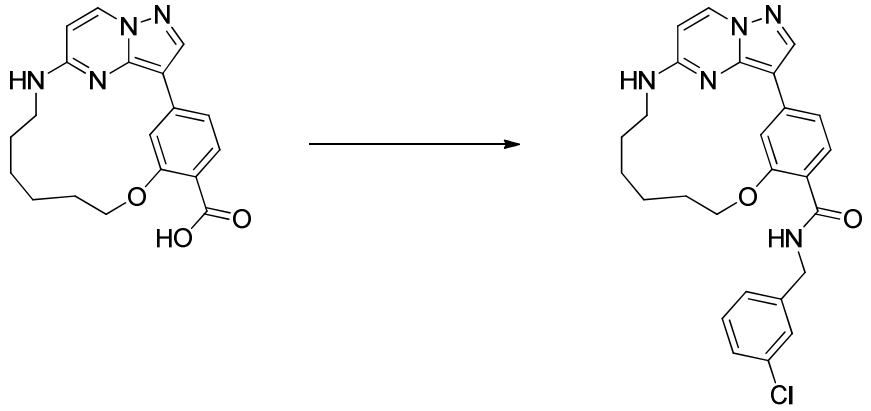

38 **139**

The title compound was synthesized according to the procedure of **61** using **38** (50 mg, 1.0 eq, 0.14 mmol) and (3-chlorophenyl)methanamine (21 mg, 1.1 eq, 0.15 mmol). The desired product was obtained as a white solid (52 mg, 77%).

^{1}H NMR (500 MHz, DMSO-d_6): δ 8.72 (t, J = 6.2 Hz, 1H, N*H*), 8.48 (d, J = 7.6 Hz, 1H, Het*H*), 8.42 (s, 1H, Het*H*), 8.35 (d, J = 1.5 Hz, 1H, Ph*H*), 7.96 (t, J = 6.0 Hz, 1H, N*H*), 7.78 (d, J = 8.2 Hz, 1H, Ph*H*), 7.42 – 7.34 (m, 3H, Ph*H*), 7.32 – 7.28 (m, 2H, Ph*H*), 6.27 (d, J = 7.6 Hz, 1H, Het*H*), 4.51 (d, J = 6.1 Hz, 2H, CH_2), 4.38 – 4.31 (m, 2H, CH_2), 3.37 – 3.33 (m, 2H, CH_2), 2.05 – 1.96 (m, 2H, CH_2), 1.86 – 1.77 (m, 2H, CH_2), 1.55 – 1.43 (m, 4H, CH_2) (ppm).

^{13}C NMR (126 MHz, DMSO-d_6): δ 165.15, 156.58, 156.15, 145.22, 142.81, 142.06, 137.90, 135.42, 132.92, 131.01, 130.11, 126.84, 126.47, 125.75, 118.11, 115.86, 108.55, 103.31, 100.52, 68.20, 42.08, 40.17, 23.91, 23.59, 22.95, 21.24 (ppm).

MS (ESI+) *m/z:* 478.90 $[M + H]^+$.

HRMS *m/z:* $[M + H]^+$ calcd for $C_{26}H_{27}ClN_5O_2$, 476.18478; found 476.18416.

HPLC (I): t_R = 16.725, purity ≥ 95%.

6.1.66 Synthesis of (1^3*Z*,1^4*E*)-*N*-(*tert*-butyl)-3-oxa-10-aza-1(3,5)-pyrazolo[1,5-*a*]-pyrimidina-2(1,3)-benzenacyclodecaphane-2^4-carboxamide (140).

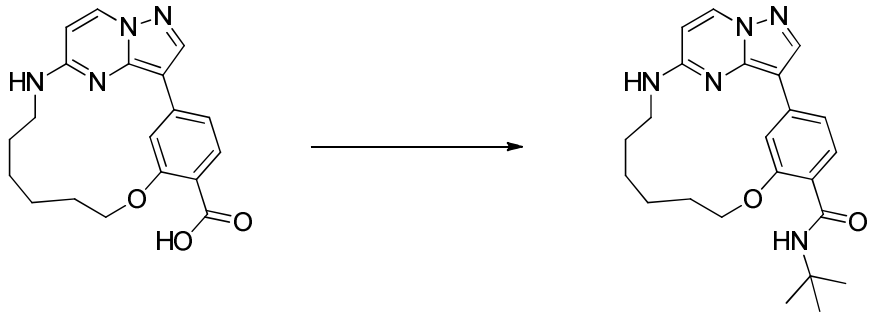

38 **140**

The title compound was synthesized according to the procedure of **61** using **38** (50 mg, 1.0 eq, 0.14 mmol) and 2-methylpropan-2-amine (11 mg, 1.1 eq, 0.15 mmol). The desired product was obtained as a slightly yellow solid (48 mg, 83%).

^{1}H NMR (500 MHz, DMSO-*d*$_6$): δ 8.47 (d, *J* = 7.6 Hz, 1H, Het*H*), 8.41 (s, 1H, Het*H*), 8.32 (d, *J* = 1.5 Hz, 1H, Ph*H*), 7.95 (t, *J* = 5.9 Hz, 1H, N*H*), 7.90 (s, 1H, N*H*), 7.83 (d, *J* = 8.2 Hz, 1H, Ph*H*), 7.38 (dd, *J* = 8.2, 1.5 Hz, 1H, Ph*H*), 6.26 (d, *J* = 7.5 Hz, 1H, Het*H*), 4.35 – 4.25 (m, 2H, C*H*$_2$), 3.32 – 3.23 (m, 2H, C*H*$_2$), 2.01 – 1.92 (m, 2H, C*H*$_2$), 1.84 – 1.75 (m, 2H, C*H*$_2$), 1.56 – 1.43 (m, 4H, C*H*$_2$), 1.38 (s, 9H, C(C*H*$_3$)$_3$) (ppm).

^{13}C NMR (126 MHz, DMSO-*d*$_6$): δ 163.67, 156.37, 156.13, 145.18, 142.02, 137.68, 135.40, 130.90, 118.84, 116.19, 109.15, 103.26, 100.50, 68.84, 50.14, 28.69, 24.09, 23.08, 21.27 (ppm).

MS (ESI+) *m/z:* 408.30 $[M + H]^+$.

HRMS *m/z:* $[M + H]^+$ calcd for $C_{23}H_{30}N_5O_2$, 408.23940; found 408.23908.

HPLC (I): t_R = 16.633, purity ≥ 95%.

6.1.67 Synthesis of 2-(4-((3-bromopyrazolo[1,5-*a*]pyrimidin-5-yl)amino)phenyl)-ethanol (123).

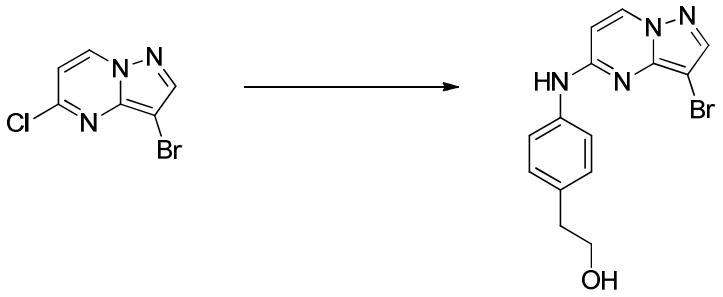

25 **123**

The title compound was synthesized according to the procedure of **26** using 2-(4-aminophenyl)ethanol (974 mg, 1.1 eq, 7.10 mmol). The desired product was obtained as yellow solid (1.42 g, 66%).

^{1}H NMR (250 MHz, DMSO-d_6): δ 9.79 (s, 1H, N*H*), 8.64 (d, J = 7.5 Hz, 1H, Het*H*), 8.00 (s, 1H, Het*H*), 7.84 – 7.74 (m, 2H, Ph*H*), 7.25 – 7.16 (m, 2H, Ph*H*), 6.53 (d, J = 7.6 Hz, 1H, Het*H*), 4.63 (t, J = 5.2 Hz, 1H, O*H*), 3.66 – 3.53 (m, 2H, CH_2), 2.70 (t, J = 7.2 Hz, 2H, CH_2) (ppm).

6.1.68 Synthesis of 3-bromo-*N*-(4-(2-((*tert*-butyldimethylsilyl)oxy)ethyl)phenyl)-pyrazolo[1,5-*a*]pyrimidin-5-amine (125).

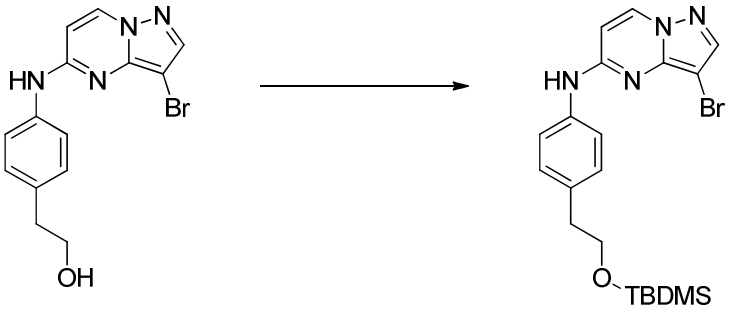

123 **125**

The title compound was synthesized according to the procedure of **27** using 2-(4-((3-bromopyrazolo[1,5-*a*]pyrimidin-5-yl)amino)phenyl)ethanol **123** (1.52 g, 1.0 eq, 4.56 mmol). The desired product was obtained as slightly yellow solid (1.96 g, 96%).

^{1}H NMR (250 MHz, $CDCl_3$-*d*): δ 9.80 (s, 1H, N*H*), 8.65 (d, *J* = 7.5 Hz, 1H, Het*H*), 8.01 (s, 1H, Het*H*), 7.86 – 7.75 (m, 2H, Ph*H*), 7.26 – 7.16 (m, 2H, Ph*H*), 6.53 (d, *J* = 7.6 Hz, 1H, Het*H*), 3.76 (t, *J* = 6.9 Hz, 2H, CH_2), 2.72 (t, *J* = 6.9 Hz, 2H, CH_2), 0.84 (s, 9H, C(CH_3)$_3$), -0.03 (s, 6H, Si(CH_3)$_2$) (ppm).

6.1.69 Synthesis of *tert*-butyl (3-bromopyrazolo[1,5-*a*]pyrimidin-5-yl)(4-(2-((*tert*-butyldi-methyl-silyl)oxy)ethyl)phenyl)carbamate (127).

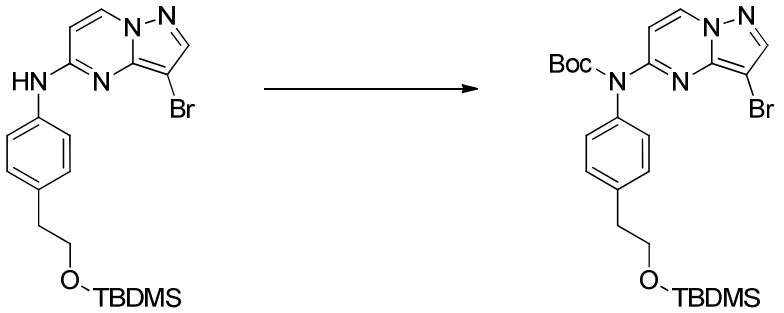

125 **127**

The title compound was synthesized according to the procedure of **28** using 3-bromo-*N*-(4-(2-((*tert*-butyldimethylsilyl)oxy)ethyl)phenyl)pyrazolo[1,5-*a*]pyrimidin-5-amine **125** (1.95 g,1.0 eq, 4.36 mmol). The desired product was obtained as yellow solid (2.16 g, 90%).

^{1}H NMR (250 MHz, $CDCl_3$-*d*): δ 8.51 (d, *J* = 7.6 Hz, 1H, Het*H*), 8.03 (s, 1H, Het*H*), 7.34 – 7.27 (m, 3H, Het*H*, Ph*H*), 7.24 – 7.17 (m, 2H, Ph*H*), 3.90 (t, *J* = 6.8 Hz, 2H, CH_2), 2.91 (t, *J* = 6.8 Hz, 2H, CH_2), 1.53 (s, 9H, C(CH_3)$_3$), 0.94 (s, 9H, C(CH_3)$_3$), 0.05 (s, 6H, Si(CH_3)$_2$) (ppm).

6.1.70 Synthesis of methyl 4-(5-((*tert*-butoxycarbonyl)(4-(2-((*tert*-butyldimethylsilyl)oxy)ethyl)-phenyl)amino)pyrazolo[1,5-*a*]pyrimidin-3-yl)-2-hydroxybenzoate (129).

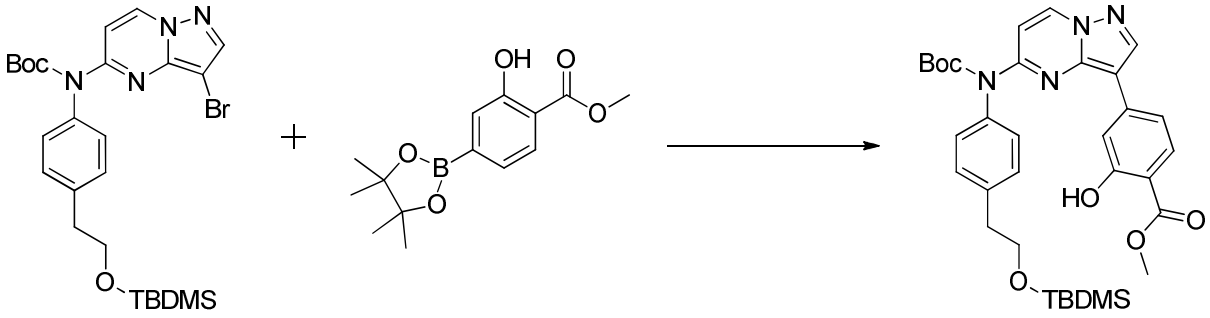

127 **32** **129**

The title compound was synthesized according to the procedure of **33** using *tert*-butyl (3-bromopyrazolo[1,5-*a*]pyrimidin-5-yl)(4-(2-((*tert*-butyldimethylsilyl)oxy)ethyl)phenyl) carbamate **127** (197 mg, 1.0 eq, 0.36 mmol). The desired product was obtained as slightly yellow solid (179 mg, 80%).

^{1}H NMR (250 MHz, $CDCl_3$-*d*): δ 10.65 (s, 1H, O*H*), 8.53 (d, J = 7.8 Hz, 1H, Het*H*), 8.34 (s, 1H, Het*H*), 7.74 – 7.56 (m, 2H, Het*H*, Ph*H*), 7.39 – 7.26 (m, 3H, Ph*H*), 7.26 – 7.11 (m, 3H, Ph*H*), 3.95 – 3.87 (m, 5H, CH_2, OCH_3), 2.93 (t, J = 7.0 Hz, 2H, CH_2), 1.46 (s, 9H, C(CH_3)$_3$), 0.89 (s, 9H, C(CH_3)$_3$), 0.01 (s, 6H, Si(CH_3)$_2$) (ppm).

6.1.71 Synthesis of methyl 4-(5-((*tert*-butoxycarbonyl)(4-(2-hydroxyethyl)phenyl)-amino)-pyrazolo[1,5-*a*]pyrimidin-3-yl)-2-hydroxybenzoate (131).

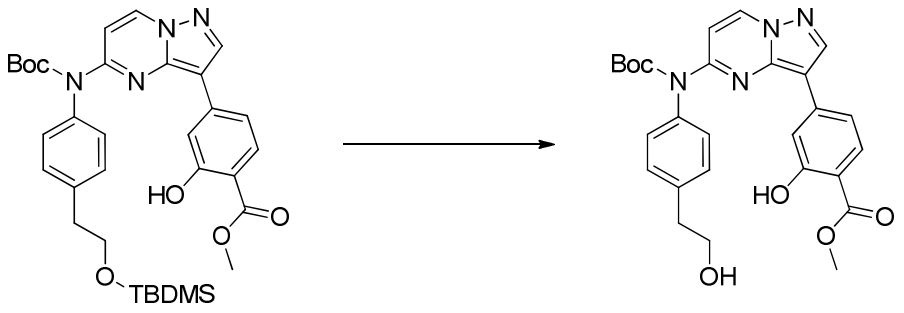

129 **131**

The title compound was synthesized according to the procedure of **34** using methyl 4-(5-((*tert*-butoxycarbonyl)(4-(2-((*tert*-butyldimethylsilyl)oxy)ethyl)phenyl)amino)pyrazolo-[1,5-*a*]pyrimidin-3-yl)-2-hydroxybenzoate **129** (1.38 g, 1.0 eq, 2.23 mmol). Purification was done by flash silica gel column chromatography with a mobile phase of *n*-hexane and ethyl acetate (ratio gradually ranging from 3:1 to 0:1). The yellow solid (939 mg, 83%) was the desired product.

^{1}H NMR (250 MHz, $CDCl_3$-*d*): δ 10.73 (s, 1H, O*H*), 8.53 (d, J = 7.8 Hz, 1H, Het*H*), 8.32 (s, 1H, Het*H*), 7.76 (d, J = 7.8 Hz, 1H, Het*H*), 7.64 (d, J = 8.4 Hz, 1H, Ph*H*), 7.42 – 7.34 (m, 2H, Ph*H*), 7.28 (d, J = 1.7 Hz, 1H, Ph*H*), 7.24 – 7.12 (m, 3H, Ph*H*), 3.96 (q, J = 6.1 Hz, 2H, CH_2), 3.92 (s, 3H, OCH_3), 2.97 (t, J = 6.2 Hz, 2H, CH_2), 2.00 (t, J = 6.1 Hz, 1H, O*H*), 1.45 (s, 9H, C(CH_3)$_3$) (ppm).

6.1.72 Synthesis of 3-(*tert*-butyl) 14-methyl (2^3Z,2^4E)-7-oxa-3-aza-2(3,5)-pyrazolo-[1,5-*a*]pyrimidina-1(1,3),4(1,4)-dibenzenacycloheptaphane-1^4,3-dicarboxylate (133).

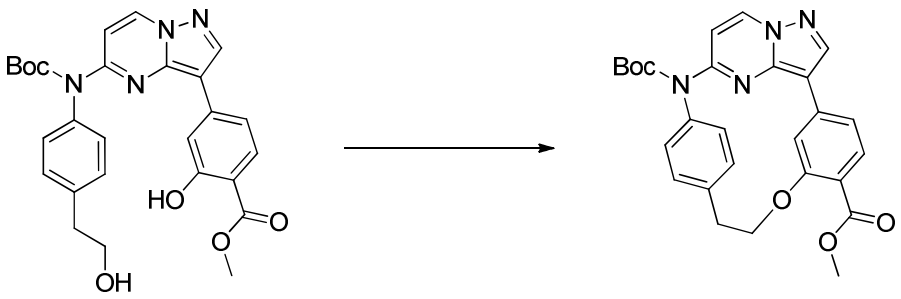

131 **133**

The title compound was synthesized according to the procedure of **35** using methyl 4-(5-((*tert*-butoxycarbonyl)(4-(2-hydroxyethyl)phenyl)amino)pyrazolo[1,5-*a*]pyrimidin-3-yl)-2-hydroxy-benzoate **131** (800 mg, 1.0 eq, 1.59 mmol). Purification was done by flash silica gel column chromatography with a mobile phase of *n*-hexane and ethyl acetate (ratio gradually ranging from 4:1 to 0:1). The obtained yellow solid (352 mg, 46%) was the desired product.

^{1}H NMR (500 MHz, DMSO-d_6): δ 9.03 (d, J = 7.9 Hz, 1H, Het*H*), 8.63 (s, 1H, Het*H*), 7.97 (d, J = 7.9 Hz, 1H, Het*H*), 7.62 (d, J = 8.2 Hz, 1H, Ph*H*), 7.49 (dd, J = 8.3, 1.8 Hz, 1H, Ph*H*), 7.43 (d, J = 8.1 Hz, 2H, Ph*H*), 7.22 (d, J = 8.2 Hz, 2H, Ph*H*), 6.79 (d, J = 1.7 Hz, 1H, Ph*H*), 3.82 (s, 3H, OCH_3), 2.98 (t, J = 5.1 Hz, 2H, CH_2), 1.48 (s, 9H, $C(CH_3)_3$) (ppm).

^{13}C NMR (126 MHz, DMSO-d_6): δ 13C NMR (126 MHz, DMSO) δ 165.51, 160.67, 153.97, 152.26, 143.26, 142.37, 140.36, 139.08, 138.17, 137.10, 130.82, 130.70, 128.57, 120.76, 120.24, 119.64, 105.13, 101.80, 82.67, 78.59, 51.84, 36.63, 27.74 (ppm).

MS (ESI+) *m/z:* 367.20 $[M - Boc - Me]^+$.

HRMS *m/z:* $[M + Na]^+$ calcd for $C_{27}H_{26}N_4NaO_5$, 509.17954; found 509.17889.

HPLC (I): t_R = 3.700 , purity ≥ 95%.

6.1.73 Synthesis of (2^3*Z*,2^4*E*)-3-(*tert*-butoxycarbonyl)-7-oxa-3-aza-2(3,5)-pyrazolo[1,5-*a*]pyrimidina-1(1,3),4(1,4)-dibenzenacycloheptaphane-1^4-carboxylic acid (135).

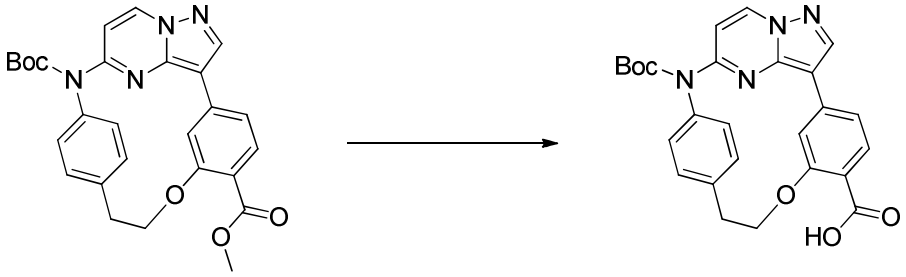

133 **135**

The title compound was synthesized according to the procedure of **37** using **133** (40 mg, 1.0 eq, 0.08 mmol). The crude product was purified by flash silica gel column chromatography with a mobile phase of *n*-hexane and ethyl acetate with the addition of 1% acetic acid (ratio gradually ranging from 7:3 to 0:1). The title compound was obtained as a white solid (29 mg, 75%).

^{1}H NMR (500 MHz, DMSO-d_6): δ 12.57 (s, 1H, COO*H*), 9.03 (d, J = 7.9 Hz, 1H, Het*H*), 8.61 (s, 1H, Het*H*), 7.97 (d, J = 7.9 Hz, 1H, Het*H*), 7.63 (d, J = 8.1 Hz, 1H, Ph*H*), 7.46 (dd, J = 8.3, 1.8 Hz, 1H, Ph*H*), 7.43 (d, J = 8.2 Hz, 2H, Ph*H*), 7.22 (d, J = 8.2 Hz, 2H, Ph*H*), 6.78 (d, J = 1.7 Hz, 1H, Ph*H*), 2.97 (t, J = 5.1 Hz, 2H, CH_2), 1.48 (s, 9H, $C(CH_3)_3$) (ppm).

^{13}C NMR (126 MHz, DMSO-d_6): δ 166.62, 160.75, 153.89, 152.27, 143.17, 142.30, 140.42, 139.05, 137.71, 137.06, 130.95, 130.80, 128.54, 121.76, 120.26, 119.51, 105.27, 101.75, 82.63, 78.32, 36.62, 27.74 (ppm).

MS (ESI+) *m/z:* 473.20 $[M + H]^+$.

HRMS *m/z:* $[M + Na]^+$ calcd for $C_{26}H_{24}N_4NaO_5$, 495.16389; found 495.16305.

HPLC (I): t_R = 16.228, purity ≥ 95%.

6.1.74 Synthesis of methyl (2^3*Z*,2^4*E*)-7-oxa-3-aza-2(3,5)-pyrazolo[1,5-*a*]-pyrimidina-1(1,3),4(1,4)-dibenzenacycloheptaphane-1^4-carboxylate (137).

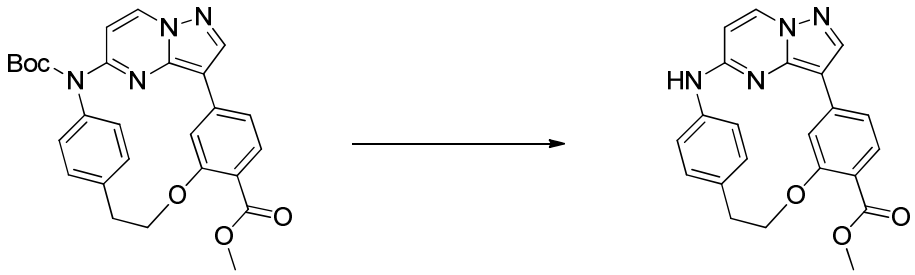

133 **137**

The title compound was synthesized according to the procedure of **36** using **133** (330 mg, 1.0 eq, 0.68 mmol). The desired product was obtained as a white solid (203 mg, 77%).

^{1}H NMR (500 MHz, DMSO-d_6): δ 9.60 (s, 1H, N*H*), 8.63 (d, *J* = 7.6 Hz, 1H, Het*H*), 8.36 (s, 1H, Het*H*), 7.59 (d, *J* = 8.2 Hz, 1H, Ph*H*), 7.41 (d, *J* = 8.2 Hz, 2H, Ph*H*), 7.38 (dd, *J* = 8.2, 1.7 Hz, 2H, Ph*H*), 7.23 (d, *J* = 1.7 Hz, 1H, Ph*H*), 7.14 (d, *J* = 8.2 Hz, 2H, Ph*H*), 6.52 (d, *J* = 7.6 Hz, 1H, Het*H*), 3.81 (s, 3H, OCH_3), 2.96 (t, *J* = 5.0 Hz, 2H, CH_2) (ppm).

^{13}C NMR (126 MHz, DMSO-d_6): δ 165.52, 160.63, 157.98, 144.57, 141.94, 139.98, 139.40, 138.66, 136.22, 130.82, 130.49, 129.74, 120.25, 119.63, 118.88, 102.38, 99.47, 78.41, 51.70, 36.66 (ppm).

MS (ESI+) *m/z:* 386.40 $[M + H]^+$.

HRMS *m/z:* $[M + H]^+$ calcd for $C_{22}H_{19}N_4O_3$, 387.14517; found 387.14491.

HPLC (I): t_R = 15.170 , purity ≥ 95%.

6.1.75 Synthesis of (2^3Z,2^4E)-7-oxa-3-aza-2(3,5)-pyrazolo[1,5-*a*]pyrimidina-1(1,3),4(1,4)-dibenzenacycloheptaphane-1^4-carboxylic acid (39).

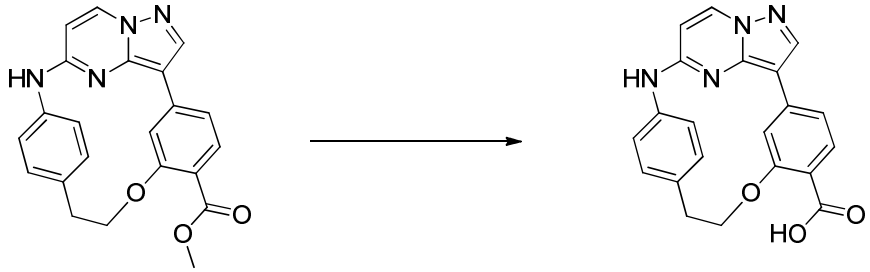

137 **39**

The title compound was synthesized according to the procedure of **37** using **137** (230 mg, 1.0 eq, 0.60 mmol). The desired product was obtained as a white solid (192 mg, 87%).

^{1}H NMR (500 MHz, DMSO-d_6): δ 12.48 (s, 1H, COO*H*), 9.60 (s, 1H, N*H*), 8.62 (d, J = 7.6 Hz, 1H, Het*H*), 8.34 (s, 1H, Het*H*), 7.59 (d, J = 8.2 Hz, 1H, Ph*H*), 7.40 (d, J = 8.2 Hz, 2H, Ph*H*), 7.35 (dd, J = 8.2, 1.8 Hz, 1H, Ph*H*), 7.21 (d, J = 1.7 Hz, 1H, Ph*H*), 7.14 (d, J = 7.9 Hz, 2H), 6.52 (d, J = 7.6 Hz, 1H, Het*H*), 2.95 (t, J = 5.0 Hz, 2H, CH_2) (ppm).

^{13}C NMR (126 MHz, DMSO-d_6): δ 166.63, 160.73, 157.94, 144.50, 141.87, 140.04, 138.98, 138.67, 136.18, 130.78, 129.73, 120.58, 120.29, 118.77, 102.50, 99.45, 78.16, 36.65 (ppm).

MS (ESI+) *m/z:* 373.20 $[M + H]^+$.

HRMS *m/z:* $[M + H]^+$ calcd for $C_{21}H_{17}N_4O_3$, 373.12952; found 373.12944.

HPLC (I): t_R = 13.602, purity ≥ 95%.

6.1.76 Synthesis of (2^3Z,2^4E)-*N*-benzyl-7-oxa-3-aza-2(3,5)-pyrazolo[1,5-*a*]-pyrimidina-1(1,3),4-(1,4)-dibenzenacycloheptaphane-1^4-carboxamide (141).

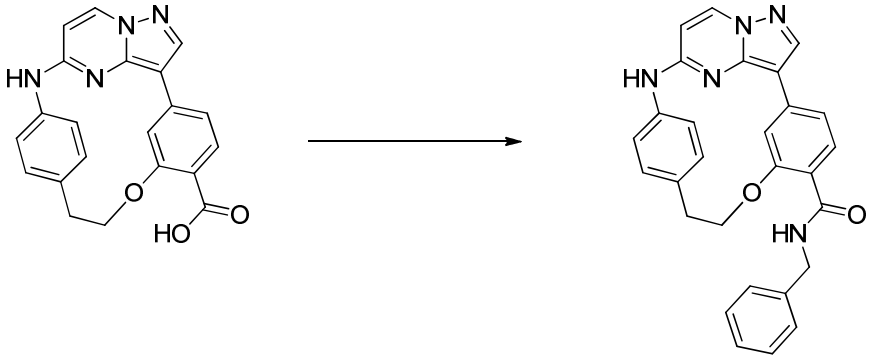

39 **141**

The title compound was synthesized according to the procedure of **61** using **39** (50 mg, 1.0 eq, 0.13 mmol) and benzylamine (16 mg, 1.1 eq, 0.15 mmol). The desired product was obtained as a white solid (49 mg, 79%).

^{1}H NMR (500 MHz, DMSO-d_6): δ 9.55 (s, 1H, N*H*), 8.64 (t, J = 6.0 Hz, 1H, N*H*), 8.62 (d, J = 7.6 Hz, 1H, Het*H*), 8.34 (s, 1H, Het*H*), 7.54 (d, J = 8.1 Hz, 1H, Ph*H*), 7.46 – 7.32 (m, 7H, Ph*H*), 7.30 – 7.24 (m, 1H, Ph*H*), 7.19 – 7.11 (m, 3H, Ph*H*), 6.51 (d, J = 7.6 Hz, 1H, Het*H*), 4.52 (d, J = 6.0 Hz, 2H, CH_2), 2.93 (t, J = 4.9 Hz, 2H, CH_2) (ppm).

^{13}C NMR (126 MHz, DMSO-d_6): δ 13C NMR (126 MHz, DMSO) δ 165.26, 158.63, 157.90, 144.32, 141.75, 139.82, 139.74, 138.89, 137.52, 136.16, 130.72, 129.87, 129.23, 128.32, 127.34, 126.76, 123.79, 119.11, 119.06, 102.62, 99.40, 79.16, 42.61, 36.54 (ppm).

MS (ESI+) *m/z:* 462.20 $[M + H]^+$.

HRMS *m/z:* $[M + H]^+$ calcd for $C_{28}H_{24}N_5O_2$, 462.19245; found 462.19202.

HPLC (I): t_R = 15.533, purity ≥ 95%.

6.1.77 Synthesis of (2^3Z,2^4E)-*N*-(3-chlorobenzyl)-7-oxa-3-aza-2(3,5)-pyrazolo[1,5-*a*]pyrimidina-1(1,3),4(1,4)-dibenzenacycloheptaphane-1^4-carboxamide (142).

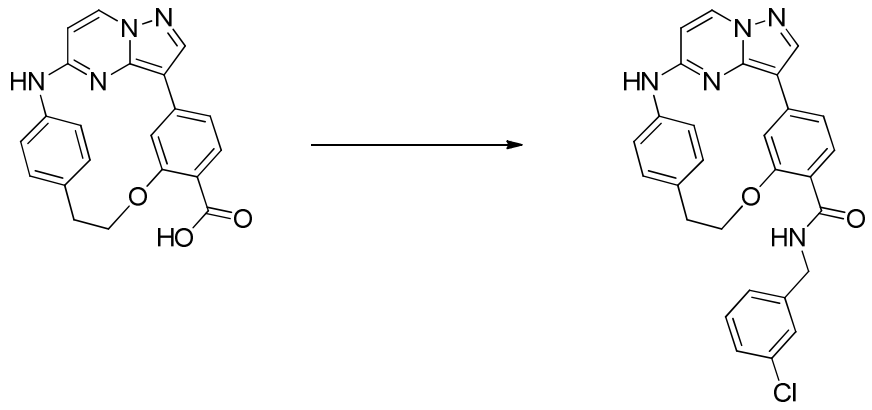

39 **142**

The title compound was synthesized according to the procedure of **61** using **39** (50 mg, 1.0 eq, 0.13 mmol) and (3-chlorophenyl)methanamine (21 mg, 1.1 eq, 0.15 mmol). The desired product was obtained as a white solid (50 mg, 75%).

^{1}H NMR (500 MHz, DMSO-d_6): δ 9.55 (s, 1H, N*H*), 8.72 (t, J = 6.1 Hz, 1H, N*H*), 8.62 (d, J = 7.6 Hz, 1H, Het*H*), 8.34 (s, 1H, Het*H*), 7.51 (d, J = 8.1 Hz, 1H, Ph*H*), 7.45 (t, J = 2.0 Hz, 1H, Ph*H*), 7.44 – 7.36 (m, 4H, Ph*H*), 7.36 – 7.32 (m, 2H, Ph*H*), 7.17 (d, J = 1.7 Hz, 1H, Ph*H*), 7.15 (d, J = 7.8 Hz, 2H, Ph*H*), 6.51 (d, J = 7.6 Hz, 1H, Het*H*), 4.51 (d, J = 6.1 Hz, 2H, CH_2), 2.97 (t, J = 4.9 Hz, 2H, CH_2) (ppm).

^{13}C NMR (126 MHz, DMSO-d_6): δ 13C NMR (126 MHz, DMSO) δ 165.52, 158.60, 157.90, 144.32, 142.46, 141.75, 139.82, 138.90, 137.55, 136.17, 132.97, 130.72, 130.19, 129.88, 129.13, 127.16, 126.67, 126.03, 123.85, 119.11, 119.04, 102.62, 99.41, 79.21, 42.11, 36.58 (ppm).

MS (ESI+) *m/z:* 496.20 $[M + H]^+$.

HRMS *m/z:* $[M + H]^+$ calcd for $C_{28}H_{23}ClN_5O_2$, 496.15348; found 496.15289.

HPLC (I): t_R = 15.177, purity ≥ 95%.

6.1.78 Synthesis of (2^3*Z*,2^4*E*)-*N*-(*tert*-butyl)-7-oxa-3-aza-2(3,5)-pyrazolo[1,5-*a*]-pyrimidina-1(1,3),4(1,4)-dibenzenacycloheptaphane-1^4-carboxamide (143).

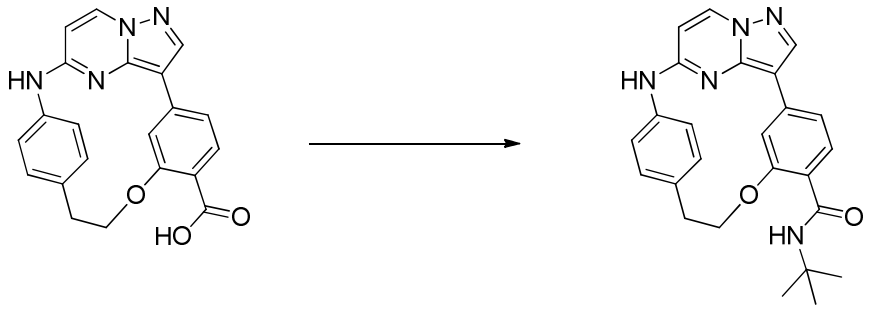

39 **143**

The title compound was synthesized according to the procedure of **61** using **39** (50 mg, 1.0 eq, 0.13 mmol) and 2-methylpropan-2-amine (11 mg, 1.1 eq, 0.15 mmol). The desired product was obtained as a beige solid (49 mg, 79%).

^{1}H NMR (500 MHz, DMSO-d_6): δ 9.56 (s, 1H, N*H*), 8.62 (d, J = 7.5 Hz, 1H, Het*H*), 8.34 (s, 1H, Het*H*), 7.95 (s, 1H), 7.55 (d, J = 8.1 Hz, 1H, Ph*H*), 7.43 (d, J = 7.9 Hz, 2H, Ph*H*), 7.38 (dd, J = 8.2, 1.7 Hz, 1H, Ph*H*), 7.18 – 7.13 (m, 3H, Ph*H*), 6.51 (d, J = 7.6 Hz, 1H, Het*H*), 3.81 (s, 1H), 3.00 (t, J = 4.9 Hz, 2H, CH_2), 1.42 (s, 9H, C(CH_3)$_3$) (ppm).

^{13}C NMR (126 MHz, DMSO-d_6): δ 13C NMR (126 MHz, DMSO) δ 164.02, 158.31, 157.91, 144.31, 141.74, 139.67, 138.94, 137.46, 136.17, 130.72, 129.88, 129.26, 123.95, 119.24, 118.89, 102.58, 99.39, 78.94, 50.23, 36.54, 28.58 (ppm).

MS (ESI+) *m/z:* 428.20 $[M + H]^+$.

HRMS *m/z:* $[M + H]^+$ calcd for $C_{25}H_{26}N_5O_2$, 428.20810; found 428.20770.

HPLC (I): t_R = 15.962, purity ≥ 95%.

6.1.79 Synthesis of methyl (1^3Z,1^4E)-9-(methylcarbamoyl)-3,6-dioxa-9-aza-1(3,5)-pyrazolo[1,5-*a*]pyrimidina-2(1,3)-benzenacyclononaphane-2^4-carboxylate (144).

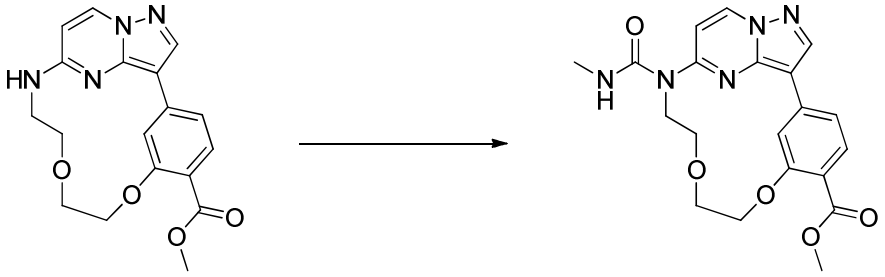

36 **144**

A solution of **36** (50 mg, 1.0 eq, 0.14 mmol) and dry triethylamine (29 mg, 2.0 eq, 0.39 mmol) in dry dichloromethane (3 mL) was cooled to 0 °C under argon atmosphere. Triphosgene (13 mg, 0.3 eq, 0.04 mmol) was added in one under stirring. After stirring for 1 h at 0 °C, methylamine 2 M in methanol (70 µL, 1.0 eq, 0.14 mmol) was added and kept for 1 h at room temperature. Subsequently, quenching was performed with saturated ammonium chloride solution. Dichloromethane was added, the phases were separated and the organic phase was washed with brine. After drying over $MgSO_4$, the crude product was purified by flash silica gel column chromatography with a mobile phase of ethyl acetate an ethanol (ratio gradually ranging from 1:0 to 0:1). The slightly yellow solid obtained was the desired compound (47 mg, 81%).

^{1}H NMR (500 MHz, DMSO-d_6): δ 8.87 (d, J = 7.8 Hz, 1H, Het*H*), 8.76 (d, J = 1.5 Hz, 1H, Ph*H*), 8.63 (s, 1H, Het*H*), 7.69 (d, J = 8.1 Hz, 1H, Ph*H*), 7.63 (q, J = 4.3 Hz, 1H, N*H*), 7.40 (dd, J = 8.1, 1.5 Hz, 1H, Ph*H*), 7.36 (d, J = 7.8 Hz, 1H, Het*H*), 4.38 (t, J = 6.4 Hz, 2H, CH_2), 4.13 (t, J = 7.0 Hz, 2H, CH_2), 3.93 – 3.86 (m, 4H, CH_2), 3.77 (s, 3H, OCH_3), 2.74 (d, J = 4.3 Hz, 3H, CH_3) (ppm).

^{13}C NMR (126 MHz, DMSO-d_6): δ 165.76, 158.74, 155.73, 154.51, 143.46, 142.66, 137.98, 135.75, 131.32, 116.45, 116.31, 112.26, 105.70, 104.22, 67.17, 66.35, 65.89, 51.67, 45.39, 27.32 (ppm).

MS (ESI+) *m/z:* 412.15 $[M + H]^+$.
HRMS *m/z:* $[M + H]^+$ calcd for $C_{20}H_{22}N_5O_5$, 412.16155; found 412.16090.
HPLC (I): t_R = 7.946 purity ≥ 95%.

6.1.80 Synthesis of methyl (1^3Z,1^4E)-9-(ethylcarbamoyl)-3,6-dioxa-9-aza-1(3,5)-pyrazolo[1,5-*a*]pyrimidina-2(1,3)-benzenacyclononaphane-2^4-carboxylate (145).

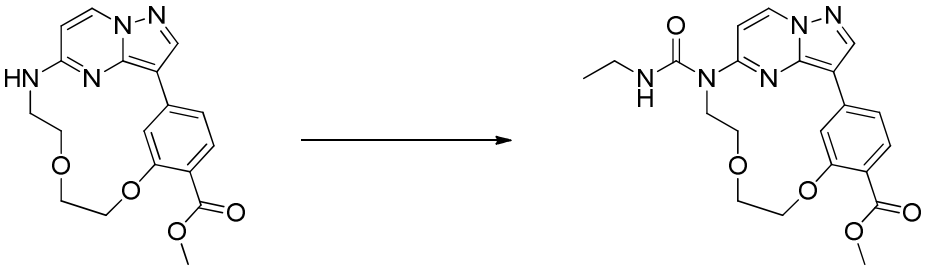

36 **145**

A solution of **36** (40 mg, 1.0 eq, 0.12 mmol) and dry triethylamine (23 mg, 2.0 eq, 0.23 mmol) in dry dichloromethane (2.5 mL) was cooled to 0 °C under argon atmosphere. Triphosgene (13 mg, 0.4 eq, 0.45 mmol) was added in one under stirring. After stirring for 1 h at 0 °C, further dry triethylamine (23 mg, 2.0 eq, 0.23 mmol) and ethylamine 2 M in ethanol (56 µL, 1.0 eq, 0.11 mmol) were added. The reaction mixture was stirred for 16 h at room temperature. After the further addition of ethylamine 2 M in ethanol (56 µL, 1.0 eq, 0.11 mmol), stirring was carried out for 48 h at room temperature. Subsequently, it was quenched with saturated ammonium chloride solution. Dichloromethane was added, the phases separated, and the organic phase was washed with brine. After drying over MgSO4, the crude product was purified by flash silica gel column chromatography with a mobile phase of *n*-hexane, ethyl acetate and ethanol (ratio gradually ranging from 1:0:0 over 0:1:0 to 0:0:1). The desired product was obtained as a white solid (30 mg, 62%).

^{1}H NMR (500 MHz, DMSO-d_6): δ 8.86 (d, J = 7.8 Hz, 1H, Het*H*), 8.76 (s, 1H, Ph*H*), 8.63 (s, 1H, Het*H*), 7.72 (t, J = 5.4 Hz, 1H, N*H*), 7.69 (d, J = 8.1 Hz, 1H, Ph*H*), 7.40 (d, J = 8.1 Hz, 1H, Ph*H*), 7.30 (d, J = 7.8 Hz, 1H, Het*H*), 4.38 (t, J = 6.4 Hz, 2H, CH_2), 4.14 (t, J = 6.9 Hz, 2H, CH_2), 3.92 – 3.86 (m, 4H, CH_2), 3.77 (s, 3H, OCH_3), 3.26 – 3.17 (m, 2H, CH_2), 1.12 (t, J = 7.2 Hz, 3H, CH_3) (ppm).

^{13}C NMR (126 MHz, DMSO-d_6): δ 165.73, 158.70, 155.03, 154.56, 143.46, 142.61, 137.97, 135.68, 131.29, 116.40, 116.25, 112.18, 105.66, 104.27, 67.09, 66.24, 65.85, 51.63, 51.53, 45.31, 35.21, 14.82 (ppm).

MS (ESI+) *m/z:*426.20 $[M + H]^+$.
HRMS *m/z:* $[M + H]^+$ calcd for $C_{21}H_{24}N_5O_5$, 426.17720; found 426.17648.
HPLC (I): t_R = 8.318 purity ≥ 95%.

6.1.81 Synthesis of methyl (1^3Z,1^4E)-9-(*tert*-butylcarbamoyl)-3,6-dioxa-9-aza-1(3,5)-pyrazolo-[1,5-*a*]pyrimidina-2(1,3)-benzenacyclononaphane-2^4-carboxylate (146).

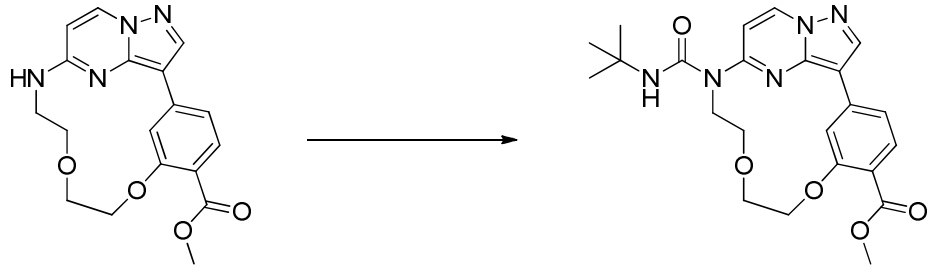

36 **146**

The title compound was synthesized according to the procedure of **144** using 2-methylpropan-2-amine (10 mg, 1.0 eq, 0.15 mmol). Purification was done by flash silica gel column chromatography with a mobile phase of ethyl acetate and ethanol (ratio gradually ranging from 1:0 to 0:1). The title compound was obtained as a slightly yellow solid (49 mg, 77%).

^{1}H NMR (500 MHz, DMSO-d_6): δ 8.84 – 8.80 (m, 2H, Het*H*, Ph*H*), 8.62 (s, 1H, Het*H*), 7.70 (d, J = 8.1 Hz, 1H, Ph*H*), 7.44 (s, 1H, N*H*), 7.40 (dd, J = 8.2, 1.4 Hz, 1H, Ph*H*), 6.98 (d, J = 7.7 Hz, 1H, Het*H*), 4.38 (t, J = 6.5 Hz, 2H, CH_2), 4.12 (t, J = 6.9 Hz, 2H, CH_2), 3.91 (t, J = 6.5 Hz, 2H, CH_2), 3.86 (t, J = 6.8 Hz, 2H, CH_2), 3.77 (s, 3H, OCH_3), 1.35 (s, 9H, C(CH_3)$_3$) (ppm).

^{13}C NMR (126 MHz, DMSO-d_6): δ 165.79, 158.69, 154.93, 154.33, 143.76, 142.62, 138.11, 135.77, 131.38, 116.40, 116.20, 112.05, 105.46, 103.74, 67.08, 66.11, 51.69, 50.90, 45.77, 28.44 (ppm).

MS (ESI+) *m/z:* 454.20 $[M + H]^+$.

HRMS *m/z:* $[M + H]^+$ calcd for $C_{23}H_{28}N_5O_5$, 454.20850; found 454.20758.

HPLC (I): t_R = 9.115 purity ≥ 95%.

6.1.82 Synthesis of methyl (1^3Z,1^4E)-9-(dimethylcarbamoyl)-3,6-dioxa-9-aza-1(3,5)-pyrazolo-[1,5-*a*]pyrimidina-2(1,3)-benzenacyclononaphane-2^4-carboxylate (147).

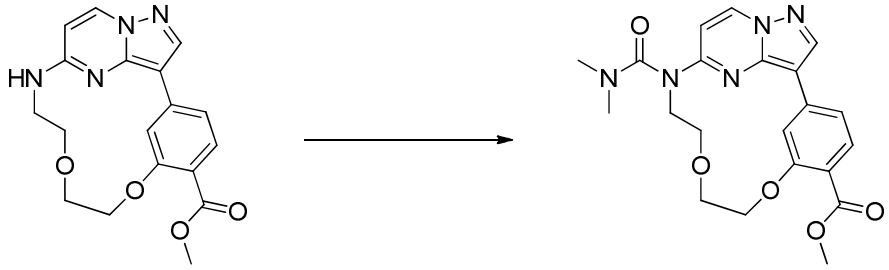

36 **147**

A solution of **36** (100 mg, 1.0 eq, 0.28 mmol) and dry triethylamine (114 mg, 4.0 eq, 1.13 mmol) in dry dichloromethane (3 mL) was cooled to 0 °C under argon atmosphere. Triphosgene (25 mg, 0.3 eq, 0.09 mmol) was added in one and the mixture was stirred for 1 h at room temperature. Dimethylamine 2 M in tetrahydrofuran (141 µL, 1.0 eq, 0.28 mmol) was added and it was stirred for 1 h at room temperature. Subsequently, quenching was performed with saturated ammonium chloride solution. Dichloromethane was added, the phases were separated and the organic phase was washed with brine. After drying over $MgSO_4$, the crude product was purified by flash silica gel column chromatography with a mobile phase of *n*-hexane, ethyl acetate and ethanol (ratio gradually ranging from 1:4:0 over 0:1:0 to 0:0:1). The slightly yellow solid obtained was the desired compound (77 mg, 64%).

^{1}H NMR (500 MHz, DMSO-d_6): δ 8.82 (d, J = 7.6 Hz, 1H, Het*H*), 8.72 (d, J = 1.5 Hz, 1H, Ph*H*), 8.58 (s, 1H, Het*H*), 7.70 (d, J = 8.1 Hz, 1H, Ph*H*), 7.37 (dd, J = 8.1, 1.4 Hz, 1H, Ph*H*), 6.55 (d, J = 7.7 Hz, 1H, Het*H*), 4.39 (t, J = 7.0 Hz, 2H, CH_2), 3.99 – 3.90 (m, 6H, CH_2), 3.77 (s, 3H, OCH_3), 2.95 (s, 6H, CH_3) (ppm).

^{13}C NMR (126 MHz, DMSO-d_6): δ 165.68, 158.20, 157.20, 153.72, 144.02, 142.75, 138.08, 136.94, 131.50, 116.22, 115.92, 111.56, 105.18, 100.34, 66.08, 65.50, 65.13, 51.62, 45.94, 37.23 (ppm).

MS (ESI+) *m/z:* 426.15 $[M + H]^+$.
HRMS *m/z:* $[M + H]^+$ calcd for $C_{21}H_{24}N_5O_5$, 426.17720; found 426.17660.
HPLC (I): t_R = 8.127 purity ≥ 95%.

6.1.83 Synthesis of methyl (1^3Z,1^4E)-9-(4-methylpiperazine-1-carbonyl)-3,6-dioxa-9-aza-1(3,5)-pyrazolo[1,5-*a*]pyrimidina-2(1,3)-benzenacyclo nonaphane-2^4-carboxylate (148).

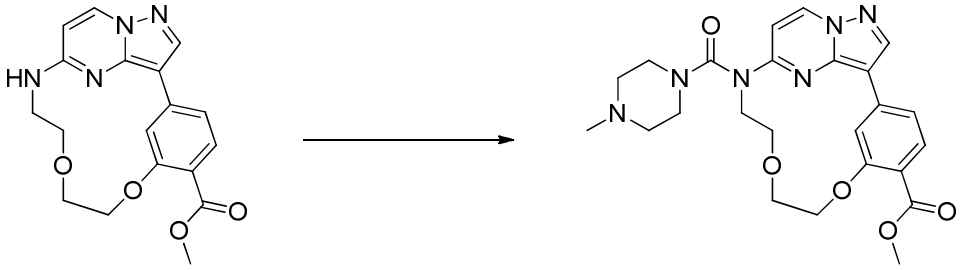

36 **148**

The title compound was synthesized according to the procedure of **147** using 1-methylpiperazine (28 mg, 1.0 eq, 0.28 mmol). Purification was done by flash silica gel column chromatography with a mobile phase of ethyl acetate and ethanol (ratio gradually ranging from 1:0 to 0:1). The desired product was obtained as a bright yellow solid (89 mg, 66%).

^{1}H NMR (500 MHz, DMSO-d_6): δ 8.85 (d, J = 7.7 Hz, 1H, Het*H*), 8.72 (d, J = 1.5 Hz, 1H, Ph*H*), 8.61 (s, 1H, Het*H*), 7.71 (d, J = 8.1 Hz, 1H, Ph*H*), 7.38 (dd, J = 8.1, 1.4 Hz, 1H, Ph*H*), 6.64 (d, J = 7.7 Hz, 1H, Het*H*), 4.40 (t, J = 7.0 Hz, 2H, CH_2), 4.02 – 3.90 (m, 6H, CH_2), 3.77 (s, 3H, OCH_3), 3.46 – 3.41 (m, 4H, CH_2), 2.42 – 2.33 (m, 4H, CH_2), 2.21 (s, 3H, , CH_3) (ppm).

^{13}C NMR (126 MHz, DMSO-d_6): δ 165.69, 158.20, 156.23, 153.79, 143.95, 142.82, 138.02, 136.94, 131.50, 116.26, 115.99, 111.54, 105.30, 100.52, 66.04, 65.45, 65.11, 54.07, 51.63, 46.11, 45.42, 45.16 (ppm).

MS (ESI+) *m/z:* 481.20 $[M + H]^+$.

HRMS *m/z:* $[M + H]^+$ calcd for $C_{24}H_{29}N_6O_5$, 481.21939; found 481.21862.

HPLC (I): t_R = 7.065, purity ≥ 95%.

6.1.84 Synthesis of methyl (1^3Z,1^4E)-9-(morpholine-4-carbonyl)-3,6-dioxa-9-aza-1(3,5)-pyrazolo[1,5-*a*]pyrimidina-2(1,3)-benzenacyclononaphane-2^4-carboxylate (149).

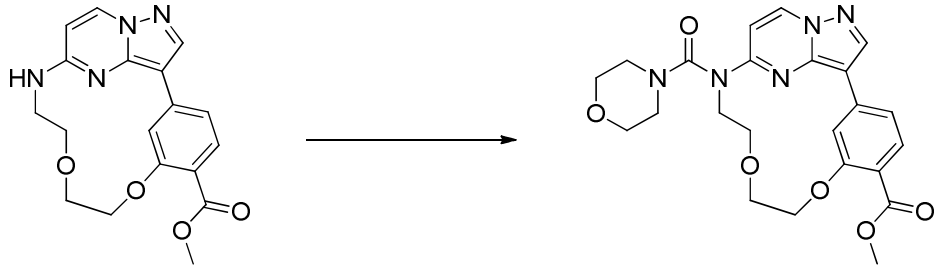

36 **149**

The title compound was synthesized according to the procedure of **147** using morpholine (12 mg, 1.0 eq, 0.14 mmol). The crude product was purified by flash silica gel column chromatography with a mobile phase of *n*-hexane, ethyl acetate and ethanol (ratio gradually ranging from 1:4:0 over 0:1:0 to 0:0:1). The title compound was obtained as a yellow solid (35 mg, 53%).

^{1}H NMR (500 MHz, DMSO-d_6): δ 8.84 (d, J = 7.7 Hz, 1H, Het*H*), 8.72 (d, J = 1.5 Hz, 1H, Ph*H*), 8.61 (s, 1H, Het*H*), 7.71 (d, J = 8.1 Hz, 1H, Ph*H*), 7.38 (dd, J = 8.1, 1.4 Hz, 1H, Ph*H*), 6.71 (d, J = 7.7 Hz, 1H, Het*H*), 4.39 (t, J = 7.0 Hz, 2H, CH_2), 4.02 – 3.98 (m, 2H, CH_2), 3.96 – 3.91 (m, 4H, CH_2), 3.77 (s, 3H, OCH_3), 3.63 (t, J = 4.9 Hz, 4H, CH_2), 3.44 (t, J = 4.8 Hz, 4H, CH_2) (ppm).

^{13}C NMR (126 MHz, DMSO-d_6): δ 165.69, 158.20, 156.36, 153.77, 143.95, 142.81, 138.01, 136.97, 131.51, 116.26, 115.99, 111.51, 105.33, 100.60, 66.03, 65.67, 65.45, 65.09, 51.63, 46.08, 45.71 (ppm).

MS (ESI+) *m/z:* 468.20 $[M + H]^+$.

HRMS *m/z:* $[M + H]^+$ calcd for $C_{23}H_{26}N_5O_6$, 468.18776; found 468.18722.

HPLC (I): t_R = 8.125 purity ≥ 95%.

6.1.85 Synthesis of methyl (1^3Z,1^4E)-9-((2-(4-methylpiperazin-1-yl)ethyl)-carbamoyl)-3,6-dioxa-9-aza-1(3,5)-pyrazolo[1,5-*a*]pyrimidina-2(1,3)-benzenacyclononaphane-2^4-carboxylate (150).

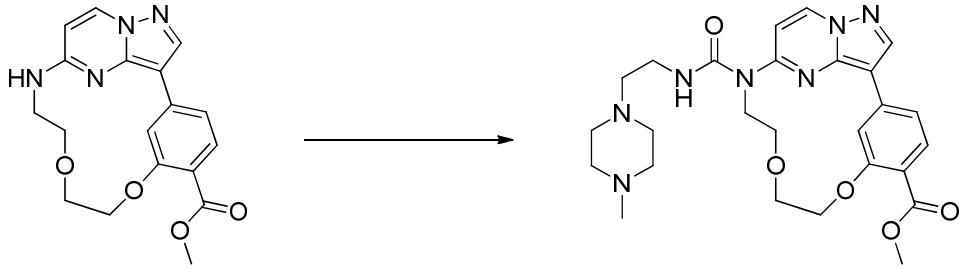

36 **150**

The title compound was synthesized according to the procedure of **147** using 2-(4-methylpiperazin-1-yl)ethanamine (40 mg, 1.0 eq, 0.28 mmol). Purification was done by flash reversed phase silica gel column chromatography with a mobile phase of acetonitrile and water (ratio gradually ranging from 5:95 to 95:5). The desired product was obtained as a white solid (115 mg, 78%).

^{1}H NMR (500 MHz, DMSO-d_6): δ 8.86 (d, J = 7.8 Hz, 1H, Het*H*), 8.79 (d, J = 1.5 Hz, 1H, Ph*H*), 8.63 (s, 1H, Het*H*), 7.71 – 7.66 (m, 2H, N*H*, Ph*H*), 7.42 – 7.37 (m, 2H, Het*H*, Ph*H*), 4.38 (t, J = 6.4 Hz, 2H, CH_2), 4.13 (t, J = 6.8 Hz, 2H, CH_2), 3.92 – 3.87 (m, 4H, CH_2), 3.77 (s, 3H, OCH_3), 3.33 – 3.23 (m, 4H, CH_2), 2.44 (t, J = 6.5 Hz, 4H, CH_2), 2.38 – 2.24 (m, 4H, CH_2), 2.15 (s, 3H, CH_3) (ppm).

^{13}C NMR (126 MHz, DMSO-d_6): δ 165.75, 158.73, 155.10, 154.70, 143.53, 142.62, 138.00, 135.67, 131.32, 116.40, 116.24, 112.21, 105.63, 104.21, 67.26, 67.18, 66.27, 66.13, 56.75, 54.84, 52.57, 51.65, 45.79, 45.43, 37.58 (ppm).

MS (ESI+) *m/z:* 524.35 $[M + H]^+$.

HRMS *m/z:* $[M + H]^+$ calcd for $C_{26}H_{34}N_7O_5$, 524.26159; found 524.26083.

HPLC (I): t_R = 6.748 purity ≥ 95%.

6.1.86 Synthesis of (1^3*Z*,1^4*E*)-9-(methylcarbamoyl)-3,6-dioxa-9-aza-1(3,5)-pyrazolo[1,5-*a*]pyrimidina-2(1,3)-benzenacyclononaphane-2^4-carboxylic acid (151).

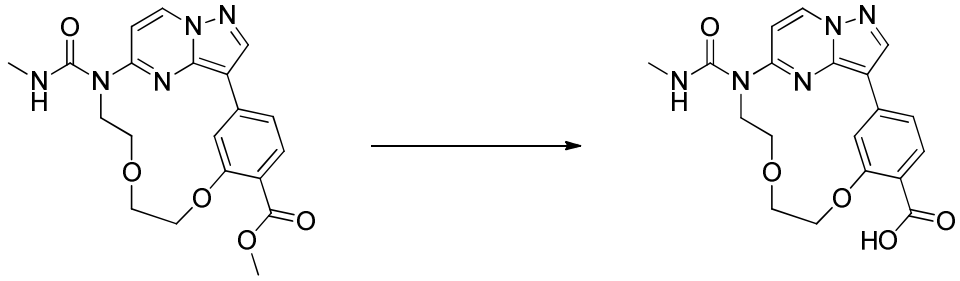

144 **151**

The title compound was synthesized according to the procedure of **60** using **144** (42 mg, 1.0 eq, 0.10 mmol). Purification was done by flash reversed phase silica gel column chromatography with a mobile phase of acetonitrile and water (ratio gradually ranging from 5:95 to 100:0). The desired product was obtained as a slightly yellow solid (18 mg, 44%).

^{1}H NMR (500 MHz, DMSO-d_6): δ 12.28 (s, 1H, COO*H*), 8.87 (d, J = 7.8 Hz, 1H, Het*H*), 8.74 (d, J = 1.5 Hz, 1H, Ph*H*), 8.63 (s, 1H, Het*H*), 7.70 (d, J = 8.0 Hz, 1H, Ph*H*), 7.63 (q, J = 4.3 Hz, 1H, N*H*), 7.39 (dd, J = 8.1, 1.5 Hz, 1H, Ph*H*), 7.36 (d, J = 7.7 Hz, 1H, Het*H*), 4.39 (t, J = 6.3 Hz, 2H, CH_2), 4.14 (t, J = 7.0 Hz, 2H, CH_2), 3.91 – 3.88 (m, 4H, CH_2), 2.74 (d, J = 4.3 Hz, 3H, CH_3) (ppm).

^{13}C NMR (126 MHz, DMSO-d_6): δ 166.84, 158.64, 155.72, 154.42, 143.37, 142.59, 137.55, 135.72, 131.48, 117.44, 116.41, 112.17, 105.80, 104.16, 67.10, 66.34, 65.83, 45.35, 27.31 (ppm).

MS (ESI+) *m/z:* 398.10 $[M + H]^+$.

HRMS *m/z:* $[M + H]^+$ calcd for $C_{19}H_{20}N_5O_5$, 398.14590; found 398.14601.

HPLC (I): t_R = 7.289 purity ≥ 95%.

6.1.87 Synthesis of (1^3Z,1^4E)-9-(ethylcarbamoyl)-3,6-dioxa-9-aza-1(3,5)-pyrazolo-[1,5-*a*]- pyrimidina-2(1,3)-benzenacyclononaphane-2^4-carboxylic acid (152).

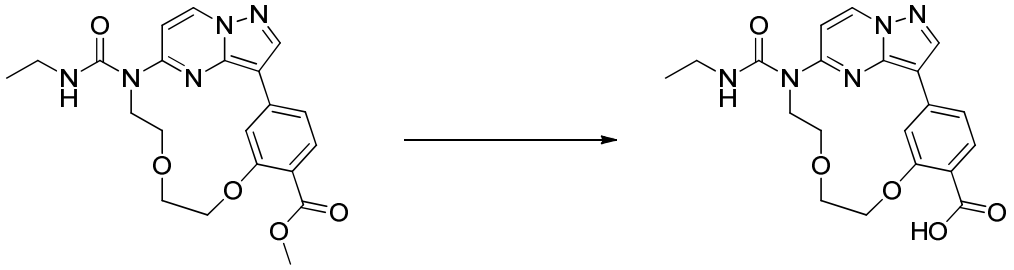

145 **152**

145 (60 mg, 1.0 eq, 0.14 mmol) and trimethyltin hydroxide (179 mg, 7.0 eq, 0.99 mmol) were solved in dichloroethane (4 mL) and the reaction mixture was stirred for 20 h under microwave radiation at 90 °C. Subsequently, the solvent was removed under reduced pressure and the residue was taken up in ethyl acetate. It was washed with 1 M HCl, the organic phase was washed with brine, dried over $MgSO_4$ and the solvent was removed in vacuo. The crude product was purified by flash reversed phase silica gel column chromatography with a mobile phase of acetonitrile and water (ratio gradually ranging from 5:95 to 100:0). The desired product was obtained as a white solid (24 mg, 41%).

^{1}H NMR (500 MHz, DMSO-d_6): δ 12.31 (s, 1H, COO*H*), 8.87 (d, J = 7.8 Hz, 1H, Het*H*), 8.75 (d, J = 1.5 Hz, 1H, Ph*H*), 8.63 (s, 1H, Het*H*), 7.76 – 7.67 (m, 2H, N*H*, Ph*H*), 7.40 (dd, J = 8.1, 1.5 Hz, 1H, Ph*H*), 7.30 (d, J = 7.8 Hz, 1H, Het*H*), 4.39 (t, J = 6.3 Hz, 2H, CH_2), 4.15 (t, J = 6.9 Hz, 2H, CH_2), 3.94 – 3.86 (m, 4H, CH_2), 3.26 – 3.17 (m, 2H, CH_2), 1.12 (t, J = 7.2 Hz, 3H, CH_3) (ppm).

^{13}C NMR (126 MHz, DMSO-d_6): δ 166.81, 158.65, 155.06, 154.52, 143.41, 142.58, 137.58, 135.68, 131.48, 117.35, 116.41, 112.16, 105.78, 104.25, 67.09, 66.31, 65.85, 45.34, 35.20, 14.83 (ppm).

MS (ESI+) *m/z:* 412.15 $[M + H]^+$.

HRMS *m/z:* $[M + H]^+$ calcd for $C_{20}H_{22}N_5O_5$, 412.16155; found 412.16101.

HPLC (I): t_R = 7.611, purity ≥ 95%.

6.1.88 Synthesis of (1^3Z,1^4E)-9-(*tert*-butylcarbamoyl)-3,6-dioxa-9-aza-1(3,5)-pyrazolo[1,5-*a*]pyrimidina-2(1,3)-benzenacyclononaphane-2^4-carboxylic acid (153).

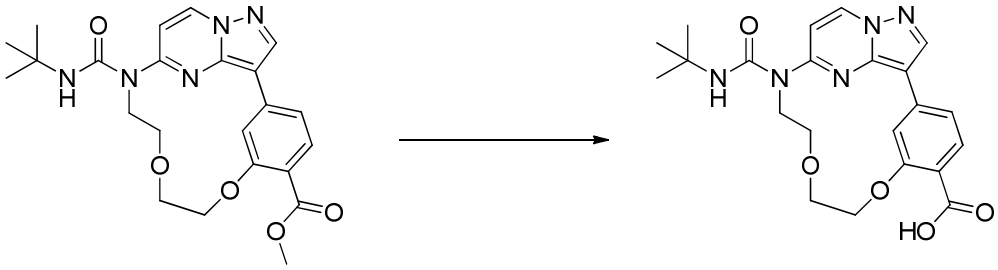

146 **153**

The title compound was synthesized according to the procedure of **152** using **146** (40 mg, 1.0 eq, 0.09 mmol). Purification was done by flash revered phase silica gel column chromatography with a mobile phase of acetonitrile and water (ratio gradually ranging from 5:95 to 100:0). The desired product was obtained as a white solid (16 mg, 41%).

^{1}H NMR (500 MHz, DMSO-d_6): δ 12.25 (s, 1H, COO*H*), 8.82 (d, J = 7.7 Hz, 1H, Het*H*), 8.79 (d, J = 1.5 Hz, 1H, Ph*H*), 8.61 (s, 1H, Het*H*), 7.71 (d, J = 8.1 Hz, 1H, Ph*H*), 7.44 (s, 1H, N*H*), 7.39 (dd, J = 8.1, 1.4 Hz, 1H, Ph*H*), 6.97 (d, J = 7.7 Hz, 1H, Het*H*), 4.38 (t, J = 6.5 Hz, 2H, CH_2), 4.12 (t, J = 6.9 Hz, 2H, CH_2), 3.93 – 3.84 (m, 4H, CH_2), 1.35 (s, 9H, , C(CH_3)$_3$) (ppm).

^{13}C NMR (126 MHz, DMSO-d_6): δ 166.80, 158.62, 154.84, 154.32, 143.68, 142.54, 137.72, 135.72, 131.55, 117.18, 116.35, 111.93, 105.54, 103.67, 66.98, 66.03, 50.87, 45.73, 28.43 (ppm).

MS (ESI+) *m/z:* 440.20 $[M + H]^+$.

HRMS *m/z:* $[M + H]^+$ calcd for $C_{22}H_{26}N_5O_5$, 440.19285; found 440.19271.

HPLC (I): t_R = 8.413, purity ≥ 95%.

6.1.89 Synthesis of (1^3Z,1^4E)-9-(dimethylcarbamoyl)-3,6-dioxa-9-aza-1(3,5)-pyrazolo[1,5-*a*]- pyrimidina-2(1,3)-benzenacyclononaphane-2^4-carboxylic acid (154).

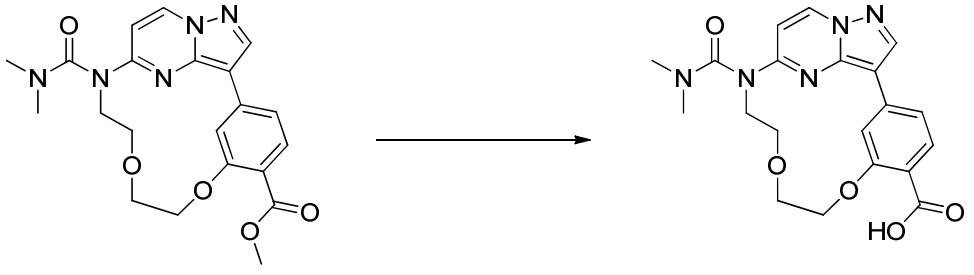

147 **154**

The title compound was synthesized according to the procedure of **152** using **147** (73 mg, 1.0 eq, 0.17 mmol). The crude product was purified by flash revered phase silica gel column chromatography with a mobile phase of acetonitrile and water (ratio gradually ranging from 5:95 to 95:5). The obtained white solid (32 mg, 45%) was the desired compound.

^{1}H NMR (500 MHz, DMSO-d_6): δ 12.34 (s, 1H, COO*H*), 8.83 (d, J = 7.7 Hz, 1H, Het*H*), 8.71 (d, J = 1.7 Hz, 1H, Ph*H*), 8.59 (s, 1H, Het*H*), 7.72 (d, J = 8.1 Hz, 1H, Ph*H*), 7.37 (dd, J = 8.1, 1.4 Hz, 1H, Ph*H*), 6.55 (d, J = 7.7 Hz, 1H, Het*H*), 4.40 (t, J = 6.9 Hz, 2H, CH_2), 4.00 – 3.91 (m, 6H, CH_2), 2.95 (s, 6H, CH_3) (ppm).

^{13}C NMR (126 MHz, DMSO-d_6): δ 166.76, 158.17, 157.23, 153.67, 143.97, 142.72, 137.66, 136.94, 131.68, 117.08, 116.22, 111.56, 105.31, 100.32, 66.05, 65.49, 65.19, 45.95, z37.24 (ppm).

MS (ESI+) *m/z:* 412.15 $[M + H]^+$.

HRMS *m/z:* $[M + H]^+$ calcd for $C_{20}H_{22}N_5O_5$, 412.16155; found 412.16120.

HPLC (I): t_R = 7.414 purity ≥ 95%.

6.1.90 Synthesis of (1^3Z,1^4E)-9-(4-methylpiperazine-1-carbonyl)-3,6-dioxa-9-aza-1(3,5)-pyrazolo[1,5-*a*]pyrimidina-2(1,3)-benzenacyclononaphane-2^4-carboxylic acid (155).

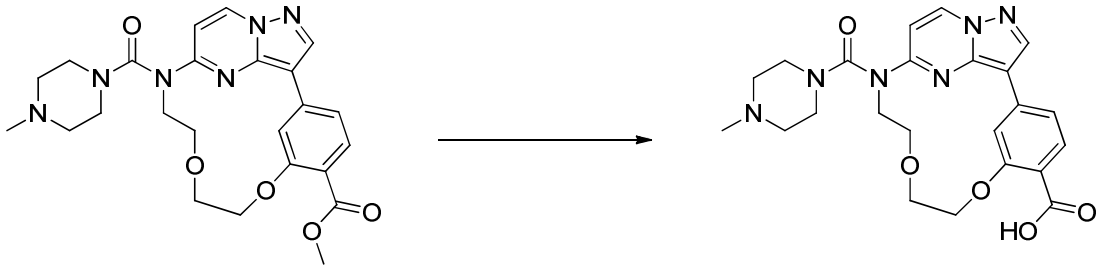

148 **155**

The title compound was synthesized according to the procedure of **152** using **148** (80 mg, 1.0 eq, 0.17 mmol). Purification was done by flash revered phase silica gel column chromatography with a mobile phase of acetonitrile and water (ratio gradually ranging from 1:9 to 9:1). The title compound was yielded as a white solid (39 mg, 50%).

^{1}H NMR (500 MHz, DMSO-d_6): δ 12.06 (s, 1H, COO*H*), 8.85 (d, J = 7.7 Hz, 1H, Het*H*), 8.71 (d, J = 1.6 Hz, 1H, Ph*H*), 8.61 (s, 1H, Het*H*), 7.72 (d, J = 8.1 Hz, 1H, Ph*H*), 7.37 (dd, J = 8.1, 1.4 Hz, 1H, Ph*H*), 6.65 (d, J = 7.7 Hz, 1H, Het*H*), 4.40 (t, J = 7.0 Hz, 2H, CH_2), 4.03 – 3.90 (m, 6H, CH_2), 3.47 – 3.42 (m, 4H, CH_2), 2.48 – 2.33 (m, 4H, CH_2), 2.25 (s, 3H, CH_3) (ppm).

^{13}C NMR (126 MHz, DMSO-d_6): δ 166.74, 158.18, 156.28, 153.74, 143.89, 142.78, 137.65, 136.93, 131.70, 117.02, 116.25, 111.50, 105.43, 100.52, 65.99, 65.43, 65.15, 53.96, 46.13, 45.28, 45.03 (ppm).

MS (ESI+) *m/z:* 467.25 $[M + H]^+$.

HRMS *m/z:* $[M + Na]^+$ calcd for $C_{23}H_{26}N_6NaO_5$, 489.18569; found 489.18499.

HPLC (I): t_R = 6.473 purity ≥ 95%.

6.1.91 Synthesis of (1^3Z,1^4E)-9-(morpholine-4-carbonyl)-3,6-dioxa-9-aza-1(3,5)-pyrazolo[1,5-*a*]- pyrimidina-2(1,3)-benzenacyclononaphane-2^4-carboxylic acid (156).

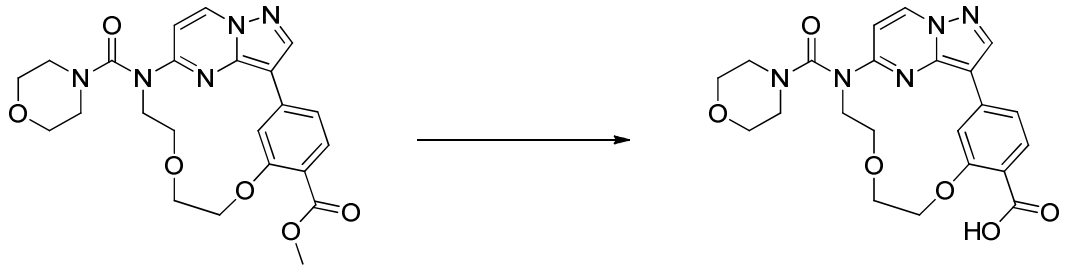

149 **156**

The title compound was synthesized according to the procedure of **152** using **149** (53 mg, 1.0 eq, 0.11 mmol). Purification was done by flash revered phase silica gel column chromatography with a mobile phase of acetonitrile and water (ratio gradually ranging from 5:95 to 95:5). The desired product was obtained as a yellow solid (16 mg, 31%).

^{1}H NMR (500 MHz, DMSO-d_6): δ 12.36 (s, 1H, COO*H*), 8.84 (d, J = 7.7 Hz, 1H, Het*H*), 8.68 (s, 1H, Ph*H*), 8.59 (s, 1H, Het*H*), 7.67 (d, J = 7.3 Hz, 1H, Ph*H*), 7.35 (d, J = 8.0 Hz, 1H, Ph*H*), 6.71 (d, J = 7.7 Hz, 1H, Het*H*), 4.38 (t, J = 7.1 Hz, 2H, CH_2), 4.04 – 3.89 (m, 6H, CH_2), 3.65 – 3.60 (m, 4H, CH_2), 3.44 (t, J = 4.8 Hz, 4H, CH_2) (ppm).

^{13}C NMR (126 MHz, DMSO-d_6): δ 156.42, 153.66, 143.82, 142.71, 136.93, 131.49, 116.20, 111.58, 105.54, 100.55, 65.96, 65.68, 65.43, 65.17, 46.11, 45.73, 40.43 (ppm).

MS (ESI+) *m/z:* 454.15 $[M + H]^+$.

HRMS *m/z:* $[M + Na]^+$ calcd for $C_{22}H_{24}N_5O_6$, 454.17211; found 454.17144.

HPLC (I): t_R = 7.423 purity ≥ 95%.

6.1.92 Synthesis of dimethyl (1^3Z,1^4E)-3,6-dioxa-9-aza-1(3,5)-pyrazolo[1,5-*a*]-pyrimidina-2(1,3)-benzenacyclononaphane-2^4,9-dicarboxylate (165).

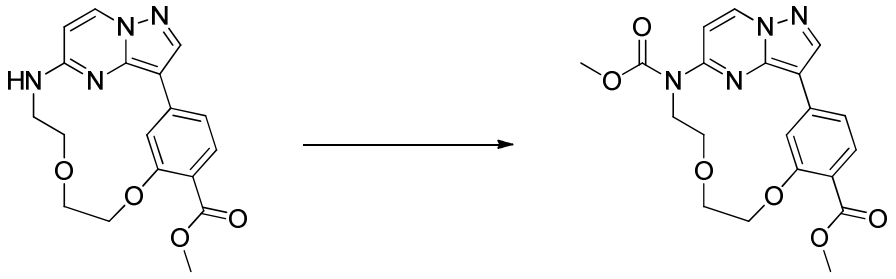

36 **165**

The title compound was synthesized according to the procedure of **147** using sodium methoxide 25% in methanol (61 mg, 1.0 eq, 0.28 mmol). The crude product was purified by flash silica gel column chromatography with a mobile phase of *n*-hexane, ethyl acetate and ethanol (ratio gradually ranging from 1:4:0 over 0:1:0 to 0:0:1). The obtained yellow solid (98 mg, 84%) was the desired compound.

^{1}H NMR (500 MHz, DMSO-d_6): δ 9.06 (d, J = 7.7 Hz, 1H, Het*H*), 8.77 (d, J = 1.6 Hz, 1H, Ph*H*), 8.73 (s, 1H, Het*H*), 7.70 (d, J = 8.1 Hz, 1H, Ph*H*), 7.62 (d, J = 7.8 Hz, 1H, Het*H*), 7.44 (dd, J = 8.1, 1.4 Hz, 1H, Ph*H*), 4.39 (t, J = 6.1 Hz, 2H, CH_2), 4.15 (t, J = 6.7 Hz, 2H, CH_2), 3.93 (t, J = 6.7 Hz, 2H) , CH_2, 3.88 (t, J = 6.0 Hz, 2H, CH_2), 3.85 (s, 3H, OCH_3), 3.78 (s, 3H, OCH_3) (ppm).

^{13}C NMR (126 MHz, DMSO-d_6): δ 165.77, 158.86, 154.30, 153.17, 143.15, 142.94, 137.52, 136.80, 131.23, 116.70, 116.65, 112.69, 106.46, 103.87, 67.58, 66.88, 66.48, 53.84, 51.69, 46.51 (ppm).

MS (ESI+) *m/z:* 413.10 $[M + H]^+$.

HRMS *m/z:* $[M + H]^+$ calcd for $C_{20}H_{21}N_4O_6$, 413.14556; found 413.14470.

HPLC (I): t_R = 8.921 purity ≥ 95%.

6.1.93 Synthesis of 9-ethyl 2^4-methyl (1^3Z,1^4E)-3,6-dioxa-9-aza-1(3,5)-pyrazolo-[1,5-*a*]pyrimidina-2(1,3)-benzenacyclononaphane-2^4,9-dicarboxylate (166).

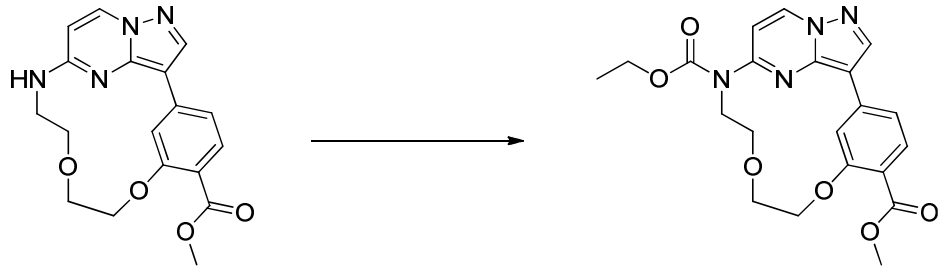

36 **166**

The title compound was synthesized according to the procedure of **147** using sodium ethoxide 21% in ethanol (91 mg, 1.0 eq, 0.28 mmol). Purification was done by flash silica gel column chromatography with a mobile phase of *n*-hexane, ethyl acetate and ethanol (ratio gradually ranging from 1:0:0 over 0:1:0 to 0:0:1). The title compound was obtained as a yellow solid (78 mg, 65%).

^{1}H NMR (500 MHz, DMSO-d_6): δ 9.06 (d, J = 7.8 Hz, 1H, Het*H*), 8.78 (d, J = 1.6 Hz, 1H, Ph*H*), 8.74 (s, 1H, Het*H*), 7.70 (d, J = 8.1 Hz, 1H, Ph*H*), 7.62 (d, J = 7.8 Hz, 1H, Het*H*), 7.45 (dd, J = 8.1, 1.5 Hz, 1H, Ph*H*), 4.39 (t, J = 6.0 Hz, 2H, CH_2), 4.30 (q, J = 7.1 Hz, 2H, CH_2), 4.16 (t, J = 6.6 Hz, 2H, CH_2), 3.94 (t, J = 6.6 Hz, 2H, CH_2), 3.89 (t, J = 6.0 Hz, 2H, CH_2), 3.78 (s, 3H, OCH_3), 1.32 (t, J = 7.1 Hz, 3H, CH_3) (ppm).

^{13}C NMR (126 MHz, DMSO-d_6): δ 165.78, 158.87, 153.72, 153.24, 143.15, 142.97, 137.54, 136.75, 131.23, 116.71, 116.66, 112.74, 106.45, 103.96, 67.61, 66.91, 66.53, 62.77, 51.68, 46.49 (ppm).

MS (ESI+) *m/z:* 427.15 $[M + H]^+$.

HRMS *m/z:* $[M + H]^+$ calcd for $C_{21}H_{23}N_4O_6$, 427.16121; found 427.16038.

HPLC (I): t_R = 9.377 purity ≥ 95%.

6.1.94 Synthesis of (1^3Z,1^4E)-9-(methoxycarbonyl)-3,6-dioxa-9-aza-1(3,5)-pyrazolo[1,5-*a*]pyrimidina-2(1,3)-benzenacyclononaphane-2^4-carboxylic acid (167).

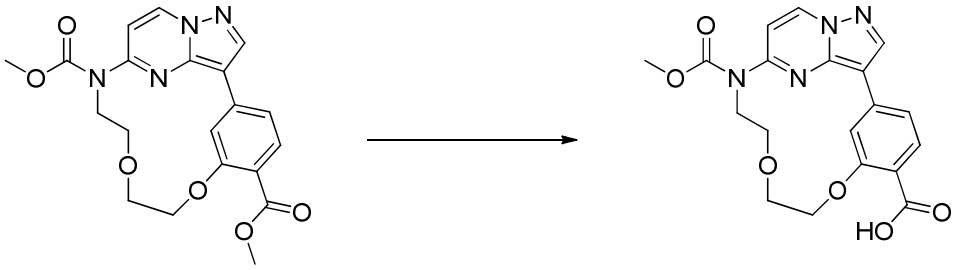

165 **167**

The title compound was synthesized according to the procedure of **152** using **165** (90 mg, 1.0 eq, 0.22 mmol). Purification was done by flash revered phase silica gel column chromatography with a mobile phase of acetonitrile and water (ratio gradually ranging from 5:95 to 95:5). The desired product was obtained as a slightly yellow solid (18 mg, 21%).

^{1}H NMR (500 MHz, DMSO-d_6): δ 12.35 (s, 1H, COO*H*), 9.04 (d, J = 7.8 Hz, 1H, Het*H*), 8.72 (d, J = 1.6 Hz, 1H, Ph*H*), 8.71 (s, 1H, Het*H*), 7.68 (d, J = 8.0 Hz, 1H, Ph*H*), 7.61 (d, J = 7.8 Hz, 1H, Het*H*), 7.41 (dd, J = 8.1, 1.5 Hz, 1H, Ph*H*), 4.38 (t, J = 6.1 Hz, 2H, CH_2), 4.14 (t, J = 6.7 Hz, 2H, CH_2), 3.92 (t, J = 6.7 Hz, 2H, CH_2), 3.88 (t, J = 6.1 Hz, 2H, CH_2), 3.85 (s, 3H, OCH_3) (ppm).

^{13}C NMR (126 MHz, DMSO-d_6): δ 158.64, 154.28, 153.03, 143.05, 142.82, 136.90, 136.74, 131.30, 116.58, 112.53, 106.57, 103.73, 67.42, 66.80, 66.36, 53.82, 46.42 (ppm).

MS (ESI+) *m/z:* 399.05 $[M + H]^+$.

HRMS *m/z:* $[M + Na]^+$ calcd for $C_{19}H_{19}N_4O_6$, 399.12991; found 399.12970.

HPLC (I): t_R = 8.095, purity ≥ 95%.

6.1.95 Synthesis of (1^3Z,1^4E)-9-(ethoxycarbonyl)-3,6-dioxa-9-aza-1(3,5)-pyrazolo-[1,5-*a*]pyrimidine-2(1,3)-benzenacyclononaphane-2^4-carboxylic acid (168).

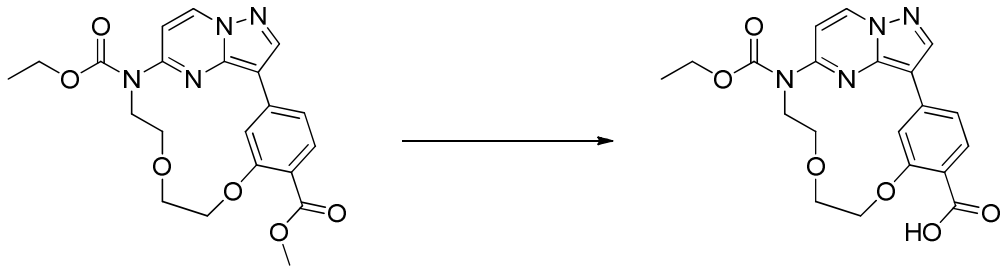

166 **168**

The title compound was synthesized according to the procedure of **152** using **166** (70 mg, 1.0 eq, 0.22 mmol). The crude product was purified by flash revered phase silica gel column chromatography with a mobile phase of acetonitrile and water (ratio gradually ranging from 5:95 to 95:5). The yellow solid (19 mg, 28%) was the desired compound.

^{1}H NMR (500 MHz, DMSO-d_6): δ 9.04 (d, J = 7.7 Hz, 1H, Het*H*), 8.73 (d, J = 1.6 Hz, 1H, Ph*H*), 8.71 (s, 1H, Het*H*), 7.69 (d, J = 8.0 Hz, 1H, Ph*H*), 7.61 (d, J = 7.8 Hz, 1H, Het*H*), 7.41 (dd, J = 8.1, 1.5 Hz, 1H, Ph*H*), 4.39 (t, J = 6.1 Hz, 2H), 4.29 (q, J = 7.1 Hz, 2H, CH_2), 4.14 (t, J = 6.7 Hz, 2H, CH_2), 3.93 (t, J = 6.7 Hz, 2H, CH_2), 3.88 (t, J = 6.1 Hz, 2H, CH_2), 1.31 (t, J = 7.1 Hz, 3H, CH_3) (ppm).

^{13}C NMR (126 MHz, DMSO-d_6): δ 166.92, 158.69, 153.72, 153.11, 143.05, 142.87, 136.97, 136.70, 131.33, 118.17, 116.62, 112.59, 106.57, 103.85, 67.48, 66.86, 66.43, 62.76, 46.42, 14.13 (ppm).

MS (ESI+) *m/z:* 413.10 $[M + H]^+$.

HRMS *m/z:* $[M + Na]^+$ calcd for $C_{20}H_{21}N_4O_6$, 413.14556; found 413.14567.

HPLC (I): t_R = 8.622, purity ≥ 95%.

6.2 Differential scanning fluorimetry assay

Thermal melting experiments were carried out, as described previously[194], with an Mx3005p realtime PCR machine (Agilent). Proteins were buffered in 25 mM HEPES (pH 7.5), 500 mM NaCl and were assayed in a 96-wellplate at a final concentration of 2 µM in a 20 µL volume. Inhibitors were added at a final concentration of 10 µM. SYPRO-Orange (Molecular Probes) was added as a fluorescence probe at a dilution of 1 in 5000. Excitation and emission filters were set to 465 nm and 590 nm, respectively. The temperature was raised with a step of 3 °C per minute, and fluorescence readings were taken at each interval. The temperature dependence of the fluorescence was approximated by the equation

$$Y_{(T)} = y_F + [(y_U + y_F)/(1 + \exp(\Delta uG_{(T)}/RT))]$$

where ΔuG is the difference in unfolding free energy between the folded and unfolded state, R is the gas constant, and y_F and y_U are the fluorescence intensity of the probe in the presence of completely folded and unfolded protein, respectively[217]. The baselines of the denatured and native state were approximated by a linear fit. The observed temperature shifts, ΔT_m^{obs}, for each inhibitor were recorded as the difference between the transition midpoints of sample and reference wells containing protein without inhibitor and were determined by nonlinear least-squares fit. Measurements were performed in triplicate.

7. Abbreviations and acronyms

%Ctrl	percent of control
$(Pd_2dba)_3$	tris(dibenzylideneacetone)dipalladium(0)
°C	degree Celsius
µm	micrometers
µM	micromole
2-MTHF	2-methyltetrahydrofuran
4-DMAP	4-(dimethylamino)pyridine
AAK1	AP-2-Associated protein Kinase
ABL	Abelson murine Leukemia viral oncogene homolog
ACE2	Angiotensin-Converting Enzyme 2
ACN	acetonitrile
ADP	Adenosine Diphosphate
AGC	protein kinase A, G and C families
ALK2/3	Anaplastic Lymphoma Kinase 2/3
ANLN	anillin actin binding protein
ANT2	anti-apoptotic oncoprotein Adenine Nucleotide Translocase 2
AP1/2	Adapter Protein 1/2
AP-MS	Affinity-Purification Mass Spectrometry
ATP	Adenosine Triphosphate
AurB	Aurora kinase B
AXK	adenine-X-lysine
B_2pin_2	bis(pinacolato)diborone
BCR	Breakpoint Cluster Region protein
Bid	BH3 interacting domain death agonist
BIKE	BMP-2-inducible protein kinase
Boc	*tert*-butyl carbamate
BRAF	serine/threonine-protein kinase B-raf
BRET	Bioluminescent Resonance Energy Transfer
Brine	aqueous NaCl saturated
BTC	bis(trichloromethyl) carbonate (triphosgene)
CAMK	Calcium/Calmodulin-dependent Kinase
CaMK2b	Calcium/Calmodulin-dependent protein Kinase 2 subunit β
CCPs	Clathrin-Coated Pits
CCVs	Clathrin-Coated Vesicles

CDC	Cell Division Cycle kinase
$CDCl_3$-*d*	dichloromethane deuterated
CDK	Cycline-Dependent Kinase
CHK1	Checkpoint Kinase 1
CK1/2	Casein Kinase 1/2
CLK3	CDC-Like Kinase 3
CMGC	Cycline-dependent kinase, Mitogen-activated protein kinase, Glycogene synthase kinase, Casein kinase 2
COVID-19	Coronavirus Disease 2019
Ct	cycle threshold (qPCR)
d	doublet
DAPK1/2/3	Death-Associated Protein Kinase 1/2/3
DCE	dichloroethane
DCM	dichloromethane
dd	double doublet
DEAD	diethyl azodicarboxylate
DENV	Dengue Virus
DFG	aspartic acid-phenylalanine-glycine
DIAD	disopropyl azodicarboxylate
DMF	dimethylformamide
DMSO	dimethylsulfoxide
DMSO-*d6*	dimethylsulfoxide deuterated
DNA	Deoxyribonucleic Acid
DPF	aspartic acid-proline-phenylalanine
DPPA	diphenylphosphoryl azide
DRAK1/2	Death-associated protein kinase-Related Apoptosis-inducing protein Kinase 1/2
DSF	Differential Scanning Fluorimetry
DWG	aspartic acid-tryptophan-glycine
DYRK	Dual-specificity Tyrosine Regulated Kinase
EBOV	Ebola Virus
EC_{50}	half-maximal effective concentration
EGFR	Epidermal Growth Factor Receptor
EH	Eps15-Homology domain
EHD1/5	EH Domain-containing protein 1/5
ePK	eukaryotic Protein Kinase
EPS15	Epidermal growth factor receptor Substrate 15

eq	equivalent
ESI	Electrospray Ionization
FDA	U.S. Food and Drug Administration
FHA	Forkhead-Associated domain
FGFR2	Fibroblast Growth Factor Receptor 2
FLT3	Fms-Like Tyrosine kinase 3
FMS	Feline McDonough Sarcoma
FRET	Fluorescence Resonance Energy Transfer
g	gram
GAK	cyclin G-Associated protein Kinase
GBM	Glioblastoma Multiforme
GSK3B	Glycogen Synthase Kinase 3 β
GTP	Guanosine Triphosphate
h	hour
HATU	(1-[bis(dimethylamino)methylene]-1H-1,2,3-triazolo[4,5-*b*]pyridinium 3-oxide hexa-fluorophosphate
HCl	hydrochloric acid
HCV	Hepatitis C Virus
HIPK(3)	Homeodomain-Interacting Protein Kinase (3)
HNSCC	Head and Neck Squamous Carcinoma
HOAt	1-hydroxy-7-azabenzotriazole
HPLC	High Performance Liquid Chromatography
HRD	histidine-arginine-aspartic acid
Hz	Hertz
IC_{50}	half maximum inhibitory concentration
IKKε	inhibitor of nuclear factor kappa-B kinase subunit epsilon
INSR	Insuline Receptor
ITC	Isothermal Titration Calorimetry
J	coupling constant
JAK1/2	Janus Kinase 1/2
K_3PO_4	potassium phosphate
K_D	dissociation constant
kDA	kilodalton
K_i	inhibitory constant
KIT	mast/stem cell growth factor receptor Kit
KOAc	potassium acetate

LiOH · H2O	lithium hydroxide monohydrate
LOK	Lymphocyte-Oriented Kinase
M	molarity
m	multiplet
m/z	mass-to-charge ratio
MALDI-HRMS	Matrix-Assisted Laser Desorption/Ionization High-Resolution Mass Spectrometry
MAPK/MEK	Mitogen-Activated Protein Kinase
MDC1	Mediator of DNA damage Checkpoint protein 1
Me_3SnOH	trimethyltin hydroxide
MeOH	methanol
mg	milligram
$MgSO_4$	magnesium sufate
MH2	C-terminal Mad Homology 2 domain
MHz	Megahertz
min	minutes
mL	milliliters
mmol	millimole
MNK1/2	MAP kinase-interacting serine/threonine-protein Kinase 1/2
mol	mole
MRE11	double-strand break repair protein Meiotic Recombination 11
MRLC	Myosin Regulatory Light Chain
MRN	protein complex (MRE11, RAD50, NBN)
MS	Mass Spectrometry
MST2	Mammalian STE20-like kinase 2
mTOR	mechanistic Target Of Rapamycin
MTT	3-(4,5-dimethylthiazol-2-yl)-2,5-diphenyltetrazolium bromide
N	normality
n	reaktion stoichiometry
n.d.	not determined
Na_2SO_4	sodium sulfate
NaCl	sodium chloride
NAK	Numb-Associated protein Kinase
NBN	nibrin
NBS	*N*-bromosuccinimide
NCI	National Cancer Institute

nm	nanometers
nM	nanomol
NMR	Nuclear Magnetic Resonance spectroscopy
NSP10	Nonstructural Protein 10
NUMB	protein numb homolog
p53	cellular tumor antigen p53
PAK2/4	p21-Activated Kinase 2/4
PCR	Polymerase Chain Reaktion
Pd(dppf)Cl_2 · DCM	[1,1′-bis(diphenylphosphino)ferrocene]dichloropalladium(II) complex with dichloromethane
PDGFR	Platelet-Derived Growth Factor Receptor
PEG	Polyrthylene Glycol
PI3K	Phosphoinositide 3 Kinases
PIM1	proto-oncogene serine/threonine-protein kinase Pim-1
PKA	Protein Kinase A
PKC	Protein Kinase C
PKG	Protein kinase G
PPh_3	triphenylphosphine
ppm	Parts Per Million
PTB	Phosphotyrosine-Binding domain
PyBOP	(benzotriazol-1-yloxy)tripyrrolidinophosphonium hexafluorophosphate
q	quartet
qPCR	quantitative real-time PCR
RAD51	DNA repair protein RAD51
RCM	Ring-Closing Metathesis
RET	Receptor Tyrosine protein kinase
RFU	Relative Fluorescence Units
RIPK2	Receptor-Interacting serine/threonine Protein Kinase 2
RNA	Ribonucleic Acid
ROCK	Rho-associated protein Kinase
ROS1	receptor tyrosine kinase encoded by gene ROS1
RPE	Retinal Pigment Epithelium
rt	room temperature
RTK	Receptor Tyrosine Kinase
s	singlet
S_{35}	Selectivity-Score with a threshold of 35 %Ctrl

SAR	Structure-Activity Relationship
SARS-CoV-2	Severe Acute Respiratory Syndrome Coronavirus type 2
SDS-PAGE	Sodium Dodecyl Sulfate Polyacrylamide Gel Electrophoresis
SGC	Structural Genomics Consortium
Smad3	Small Mothers Against Decapentaplegic 3
SPS	Scintillation Proximity assay
STE	(MAPK cascade families (Sterile 7/ MAP2K, Sterile 11/MAP3K and Sterile 20/MAP4K))
STK16	myristoylated and palmitoylated Serine/Threonine protein Kinase 16
STK17A	Serine/Threonine protein Kinase 17A
STK2/20	Serine/Threonine protein kinase 2/20
STLK3	Sterile-20-Like Kinase
STPK	Serine/Threonine-specific Protein Kinase
t	triplet
TBAF	tetrabutylammonium fluoride
TBB	4,5,6,7-tetrabromobenzotriazole
TBDMSCl	*tert*-butyldimethylsilyl chloride
TBK1	TANK-Binding Kinase 1
TCOF1	Treacle ribosome biogenesis Factor 1
TEA	triethylamine
Tf_2O	trifluoromethanesulfonic anhydride
TFA	trifluoroacetic acid
TGF-β	Transforming Growth Factor β
TGN	Trans-Golgi Network
TKL	Tyrosine Kinase Like
TLC	Thin Layer Chromatography
T_m	melting temperature
TMPRSS2	Transmembrane Protease Serine Subtype 2
TPK	Tyrosine-specific Protein Kinase
TPP	triphenylphosphine
t_R	retention time
TR-FRET	Time-Resolved Fluorescence Resonance Energy Transfer
ULK3	Unc-51-Like Kinase 3
VEGFR	Vascular Endothelial Growth Factor
VIAK	Valine-Isoleucine-Alanine-Lysine
XPhos	2-dicyclohexylphosphino-2′,4′,6′-triisopropylbiphenyl

Abbreviations and acronyms

ΔG	free binding energy
ΔH	enthalpy
ΔS	entropy
ΔT_m	T_m-shift

Amino acids

Amino acid	Three letter code	One letter code
Alanine	Aln	A
Arginine	Arg	R
Asparagine	Asn	N
Aspartic acid	Asp	D
Cysteine	Cys	C
Glutamic acide	Glu	E
Glutamine	Glu	Q
Glycine	Gly	G
Histidine	His	H
Isoleucine	Ile	I
Leucine	Leu	L
Lysine	Lys	K
Methionine	Met	M
Phenylalanine	Phe	F
Proline	Pro	P
Serine	Ser	S
Threonine	Thr	T
Tryptophan	Trp	W
Tyrosine	Tyr	Y
Valine	Val	V

8. References

1. Sung, H. *et al.* Global cancer statistics 2020: GLOBOCAN estimates of incidence and mortality worldwide for 36 cancers in 185 countries. *CA. Cancer J. Clin.* **71**, 209– 249 (2021).
2. Collett, M. S. & Erikson, R. L. Protein kinase activity associated with the avian sarcoma virus src gene product. *Proc. Natl. Acad. Sci. U. S. A.* **75**, 2021–2024 (1978).
3. Castagna, M. *et al.* Direct activation of calcium-activated, phospholipid-dependent protein kinase by tumor-promoting phorbol esters. *J. Biol. Chem.* **257**, 7847–7851 (1982).
4. Hidaka, H., Inagaki, M., Kawamoto, S. & Sasaki, Y. Isoquinolinesulfonamides, Novel and Potent Inhibitors of Cyclic Nucleotide Dependent Protein Kinase and Protein Kinase C. *Biochemistry* **23**, 5036–5041 (1984).
5. Ward, N. E. & O'Brian, C. A. Kinetic analysis of protein kinase C inhibition by staurosporine: evidence that inhibition entails inhibitor binding at a conserved region of the catalytic domain but not competition with substrates. *Mol. Pharmacol.* **41**, 387–392 (1992).
6. Craig Venter, J. *et al.* The sequence of the human genome. *Science (80-.).* **291**, 1304–1351 (2001).
7. Manning, G., Whyte, D. B., Martinez, R., Hunter, T. & Sudarsanam, S. The protein kinase complement of the human genome. *Science* **298**, 1912–1934 (2002).
8. Ferguson, F. M. & Gray, N. S. Kinase inhibitors: The road ahead. *Nature Reviews Drug Discovery* **17**, 353–376 (2018).
9. Müller, S. & Knapp, S. Targeting kinases for the treatment of inflammatory diseases. *Expert Opinion on Drug Discovery* **5**, 867–881 (2010).
10. FISCHER, E. H. & KREBS, E. G. Conversion of phosphorylase b to phosphorylase a in muscle extracts. *J. Biol. Chem.* **216**, 121–132 (1955).
11. Gross, S., Rahal, R., Stransky, N., Lengauer, C. & Hoeflich, K. P. Targeting cancer with kinase inhibitors. *Journal of Clinical Investigation* **125**, 1780–1789 (2015).
12. Walsh, C. T., Garneau-Tsodikova, S. & Gatto, G. J. Protein posttranslational modifications: The chemistry of proteome diversifications. *Angewandte Chemie - International Edition* **44**, 7342–7372 (2005).
13. Cicenas, J., Zalyte, E., Bairoch, A. & Gaudet, P. Kinases and cancer. *Cancers* **10**, (2018).
14. Ubersax, J. A. & Ferrell, J. E. Mechanisms of specificity in protein phosphorylation. *Nature Reviews Molecular Cell Biology* **8**, 530–541 (2007).
15. Hanks, S. K. & Hunter, T. The eukaryotic protein kinase superfamily: kinase (catalytic) domain structure and classification [1]. *FASEB J.* **9**, 576–596 (1995).
16. Manning, G., Plowman, G. D., Hunter, T. & Sudarsanam, S. Evolution of protein kinase signaling from yeast to man. *Trends in Biochemical Sciences* **27**, 514–520 (2002).

17. Fabbro, D., Cowan-Jacob, S. W. & Moebitz, H. Ten things you should know about protein kinases: IUPHAR Review 14. *British Journal of Pharmacology* **172**, 2675–2700 (2015).

18. Ghoreschi, K., Laurence, A. & O'Shea, J. J. Selectivity and therapeutic inhibition of kinases: To be or not to be? *Nat. Immunol.* **10**, 356–360 (2009).

19. Hanks, S. K., Quinn, A. M. & Hunter, T. The protein kinase family: Conserved features and deduced phylogeny of the catalytic domains. *Science (80-.).* **241**, 42–52 (1988).

20. Johnson, L. N., Lowe, E. D., Noble, M. E. M. & Owen, D. J. The structural basis for substrate recognition and control by protein kinases. in *FEBS Letters* **430**, 1–11 (Elsevier B.V., 1998).

21. Nolen, B., Taylor, S. & Ghosh, G. Regulation of protein kinases: Controlling activity through activation segment conformation. *Molecular Cell* **15**, 661–675 (2004).

22. Cowan-Jacob, S. W. Structural biology of protein tyrosine kinases. *Cellular and Molecular Life Sciences* **63**, 2608–2625 (2006).

23. Taylor, S. S. & Kornev, A. P. Protein kinases: Evolution of dynamic regulatory proteins. *Trends in Biochemical Sciences* **36**, 65–77 (2011).

24. Taylor, S. S. *et al.* Catalytic subunit of cyclic AMP-dependent protein kinasestructure and dynamics of the active site cleft. in *Pharmacology and Therapeutics* **82**, 133–141 (1999).

25. Cowan-Jacob, S. W., Möbitz, H. & Fabbro, D. Structural biology contributions to tyrosine kinase drug discovery. *Current Opinion in Cell Biology* **21**, 280–287 (2009).

26. Bhullar, K. S. *et al.* Kinase-targeted cancer therapies: Progress, challenges and future directions. *Molecular Cancer* **17**, 1–20 (2018).

27. Kornev, A. P., Haste, N. M., Taylor, S. S. & Ten Eyck, L. F. Surface comparison of active and inactive protein kinases identifies a conserved activation mechanism. *Proc. Natl. Acad. Sci. U. S. A.* **103**, 17783–17788 (2006).

28. Kornev, A. P., Taylor, S. S. & Ten Eyck, L. F. A helix scaffold for the assembly of active protein kinases. *Proc. Natl. Acad. Sci. U. S. A.* **105**, 14377–14382 (2008).

29. Shibuya, M. Effect of fasudil HCl, a protein kinase inhibitor, on cerebral vasospasm. *Acta Neurochir. Suppl.* **77**, 201–204 (2001).

30. Song, H. & Gao, D. Fasudil, a Rho-associated protein kinase inhibitor, attenuates retinal ischemia and reperfusion injury in rats. *Int. J. Mol. Med.* **28**, 193–198 (2011).

31. Tamaoki, T. *et al.* Staurosporine, a potent inhibitor of phospholipid Ca++dependent protein kinase. *Biochem. Biophys. Res. Commun.* **135**, 397–402 (1986).

32. Buchdunger, E., Matter, A. & Druker, B. J. Bcr-Abl inhibition as a modality of CML therapeutics. *Biochimica et Biophysica Acta - Reviews on Cancer* **1551** (2001).

33. Roskoski, R. Properties of FDA-approved small molecule protein kinase inhibitors: A 2020 update. *Pharmacological Research* **152**, 104609 (2020).

34. Müller, S., Chaikuad, A., Gray, N. S. & Knapp, S. The ins and outs of selective kinase inhibitor development. *Nature Chemical Biology* **11**, 818–821 (2015).

35. Wu, P., Nielsen, T. E. & Clausen, M. H. FDA-approved small-molecule kinase inhibitors. *Trends in Pharmacological Sciences* **36**, 422–439 (2015).

36. Roskoski, R. A historical overview of protein kinases and their targeted small molecule inhibitors. *Pharmacological Research* **100**, 1–23 (2015).

37. Liu, Y. & Gray, N. S. Rational design of inhibitors that bind to inactive kinase conformations. *Nature Chemical Biology* **2**, 358–364 (2006).

38. Zhao, Z. *et al.* Exploration of type II binding mode: A privileged approach for kinase inhibitor focused drug discovery? *ACS Chemical Biology* **9**, 1230–1241 (2014).

39. Cowan-Jacob, S. W., Jahnke, W. & Knapp, S. Novel approaches for targeting kinases: Allosteric inhibition, allosteric activation and pseudokinases. *Future Medicinal Chemistry* **6**, 541–561 (2014).

40. Gavrin, L. K. & Saiah, E. Approaches to discover non-ATP site kinase inhibitors. *MedChemComm* **4**, 41–51 (2013).

41. Lu, X., Smaill, J. B. & Ding, K. New Promise and Opportunities for Allosteric Kinase Inhibitors. *Angew. Chemie Int. Ed.* **59**, 13764–13776 (2020).

42. Wylie, A. A. *et al.* The allosteric inhibitor ABL001 enables dual targeting of BCR-ABL1. *Nature* **543**, 733–737 (2017).

43. Karaman, M. W. *et al.* A quantitative analysis of kinase inhibitor selectivity. *Nat. Biotechnol.* **26**, 127–132 (2008).

44. Norman, R. A., Toader, D. & Ferguson, A. D. Structural approaches to obtain kinase selectivity. *Trends in Pharmacological Sciences* **33**, 273–278 (2012).

45. Arrowsmith, C. H. *et al.* The promise and peril of chemical probes. *Nature Chemical Biology* **11**, 536–541 (2015).

46. Müller, S. *et al.* Donated chemical probes for open science. *Elife* **7**, (2018).

47. Wilhelm, S. *et al.* Discovery and development of sorafenib: A multikinase inhibitor for treating cancer. *Nature Reviews Drug Discovery* **5**, 835–844 (2006).

48. Cox, K. J., Shomin, C. D. & Ghosh, I. Tinkering outside the kinase ATP box: Allosteric (type IV) and bivalent (type V) inhibitors of protein kinases. *Future Medicinal Chemistry* vol. 3 29–43 (2011).

49. Hill, Z. B., Perera, B. G. K., Andrews, S. S. & Maly, D. J. Targeting diverse signaling interaction sites allows the rapid generation of bivalent kinase inhibitors. *ACS Chem. Biol.* **7**, 487–495 (2012).

50. Driggers, E. M., Hale, S. P., Lee, J. & Terrett, N. K. The exploration of macrocycles for drug discovery - An underexploited structural class. *Nature Reviews Drug Discovery* **7**, 608–624 (2008).

51. Mallinson, J. & Collins, I. Macrocycles in new drug discovery. *Future Medicinal Chemistry* **4**, 1409–1438 (2012).

52. Mortensen, K. T., Osberger, T. J., King, T. A., Sore, H. F. & Spring, D. R. Strategies for the Diversity-Oriented Synthesis of Macrocycles. *Chemical Reviews* **119**, 10288–10317 (2019).

53. Johnson, T. W. *et al.* Discovery of (10 R)-7-Amino-12-fluoro-2,10,16-trimethyl-15-oxo-10,15,16,17- tetrahydro- 2H -8,4-(metheno)pyrazolo[4,3- h][2,5,11]-benzoxadiazacyclotetradecine-3-carbonitrile (PF-06463922), a macrocyclic inhibitor of anaplastic lymphoma kinase (ALK) and c-ros oncogene 1 (ROS1) with preclinical brain exposure and broad-spectrum potency against ALK-resistant mutations. *J. Med. Chem.* **57**, 4720–4744 (2014).

54. Kwitkowski, V. E. *et al.* FDA Approval Summary: Temsirolimus as Treatment for Advanced Renal Cell Carcinoma. *Oncologist* **15**, 428–435 (2010).

55. Marsault, E. & Peterson, M. L. Macrocycles are great cycles: Applications, opportunities, and challenges of synthetic macrocycles in drug discovery. *J. Med. Chem.* **54**, 1961–2004 (2011).

56. Mullard, A. Re-assessing the rule of 5, two decades on. *Nature Reviews Drug Discovery* **17**, 777 (2018).

57. Lipinski, C. A., Lombardo, F., Dominy, B. W. & Feeney, P. J. Experimental and computational approaches to estimate solubility and permeability in drug discovery and development settings. *Advanced Drug Delivery Reviews* **23**, 3–25 (1997).

58. Xing, L., Klug-Mcleod, J., Rai, B. & Lunney, E. A. Kinase hinge binding scaffolds and their hydrogen bond patterns. *Bioorganic Med. Chem.* **23**, 6520–6527 (2015).

59. Breslin, H. J. *et al.* Design, synthesis, and anaplastic lymphoma kinase (ALK) inhibitory activity for a novel series of 2,4,8,22-tetraazatetracyclo[14.3.1.1 3,7.1 9,13]docosa-1(20),3(22),4,6,9(21),10,12,16,18-nonaene macrocycles. *J. Med. Chem.* **55**, 449–464 (2012).

60. Cummings, M. D. & Sekharan, S. Structure-Based Macrocycle Design in Small-Molecule Drug Discovery and Simple Metrics to Identify Opportunities for Macrocyclization of Small-Molecule Ligands. *Journal of Medicinal Chemistry* **62**, 6843–6853 (2019).

61. Giordanetto, F. & Kihlberg, J. Macrocyclic drugs and clinical candidates: What can medicinal chemists learn from their properties? *J. Med. Chem.* **57**, 278–295 (2014).

62. Wu, J., Savooji, J. & Liu, D. Second- and third-generation ALK inhibitors for non-small cell lung cancer. *Journal of Hematology and Oncology* **9**, 1–7 (2016).

63. Basit, S., Ashraf, Z., Lee, K. & Latif, M. First macrocyclic 3rd-generation ALK inhibitor for treatment of ALK/ROS1 cancer: Clinical and designing strategy update of lorlatinib. *European Journal of Medicinal Chemistry* **134**, 348–356 (2017).

64. Tao, Z. F. *et al.* Structure-based design, synthesis, and biological evaluation of potent and selective macrocyclic checkpoint kinase 1 inhibitors. *J. Med. Chem.* **50**, 1514–1527 (2007).

65. William, A. D. *et al.* Discovery of kinase spectrum selective macrocycle (16E)-14-methyl-20-oxa-5, 7,14,26-tetraazatetracyclo[19.3.1.1(2,6).1(8,12)]heptacosa-1(25),2(26),3,5,8(27) ,9,11,16,21,23-decaene (SB1317/TG02), a potent inhibitor of cyclin dependent kinases (CDKs), Janus kinase 2 (JAK2), and Fms-like tyrosine kinase-3 (FLT3) for the treatment of cancer. *J. Med. Chem.* **55**, 169–196 (2012).

66. Lücking, U. *et al.* Macrocyclic aminopyrimidines as multitarget CDK and VEGF-R inhibitors with potent antiproliferative activities. *ChemMedChem* **2**, 63–77 (2007).

67. Mitsunobu, O. The Use of Diethyl Azodicarboxylate and Triphenylphosphine in Synthesis and Transformation of Natural Products. *Synthesis (Germany)* **1981** 1–28 (1981).

68. Kohli, R. M., Walsh, C. T. & Burkart, M. D. Biomimetic synthesis and optimization of cyclic peptide antibiotics. *Nature* **418**, 658–661 (2002).

69. Ishikawa, M. & Hashimoto, Y. Improvement in aqueous solubility in small molecule drug discovery programs by disruption of molecular planarity and symmetry. *J. Med. Chem.* **54**, 1539–1554 (2011).

70. Choon Woo Lee & Grubbs, R. H. Formation of macrocycles via ring-closing olefin metathesis. *J. Org. Chem.* **66**, 7155–7158 (2001).

71. Kemker, I., Schnepel, C., Schröder, D. C., Marion, A. & Sewald, N. Cyclization of RGD Peptides by Suzuki-Miyaura Cross-Coupling. *J. Med. Chem.* **62**, 7417–7430 (2019).

72. Li, H. *et al.* Synthesis of bis-macrocyclic HCV protease inhibitor mk-6325 via intramolecular sp 2- sp 3 Suzuki-Miyaura coupling and ring closing metathesis. *Org. Lett.* **17**, 1533–1536 (2015).

73. BURNETT, G. & KENNEDY, E. P. The enzymatic phosphorylation of proteins. *J. Biol. Chem.* **211**, 969–980 (1954).

74. Pinna, L. A. Protein kinase CK2: A challenge to canons. *J. Cell Sci.* **115**, 3873–3878 (2002).

75. Marin, O. *et al.* Tyrosine versus serine/threonine phosphorylation by protein kinase casein kinase-2. A study with peptide substrates derived from immunophilin Fpr3. *J. Biol. Chem.* **274**, 29260–29265 (1999).

76. Bian, Y. *et al.* Global screening of CK2 kinase substrates by an integrated phosphoproteomics workflow. *Sci. Rep.* **3**, 1–7 (2013).

77. Salvi, M., Sarno, S., Cesaro, L., Nakamura, H. & Pinna, L. A. Extraordinary pleiotropy of protein kinase CK2 revealed by weblogo phosphoproteome analysis. *Biochim. Biophys. Acta - Mol. Cell Res.* **1793**, 847–859 (2009).

78. Rabalski, A. J., Gyenis, L. & Litchfield, D. W. Molecular pathways: Emergence of protein kinase CK2 (CSNK2) as a potential target to inhibit survival and DNA damage response and repair pathways in cancer cells. *Clin. Cancer Res.* **22**, 2840–2847 (2016).

79. Meggio, F. & Pinna, L. A. One-thousand-and-one substrates of protein kinase CK2? *FASEB J.* **17**, 349–368 (2003).

80. Götz, C. & Montenarh, M. Protein kinase CK2 in development and differentiation. *Biomed. Reports* **6**, 127–133 (2017).

81. Wells, C., Drewry, D., Pickett, J. & Axtman, A. SGC-CK2-1: The First Selective Chemical Probe for the Pleiotropic Kinase CK2. *ChemRxiv* (2020).

82. Cozza, G., Meggio, F. & Moro, S. The Dark Side of Protein Kinase CK2 Inhibition. *Curr. Med. Chem.* **18**, 2867–2884 (2011).

83. Niefind, K., Guerra, B., Ermakowa, I. & Issinger, O. G. Crystal structure of human protein kinase CK2: Insights into basic properties of the CK2 holoenzyme. *EMBO J.* **20**, 5320–5331 (2001).

84. Cozza, G., Bortolato, A. & Moro, S. How druggable is protein kinase CK2? *Medicinal Research Reviews* **30**, 419–462 (2010).

85. Cristiani, A. *et al.* The Role of the N-Terminal Domain in the Regulation of the "Constitutively Active" Conformation of Protein Kinase CK2α: Insight from a Molecular Dynamics Investigation. *ChemMedChem* **6**, 1207–1216 (2011).

86. Sarno, S., Ghisellini, P. & Pinna, L. A. Unique activation mechanism of protein kinase CK2. The N-terminal segment is essential for constitutive activity of the catalytic subunit but not of the holoenzyme. *J. Biol. Chem.* **277**, 22509–22514 (2002).

87. Graham, K. C. & Litchfield, D. W. The regulatory β subunit of protein kinase CK2 mediates formation of tetrameric CK2 complexes. *J. Biol. Chem.* **275**, 5003–5010 (2000).

88. Chantalat, L. *et al.* Crystal structure of the human protein kinase CK2 regulatory subunit reveals its zinc finger-mediated dimerization. *EMBO J.* **18**, 2930–2940 (1999).

89. Lolli, G., Ranchio, A. & Battistutta, R. Active form of the protein kinase CK2 α2β2 holoenzyme is a strong complex with symmetric architecture. *ACS Chem. Biol.* **9**, 366–371 (2014).

90. Guerra, B. & Issinger, O.-G. Protein Kinase CK2 in Human Diseases. *Curr. Med. Chem.* **15**, 1870–1886 (2008).

91. Sarno, S. & Pinna, L. A. Protein kinase CK2 as a druggable target. *Mol. Biosyst.* **4**, 889–894 (2008).

92. Ruzzene, M. & Pinna, L. A. Addiction to protein kinase CK2: A common denominator of diverse cancer cells? *Biochim. Biophys. Acta - Proteins Proteomics* **1804**, 499–504 (2010).

93. Ahmad, K. A., Wang, G., Unger, G., Slaton, J. & Ahmed, K. Protein kinase CK2 - A key suppressor of apoptosis. *Adv. Enzyme Regul.* **48**, 179–187 (2008).

94. Litchfield, D. W. Protein kinase CK2: Structure, regulation and role in cellular decisions of life and death. *Biochemical Journal* **369**, 1–15 (2003).

95. Desagher, S. *et al.* Phosphorylation of Bid by casein kinases I and II regulates its cleavage by caspase 8. *Mol. Cell* **8**, 601–611 (2001).

96. Turowec, J. P. *et al.* An unbiased proteomic screen reveals caspase cleavage is positively and negatively regulated by substrate phosphorylation. *Mol. Cell. Proteomics* **13**, 1184–1197 (2014).

97. Spycher, C. *et al.* Constitutive phosphorylation of MDC1 physically links the MRE11-RAD50-NBS1 complex to damaged chromatin. *J. Cell Biol.* **181**, 227–240 (2008).

98. Chapman, J. R. & Jackson, S. P. Phospho-dependent interactions between NBS1 and MDC1 mediate chromatin retention of the MRN complex at sites of DNA damage. *EMBO Rep.* **9**, 795–801 (2008).

99. Borgo, C. & Ruzzene, M. Role of protein kinase CK2 in antitumor drug resistance. *Journal of Experimental and Clinical Cancer Research* **38**, 1–15 (2019).

100. Brear, P. *et al.* Specific inhibition of CK2α from an anchor outside the active site. *Chem. Sci.* **7**, 6839–6845 (2016).

101. Swider, R. *et al.* Synthesis, biological activity and structural study of new benzotriazole-based protein kinase CK2 inhibitors. *RSC Adv.* **5**, 72482–72494 (2015).

102. Ohno, H. *et al.* Structure–activity relationship study of 4-(thiazol-5-yl)benzoic acid derivatives as potent protein kinase CK2 inhibitors. *Bioorganic Med. Chem.* **24**, 1136–1141 (2016).

103. Cozza, G. *et al.* Cell-permeable dual inhibitors of protein kinases CK2 and PIM-1: Structural features and pharmacological potential. *Cell. Mol. Life Sci.* **71**, 3173–3185 (2014).

104. Schnitzler, A. *et al.* A π-halogen bond of dibenzofuranones with the gatekeeper phe113 in human protein kinase CK2 leads to potent tight binding inhibitors. *Pharmaceuticals* **11**, (2018).

105. Dalle Vedove, A. *et al.* A novel class of selective CK2 inhibitors targeting its open hinge conformation. *Eur. J. Med. Chem.* **195**, (2020).

106. CX-4945 Granted Orphan Drug Designation. *Oncol. Times* **39**, 23 (2017).

107. Wang, H., Davis, A., Yu, S. & Ahmed, K. Response of cancer cells to molecular interruption of the CK2 signal. *Mol. Cell. Biochem.* **227**, 167–174 (2001).

108. Siddiqui-Jain, A. *et al.* CX-4945, an orally bioavailable selective inhibitor of protein kinase CK2, inhibits prosurvival and angiogenic signaling and exhibits antitumor efficacy. *Cancer Res.* **70**, 10288–10298 (2010).

109. Chon, H. J., Bae, K. J., Lee, Y. & Kim, J. The casein kinase 2 inhibitor, CX-4945, as an anti-cancer drug in treatment of human hematological malignancies. *Frontiers in Pharmacology* **6**, (2015).

110. Dowling, J. E. *et al.* Potent and Selective CK2 Kinase Inhibitors with Effects on Wnt Pathway Signaling in Vivo. *ACS Med. Chem. Lett.* **7**, 300–305 (2016).

111. Berginski ME, Moret N, Liu C, Goldfarb D, Sorger PK, G. S. The Dark Kinase Knowledgebase: an online compendium of knowledge and experimental results of understudied kinases. *Nucleic Acids Res.* **49**, D529–D535 (2020).

112. Farag, A. K. & Roh, E. J. Death-associated protein kinase (DAPK) family modulators: Current and future therapeutic outcomes. *Medicinal Research Reviews* **39**, 349–385 (2019).

113. Shiloh, R., Bialik, S. & Kimchi, A. The DAPK family: A structure-function analysis. *Apoptosis* **19**, 286–297 (2014).

114. Bialik, S. & Kimchi, A. The death-associated protein kinases: Structure, function, and beyond. *Annual Review of Biochemistry* **75**, 189–210 (2006).

115. Sanjo, H., Kawait, T. & Akira, S. DRAKs, novel serine/threonine kinases related to death-associated protein kinase that trigger apoptosis. *J. Biol. Chem.* **273**, 29066–29071 (1998).

116. Oue, Y., Murakami, S., Isshiki, K., Tsuji, A. & Yuasa, K. Intracellular localization and binding partners of death associated protein kinase-related apoptosis-inducing protein kinase 1. *Biochem. Biophys. Res. Commun.* **496**, 1222–1228 (2018).

117. Mao, P. *et al.* Serine/threonine kinase 17A is a novel p53 target gene and modulator of cisplatin toxicity and reactive oxygen species in testicular cancer cells. *J. Biol. Chem.* **286**, 19381–19391 (2011).

118. Park, Y. *et al.* Cytoplasmic DRAK1 overexpressed in head and neck cancers inhibits TGF-β1 tumor suppressor activity by binding to Smad3 to interrupt its complex formation with Smad4. *Oncogene* **34**, 5037–5045 (2015).

119. Picado, A. *et al.* A Chemical Probe for Dark Kinase STK17B Derives Its Potency and High Selectivity through a Unique P-Loop Conformation. *J. Med. Chem.* **63**, 14626–14646 (2020)

120. Mao, P. *et al.* Serine/threonine kinase 17A is a novel candidate for therapeutic targeting in glioblastoma. *PLoS One* **8**, e81803 (2013).

121. Taylor, O. G., Brzozowski, J. S. & Skelding, K. A. Glioblastoma multiforme: An overview of emerging therapeutic targets. *Frontiers in Oncology* **9**, 963 (2019).

122. Thorne, A. H., Zanca, C. & Furnari, F. Epidermal growth factor receptor targeting and challenges in glioblastoma. *Neuro. Oncol.* **18**, 914–918 (2016).

123. Chen, A. S. *et al.* DRAK/STK17a drives neoplastic glial proliferation through modulation of MRLC signaling. *Cancer Res.* **79**, 1085–1097 (2019).

124. Reich, S. H. *et al.* Structure-based Design of Pyridone-Aminal eFT508 Targeting Dysregulated Translation by Selective Mitogen-activated Protein Kinase Interacting Kinases 1 and 2 (MNK1/2) Inhibition. *J. Med. Chem.* **61**, 3516–3540 (2018).

125. Howard, S. *et al.* Fragment-based discovery of the pyrazol-4-yl urea (AT9283), a multitargeted kinase inhibitor with potent aurora kinase activity. *J. Med. Chem.* **52**, 379–388 (2009).

126. Lefranc, J. *et al.* Discovery of BAY-985, a Highly Selective TBK1/IKKϵ Inhibitor. *J. Med. Chem.* **63**, 601–612 (2020).

127. Gao, L. J. *et al.* Discovery of dual death-associated protein related apoptosis inducing protein kinase 1 and 2 inhibitors by a scaffold hopping approach. *J. Med. Chem.* **57**, 7624–7643 (2014).

128. Sorrell, F. J., Szklarz, M., Abdul Azeez, K. R., Elkins, J. M. & Knapp, S. Family-wide Structural Analysis of Human Numb-Associated Protein Kinases. *Structure* **24**, 401–411 (2016).

129. Kaksonen, M. & Roux, A. Mechanisms of clathrin-mediated endocytosis. *Nature Reviews Molecular Cell Biology* **19**, 313–326 (2018).

130. Conner, S. D. & Schmid, S. L. Identification of an adaptor-associated kinase, AAK1, as a regulator of clathrin-mediated endocytosis. *J. Cell Biol.* **156**, 921–929 (2002).

131. Yap, C. C. & Winckler, B. Adapting for endocytosis: Roles for endocytic sorting adaptors in directing neural development. *Front. Cell. Neurosci.* **9**, 119 (2015).

132. Henderson, D. M. & Conner, S. D. A novel AAK1 splice variant functions at multiple steps of the endocytic pathway. *Mol. Biol. Cell* **18**, 2698–2706 (2007).

133. Ricotta, D., Conner, S. D., Schmid, S. L., Von Figura, K. & Höning, S. Phosphorylation of the AP2 μ subunit by AAK1 mediates high affinity binding to membrane protein sorting signals. *J. Cell Biol.* **156**, 791–795 (2002).

134. Ohno, H. *et al.* Interaction of tyrosine-based sorting signals with clathrin-associated proteins. *Science (80-.).* **269**, 1872–1875 (1995).

135. Fingerhut, A., Von Figura, K. & Höning, S. Binding of AP2 to Sorting Signals Is Modulated by AP2 Phosphorylation. *J. Biol. Chem.* **276**, 5476–5482 (2001).

136. Traub, L. M. Sorting it out: AP-2 and alternate clathrin adaptors in endocytic cargo selection. *Journal of Cell Biology* **163**, 203–208 (2003).

137. Krieger, J. R. *et al.* Identification and selected reaction monitoring (SRM) quantification of endocytosis factors associated with Numb. *Mol. Cell. Proteomics* **12**, 499–514 (2013).

138. Sorensen, E. B. & Conner, S. D. AAK1 regulates Numb function at an early step in clathrin-mediated endocytosis. *Traffic* **9**, 1791–1800 (2008).

139. Neveu, G. *et al.* Identification and Targeting of an Interaction between a Tyrosine Motif within Hepatitis C Virus Core Protein and AP2M1 Essential for Viral Assembly. *PLoS Pathog.* **8**, e1002845 (2012).

140. Neveu, G. *et al.* AP-2-Associated Protein Kinase 1 and Cyclin G-Associated Kinase Regulate Hepatitis C Virus Entry and Are Potential Drug Targets. *J. Virol.* **89**, 4387–4404 (2015).

141. Bekerman, E. *et al.* Anticancer kinase inhibitors impair intracellular viral trafficking and exert broad-spectrum antiviral effects. *J. Clin. Invest.* **127**, 1338–1352 (2017).

142. Verdonck, S. *et al.* Synthesis and Structure-Activity Relationships of 3,5-Disubstituted-pyrrolo[2,3- b]pyridines as Inhibitors of Adaptor-Associated Kinase 1 with Antiviral Activity. *J. Med. Chem.* **62**, 5810–5831 (2019).

143. Kostich, W. *et al.* Inhibition of AAK1 kinase as a novel therapeutic approach to treat neuropathic pain. *J. Pharmacol. Exp. Ther.* **358**, 371–386 (2016).

144. Abdel-Magid, A. F. Inhibitors of Adaptor-Associated Kinase 1 (AAK1) May Treat Neuropathic Pain, Schizophrenia, Parkinson's Disease, and Other Disorders. *ACS Med. Chem. Lett.* **8**, 595–597 (2017).

145. Kuai, L. *et al.* AAK1 identified as an inhibitor of neuregulin-1/ErbB4-dependent neurotrophic factor signaling using integrative chemical genomics and proteomics. *Chem. Biol.* **18**, 891–906 (2011).

146. Magro, G. SARS-CoV-2 and COVID-19: What are our options? Where should we focus our attention on to find new drugs and strategies? *Travel Medicine and Infectious Disease* **37**, 101685 (2020).

147. Puray-Chavez, M. *et al.* Systematic analysis of SARS-CoV-2 infection of an ACE2-negative human airway 1 cell 2. *bioRxiv* (2021).

148. Wang, P. G., Tang, D. J., Hua, Z., Wang, Z. & An, J. Sunitinib reduces the infection of SARS-CoV, MERS-CoV and SARS-CoV-2 partially by inhibiting AP2M1 phosphorylation. *Cell Discovery* **6**, 71 (2020).

149. Richardson, P. *et al.* Baricitinib as potential treatment for 2019-nCoV acute respiratory disease. *The Lancet* **395**, e30–e31 (2020).

150. Le Tourneau, C., Raymond, E. & Faivre, S. Sunitinib: A novel tyrosine kinase inhibitor. A brief review of its therapeutic potential in the treatment of renal carcinoma and gastrointestinal stromal tumors (GIST). *Therapeutics and Clinical Risk Management* **3**, 341–348 (2007).

151. Fridman, J. S. *et al.* Selective Inhibition of JAK1 and JAK2 Is Efficacious in Rodent Models of Arthritis: Preclinical Characterization of INCB028050. *J. Immunol.* **184**, 5298–5307 (2010).

152. Jorgensen, S. C. J., Tse, C. L. Y., Burry, L. & Dresser, L. D. Baricitinib: A Review of Pharmacology, Safety, and Emerging Clinical Experience in COVID-19. *Pharmacotherapy* **40**, 843–856 (2020).

153. Wells, C. *et al.* SGC-AAK1-1: A Chemical Probe Targeting AAK1 and BMP2K. *ACS Med. Chem. Lett.* **11**, 340–345 (2020).

154. Blom, P. M. F. & Hoflack, J. M. C. J. 2012 Macrocyclic FLT3 kinase inhibitors. Publication Date 2013/04/04. FR. Patent. WO/2013/045653.

155. Lam, K. C., Marder, T. B. & Lin, Z. Mechanism of the palladium-catalyzed borylation of aryl halides with pinacolborane. *Organometallics* **29**, 1849–1857 (2010).

156. Chow, W. K. *et al.* A decade advancement of transition metal-catalyzed borylation of aryl halides and sulfonates. *RSC Advances* **3**, 12518–12539 (2013).

157. Miyaura, N., Yamada, K. & Suzuki, A. A new stereospecific cross-coupling by the palladium-catalyzed reaction of 1-alkenylboranes with 1-alkenyl or 1-alkynyl halides. *Tetrahedron Lett.* **20**, 3437–3440 (1979).

158. Lennox, A. J. J. & Lloyd-Jones, G. C. Selection of boron reagents for Suzuki-Miyaura coupling. *This J. is Cite this Chem. Soc. Rev* **43**, 412 (2014).

159. Hooper, A., Zambon, A. & Springer, C. J. A novel protocol for the one-pot borylation/Suzuki reaction provides easy access to hinge-binding groups for kinase inhibitors. *Org. Biomol. Chem.* **14**, 963–969 (2016).

160. Mitsunobu, O., Yamada, M. & Mukaiyama, T. Preparation of Esters of Phosphoric Acid by the Reaction of Trivalent Phosphorus Compounds with Diethyl Azodicarboxylate in the Presence of Alcohols. *Bull. Chem. Soc. Jpn.* **40**, 935–939 (1967).

161. Hughes, D. L. Progress in the mitsunobu reaction. A review. *Org. Prep. Proced. Int.* **28**, 127–164 (1996).

162. Hughes, D. L., Reamer, R. A., Bergan, J. J. & Grabowski, E. J. J. A mechanistic study of the mitsunobu esterification reaction. *J. Am. Chem. Soc.* **110**, 6487–6491 (1988).

163. Nicolaou, K. C., Estrada, A. A., Zak, M., Lee, S. H. & Safina, B. S. A mild and selective method for the hydrolysis of esters with trimethyltin hydroxide. *Angew. Chemie - Int. Ed.* **44**, 1378–1382 (2005).

164. Leas, D. A. *et al.* Formation of 2-Imino Benzo[e]-1,3-oxazin-4-ones from Reactions of Salicylic Acids and Anilines with HATU: Mechanistic and Synthetic Studies. *ACS Omega* **3**, 781–787 (2018).

165. Valeur, E. & Bradley, M. Amide bond formation: Beyond the myth of coupling reagents. *Chem. Soc. Rev.* **38**, 606–631 (2009).

166. Vrettos, E. I. *et al.* Unveiling and tackling guanidinium peptide coupling reagent side reactions towards the development of peptide-drug conjugates. *RSC Adv.* **7**, 50519–50526 (2017).

167. Ghosh, A. K., Brindisi, M. & Sarkar, A. The Curtius Rearrangement: Applications in Modern Drug Discovery and Medicinal Chemistry. *ChemMedChem* **13**, 2351–2373 (2018).

168. Shioiri, T. Contribution Diphenyl Phosphorazidate (DPPA) − More Than Three Decades Later. *TCI Mail* 134 (2007).

169. Clayden, J. & Hennecke, U. α-Pyridylation of chiral amines via urea coupling, lithiation and rearrangement. *Org. Lett.* **10**, 3567–3570 (2008).

170. Kocz, R., Roestamadji, J. & Mobashery, S. A Convenient Triphosgene-Mediated Synthesis of Symmetric Carboxylic Acid Anhydrides. *J. Org. Chem.* **59**, 2913–2914 (1994).

171. Cotarca, L., Geller, T. & Répási, J. Bis(trichloromethyl)carbonate (BTC, Triphosgene): A Safer Alternative to Phosgene? *Org. Process Res. Dev.* **21**, 1439–1446 (2017).

172. Varjosaari, S. E., Suating, P. & Adler, M. J. One-Pot Synthesis of O -Aryl Carbamates. *Synth.* **48**, 43–47 (2016).

173. Fedorov, O., Niesen, F. H. & Knapp, S. Kinase inhibitor selectivity profiling using differential scanning fluorimetry. *Methods Mol. Biol.* **795**, 109–118 (2012).

174. Gao, K., Oerlemans, R. & Groves, M. R. Theory and applications of differential scanning fluorimetry in early-stage drug discovery. *Biophysical Reviews* **12**, 85–104 (2020).

175. Srivastava, V. K. & Yadav, R. Isothermal titration calorimetry. in *Data Processing Handbook for Complex Biological Data Sources* 125–137 (Elsevier, 2019).

176. Eurofins Discover X. scanMAX Kinase Assay Panal; [cited 2021 Apr 4]. Available from: https://www.discoverx.com/services/drug-discovery-development-services/kinase-profiling/kinomescan/scanmax.

177. Vasta, J. D. *et al.* Quantitative, Wide-Spectrum Kinase Profiling in Live Cells for Assessing the Effect of Cellular ATP on Target Engagement. *Cell Chem. Biol.* **25**, 206-214.e11 (2018).

178. Dale, N. C., Johnstone, E. K. M., White, C. W. & Pfleger, K. D. G. NanoBRET: The bright future of proximity-based assays. *Frontiers in Bioengineering and Biotechnology* **7**, 56 (2019).

179. Pierre, F. *et al.* Discovery and SAR of 5-(3-Chlorophenylamino)benzo[c][2,6]naphthyridine-8- carboxylic Acid (CX-4945), the first clinical stage inhibitor of protein kinase CK2 for the Treatment of Cancer. *J. Med. Chem.* **54**, 635–654 (2011).

180. Brear, P. *et al.* Specific inhibition of CK2α from an anchor outside the active site. *Chem. Sci.* **7**, 6839–6845 (2016).

181. Trembley, J. H., Wang, G., Unger, G., Slaton, J. & Ahmed, K. CK2: A key player in cancer biology. *Cellular and Molecular Life Sciences* **66**, 1858–1867 (2009).

182. Trembley, J. H. *et al.* Emergence of protein kinase CK2 as a key target in cancer therapy. *BioFactors* **36**, 187–195 (2010).

183. Lebrin, F., Chambaz, E. M. & Bianchini, L. A role for protein kinase CK2 in cell proliferation: Evidence using a kinase-inactive mutant of CK2 catalytic subunit α. *Oncogene* **20**, 2010–2022 (2001).

184. Reaction Biology. DRAK1/STK17A Kinase Assay Service; [cited 2021 Mai 21] https://www.reactionbiology.com/datasheet/drak1_stk17a_kin_malvern.

185. Koeberle, S. C. *et al.* Skepinone-L is a selective p38 mitogen-activated protein kinase inhibitor. *Nat. Chem. Biol.* **8**, 141–143 (2012).

186. Lee, M. & Dominguez, C. MAP Kinase p38Inhibitors: Clinical Results and an Intimate Look at Their Interactions with p38α Protein. *Curr. Med. Chem.* **12**, 2979–2994 (2005).

187. Asquith, C. R. M. *et al.* Identification and Optimization of 4-Anilinoquinolines as Inhibitors of Cyclin G Associated Kinase. *ChemMedChem* **13**, 48–66 (2018).

188. Henderson, S. H. *et al.* Mining Public Domain Data to Develop Selective DYRK1A Inhibitors. *ACS Med. Chem. Lett.* **11**, 1620–1626 (2020).

189. Corthell, J. T. Immunoprecipitation. in *Basic Molecular Protocols in Neuroscience: Tips, Tricks, and Pitfalls* 77–81 (Elsevier, 2014).

190. Stewart, A. & Fisher, R. A. Co-Immunoprecipitation: Isolation of Protein Signaling Complexes from Native Tissues. in *Methods in Cell Biology* **112**, 33–54 (Academic Press, 2012).

191. Gordon, D. E. *et al.* A SARS-CoV-2 protein interaction map reveals targets for drug repurposing. *Nature* **583**, 459–468 (2020).

192. Asquith, C. R. M. *et al.* SGC-GAK-1: A Chemical Probe for Cyclin G Associated Kinase (GAK). *J. Med. Chem.* **62**, 2830–2836 (2019).

193. Riva, L. *et al.* Discovery of SARS-CoV-2 antiviral drugs through large-scale compound repurposing. *Nature* **586**, 113–119 (2020).

194. Krämer, A. *et al.* Optimization of pyrazolo[1,5-a]pyrimidines lead to the identification of a highly selective casein kinase 2 inhibitor. *Eur. J. Med. Chem.* **208**, 112770 (2020).

195. Hoffmann, M. *et al.* Nafamostat mesylate blocks activation of SARS-CoV-2: New treatment option for COVID-19. *Antimicrob. Agents Chemother.* **64**, e00754-20 (2020).

196. Hoffmann, M. *et al.* SARS-CoV-2 Cell Entry Depends on ACE2 and TMPRSS2 and Is Blocked by a Clinically Proven Protease Inhibitor. *Cell* **181**, 271-280 (2020).

197. Bullock, A. N. *et al.* Structural basis of inhibitor specificity of the human protooncogene proviral insertion site in moloney murine leukemia virus (PIM-1) kinase. *J. Med. Chem.* **48**, 7604–7614 (2005).

198. Mathison, C. J. N. *et al.* Efficacy and Tolerability of Pyrazolo[1,5- a]pyrimidine RET Kinase Inhibitors for the Treatment of Lung Adenocarcinoma. *ACS Med. Chem. Lett.* **11**, 558–565 (2020).

199. Singleton, J. D. *et al.* Synthesis and biological evaluation of novel pyrazolo[1,5-a]pyrimidines: Discovery of a selective inhibitor of JAK1 JH2 pseudokinase and VPS34. *Bioorganic Med. Chem. Lett.* **30**, 126813 (2020).

200. Carvalho, D. *et al.* ALK2 inhibitors display beneficial effects in preclinical models of ACVR1 mutant diffuse intrinsic pontine glioma. *Commun. Biol.* **2**, (2019).

201. Cuny, G. D. *et al.* Structure-activity relationship study of bone morphogenetic protein (BMP) signaling inhibitors. *Bioorganic Med. Chem. Lett.* **18**, 4388–4392 (2008).

202. Tigno-Aranjuez, J. T. *et al.* In vivo inhibition of RIPK2 kinase alleviates inflammatory disease. *J. Biol. Chem.* **289**, 29651–29664 (2014).

203. Zień, P., Bretner, M., Zastąpiło, K., Szyszka, R. & Shugar, D. Selectivity of 4,5,6,7-tetrabromobenzimidazole as an ATP-competitive potent inhibitor of protein kinase CK2 from various sources. *Biochem. Biophys. Res. Commun.* **306**, 129–133 (2003).

204. Janeczko, M., Masłyk, M., Kubiński, K. & Golczyk, H. Emodin, a natural inhibitor of protein kinase CK2, suppresses growth, hyphal development, and biofilm formation of Candida albicans. *Yeast* **34**, 253–265 (2017).

205. Benanti, J. A. Create, activate, destroy, repeat: Cdk1 controls proliferation by limiting transcription factor activity. *Current Genetics* **62**, 271–276 (2016).

206. Asghar, U., Witkiewicz, A. K., Turner, N. C. & Knudsen, E. S. The history and future of targeting cyclin-dependent kinases in cancer therapy. *Nature Reviews Drug Discovery* **14**, 130–146 (2015).

207. Weirauch, U. *et al.* Functional role and therapeutic potential of the Pim-1 kinase in colon carcinoma. *Neoplasia (United States)* **15**, 783–794 (2013).

208. Tian, F., Wang, Y., Xiao, Z. & Zhu, X. Circular RNA circHIPK3 promotes NCI-H1299 and NCI-H2170 cell proliferation through mir-379 and its target IGF1. *Chinese J. Lung Cancer* **20**, 459–467 (2017).

209. Lu, H. *et al.* Circular RNA HIPK3 induces cell proliferation and inhibits apoptosis in non-small cell lung cancer through sponging miR-149. *Cancer Biol. Ther.* **21**, 113–121 (2020).

210. Durand, J., Zhang, Q. & Baldwin, A. Roles for the IKK-Related Kinases TBK1 and IKKε in Cancer. *Cells* **7**, 139 (2018).

211. Thomas, C. M. & Campbell, P. FLT3 inhibitors in acute myeloid leukemia: Current and future. *Journal of Oncology Pharmacy Practice* **25**, 163–171 (2019).

212. Larrosa-Garcia, M. & Baer, M. R. FLT3 Inhibitors in acute myeloid leukemia: Current status & future directions. *Molecular Cancer Therapeutics* **16**, 991–1001 (2017).

213. Oshima, T. *et al.* Cell-based screen identifies a new potent and highly selective CK2 inhibitor for modulation of circadian rhythms and cancer cell growth. *Sci. Adv.* **5**, (2019).

214. Tigno-Aranjuez, J. T. *et al.* In vivo inhibition of RIPK2 kinase alleviates inflammatory disease. *J. Biol. Chem.* **289**, 29651–29664 (2014).

215. Wu, P., Nielsen, T. E. & Clausen, M. H. Small-molecule kinase inhibitors: An analysis of FDA-approved drugs. *Drug Discovery Today* **21**, 5–10 (2016).

216. Zhang, J., Yang, P. L. & Gray, N. S. Targeting cancer with small molecule kinase inhibitors. *Nature Reviews Cancer* **9**, 28–39 (2009).

217. Matulis, D., Kranz, J.K., Salemme, F.R., Todd, M.J. Thermodynamic Stability of Carbonic Anhydrase: Measurements of Binding Affinity and Stoichiometry Using ThermoFluor. *Biochem.* **44**, 5258–5266 (2005).

9. List of figures

10. List of schemes

11. List of tables

12. Acknowledgements

13. Curriculum Vitae

14. Appendix

14.1 NMR spectra

Compound **25**

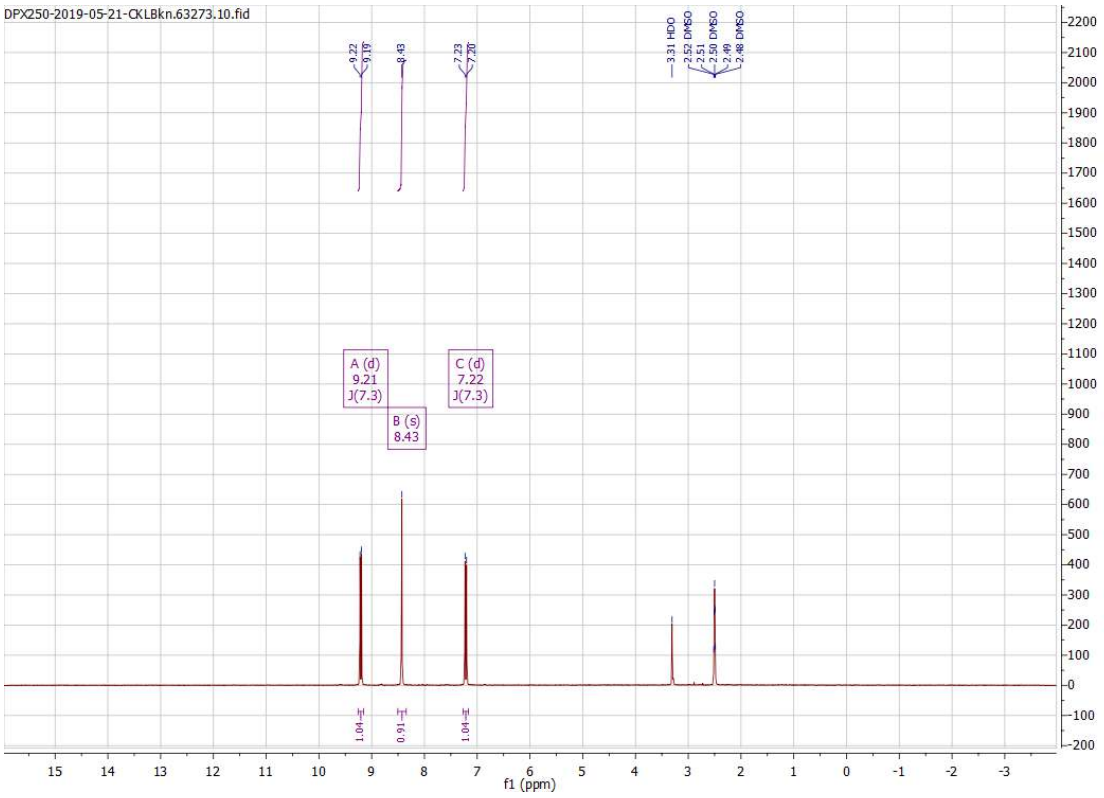

Compound **26**

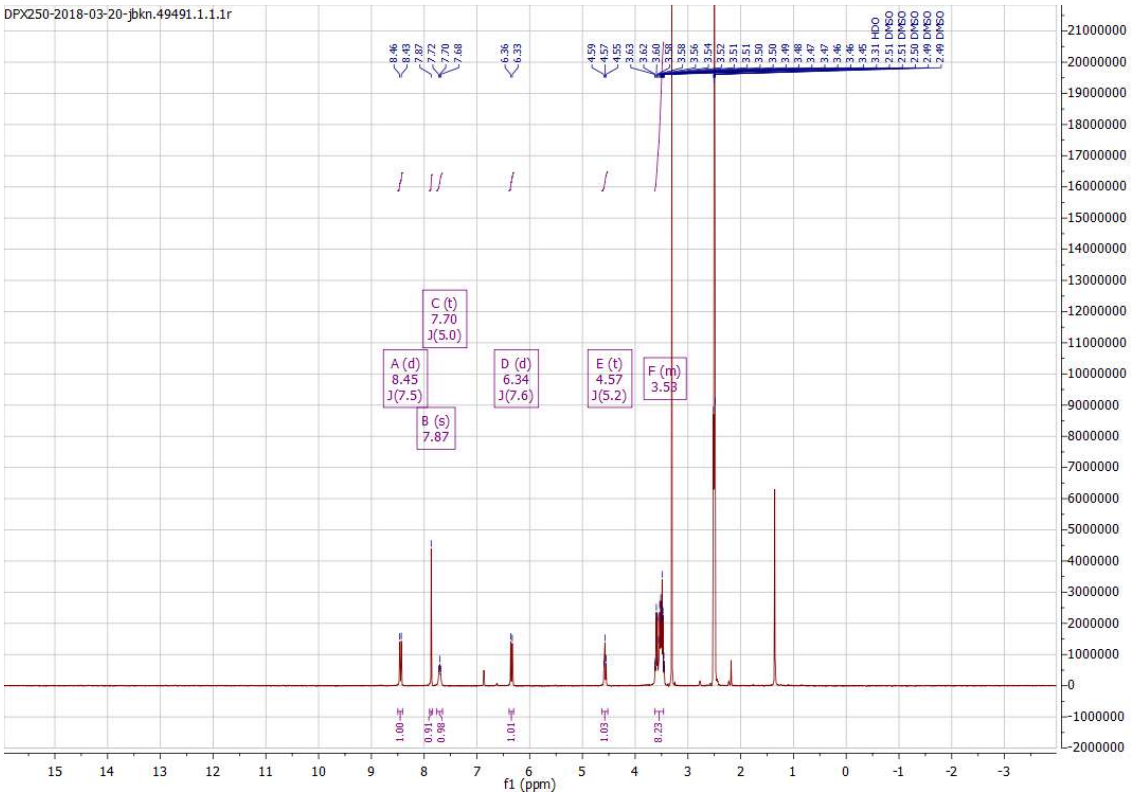

Compound **27**

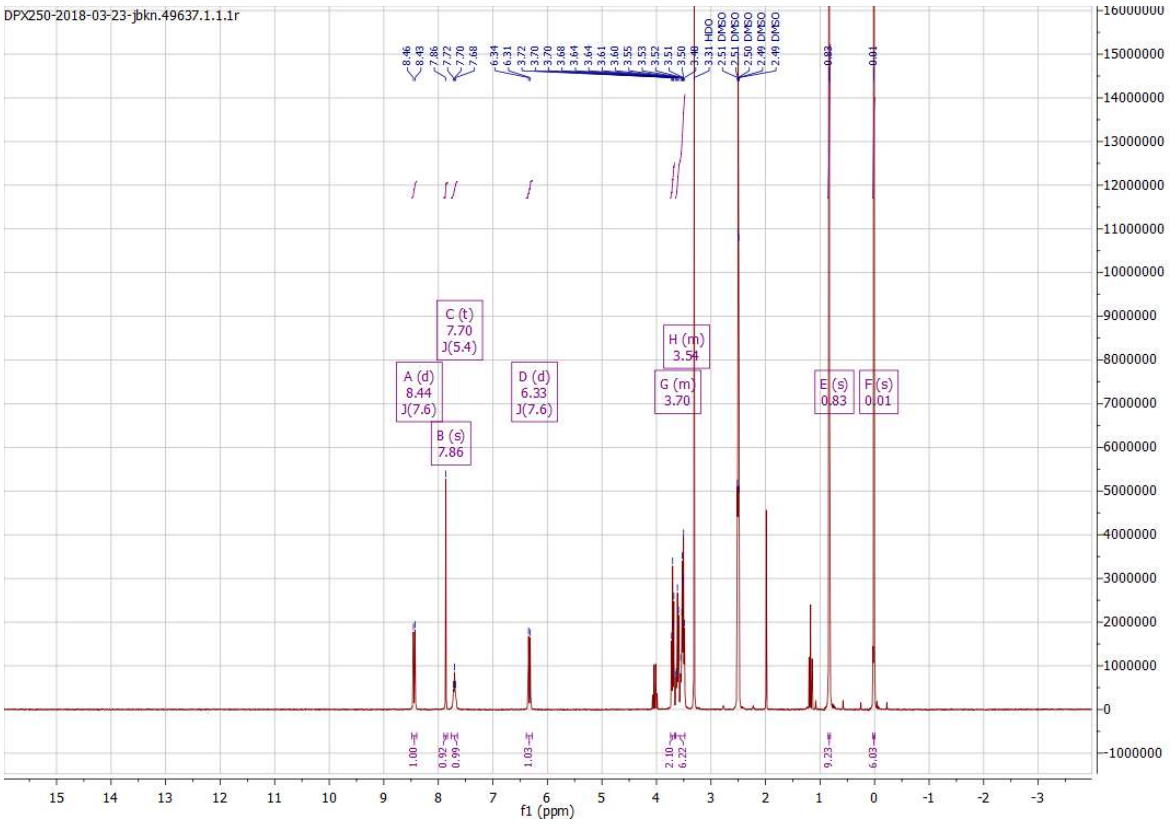

Compound **28**

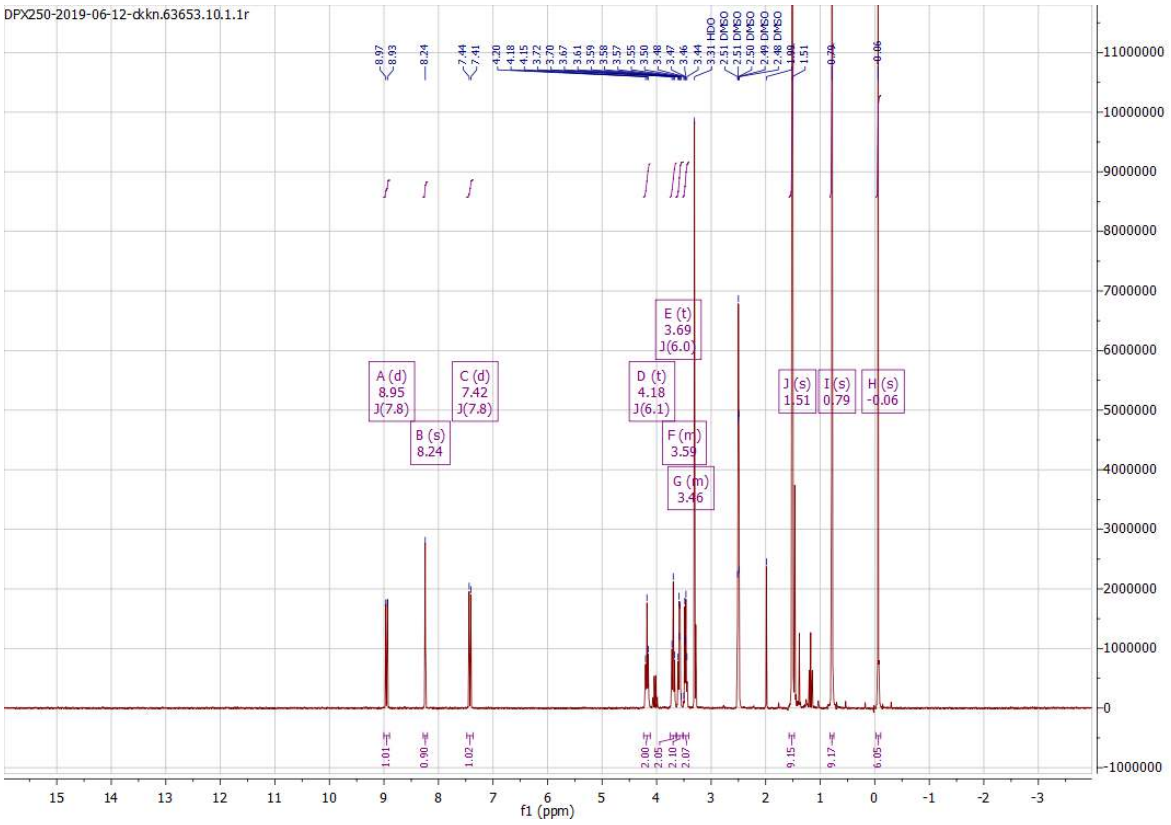

Compound **30**

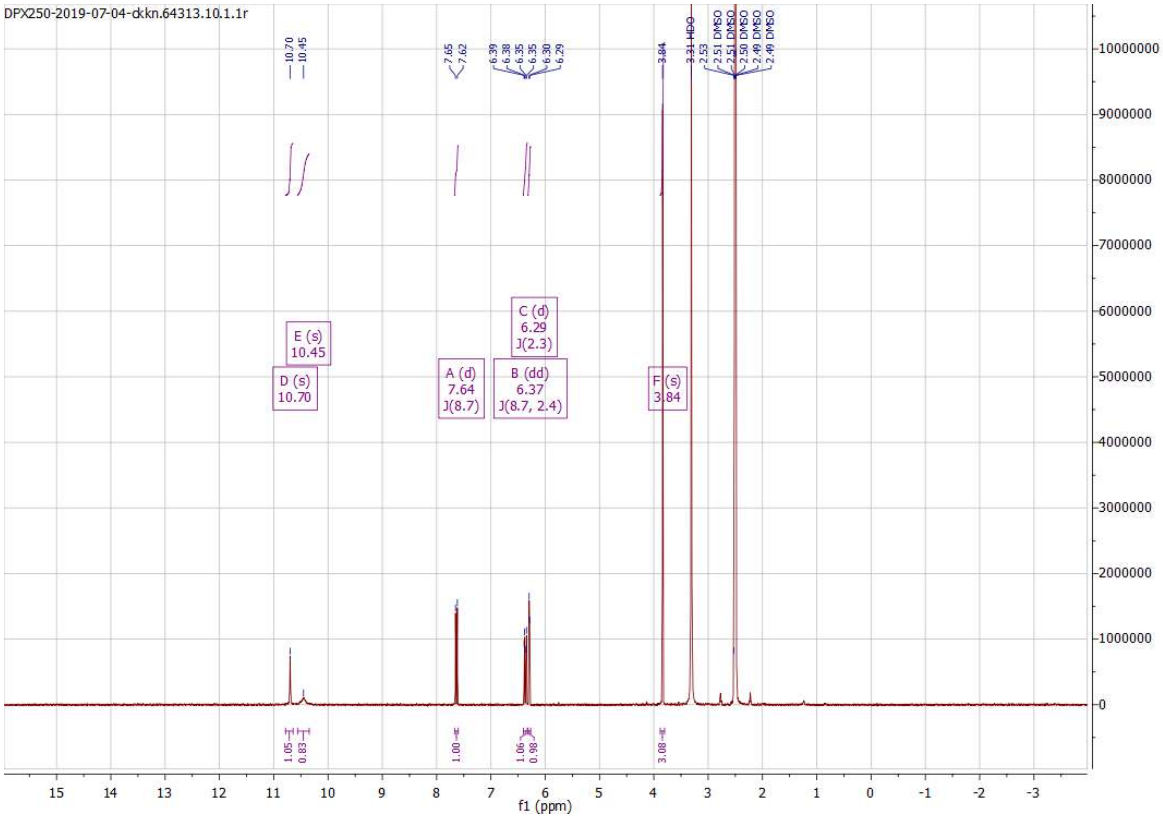

Compound **31**

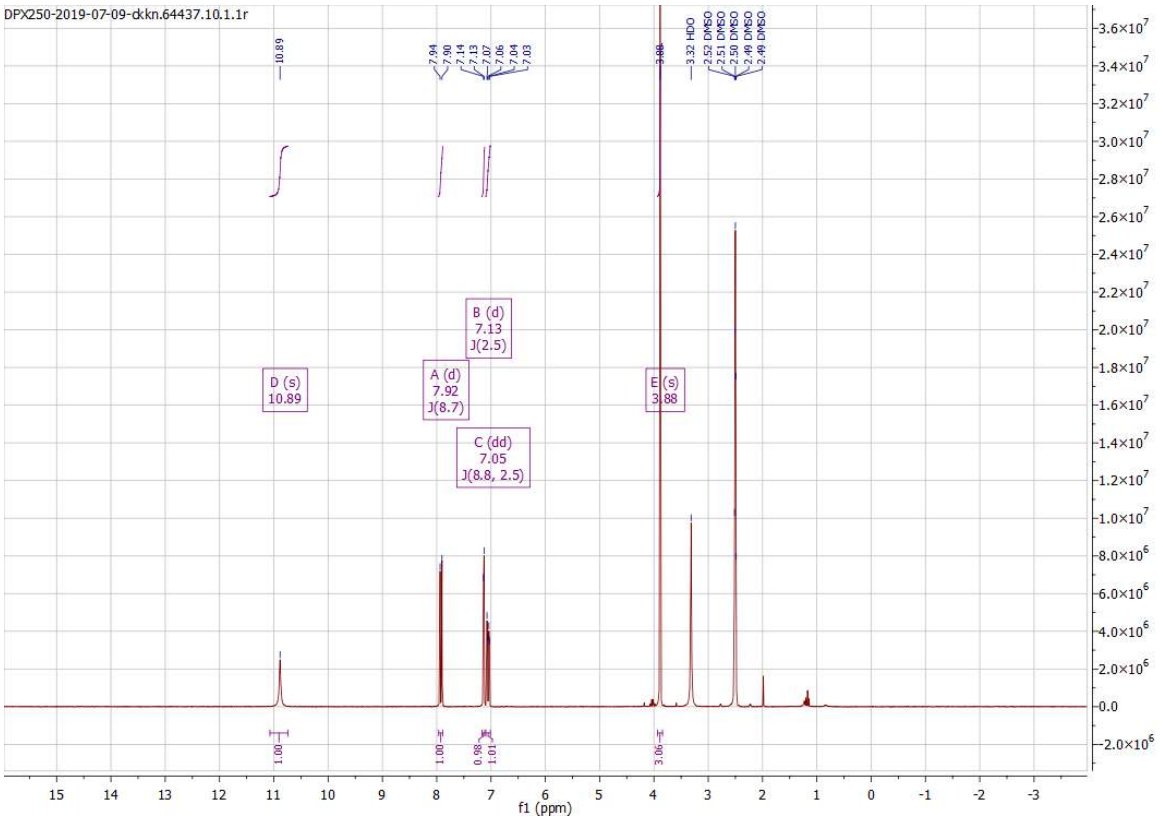

Compound **32**

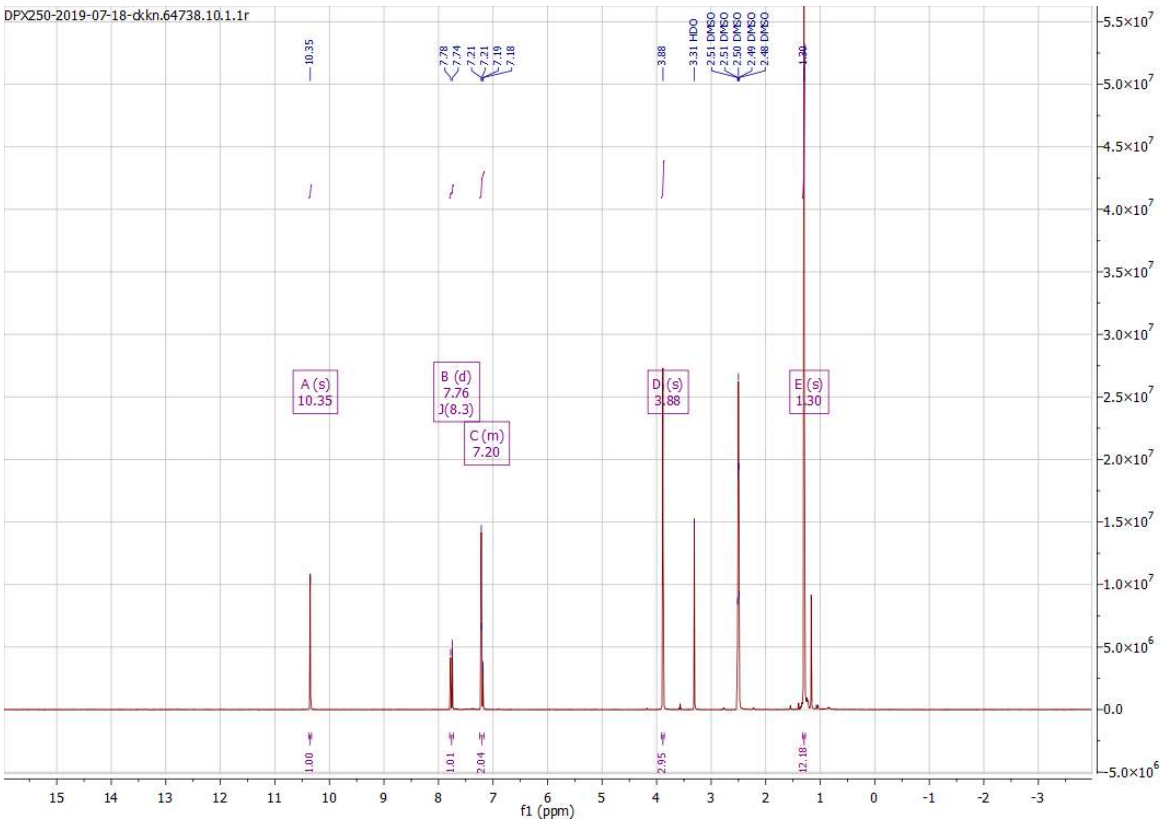

Compound **33**

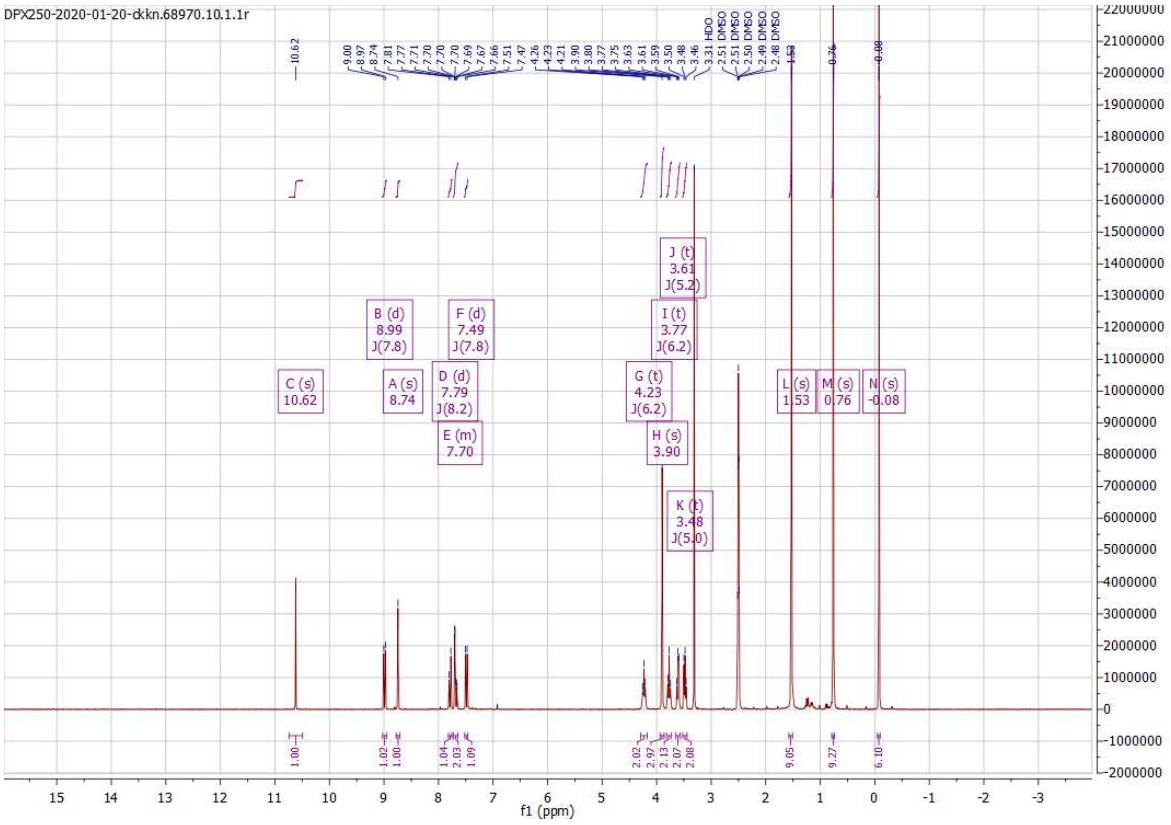

Compound **34**

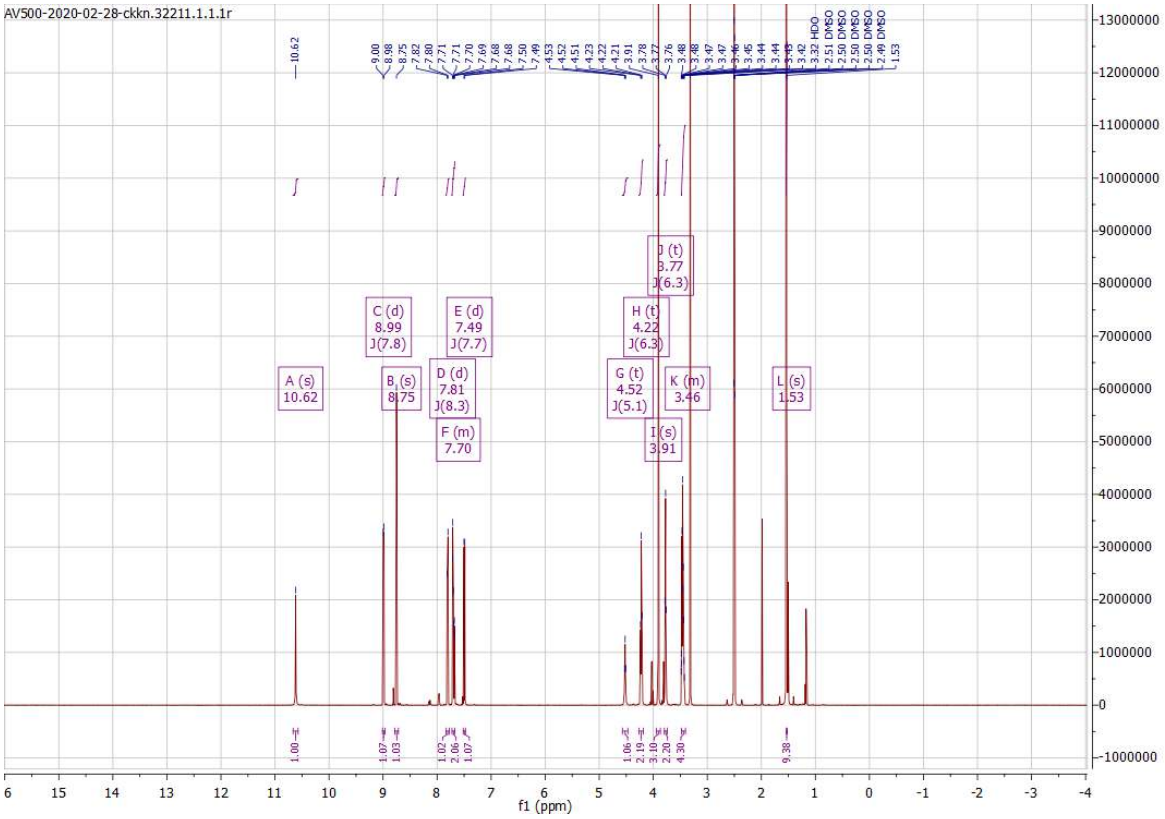
AV500-2020-02-28-ckkn.32211.1.1.1r
A (s) 10.62
B (s) 8.75
C (d) 8.99 J(7.8)
D (d) 7.81 J(8.3)
E (d) 7.49 J(7.7)
F (m) 7.70
G (t) 4.52 J(5.1)
H (t) 4.22 J(6.3)
I (s) 3.91
J (t) 3.77 J(6.3)
K (m) 3.46
L (s) 1.53
f1 (ppm)

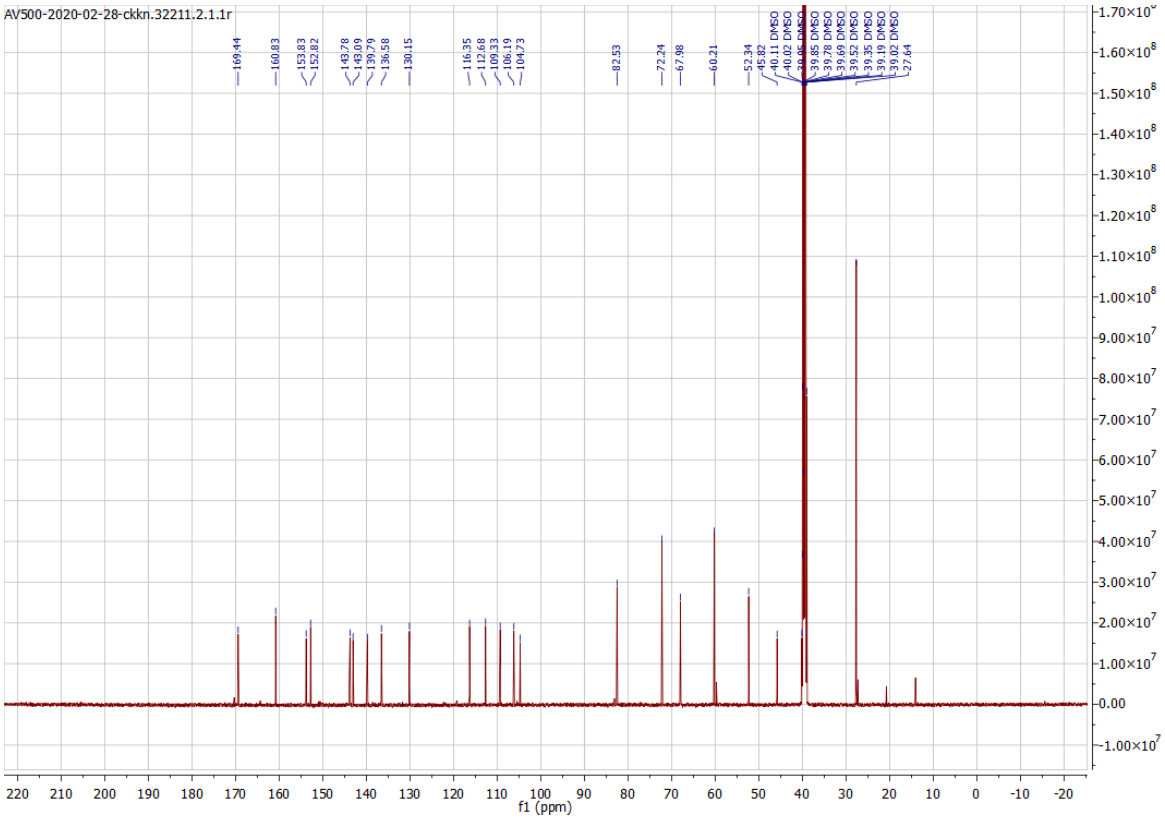
AV500-2020-02-28-ckkn.32211.2.1.1r
f1 (ppm)

Compound **35**

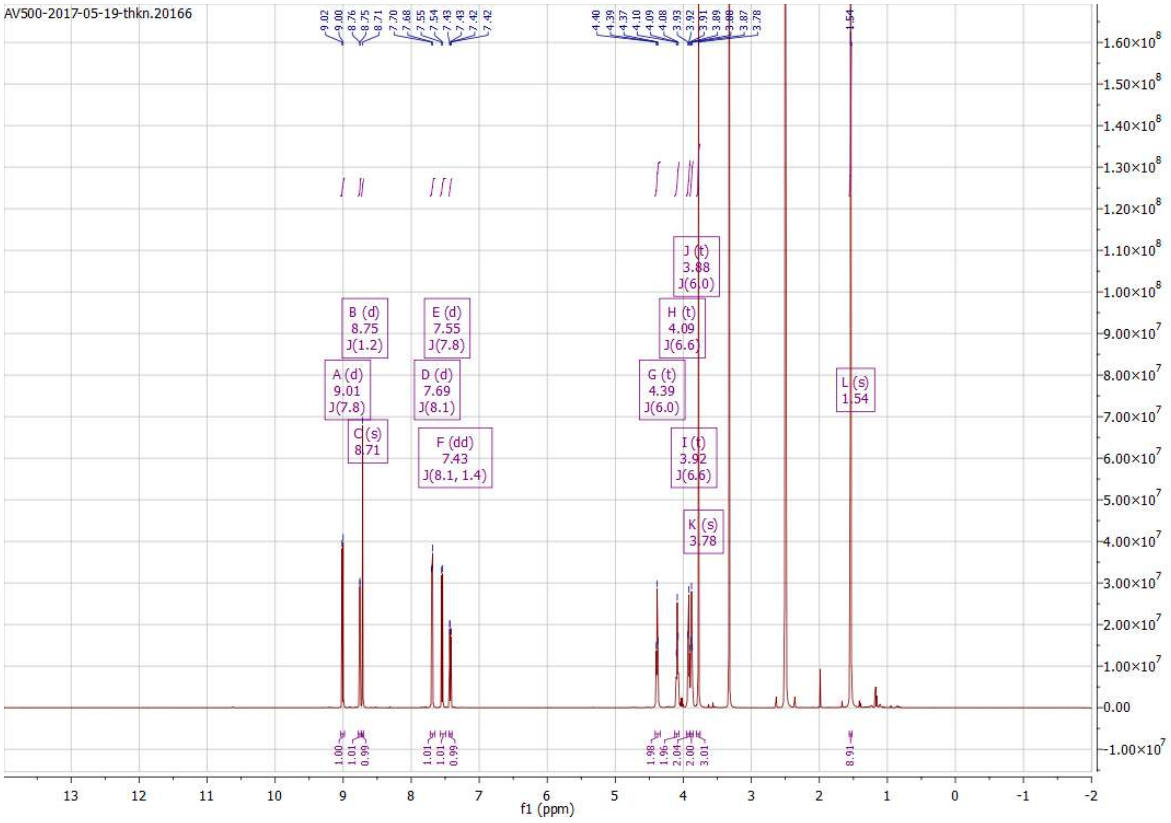
AV500-2017-05-19-thkn.20166
B (d)
8.75
J(1.2)
E (d)
7.55
J(7.8)
J (t)
3.88
J(6.0)
H (t)
4.09
J(6.6)
A (d)
9.01
J(7.8)
D (d)
7.69
J(8.1)
G (t)
4.39
J(6.0)
L (s)
1.54
C (s)
8.71
F (dd)
7.43
J(8.1, 1.4)
I (t)
3.92
J(6.6)
K (s)
3.78
f1 (ppm)

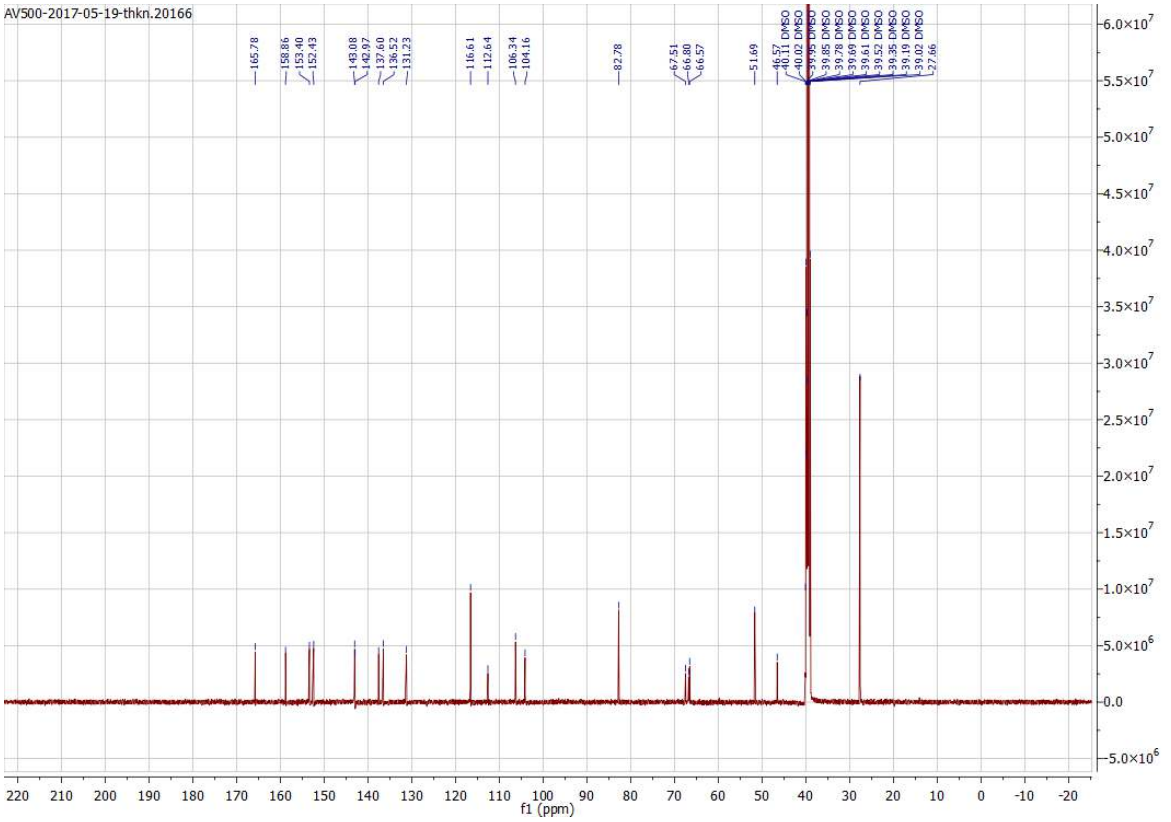
AV500-2017-05-19-thkn.20166
f1 (ppm)

Compound **46**

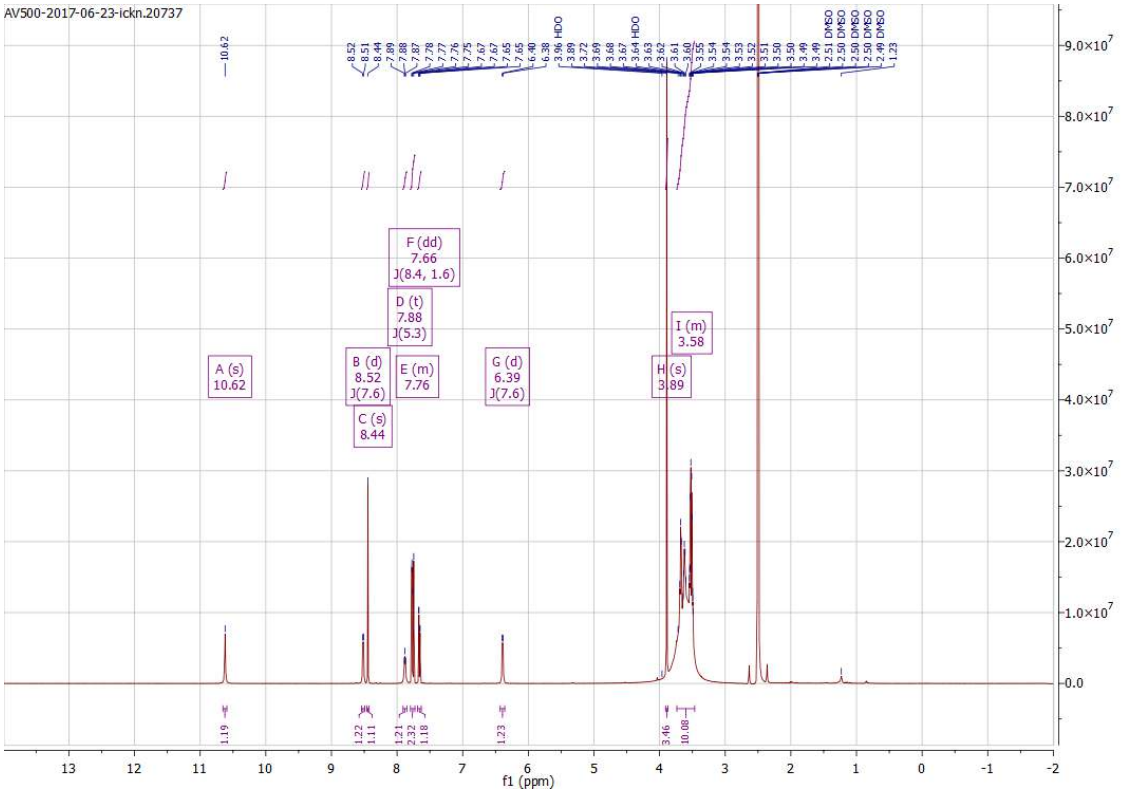
AV500-2017-06-23-ickn.20737
A (s)
10.62
B (d)
8.52
J(7.6)
C (s)
8.44
D (t)
7.88
J(5.3)
E (m)
7.76
F (dd)
7.66
J(8.4, 1.6)
G (d)
6.39
J(7.6)
H (s)
3.89
I (m)
3.58
f1 (ppm)

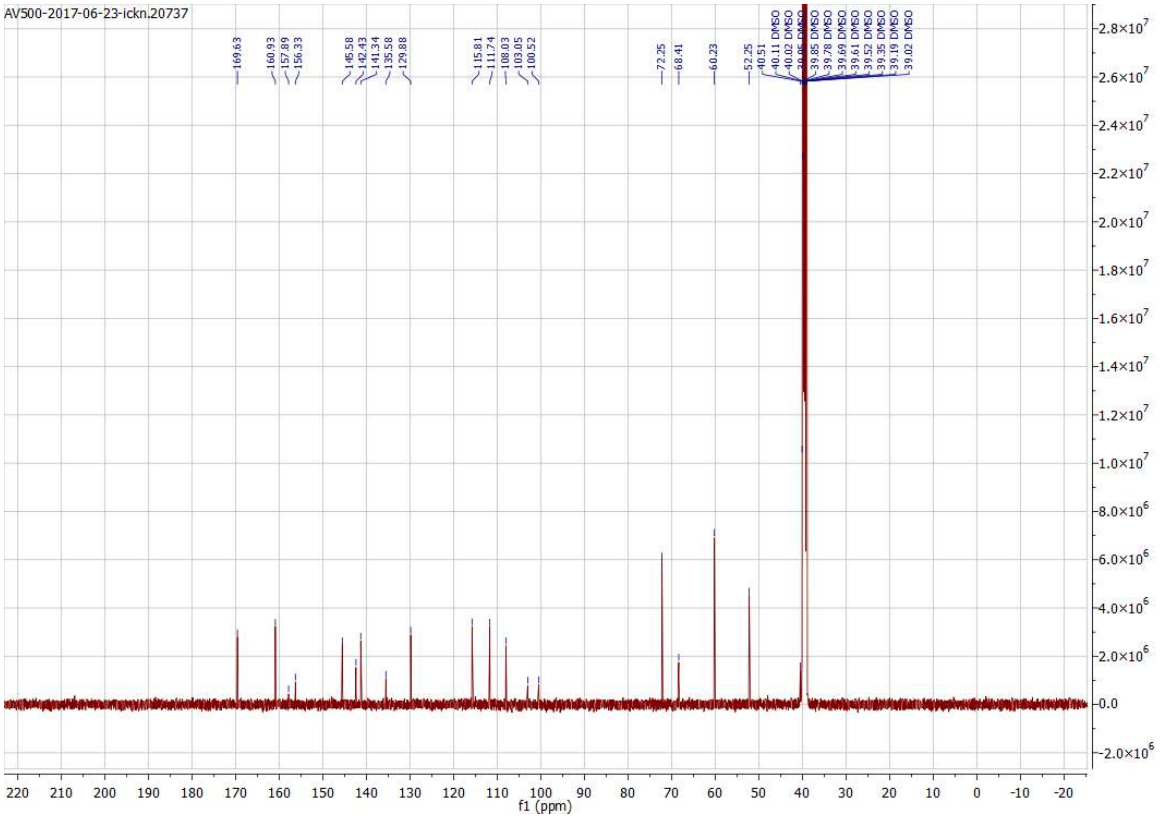
AV500-2017-06-23-ickn.20737
f1 (ppm)

Compound **47**

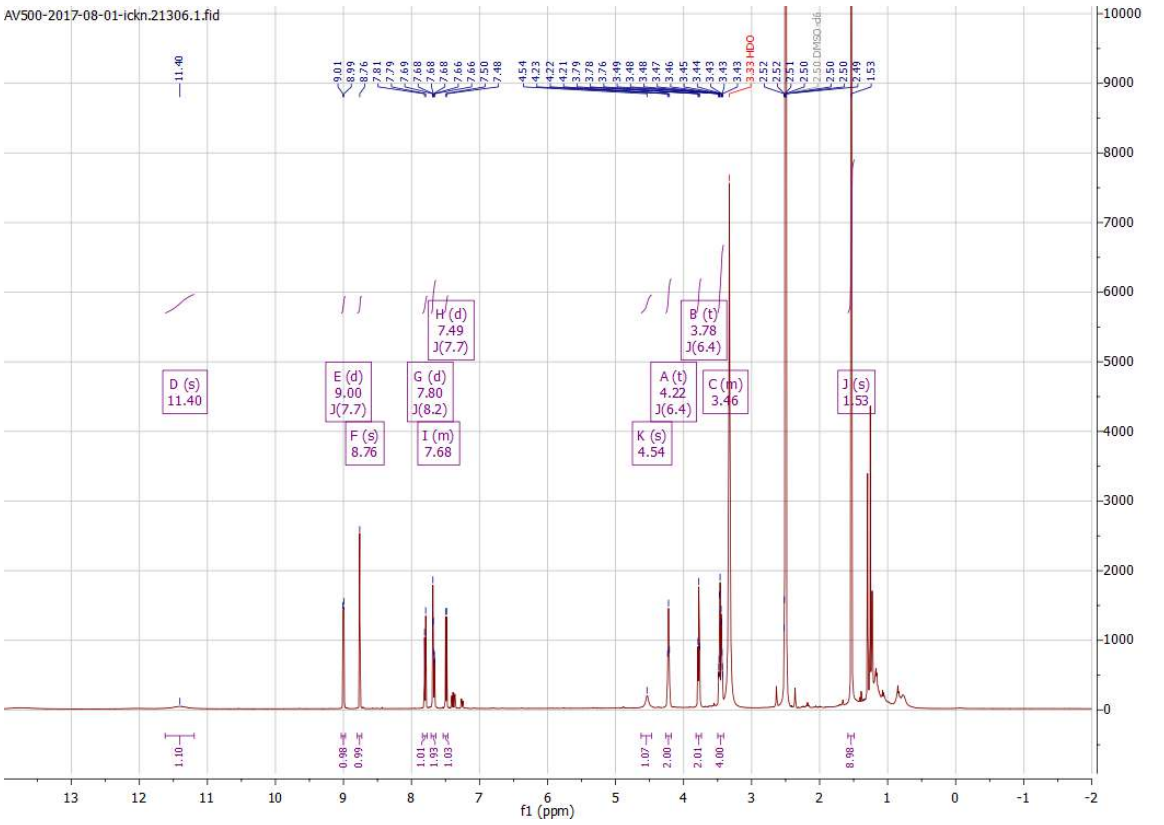
AV500-2017-08-01-ickn.21306.1.fid
D (s) 11.40
E (d) 9.00 J(7.7)
F (s) 8.76
H (d) 7.49 J(7.7)
G (d) 7.80 J(8.2)
I (m) 7.68
B (t) 3.78 J(6.4)
A (t) 4.22 J(6.4)
C (m) 3.46
K (s) 4.54
J (s) 1.53
f1 (ppm)

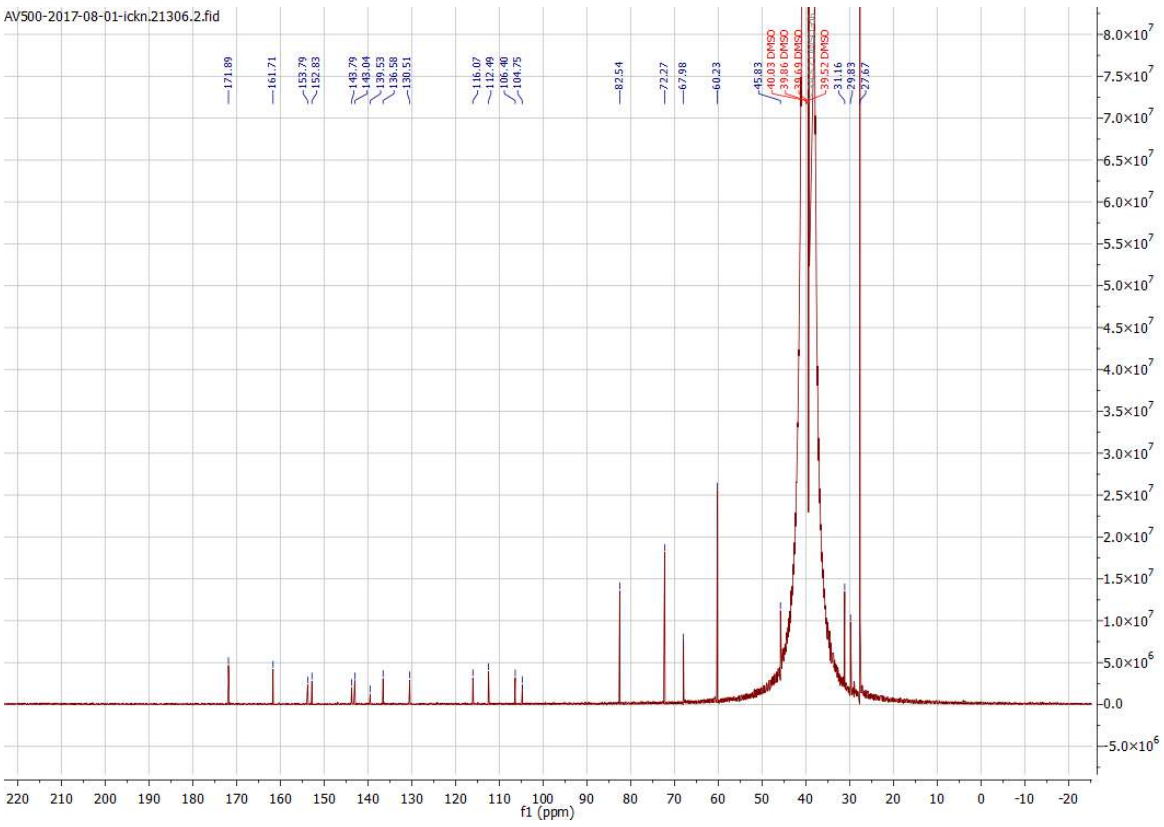
AV500-2017-08-01-ickn.21306.2.fid
f1 (ppm)

Compound **60**

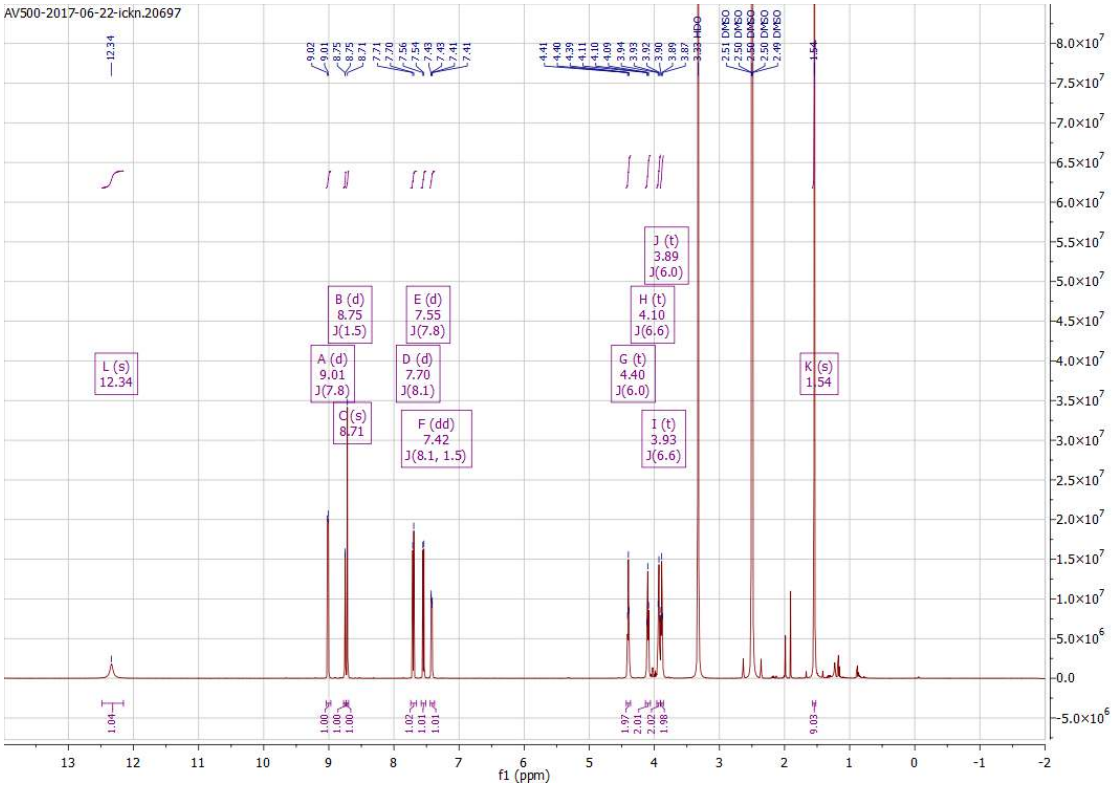
AV500-2017-06-22-ickn.20697
L (s) 12.34
A (d) 9.01 J(7.8)
B (d) 8.75 J(1.5)
C (s) 8.71
D (d) 7.70 J(8.1)
E (d) 7.55 J(7.8)
F (dd) 7.42 J(8.1, 1.5)
G (t) 4.40 J(6.0)
H (t) 4.10 J(6.6)
I (t) 3.93 J(6.6)
J (t) 3.89 J(6.0)
K (s) 1.54
f1 (ppm)

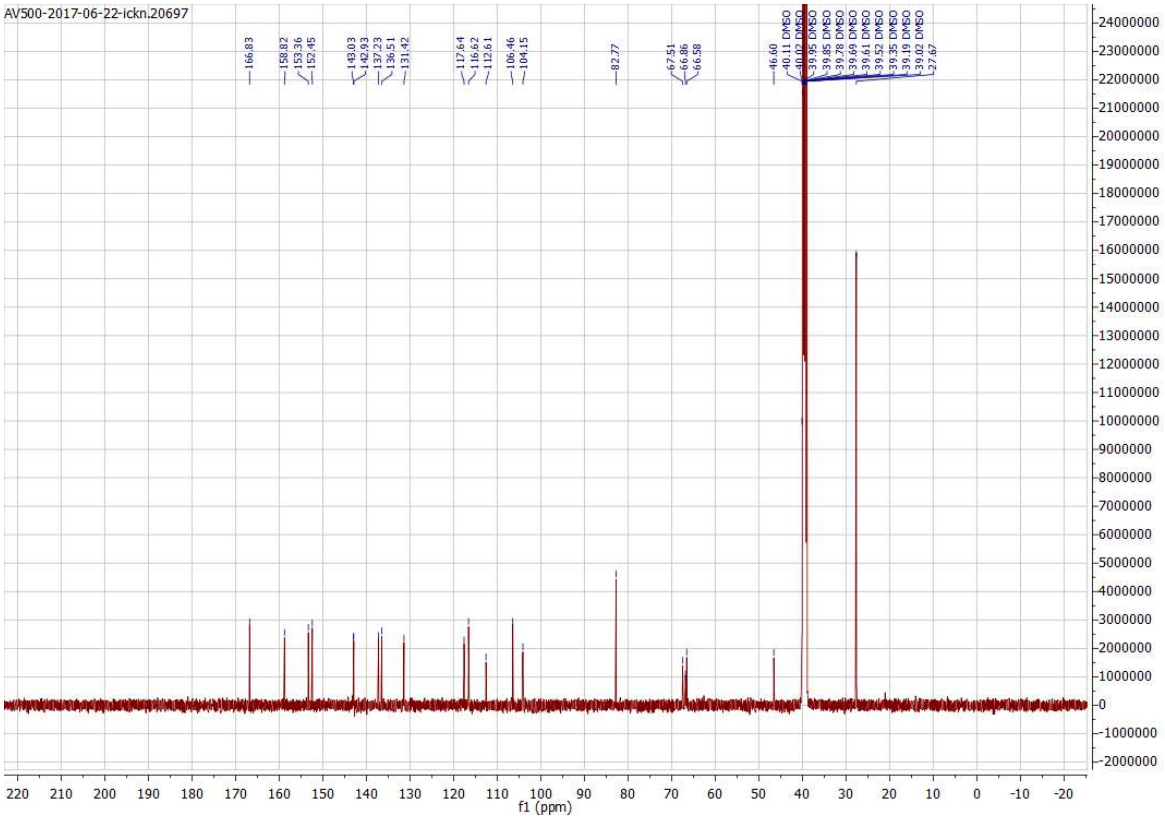
AV500-2017-06-22-ickn.20697
f1 (ppm)

Compound **36**

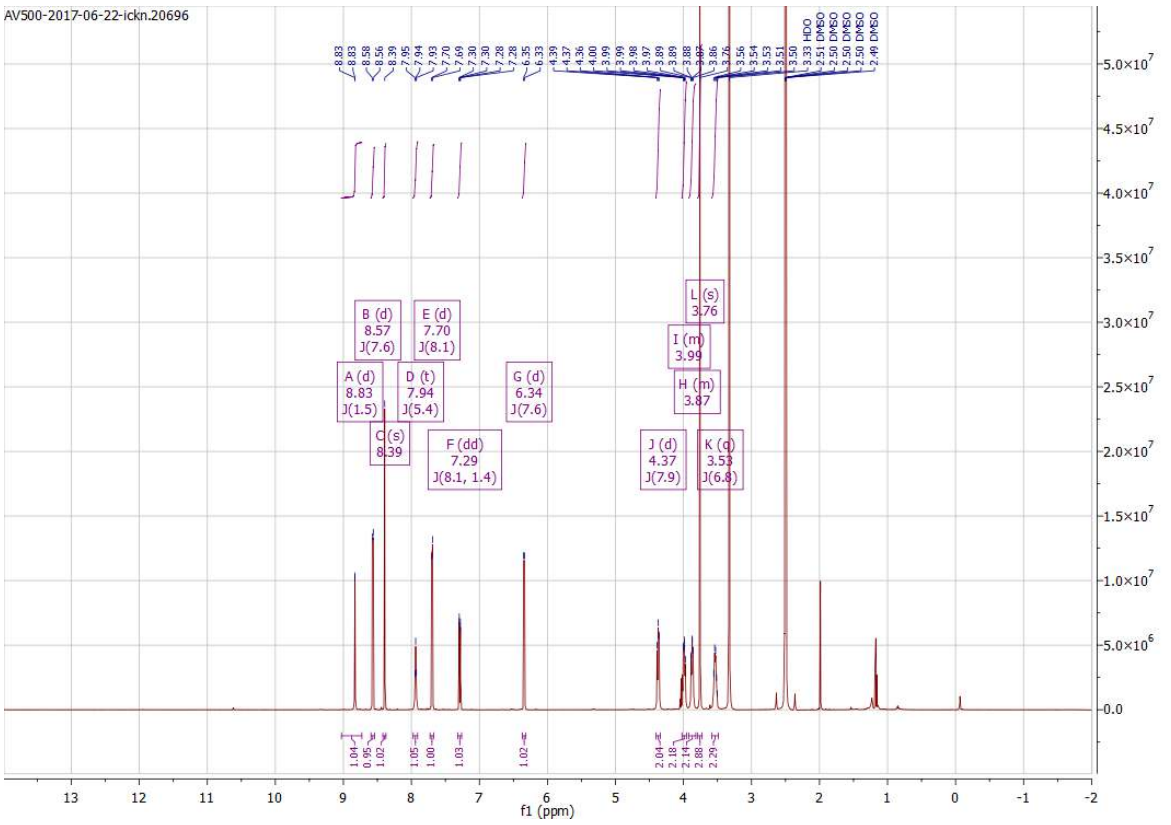
AV500-2017-06-22-ickn.20696
B (d) 8.57 J(7.6)
E (d) 7.70 J(8.1)
A (d) 8.83 J(1.5)
D (t) 7.94 J(5.4)
G (d) 6.34 J(7.6)
L (s) 3.76
I (m) 3.99
H (m) 3.87
C (s) 8.39
F (dd) 7.29 J(8.1, 1.4)
J (d) 4.37 J(7.9)
K (q) 3.53 J(6.8)
f1 (ppm)

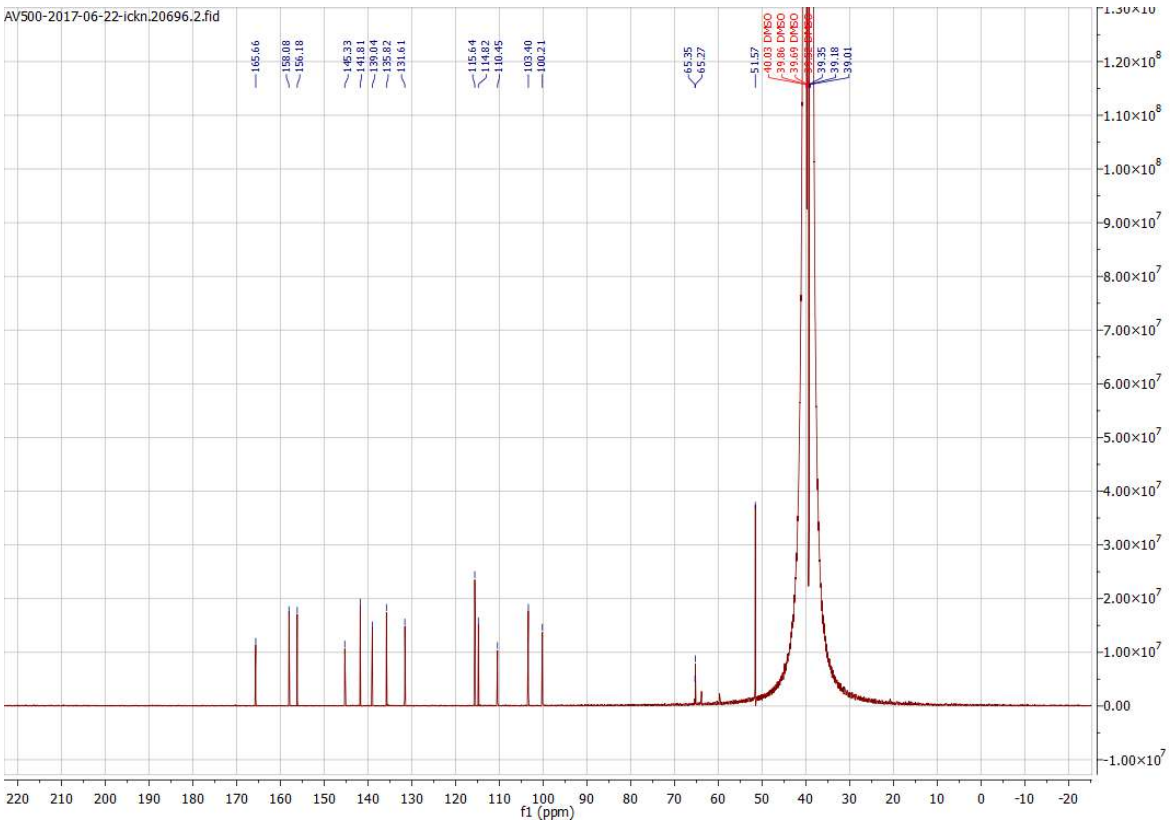
AV500-2017-06-22-ickn.20696.2.fid
f1 (ppm)

Compound **37**

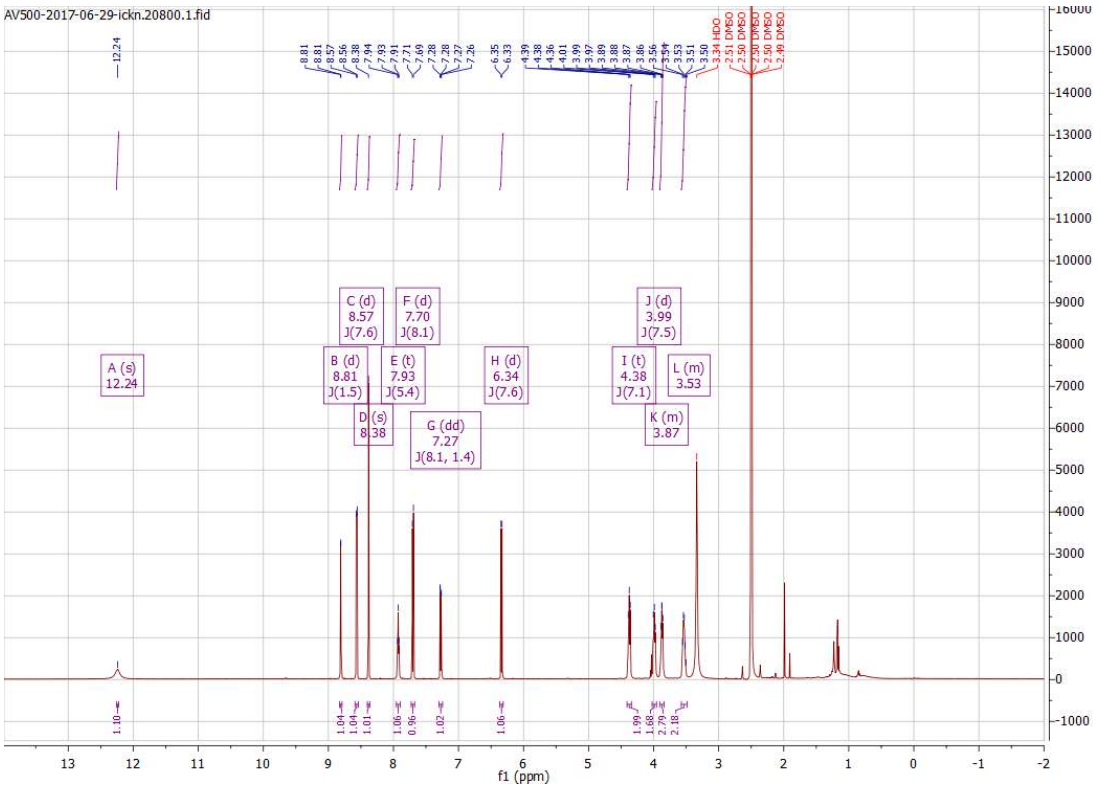
AV500-2017-06-29-ickn.20800.1.fid
A (s) 12.24
B (d) 8.81 J(1.5)
C (d) 8.57 J(7.6)
D (s) 8.38
E (t) 7.93 J(5.4)
F (d) 7.70 J(8.1)
G (dd) 7.27 J(8.1, 1.4)
H (d) 6.34 J(7.6)
I (t) 4.38 J(7.1)
J (d) 3.99 J(7.5)
K (m) 3.87
L (m) 3.53
f1 (ppm)

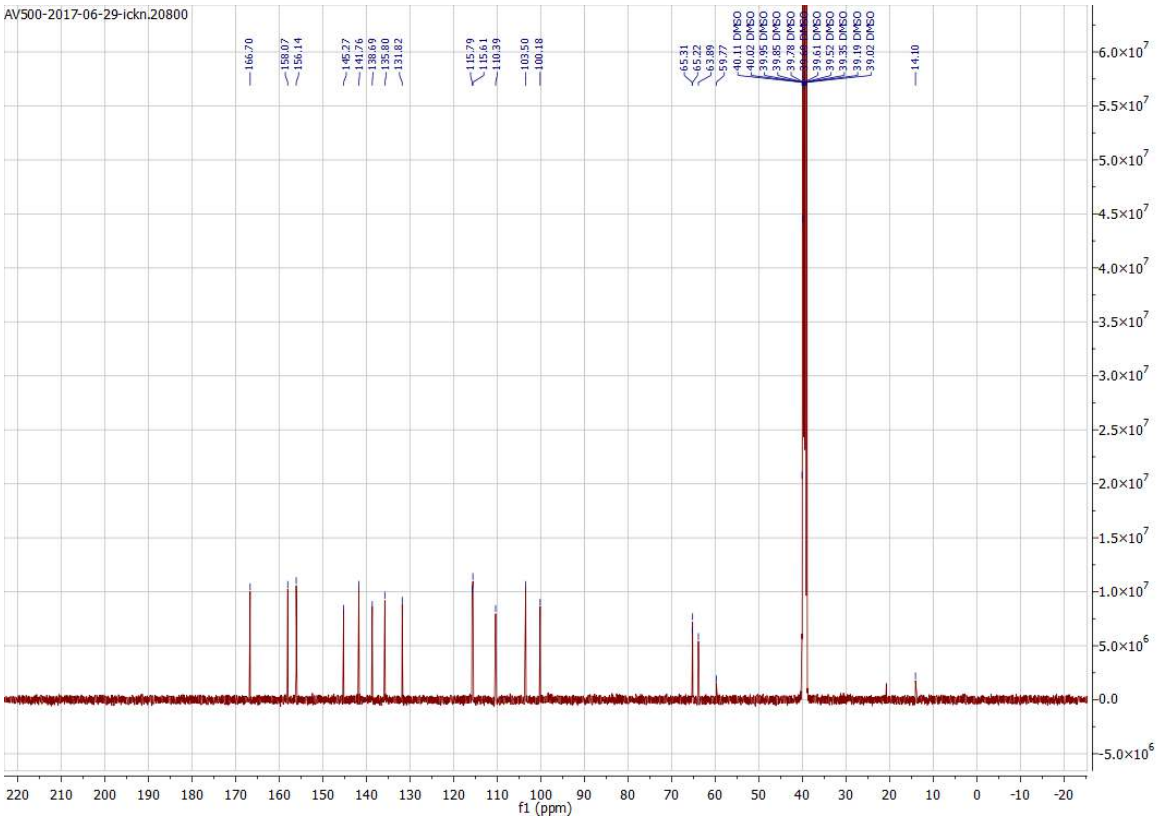
AV500-2017-06-29-ickn.20800
f1 (ppm)

Compound **61**

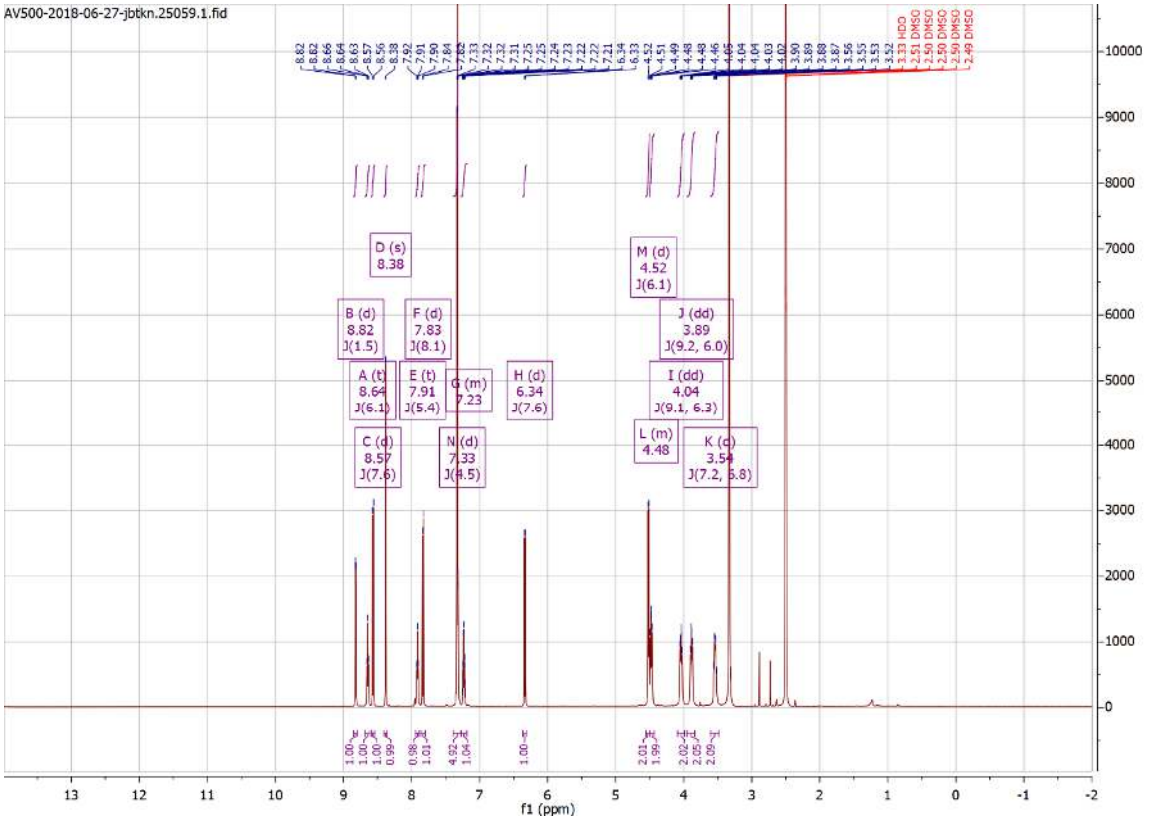
AV500-2018-06-27-jbtkn.25059.1.fid
D (s)
8.38
M (d)
4.52
J(6.1)
B (d)
8.82
J(1.5)
F (d)
7.83
J(8.1)
J (dd)
3.89
J(9.2, 6.0)
A (t)
8.64
J(6.1)
E (t)
7.91
J(5.4)
G (m)
7.23
H (d)
6.34
J(7.6)
I (dd)
4.04
J(9.1, 6.3)
C (d)
8.57
J(7.6)
N (d)
7.33
J(4.5)
L (m)
4.48
K (d)
3.54
J(7.2, 5.8)
f1 (ppm)

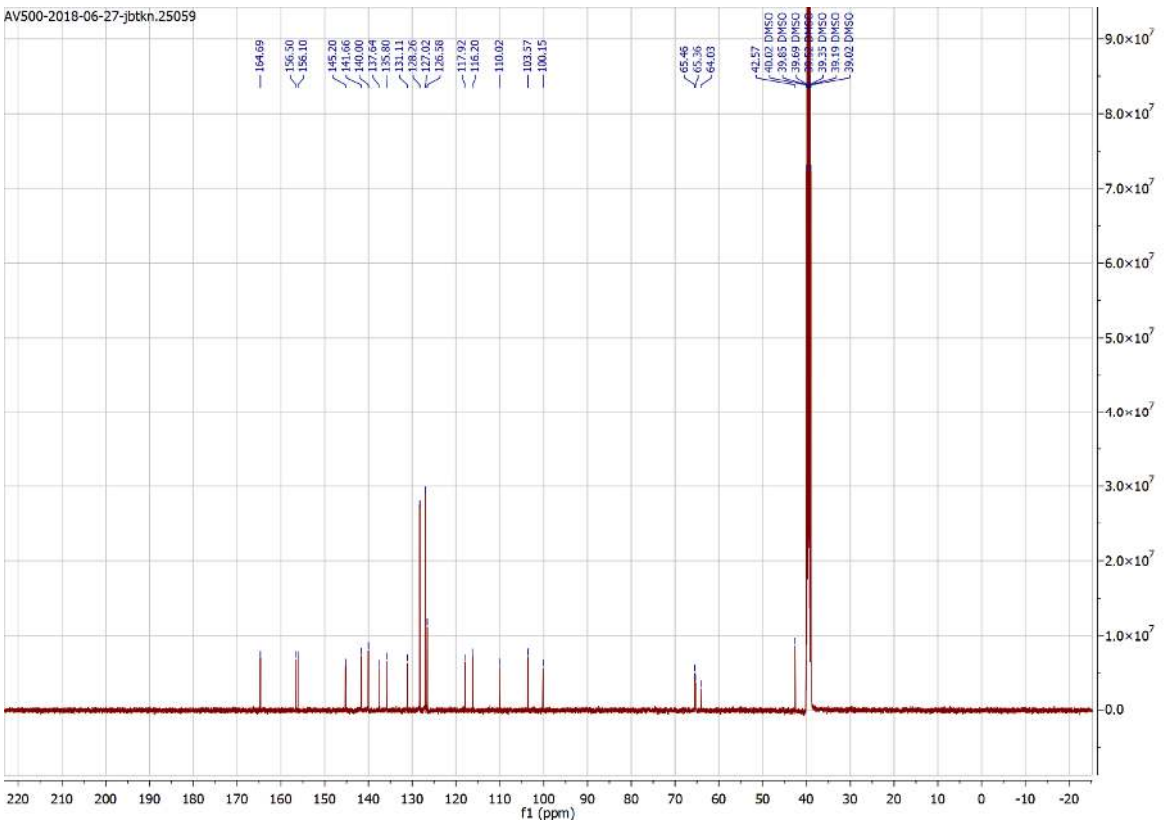
AV500-2018-06-27-jbtkn.25059
f1 (ppm)

Compound **62**

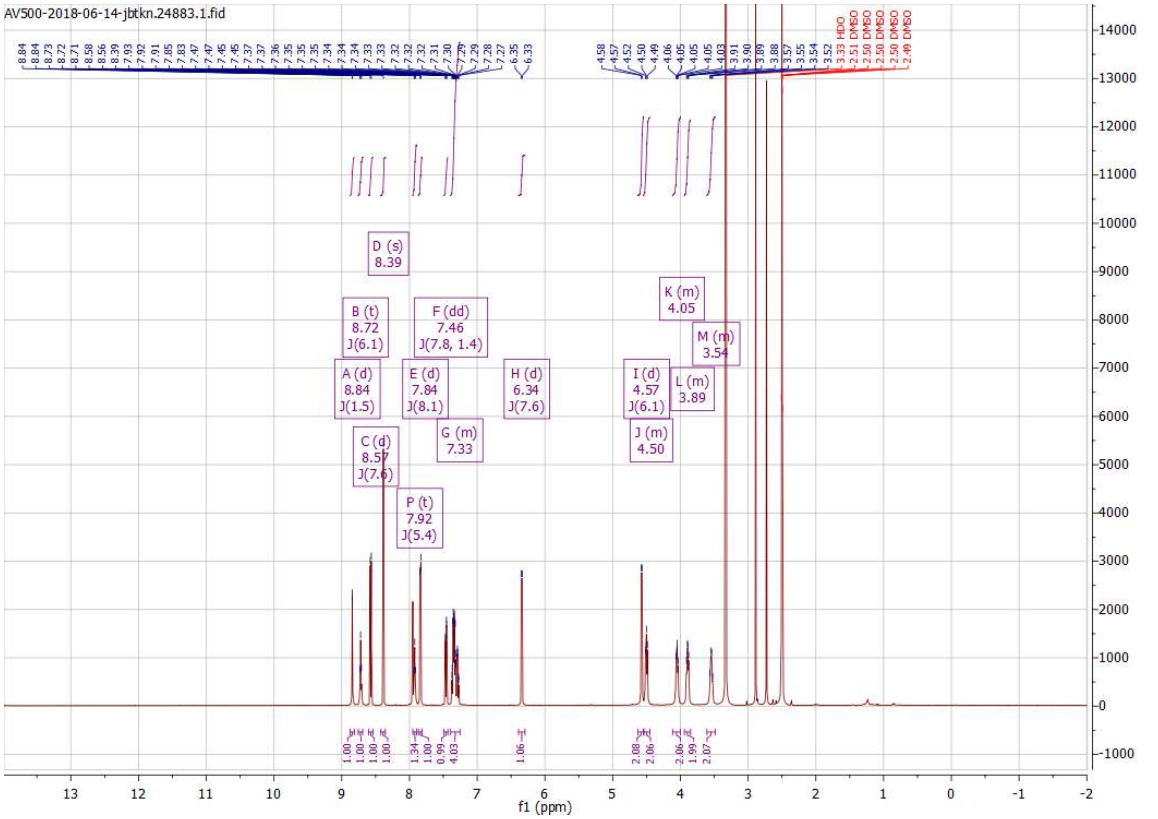
AV500-2018-06-14-jbtkn.24883.1.fid
D (s)
8.39
B (t)
8.72
J(6.1)
F (dd)
7.46
J(7.8, 1.4)
K (m)
4.05
M (m)
3.54
A (d)
8.84
J(1.5)
E (d)
7.84
J(8.1)
H (d)
6.34
J(7.6)
I (d)
4.57
J(6.1)
L (m)
3.89
G (m)
7.33
J (m)
4.50
C (d)
8.57
J(7.6)
P (t)
7.92
J(5.4)
f1 (ppm)

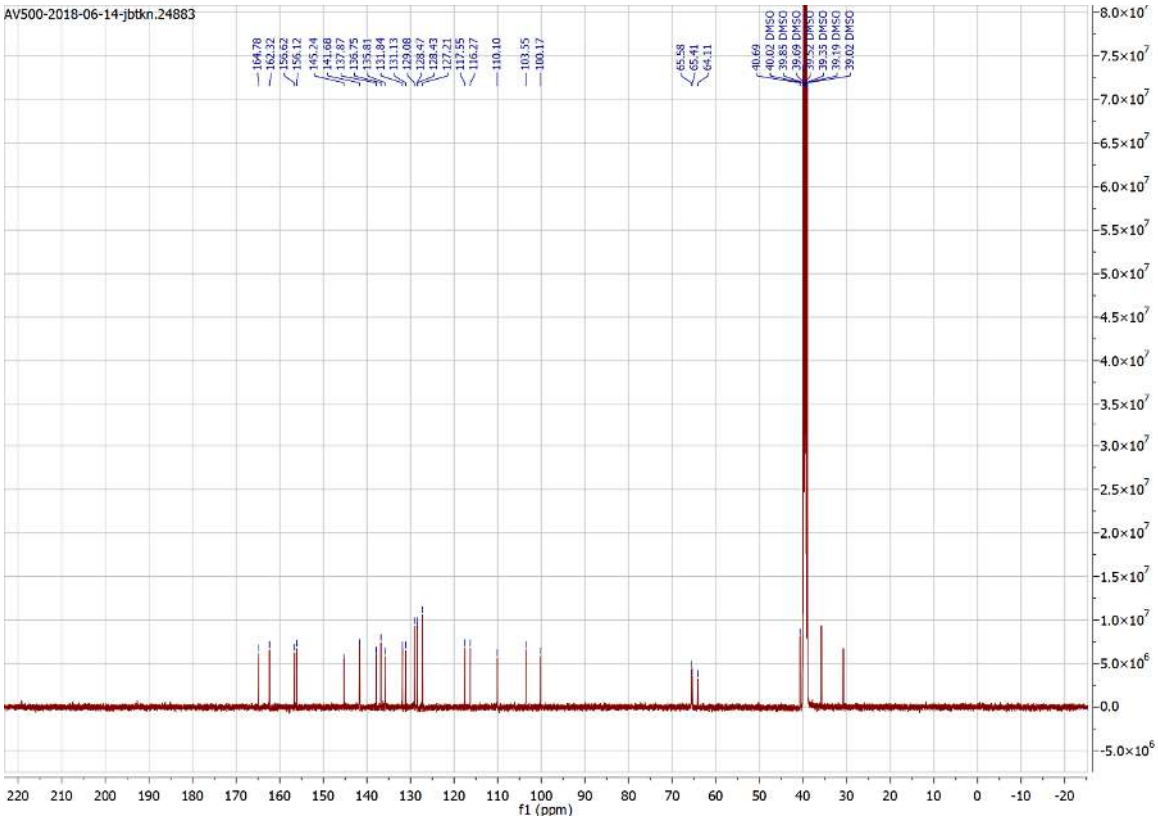
AV500-2018-06-14-jbtkn.24883
f1 (ppm)

Compound **63**

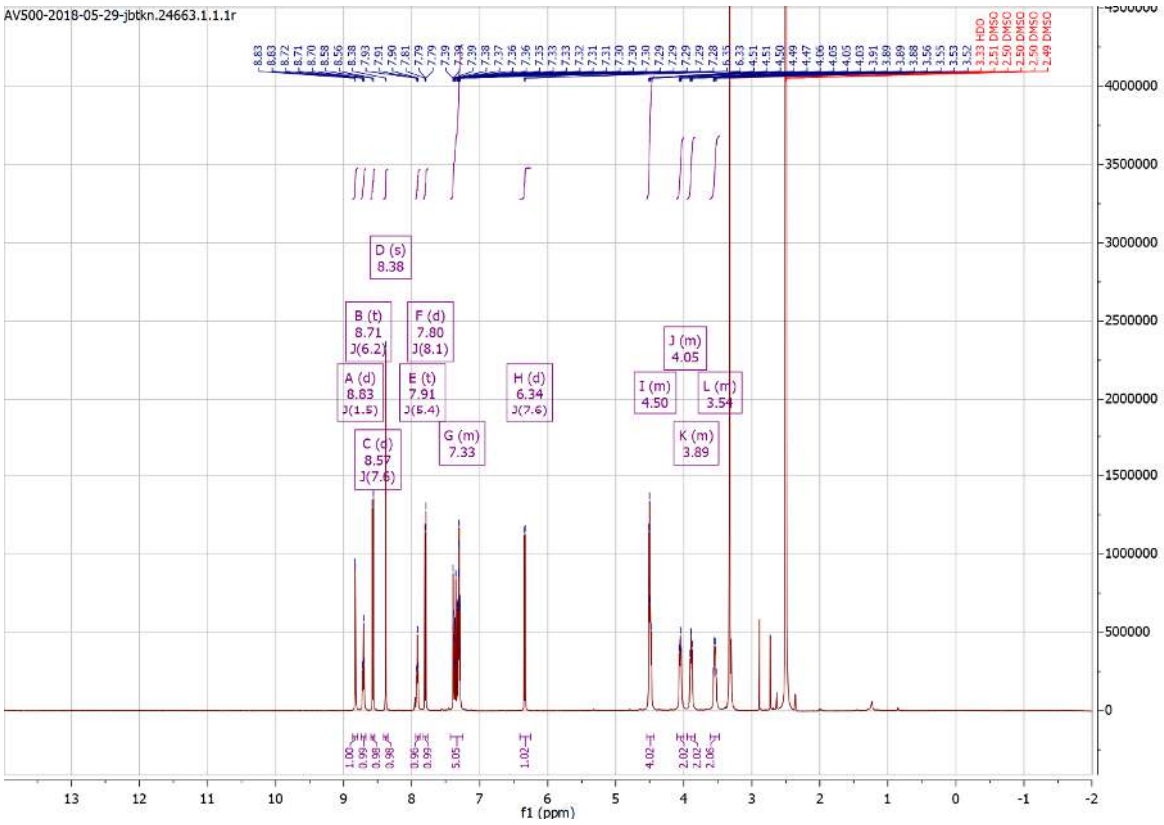
AV500-2018-05-29-jbtkn.24663.1.1.1r
D (s)
8.38
B (t)
8.71
J(6.2)
F (d)
7.80
J(8.1)
J (m)
4.05
A (d)
8.83
J(1.5)
E (t)
7.91
J(5.4)
H (d)
6.34
J(7.6)
I (m)
4.50
L (m)
3.54
C (d)
8.57
J(7.6)
G (m)
7.33
K (m)
3.89
f1 (ppm)

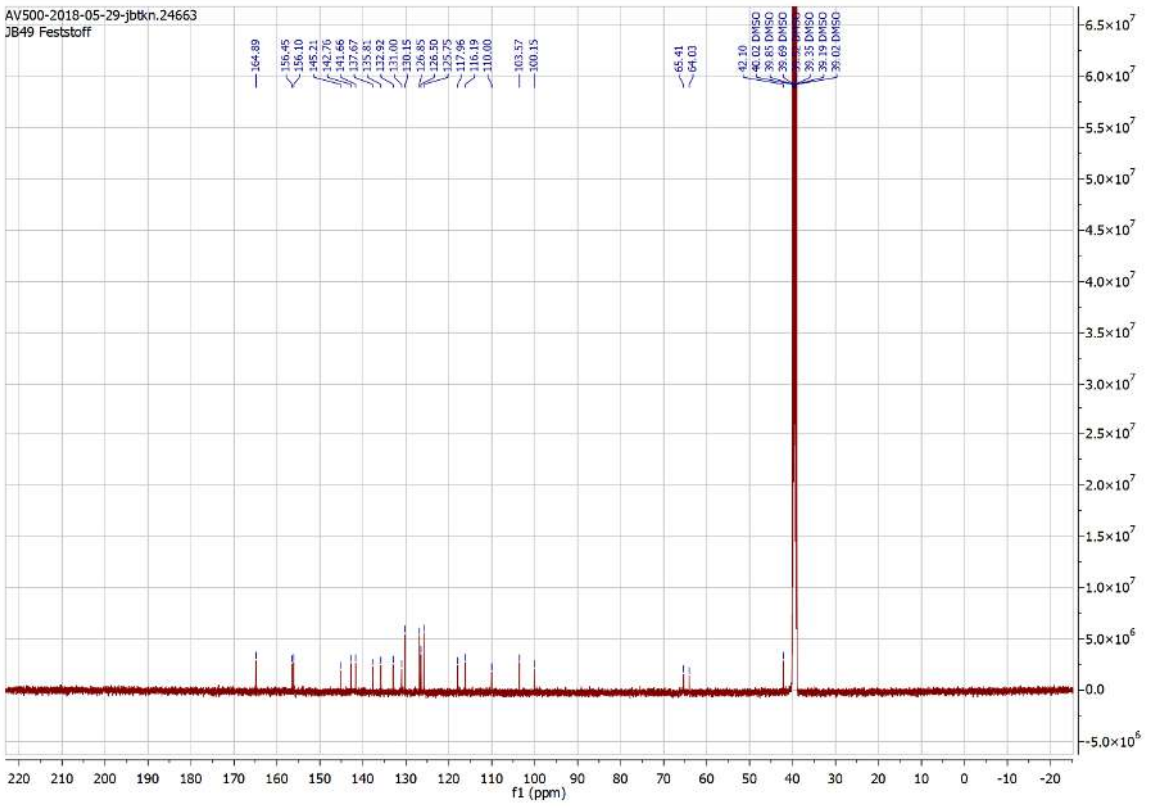
AV500-2018-05-29-jbtkn.24663
JB49 Feststoff
f1 (ppm)

Compound **64**

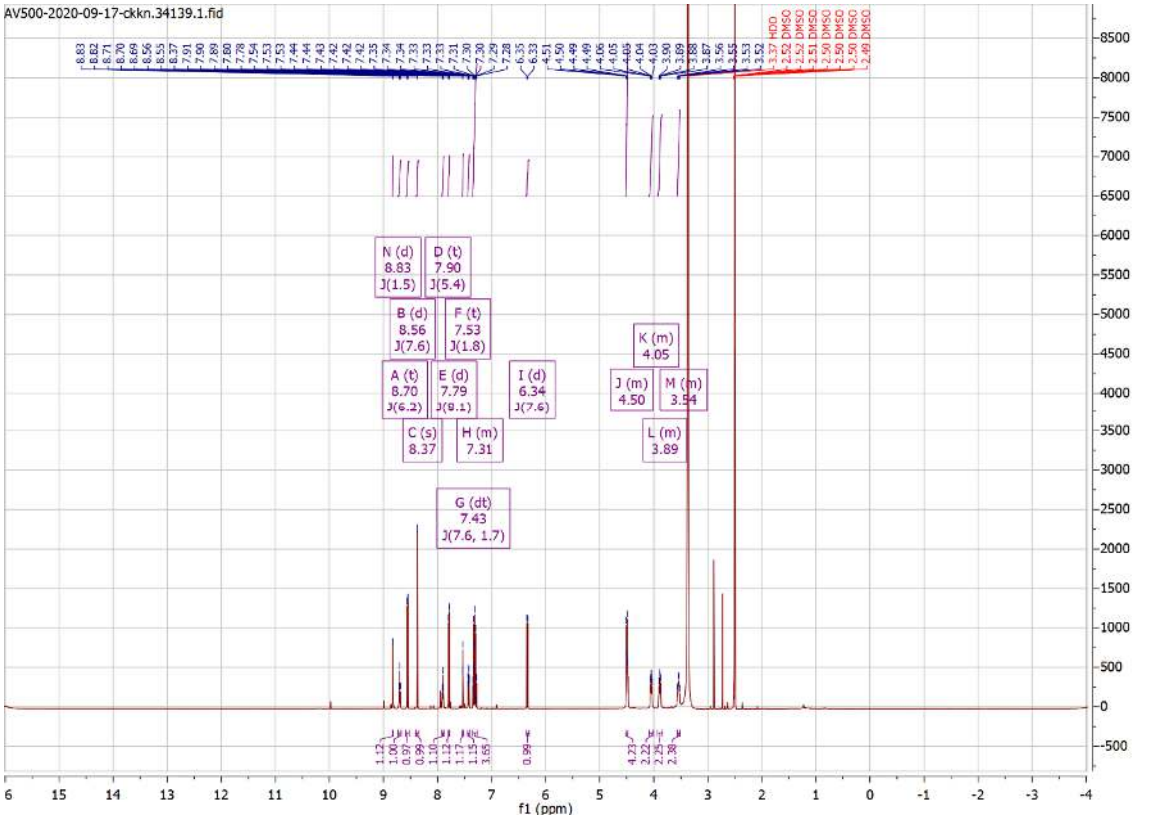
AV500-2020-09-17-ckkn.34139.1.fid
N (d) 8.83 J(1.5)
D (t) 7.90 J(5.4)
B (d) 8.56 J(7.6)
F (t) 7.53 J(1.8)
K (m) 4.05
A (t) 8.70 J(6.2)
E (d) 7.79 J(8.1)
I (d) 6.34 J(7.6)
J (m) 4.50
M (m) 3.54
C (s) 8.37
H (m) 7.31
L (m) 3.89
G (dt) 7.43 J(7.6, 1.7)
f1 (ppm)

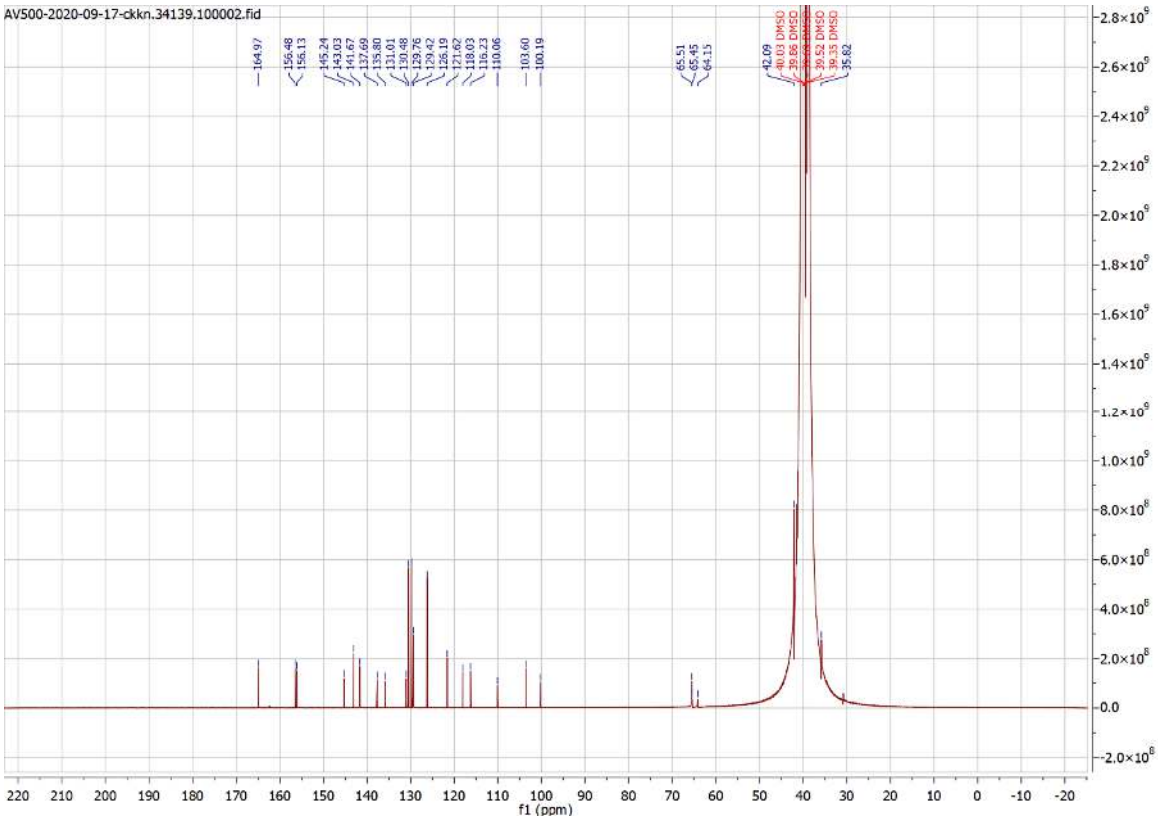
AV500-2020-09-17-ckkn.34139.100002.fid
f1 (ppm)

Compound **65**

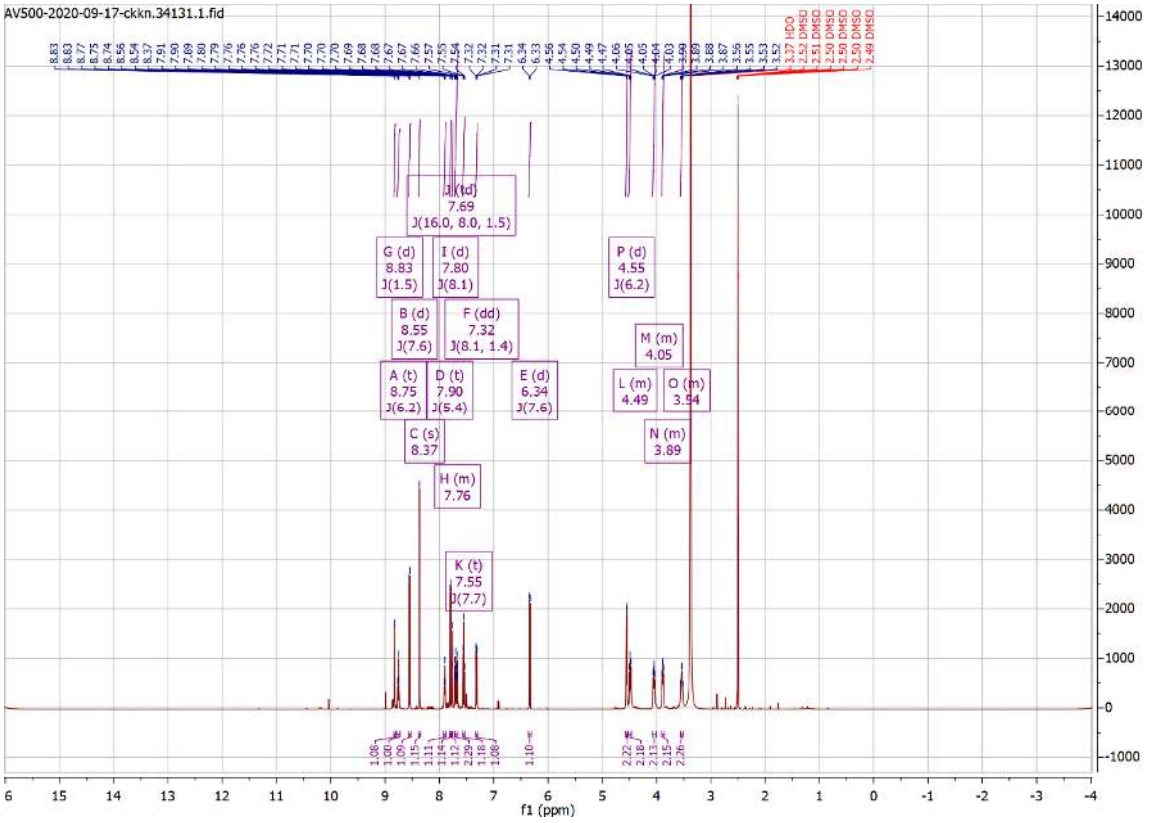
AV500-2020-09-17-ckkn.34131.1.fid
J(td)
7.69
J(16.0, 8.0, 1.5)
G (d)
8.83
J(1.5)
I (d)
7.80
J(8.1)
P (d)
4.55
J(6.2)
B (d)
8.55
J(7.6)
F (dd)
7.32
J(8.1, 1.4)
M (m)
4.05
A (t)
8.75
J(6.2)
D (t)
7.90
J(5.4)
E (d)
6.34
J(7.6)
L (m)
4.49
O (m)
3.54
C (s)
8.37
N (m)
3.89
H (m)
7.76
K (t)
7.55
J(7.7)
f1 (ppm)

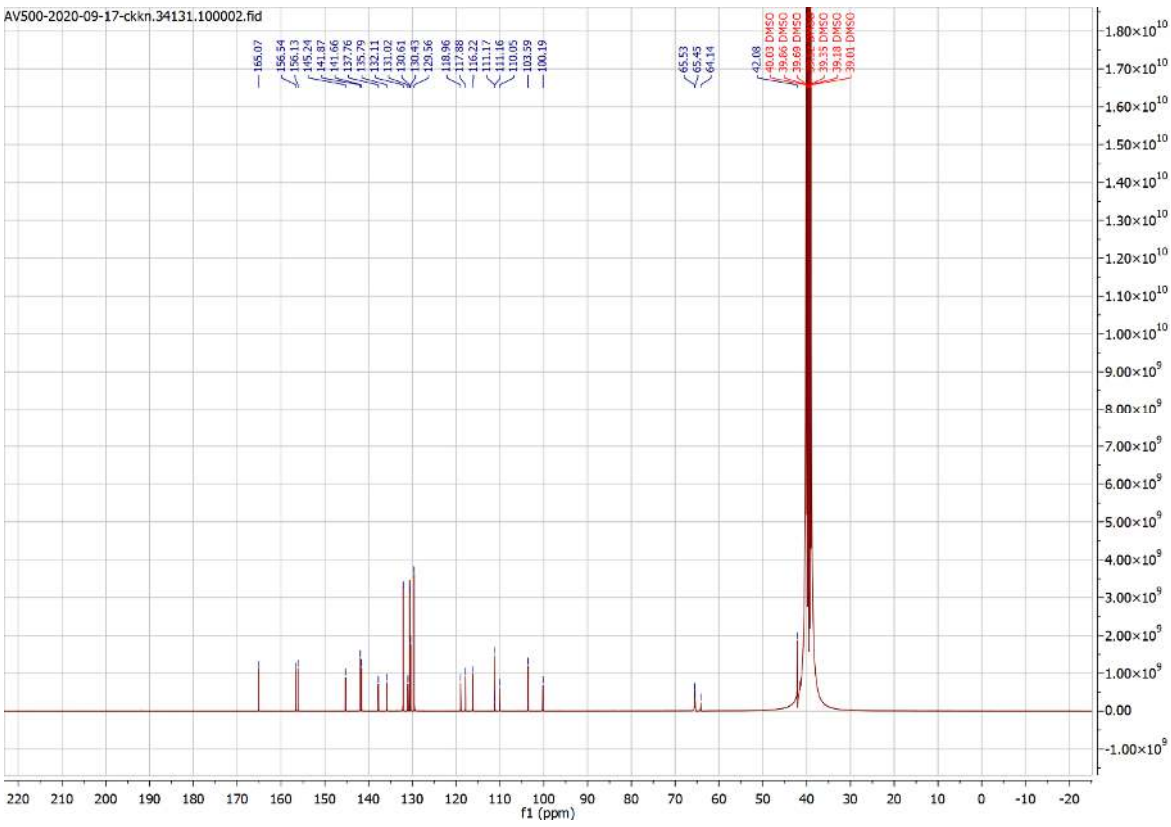
AV500-2020-09-17-ckkn.34131.100002.fid
f1 (ppm)

Compound **66**

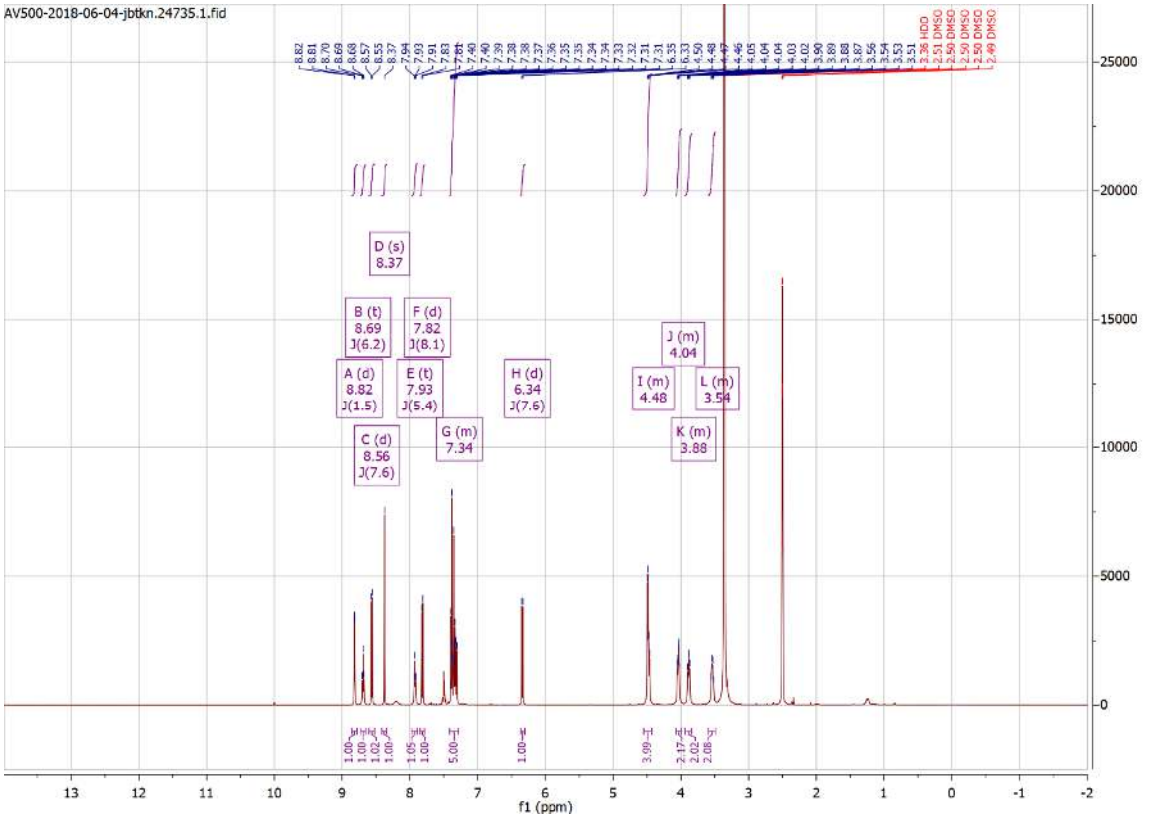
AV500-2018-06-04-jbtkn.24735.1.fid
D (s)
8.37
B (t)
8.69
J(6.2)
F (d)
7.82
J(8.1)
A (d)
8.82
J(1.5)
E (t)
7.93
J(5.4)
H (d)
6.34
J(7.6)
C (d)
8.56
J(7.6)
G (m)
7.34
J (m)
4.04
I (m)
4.48
L (m)
3.54
K (m)
3.88
f1 (ppm)

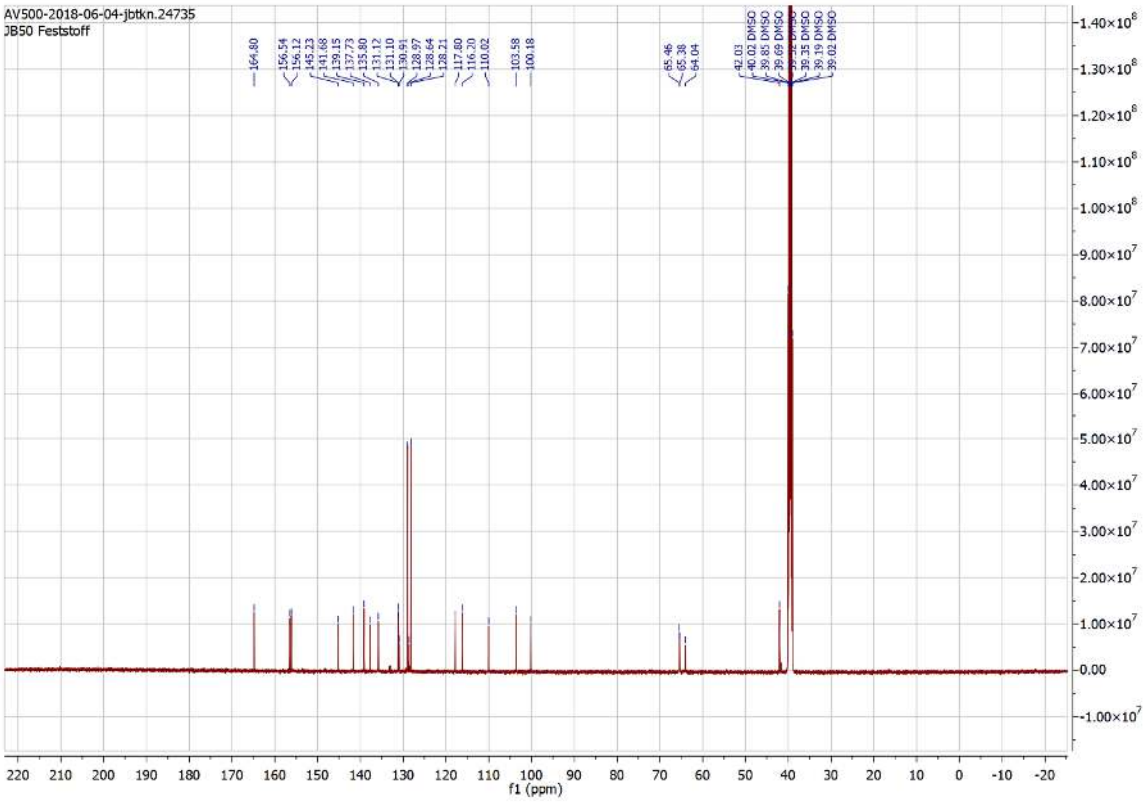
AV500-2018-06-04-jbtkn.24735
JB50 Feststoff
f1 (ppm)

Compound **67**

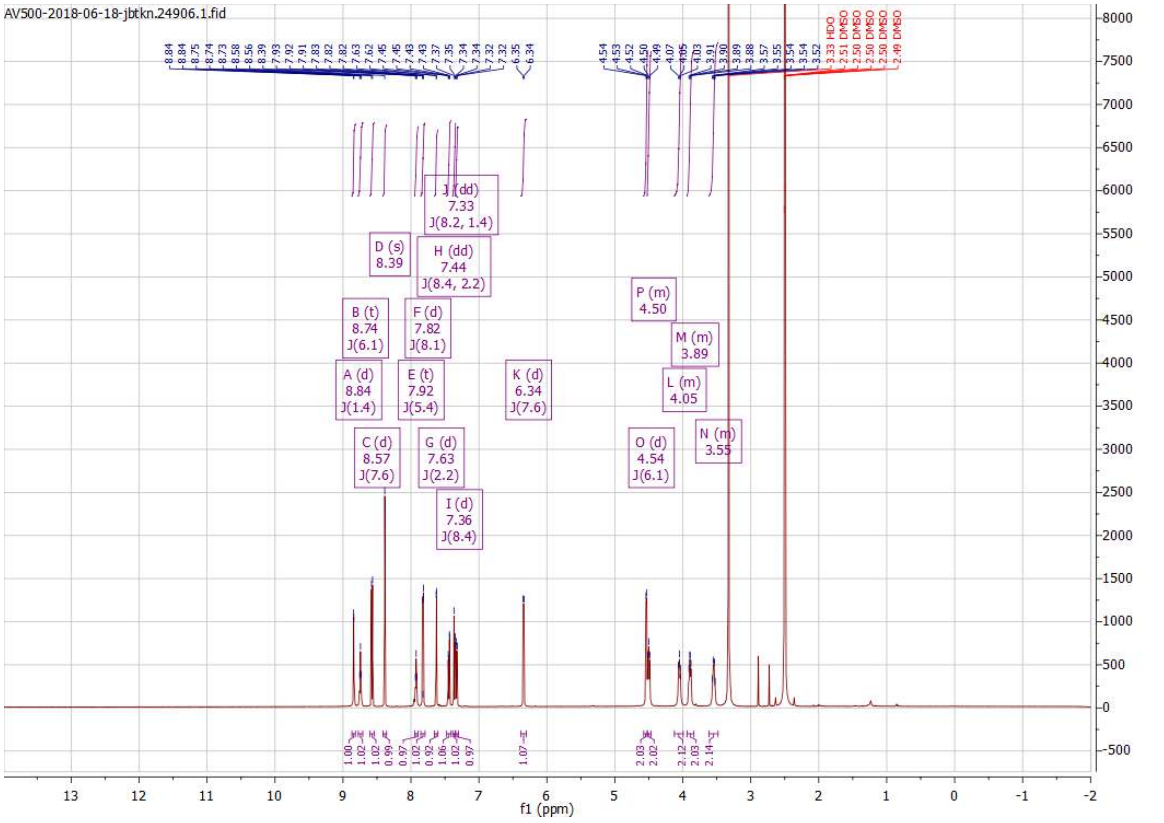
AV500-2018-06-18-jbtkn.24906.1.fid
J (dd)
7.33
J(8.2, 1.4)
D (s)
8.39
H (dd)
7.44
J(8.4, 2.2)
P (m)
4.50
B (t)
8.74
J(6.1)
F (d)
7.82
J(8.1)
M (m)
3.89
A (d)
8.84
J(1.4)
E (t)
7.92
J(5.4)
K (d)
6.34
J(7.6)
L (m)
4.05
N (m)
3.55
C (d)
8.57
J(7.6)
G (d)
7.63
J(2.2)
O (d)
4.54
J(6.1)
I (d)
7.36
J(8.4)
f1 (ppm)

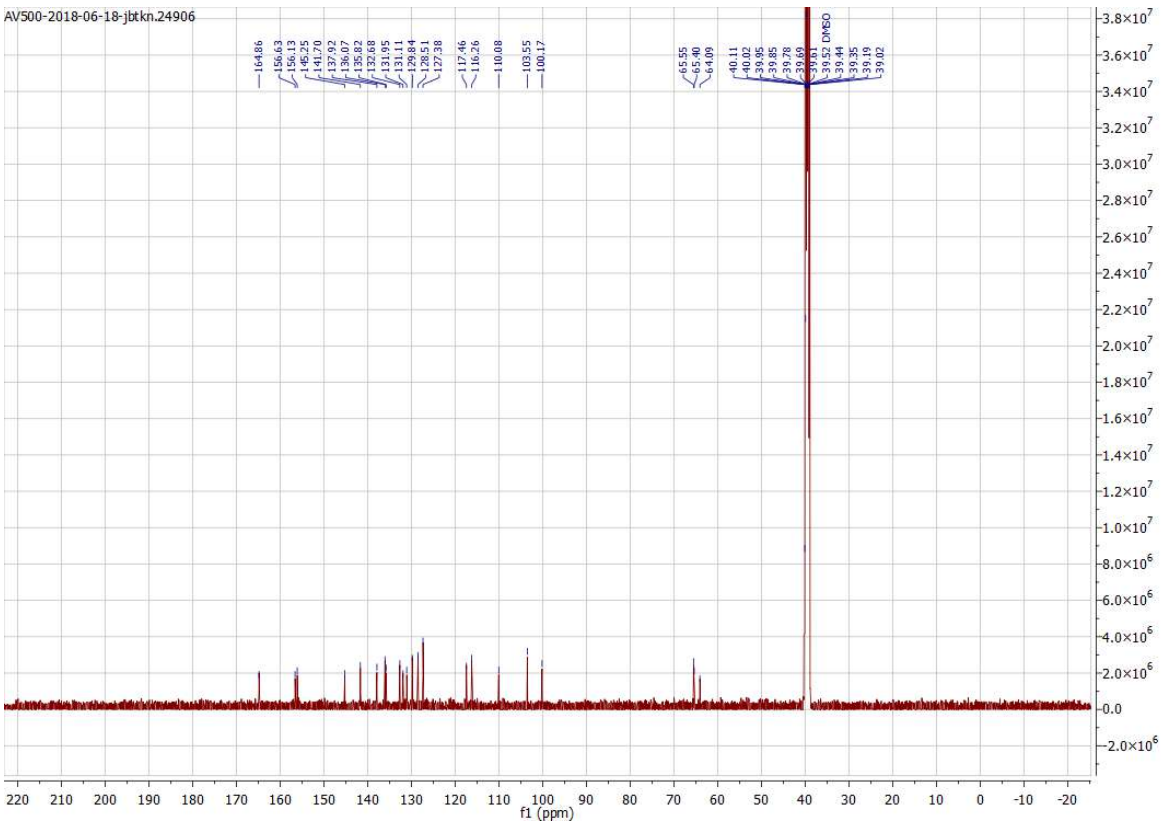
AV500-2018-06-18-jbtkn.24906
f1 (ppm)

Compound **68**

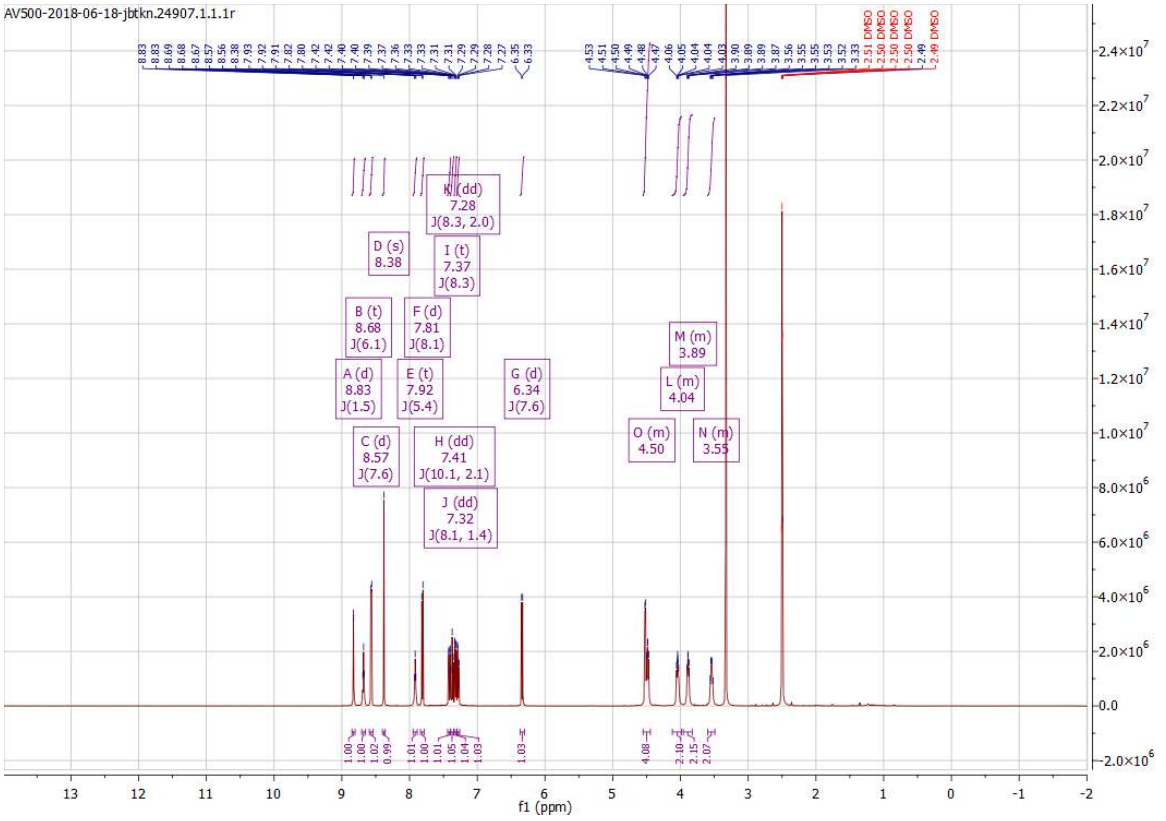
AV500-2018-06-18-jbtkn.24907.1.1.1r
K (dd)
7.28
J(8.3, 2.0)
D (s)
8.38
I (t)
7.37
J(8.3)
B (t)
8.68
J(6.1)
F (d)
7.81
J(8.1)
M (m)
3.89
A (d)
8.83
J(1.5)
E (t)
7.92
J(5.4)
G (d)
6.34
J(7.6)
L (m)
4.04
O (m)
4.50
N (m)
3.55
C (d)
8.57
J(7.6)
H (dd)
7.41
J(10.1, 2.1)
J (dd)
7.32
J(8.1, 1.4)
f1 (ppm)

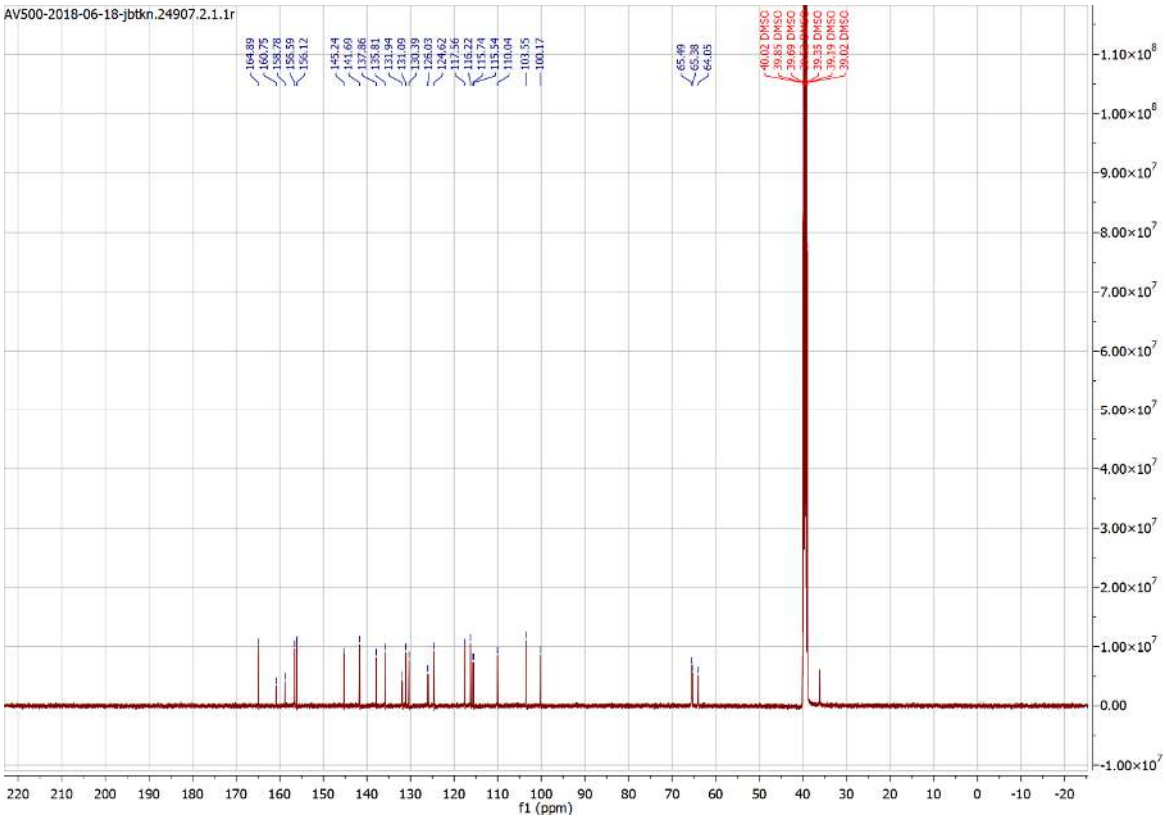
AV500-2018-06-18-jbtkn.24907.2.1.1r
f1 (ppm)

Compound **69**

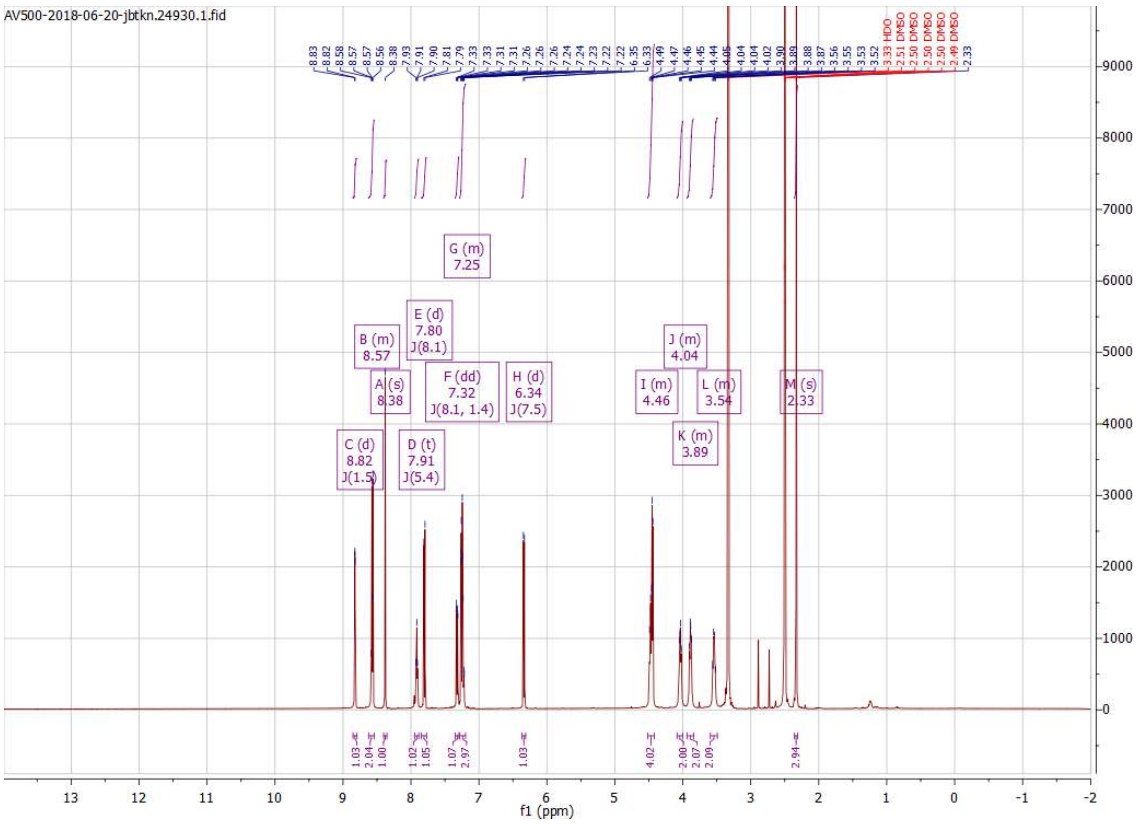
AV500-2018-06-20-jbtkn.24930.1.fid
G (m)
7.25
E (d)
7.80
J(8.1)
B (m)
8.57
A (s)
8.38
F (dd)
7.32
J(8.1, 1.4)
H (d)
6.34
J(7.5)
C (d)
8.82
J(1.5)
D (t)
7.91
J(5.4)
J (m)
4.04
I (m)
4.46
L (m)
3.54
M (s)
2.33
K (m)
3.89
f1 (ppm)

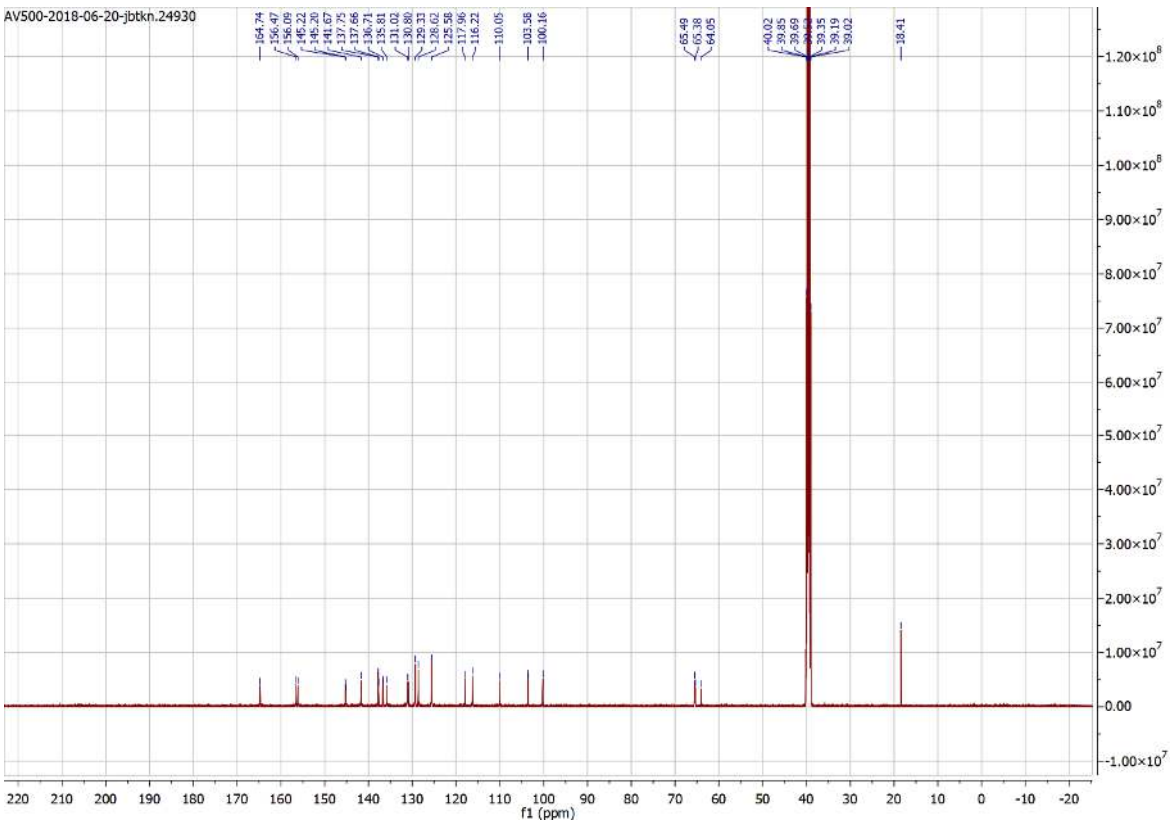
AV500-2018-06-20-jbtkn.24930
f1 (ppm)

Compound **70**

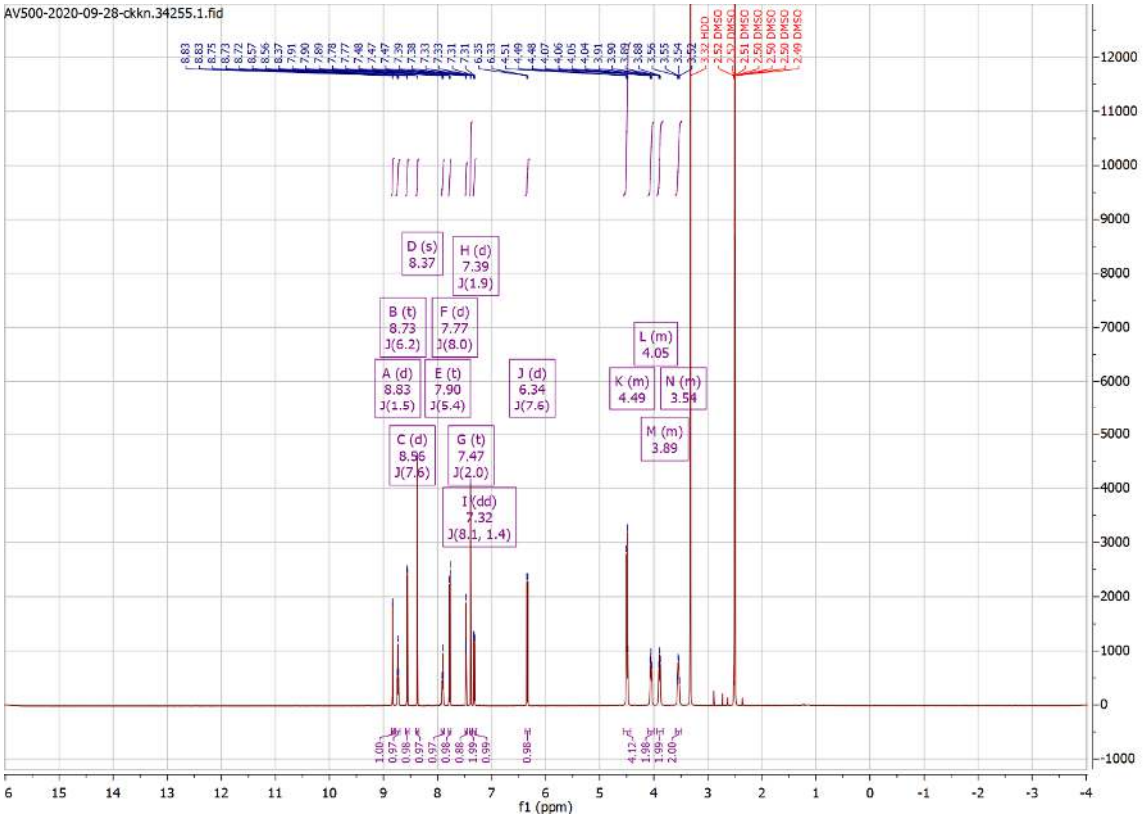
AV500-2020-09-28-ckkn.34255.1.fid
D (s) 8.37
H (d) 7.39 J(1.9)
B (t) 8.73 J(6.2)
F (d) 7.77 J(8.0)
L (m) 4.05
A (d) 8.83 J(1.5)
E (t) 7.90 J(5.4)
J (d) 6.34 J(7.6)
K (m) 4.49
N (m) 3.54
M (m) 3.89
C (d) 8.56 J(7.6)
G (t) 7.47 J(2.0)
I (dd) 7.32 J(8.1, 1.4)
f1 (ppm)

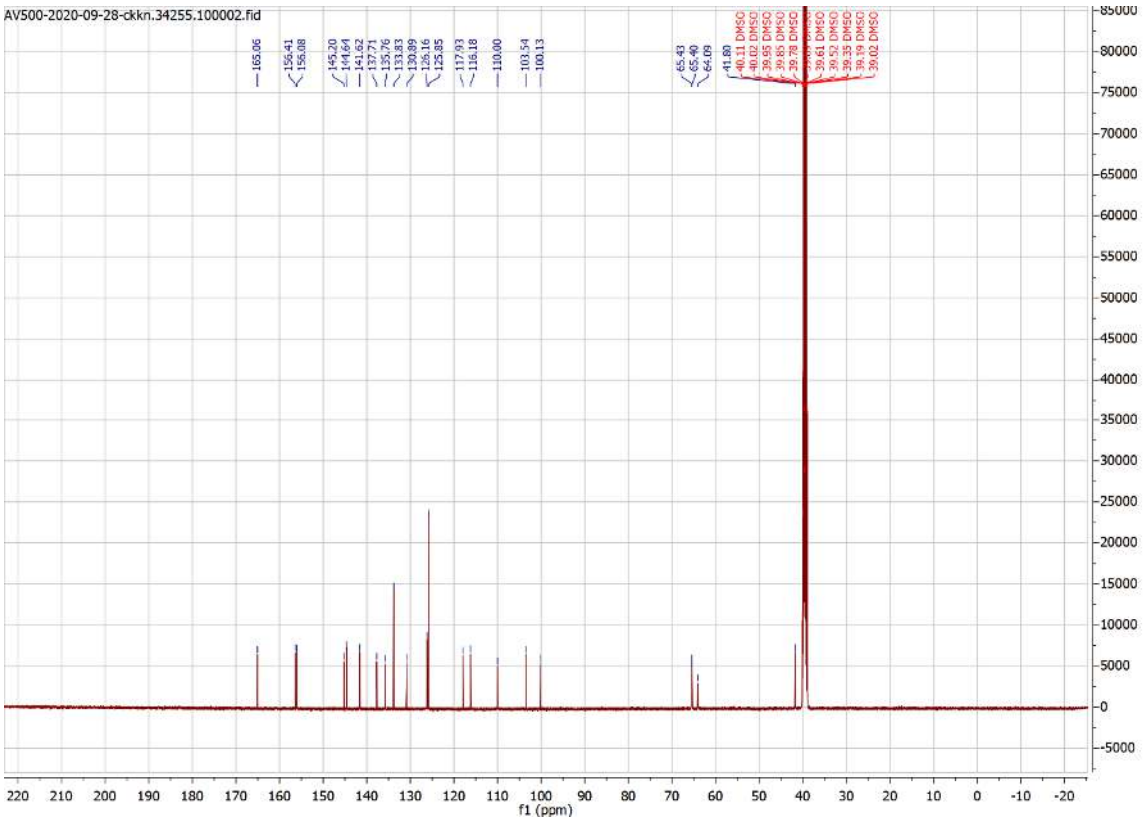
AV500-2020-09-28-ckkn.34255.100002.fid
f1 (ppm)

Compound **71**

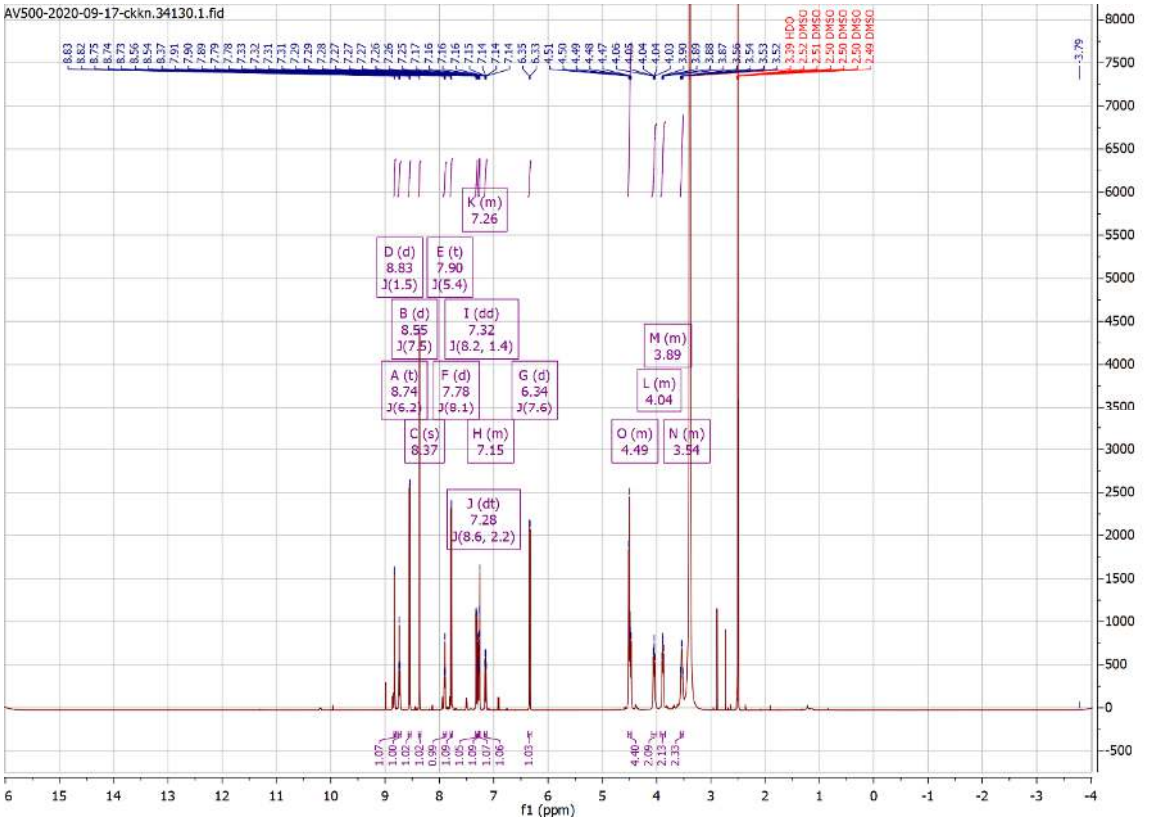
AV500-2020-09-17-ckkn.34130.1.fid
K (m) 7.26
D (d) 8.83 J(1.5)
E (t) 7.90 J(5.4)
B (d) 8.55 J(7.5)
I (dd) 7.32 J(8.2, 1.4)
M (m) 3.89
A (t) 8.74 J(6.2)
F (d) 7.78 J(8.1)
G (d) 6.34 J(7.6)
L (m) 4.04
C (s) 8.37
H (m) 7.15
O (m) 4.49
N (m) 3.54
J (dt) 7.28 J(8.6, 2.2)
f1 (ppm)

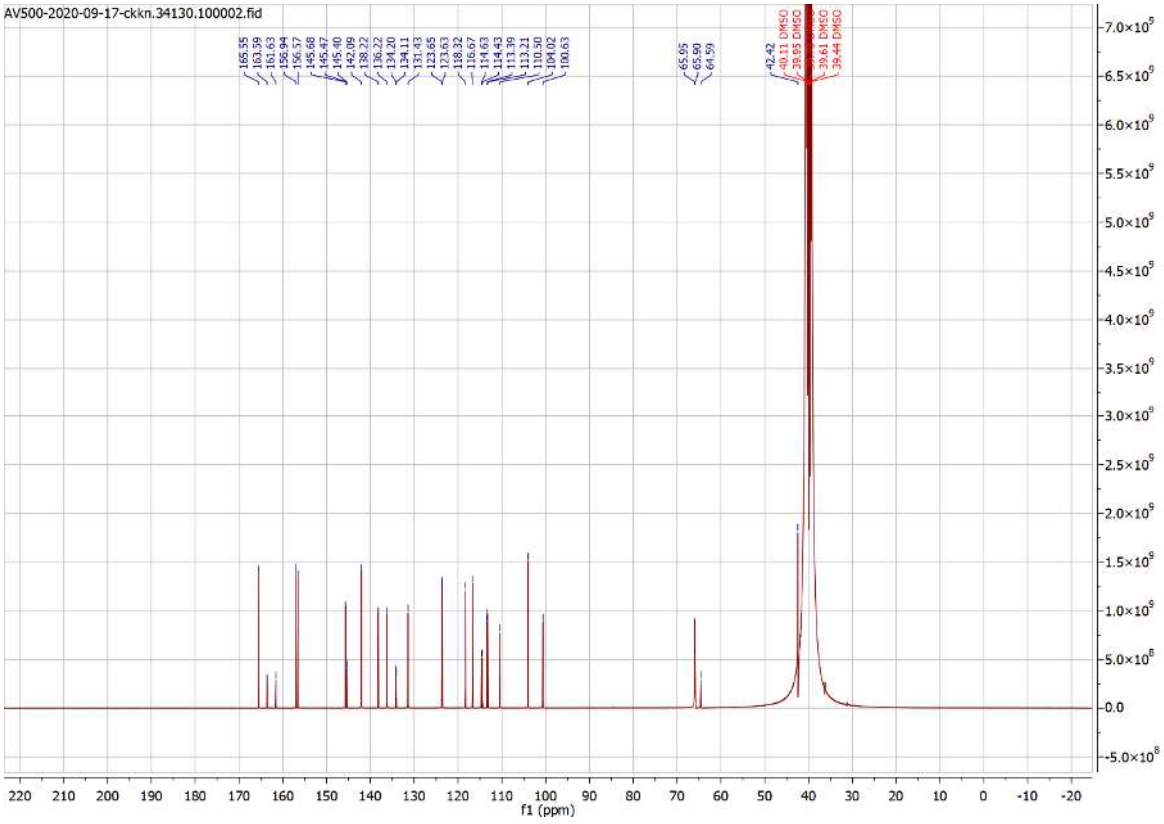
AV500-2020-09-17-ckkn.34130.100002.fid
f1 (ppm)

Compound **72**

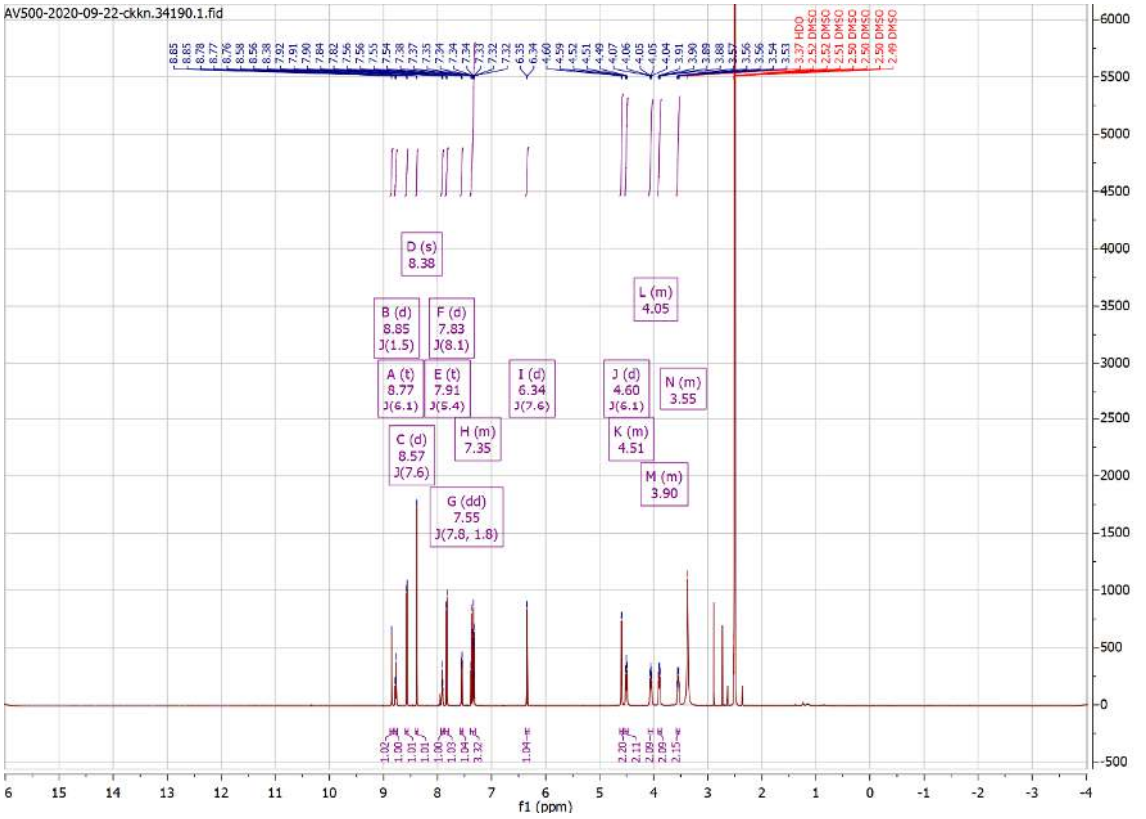
AV500-2020-09-22-ckkn.34190.1.fid
D (s)
8.38
B (d)
8.85
J(1.5)
F (d)
7.83
J(8.1)
L (m)
4.05
A (t)
8.77
J(6.1)
E (t)
7.91
J(5.4)
I (d)
6.34
J(7.6)
J (d)
4.60
J(6.1)
N (m)
3.55
C (d)
8.57
J(7.6)
H (m)
7.35
K (m)
4.51
M (m)
3.90
G (dd)
7.55
J(7.8, 1.8)
f1 (ppm)

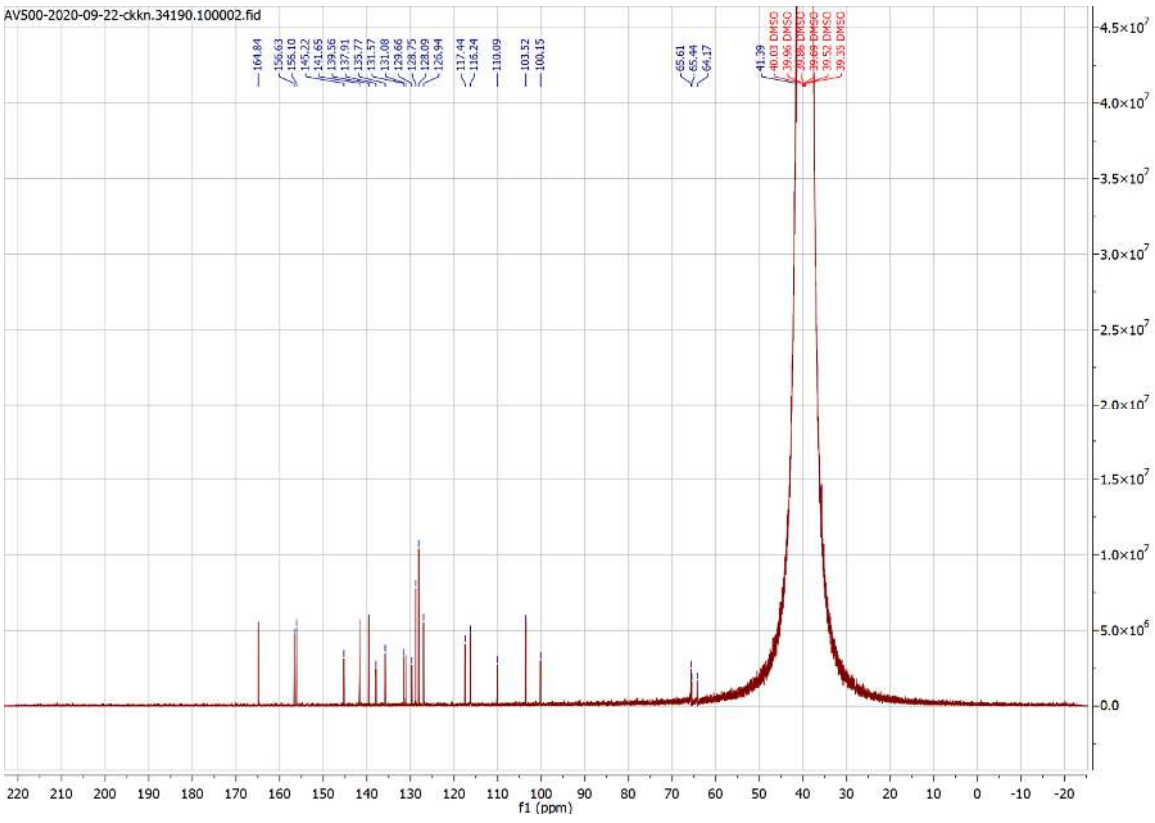
AV500-2020-09-22-ckkn.34190.100002.fid
f1 (ppm)

Compound **73**

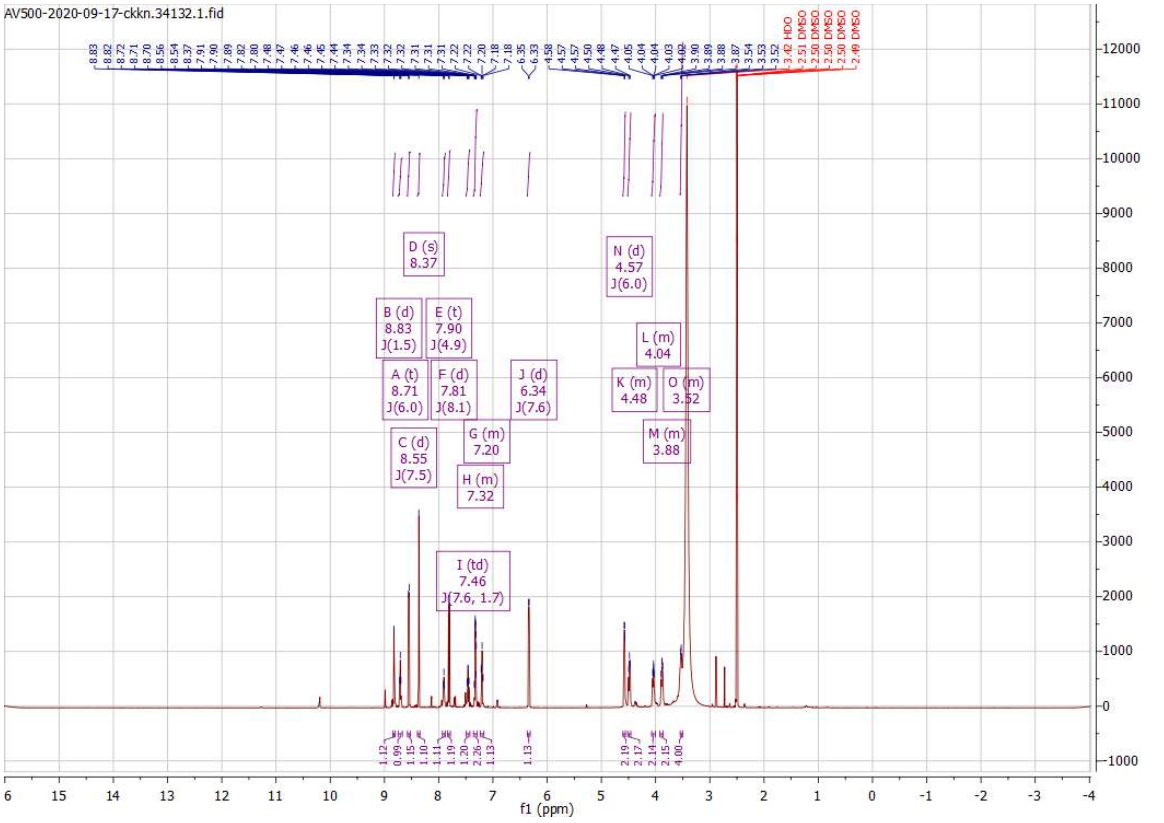
AV500-2020-09-17-ckkn.34132.1.fid
D (s)
8.37
N (d)
4.57
J(6.0)
B (d)
8.83
J(1.5)
E (t)
7.90
J(4.9)
L (m)
4.04
A (t)
8.71
J(6.0)
F (d)
7.81
J(8.1)
J (d)
6.34
J(7.6)
K (m)
4.48
O (m)
3.52
C (d)
8.55
J(7.5)
G (m)
7.20
M (m)
3.88
H (m)
7.32
I (td)
7.46
J(7.6, 1.7)
f1 (ppm)

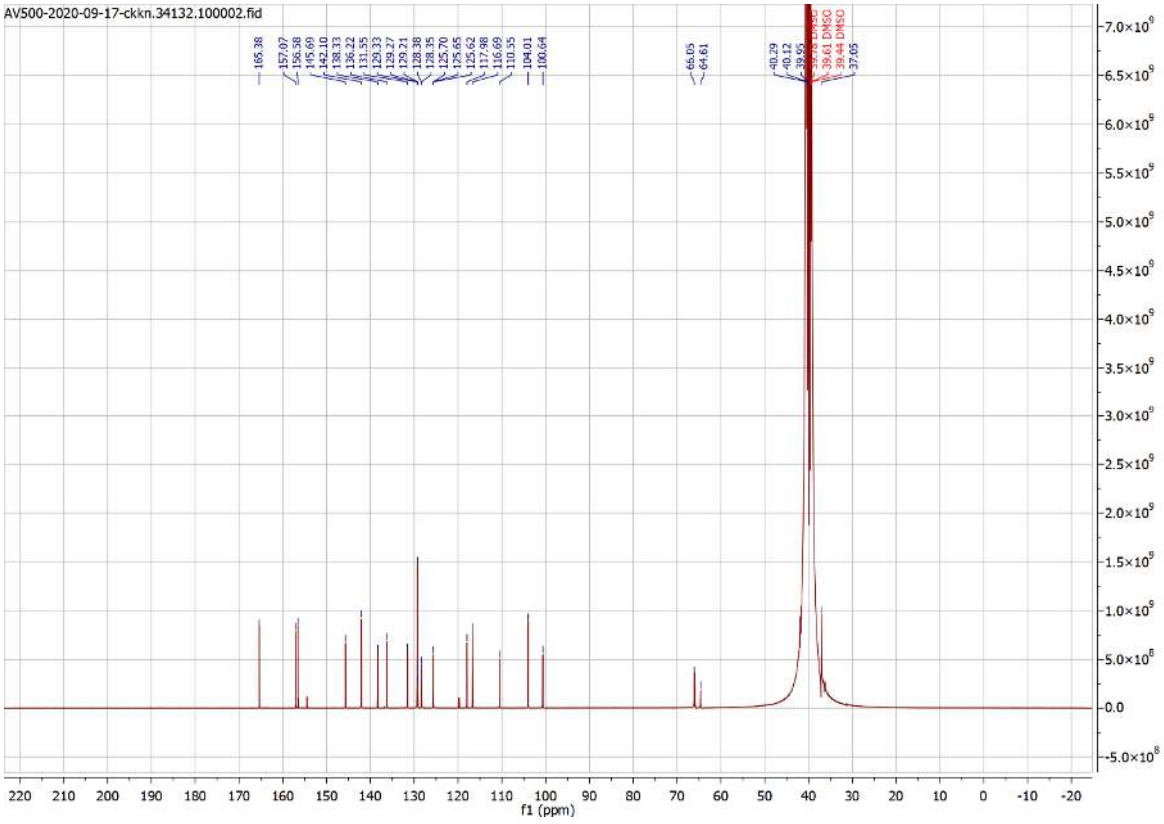
AV500-2020-09-17-ckkn.34132.100002.fid
f1 (ppm)

Compound **85**

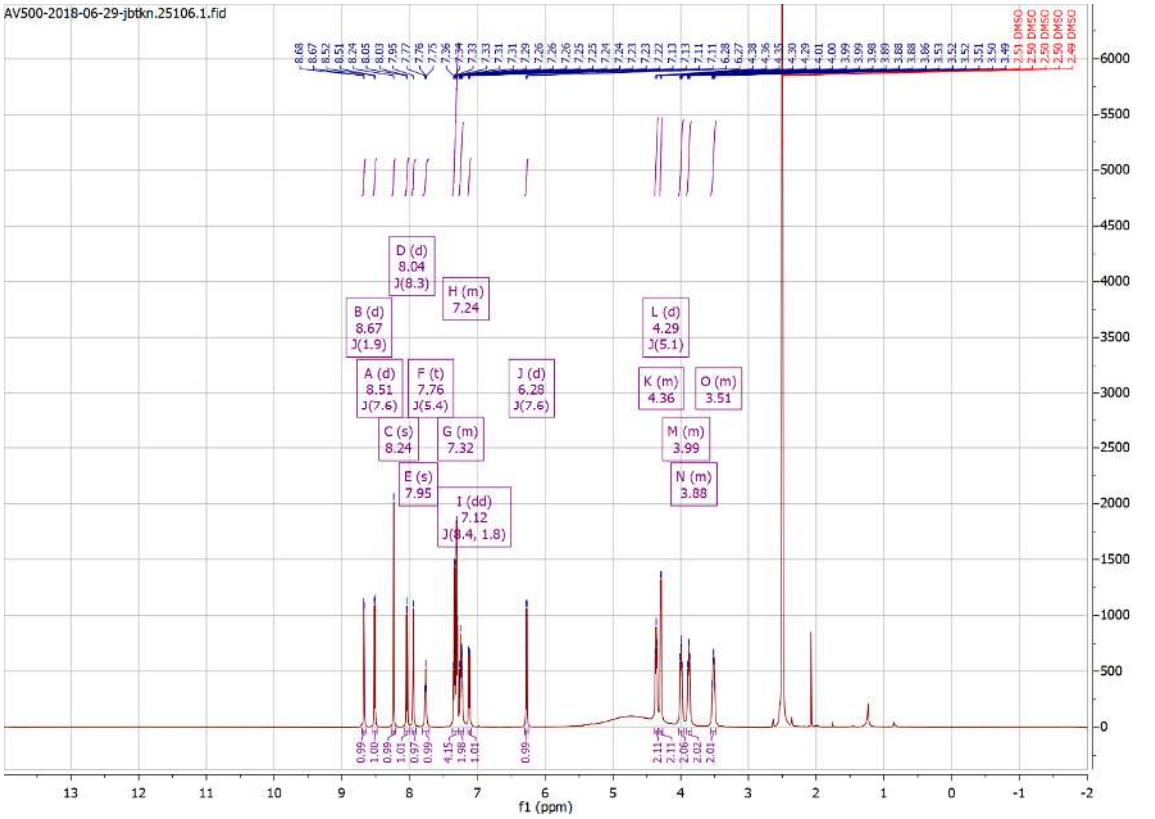
AV500-2018-06-29-jbtkn.25106.1.fid
D (d) 8.04 J(8.3)
H (m) 7.24
B (d) 8.67 J(1.9)
L (d) 4.29 J(5.1)
A (d) 8.51 J(7.6)
F (t) 7.76 J(5.4)
J (d) 6.28 J(7.6)
K (m) 4.36
O (m) 3.51
C (s) 8.24
G (m) 7.32
M (m) 3.99
E (s) 7.95
N (m) 3.88
I (dd) 7.12 J(8.4, 1.8)
f1 (ppm)

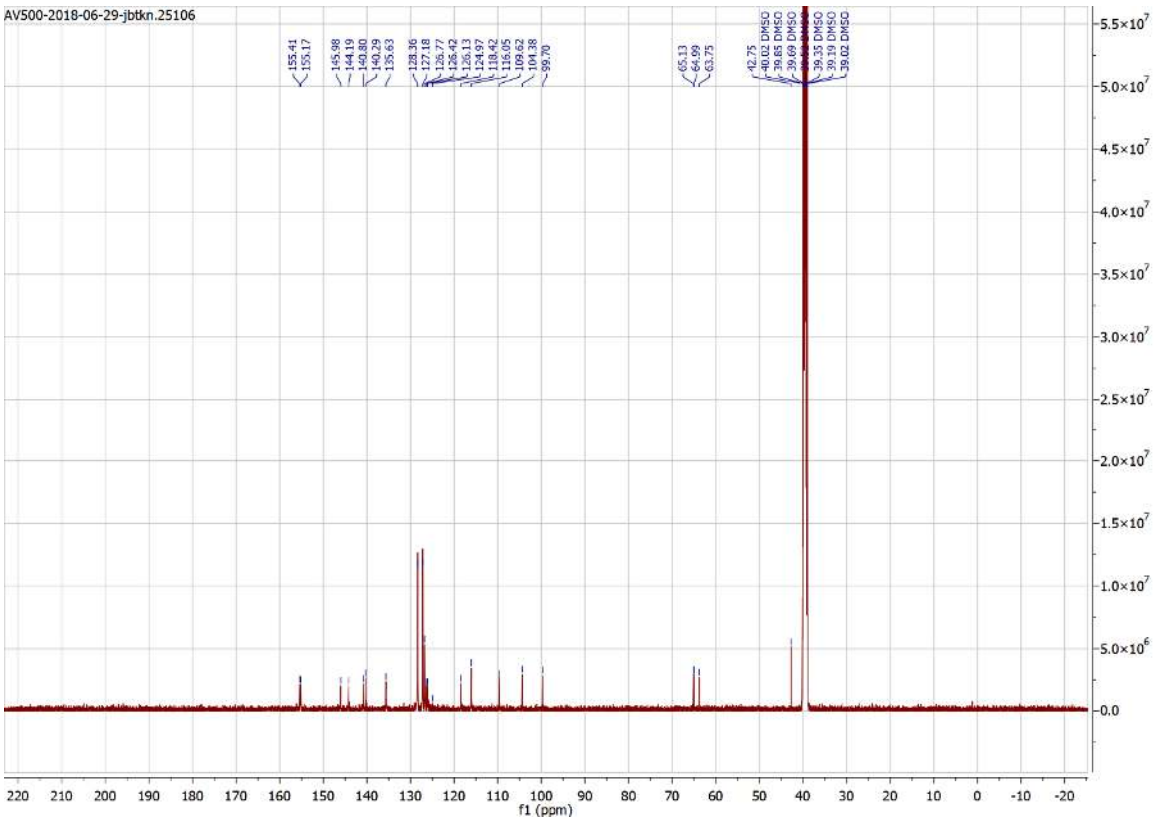
AV500-2018-06-29-jbtkn.25106
f1 (ppm)

Compound **86**

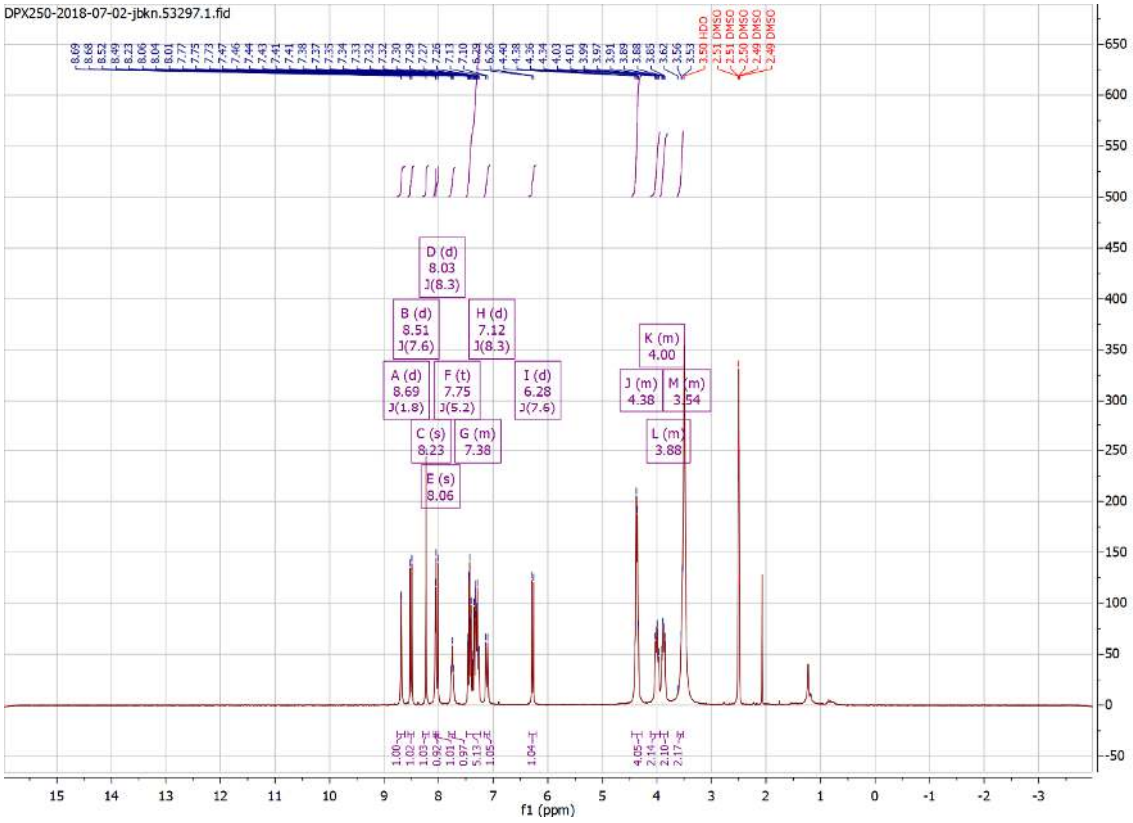
DPX250-2018-07-02-jbkn.53297.1.fid
D (d)
8.03
J(8.3)
B (d)
8.51
J(7.6)
H (d)
7.12
J(8.3)
K (m)
4.00
A (d)
8.69
J(1.8)
F (t)
7.75
J(5.2)
I (d)
6.28
J(7.6)
J (m)
4.38
M (m)
3.54
C (s)
8.23
G (m)
7.38
L (m)
3.88
E (s)
8.06
f1 (ppm)

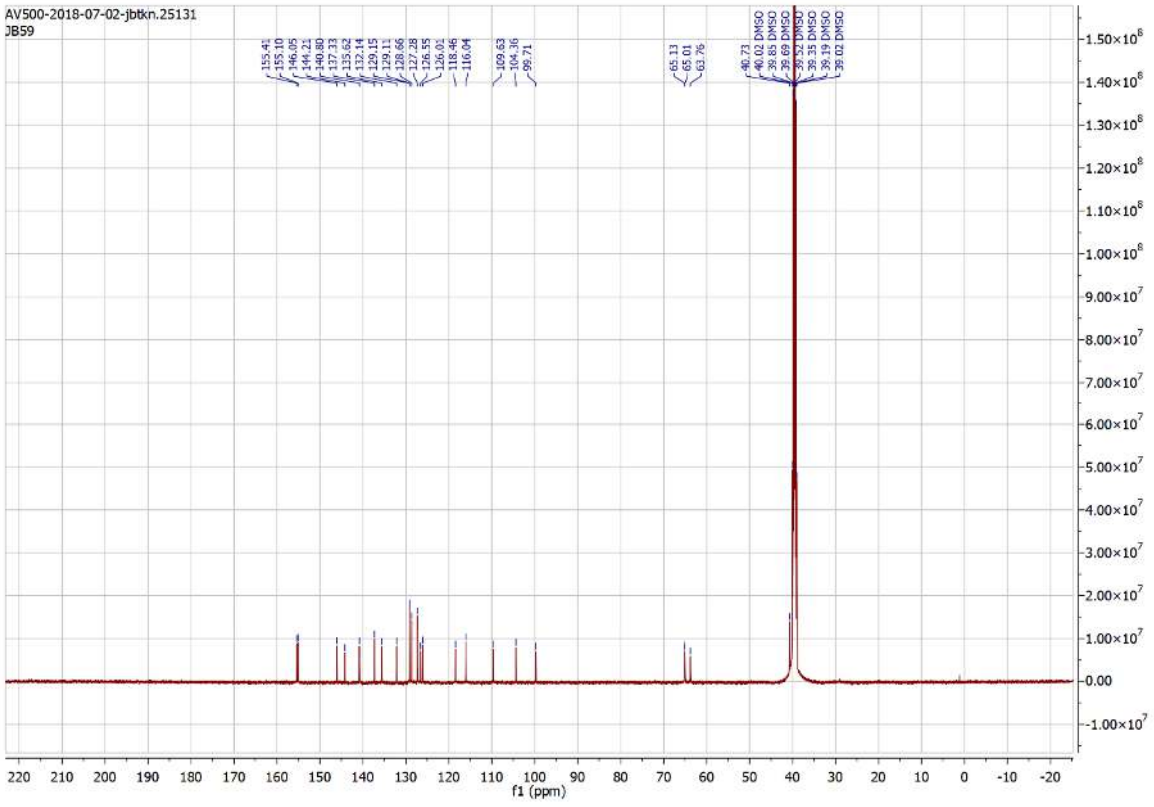
AV500-2018-07-02-jbtkn.25131
JB59
f1 (ppm)

Compound **87**

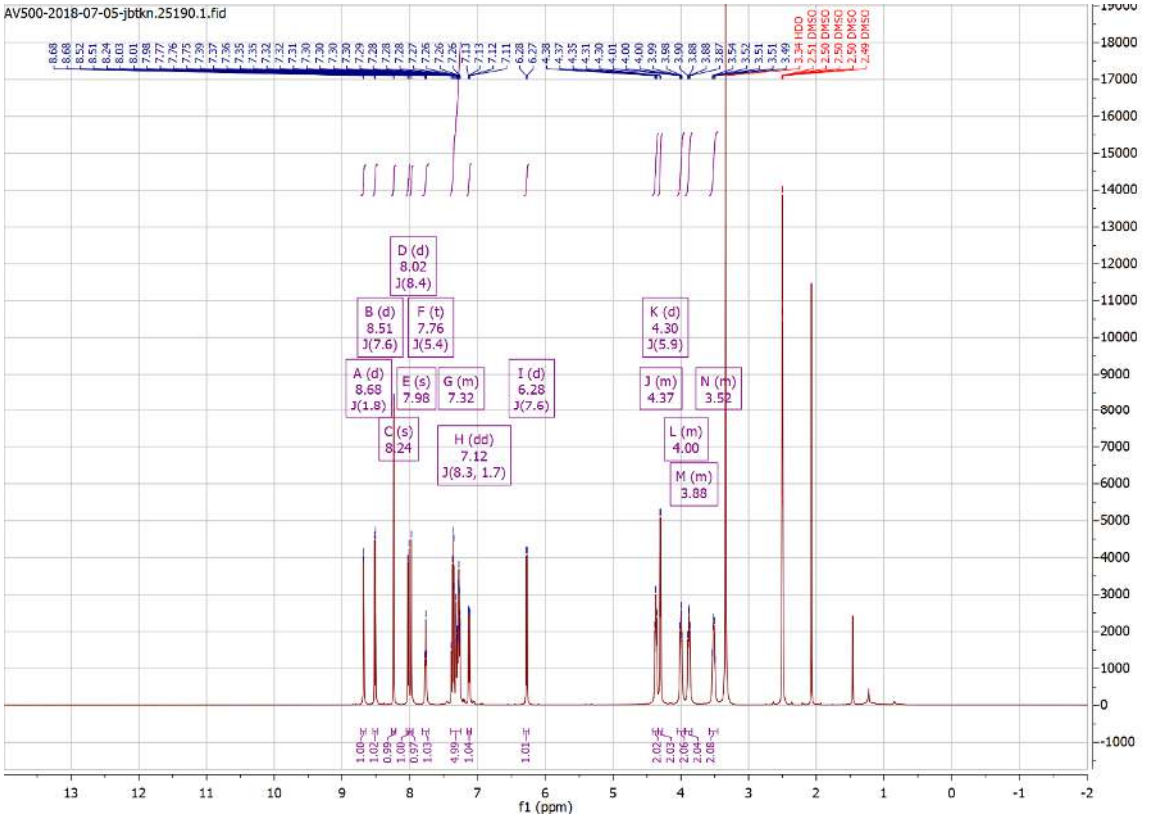
AV500-2018-07-05-jbtkn.25190.1.fid
D (d)
8.02
J(8.4)
B (d)
8.51
J(7.6)
F (t)
7.76
J(5.4)
K (d)
4.30
J(5.9)
A (d)
8.68
J(1.8)
E (s)
7.98
G (m)
7.32
I (d)
6.28
J(7.6)
J (m)
4.37
N (m)
3.52
C (s)
8.24
H (dd)
7.12
J(8.3, 1.7)
L (m)
4.00
M (m)
3.88
f1 (ppm)

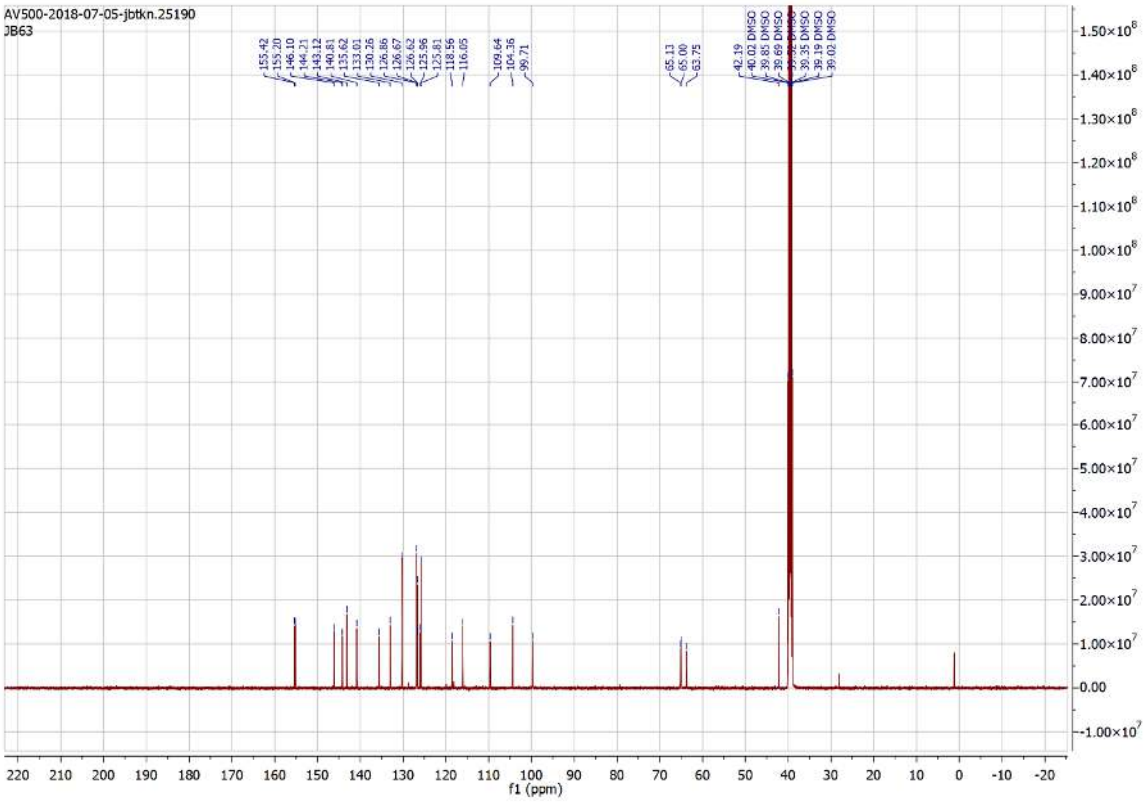
AV500-2018-07-05-jbtkn.25190
JB63
f1 (ppm)

Compound **88**

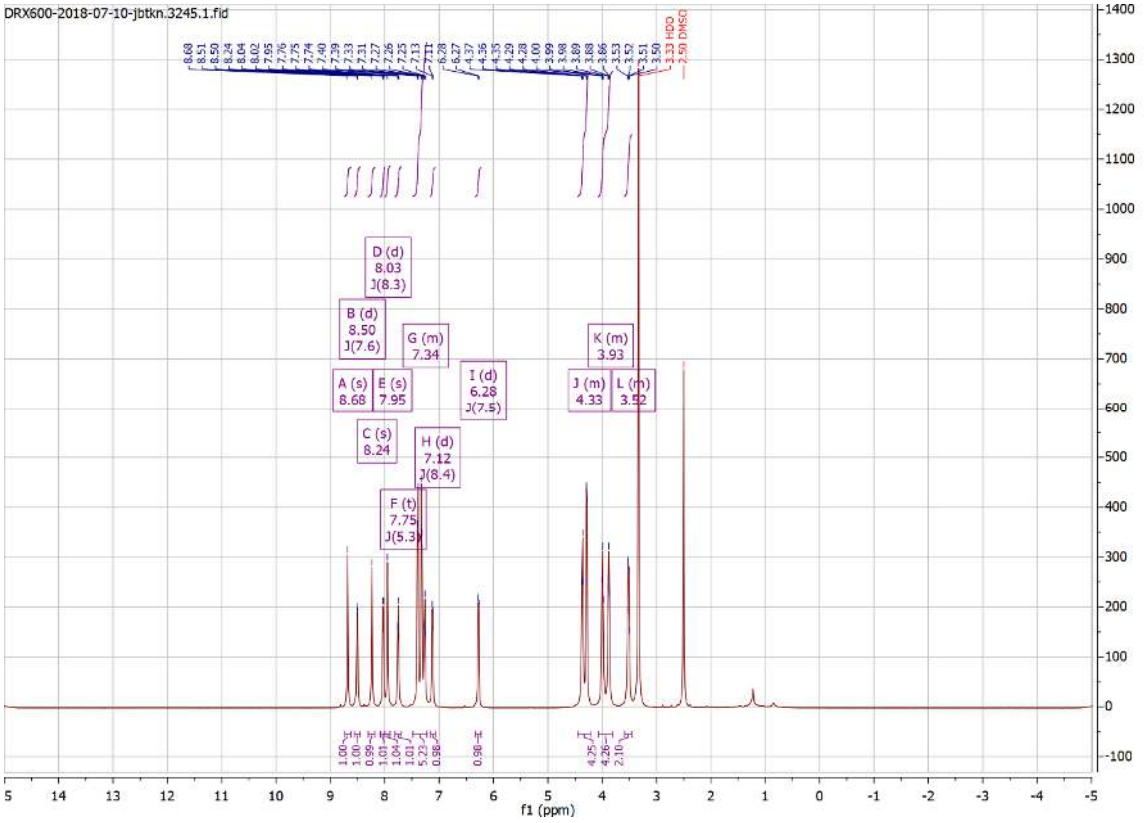
DRX600-2018-07-10-jbtkn.3245.1.fid
D (d)
8.03
J(8.3)
B (d)
8.50
J(7.6)
G (m)
7.34
K (m)
3.93
A (s)
8.68
E (s)
7.95
I (d)
6.28
J(7.5)
J (m)
4.33
L (m)
3.52
C (s)
8.24
H (d)
7.12
J(8.4)
F (t)
7.75
f1 (ppm)

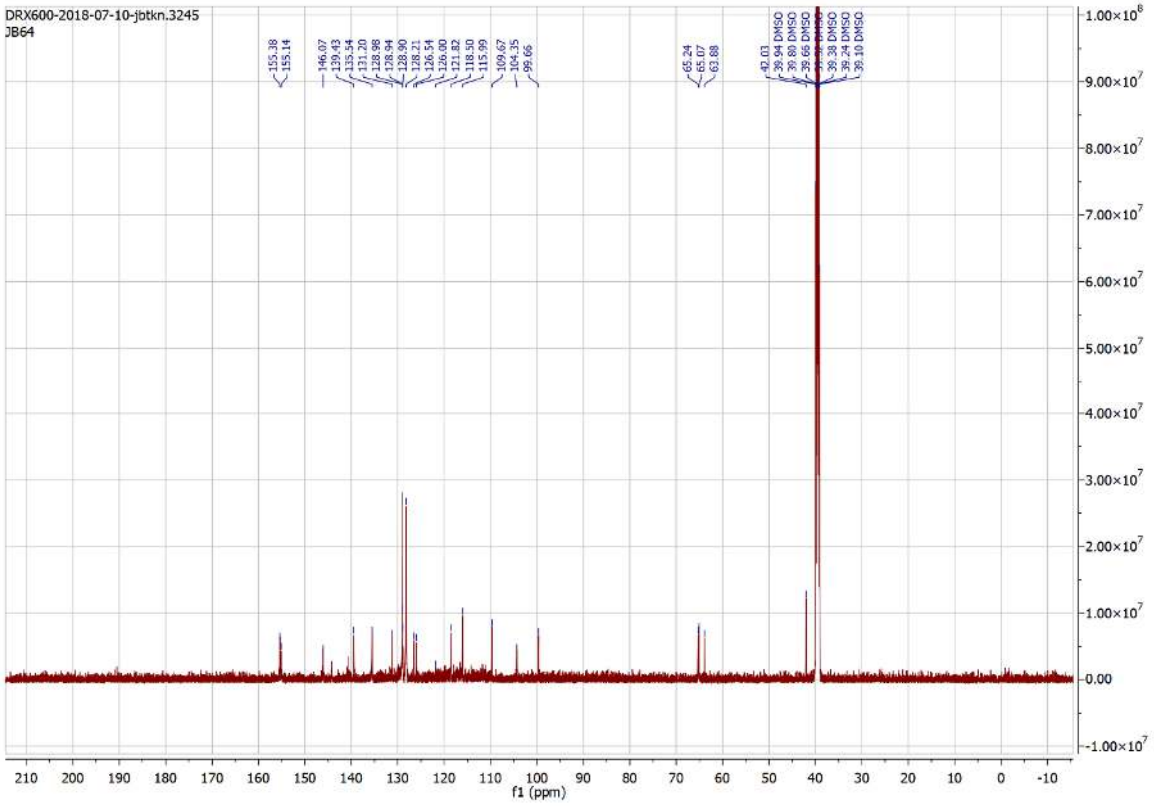
DRX600-2018-07-10-jbtkn.3245
JB64
f1 (ppm)

Compound **89**

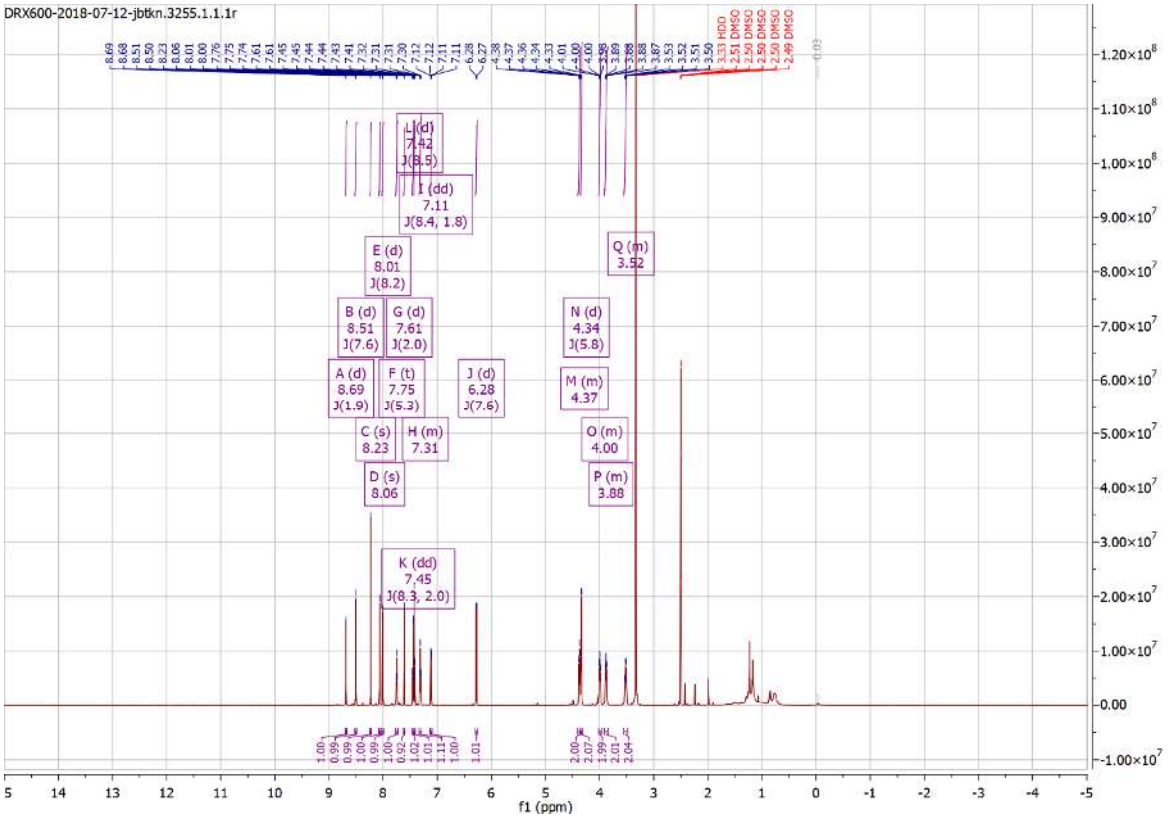
DRX600-2018-07-12-jbtkn.3255.1.1.1r
L (dd)
7.42
J(8.5)
I (dd)
7.11
J(8.4, 1.8)
E (d)
8.01
J(8.2)
Q (m)
3.52
B (d)
8.51
J(7.6)
G (d)
7.61
J(2.0)
N (d)
4.34
J(5.8)
A (d)
8.69
J(1.9)
F (t)
7.75
J(5.3)
J (d)
6.28
J(7.6)
M (m)
4.37
C (s)
8.23
H (m)
7.31
O (m)
4.00
D (s)
8.06
P (m)
3.88
K (dd)
7.45
J(8.3, 2.0)
f1 (ppm)

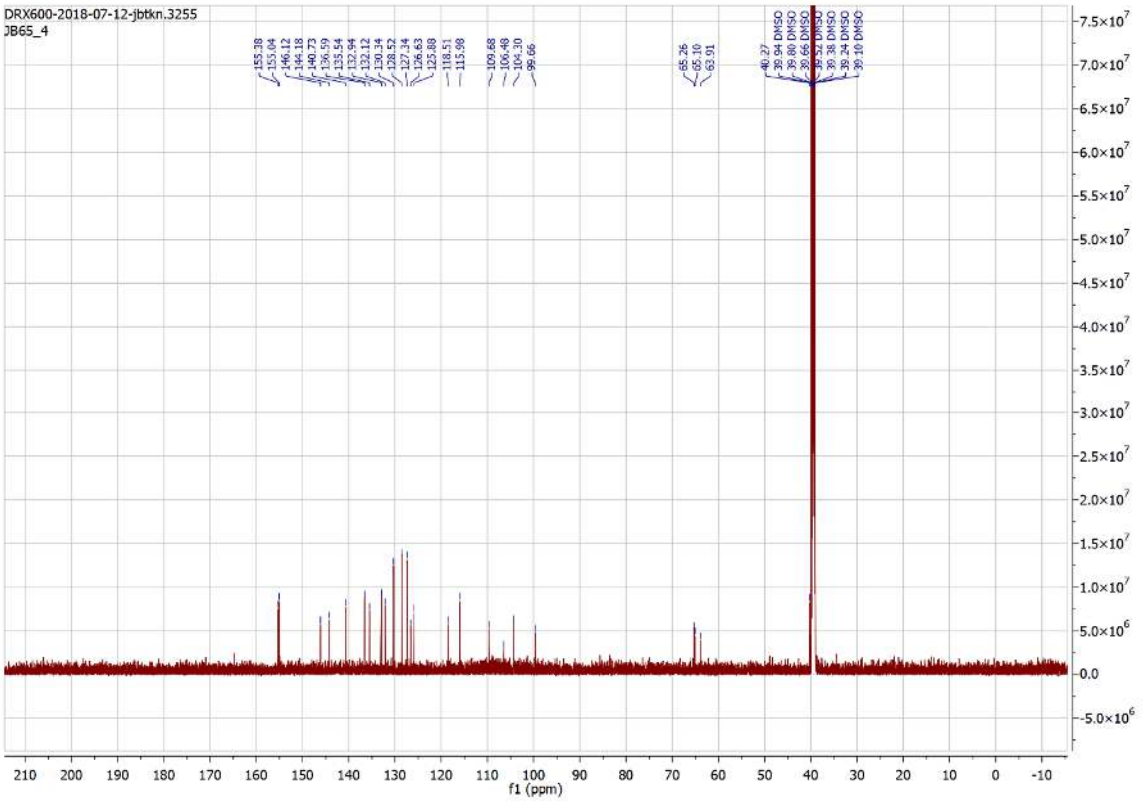
DRX600-2018-07-12-jbtkn.3255
JB65_4
f1 (ppm)

Compound **90**

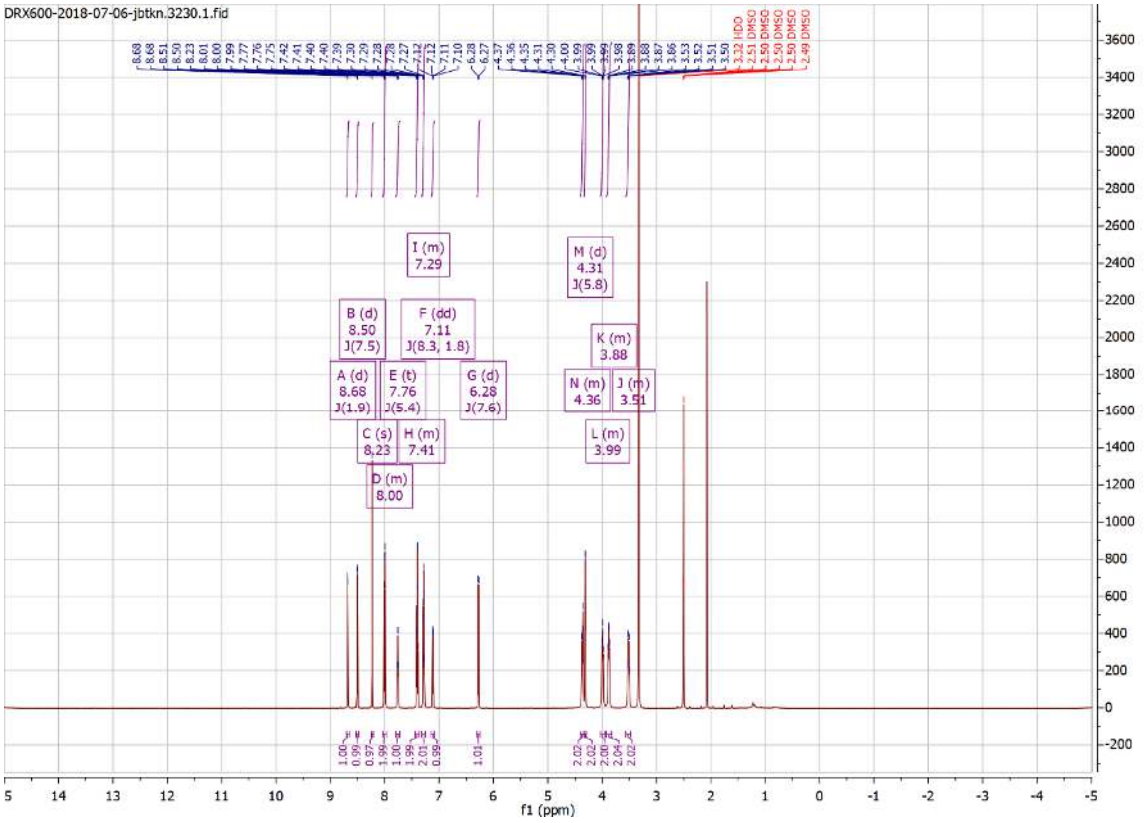
DRX600-2018-07-06-jbtkn.3230.1.fid
I (m)
7.29
M (d)
4.31
J(5.8)
B (d)
8.50
J(7.5)
F (dd)
7.11
J(8.3, 1.8)
K (m)
3.88
A (d)
8.68
J(1.9)
E (t)
7.76
J(5.4)
G (d)
6.28
J(7.6)
N (m)
4.36
J (m)
3.51
C (s)
8.23
H (m)
7.41
L (m)
3.99
D (m)
8.00
f1 (ppm)

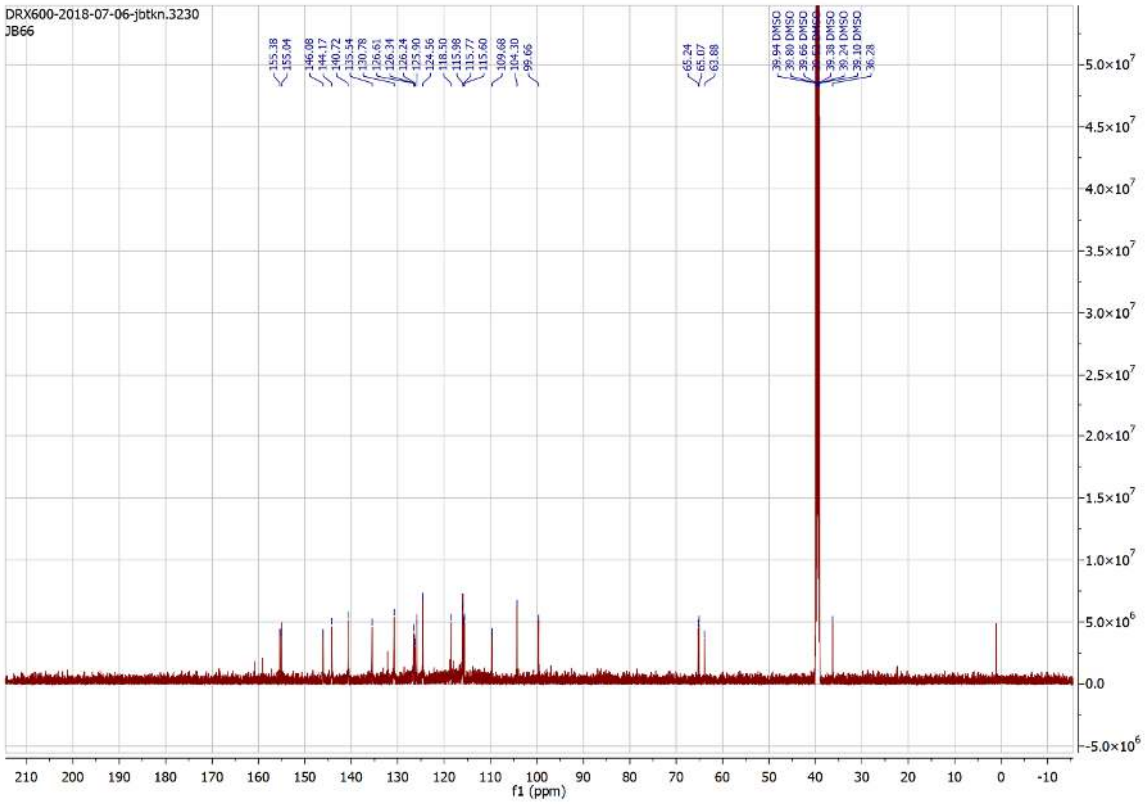
DRX600-2018-07-06-jbtkn.3230
JB66
f1 (ppm)

Compound **91**

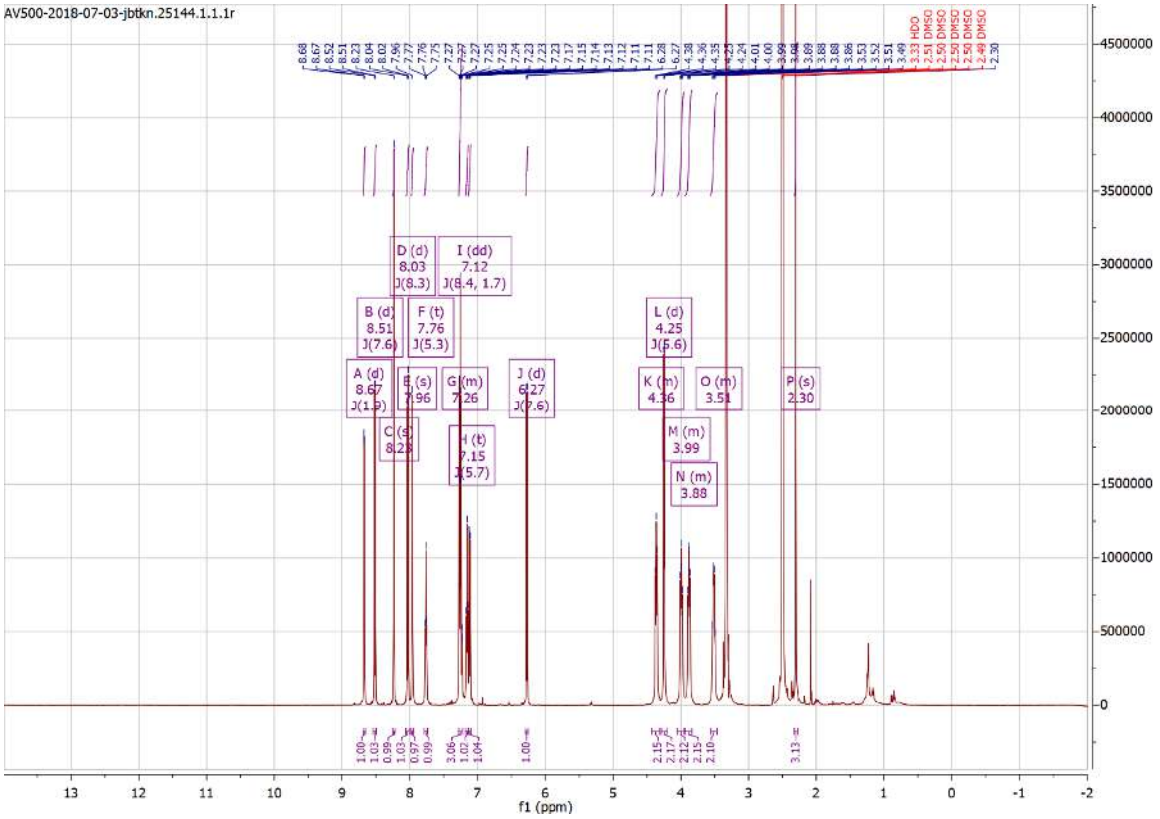
AV500-2018-07-03-jbtkn.25144.1.1.1r
f1 (ppm)

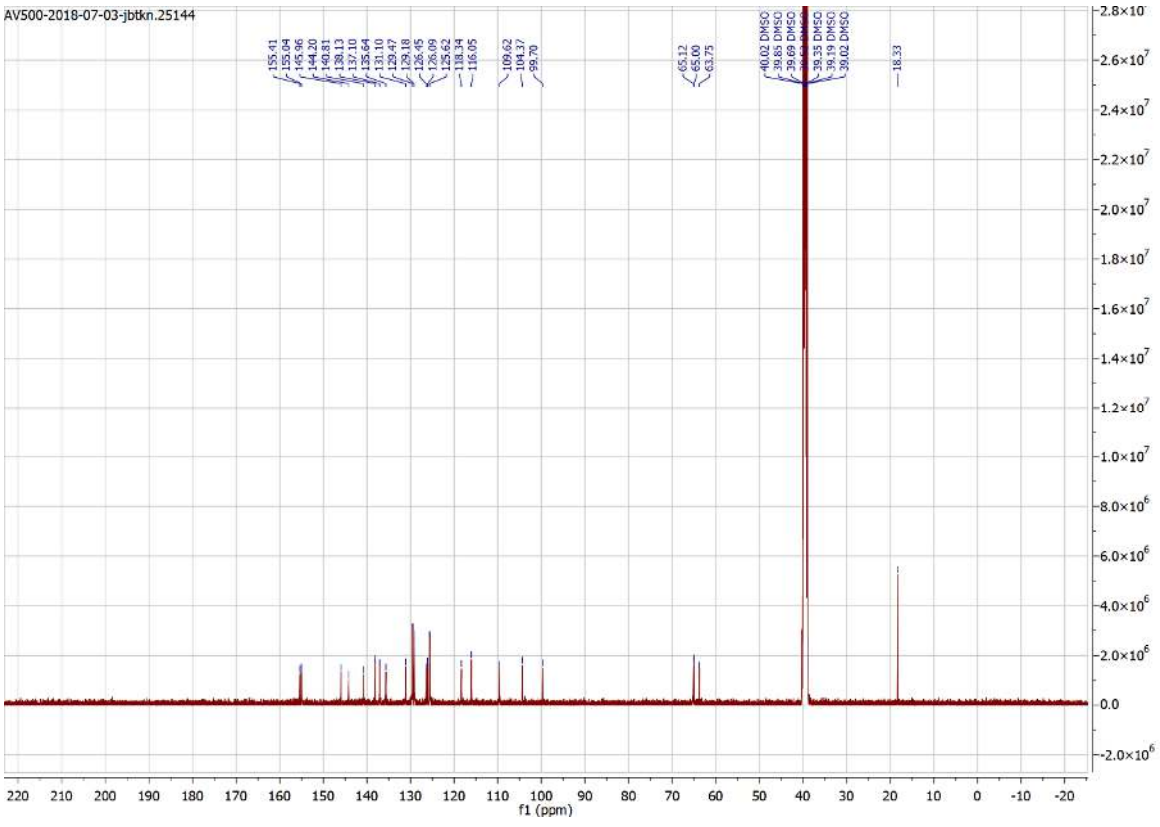
AV500-2018-07-03-jbtkn.25144
f1 (ppm)

Compound **92**

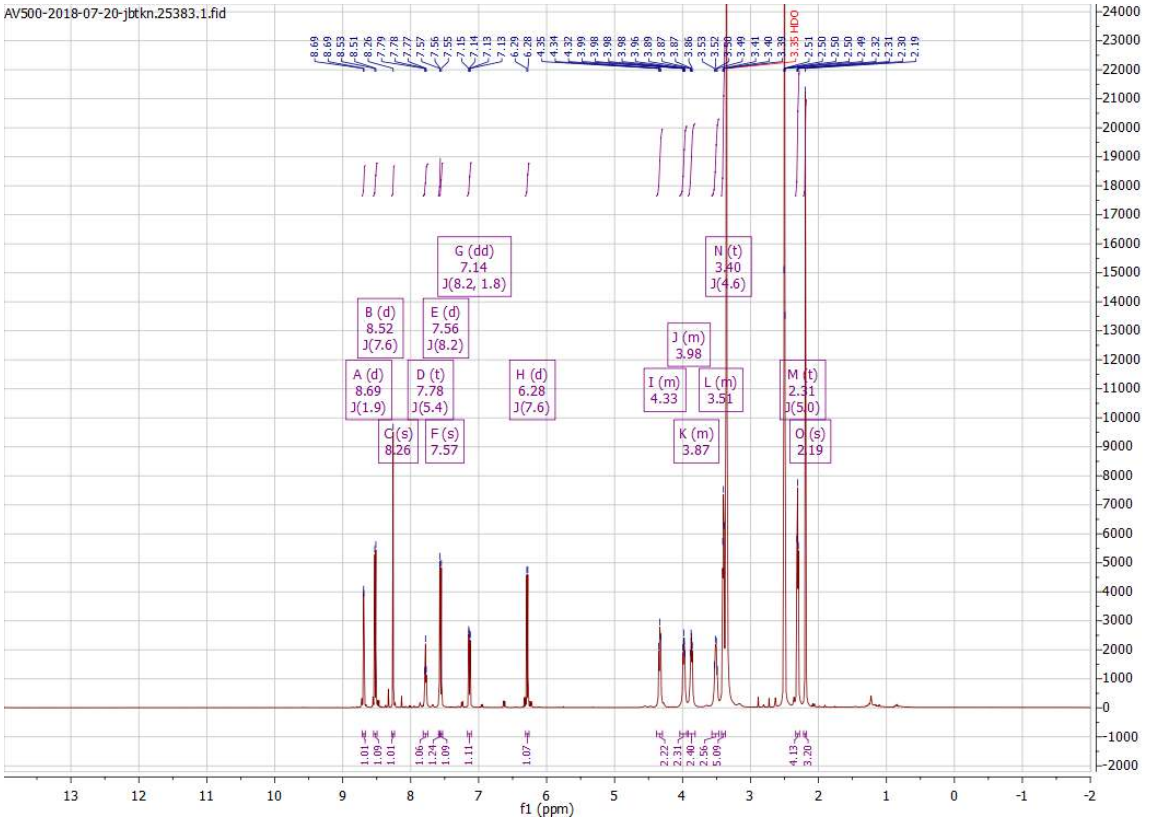
AV500-2018-07-20-jbtkn.25383.1.fid
G (dd)
7.14
J(8.2, 1.8)
N (t)
3.40
J(4.6)
B (d)
8.52
J(7.6)
E (d)
7.56
J(8.2)
J (m)
3.98
A (d)
8.69
J(1.9)
D (t)
7.78
J(5.4)
H (d)
6.28
J(7.6)
I (m)
4.33
L (m)
3.51
M (t)
2.31
J(5.0)
C (s)
8.26
F (s)
7.57
K (m)
3.87
O (s)
2.19
f1 (ppm)

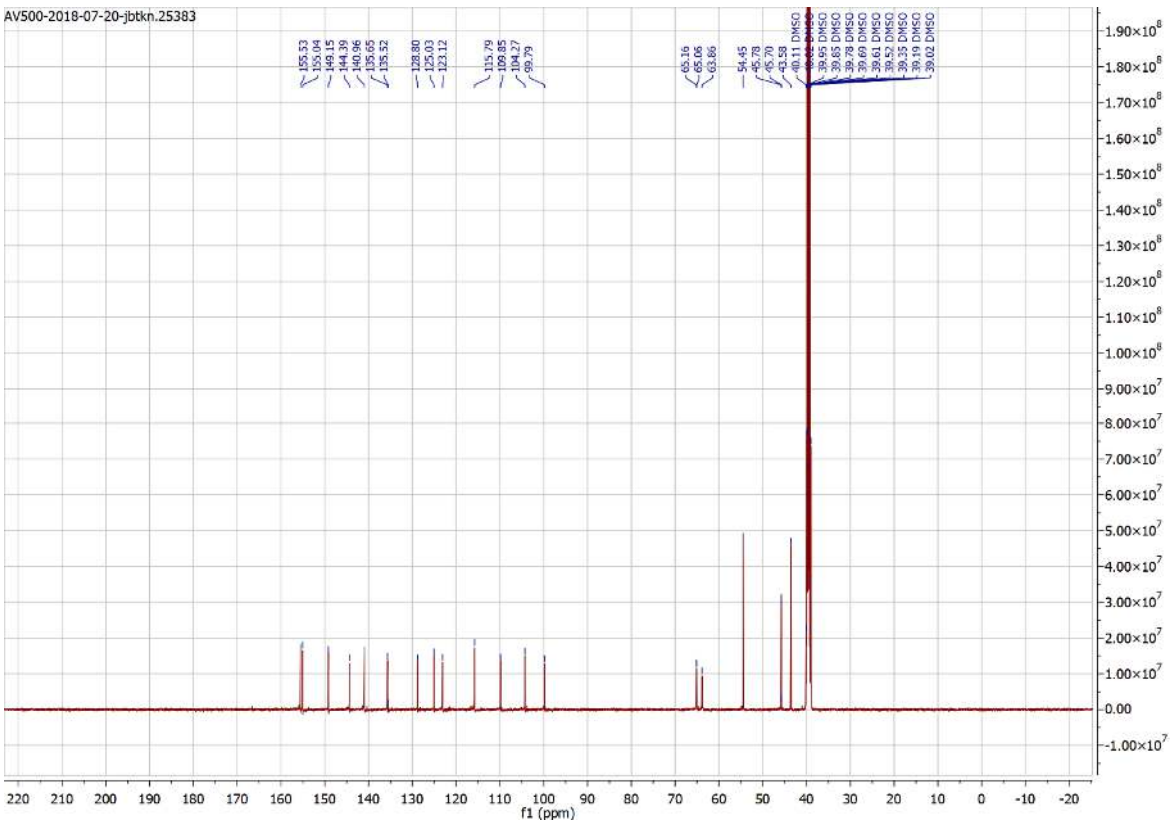
AV500-2018-07-20-jbtkn.25383
f1 (ppm)

Compound **107**

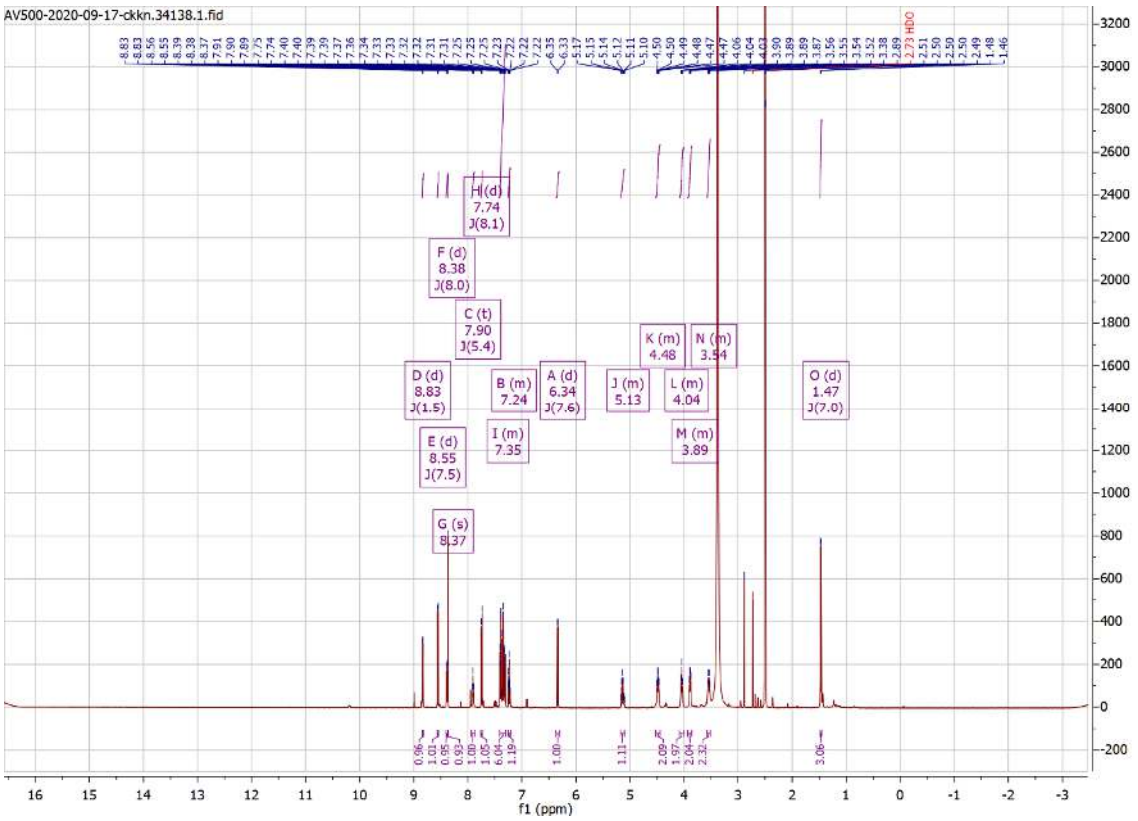

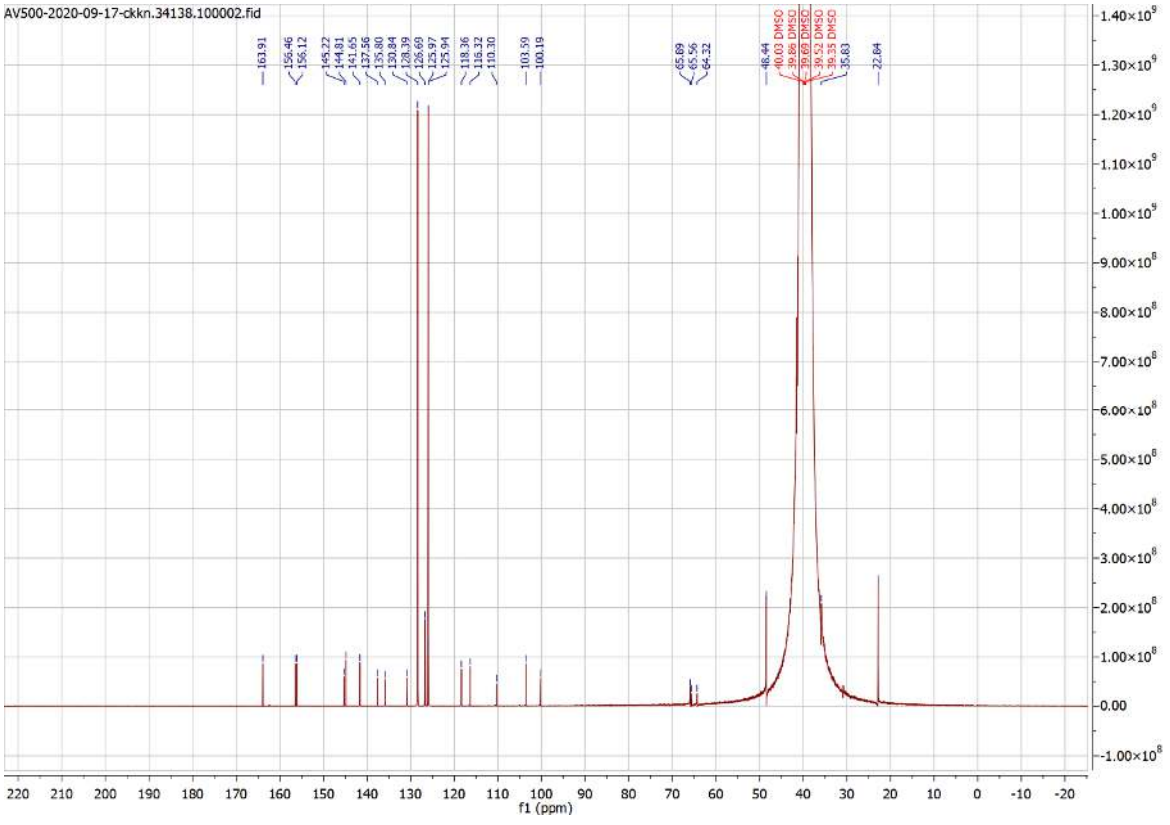

Compound **108**

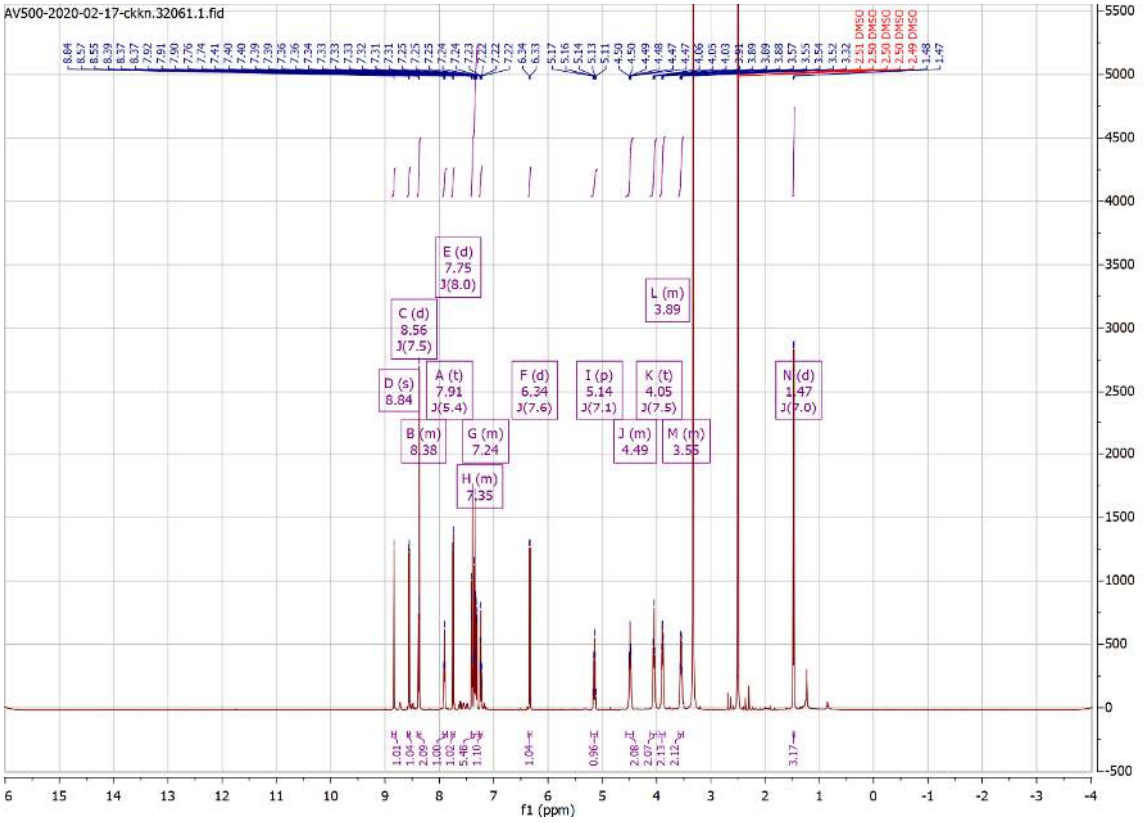

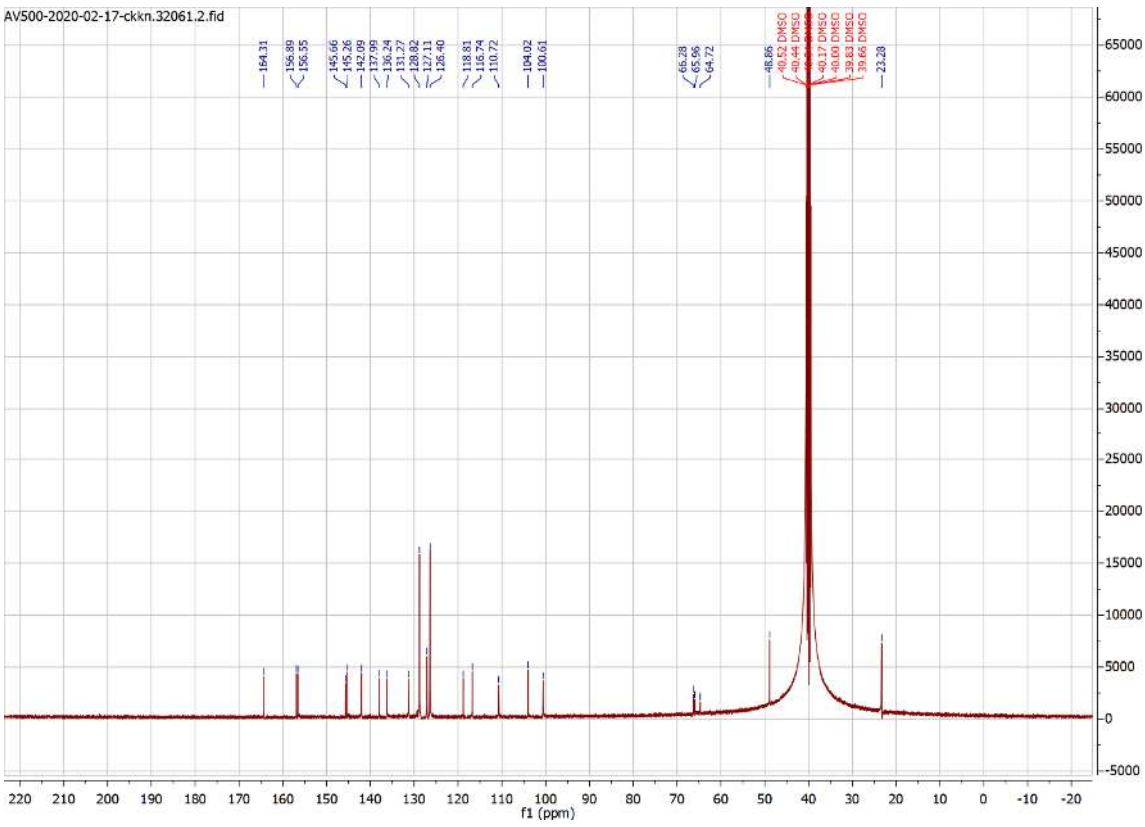

Compound **109**

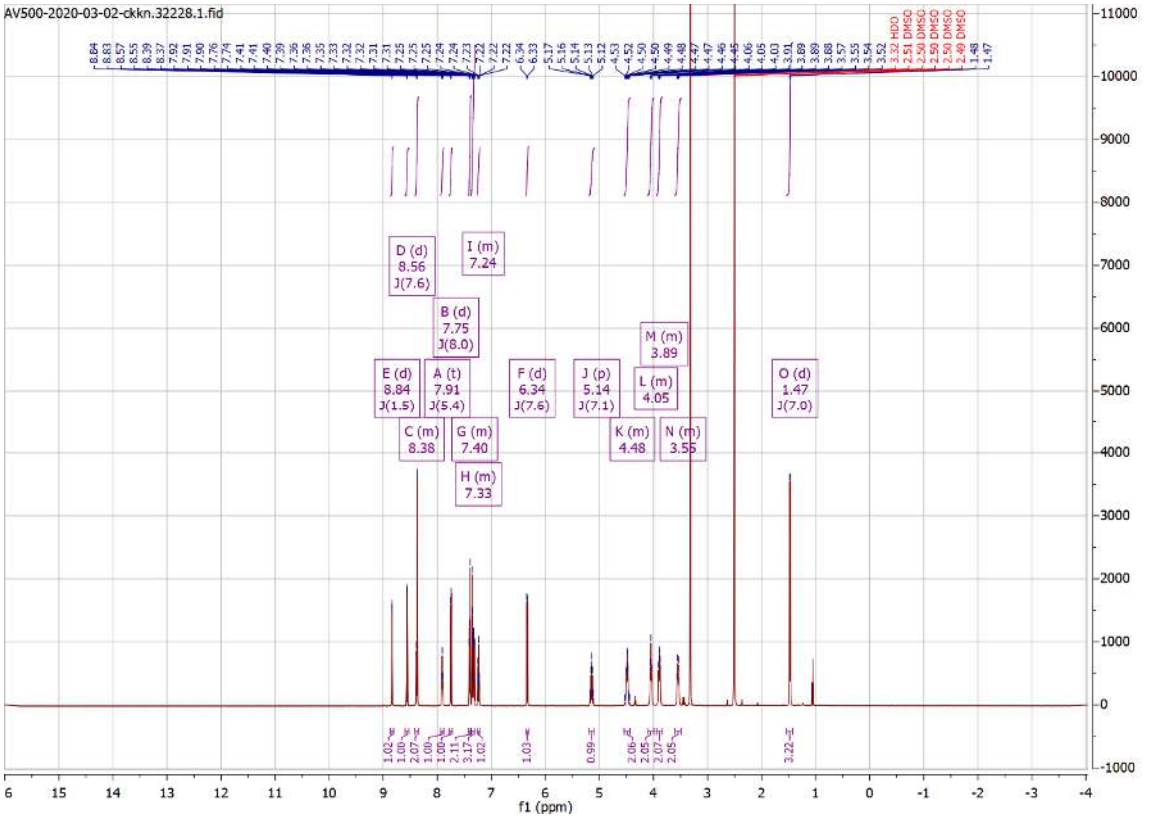

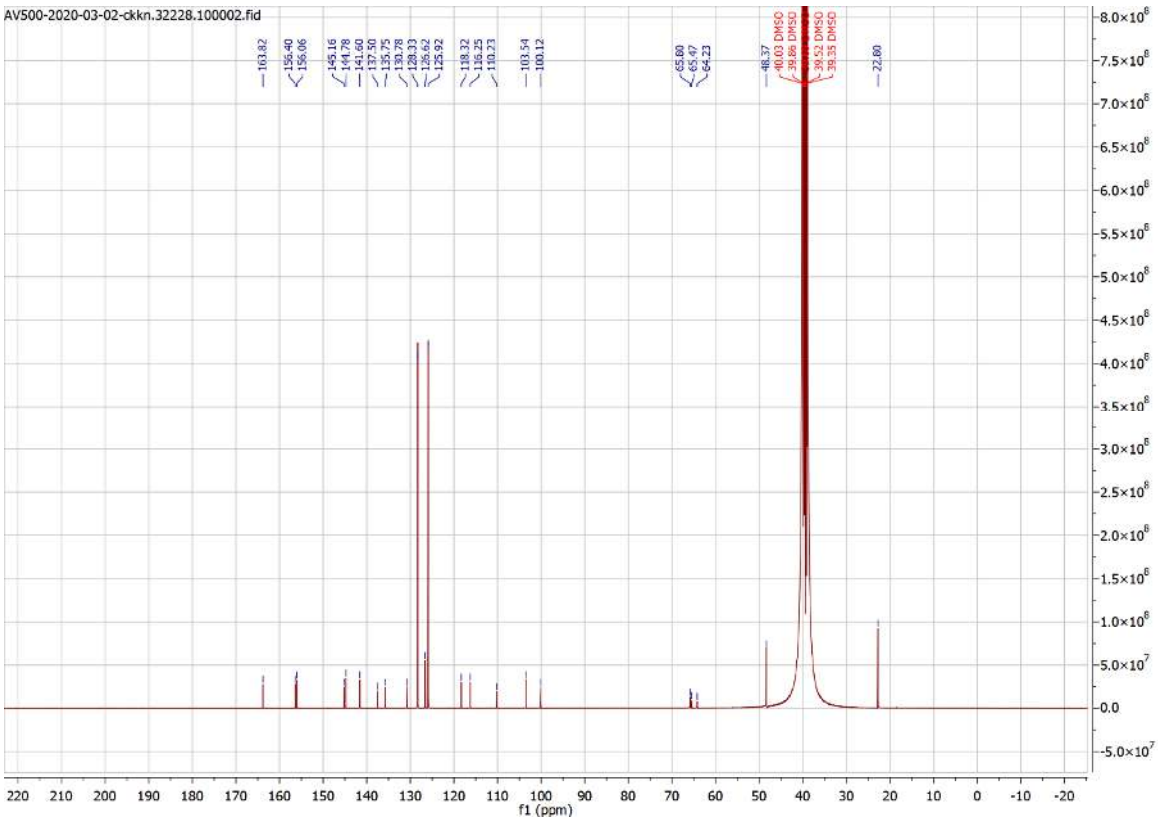

Compound **110**

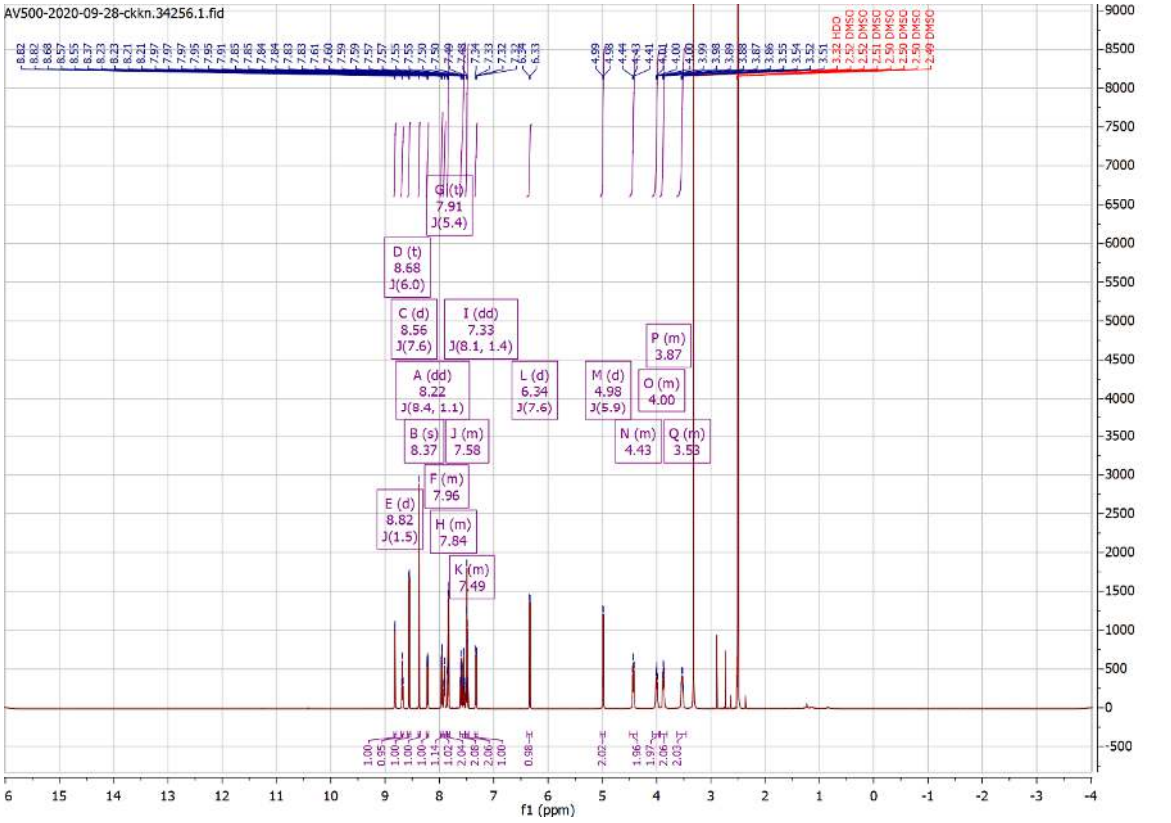

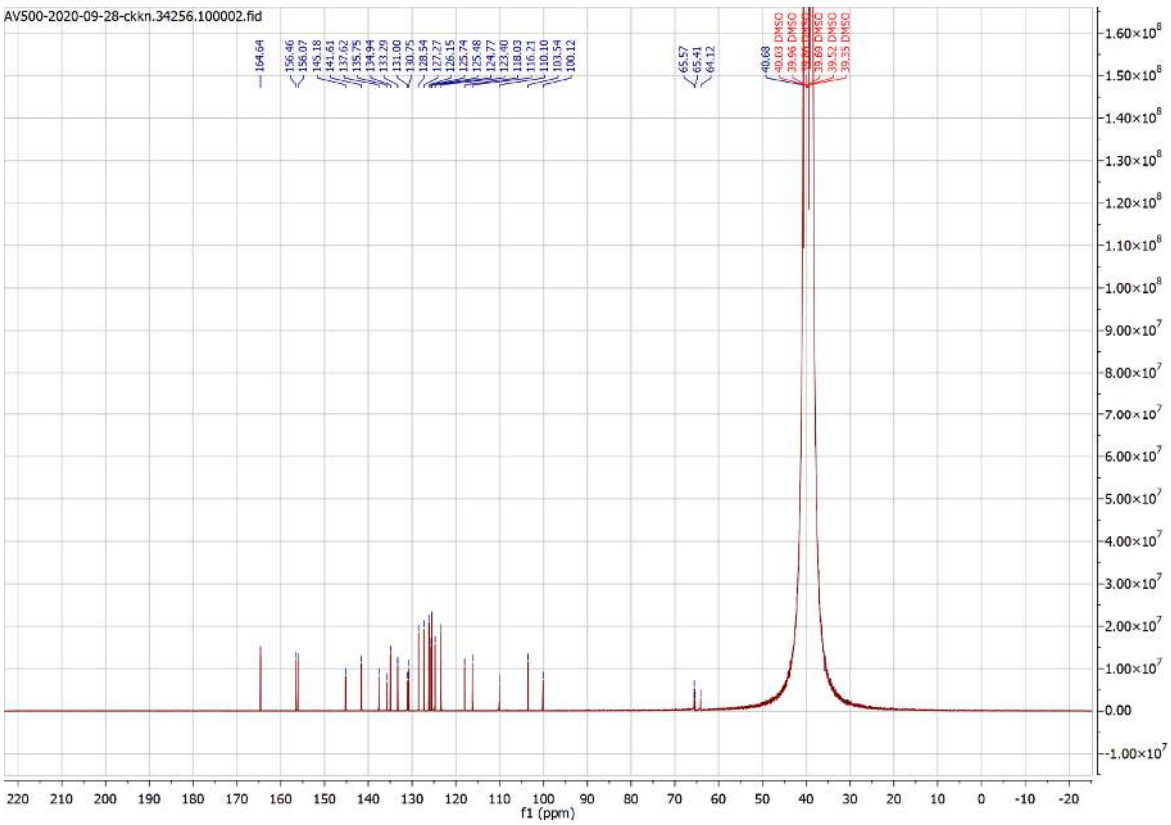

Compound **111**

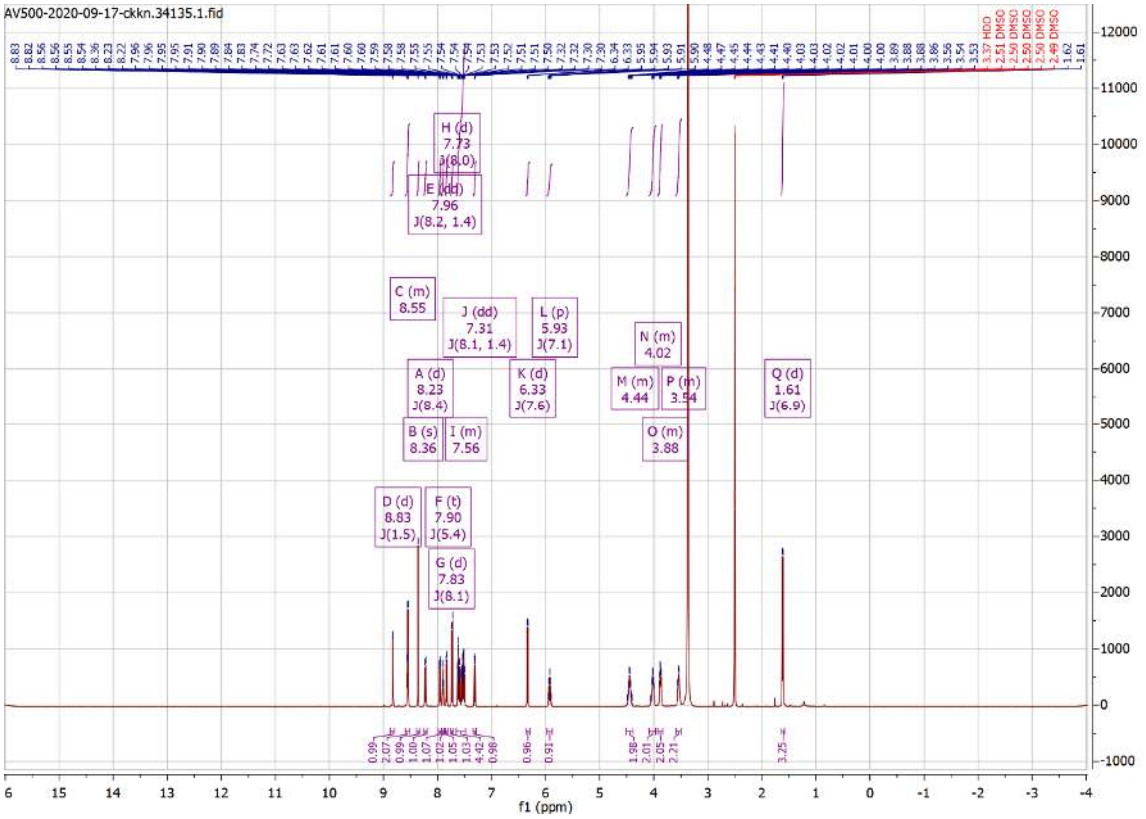

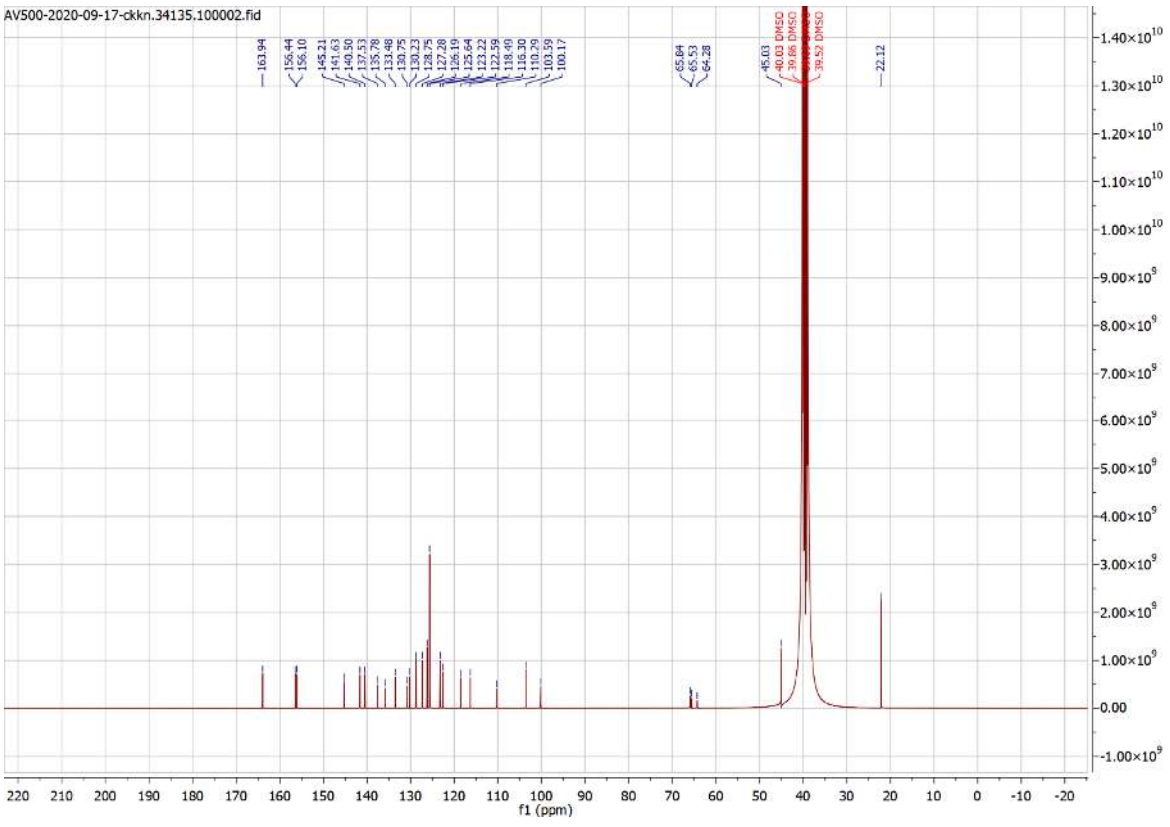

Compound **112**

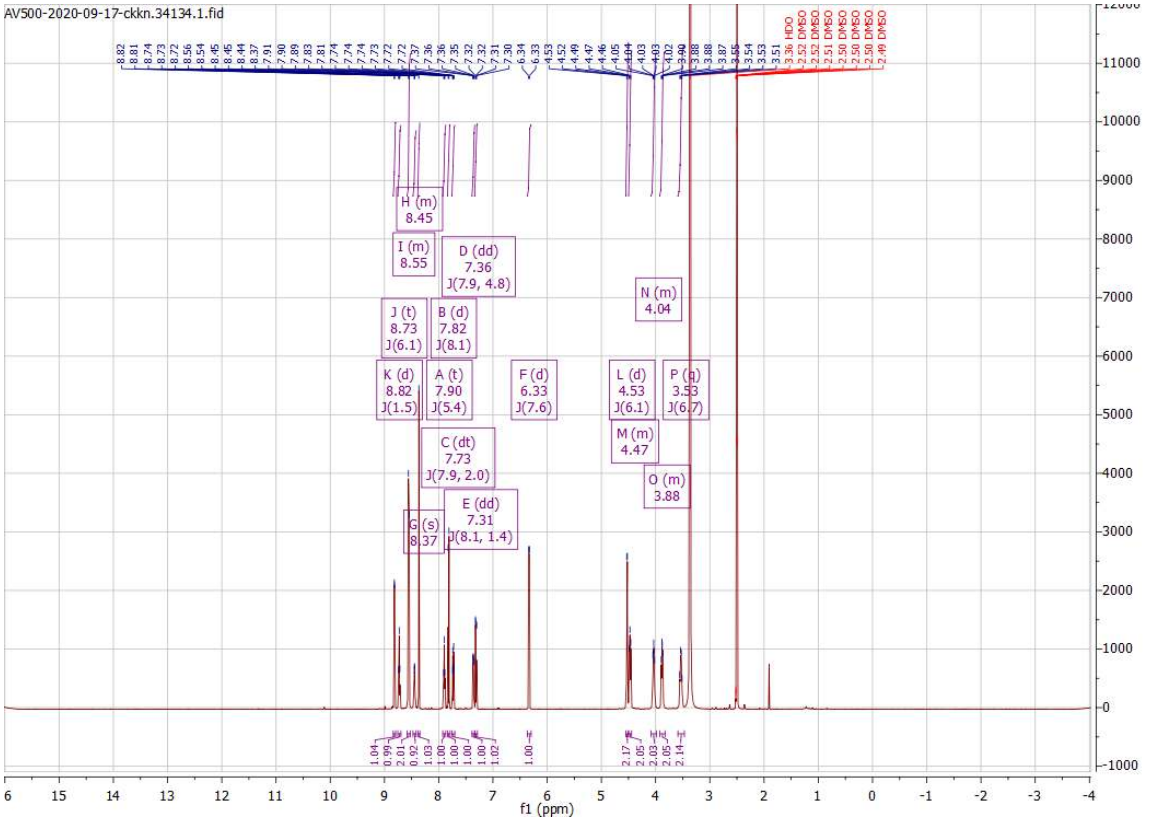

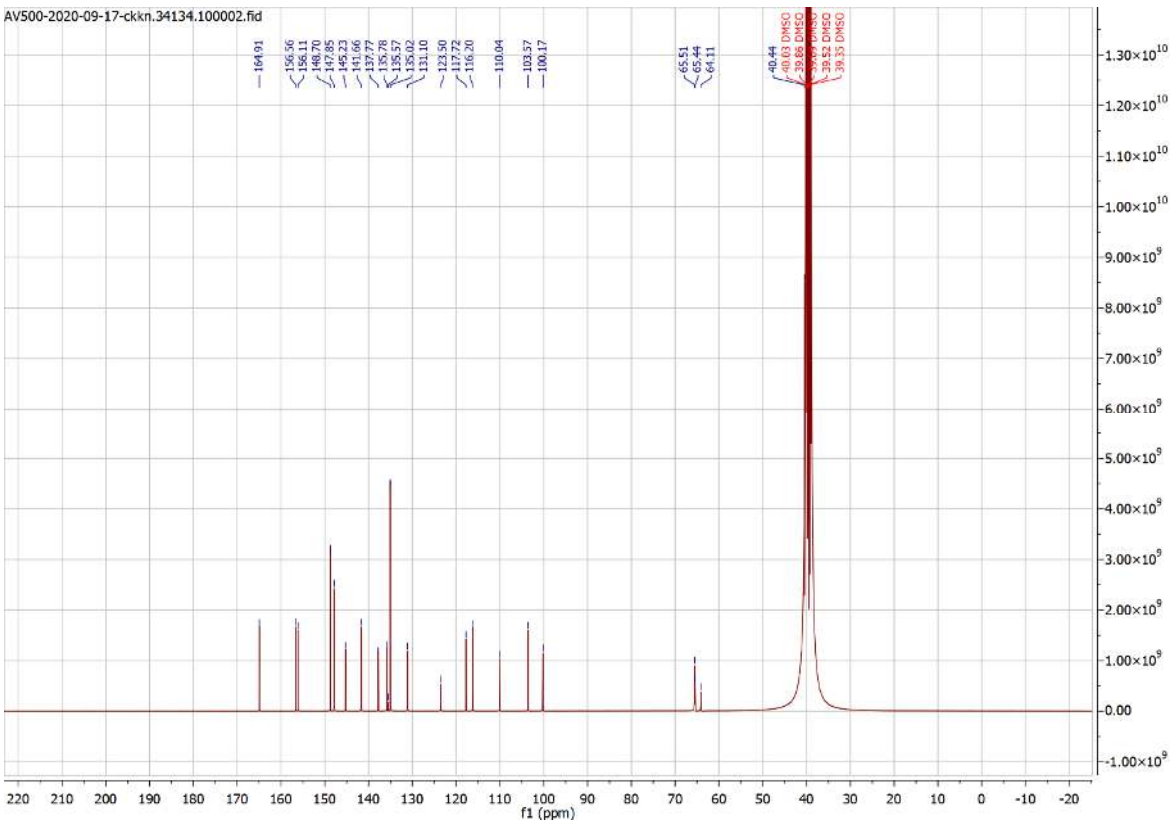

Compound **113**

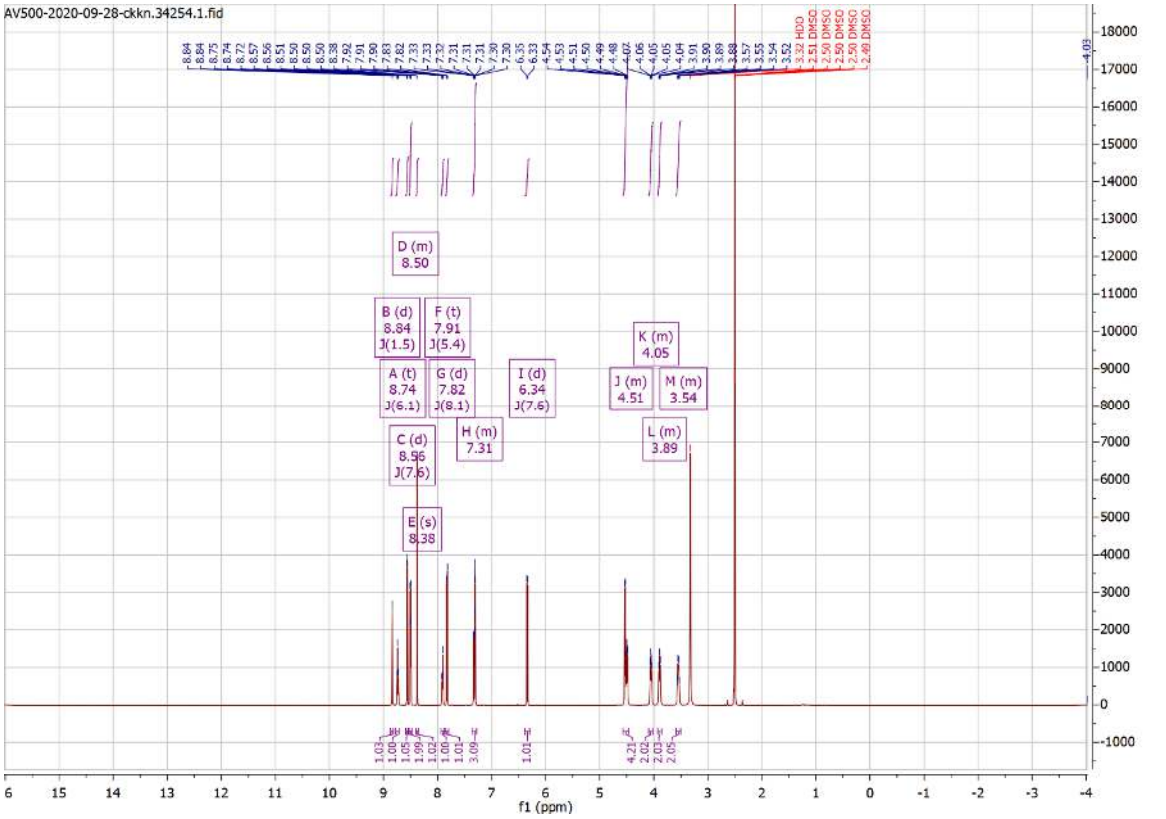

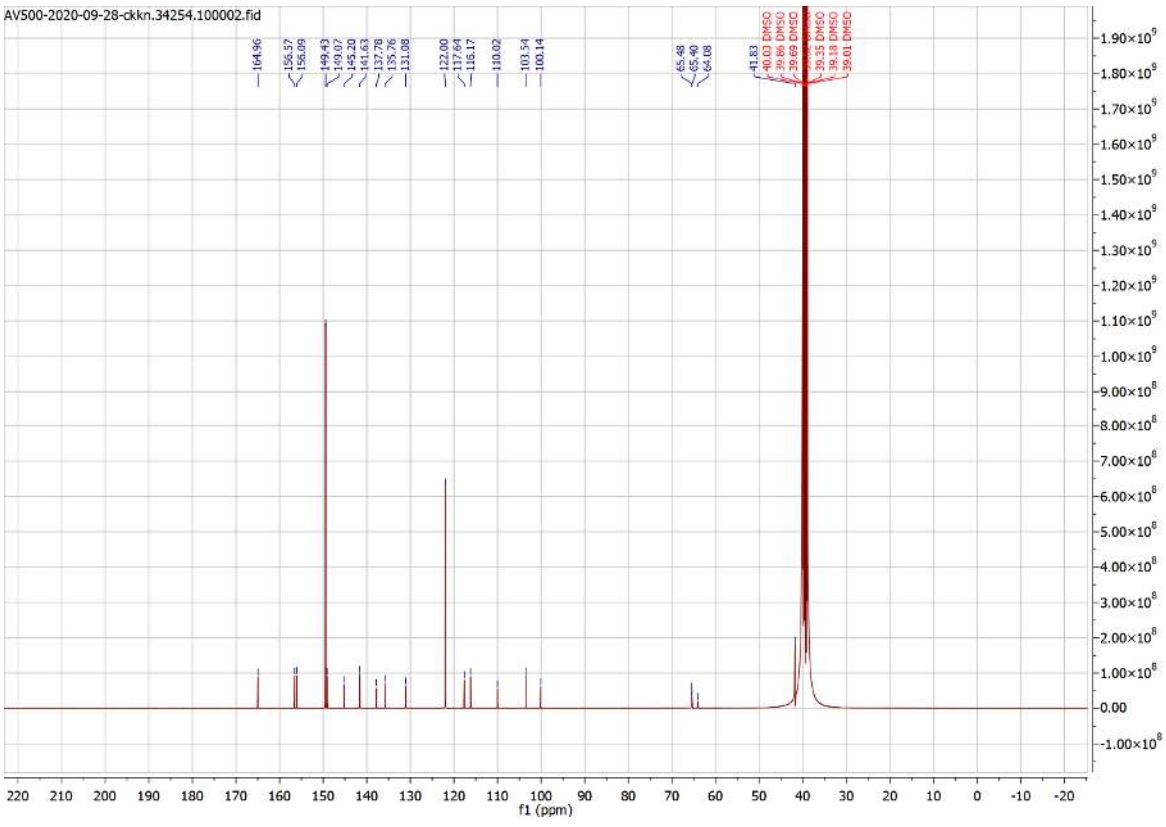

Compound **114**

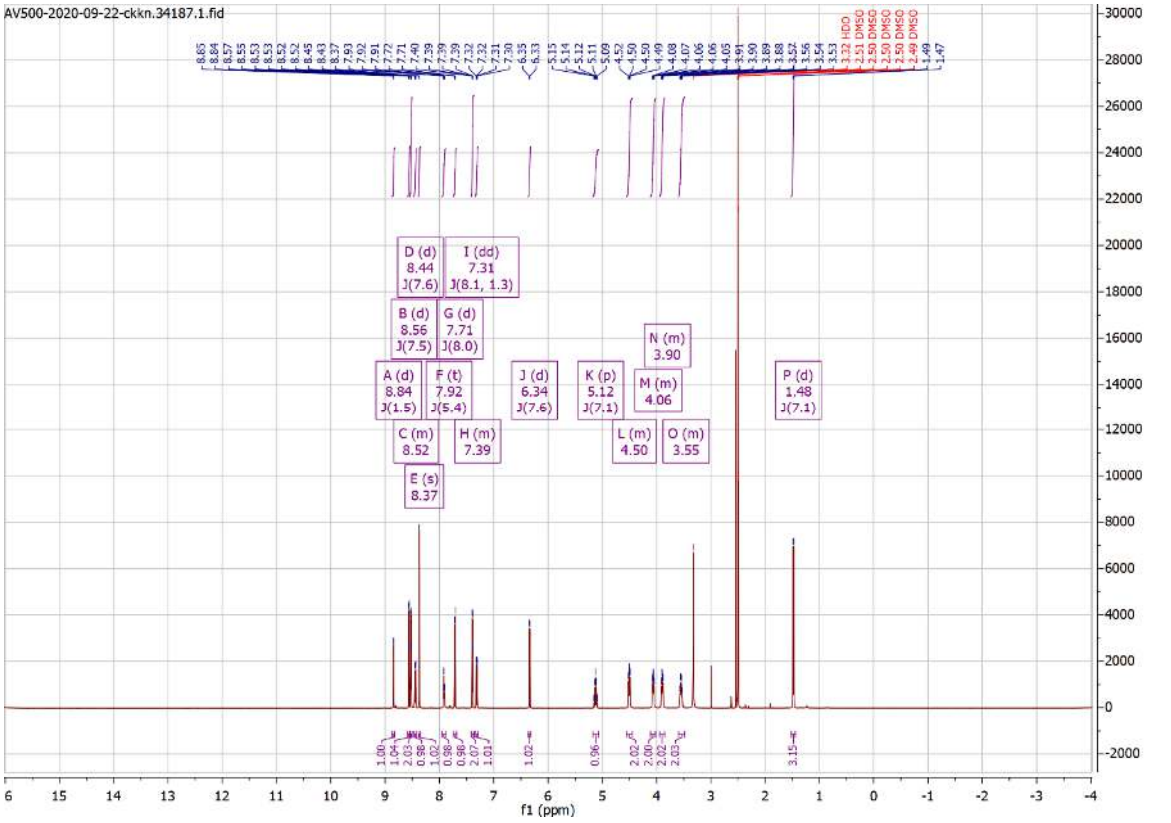

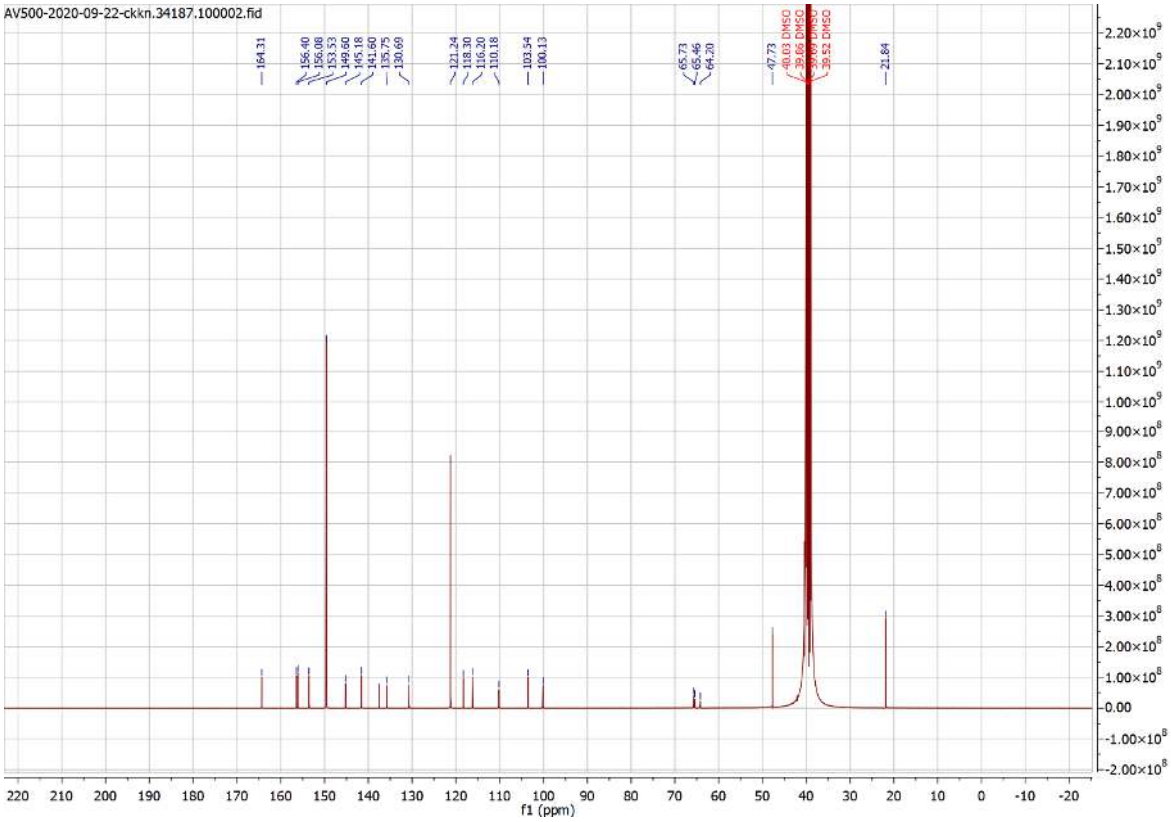

Compound **115**

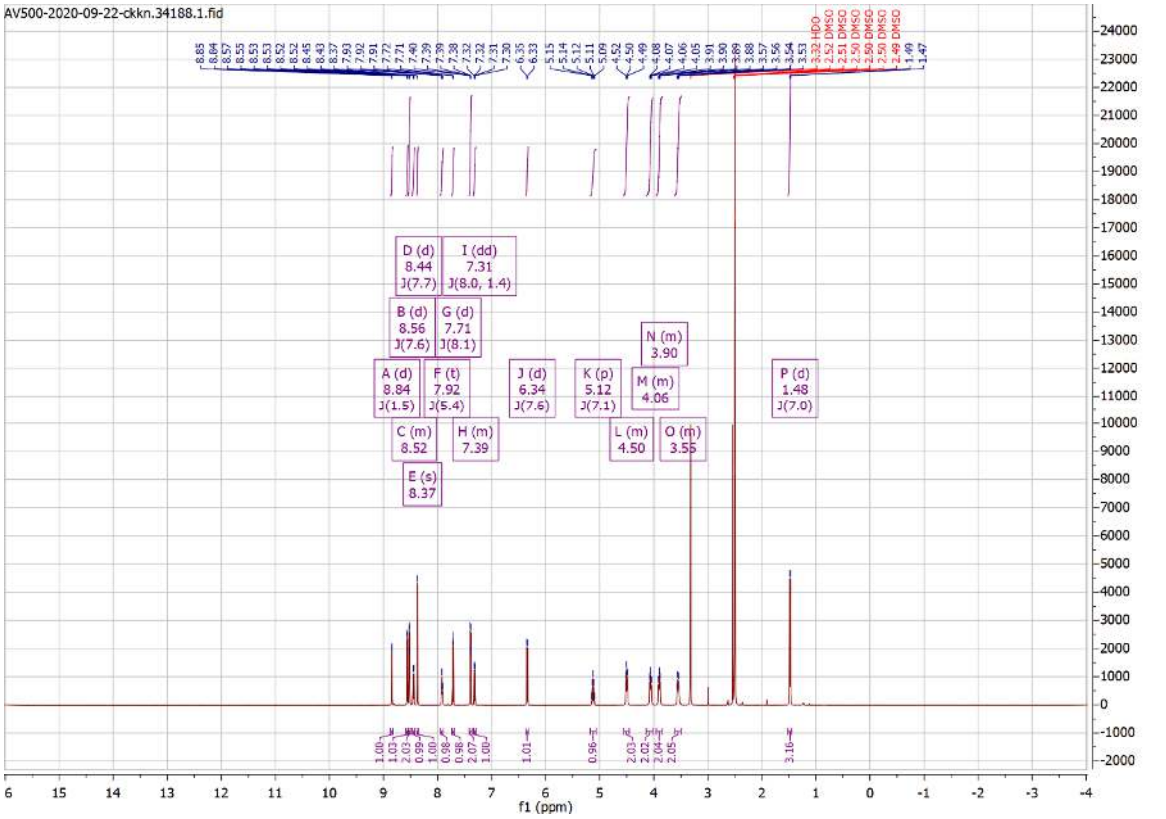

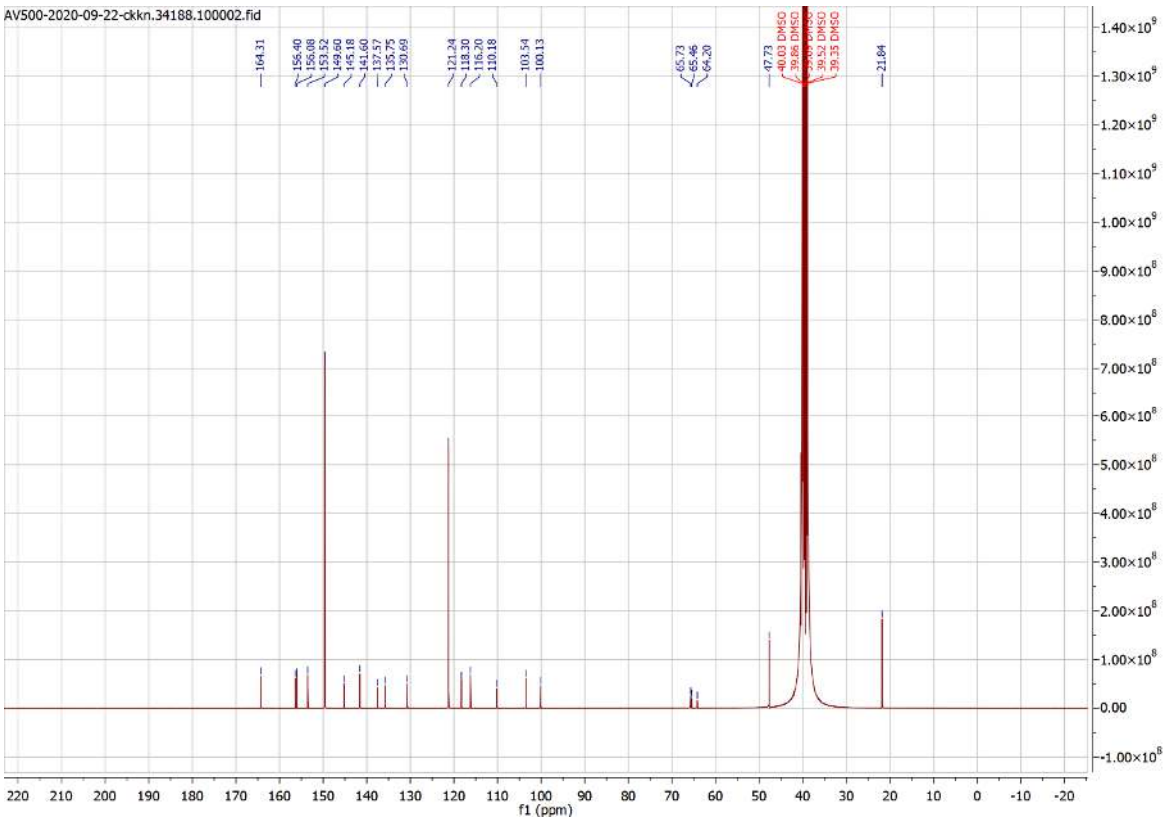

Compound **116**

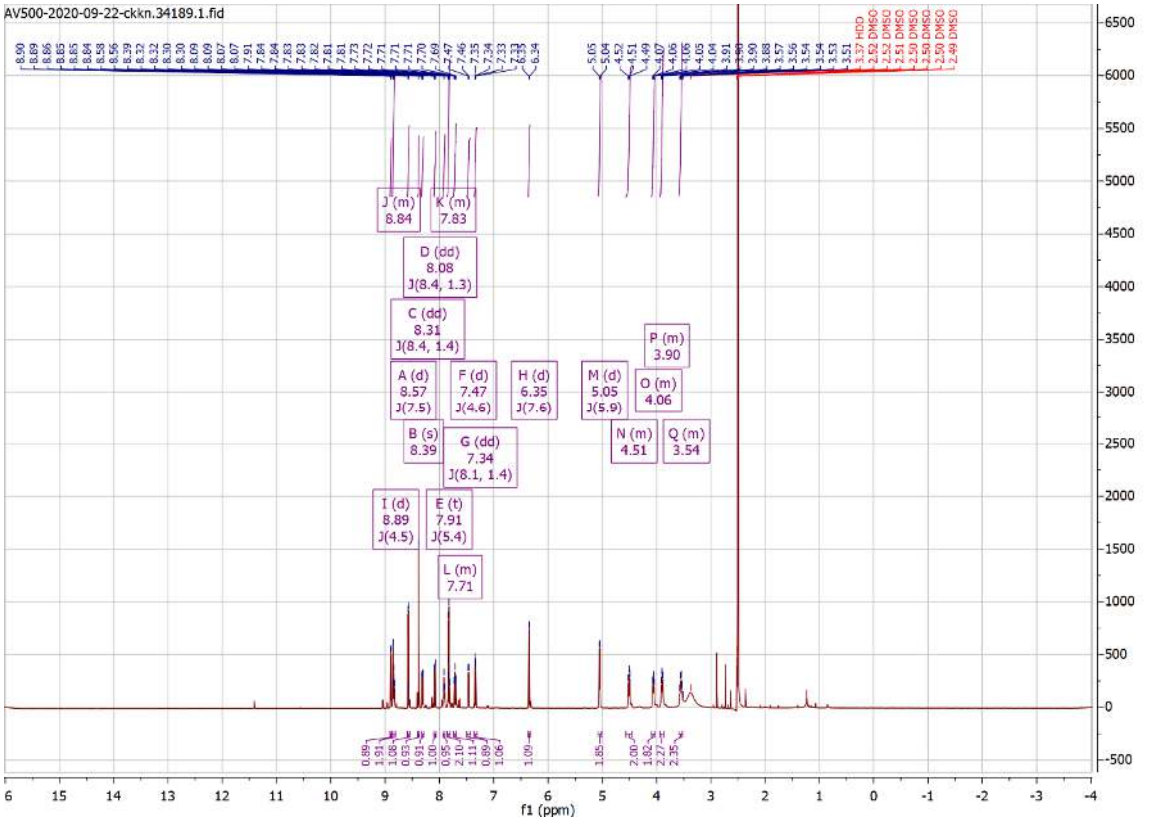

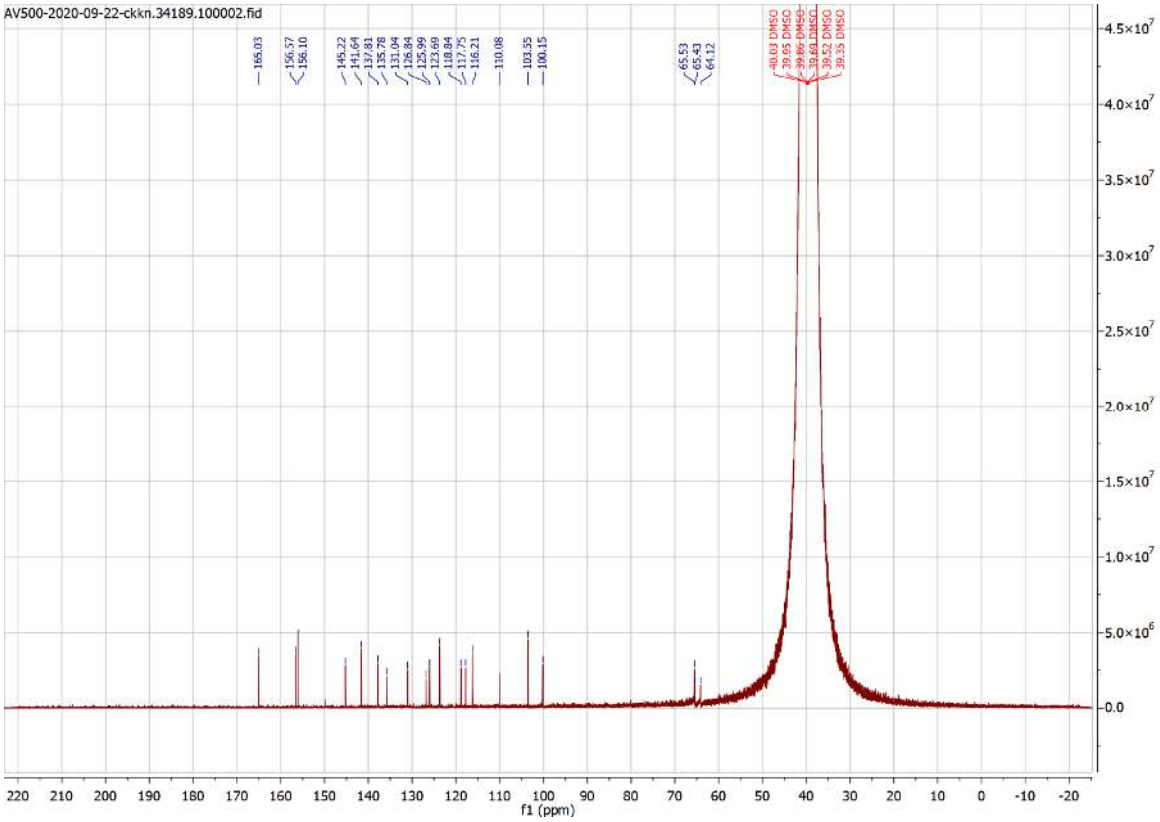

Compound **117**

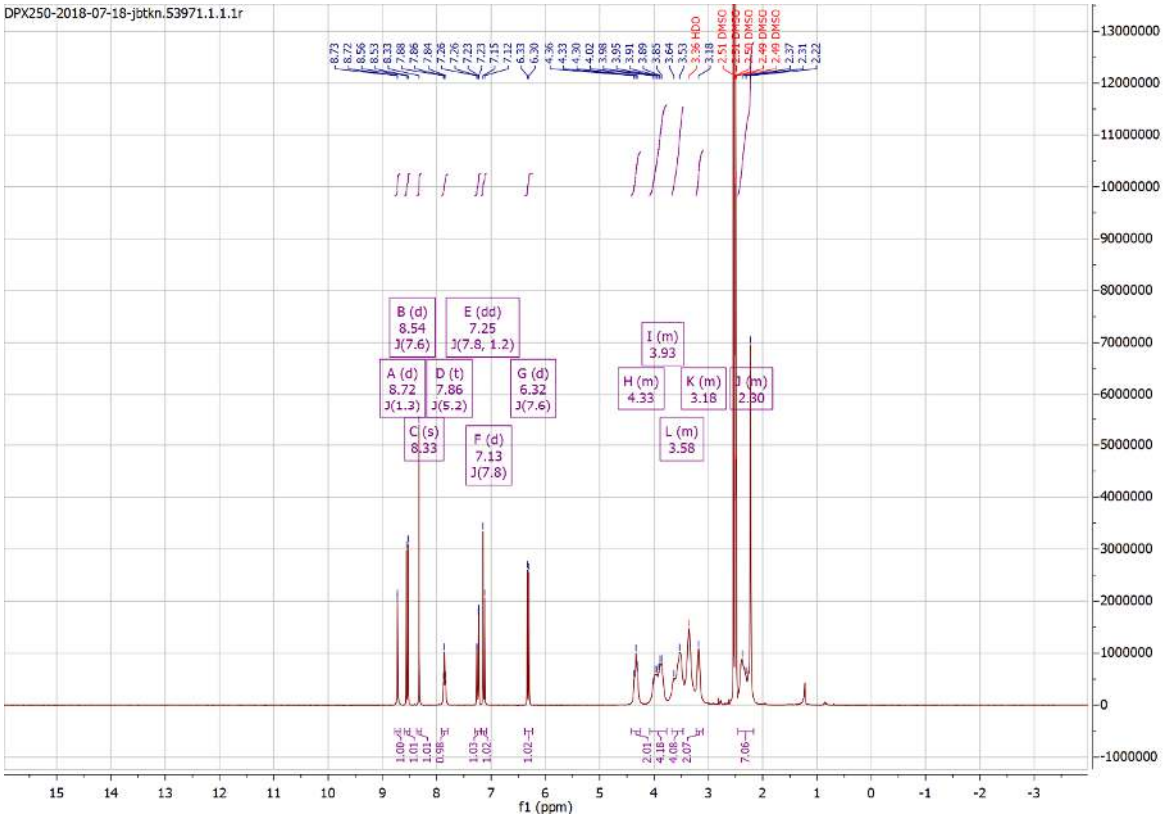

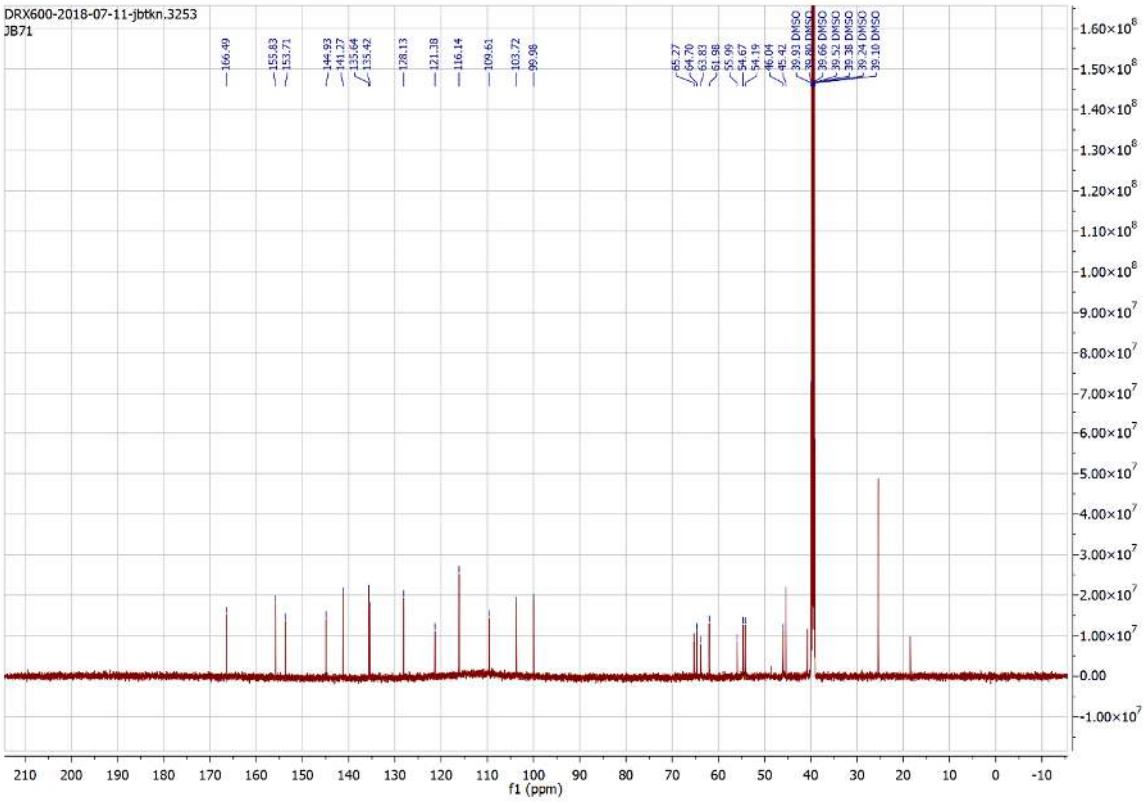

Compound **118**

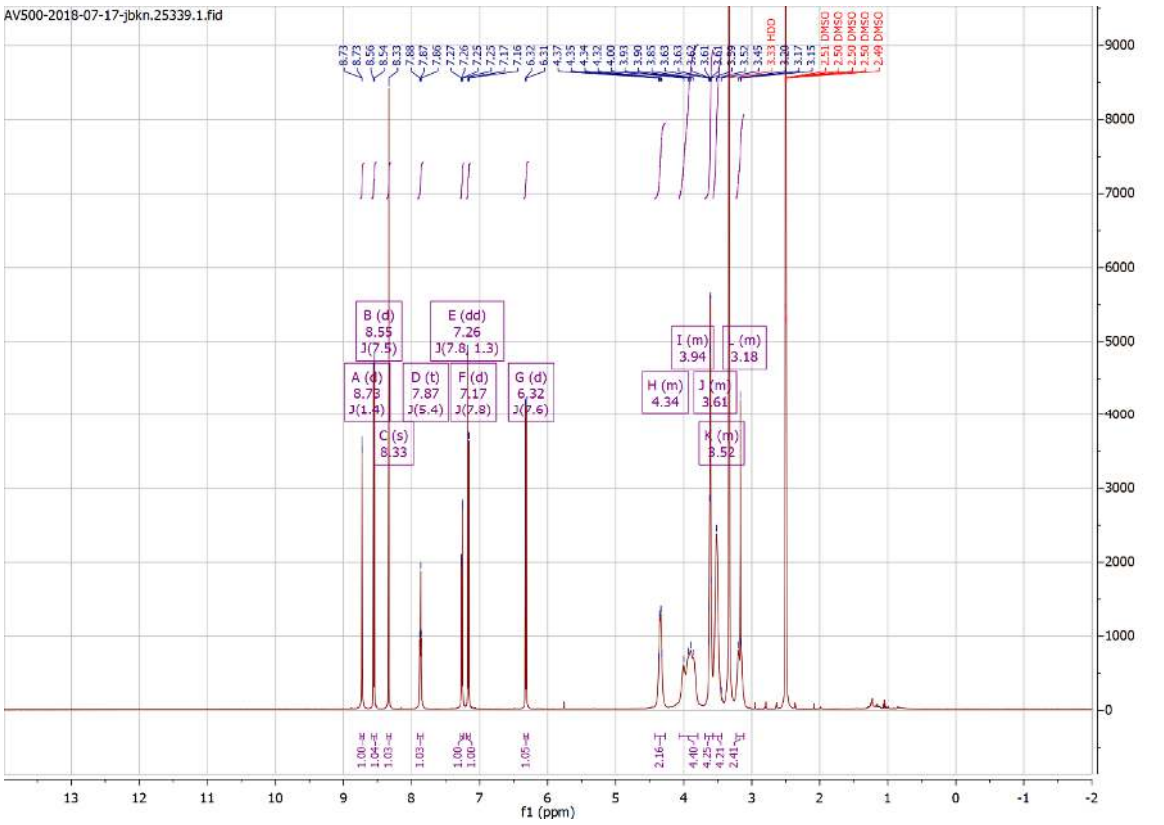

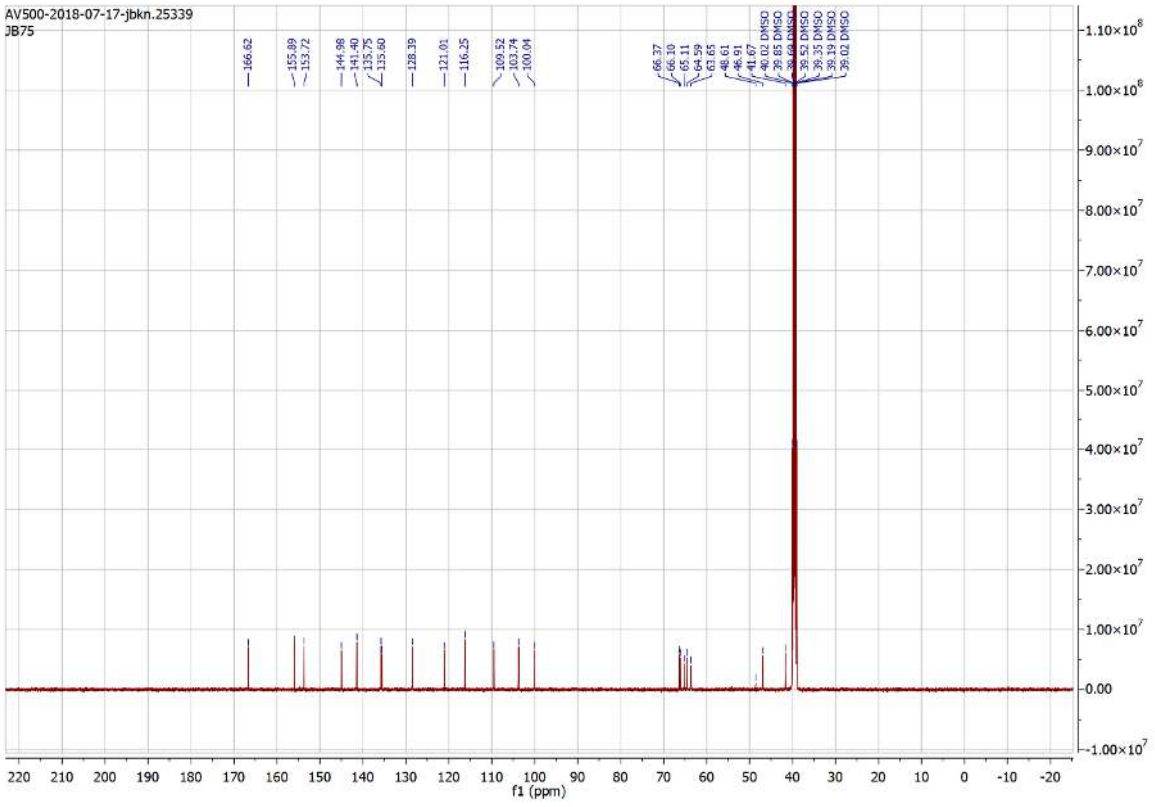

Compound **119**

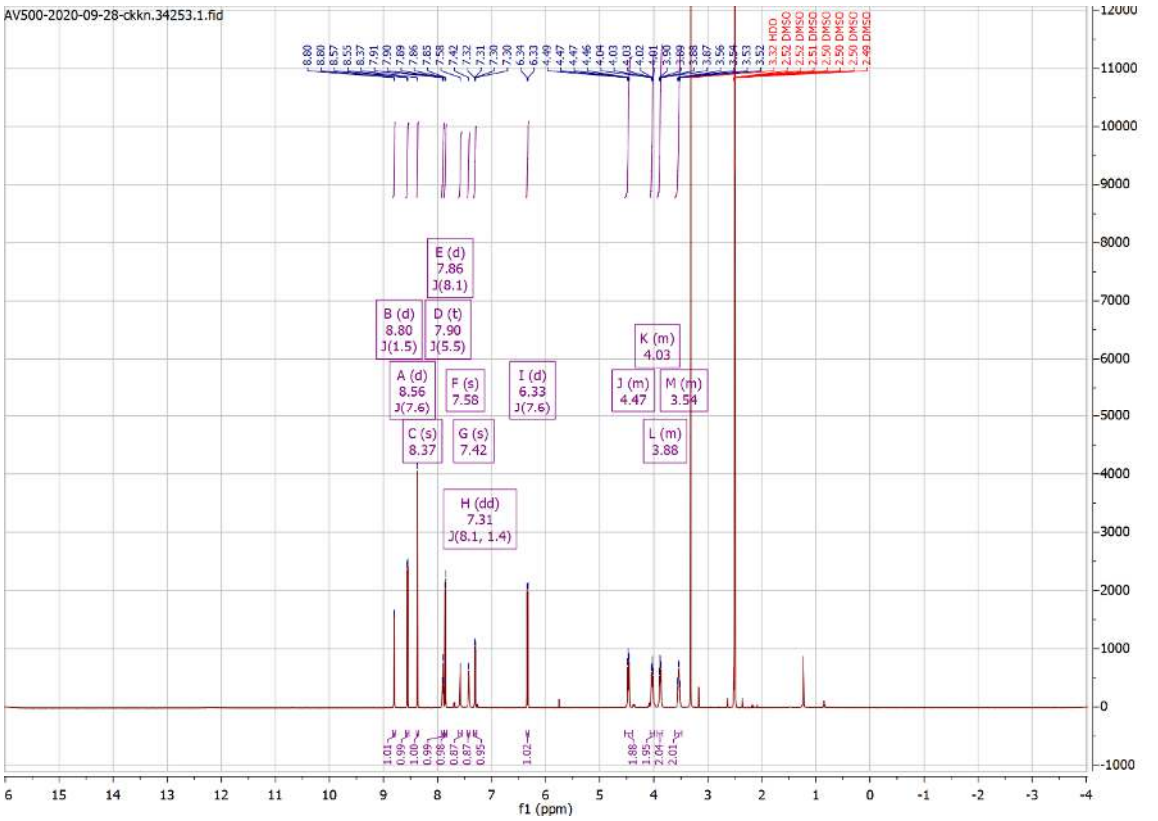

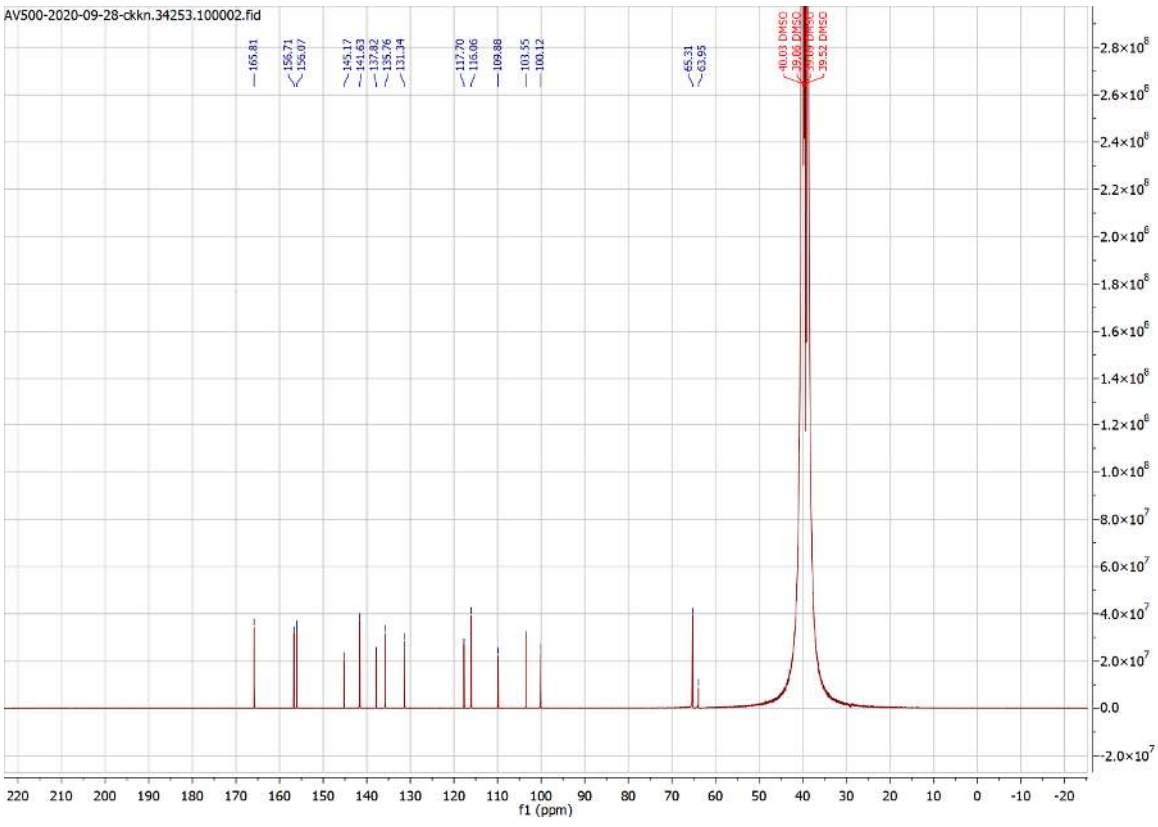

Compound **120**

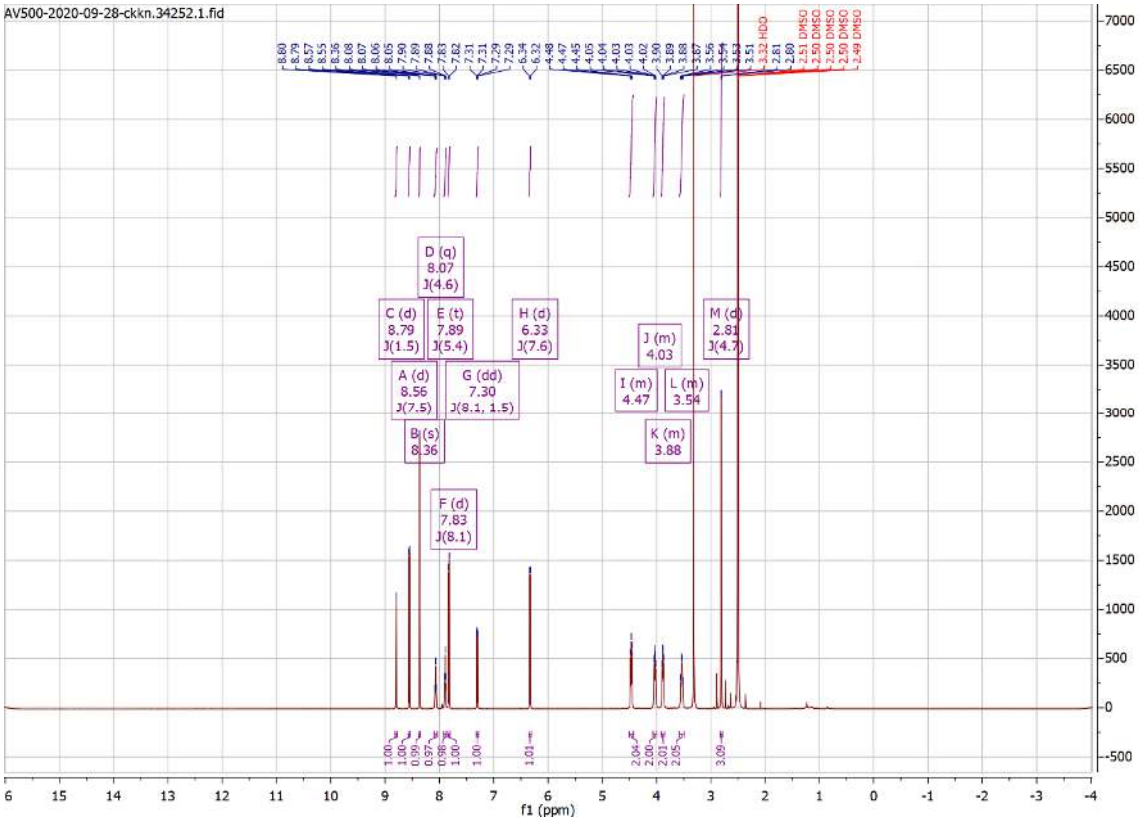

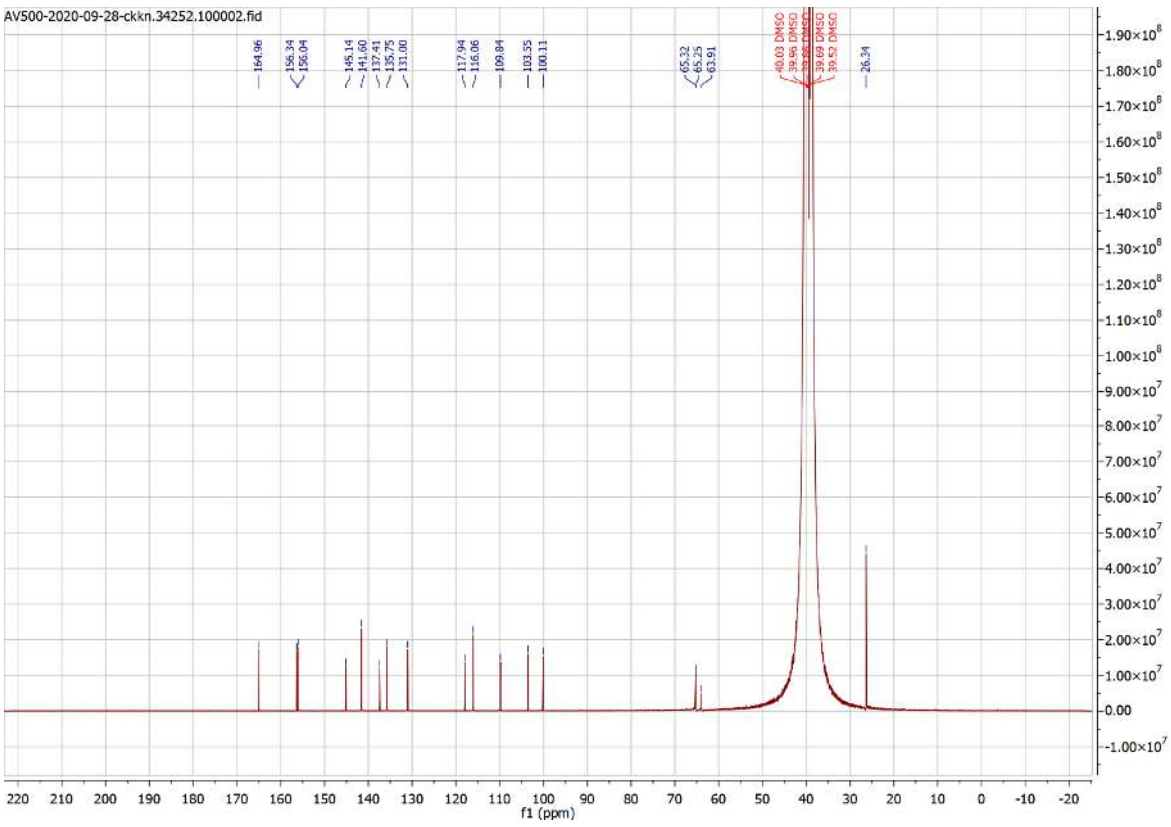

Compound **121**

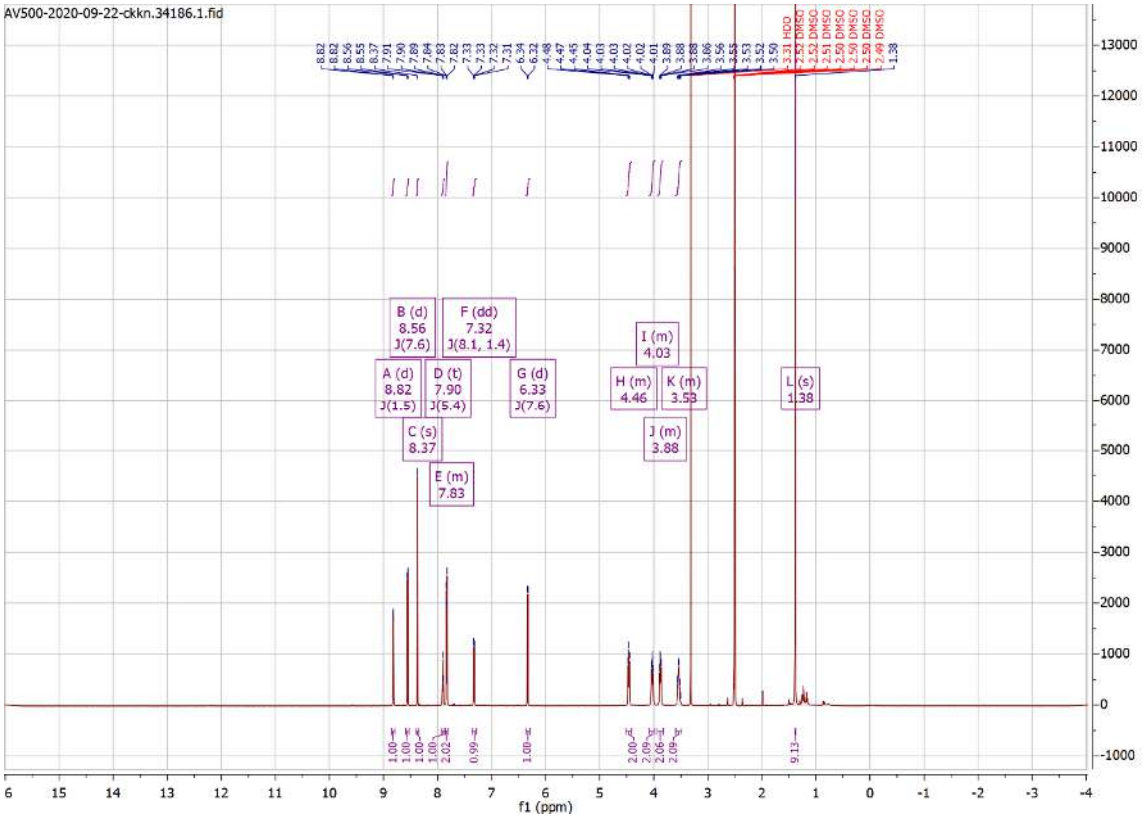

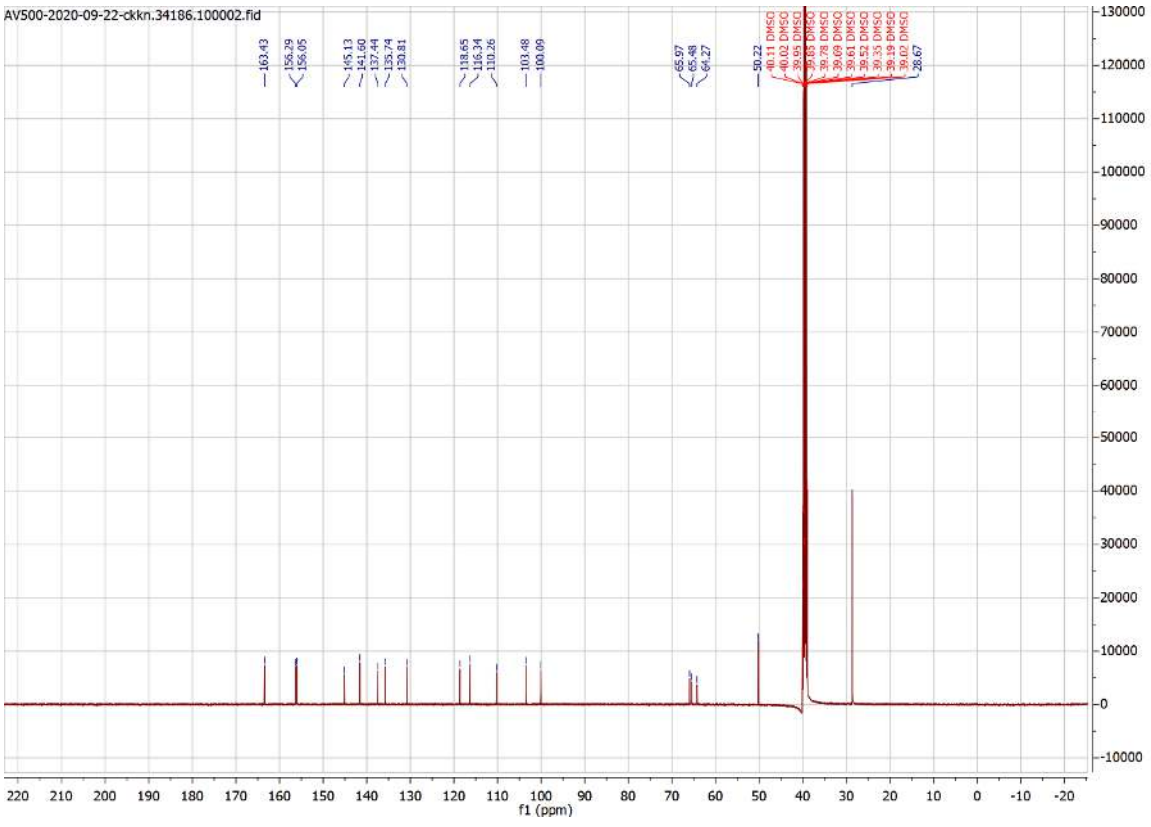

Compound **171**

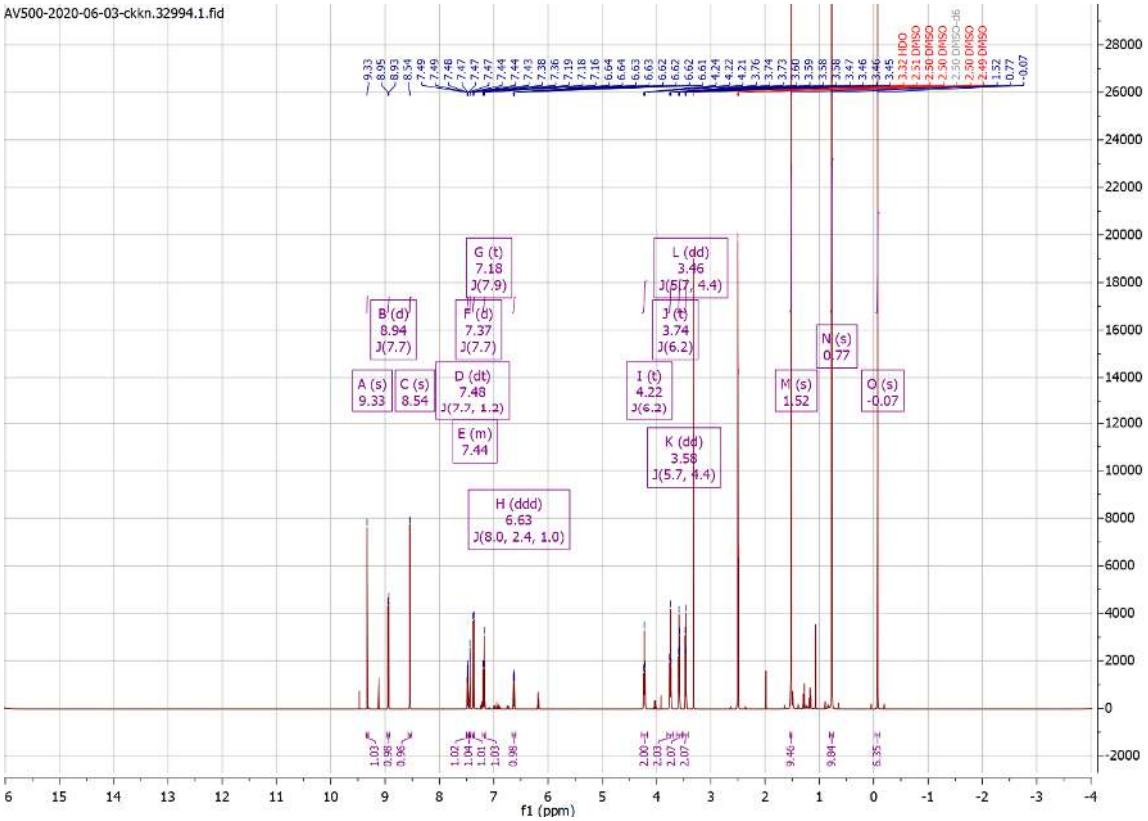

Compound **172**

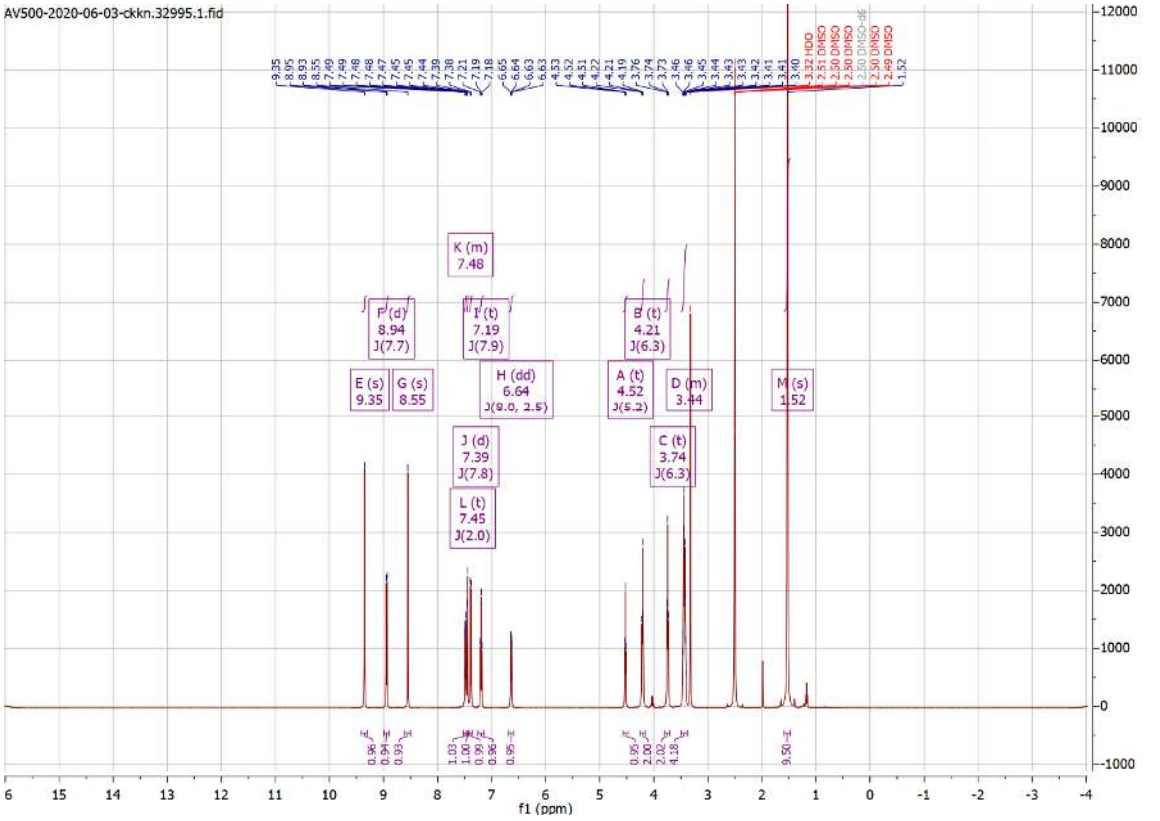

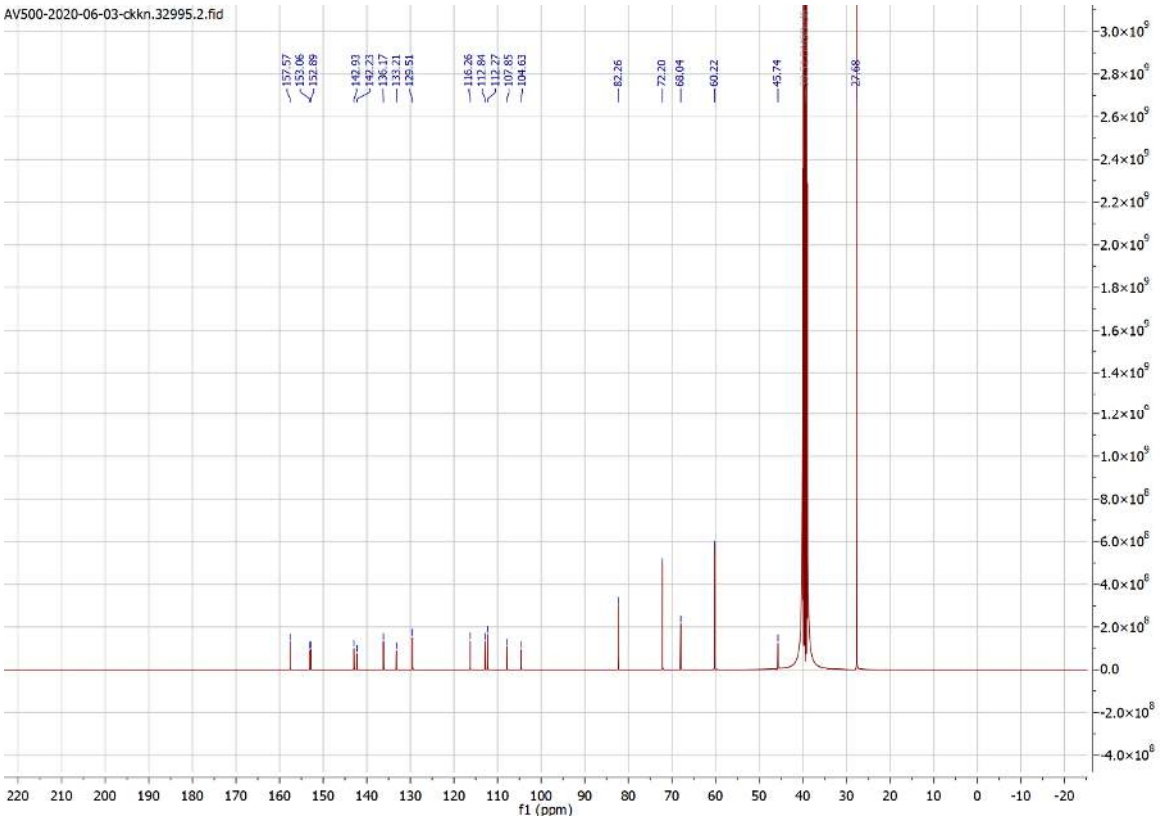

Compound **175**

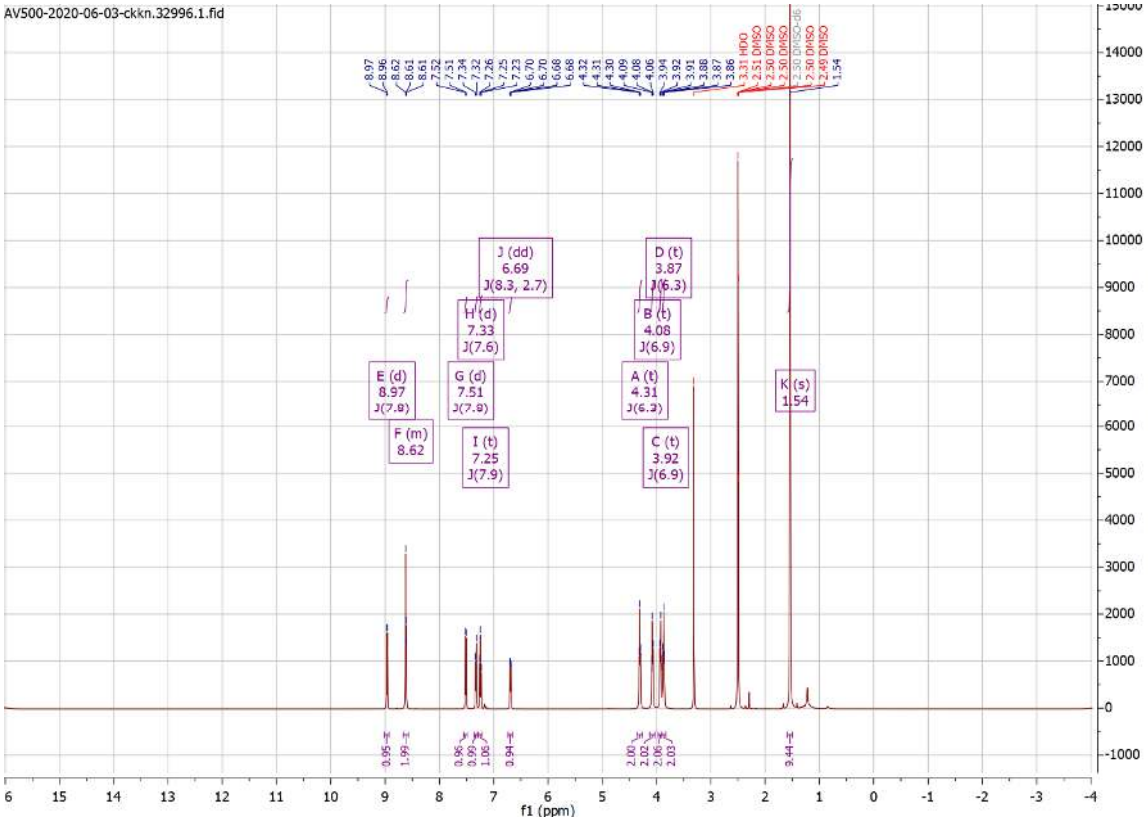

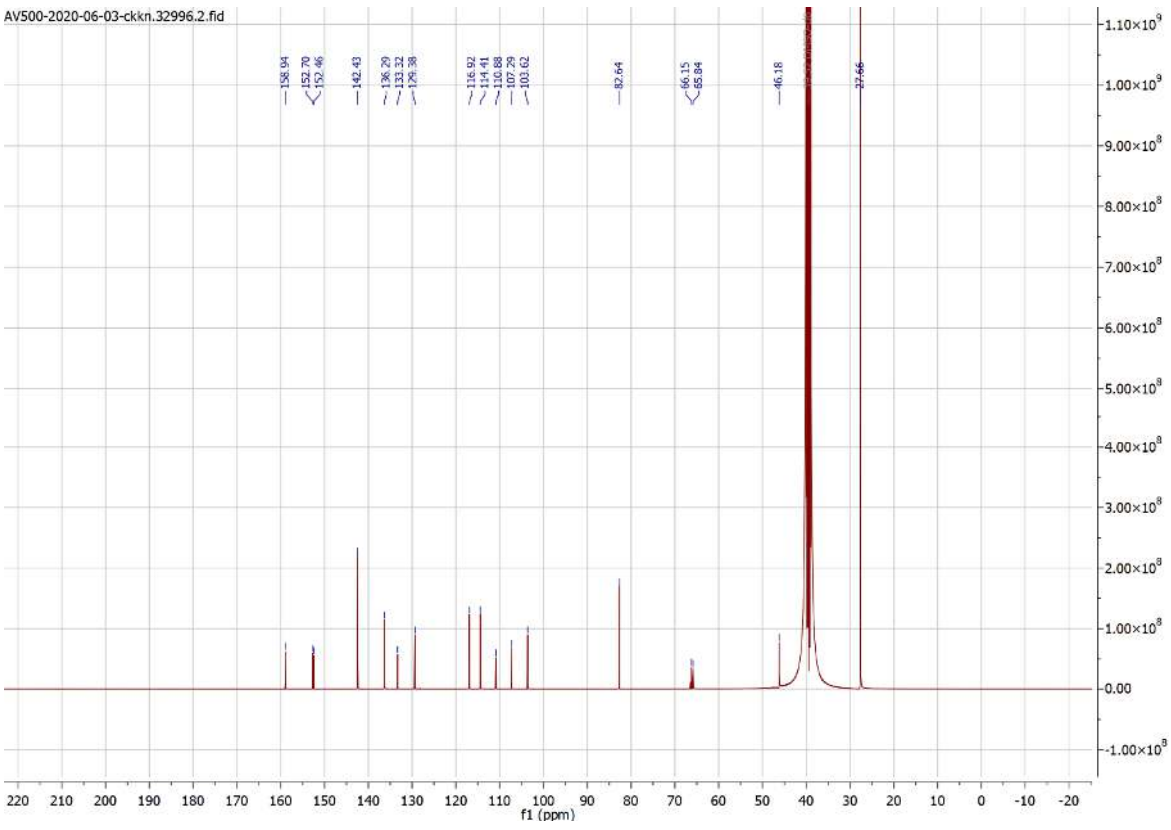

Compound **122**

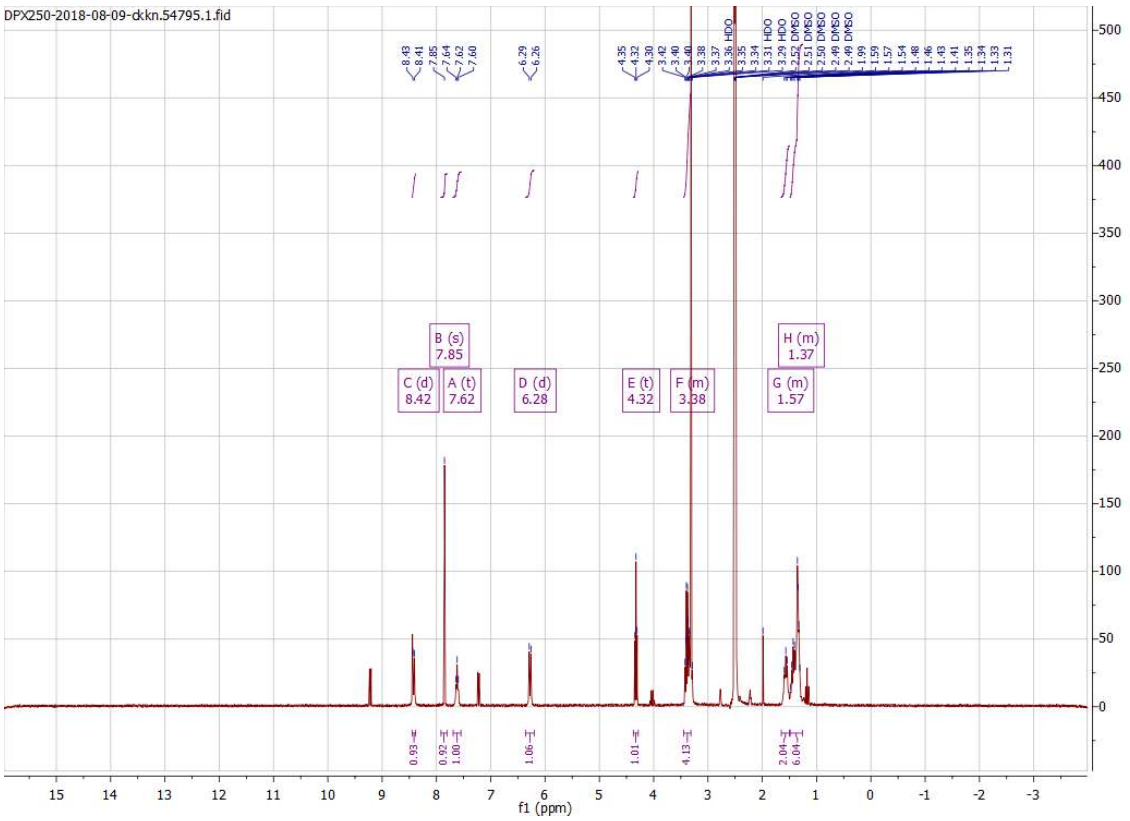

Compound **124**

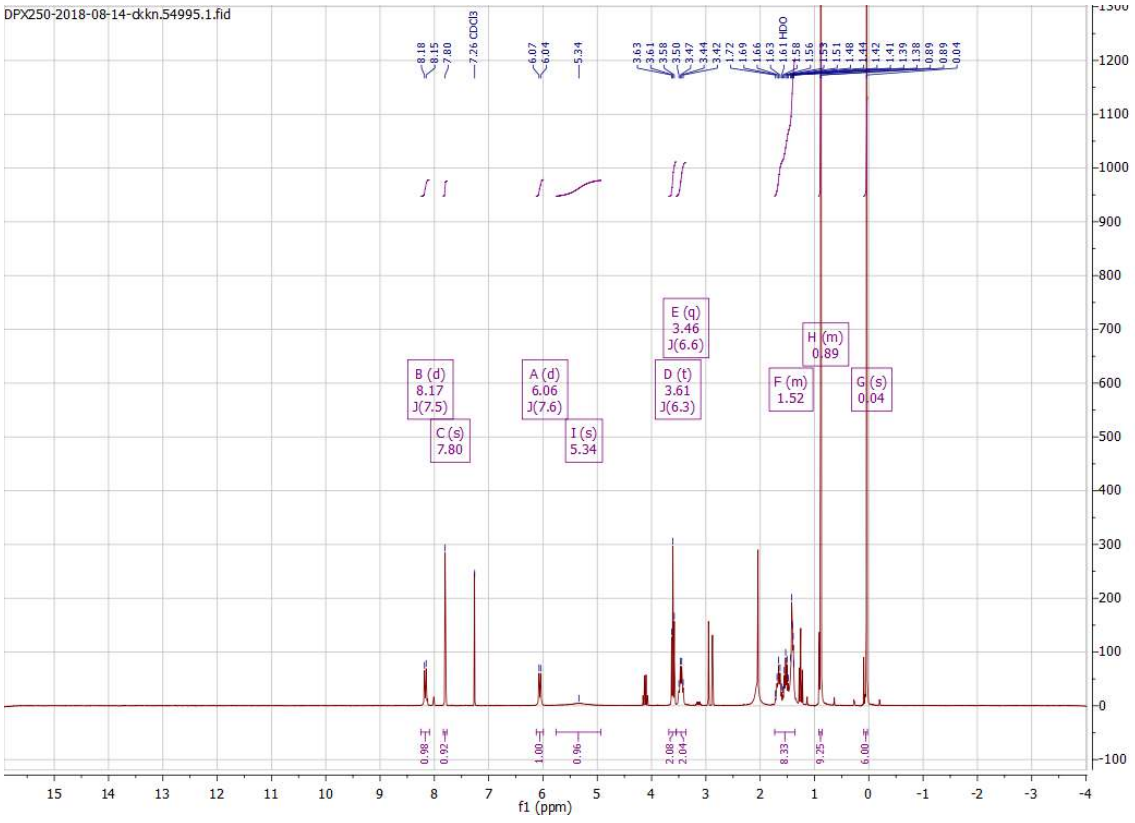

Compound **126**

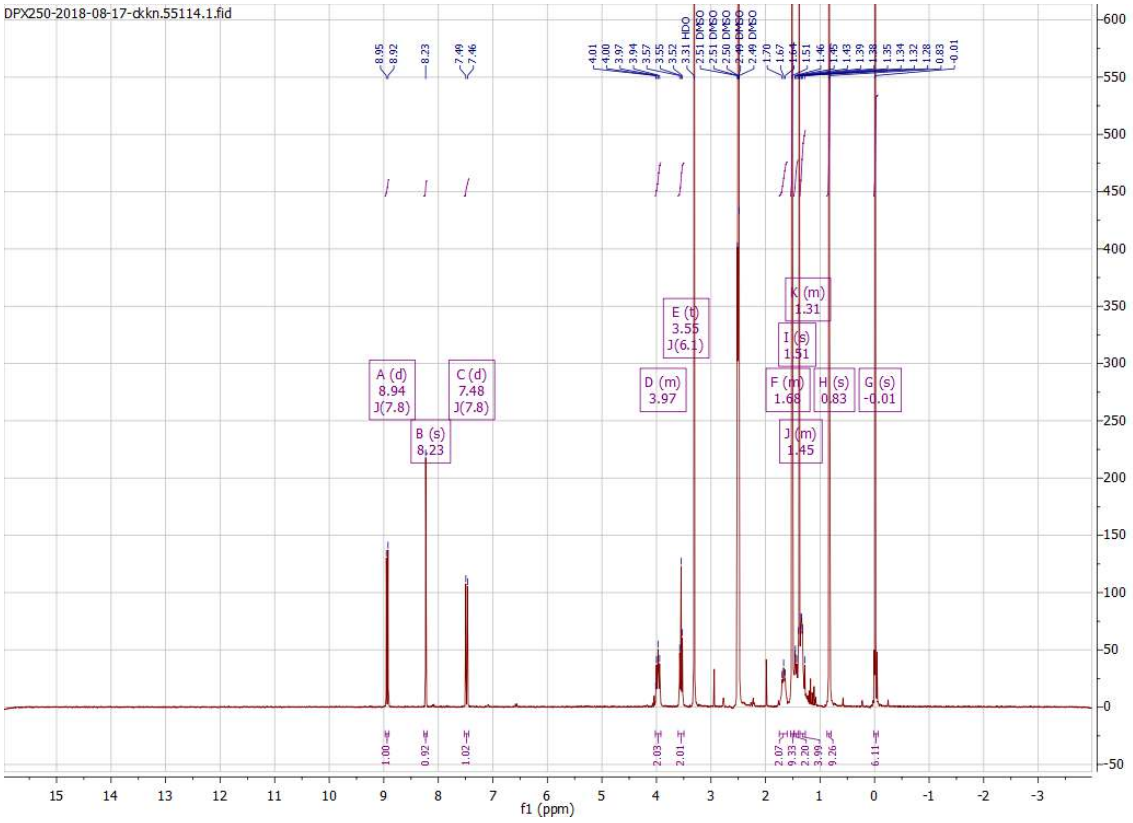

Compound **128**

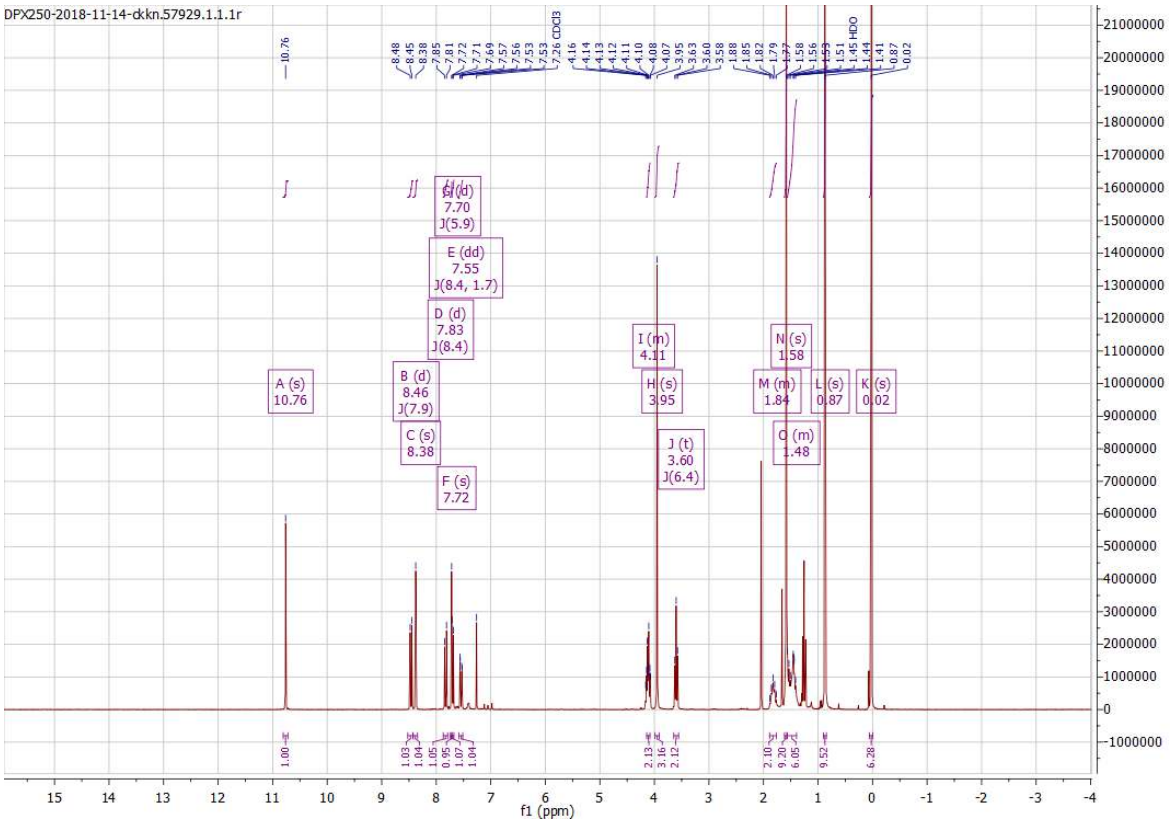

Compound **130**

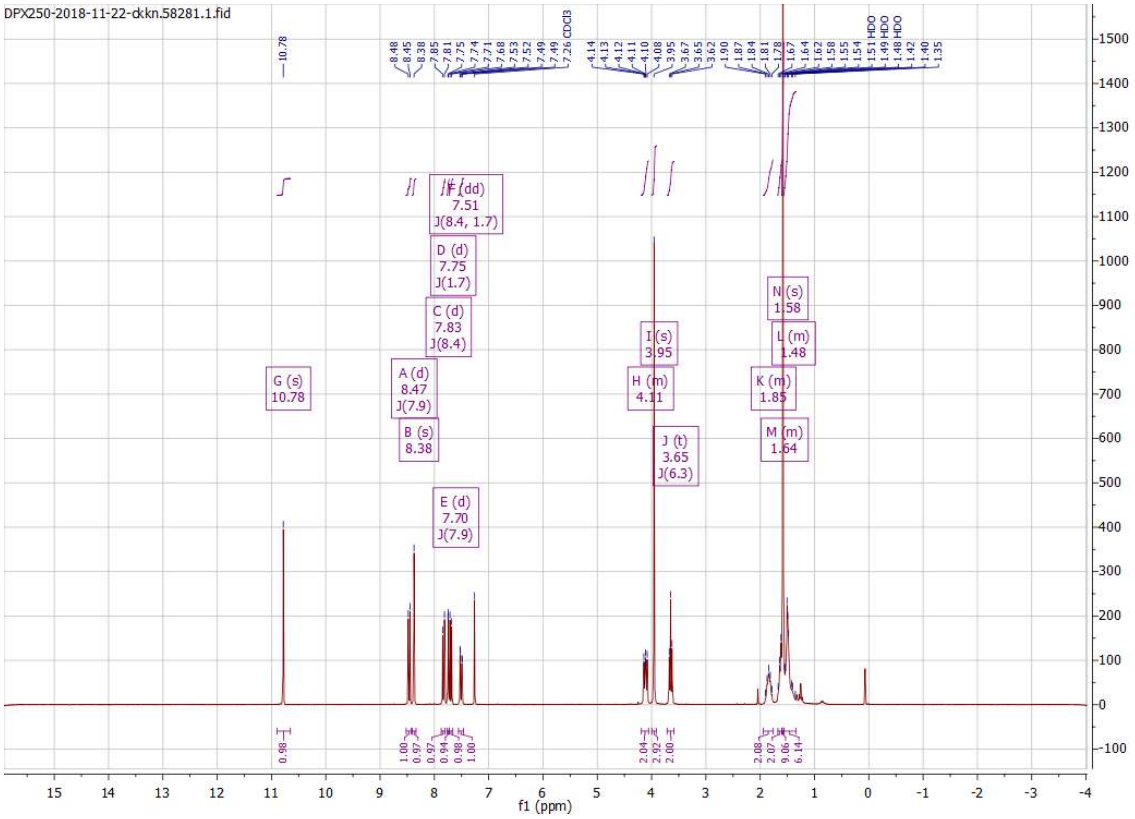

Compound **132**

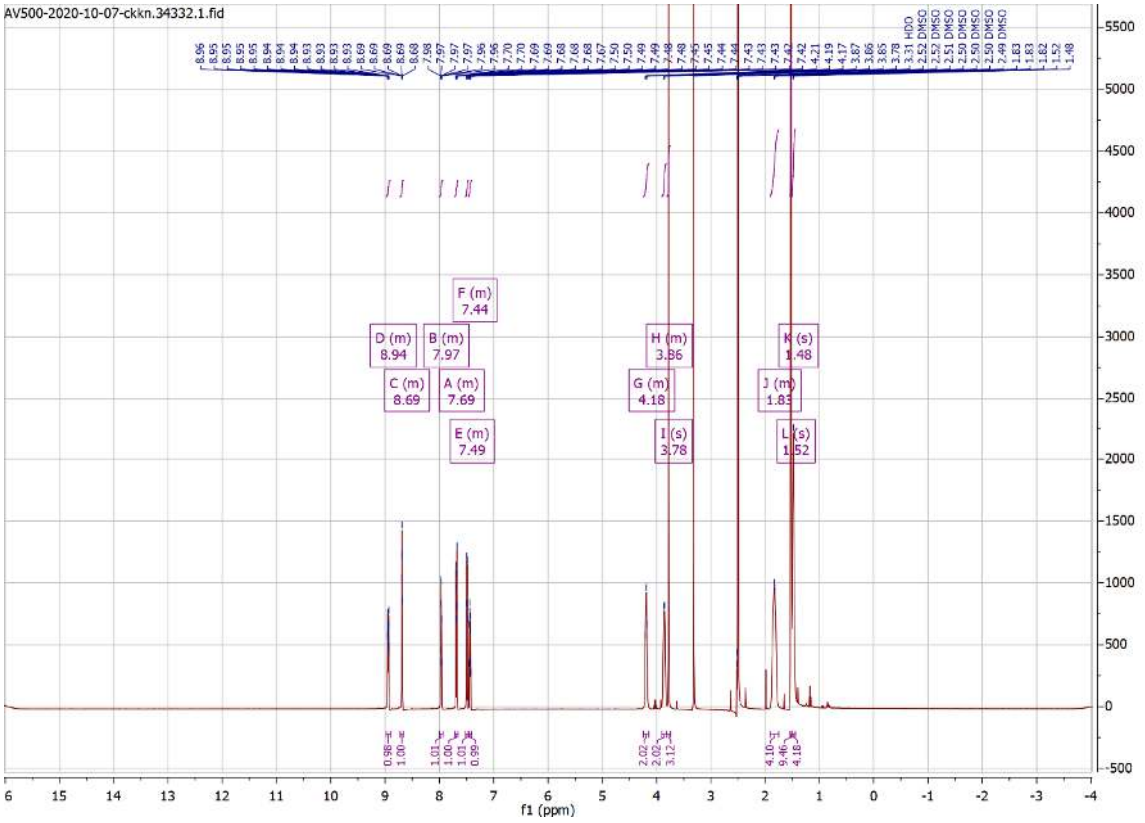

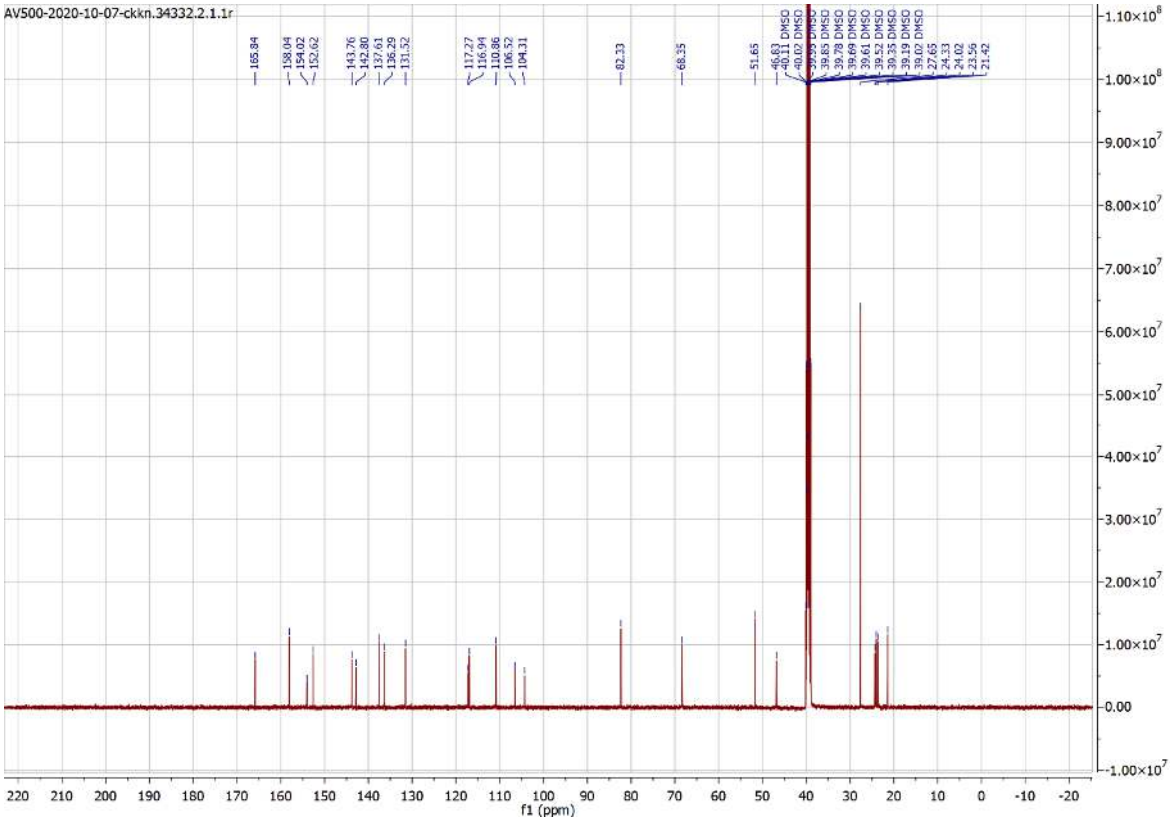

Compound **134**

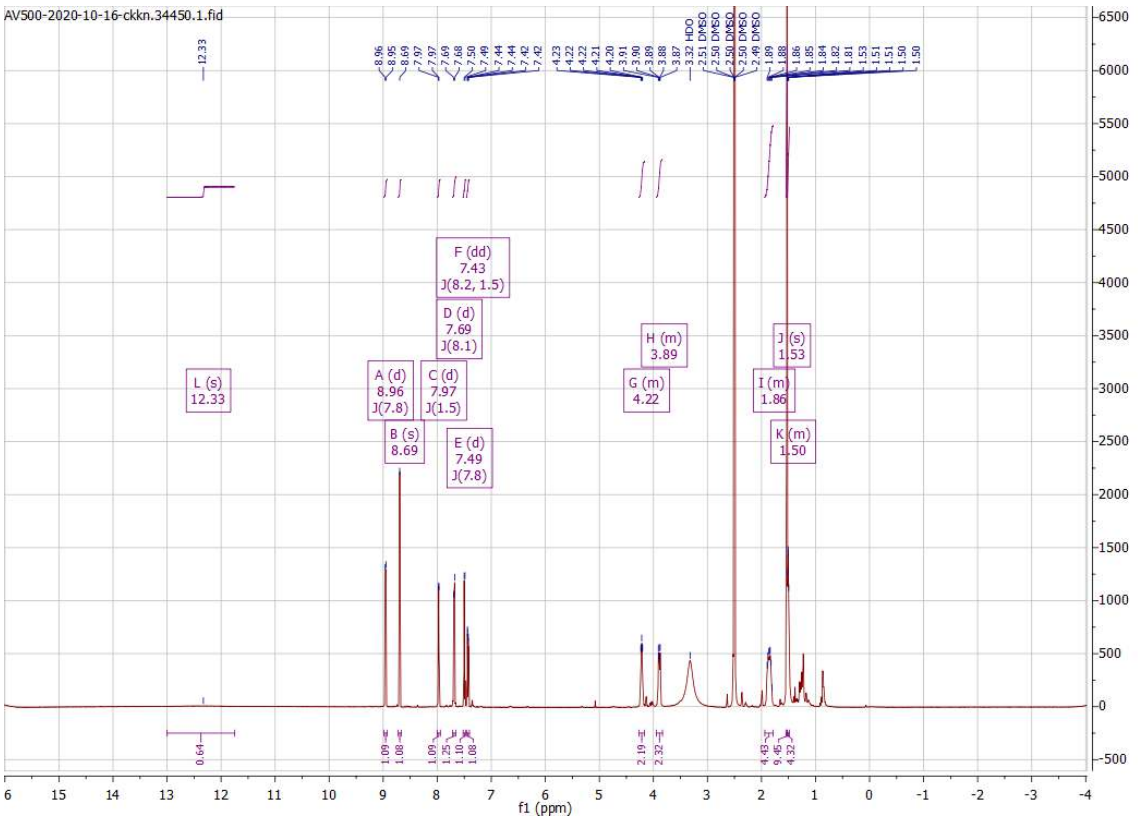

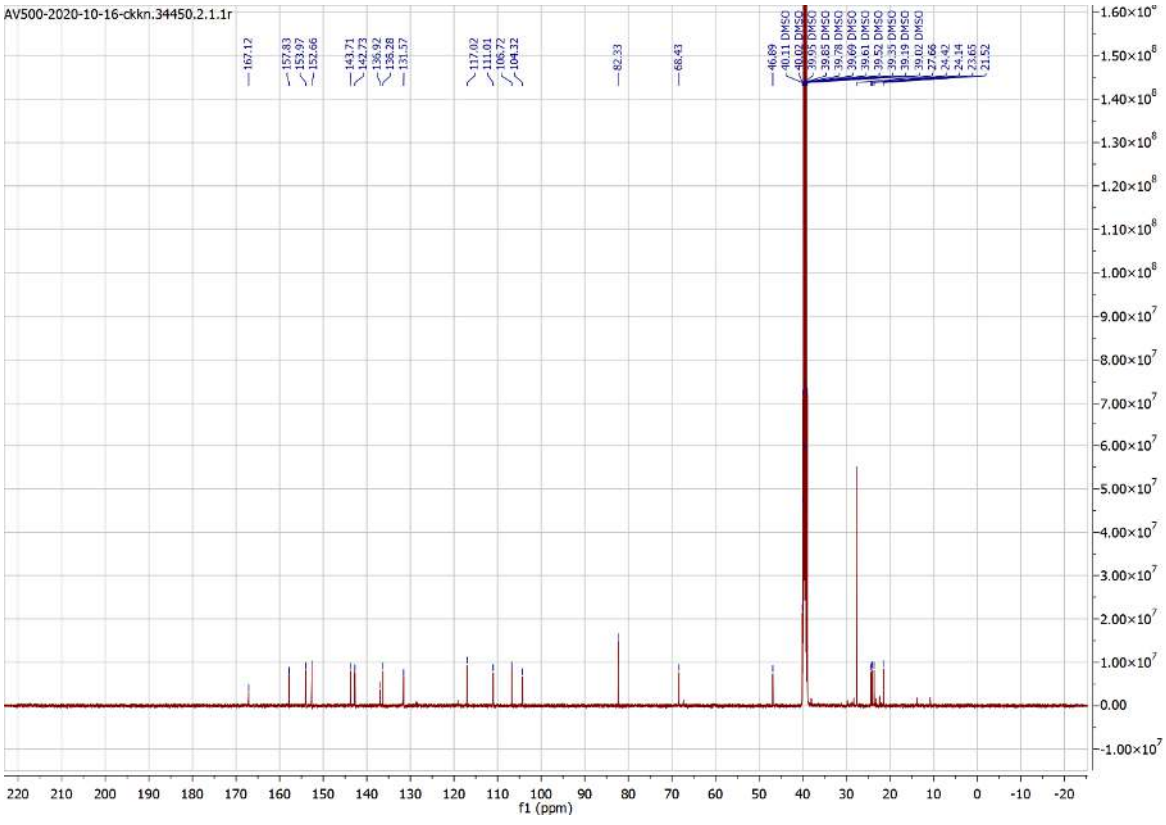

Compound **136**

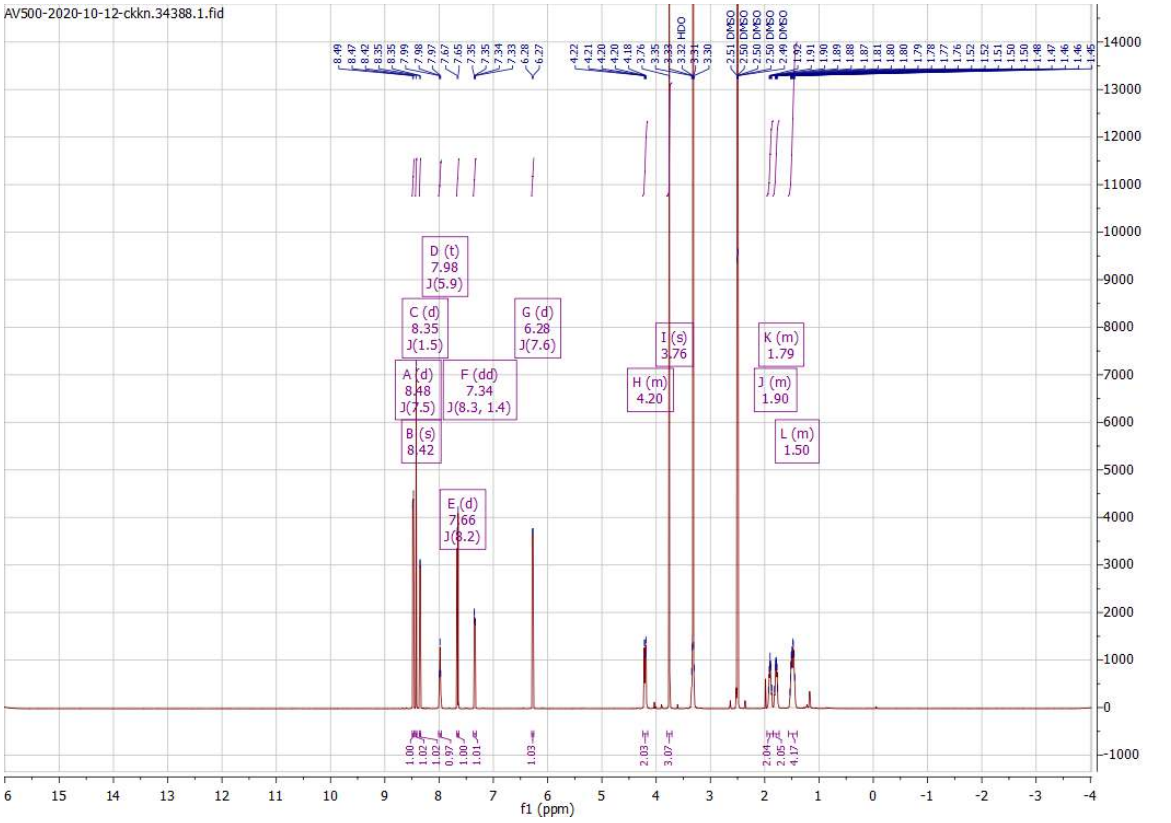

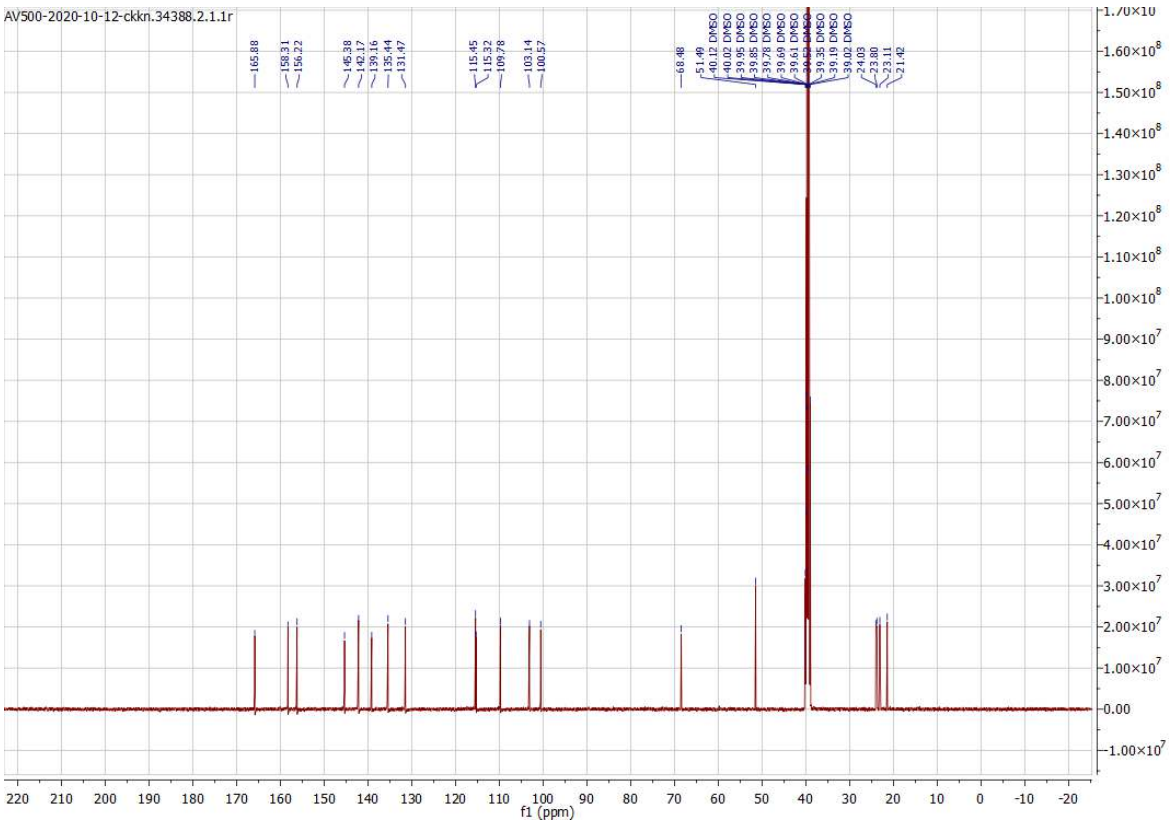

Compound **38**

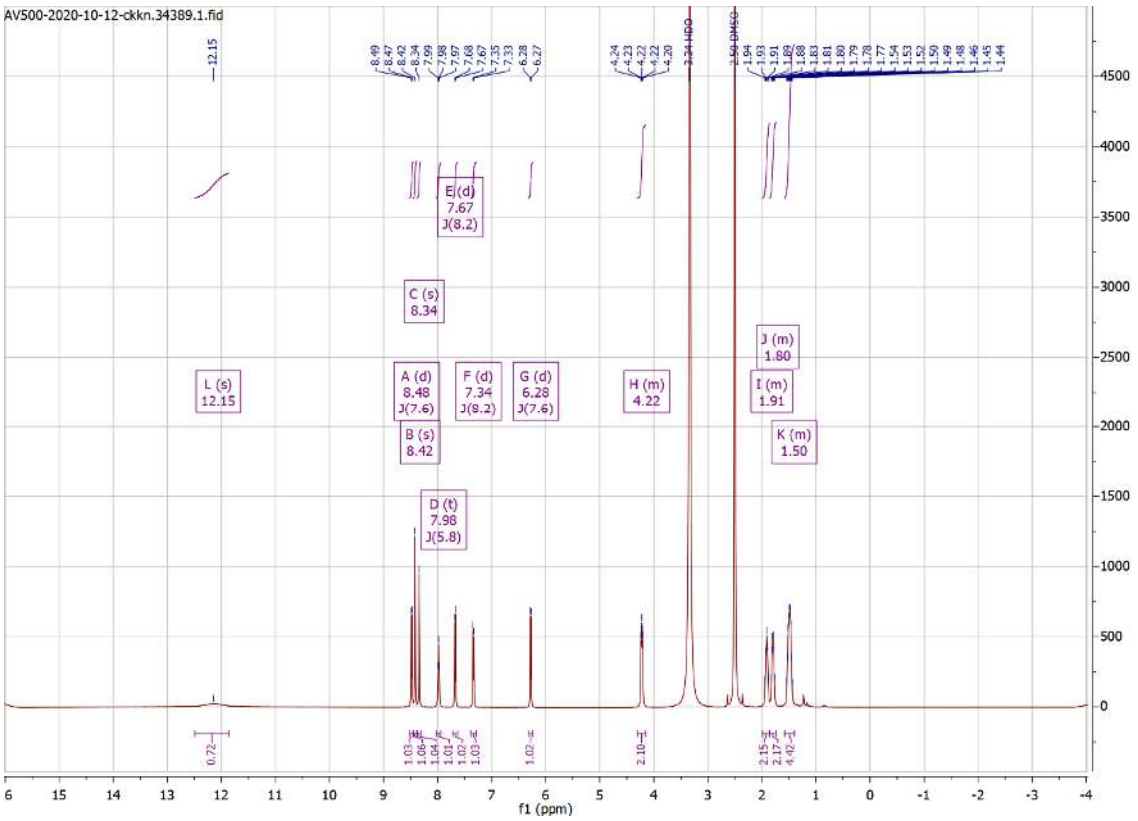
AV500-2020-10-12-ckkn.34389.1.fid
L (s) 12.15
A (d) 8.48 J(7.6)
B (s) 8.42
C (s) 8.34
D (t) 7.98 J(5.8)
E(d) 7.67 J(8.2)
F (d) 7.34 J(8.2)
G (d) 6.28 J(7.6)
H (m) 4.22
I (m) 1.91
J (m) 1.80
K (m) 1.50
f1 (ppm)

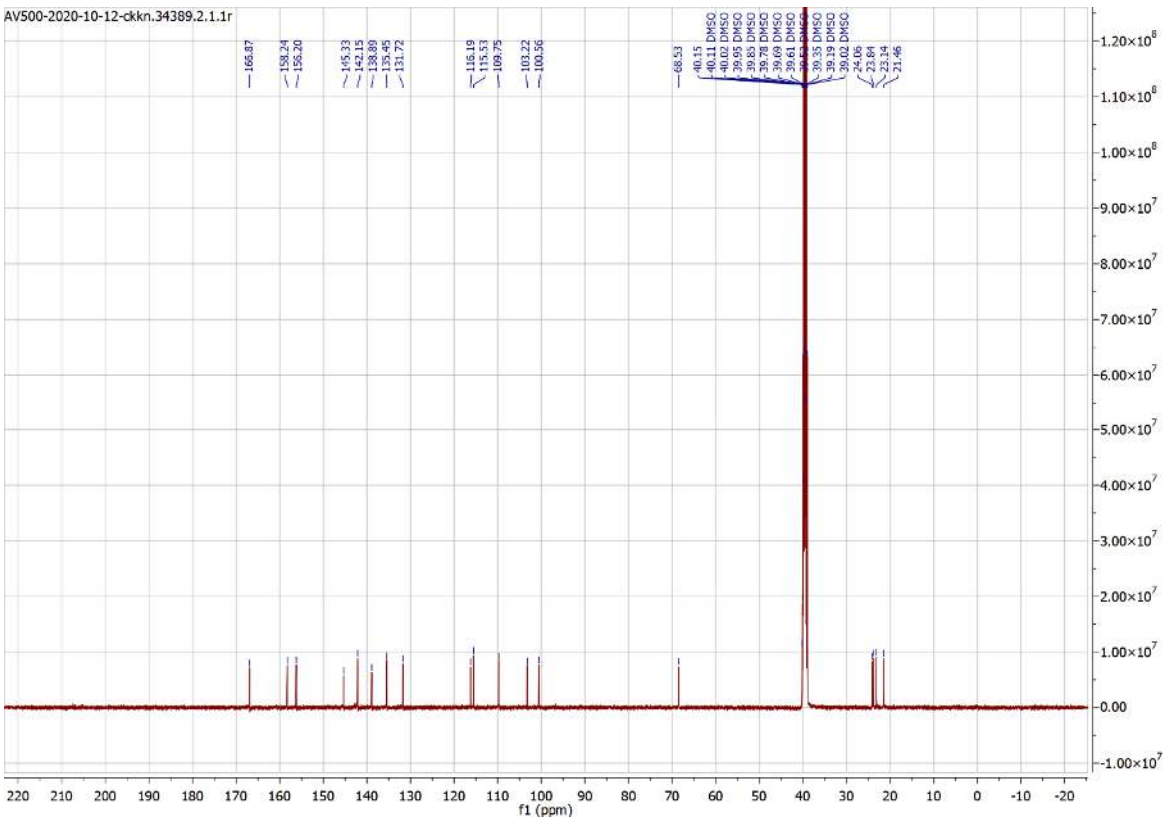
AV500-2020-10-12-ckkn.34389.2.1.1r
f1 (ppm)

Compound **138**

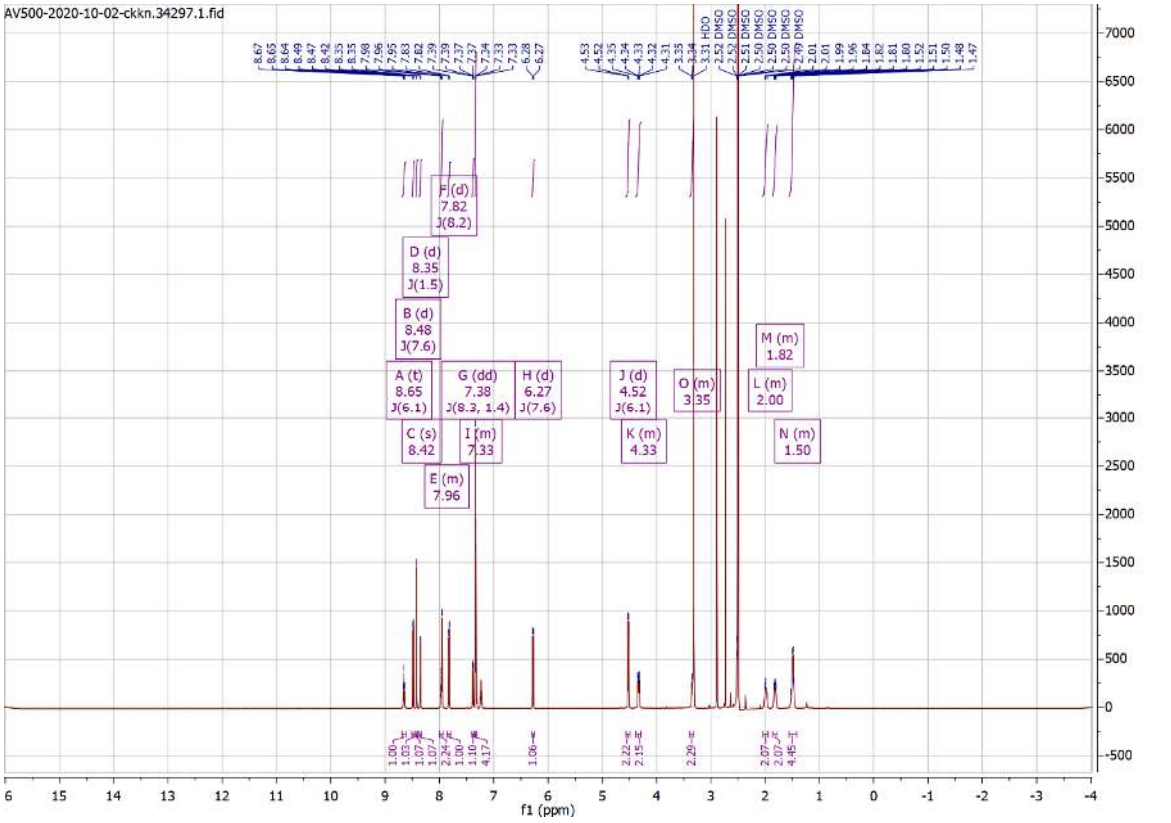

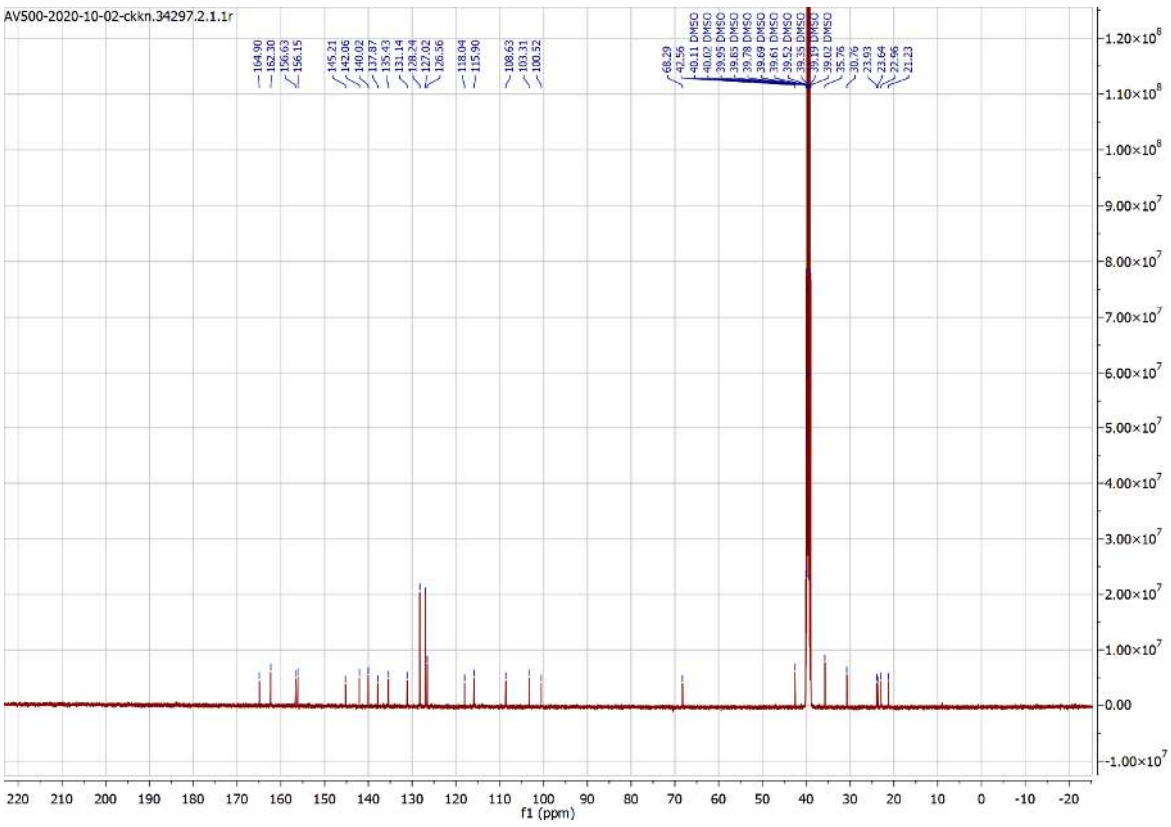

Compound **139**

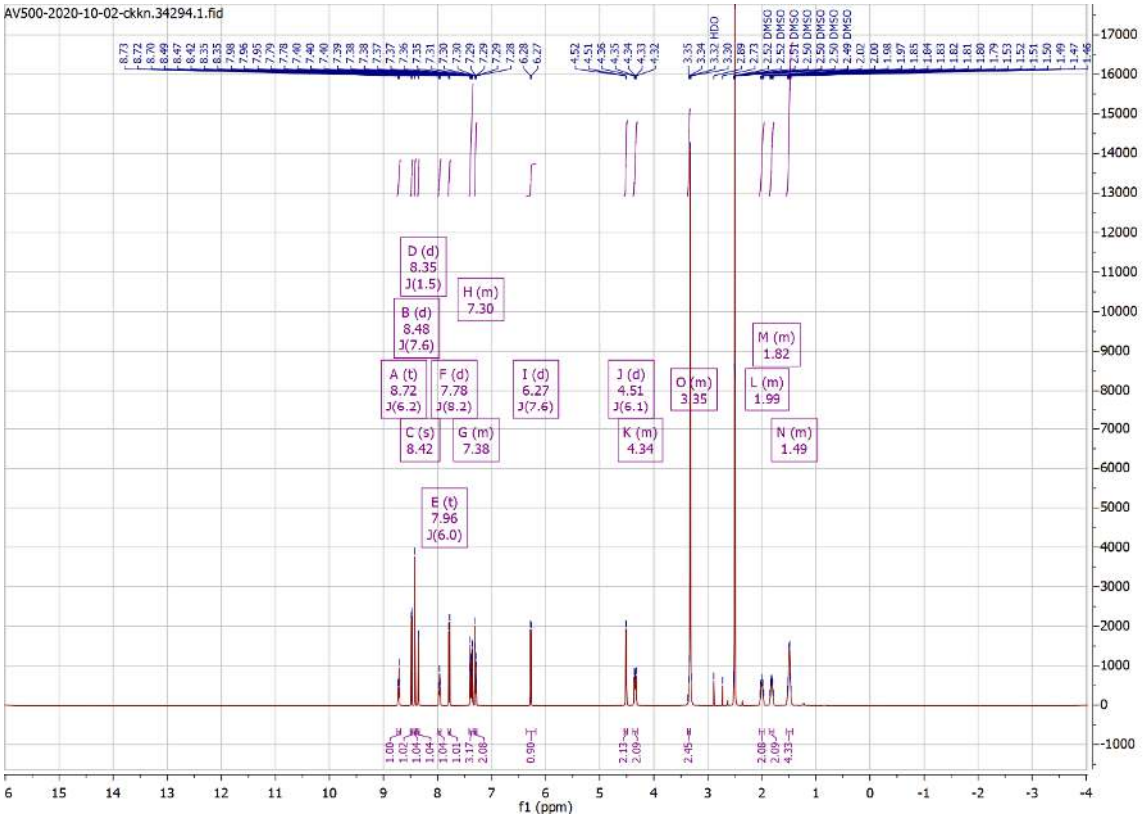

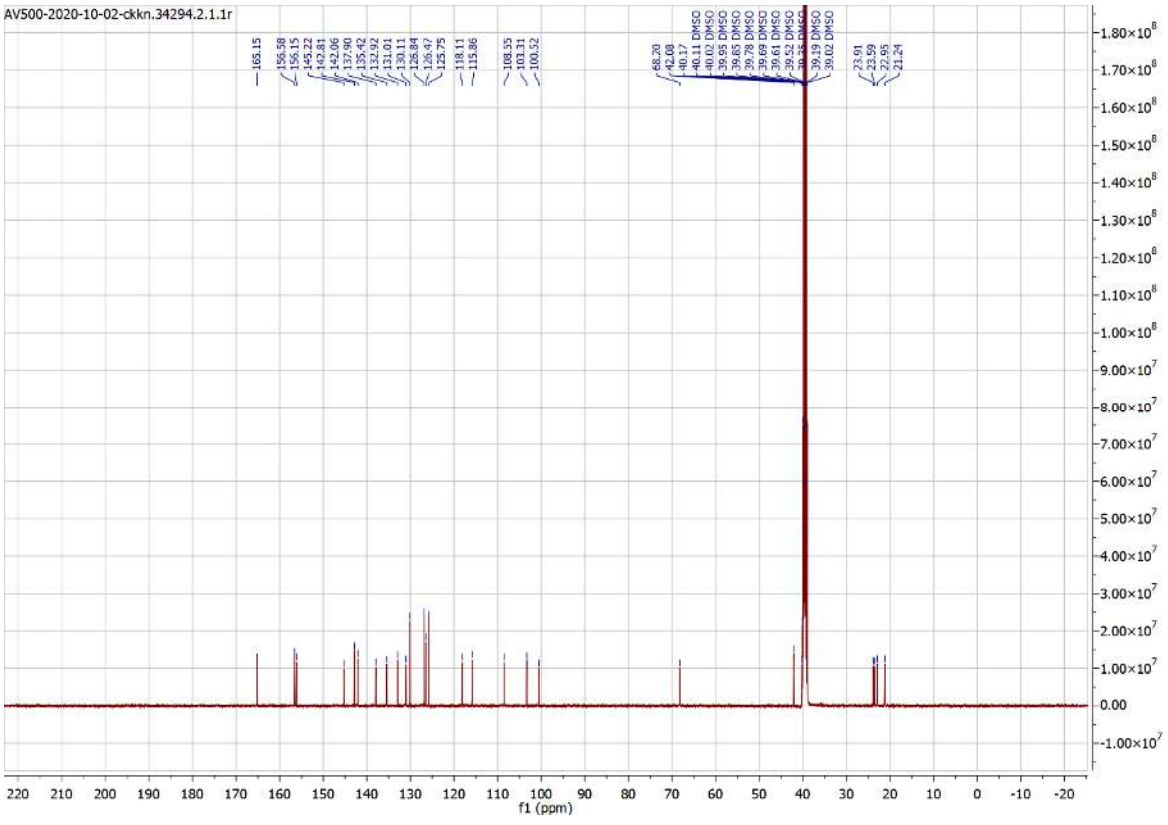

Compound **140**

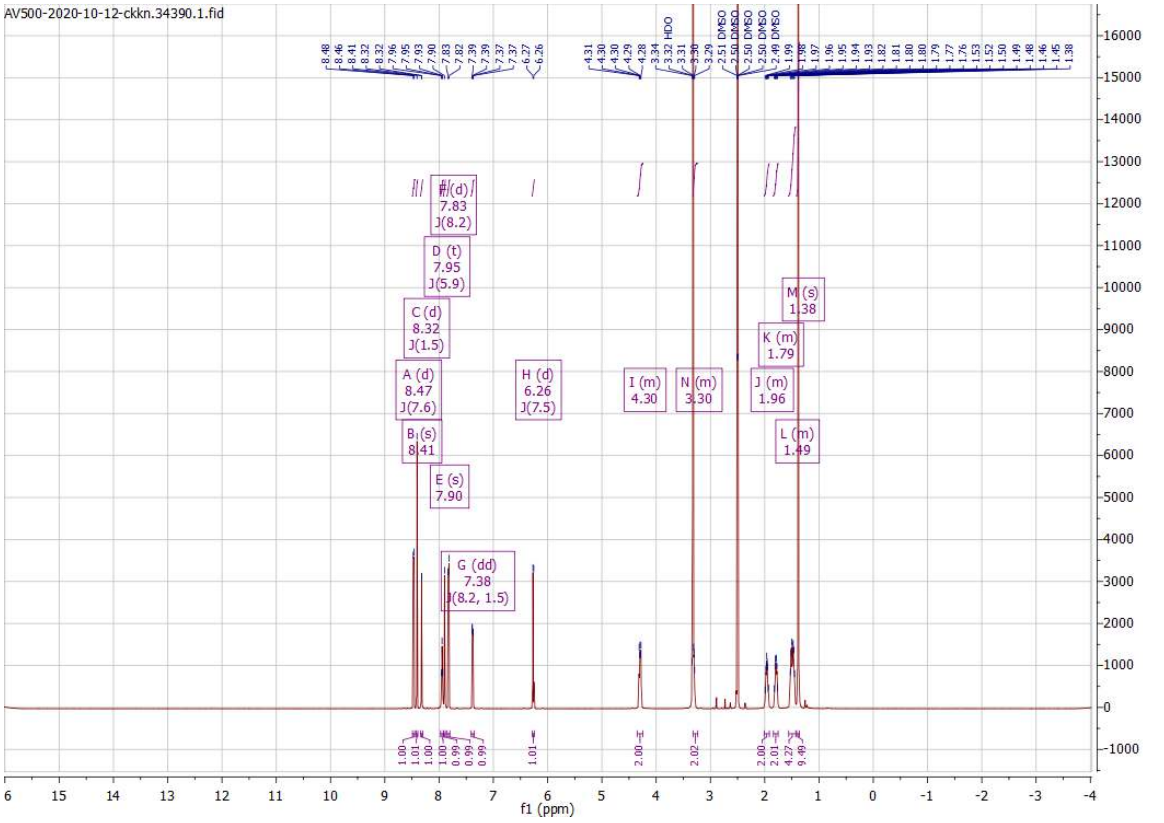

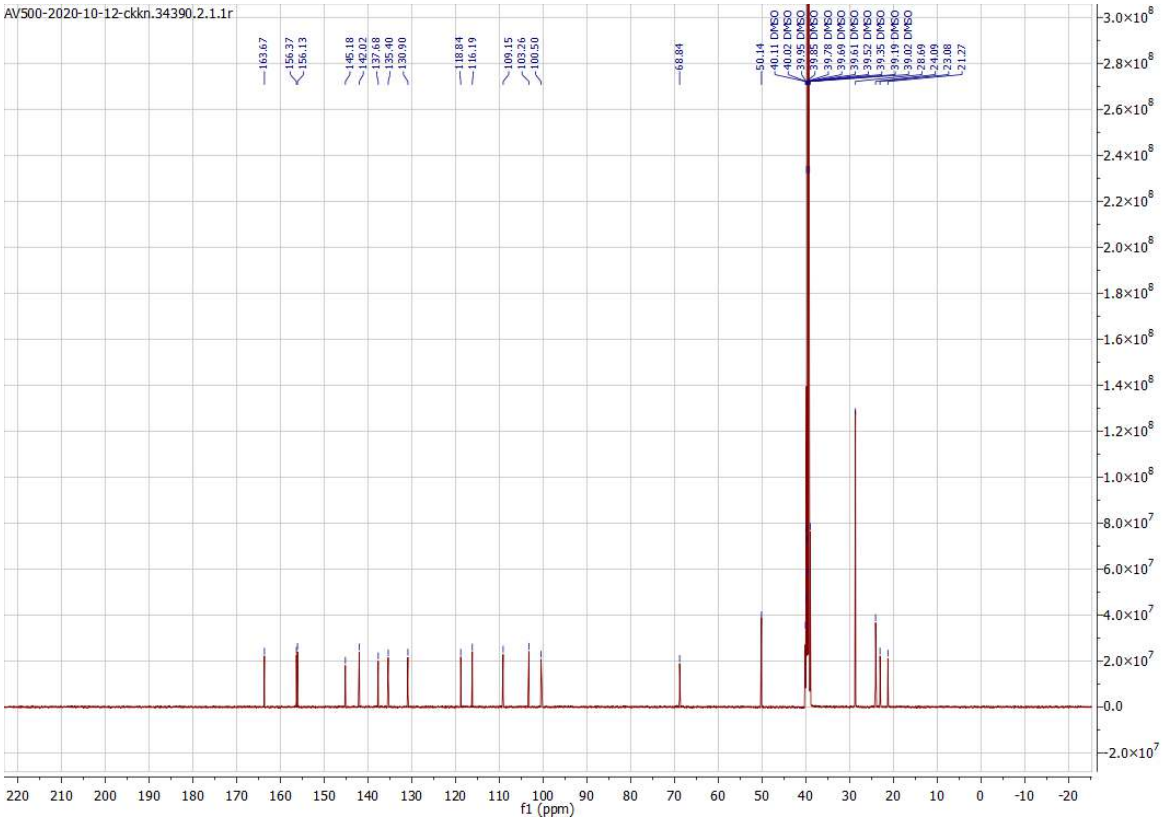

Compound **123**

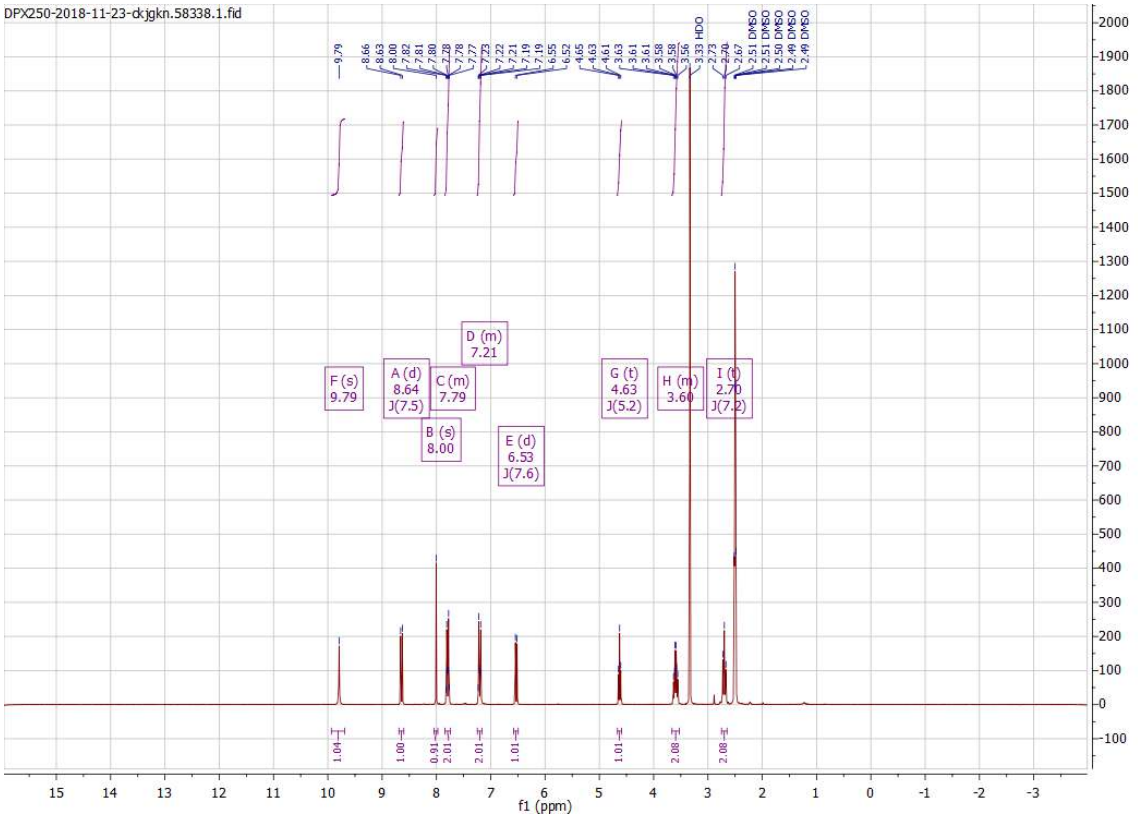

Compound **125**

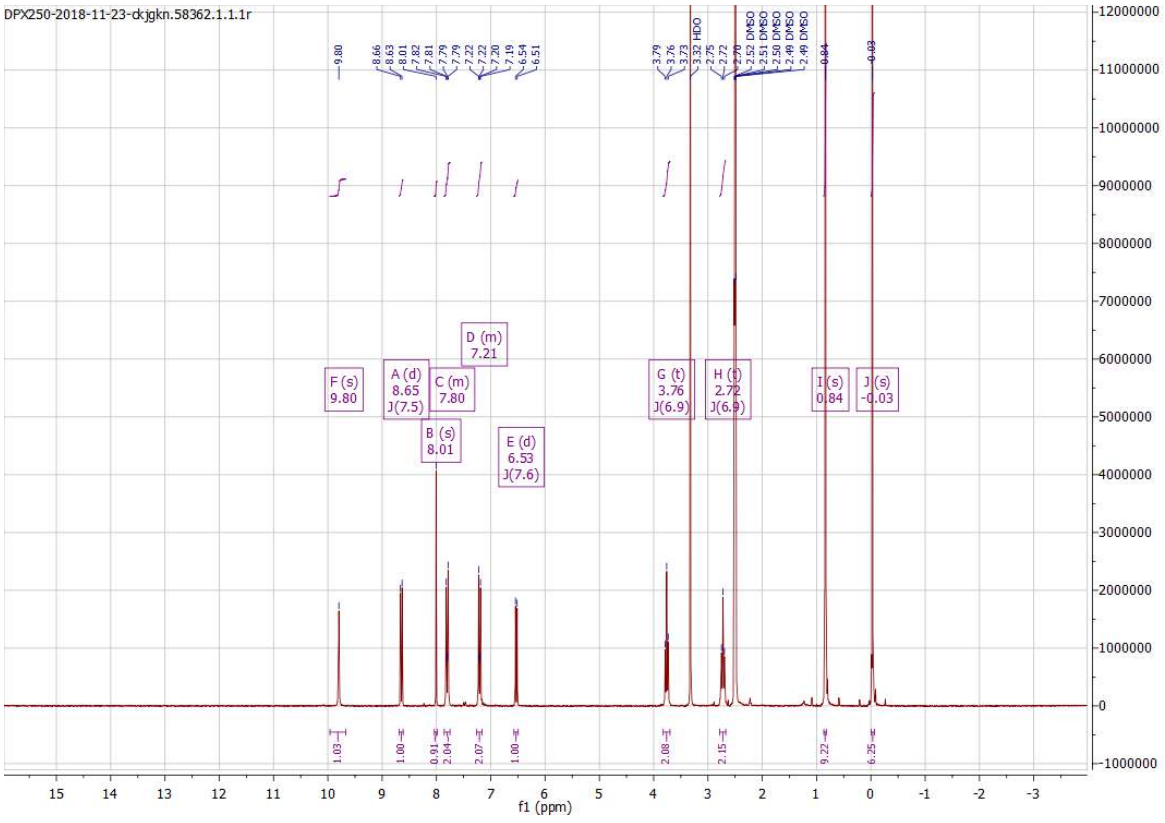

Compound **127**

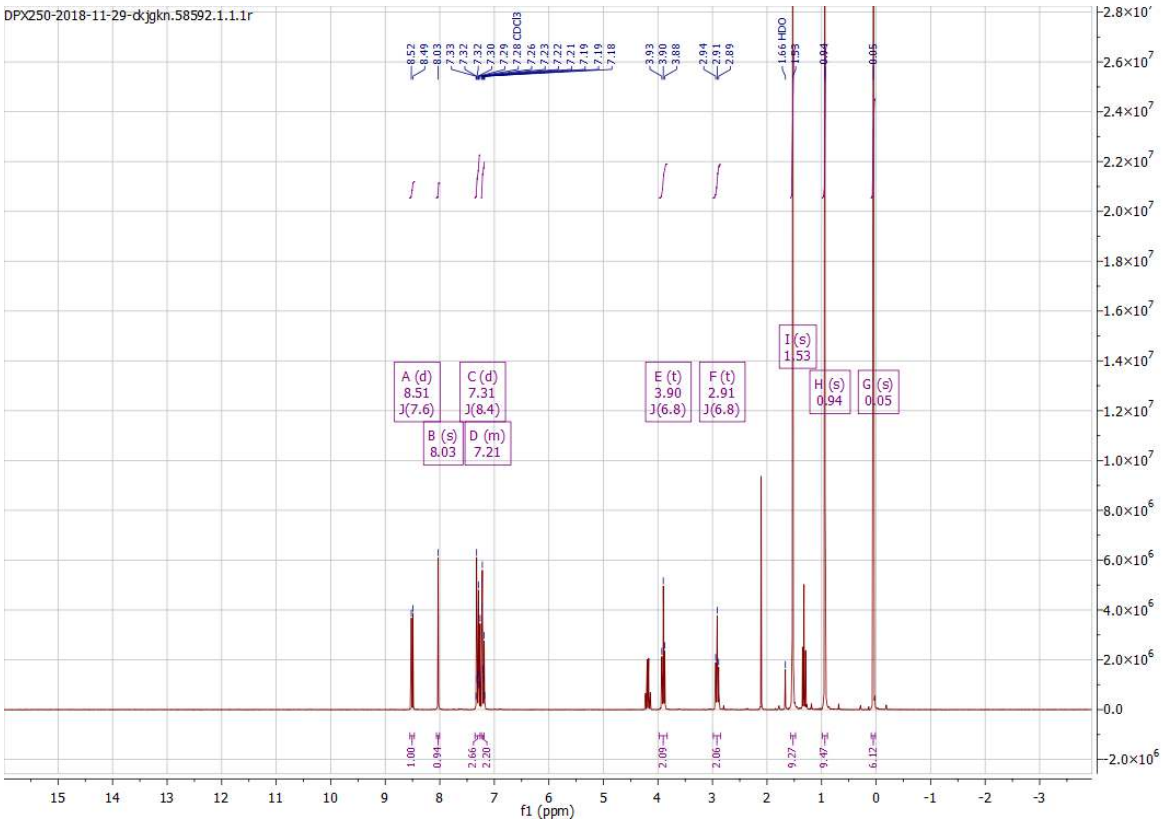

Compound **129**

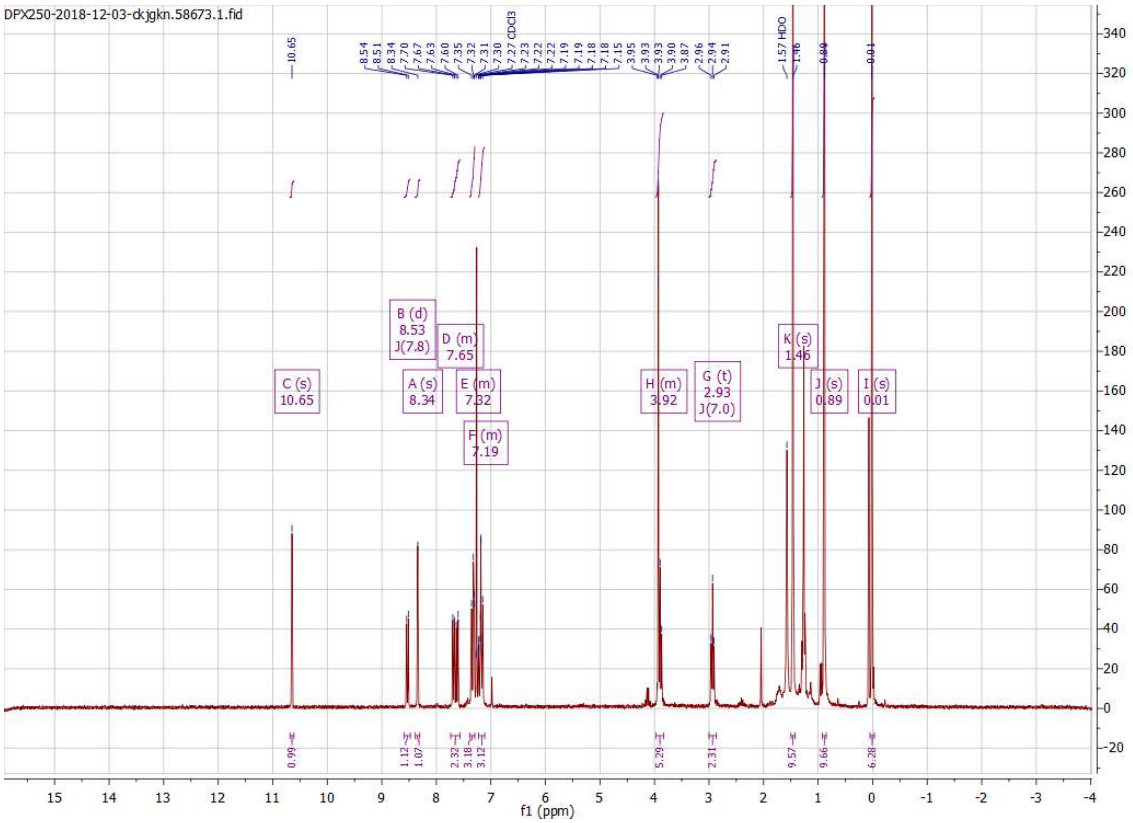

Compound **131**

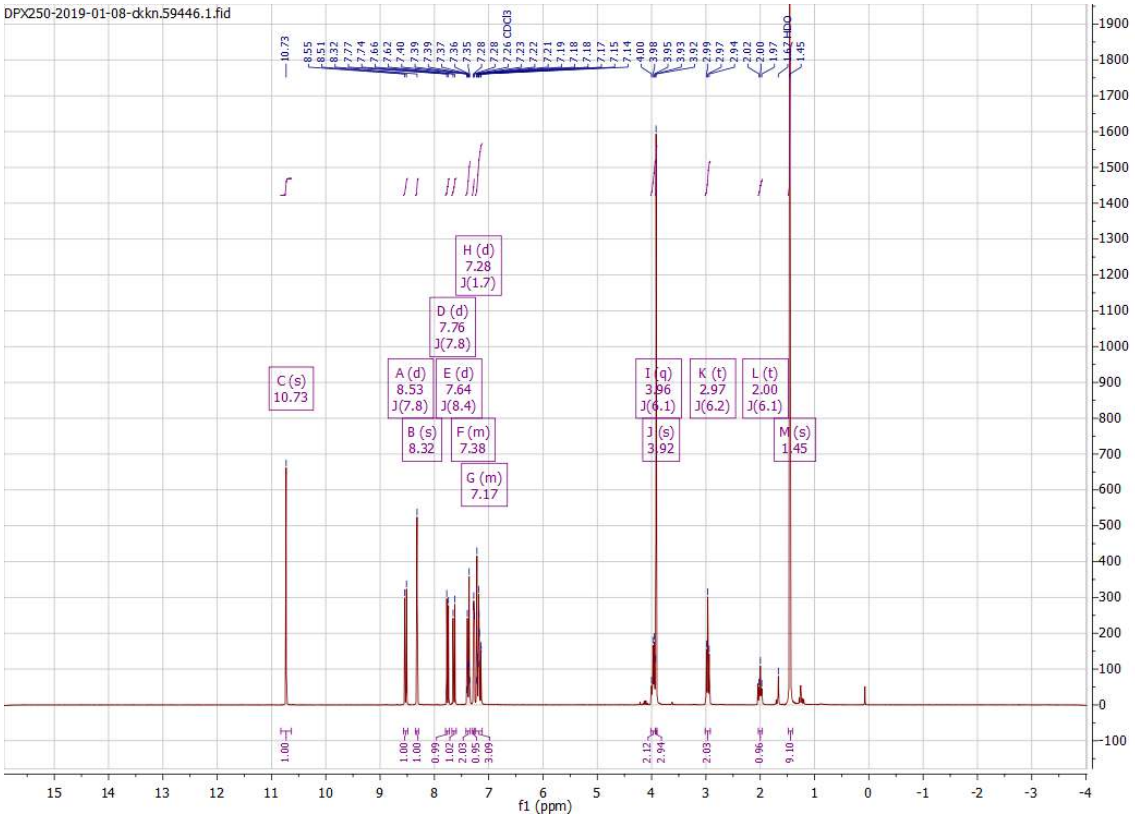

Compound **133**

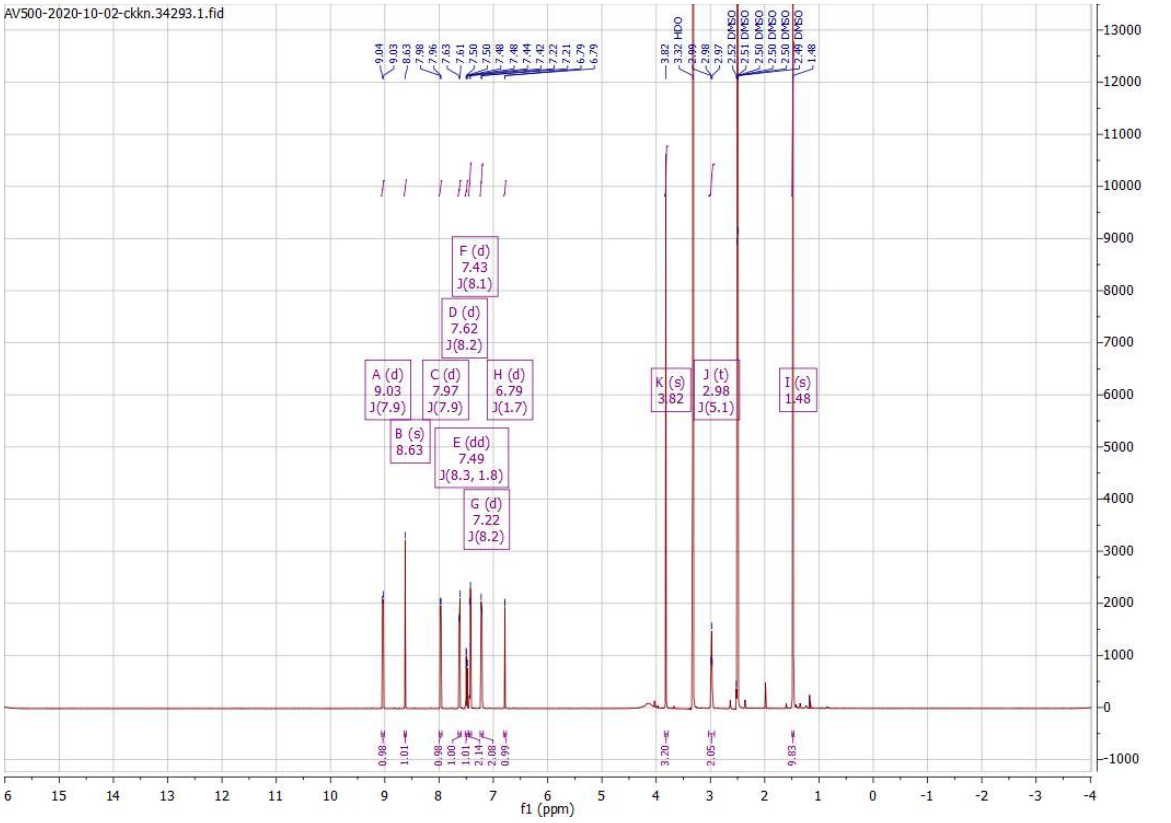

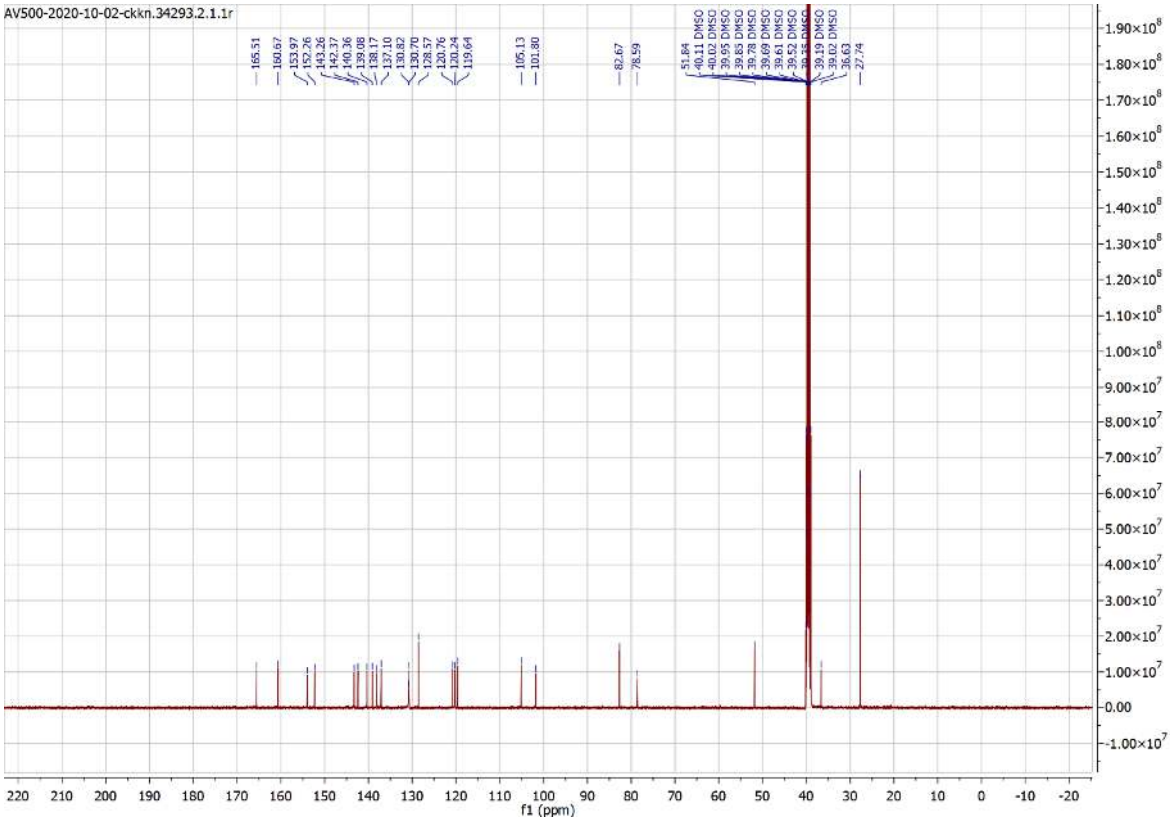

Compound **135**

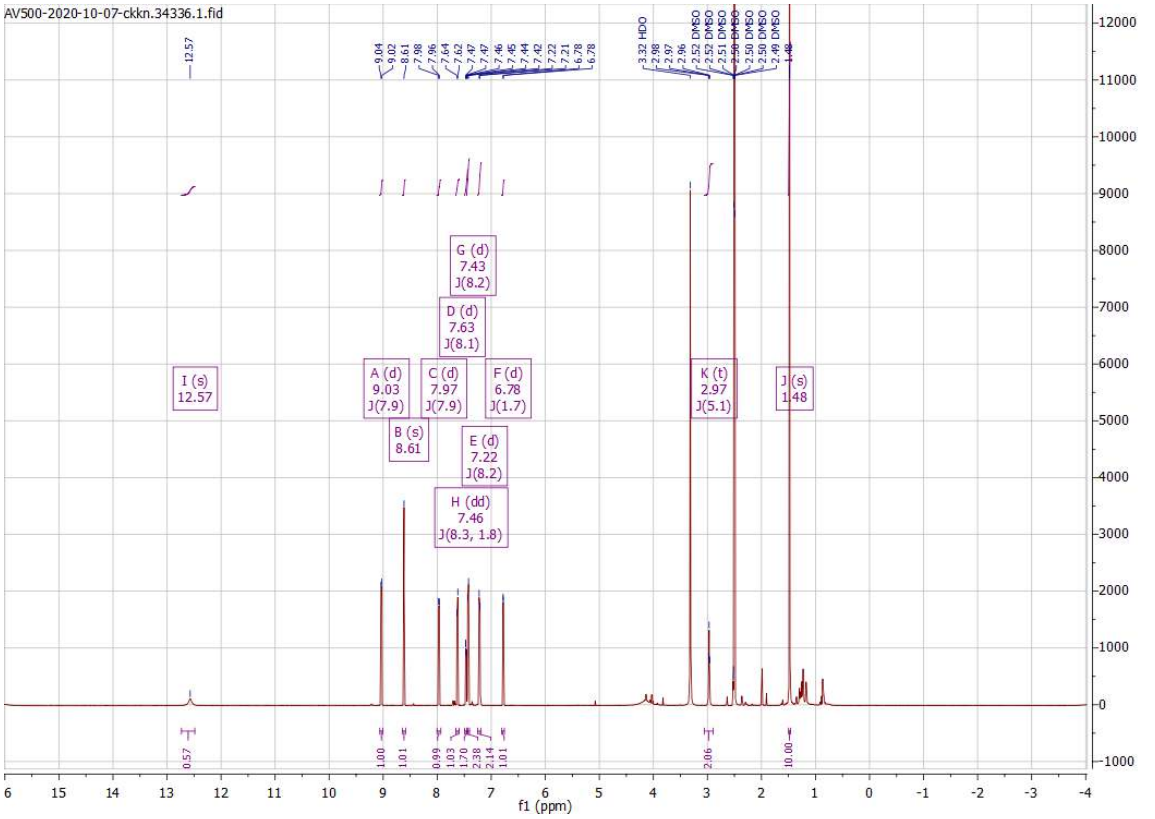

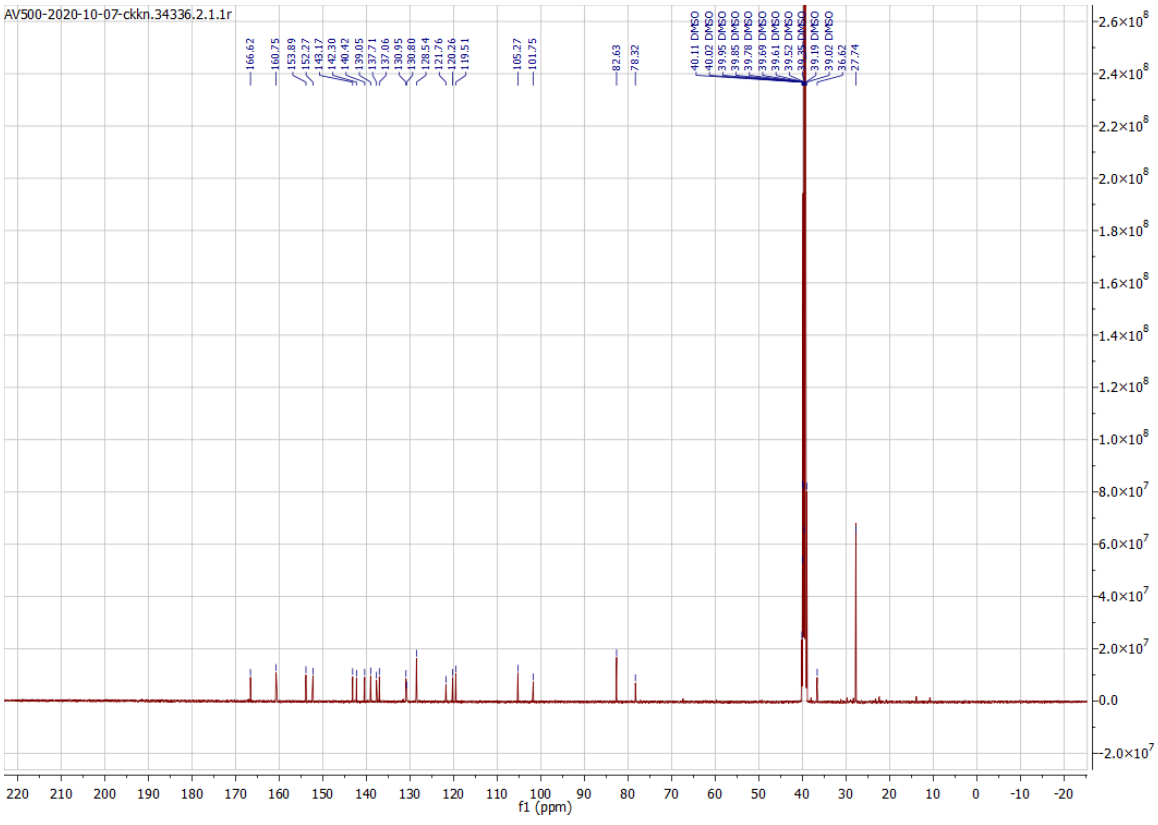

Compound **137**

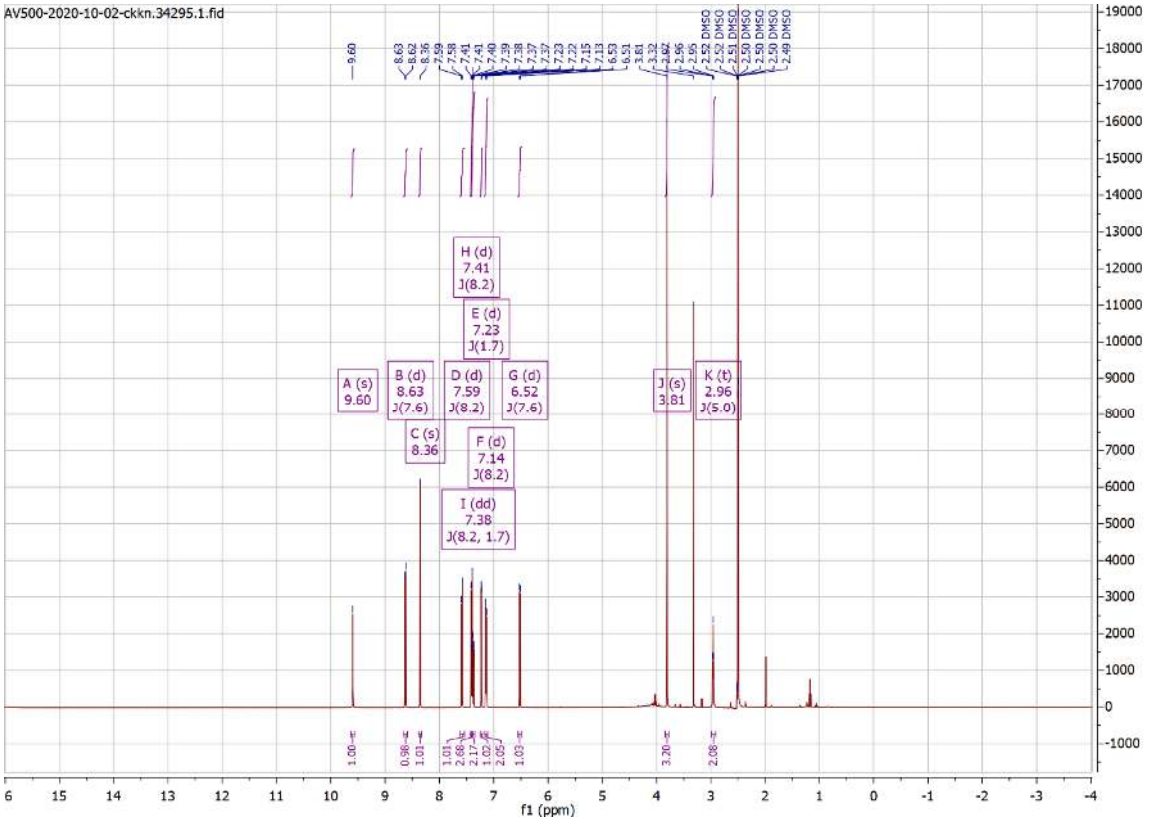

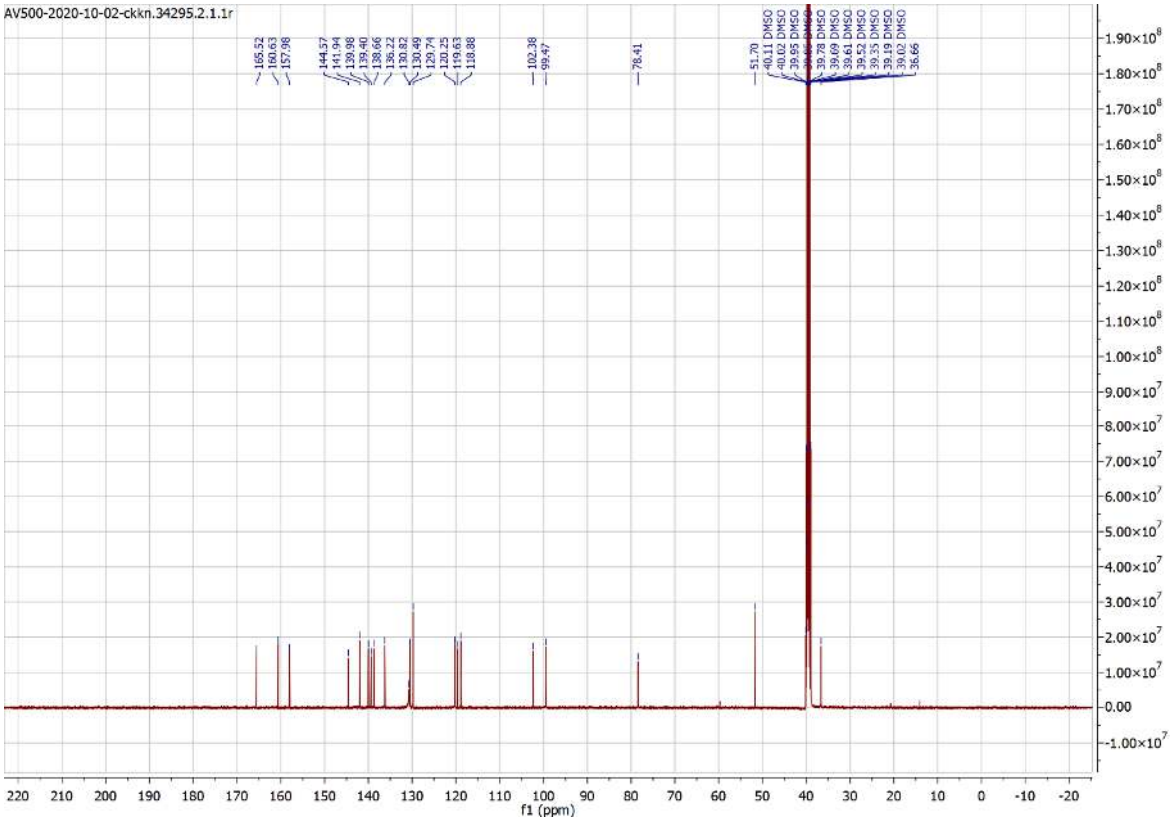

Compound **139**

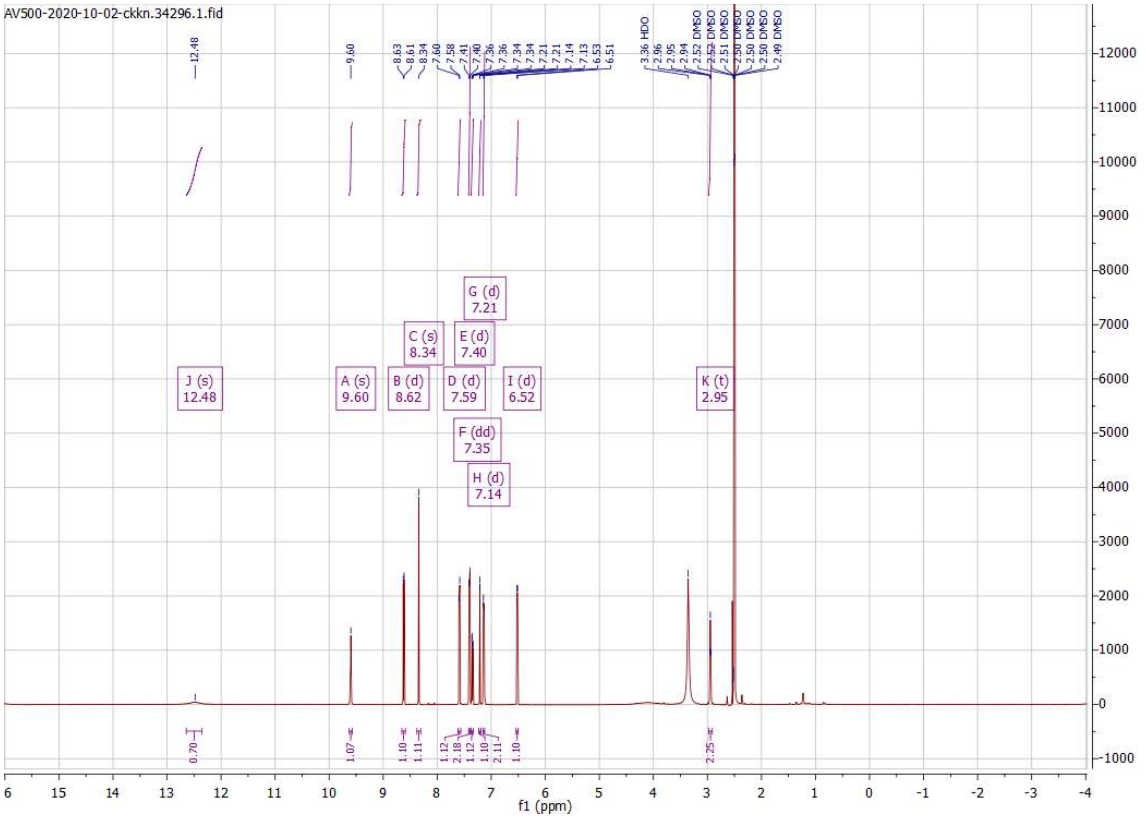

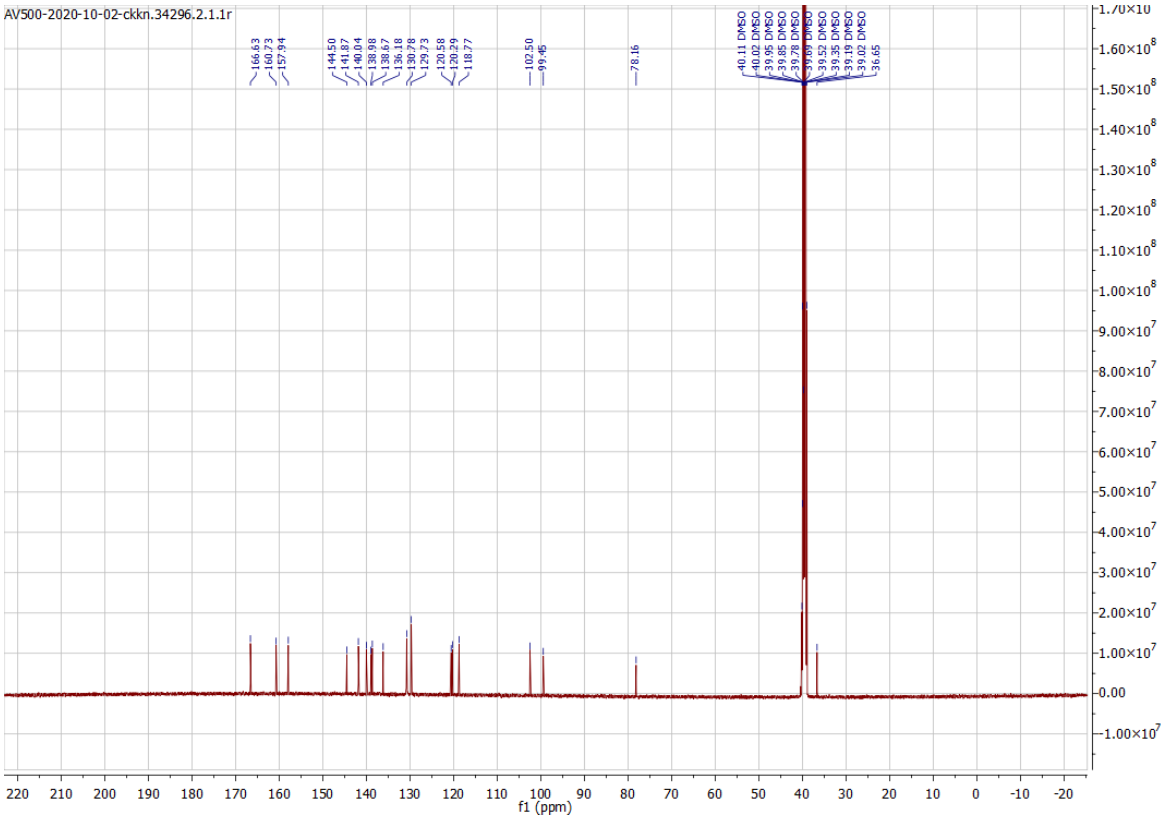

Compound **141**

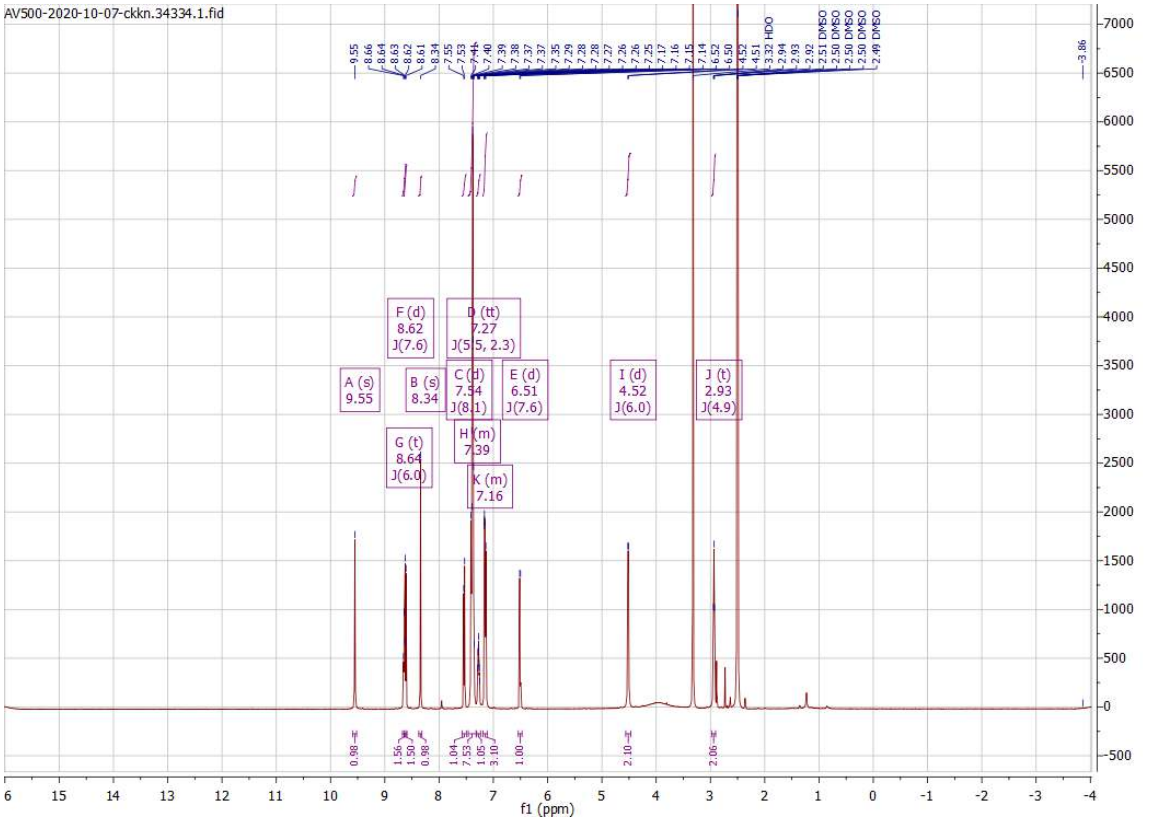

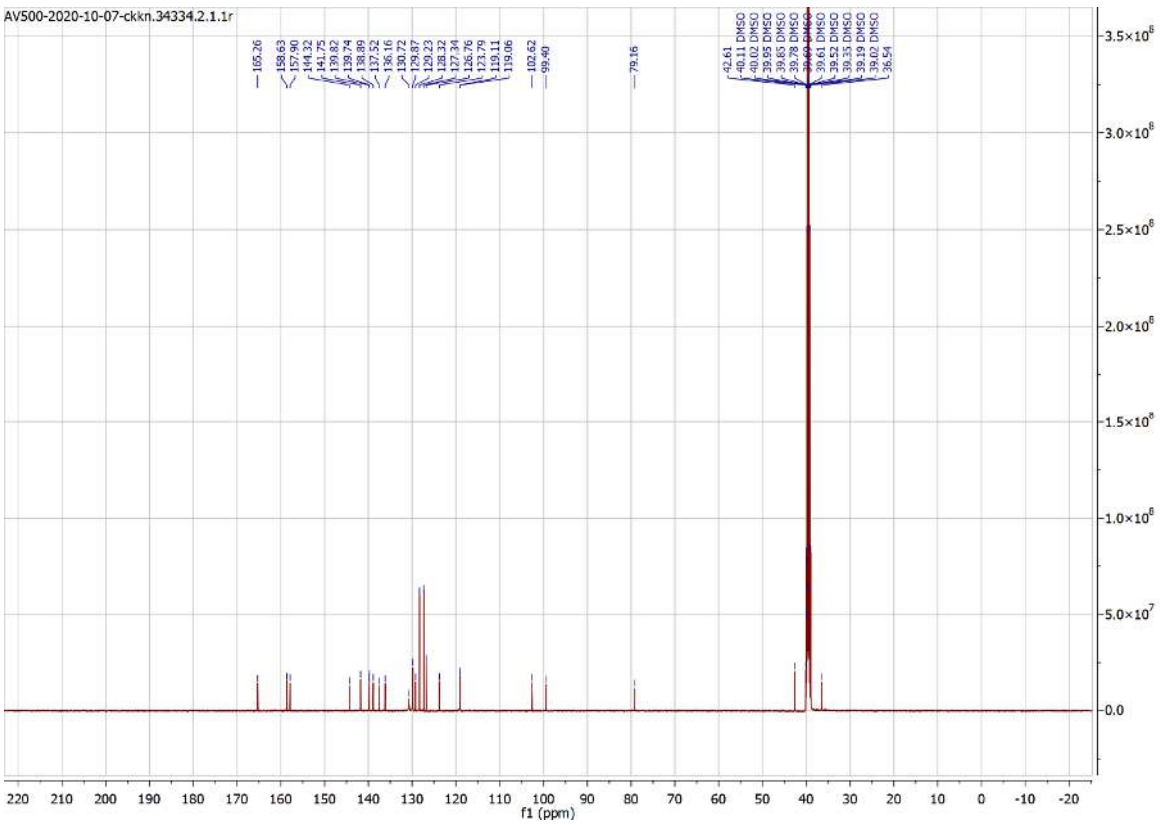

Compound **142**

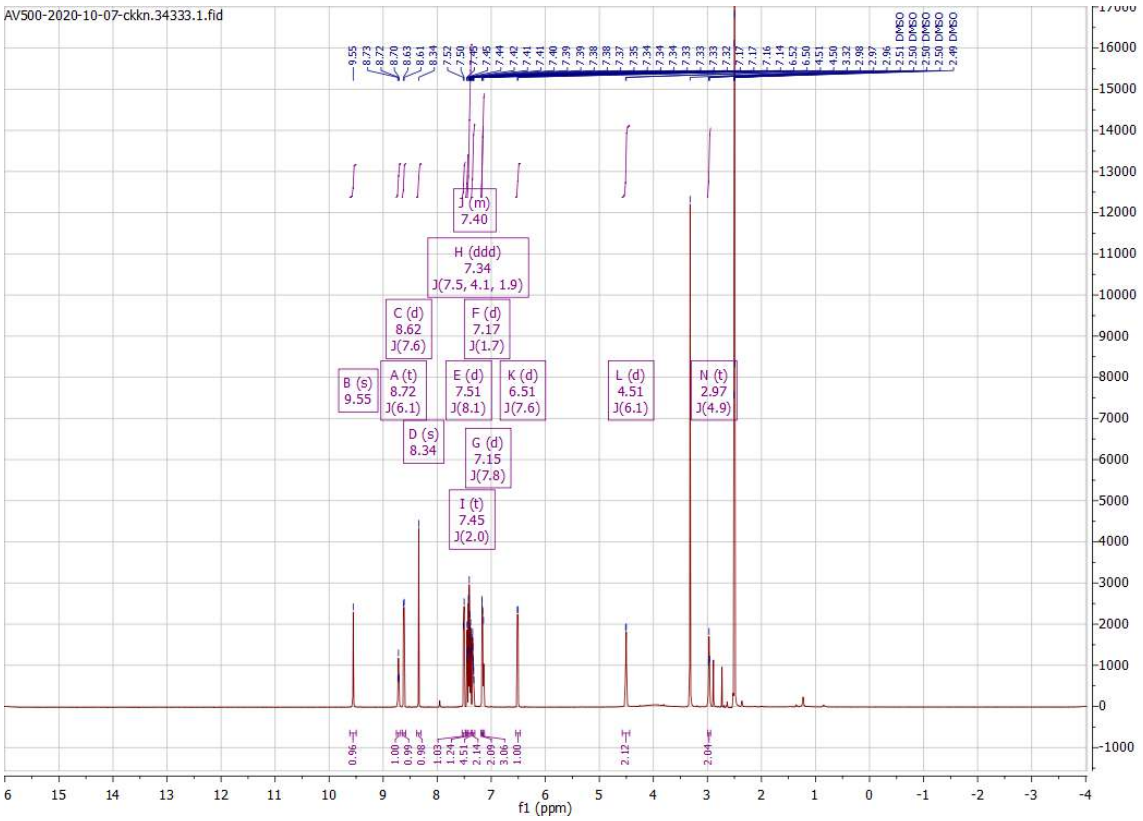

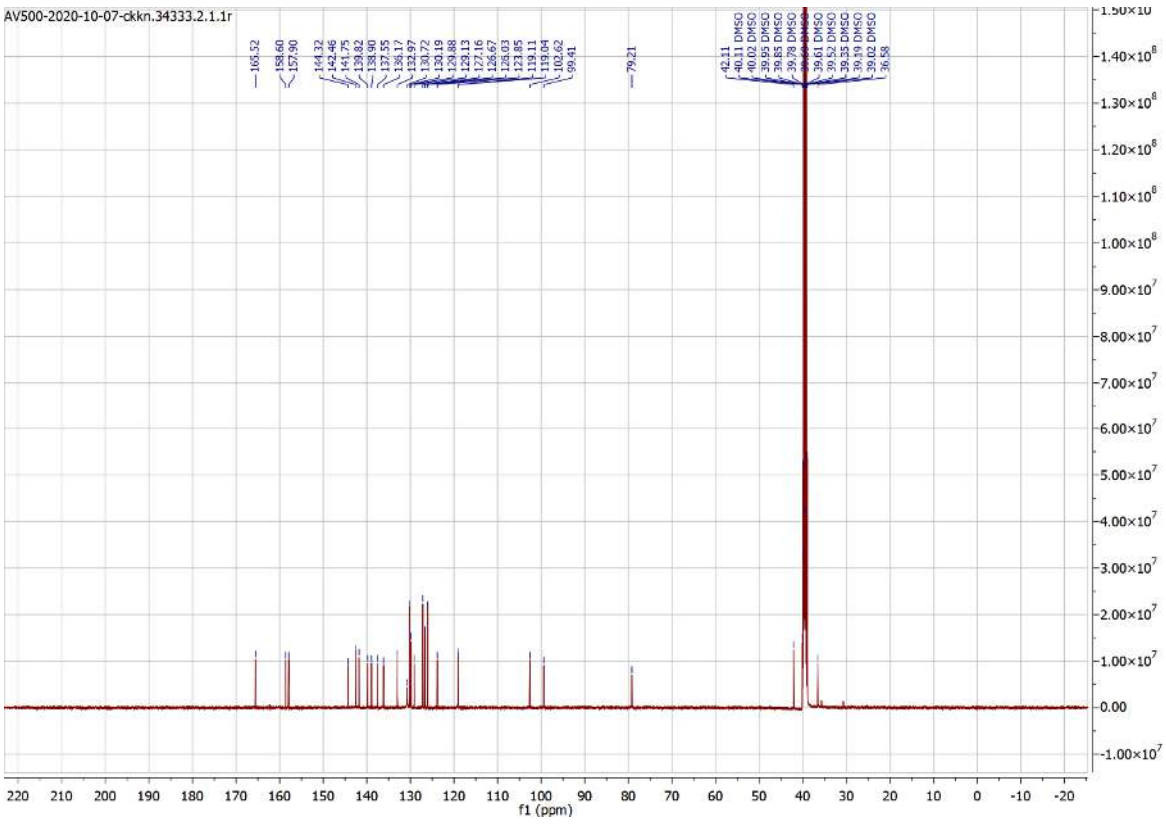

Compound **143**

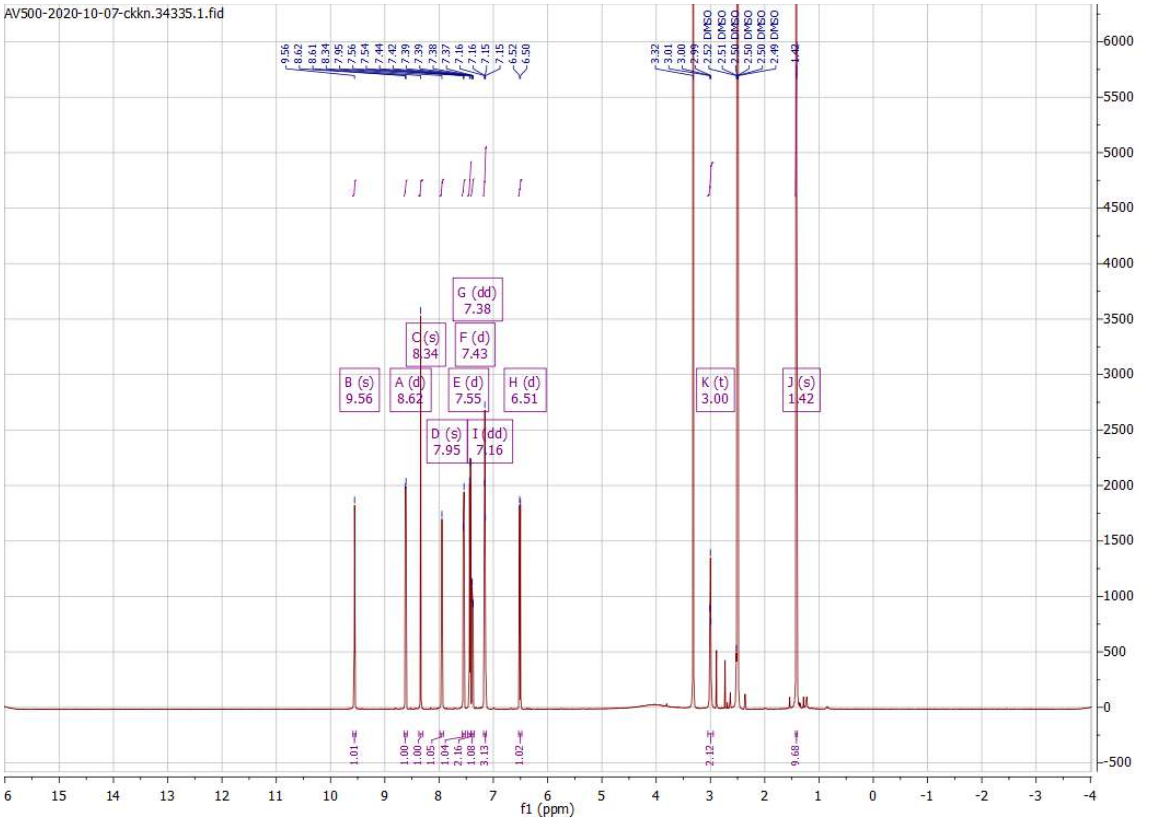

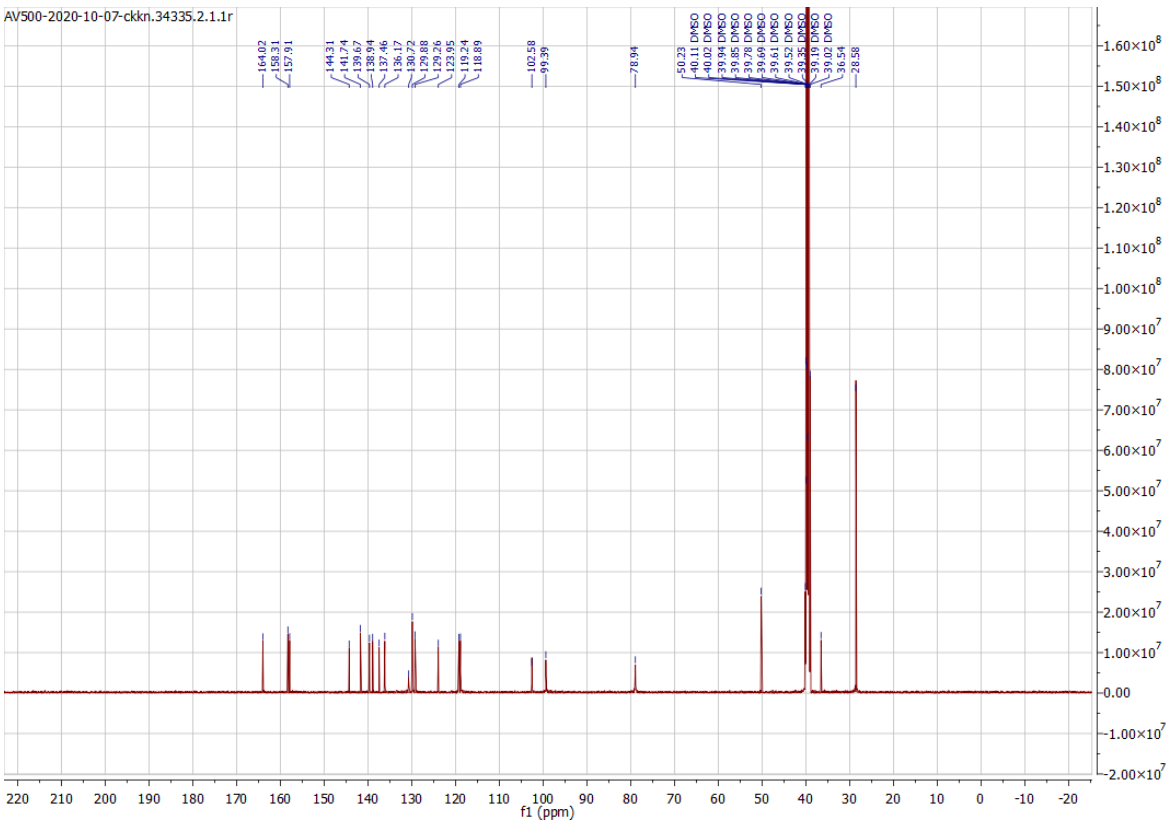

Compound **144**

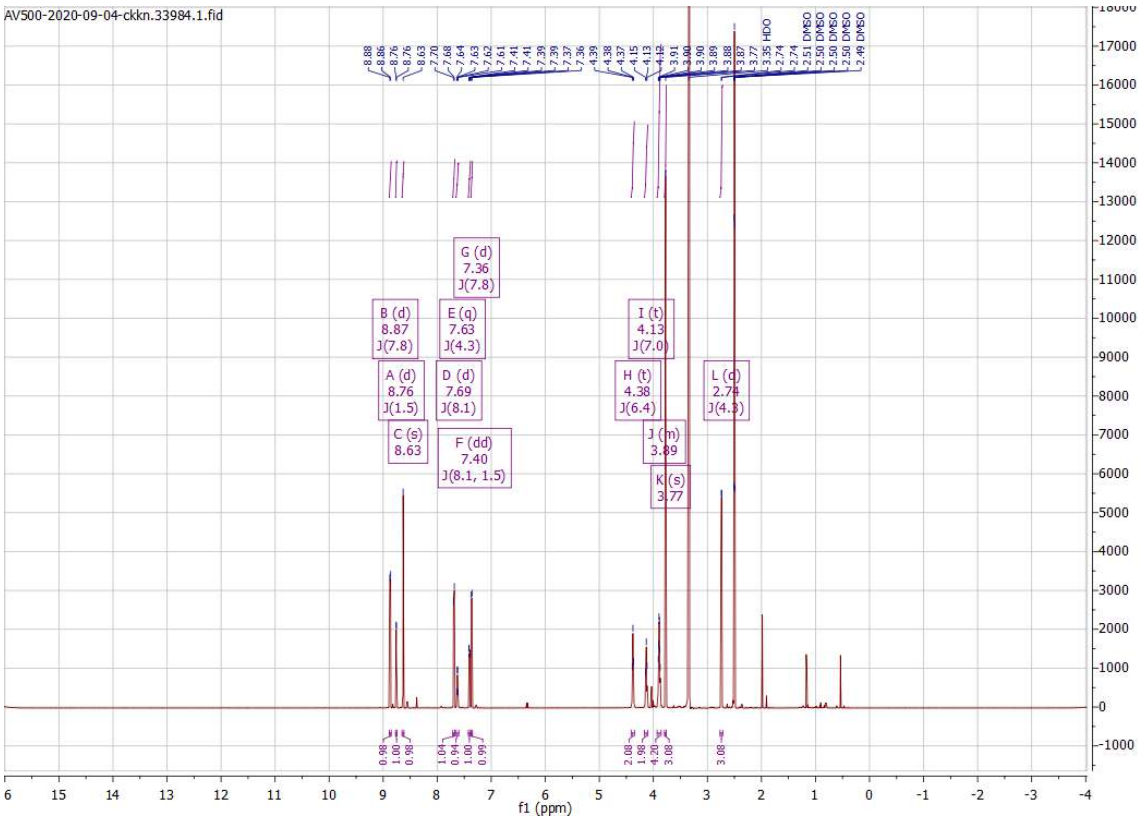

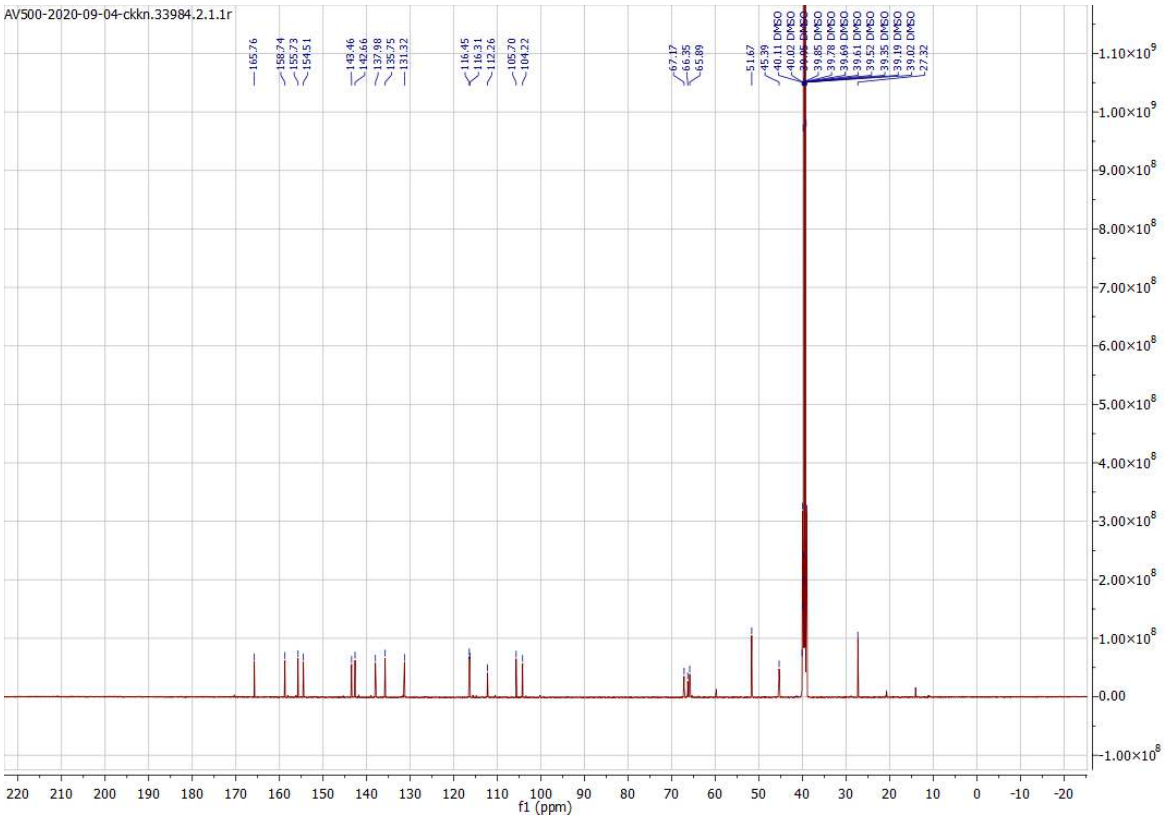

Compound **145**

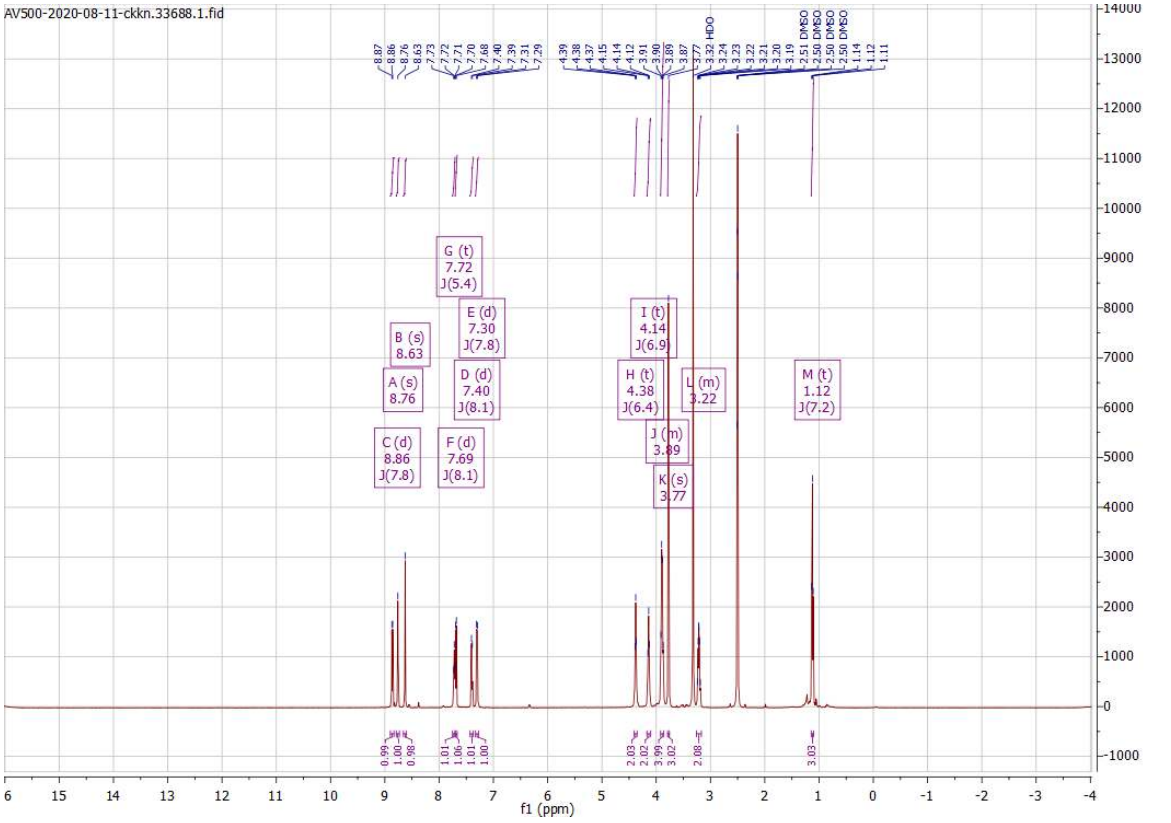

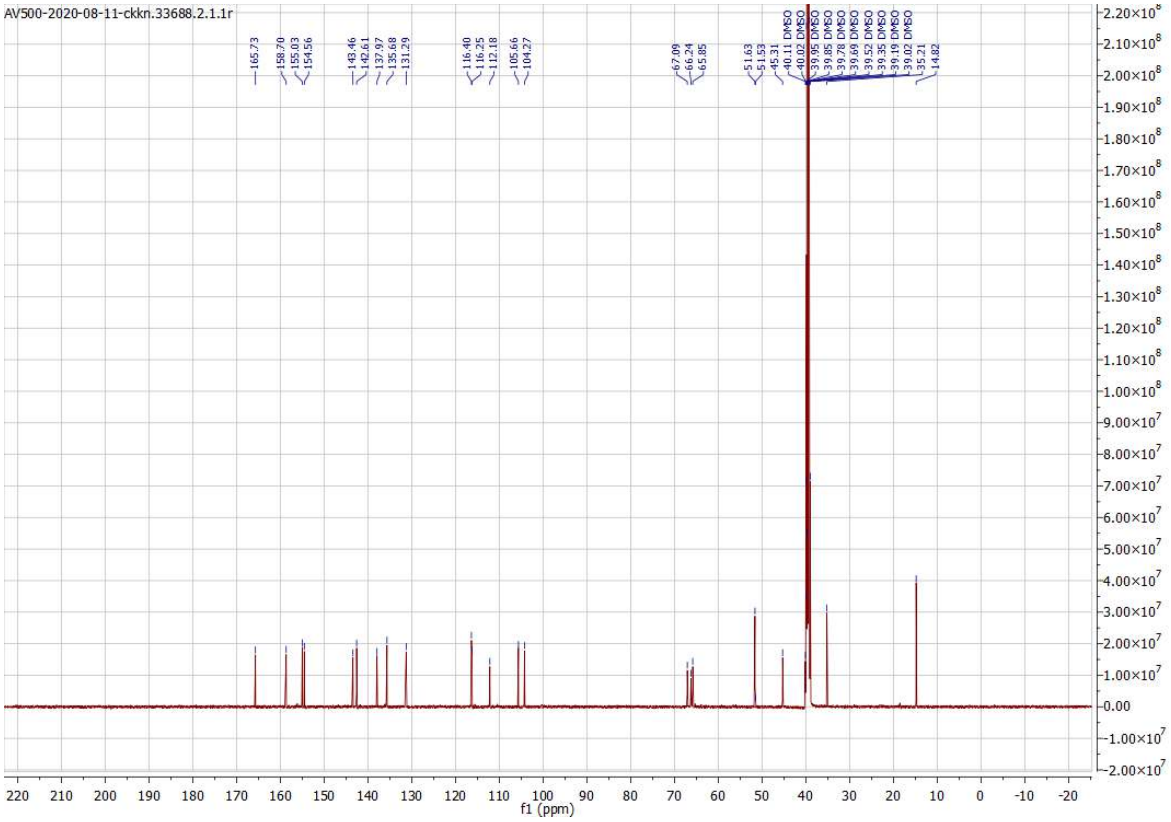

Compound **146**

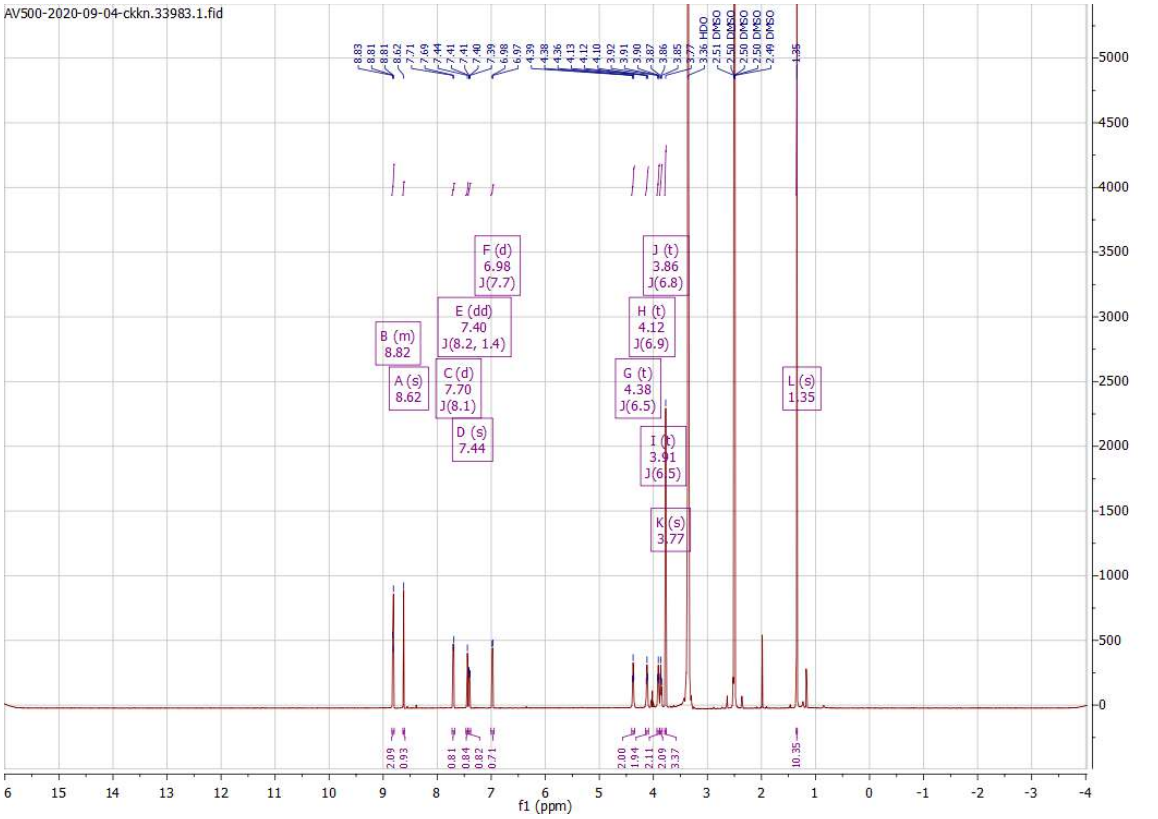

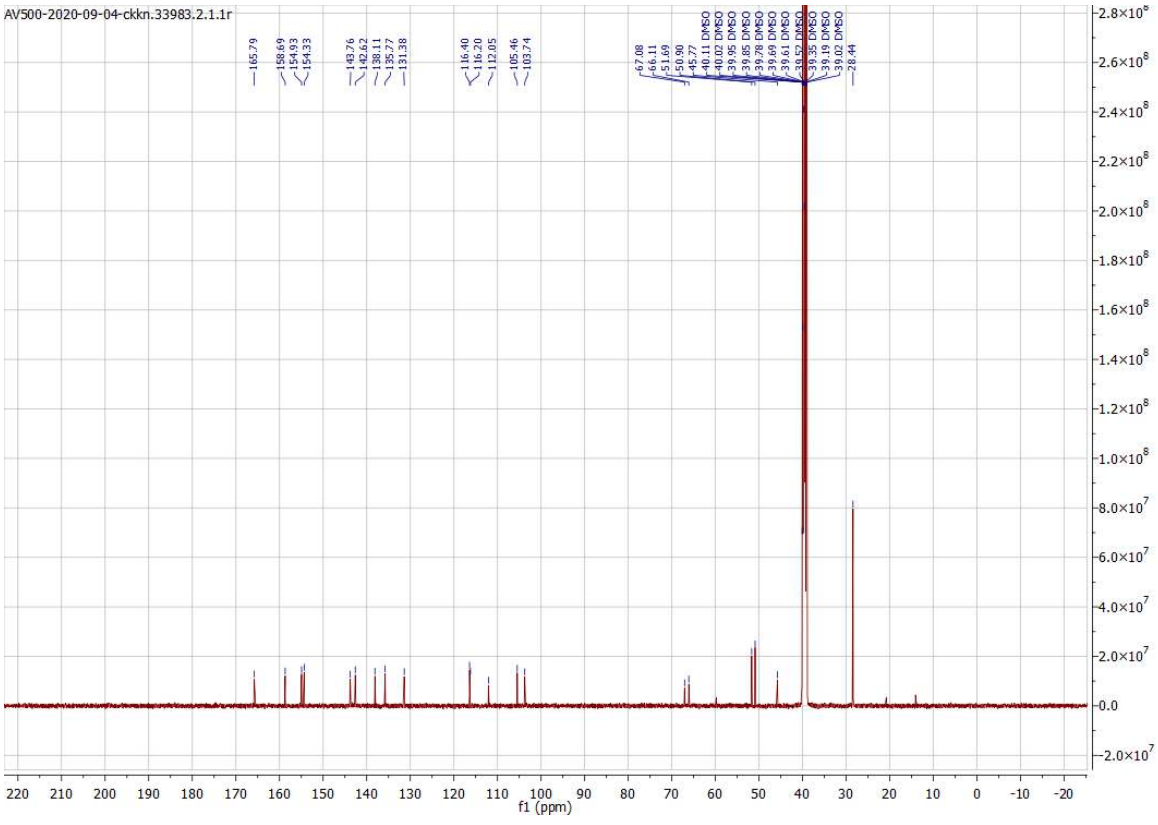

Compound **147**

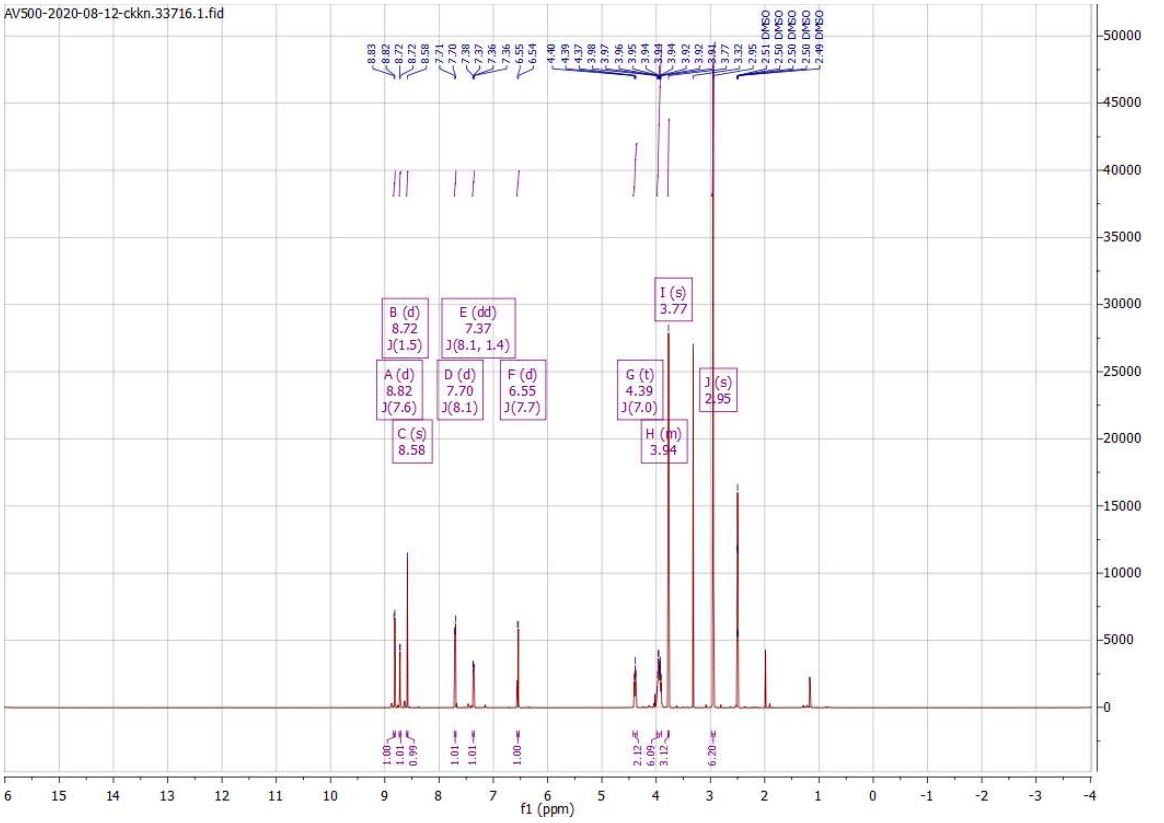

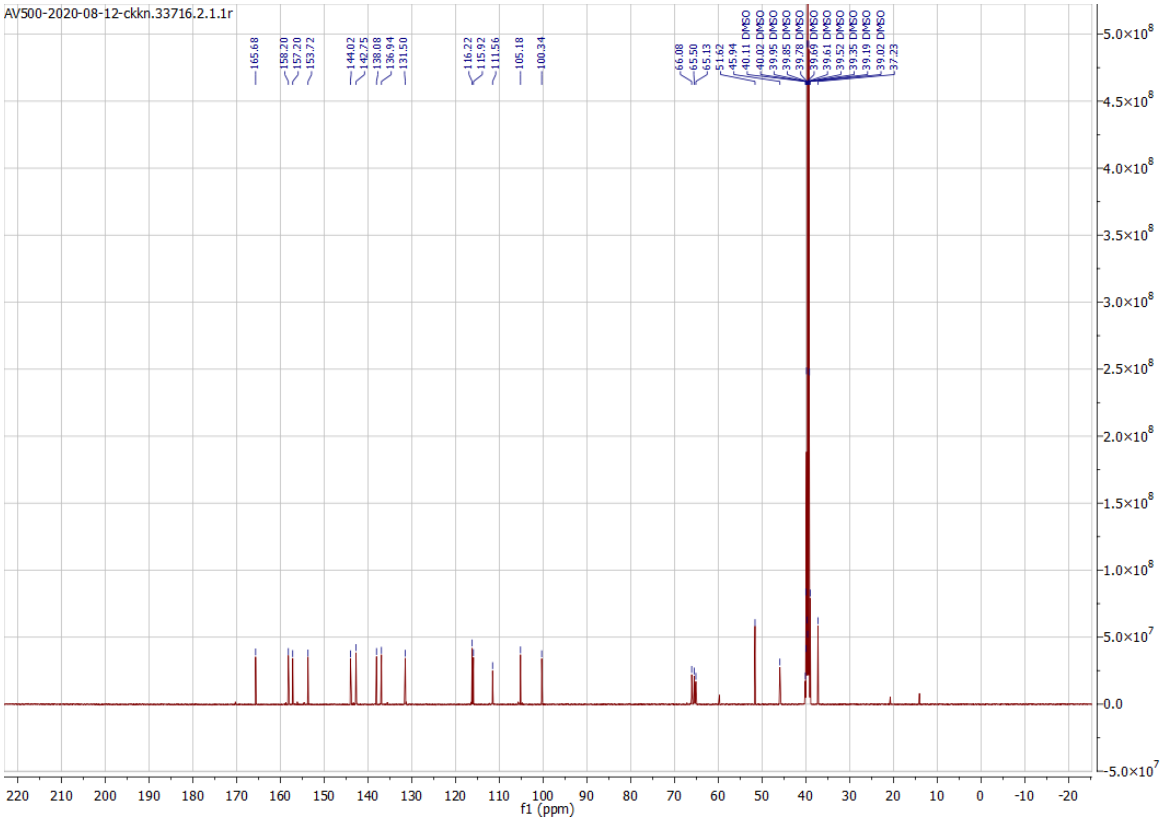

Compound **148**

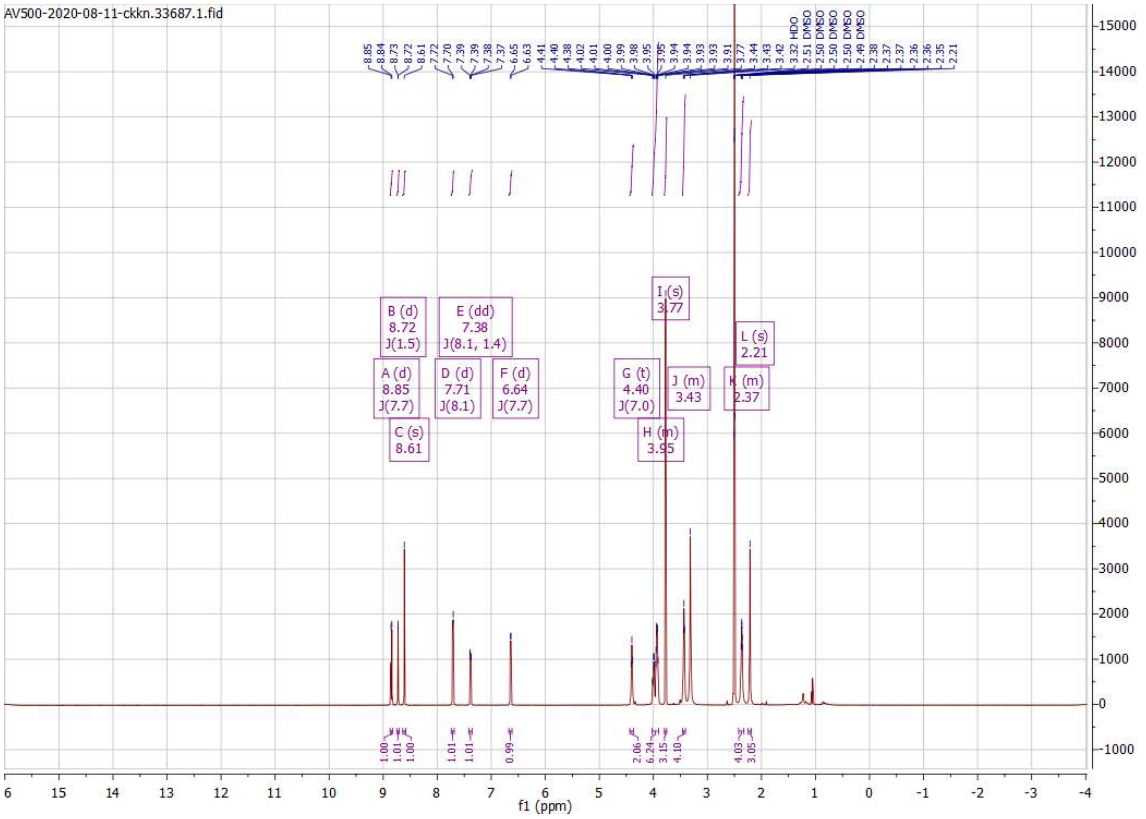

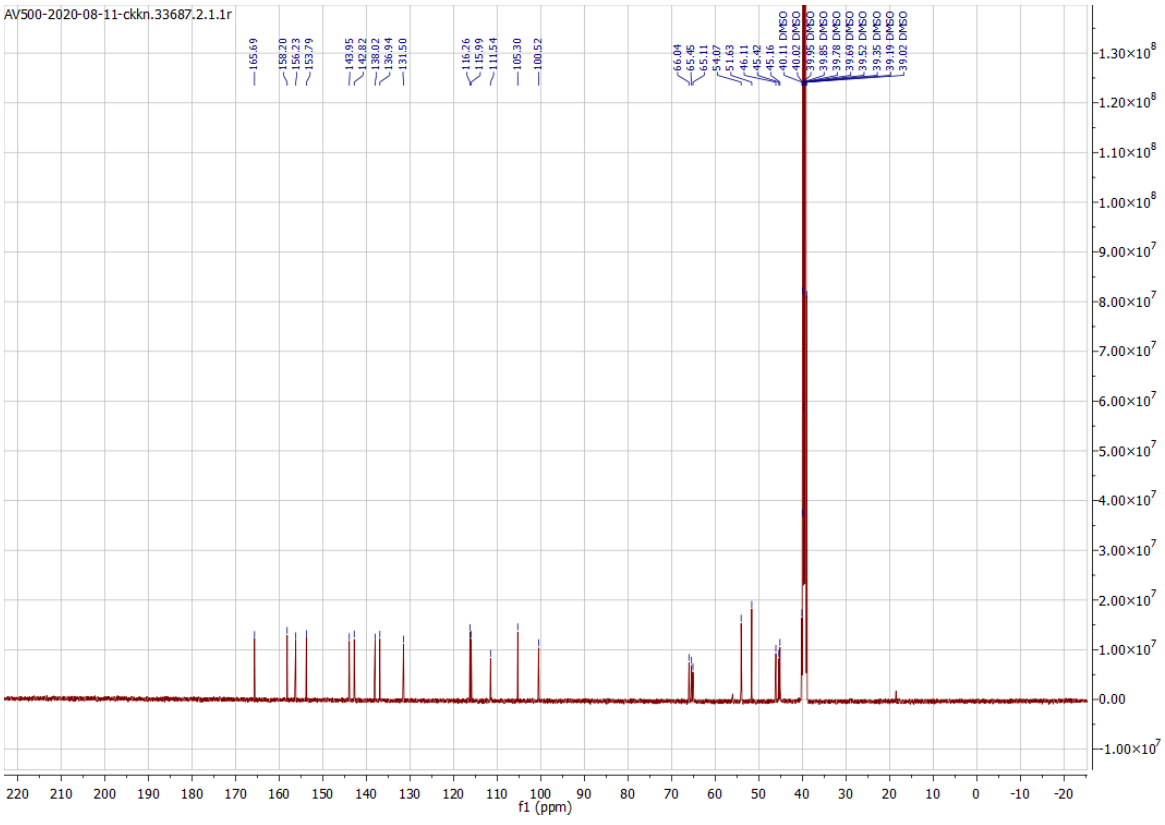

Compound **149**

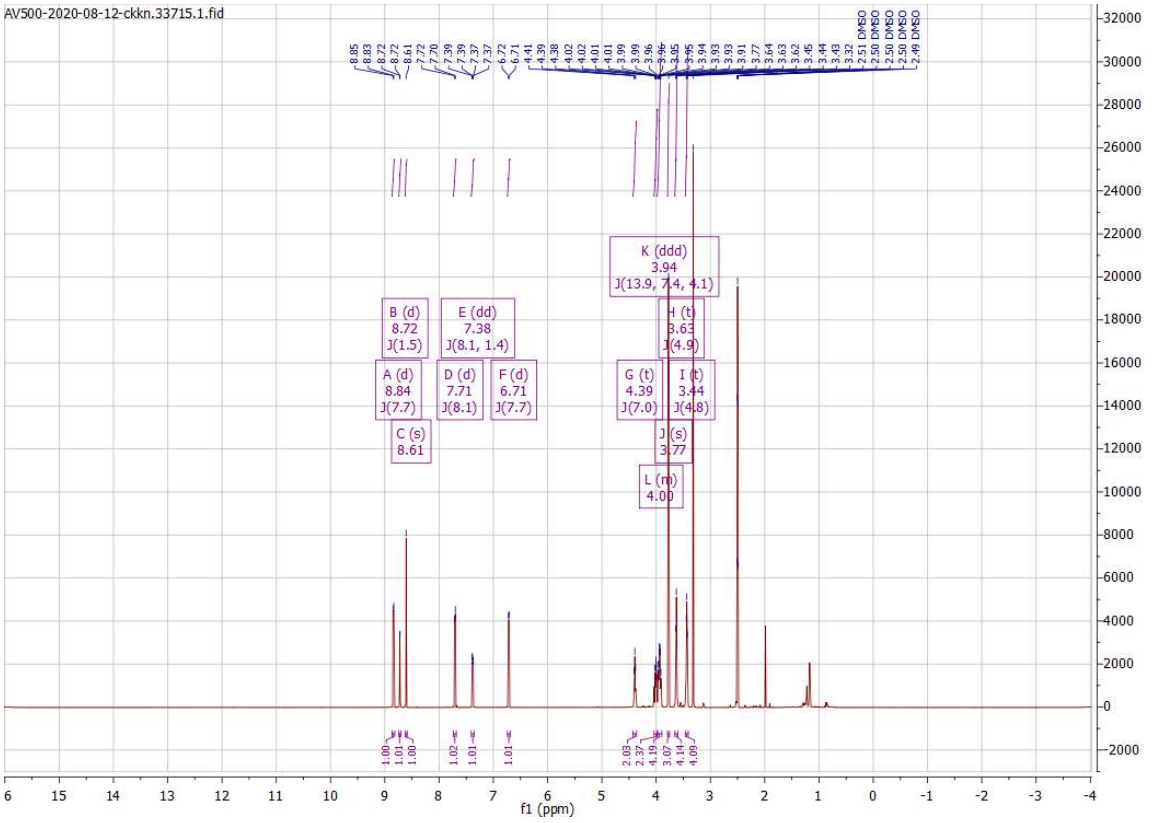

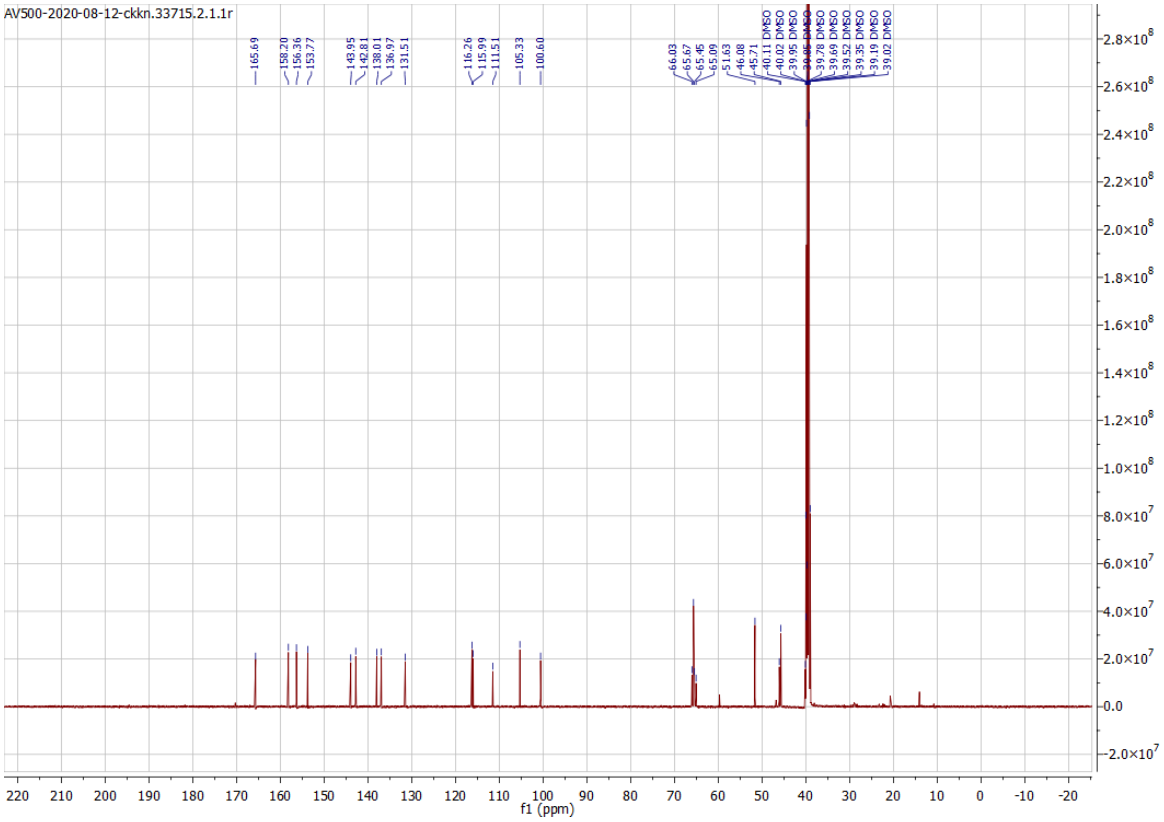

Compound **150**

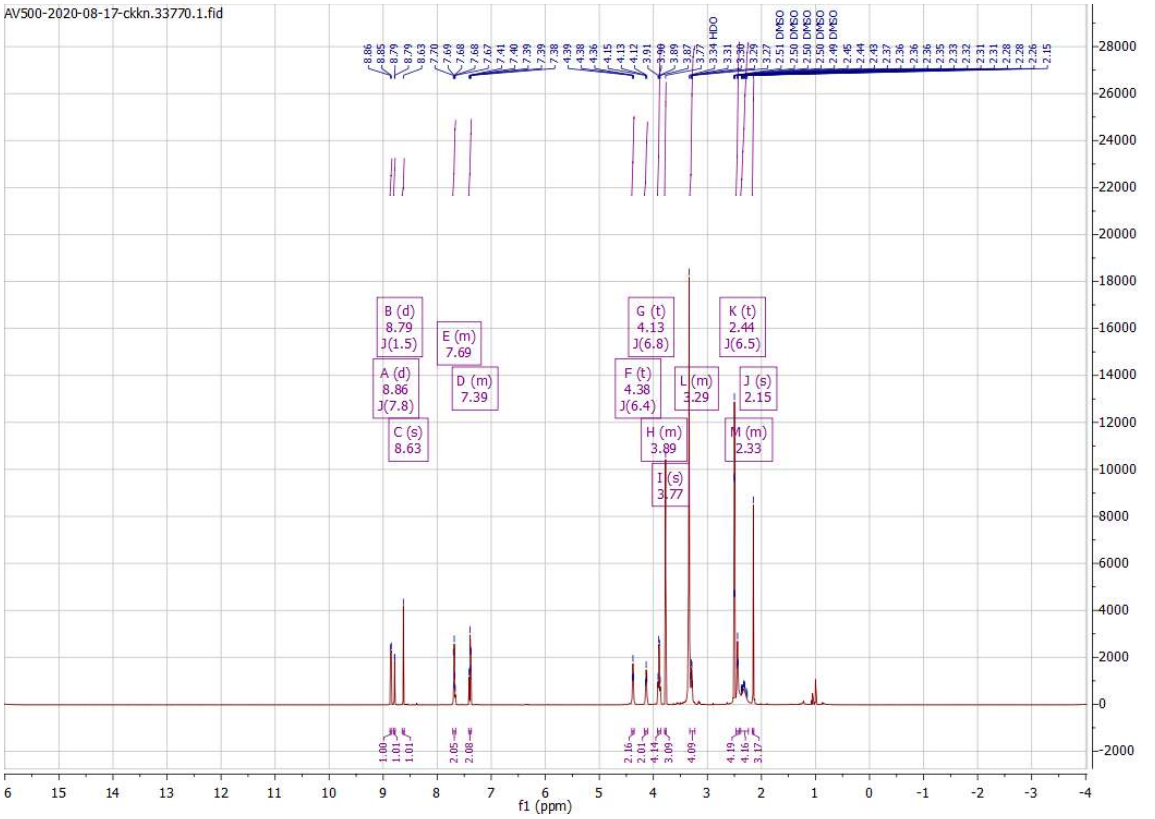

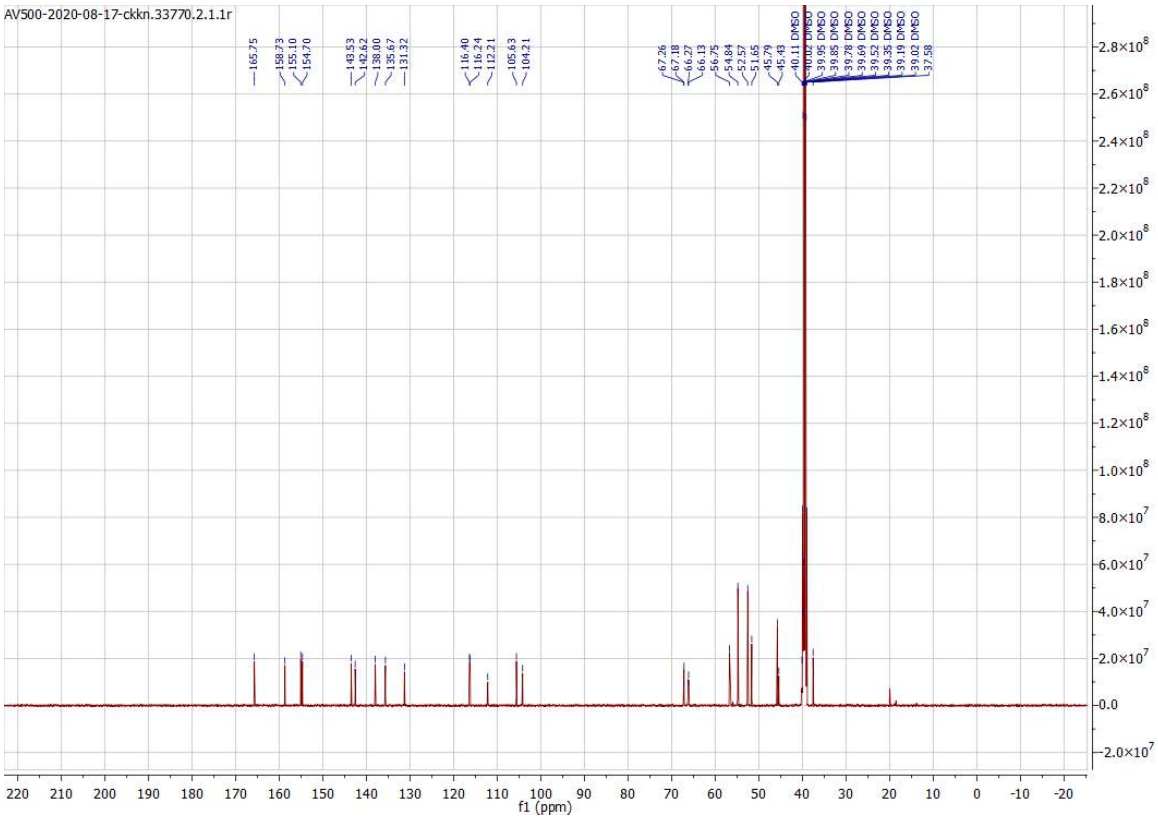

Compound **151**

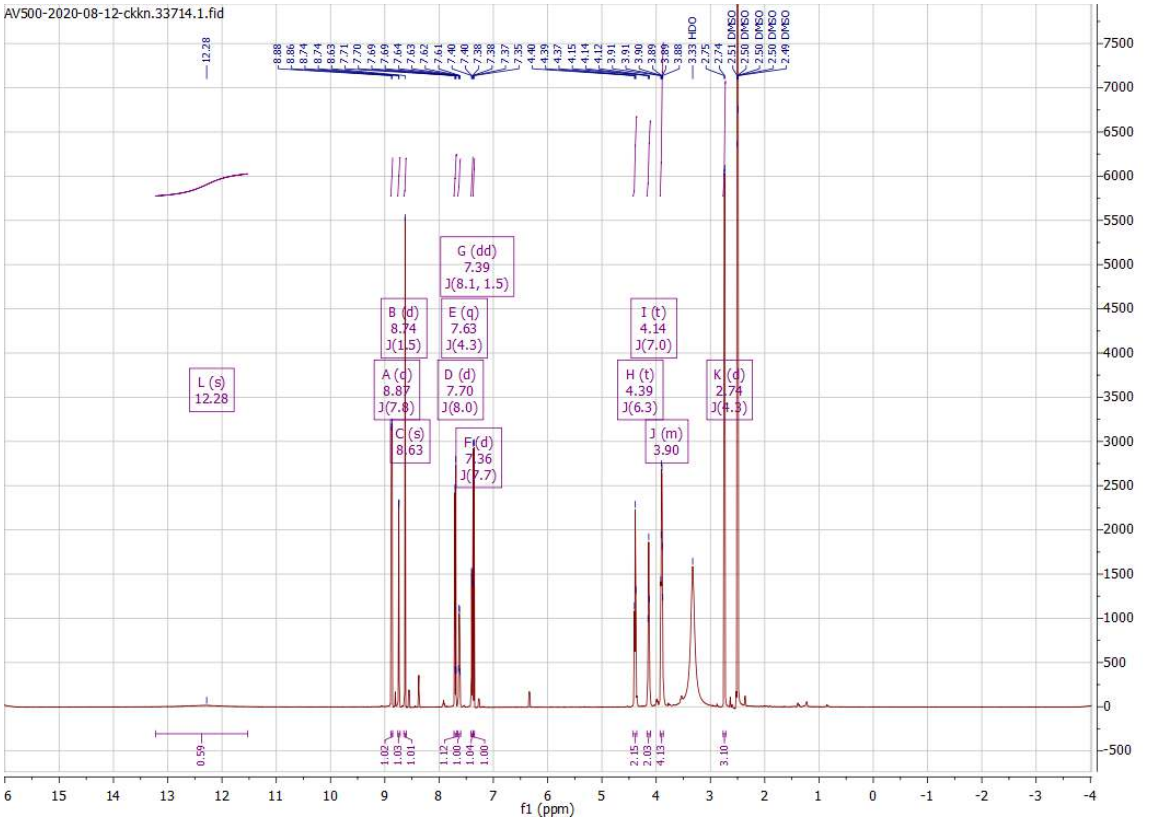

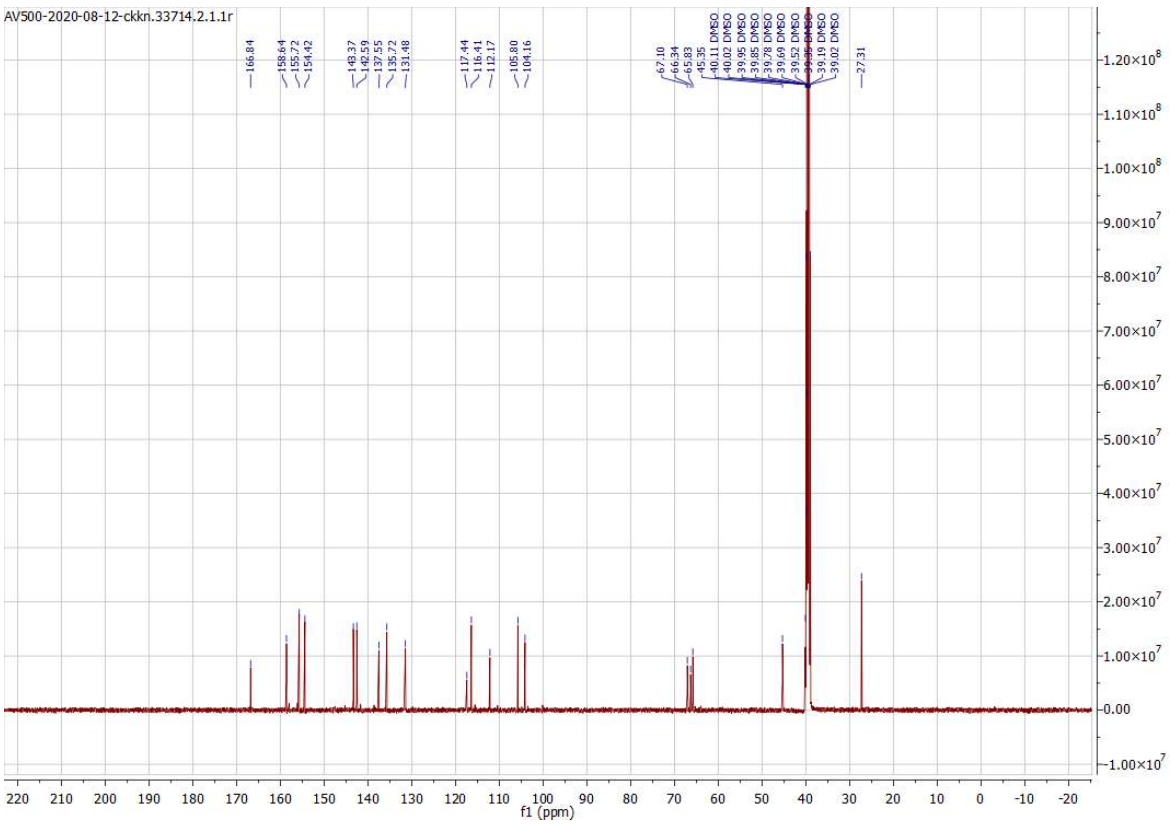

Compound **152**

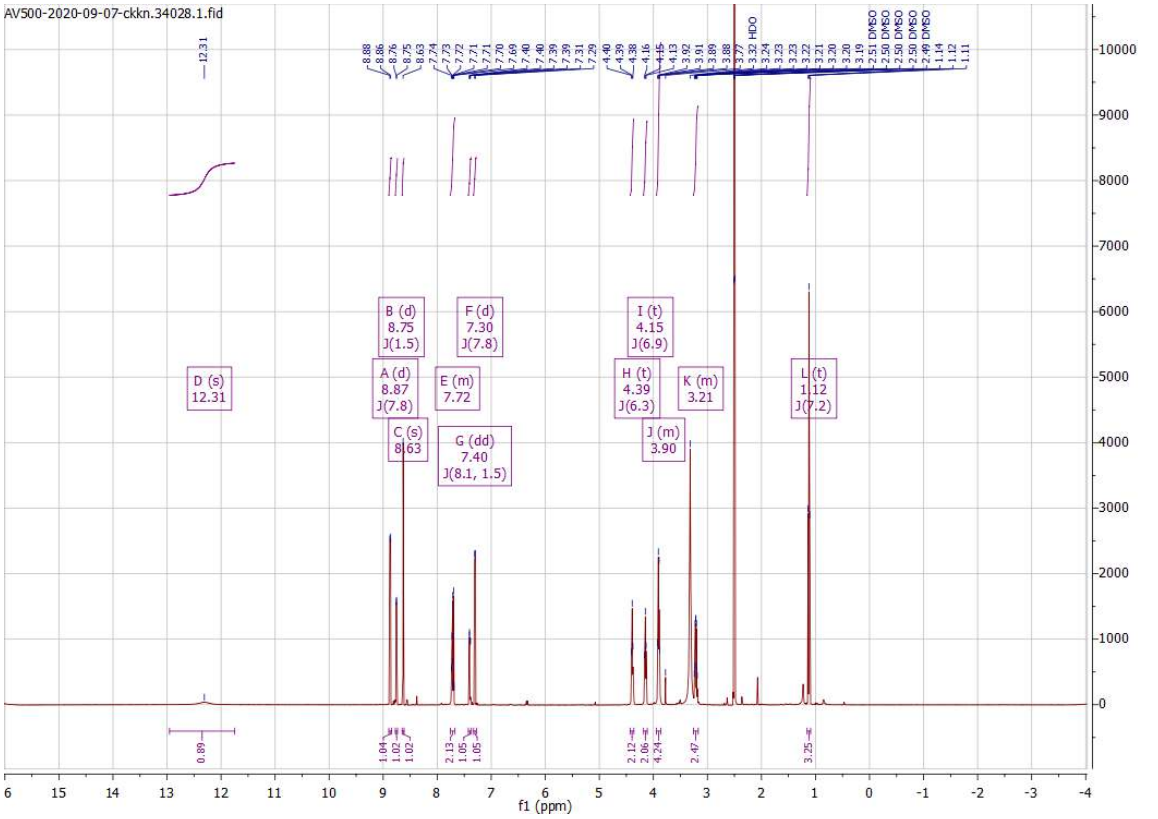

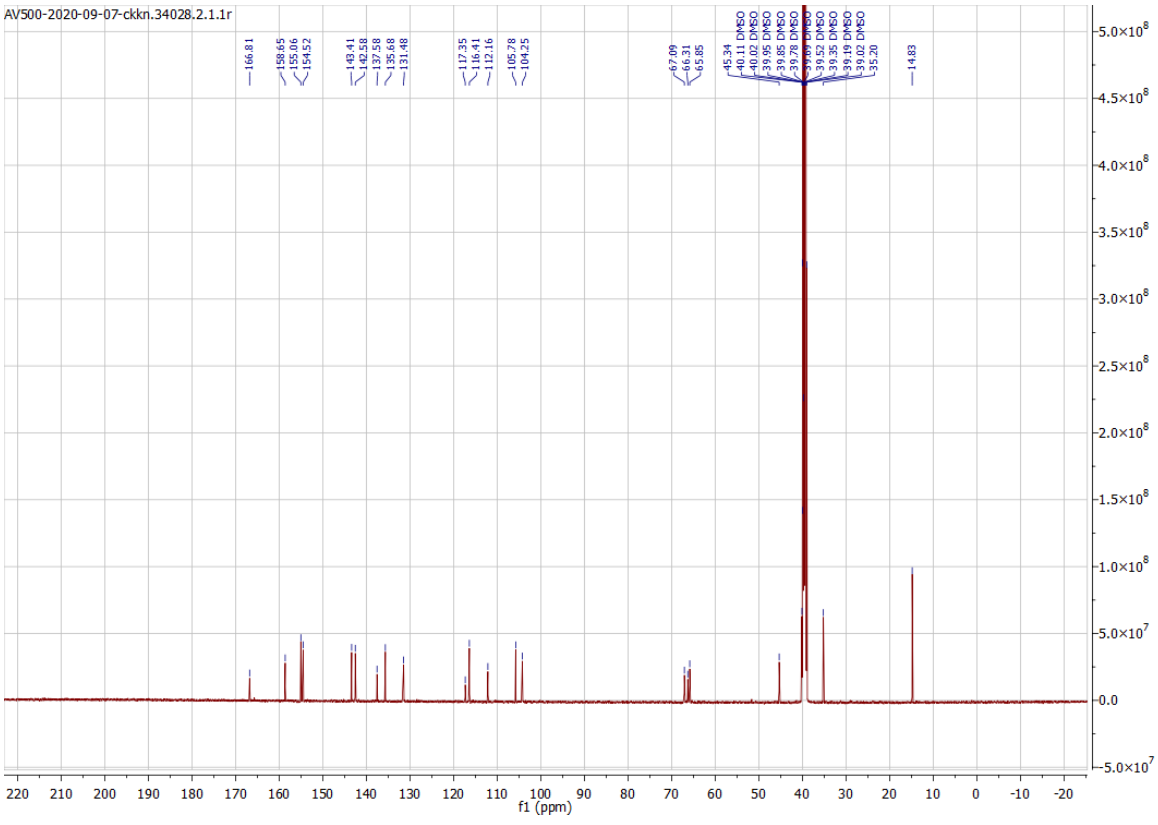

Compound **153**

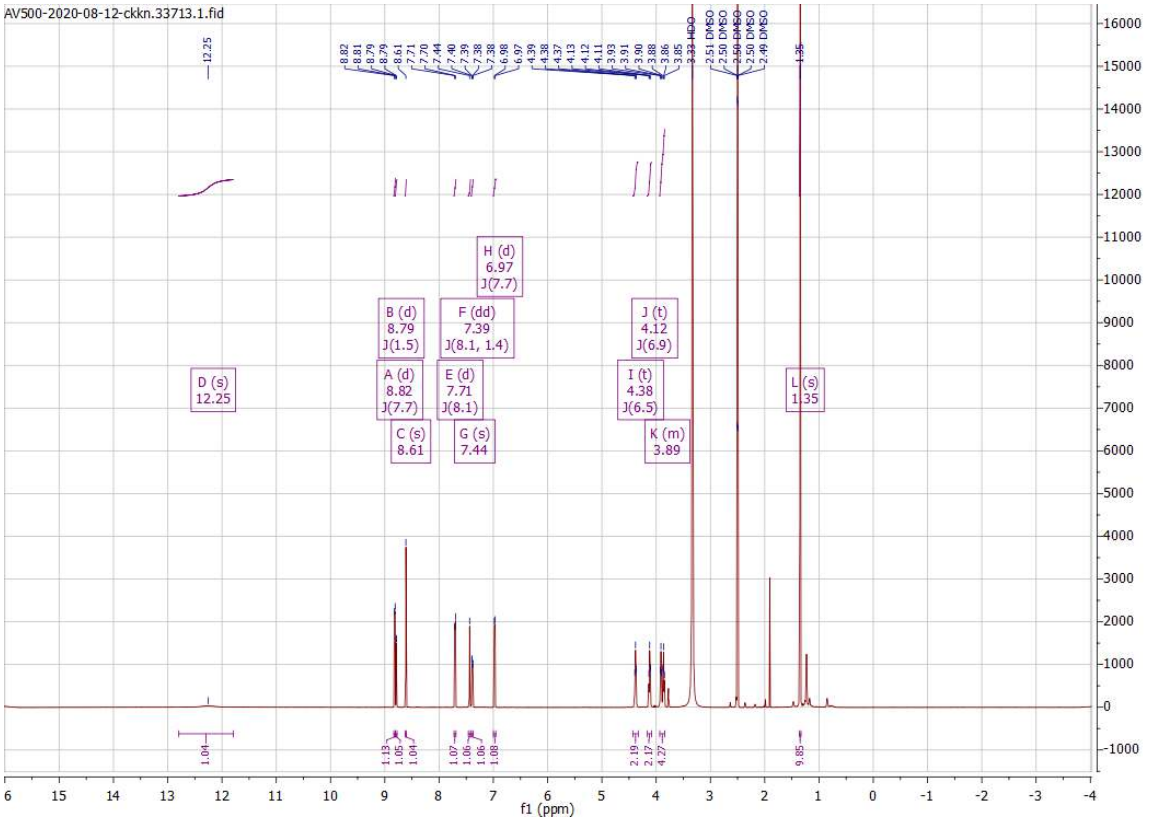

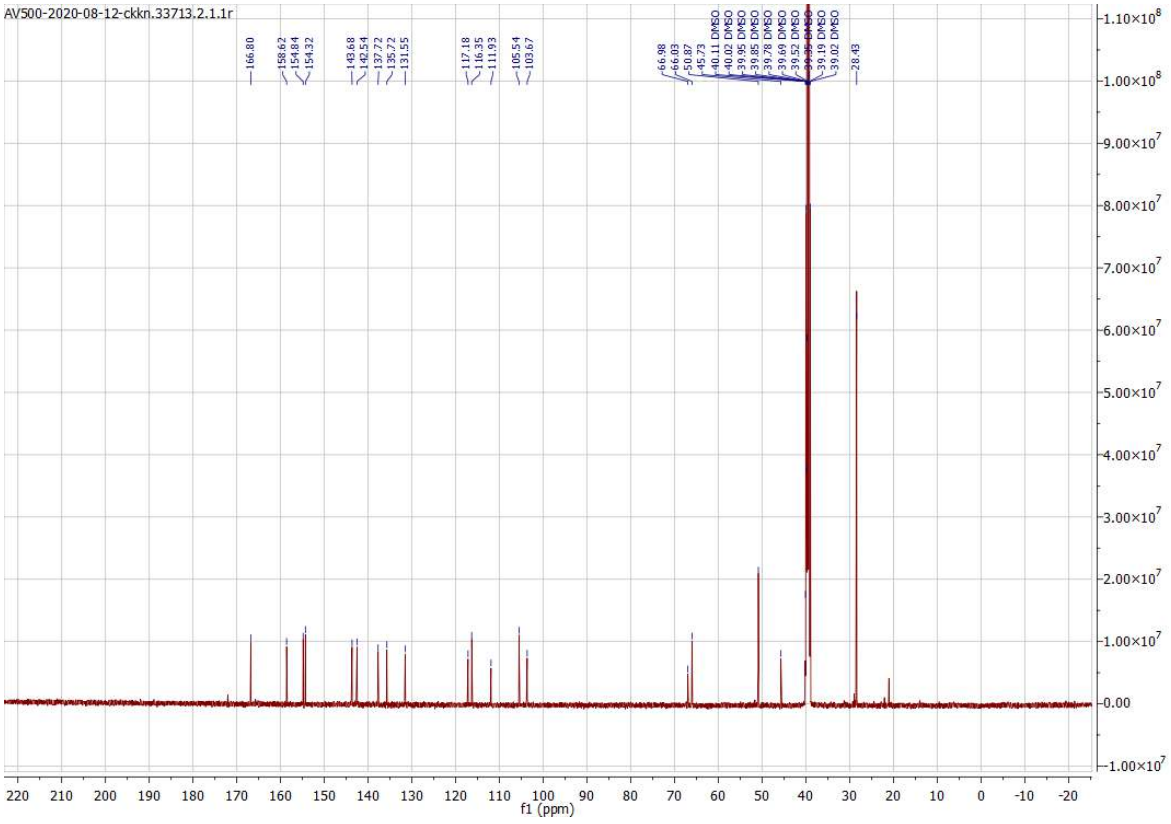

Compound **154**

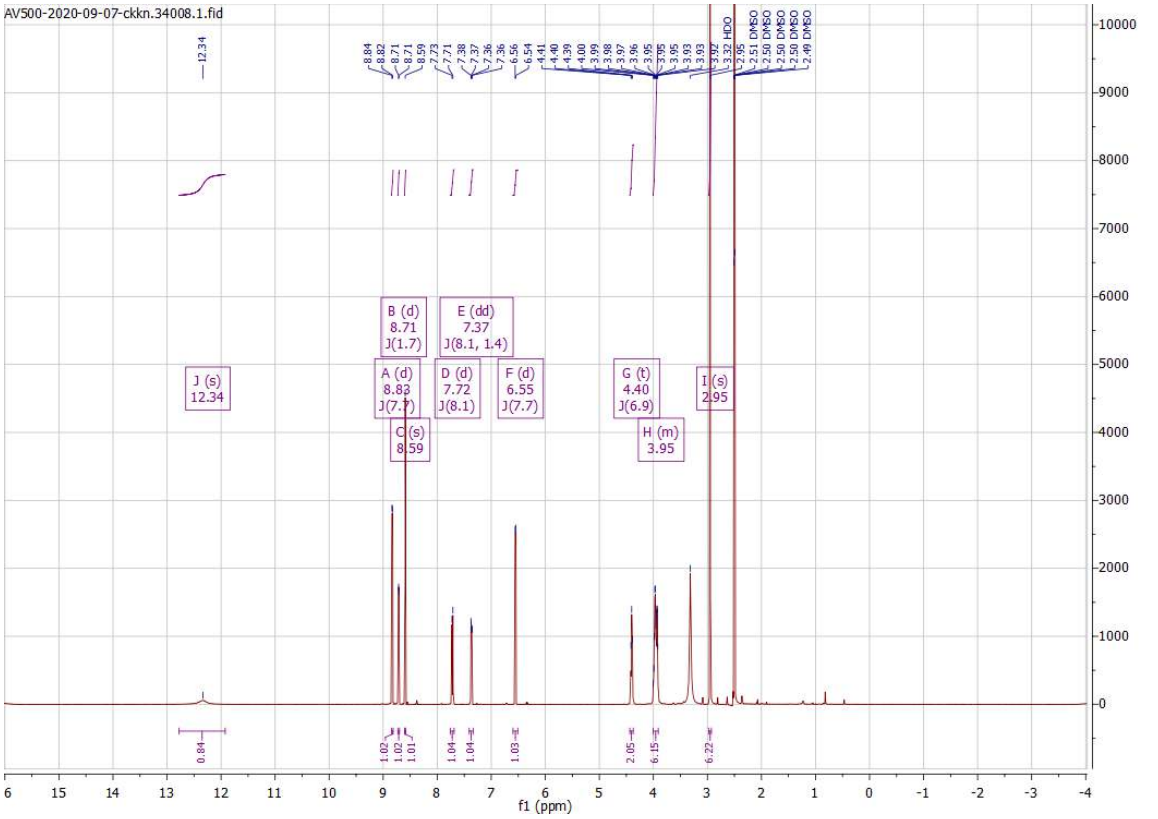

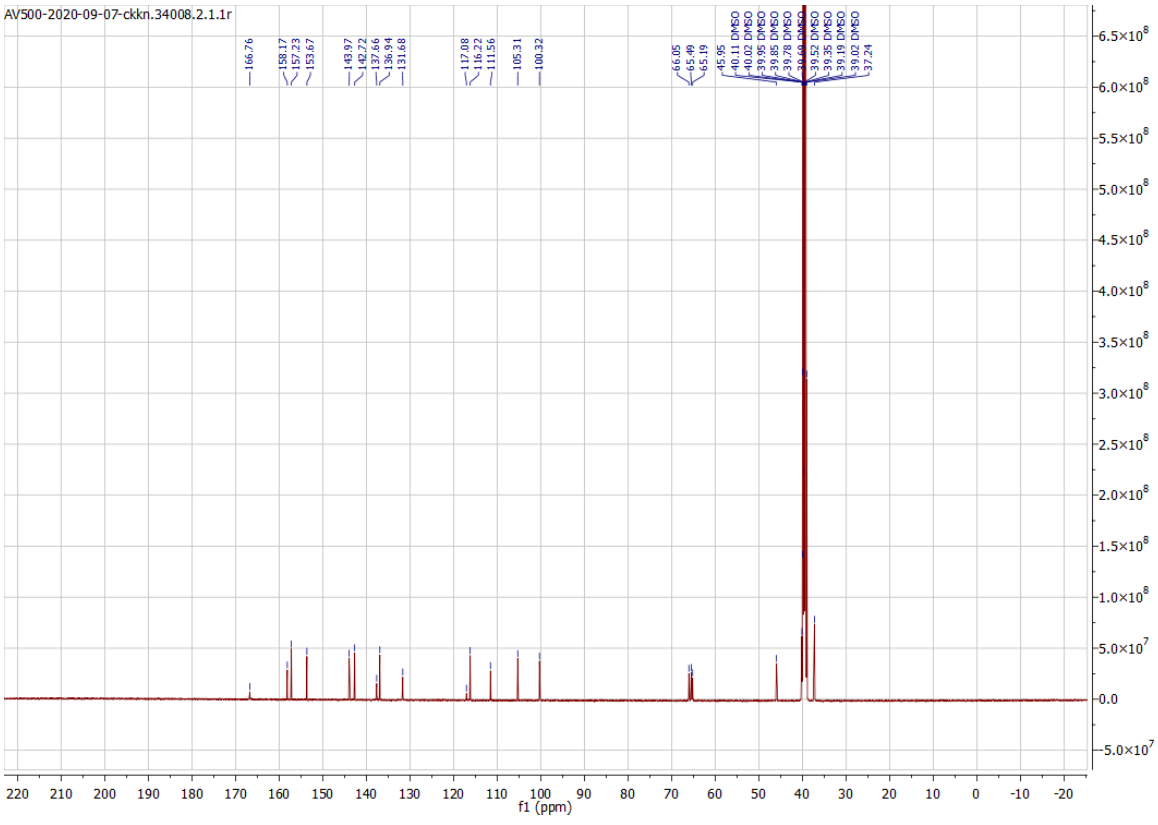

Compound **155**

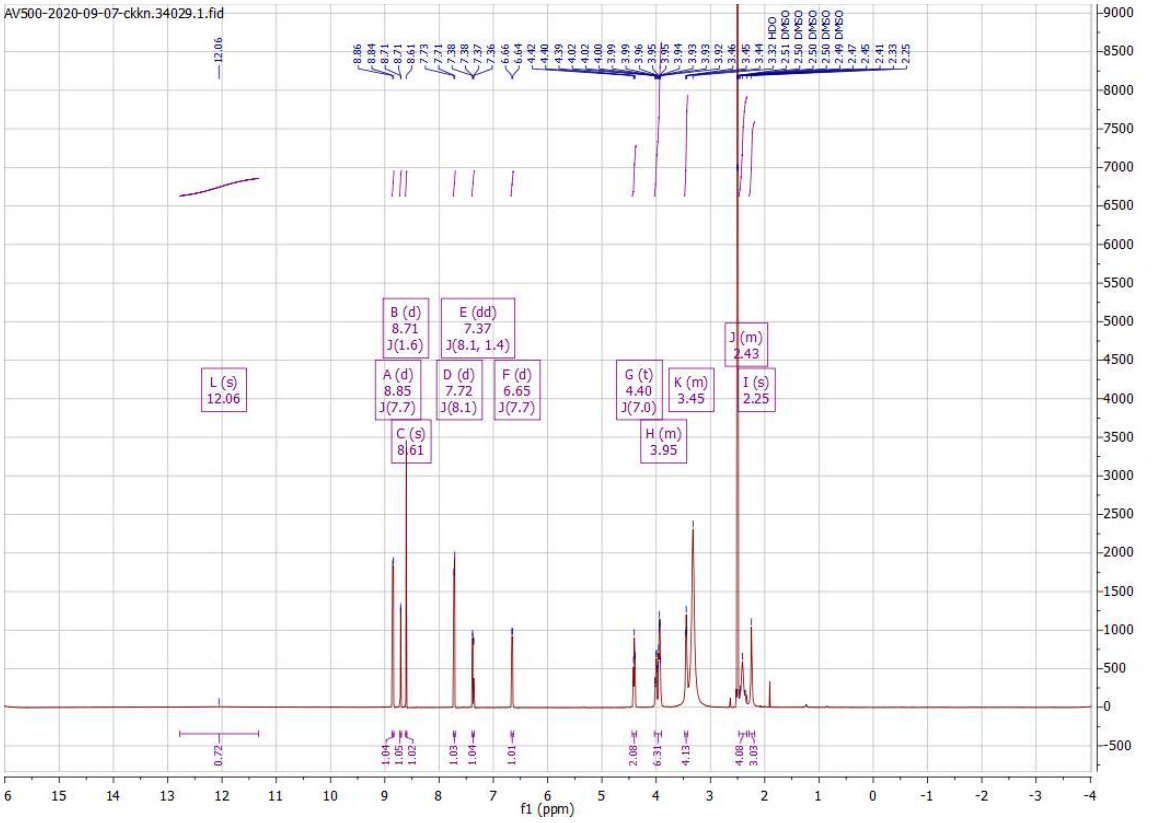

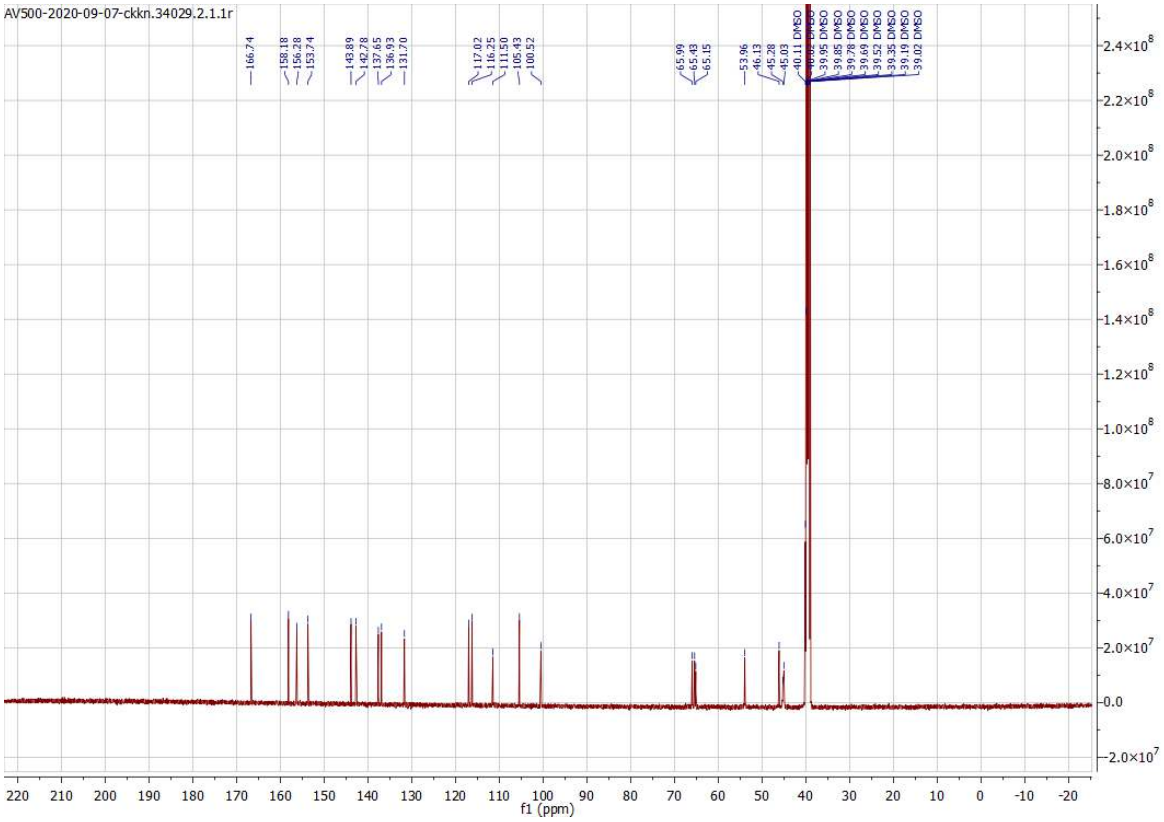

Compound **156**

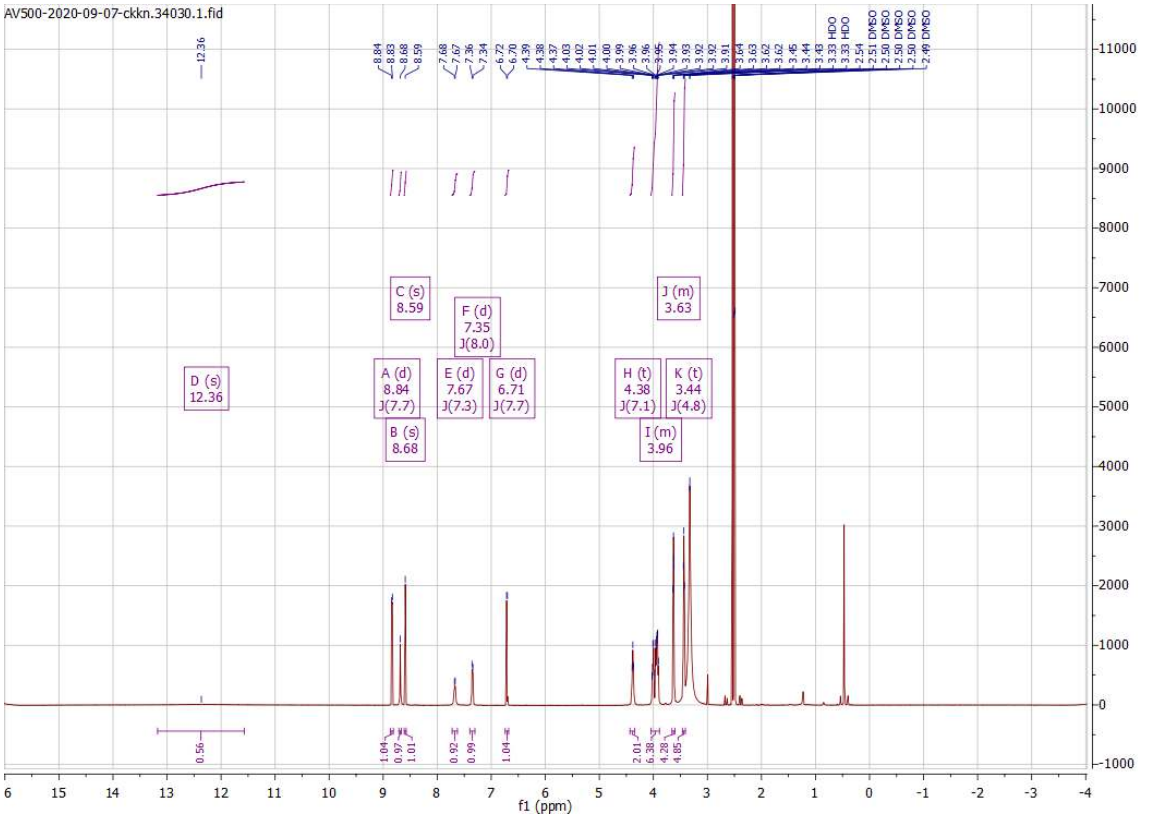

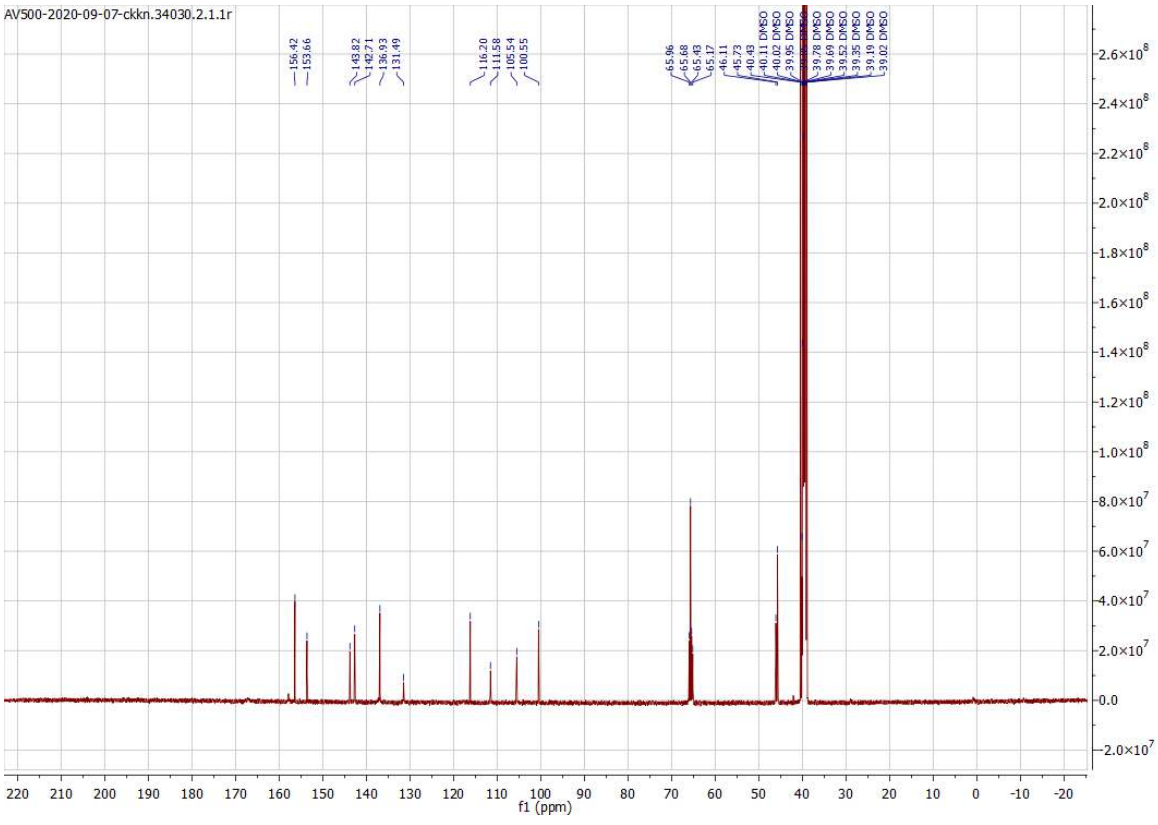

Compound **165**

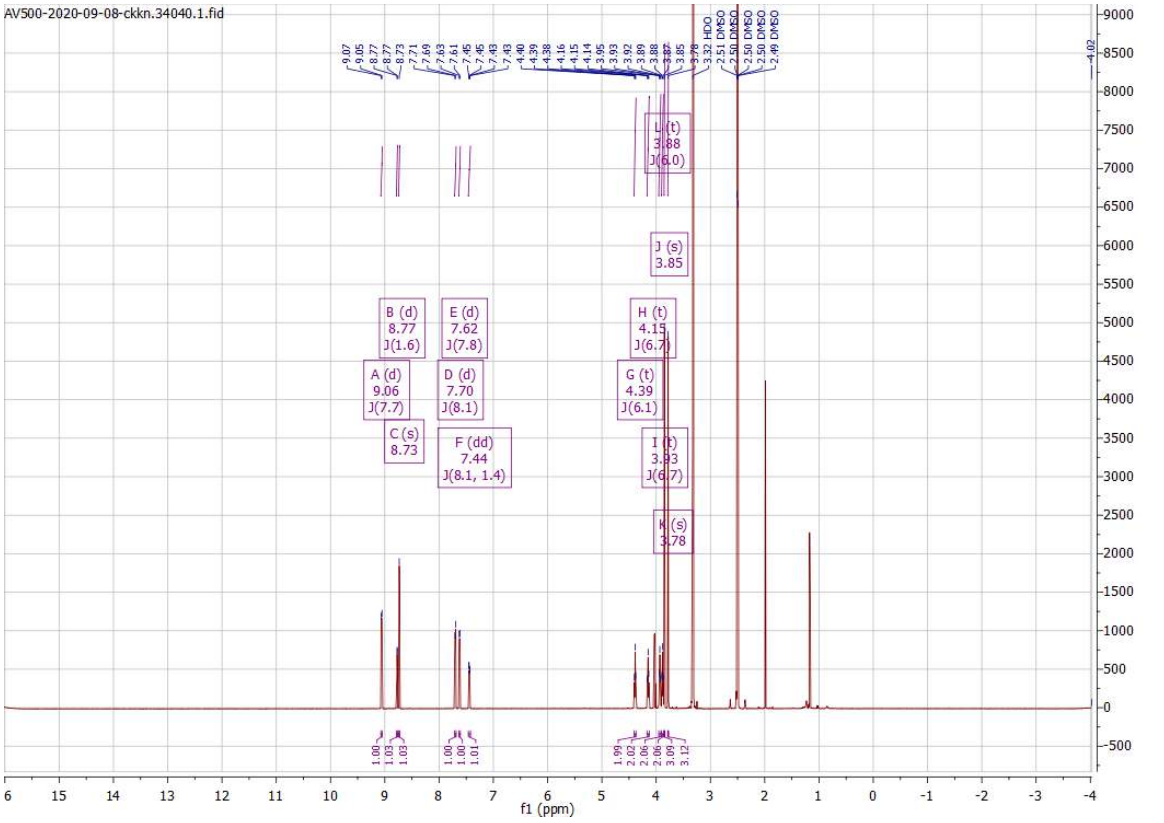

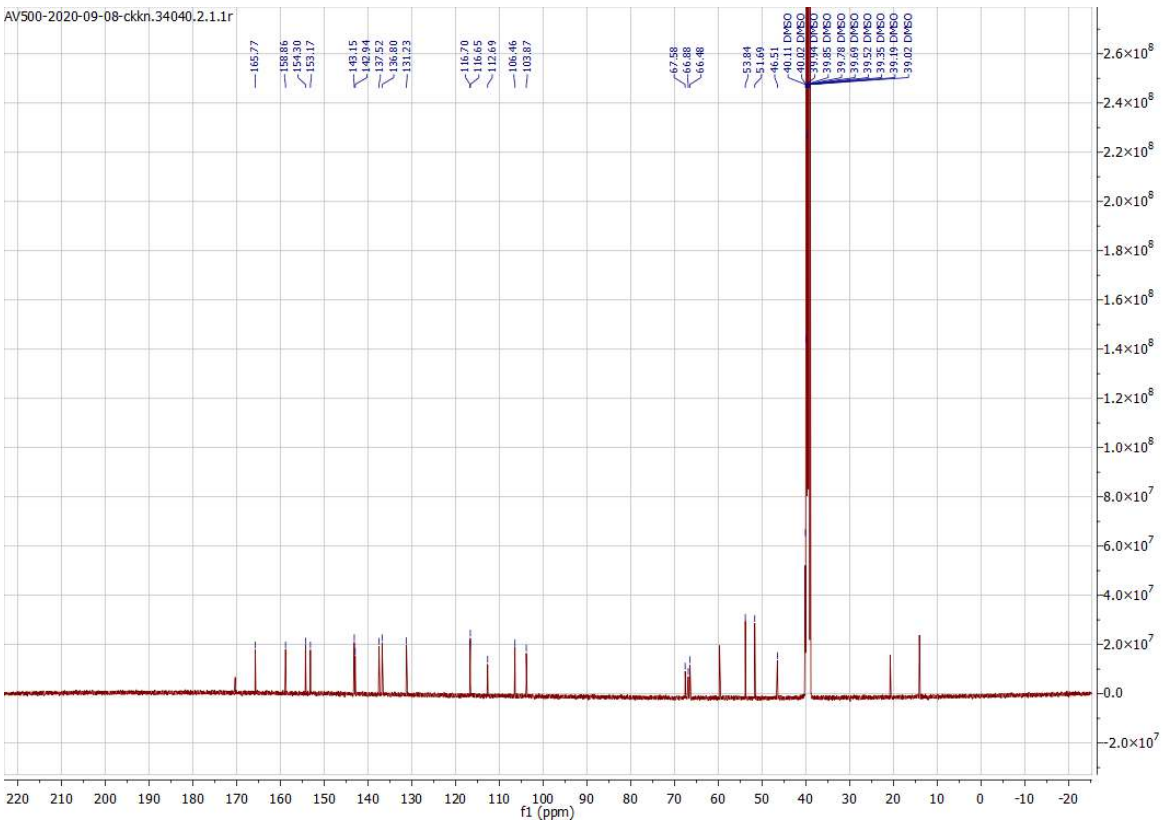

Compound **166**

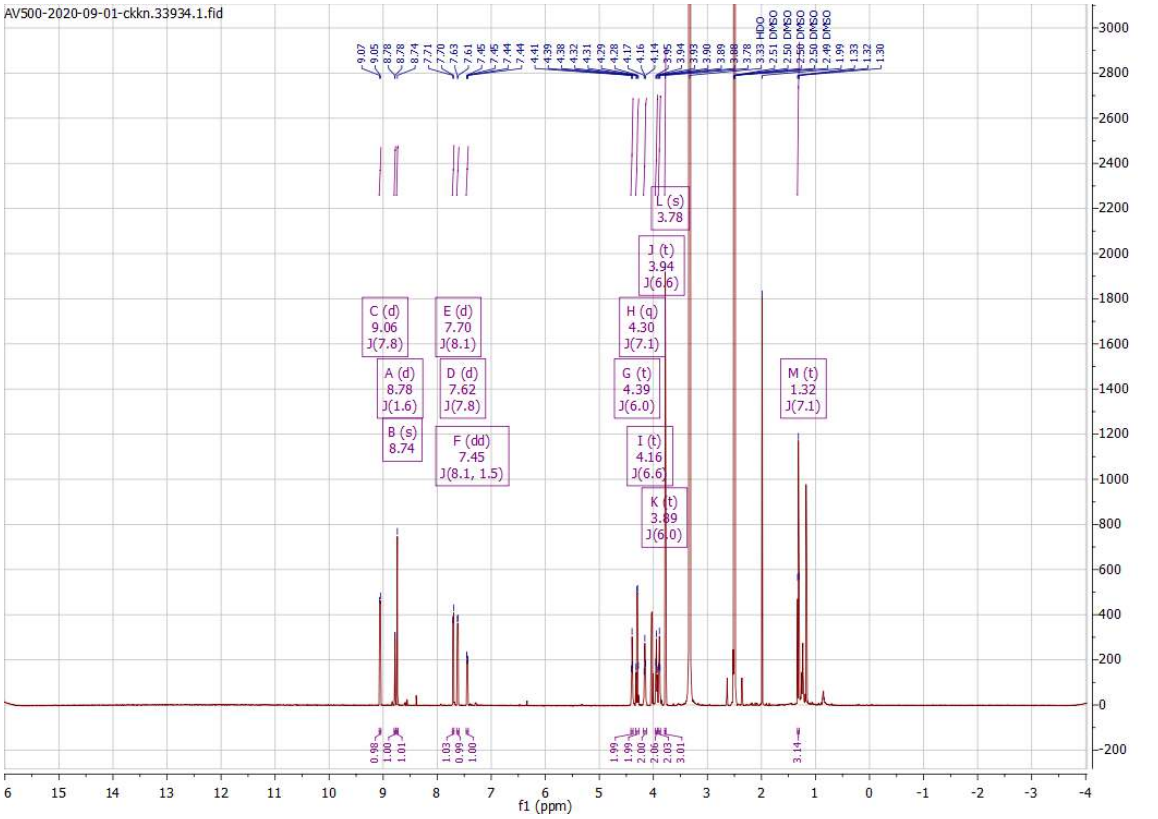

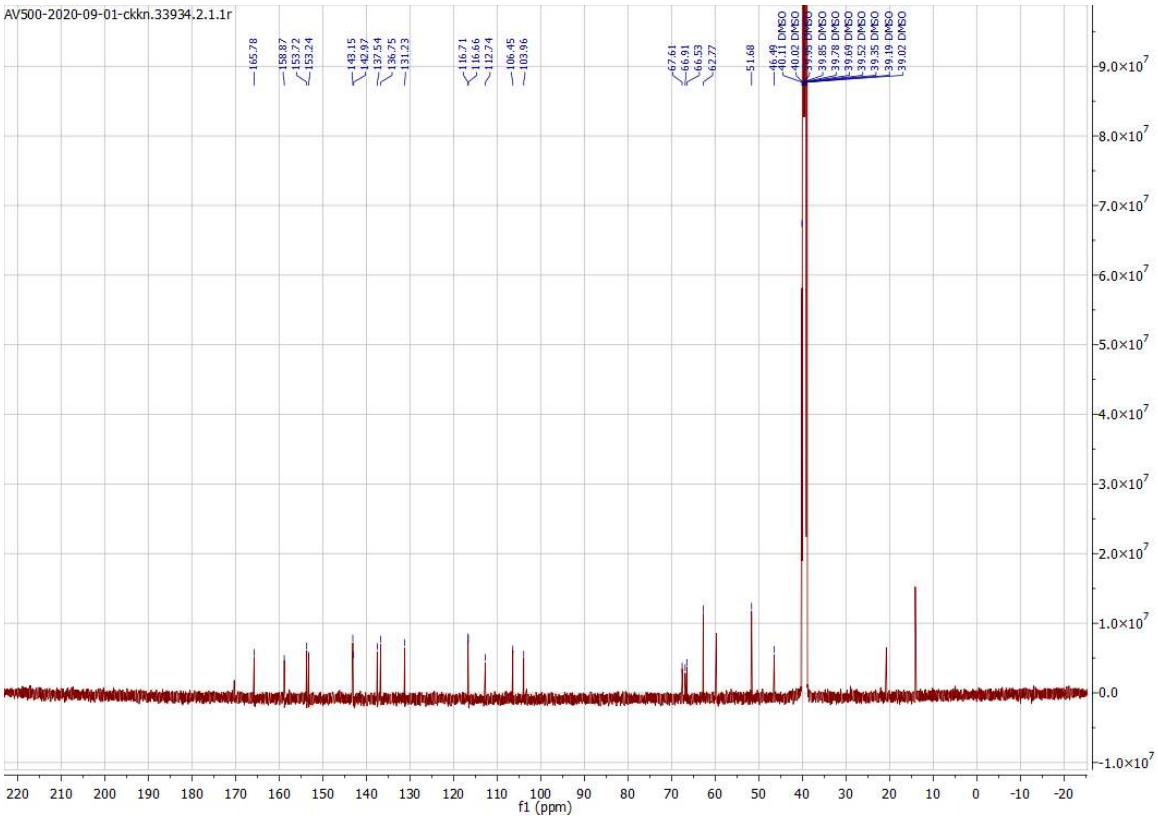

Compound **167**

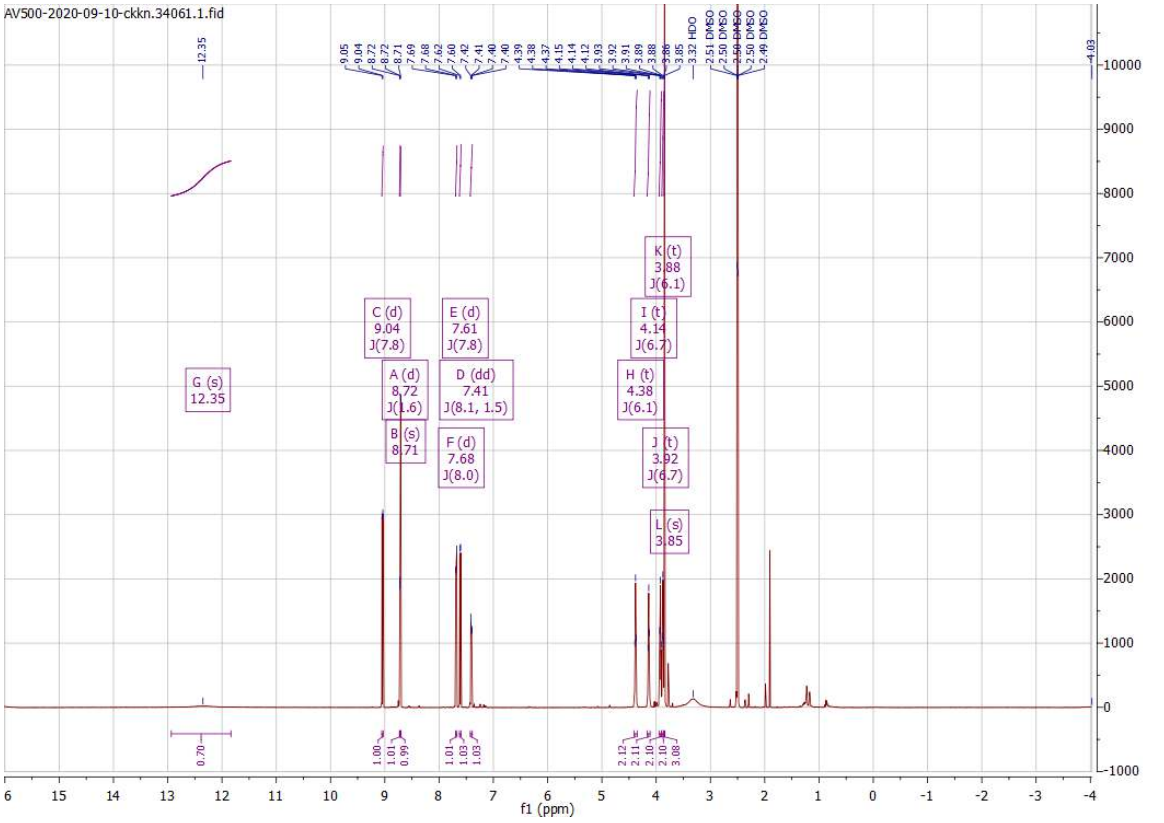

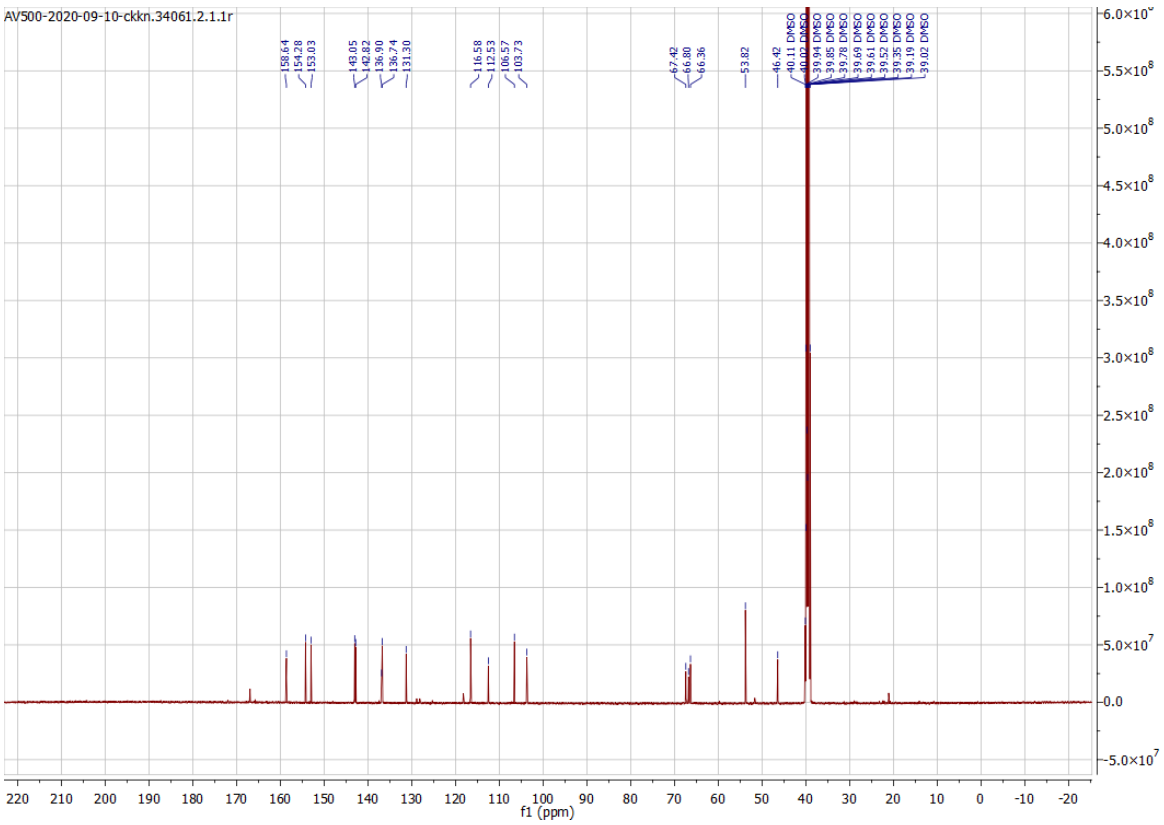

Compound **168**

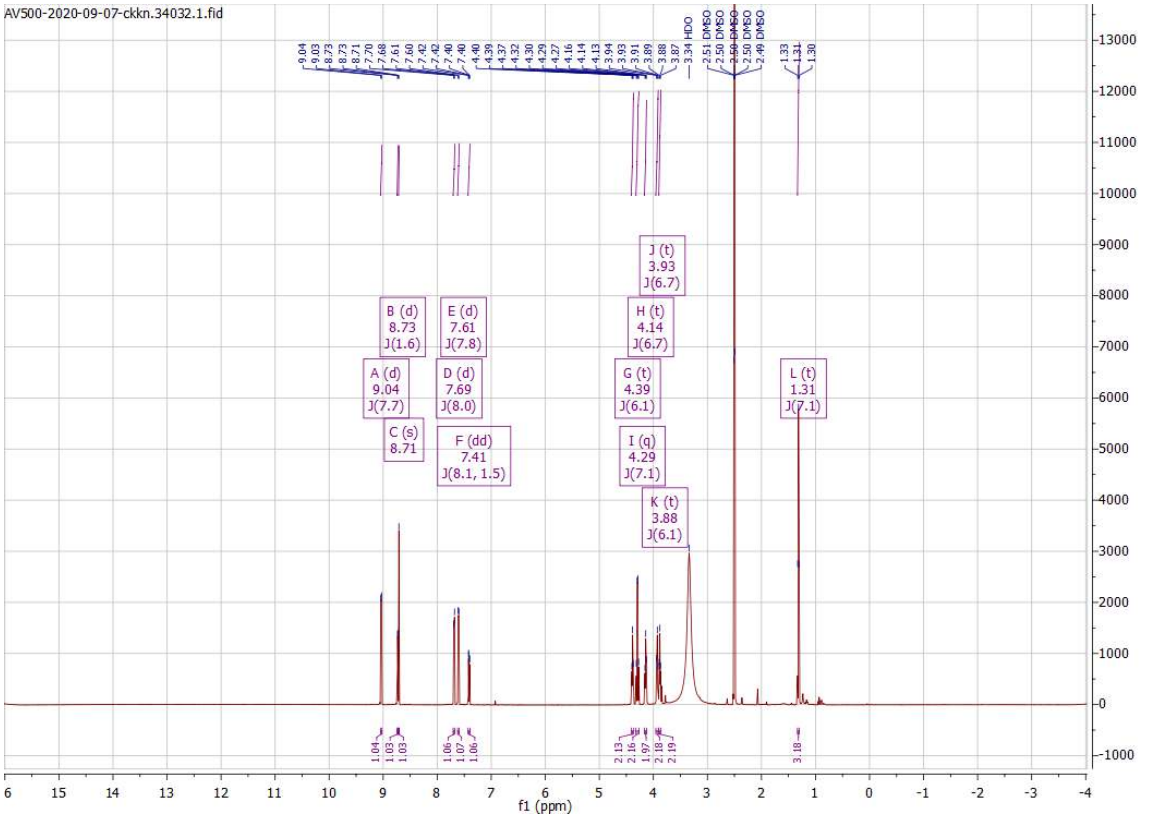

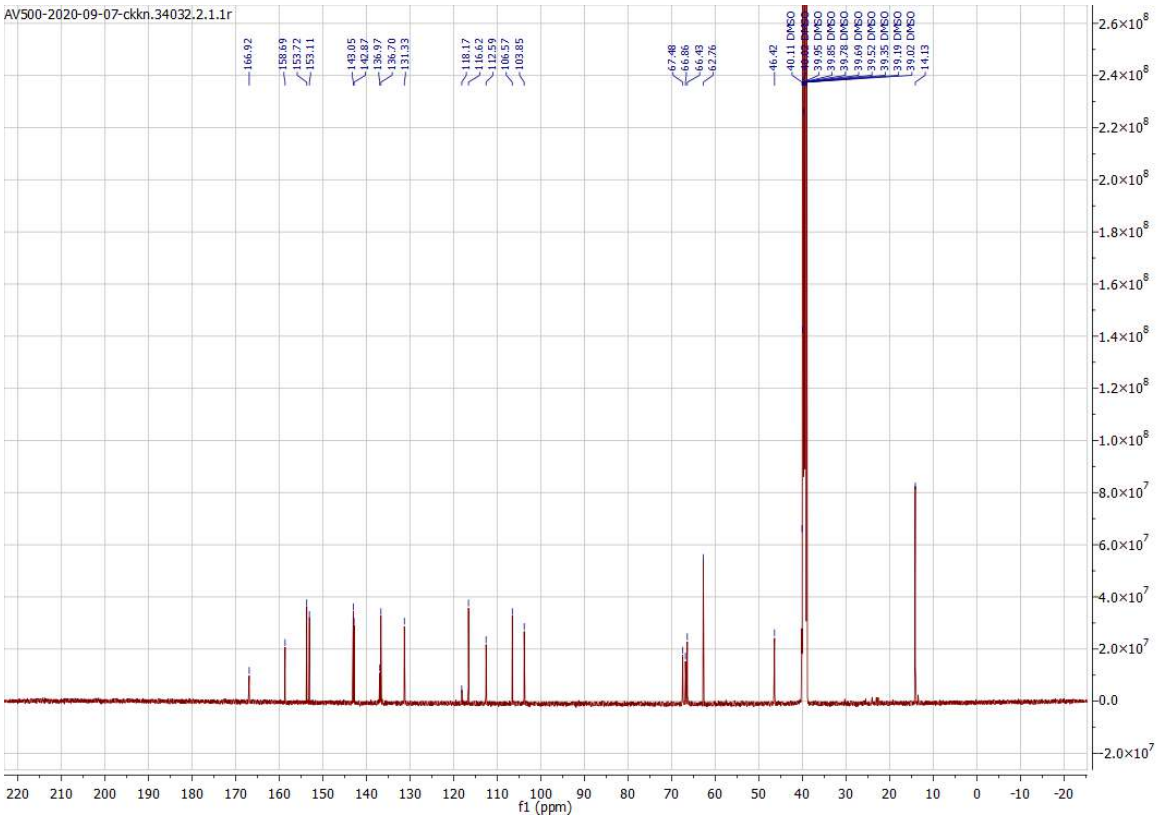

14.2 HPLC data

Compound **34**

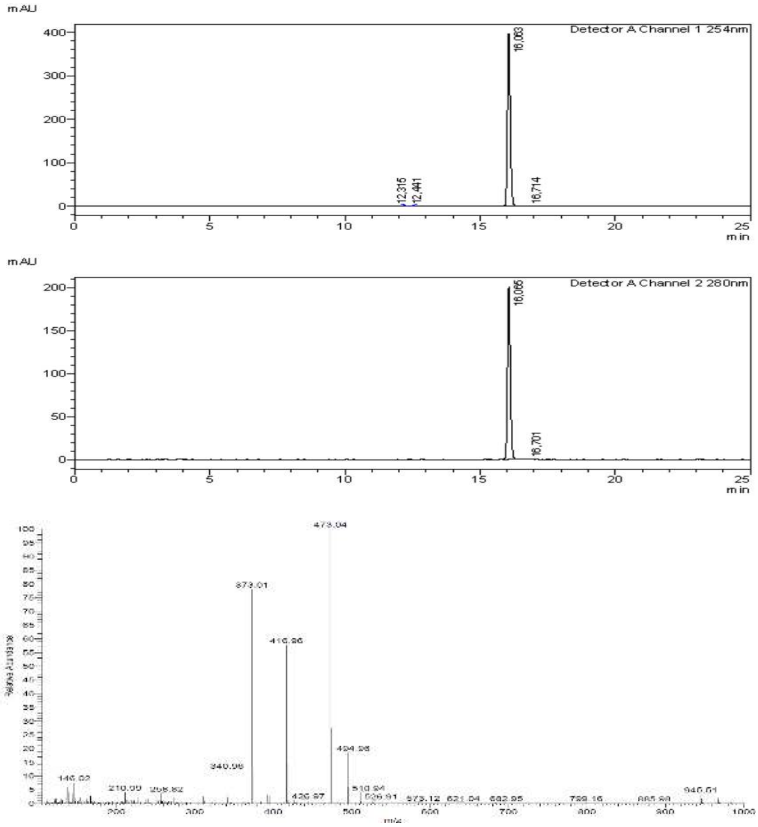

Compound **35**

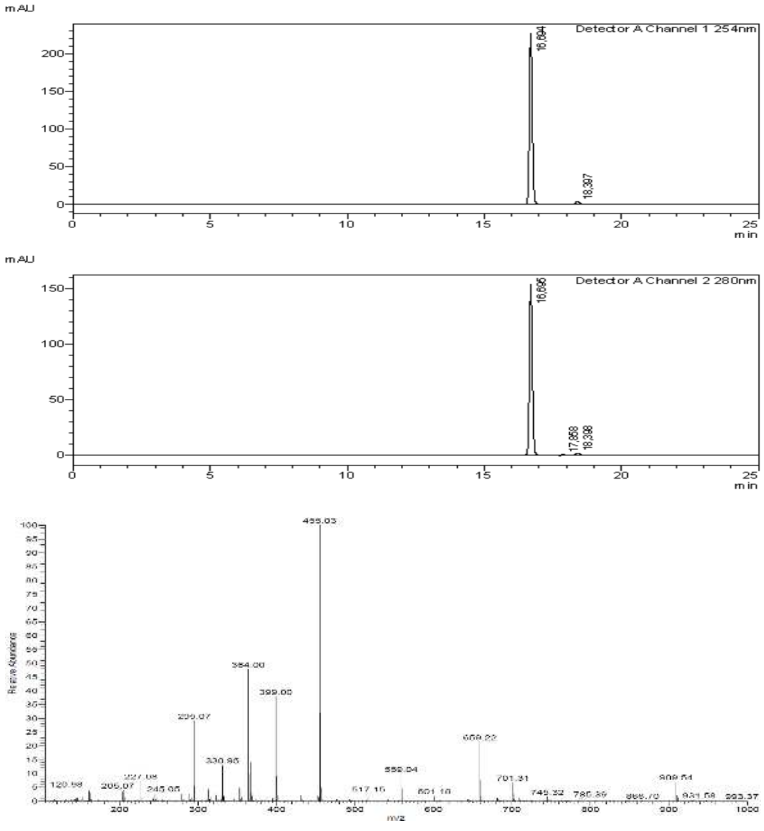

Compound **46**

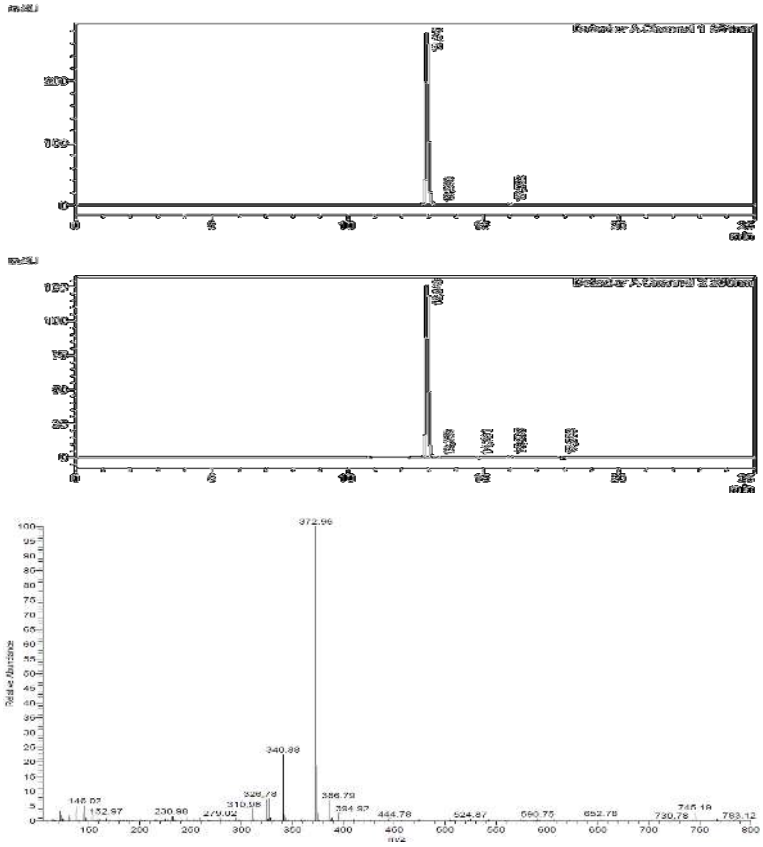

Compound **47**

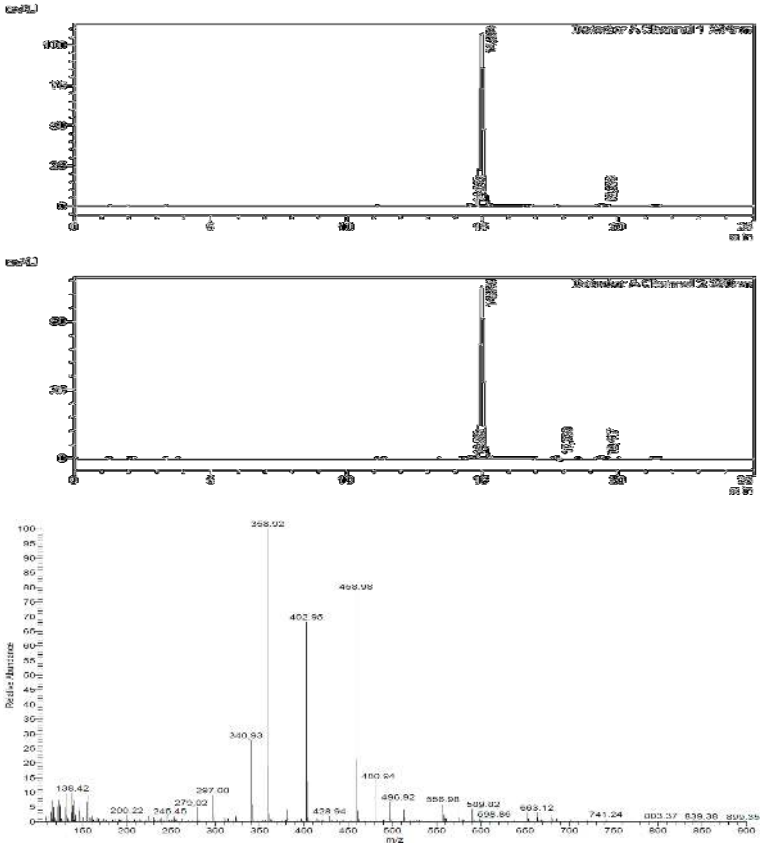

Compound **60**

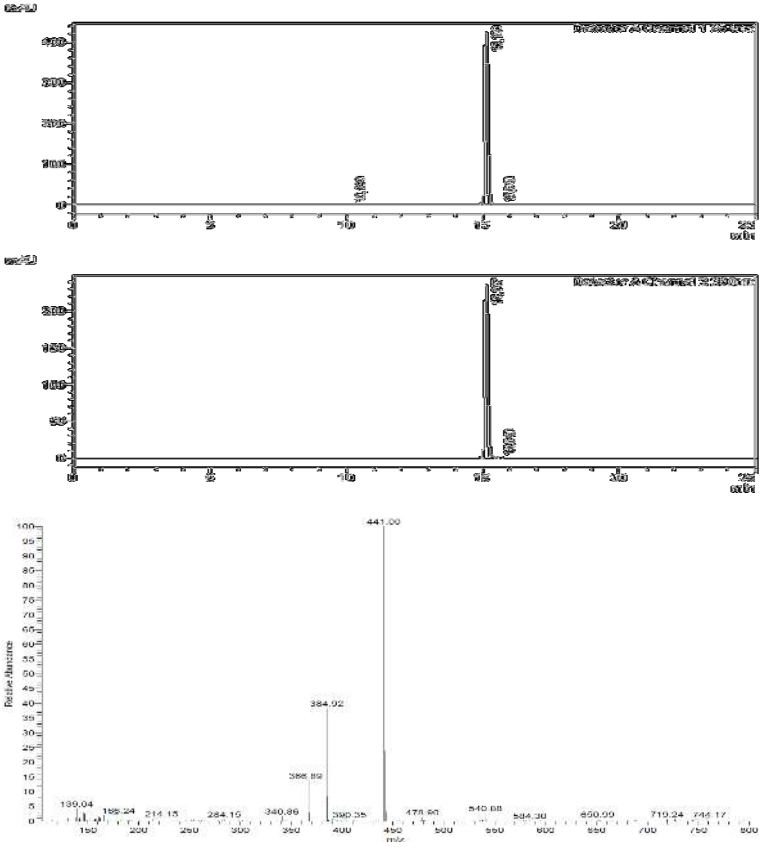

Compound **36**

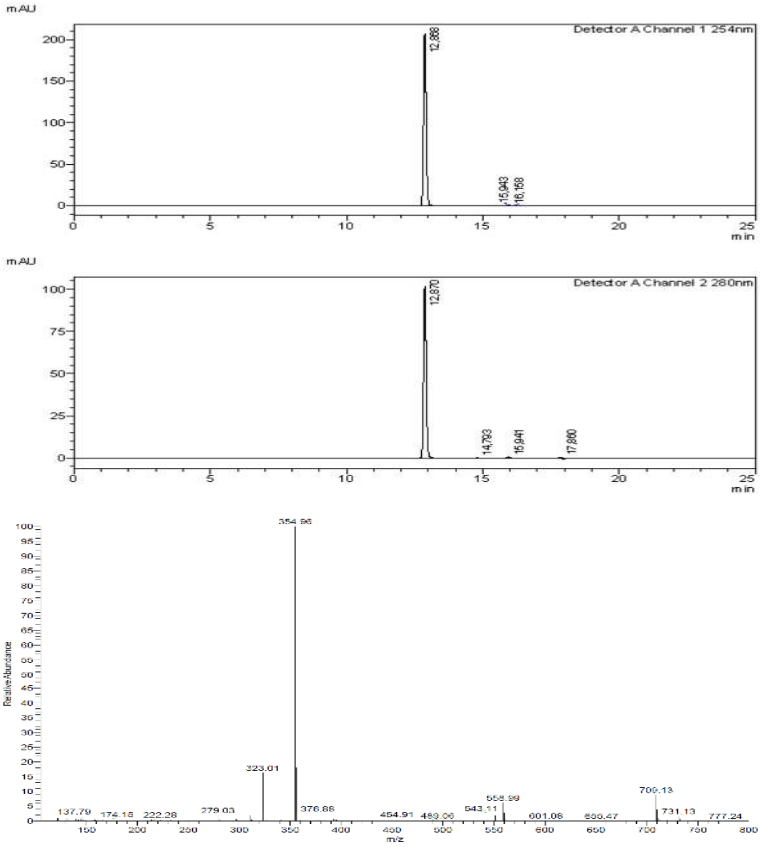

Compound **37**

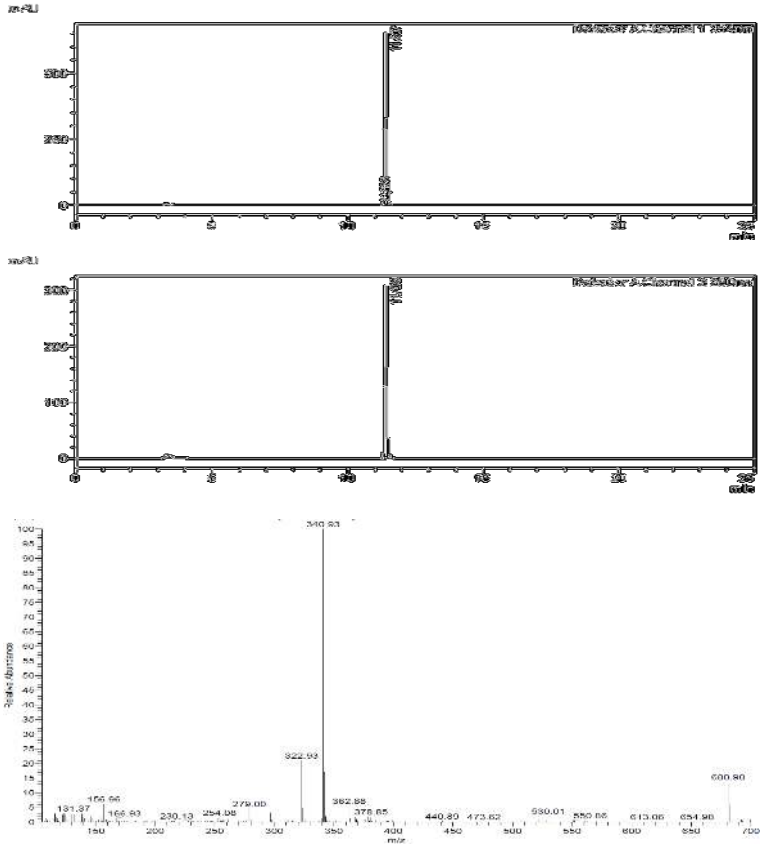

Compound **61**

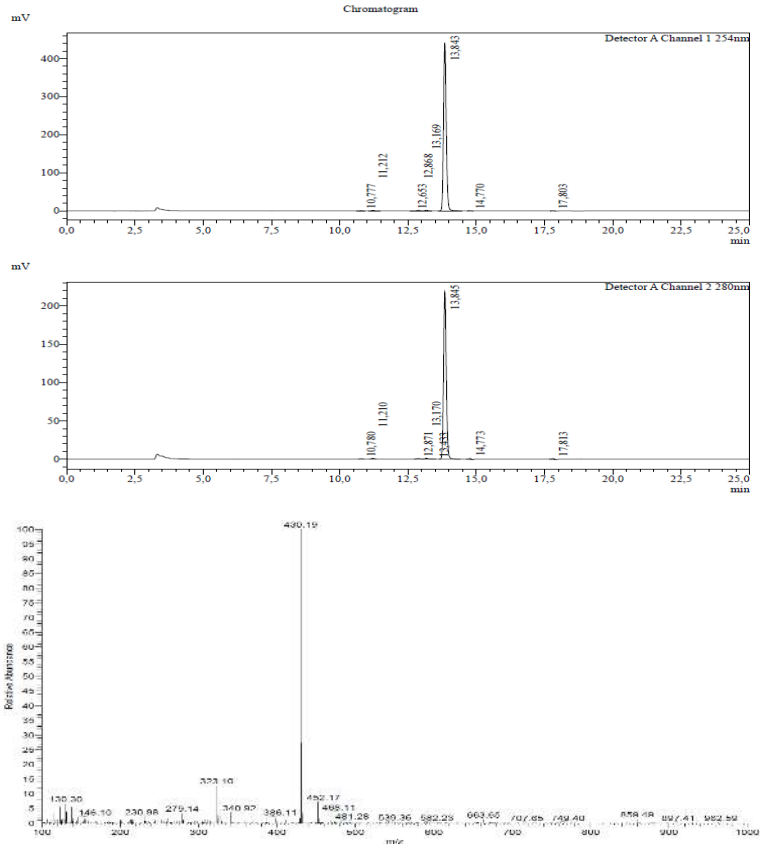

Compound **62**

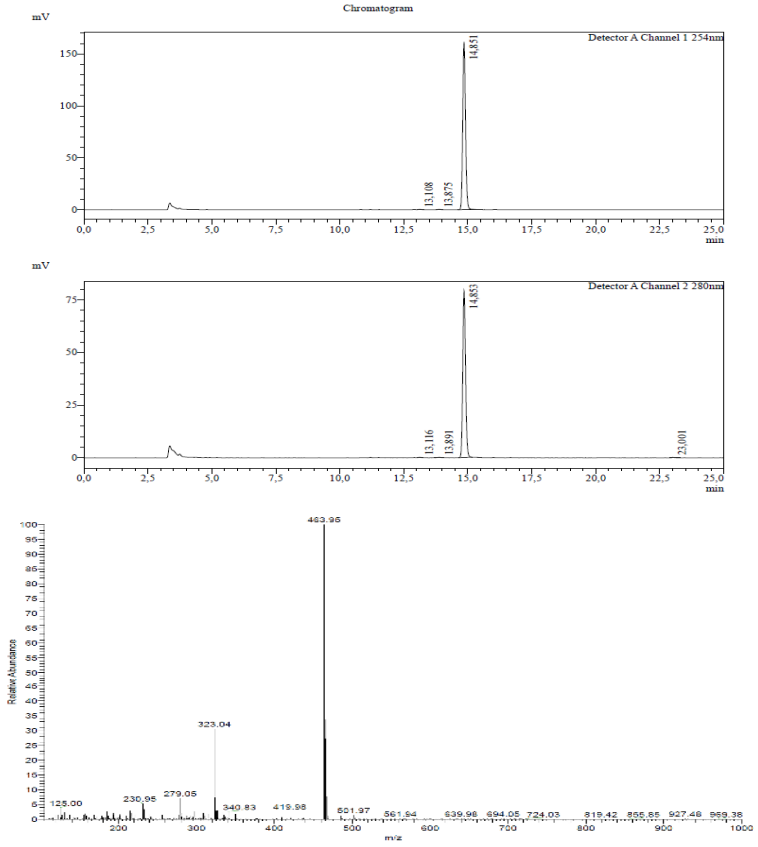

Compound **63**

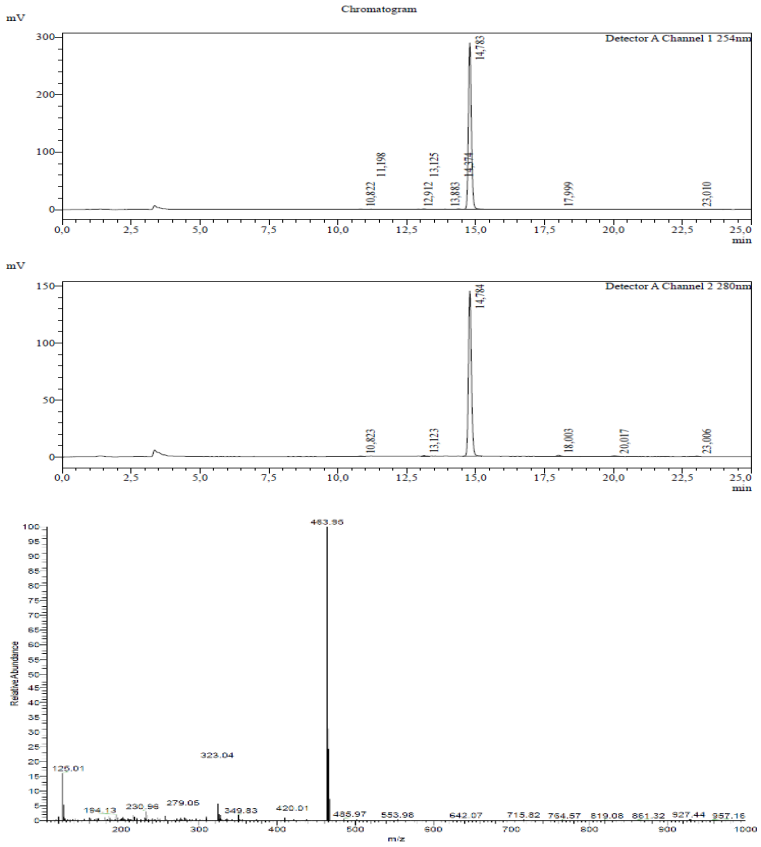

Compound **64**

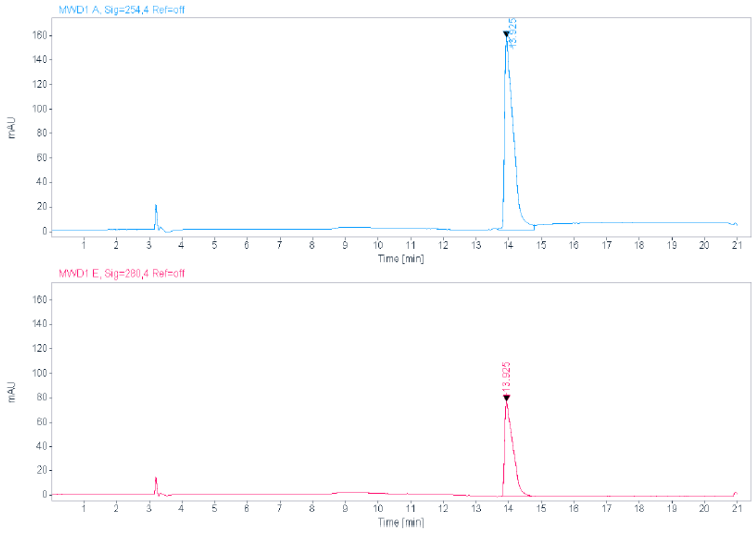

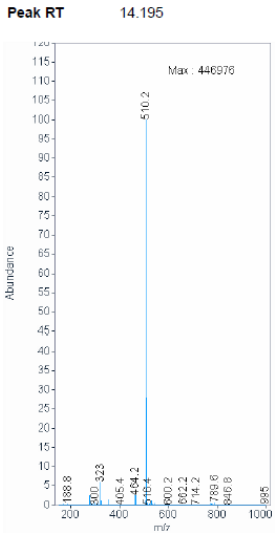

Compound **65**

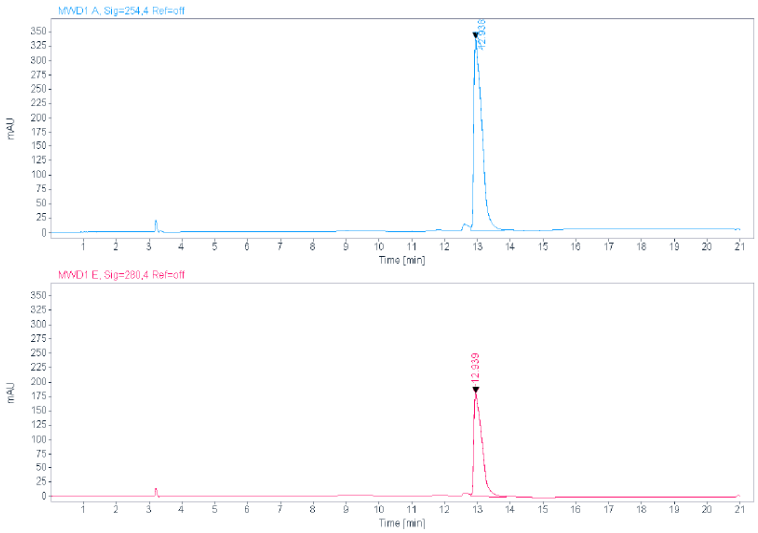

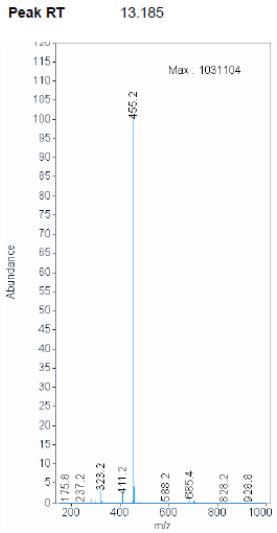

Compound **66**

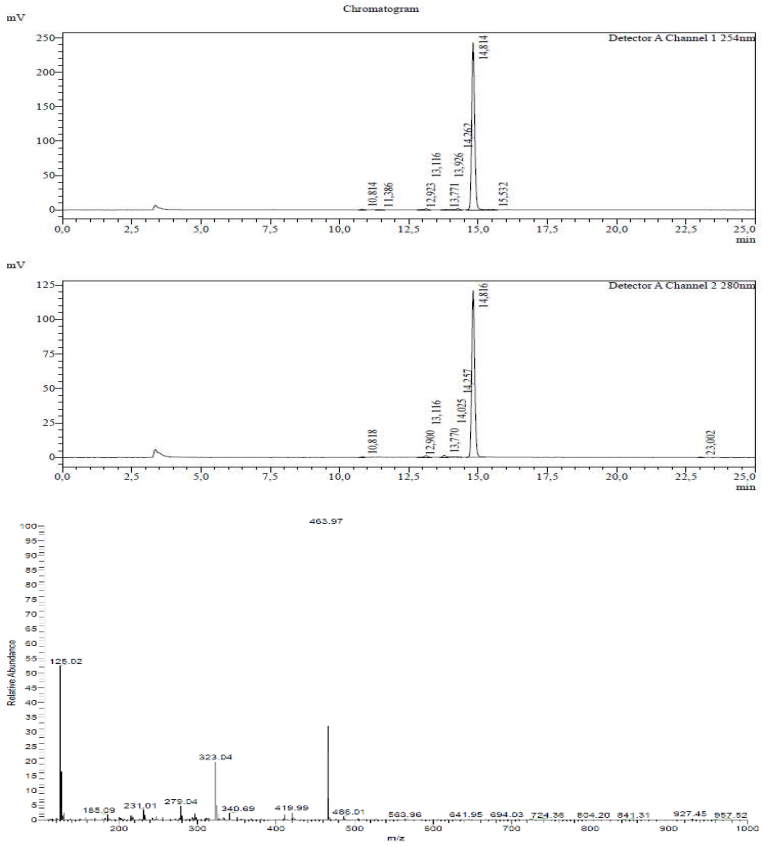

Compound **67**

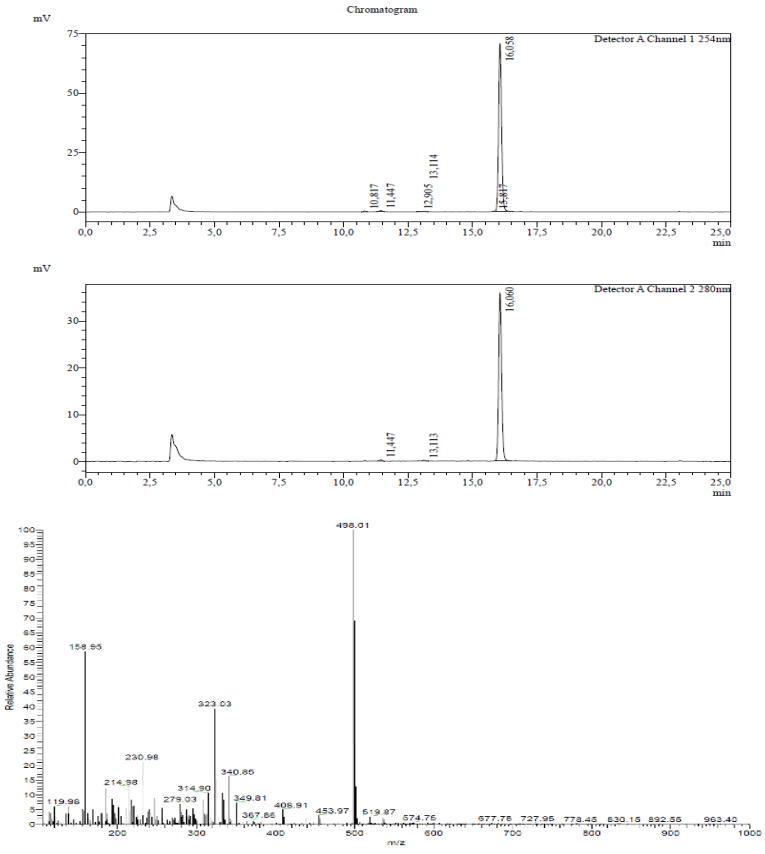

Compound **68**

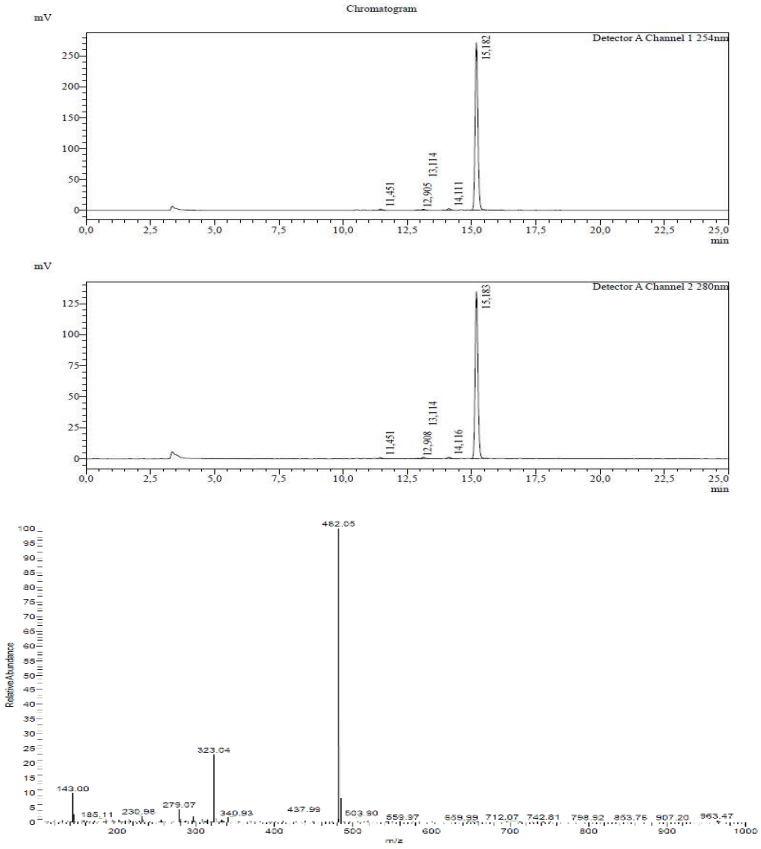

Compound **69**

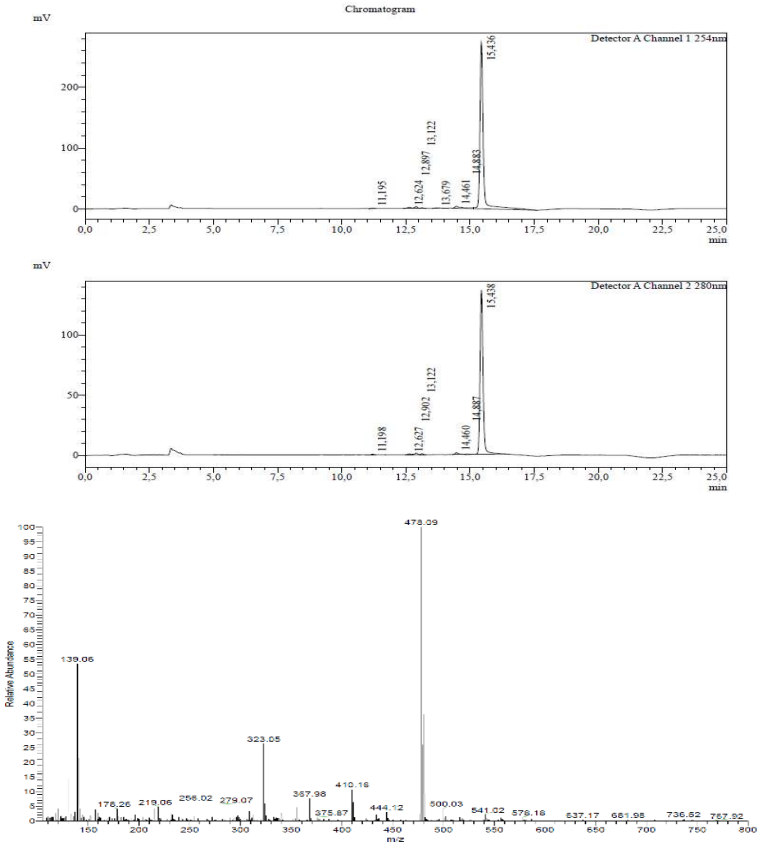

Compound **70**

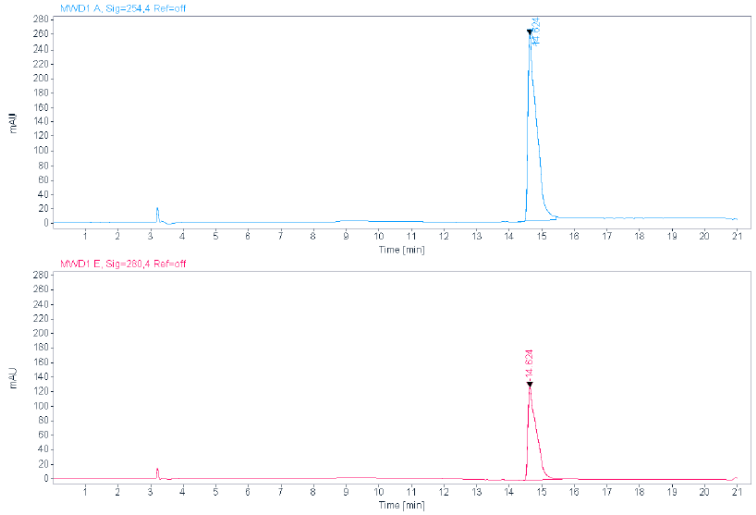

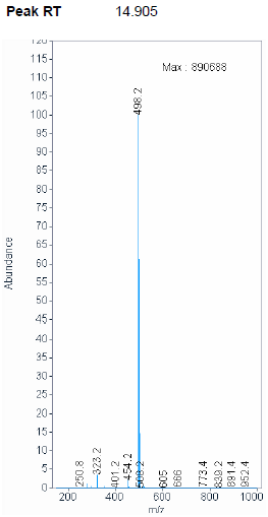

Compound **71**

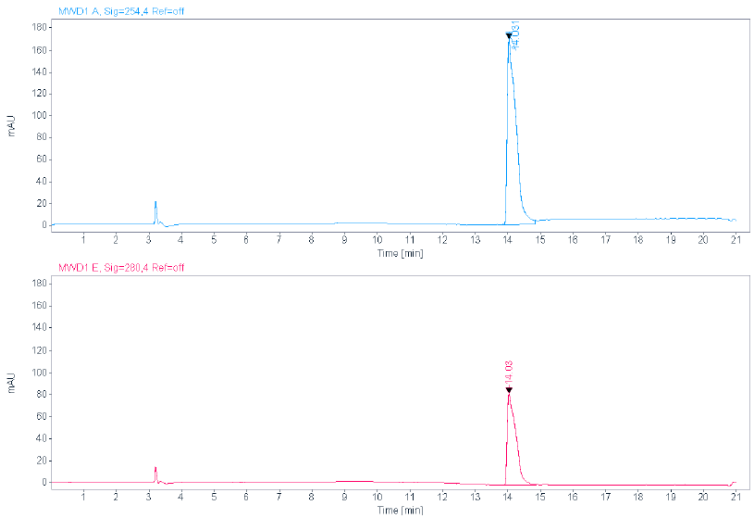

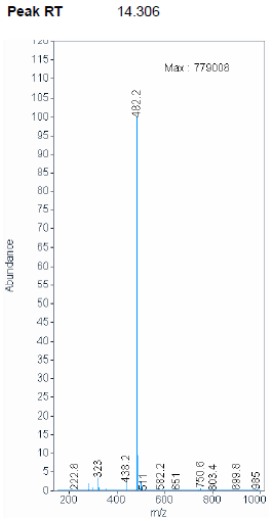

Compound **72**

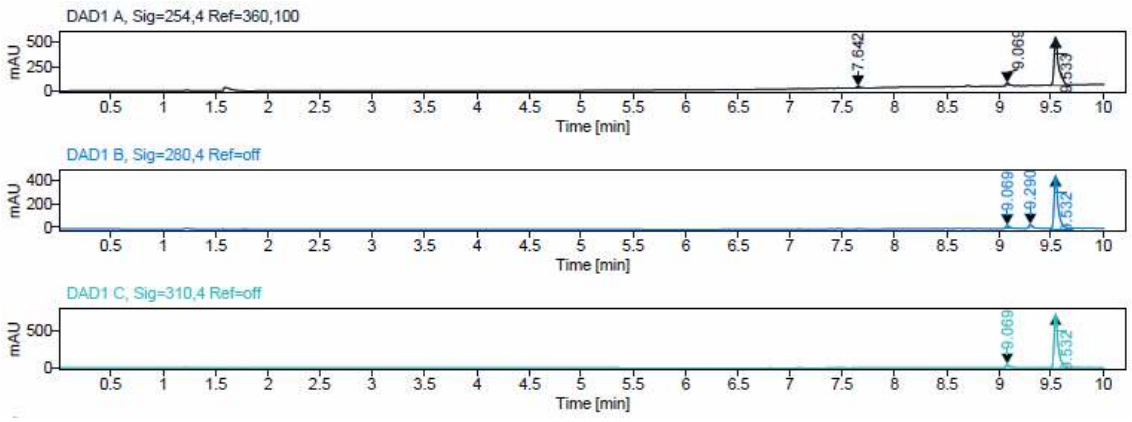

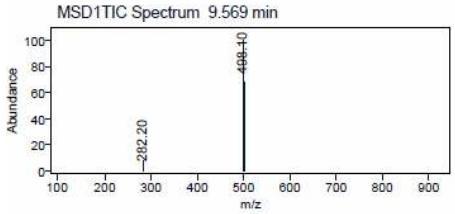

Compound **73**

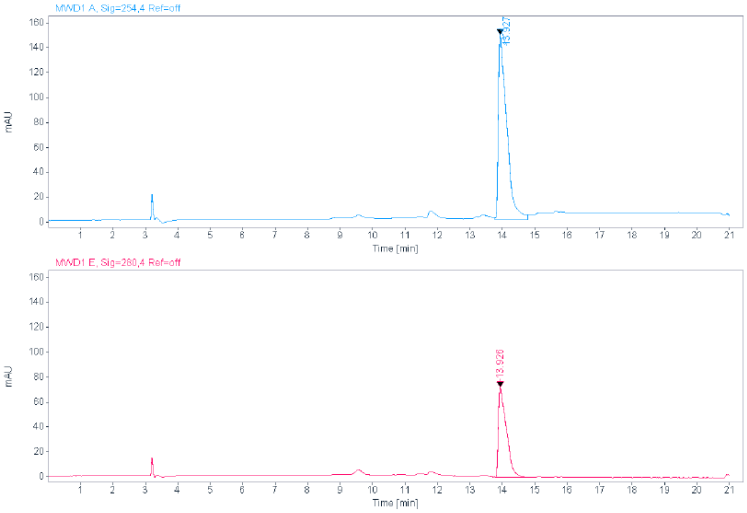

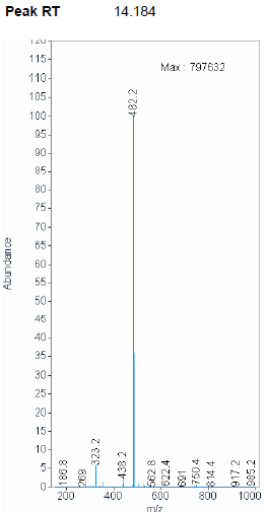

Compound **85**

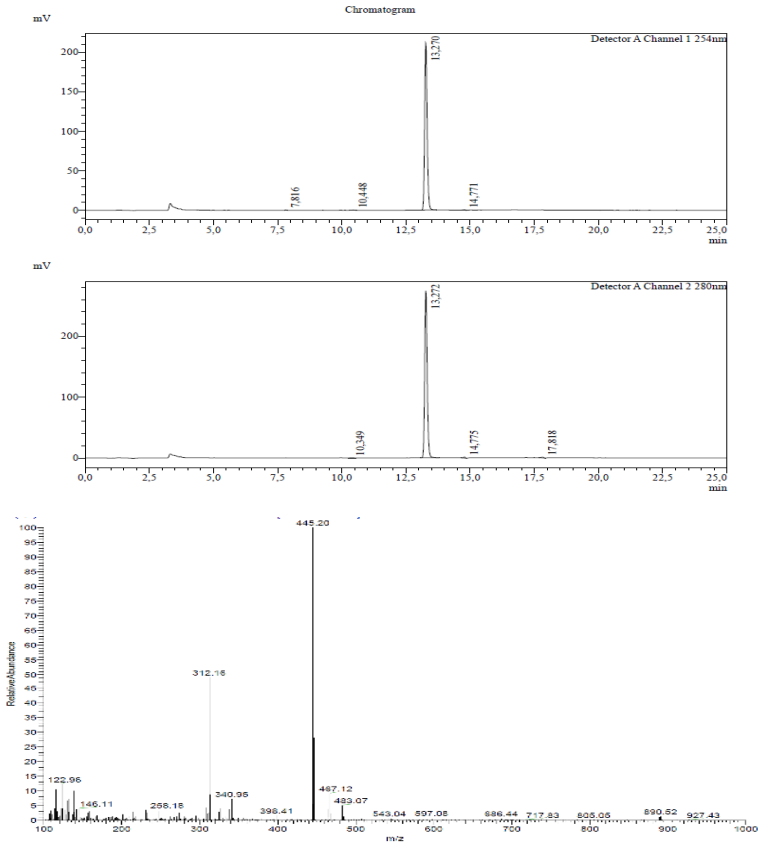

Compound **86**

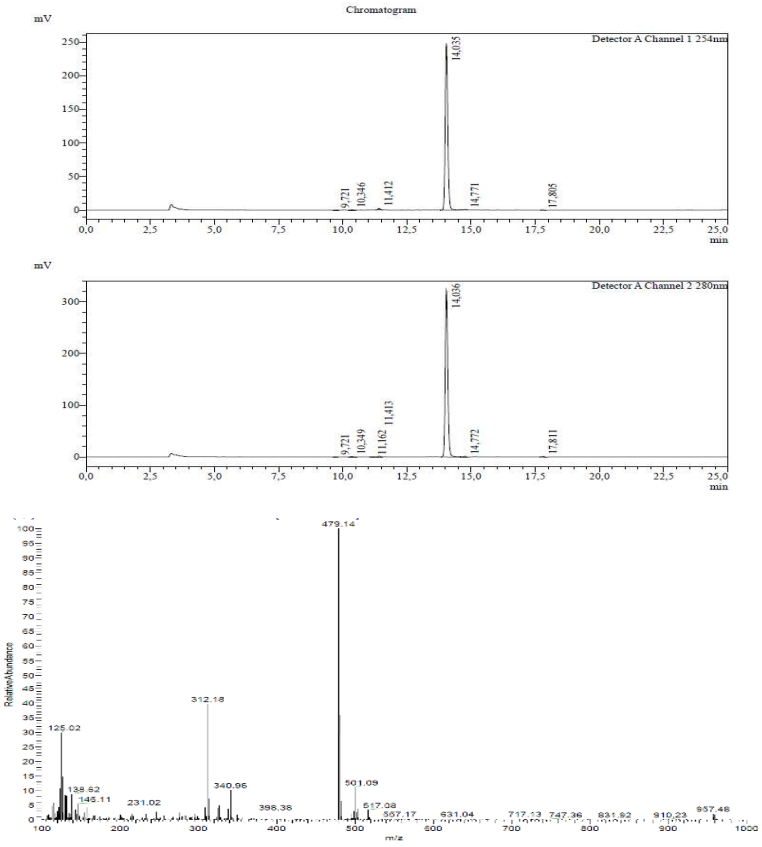

Compound **87**

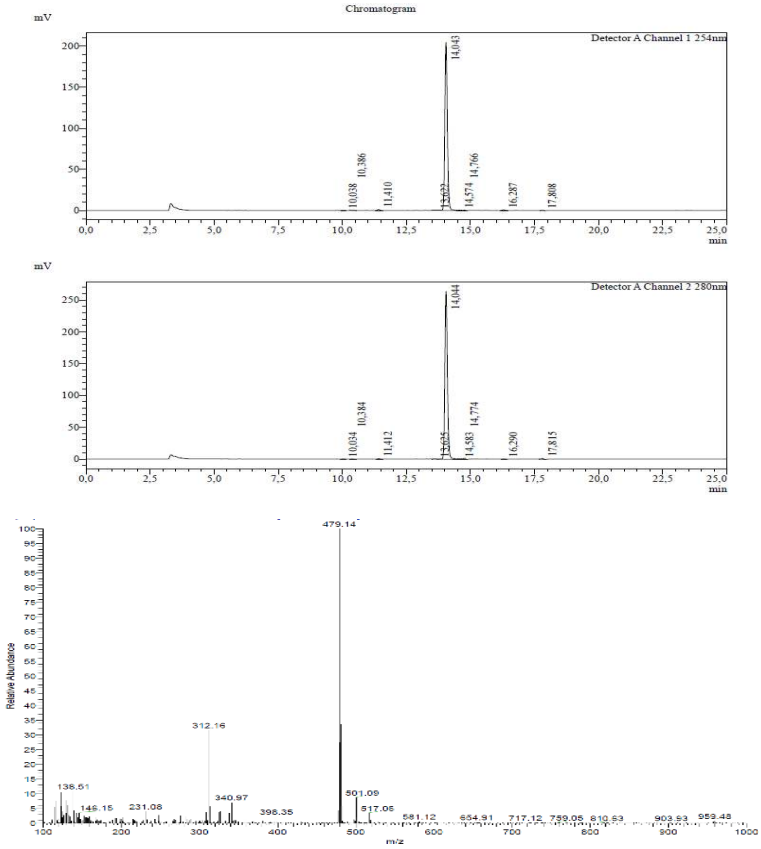

Compound **88**

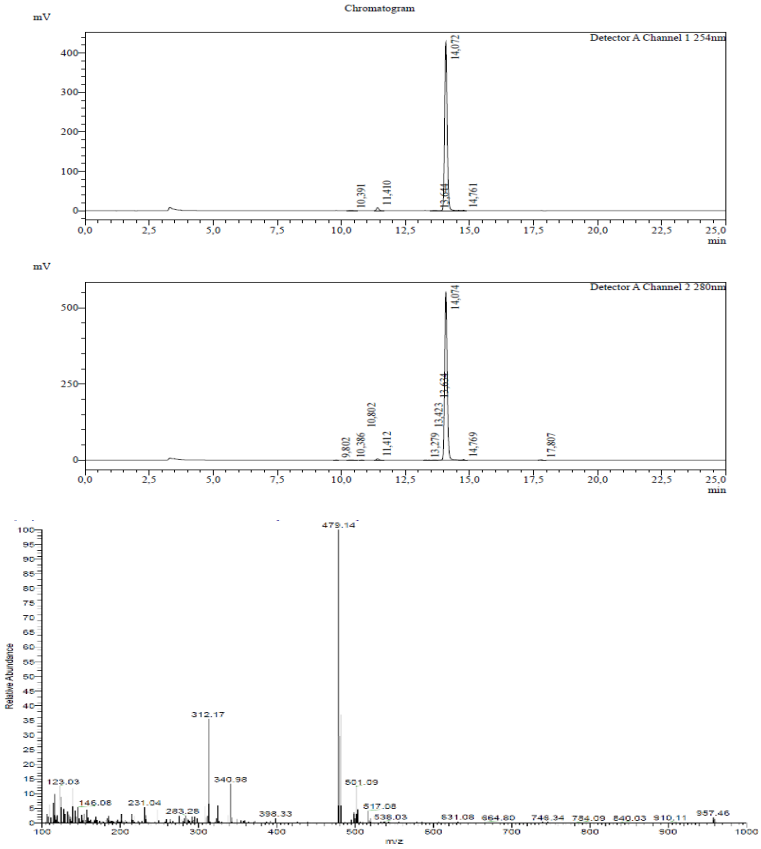

Compound **89**

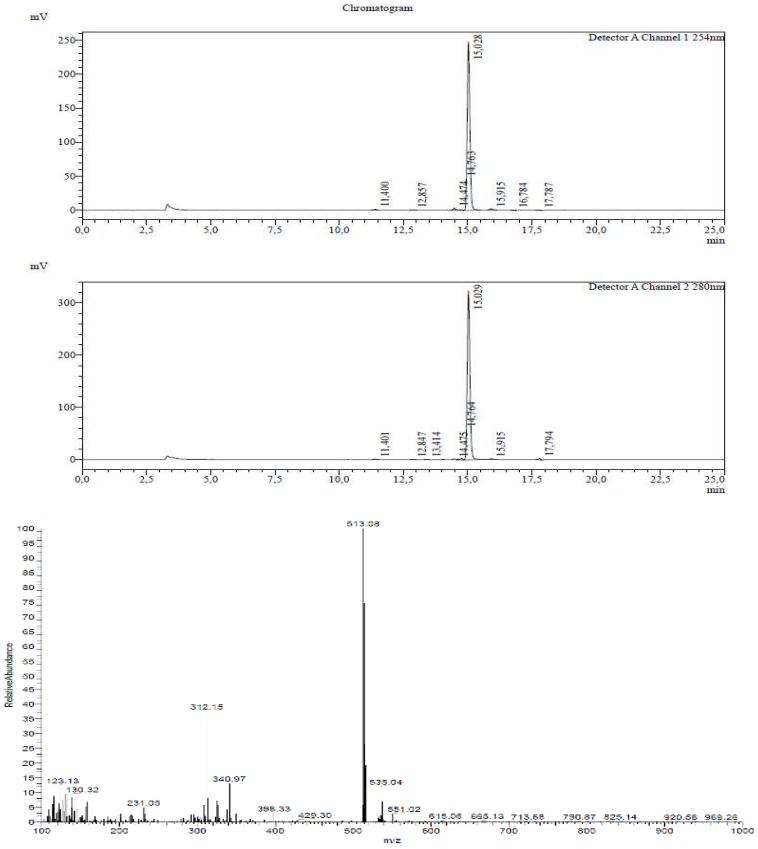

Compound **90**

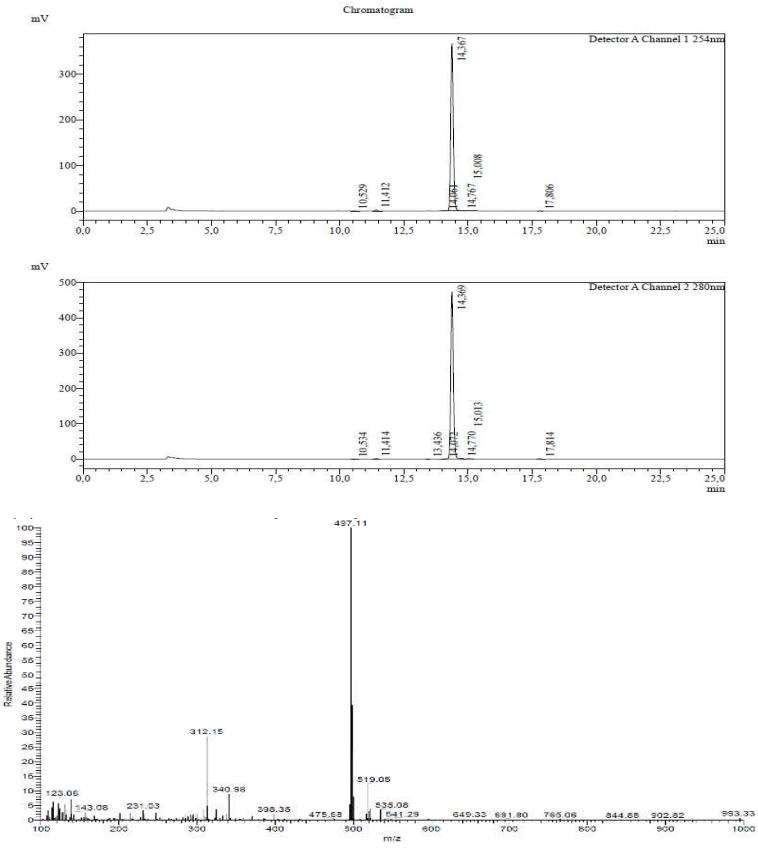

Compound **91**

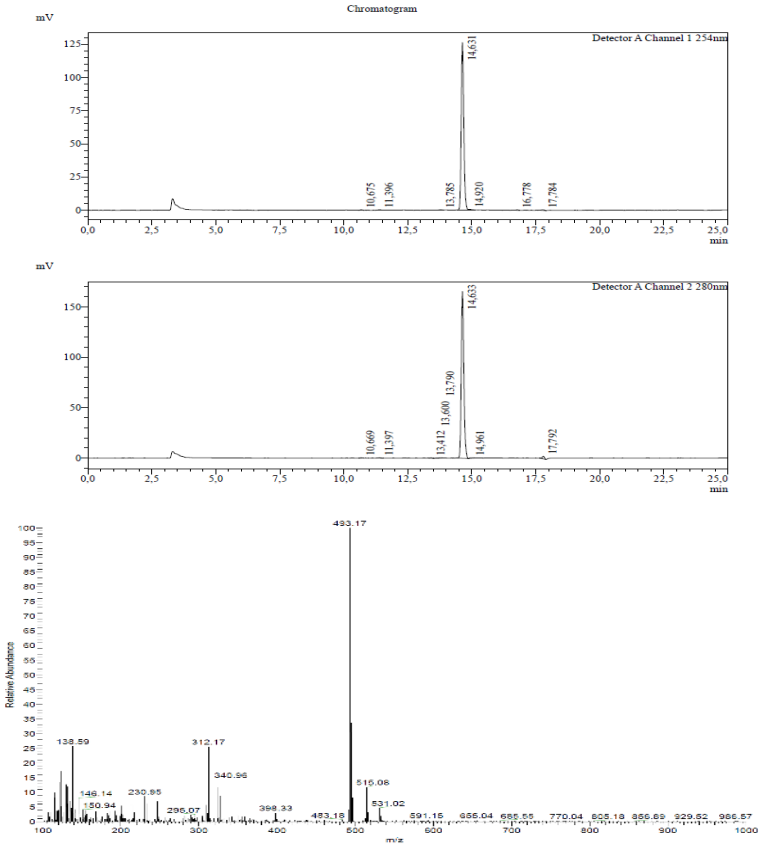

Compound **92**

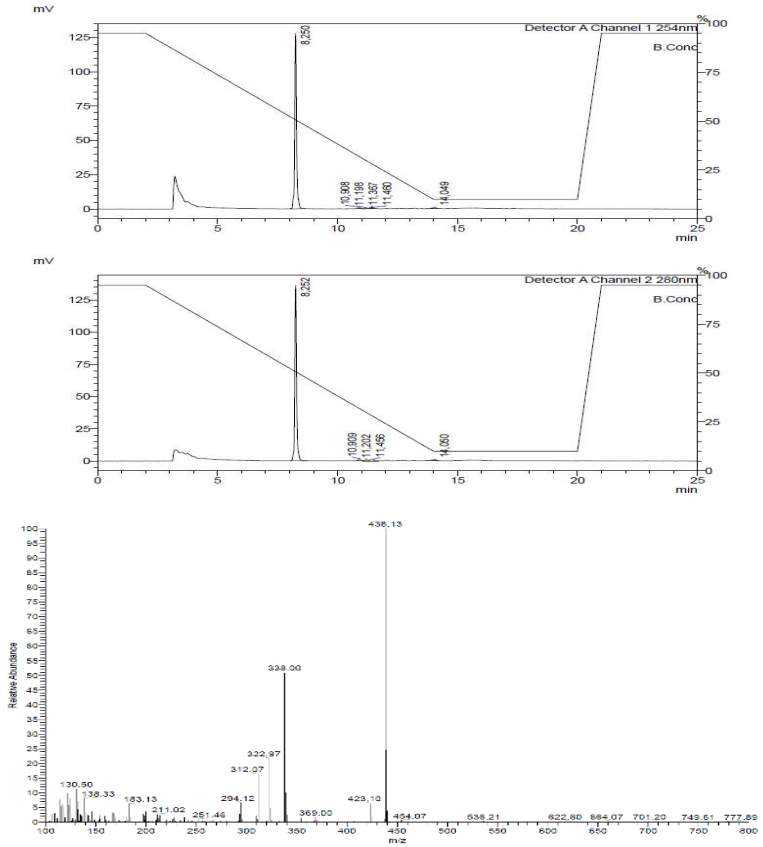

Compound **107**

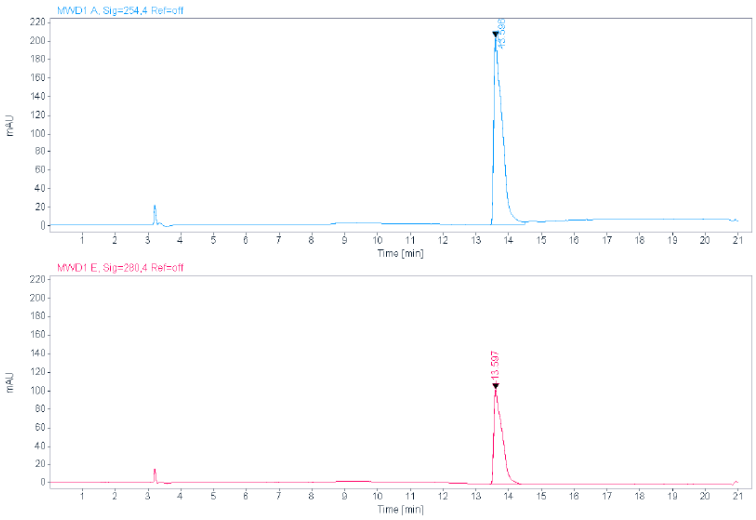

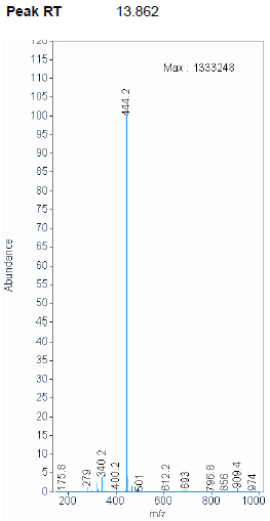

Compound **108**

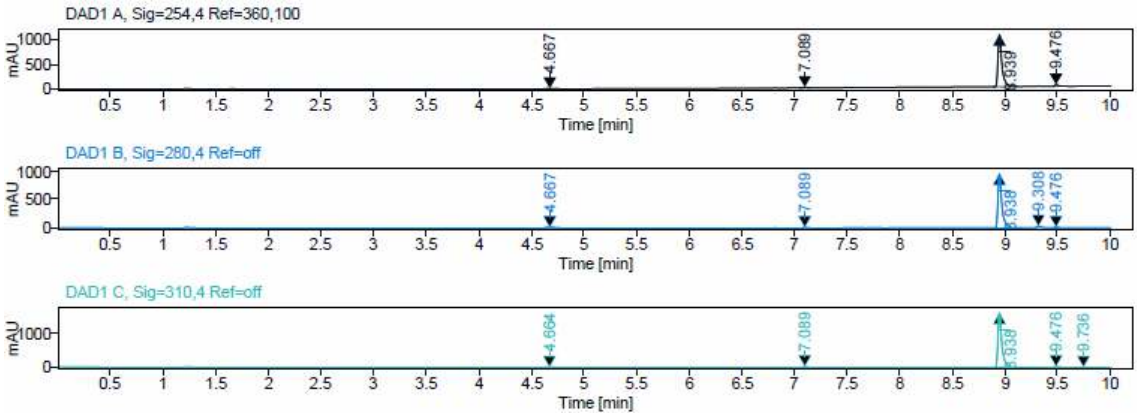

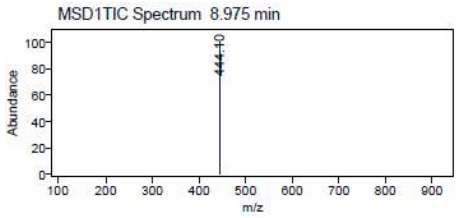

Compound **109**

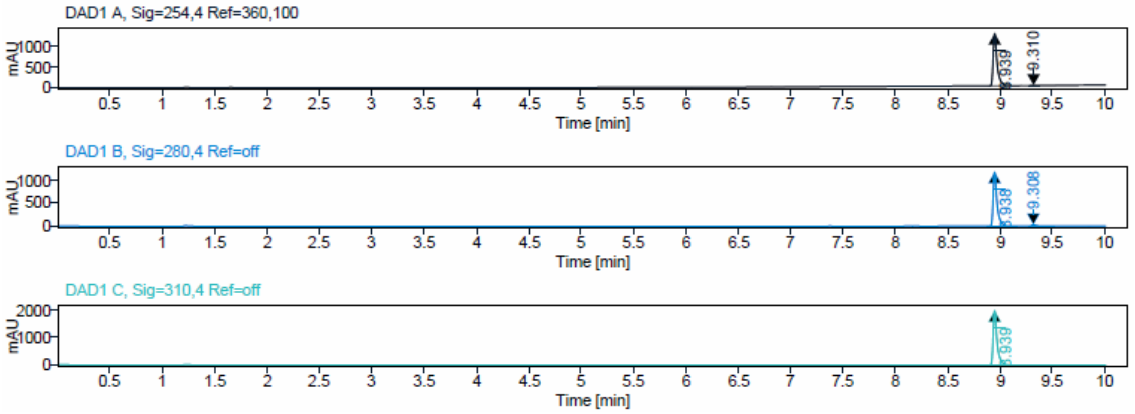

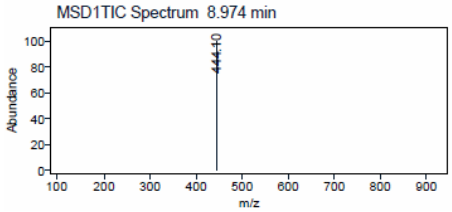

Compound **110**

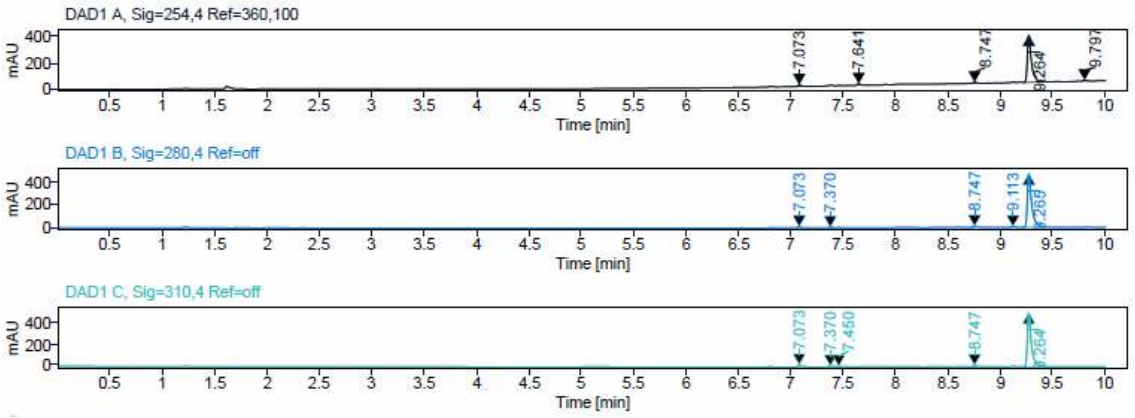

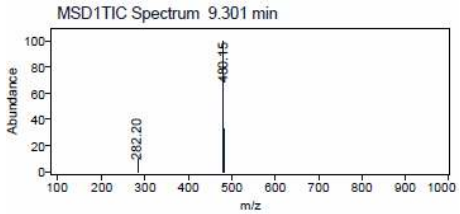

Compound **111**

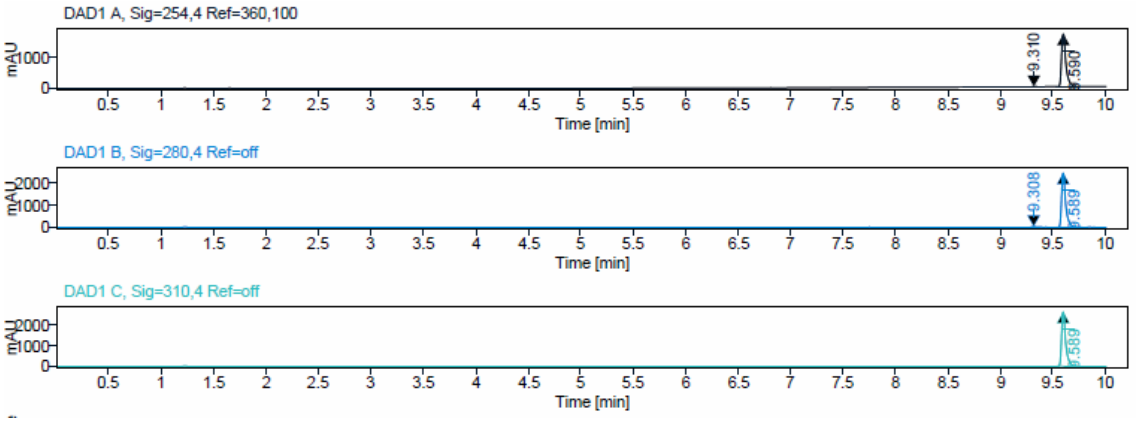

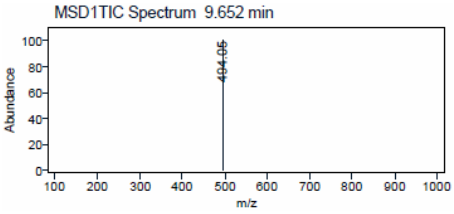

Compound **112**

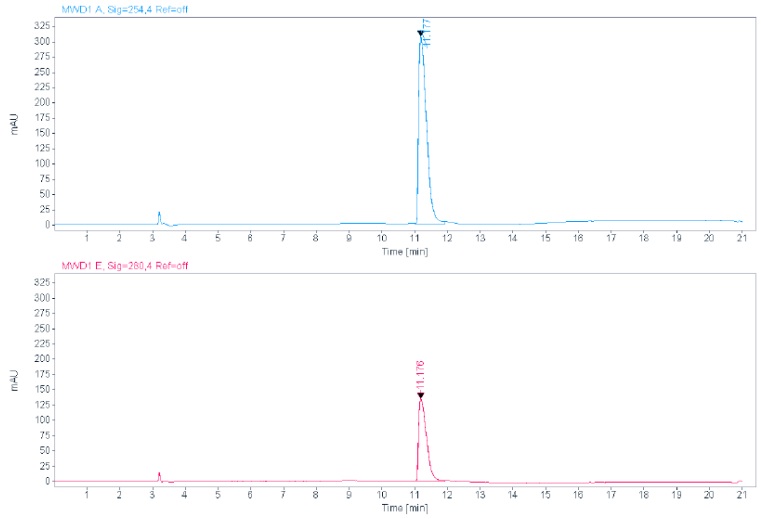

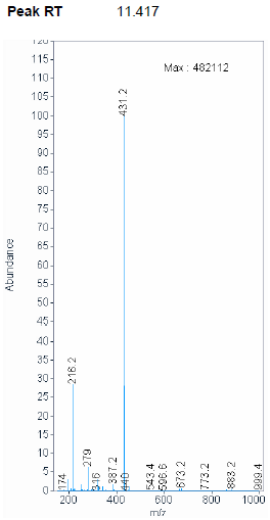

Compound **113**

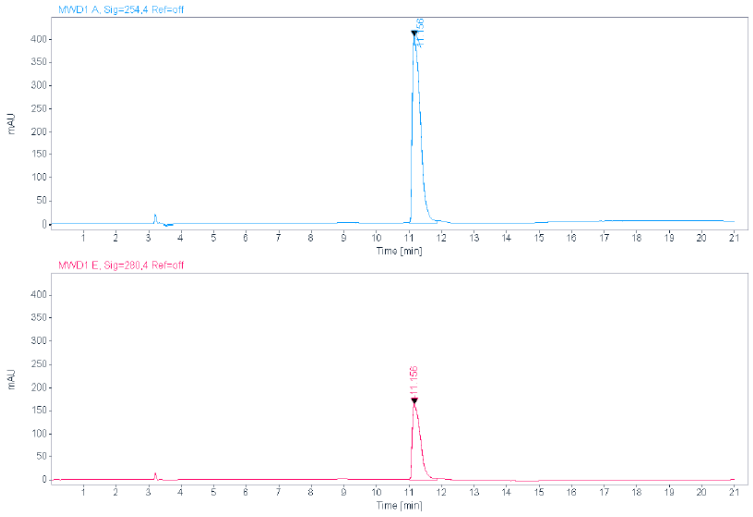

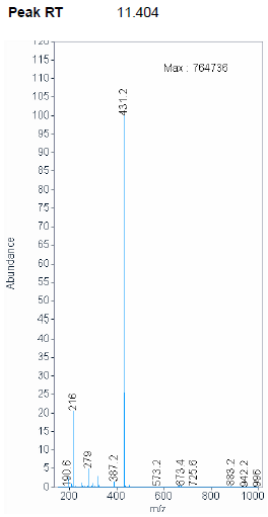

Compound **114**

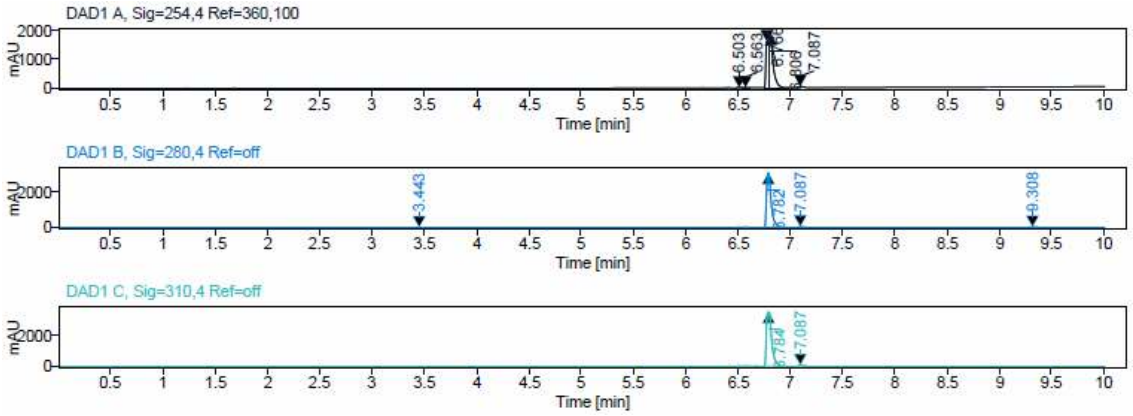

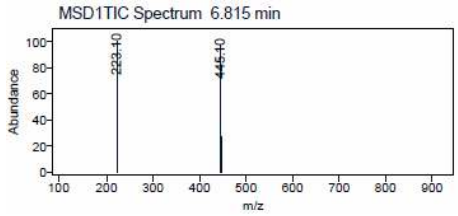

Compound **115**

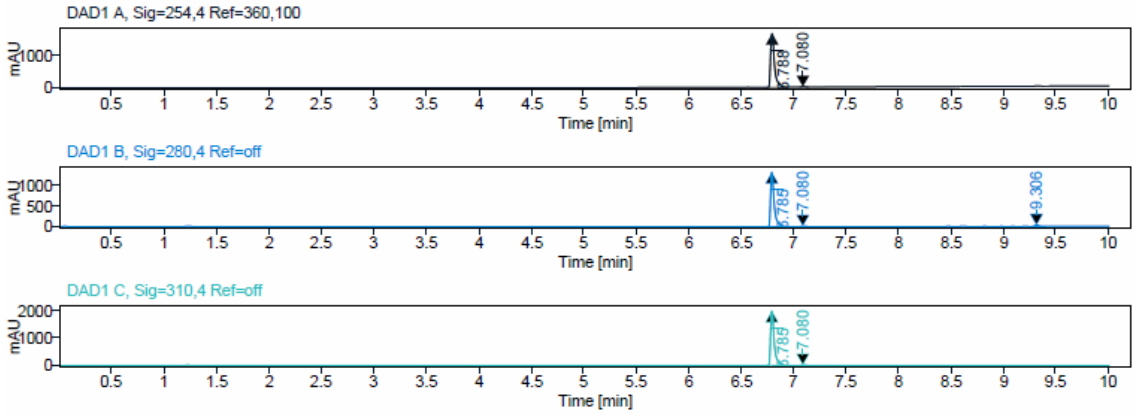

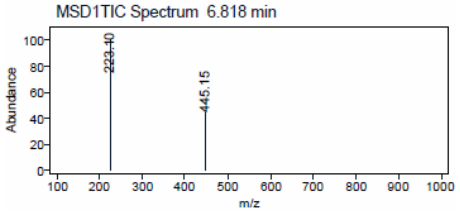

Compound **116**

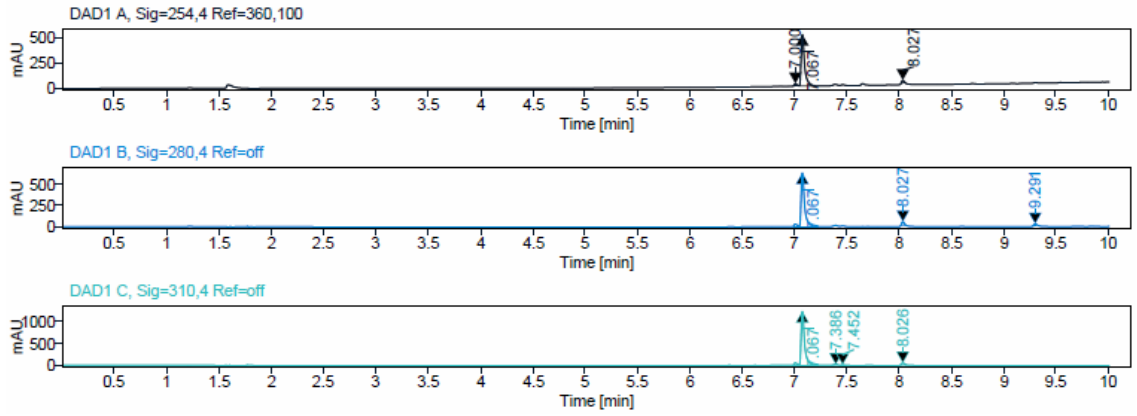

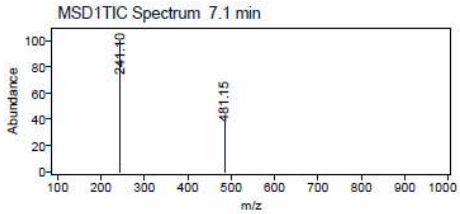

Compound **117**

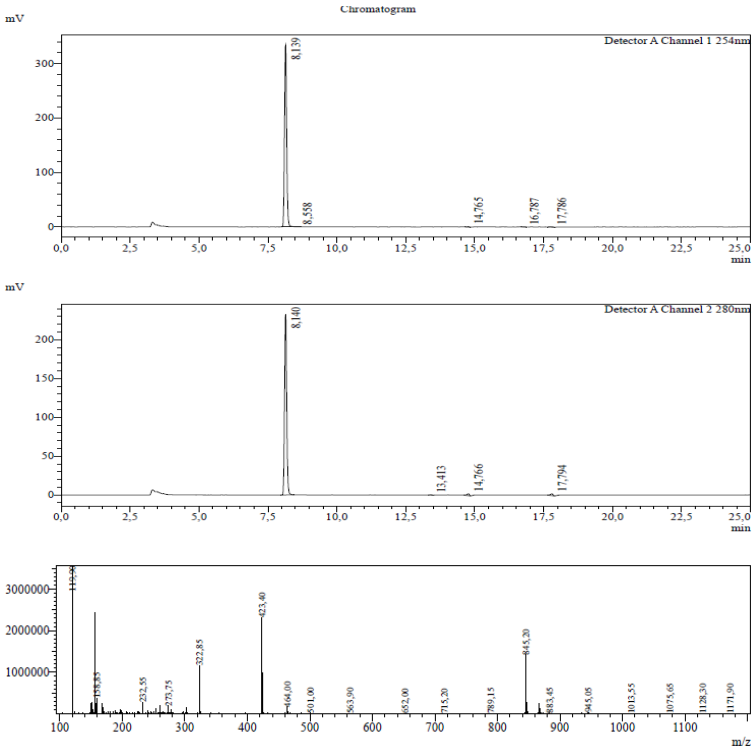

Compound **118**

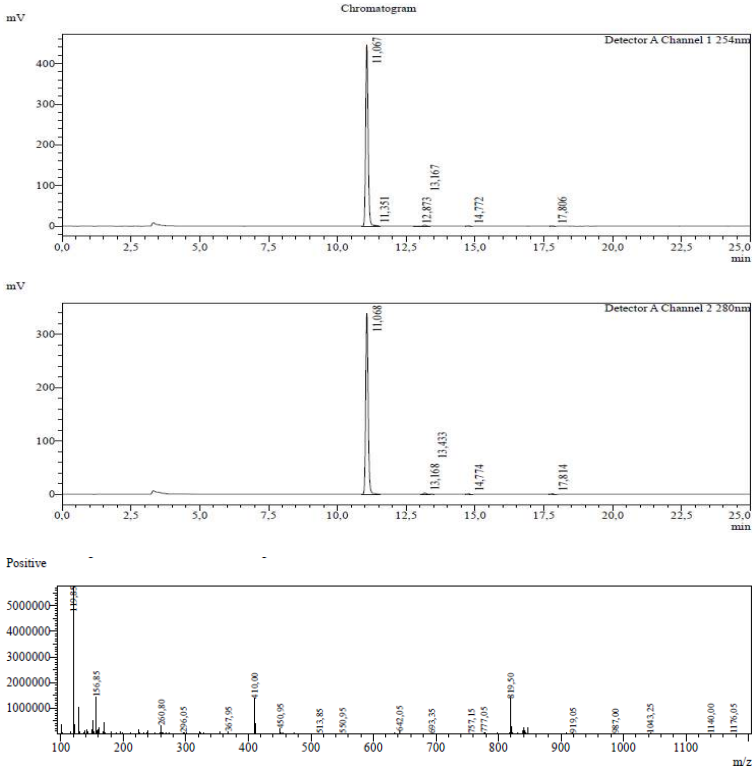

Compound **119**

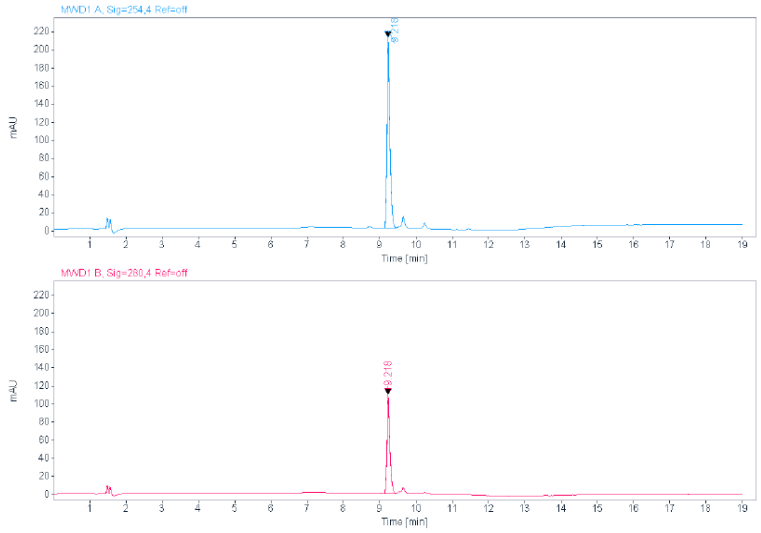

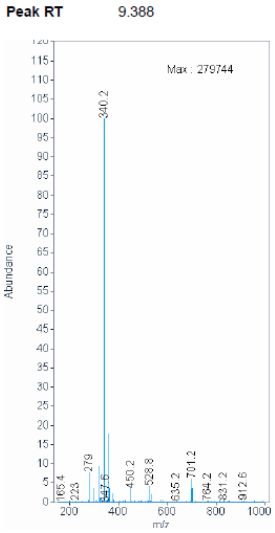

Compound **120**

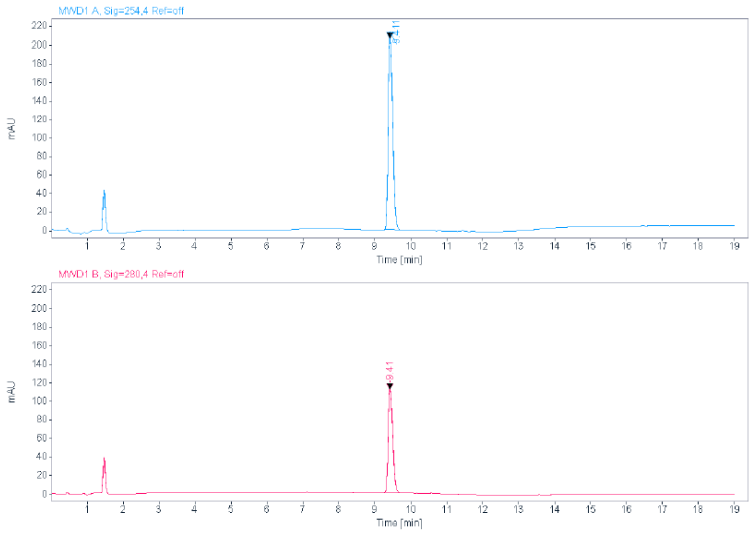

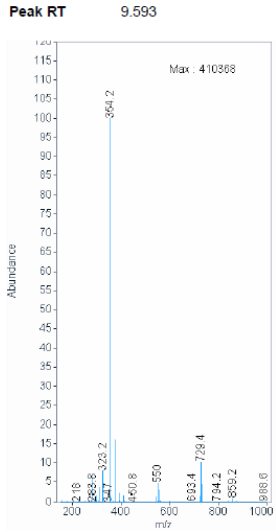

Compound **121** (CK156)

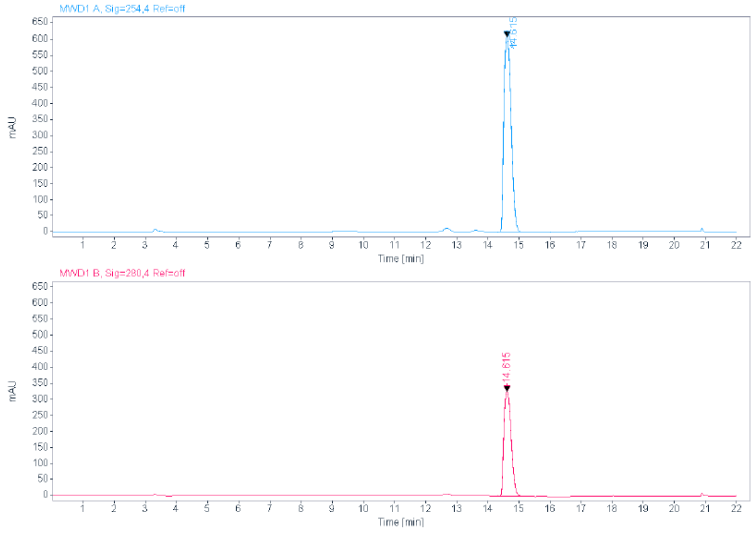

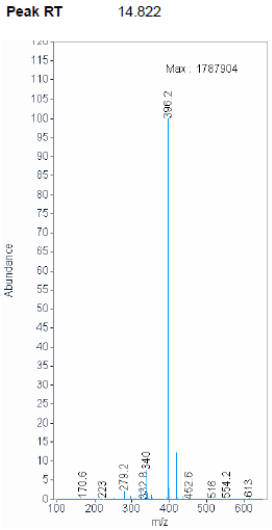

Compound **172**

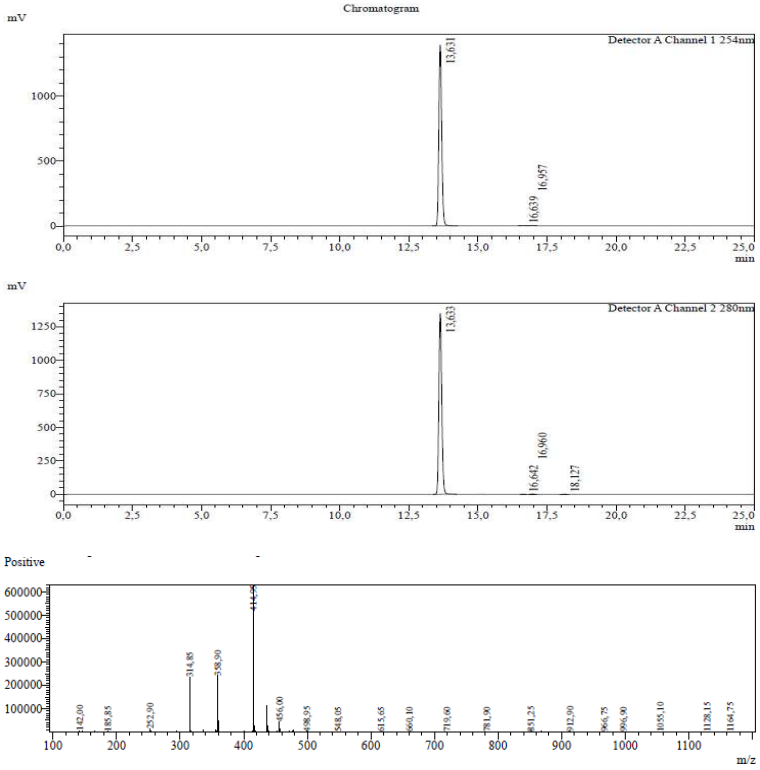

Compound **175**

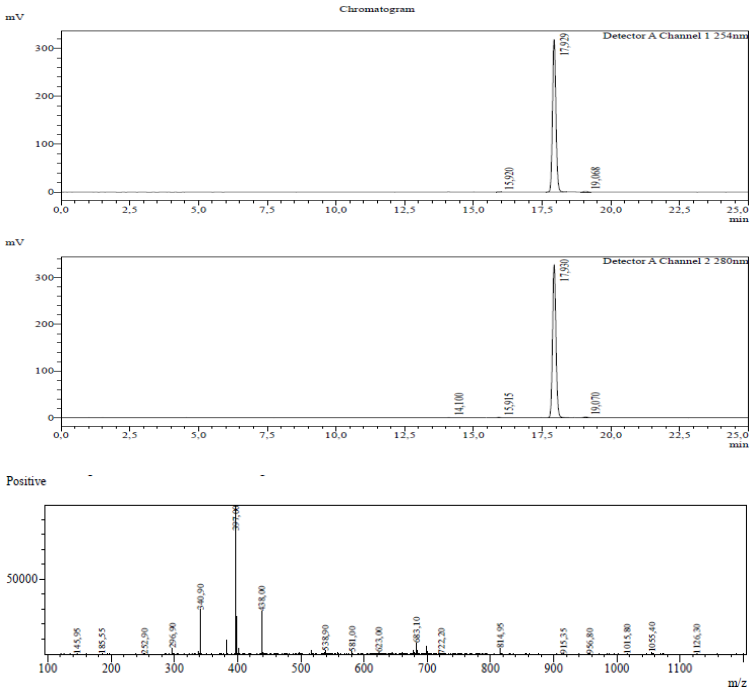

Compound **132**

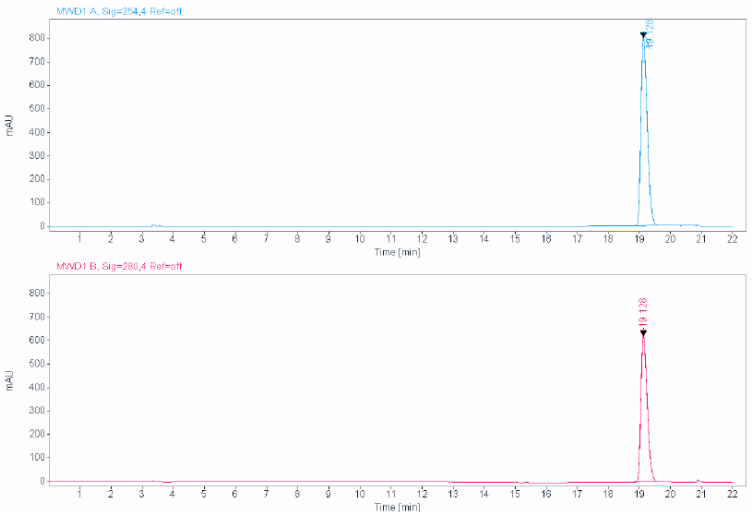

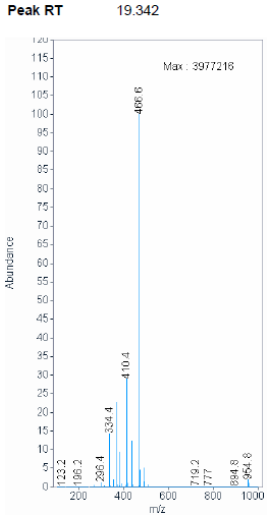

Compound **134**

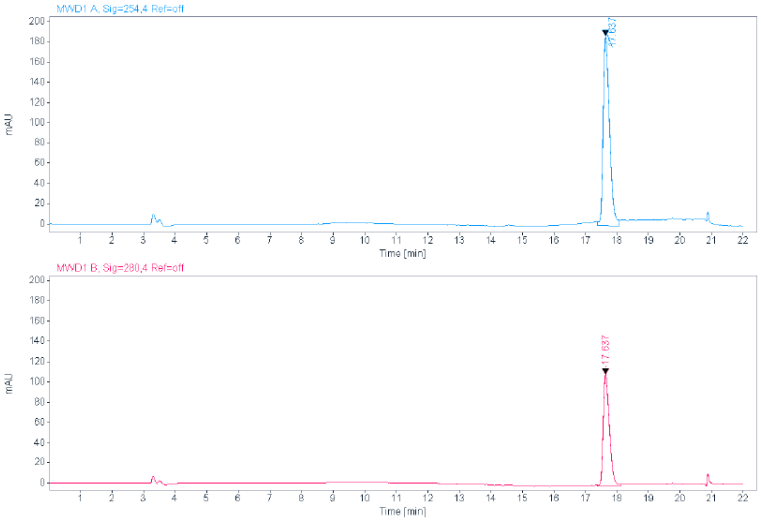

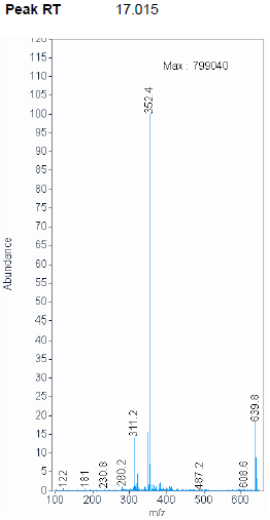

Compound **136**

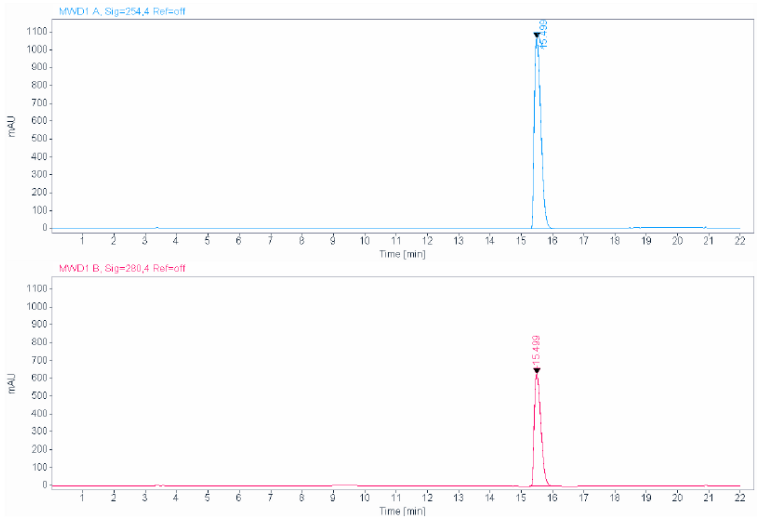

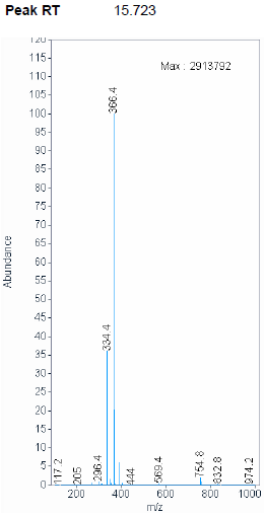

Compound **38**

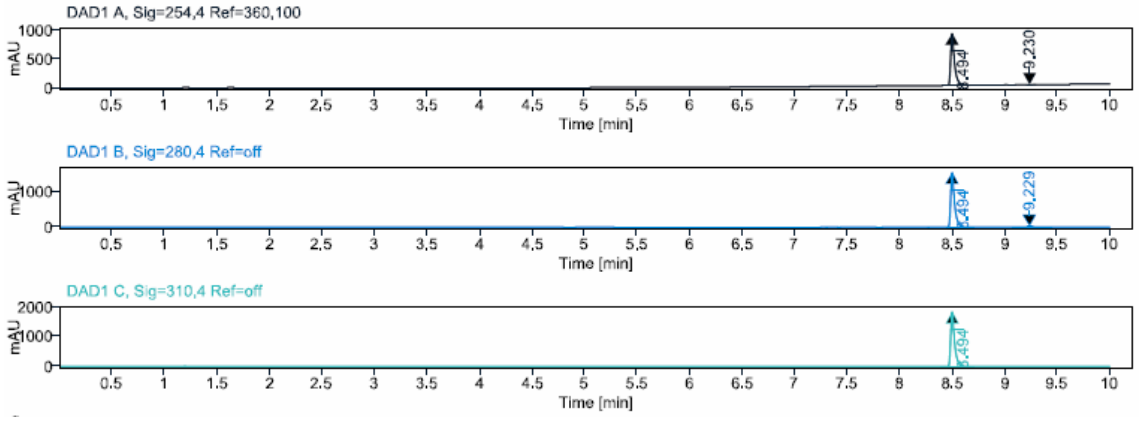

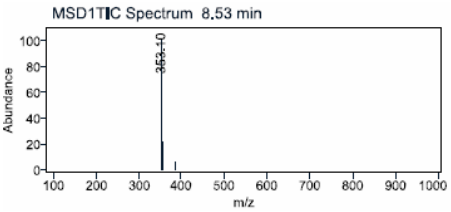

Compound **138**

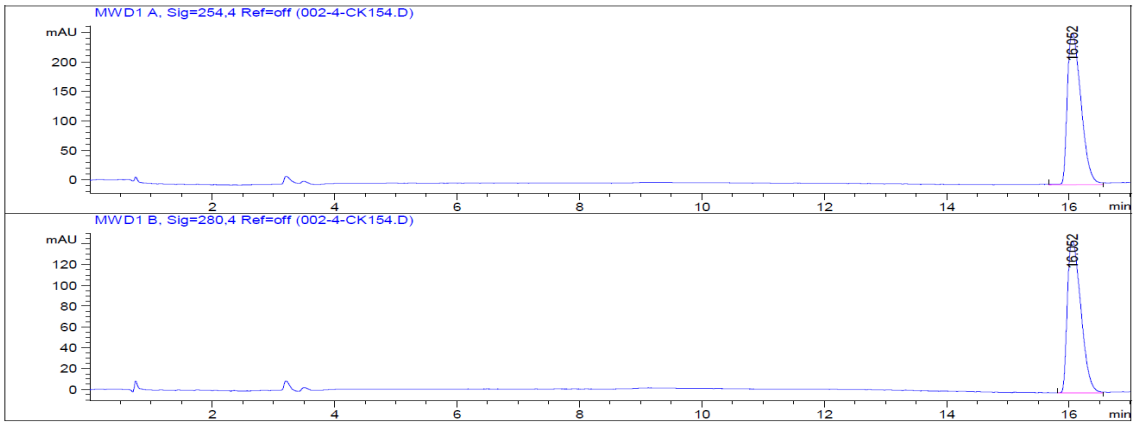

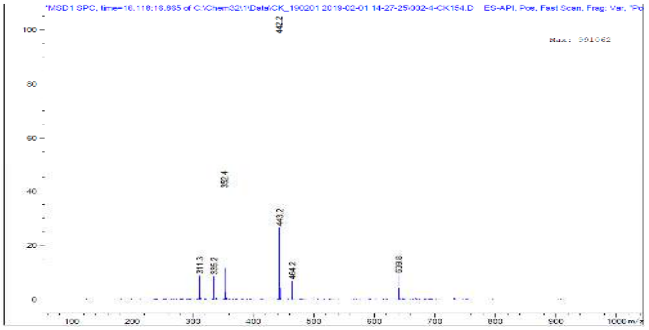

Compound **139**

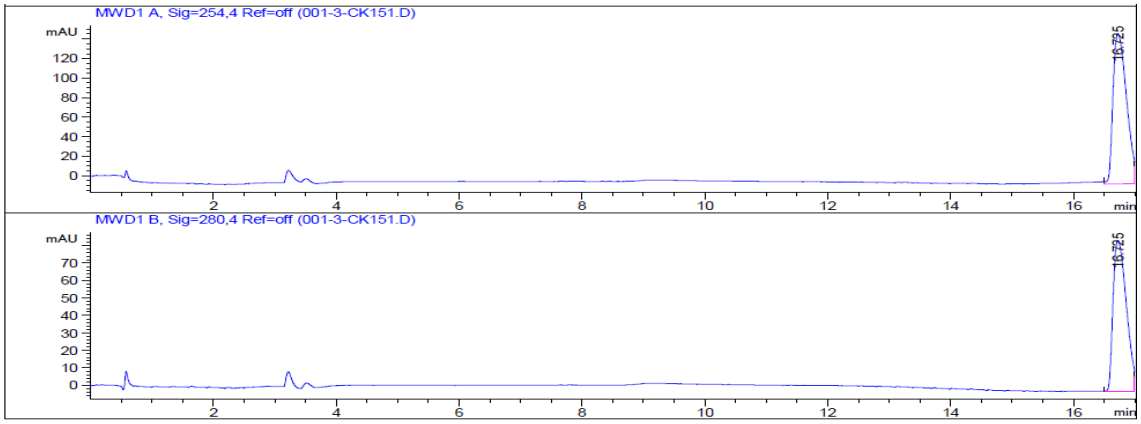

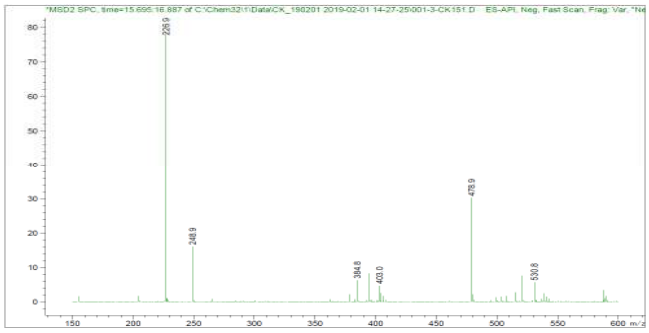

Compound **140**

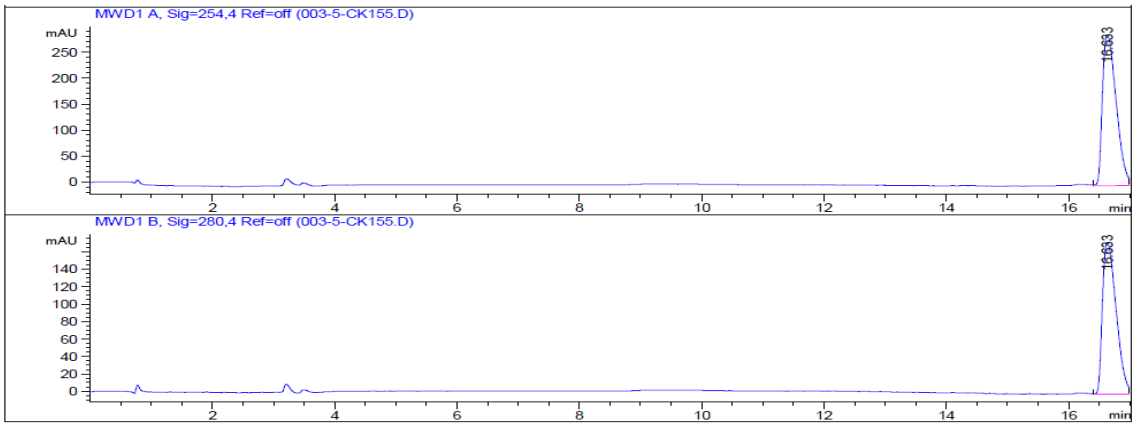

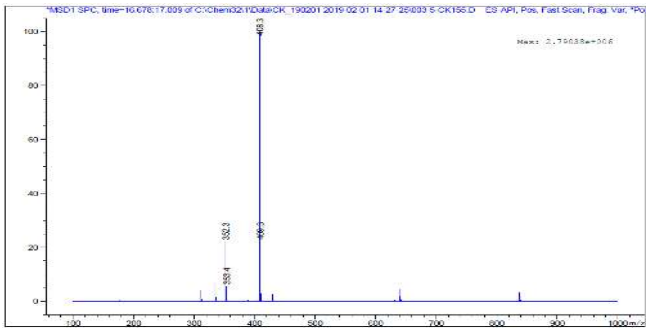

Compound **133**

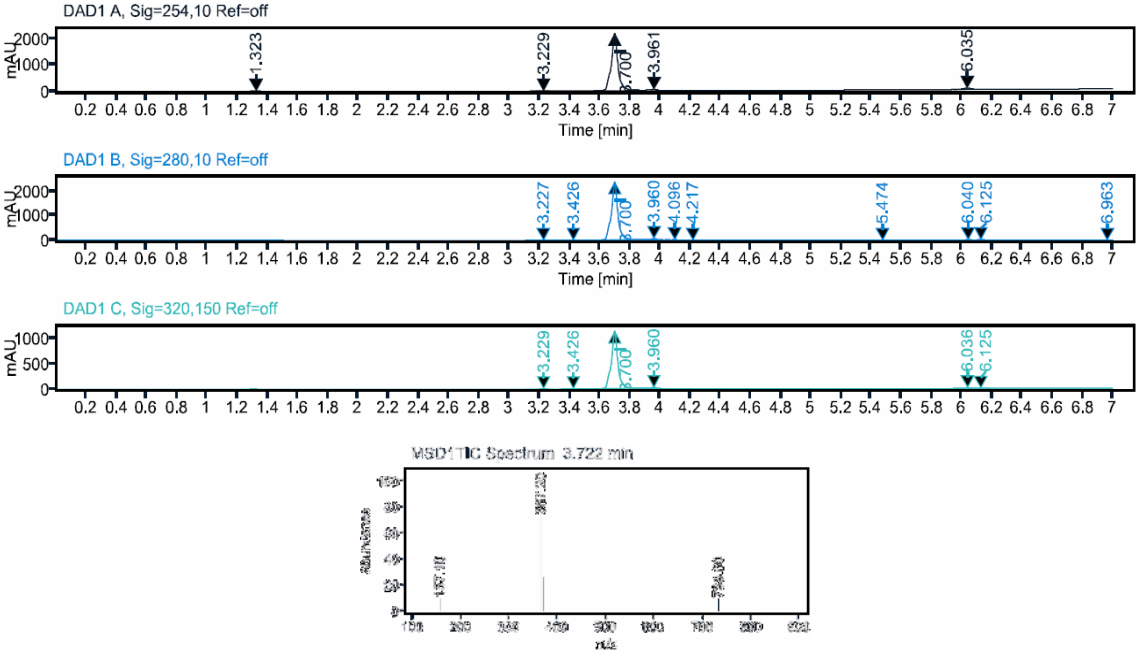

Compound **135**

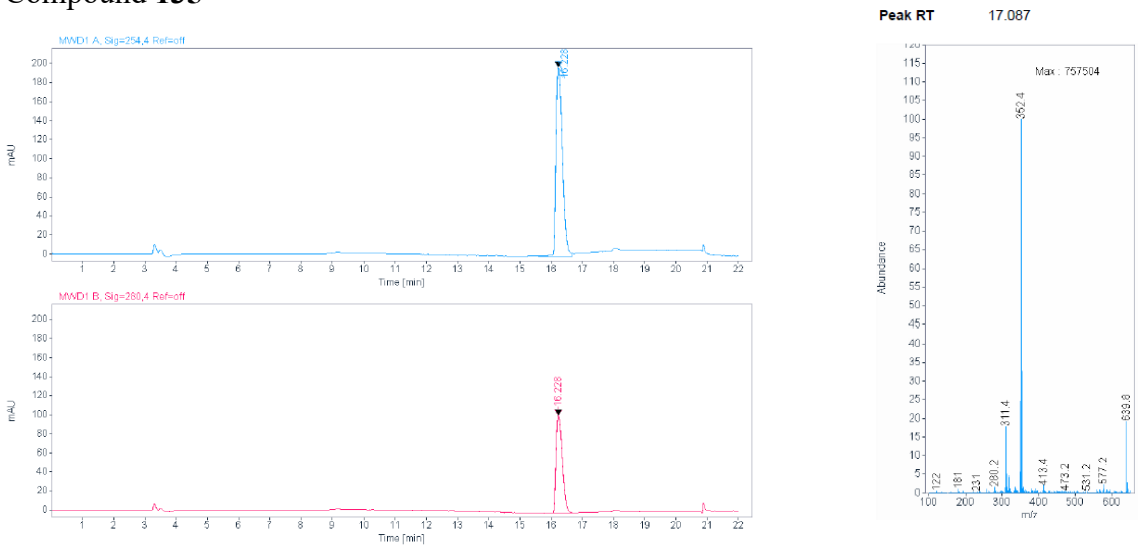

Compound **137**

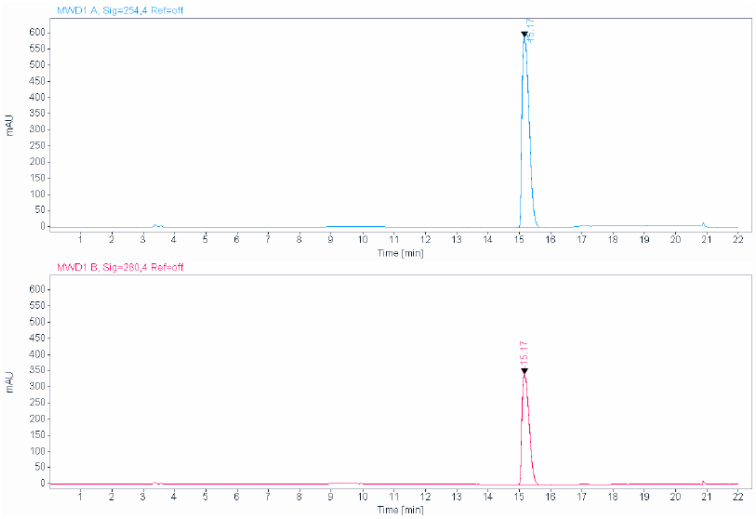

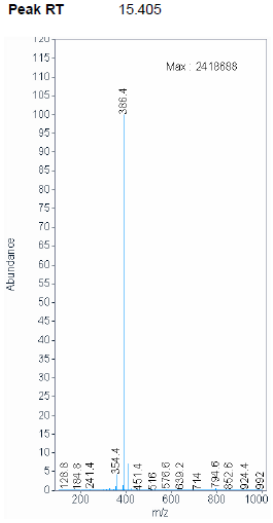

Compound **139**

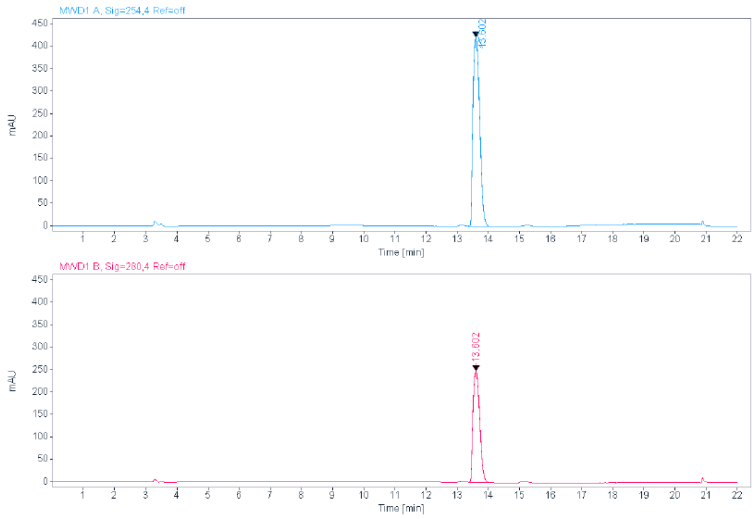

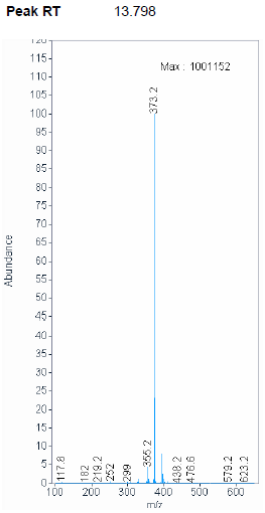

Compound **141**

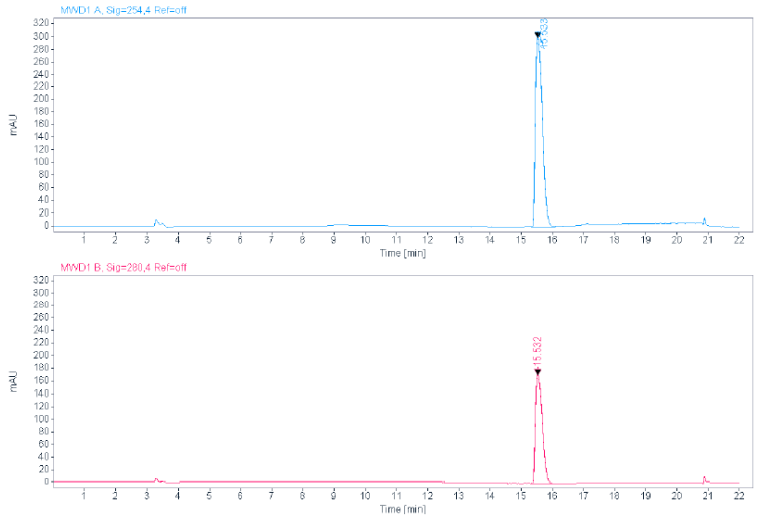

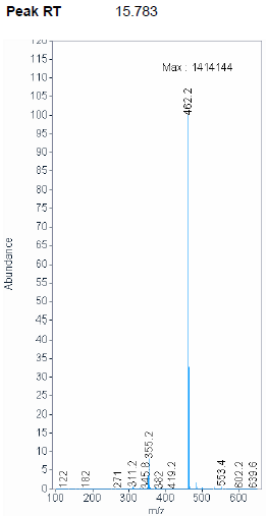

Compound **142**

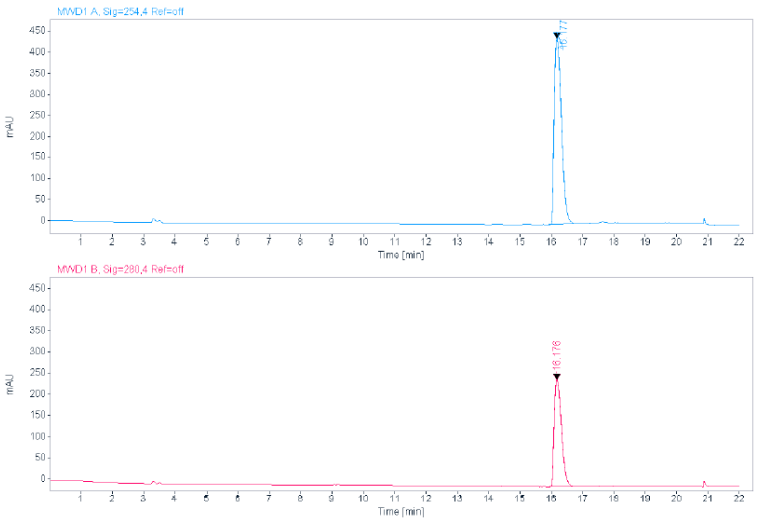

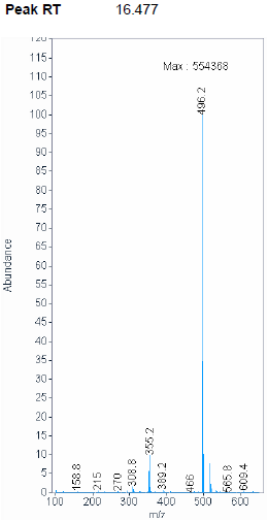

Compound **143**

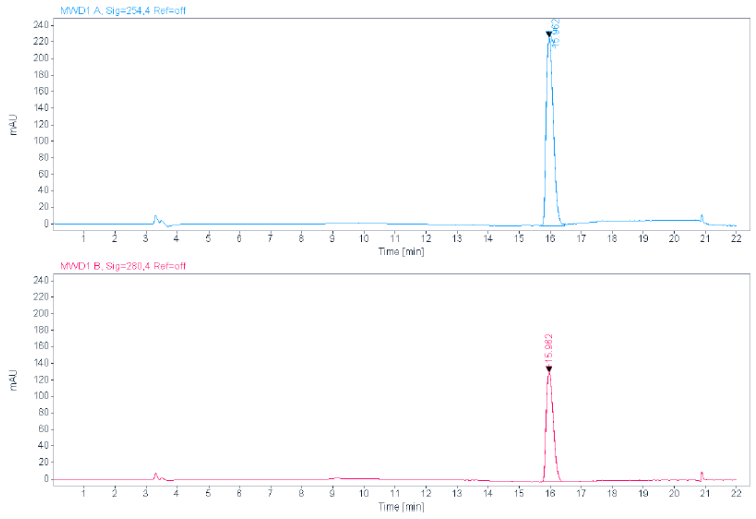

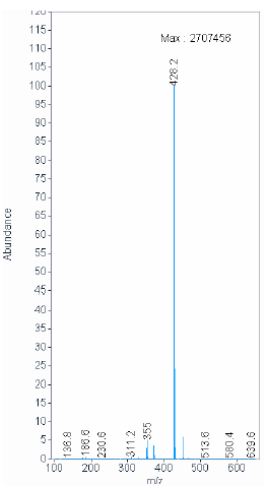

Compound **144**

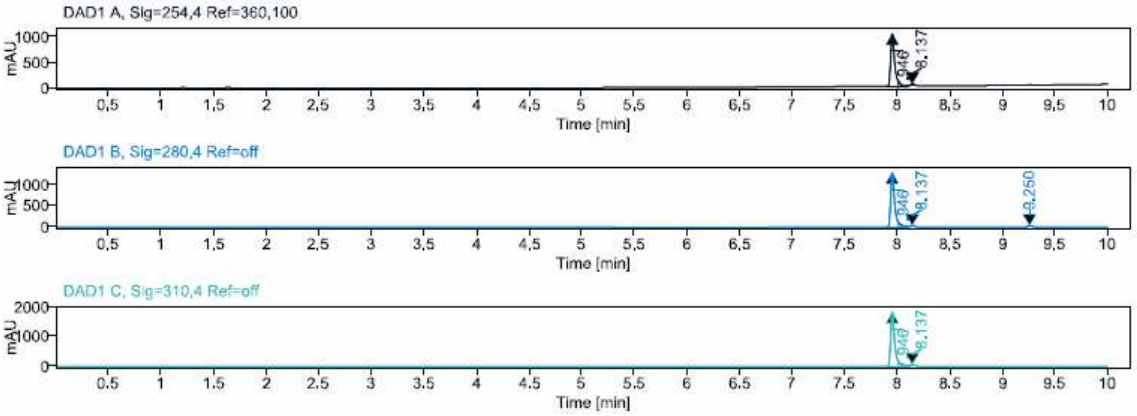

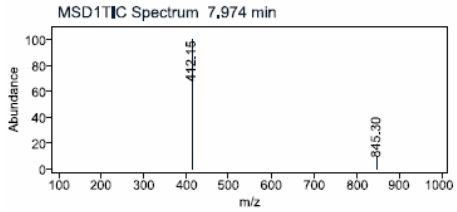

Compound **145**

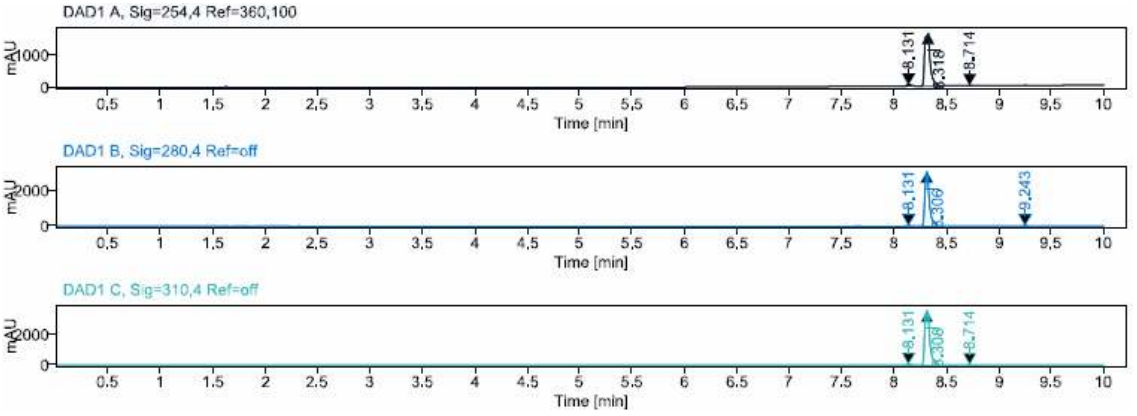

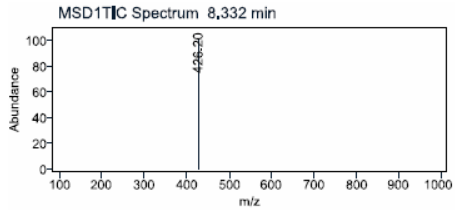

Compound **146**

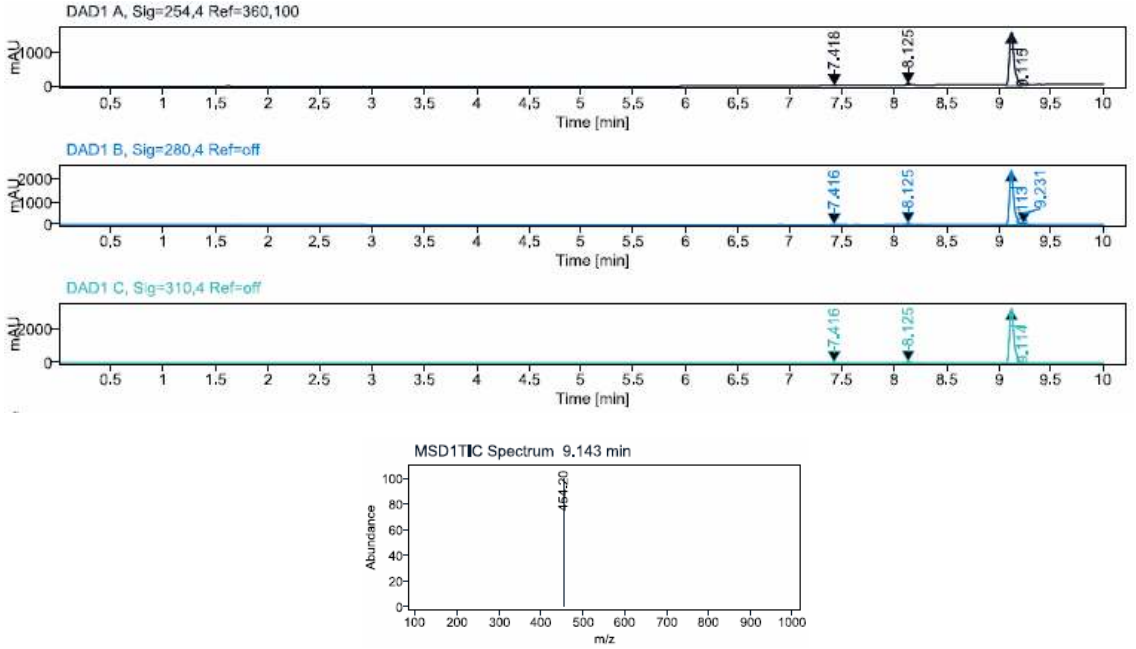

Compound **147**

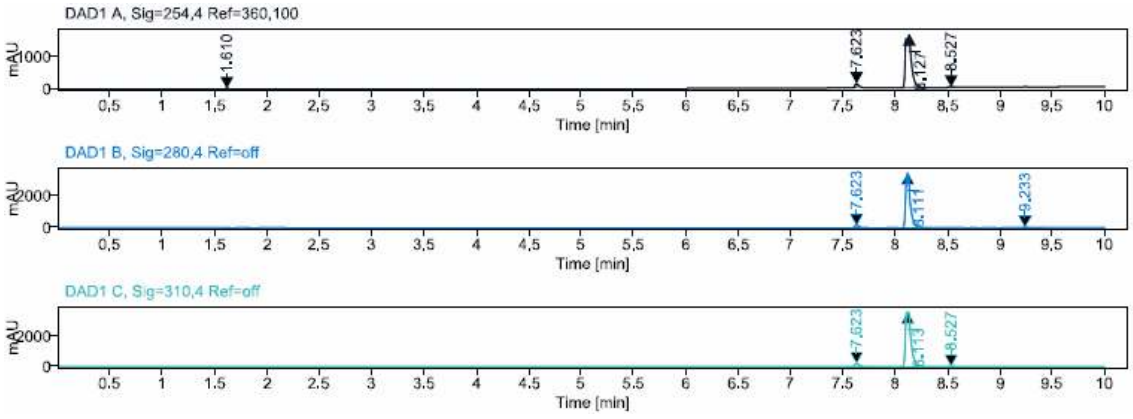

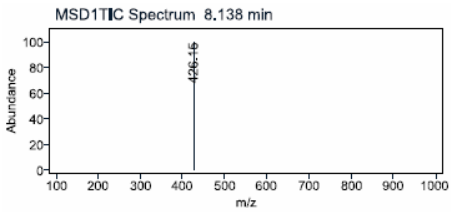

Compound **148**

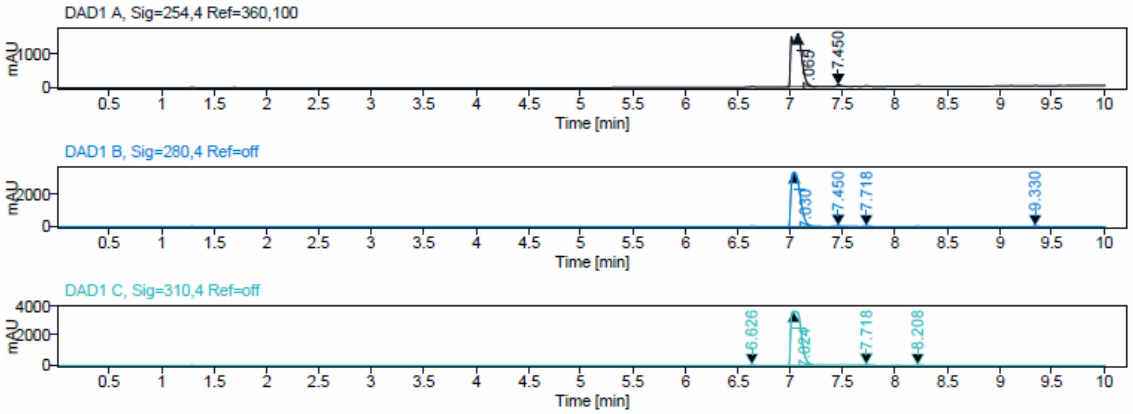

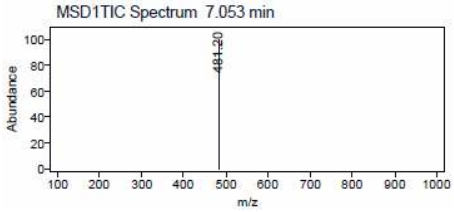

Compound **149**

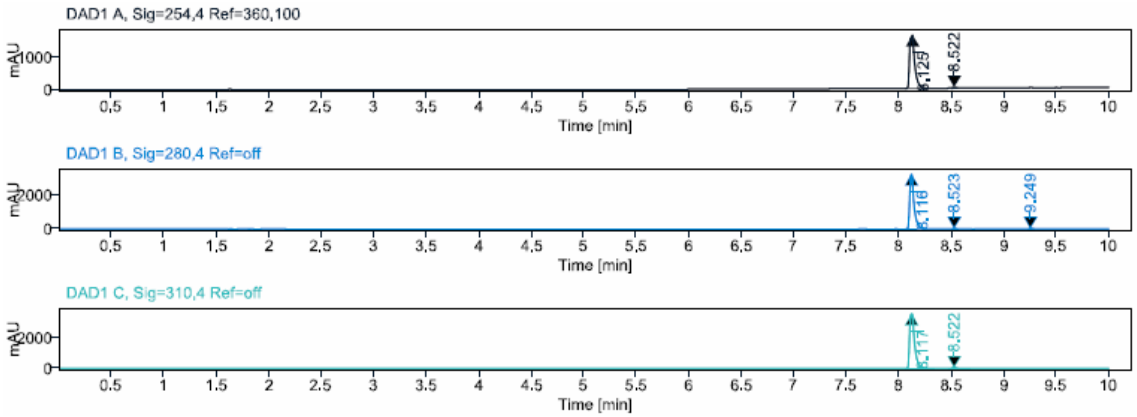

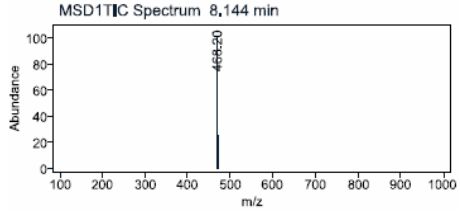

Compound **150**

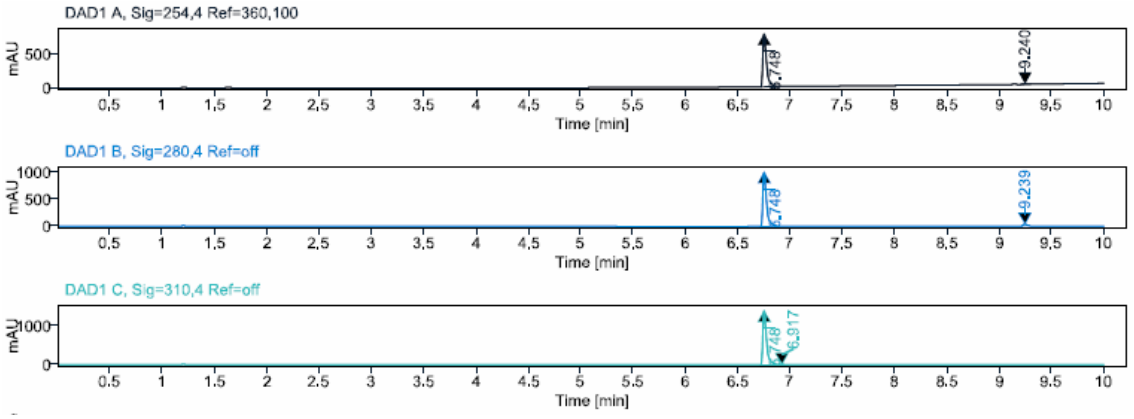

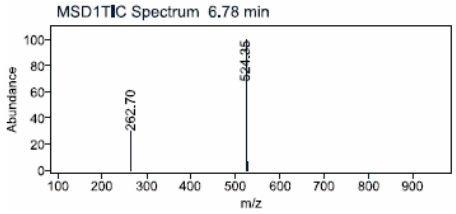

Compound **151**

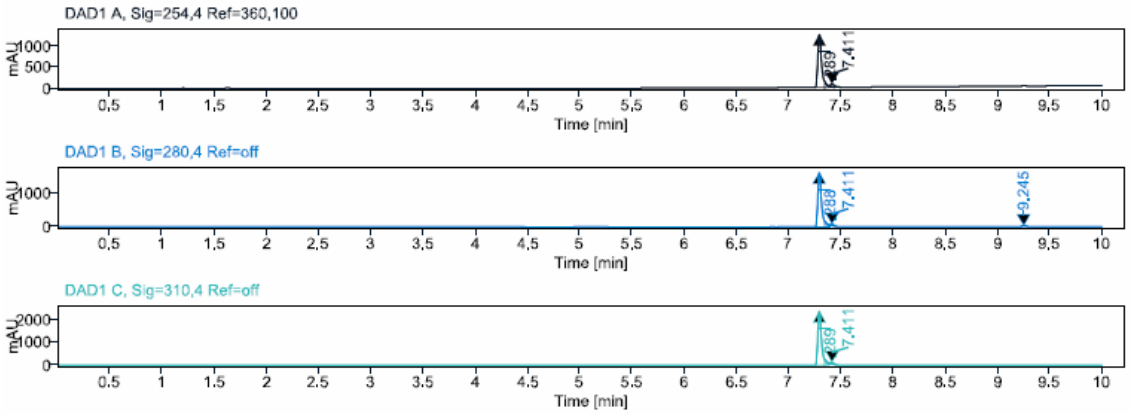

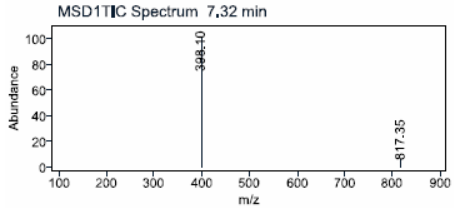

Compound **152**

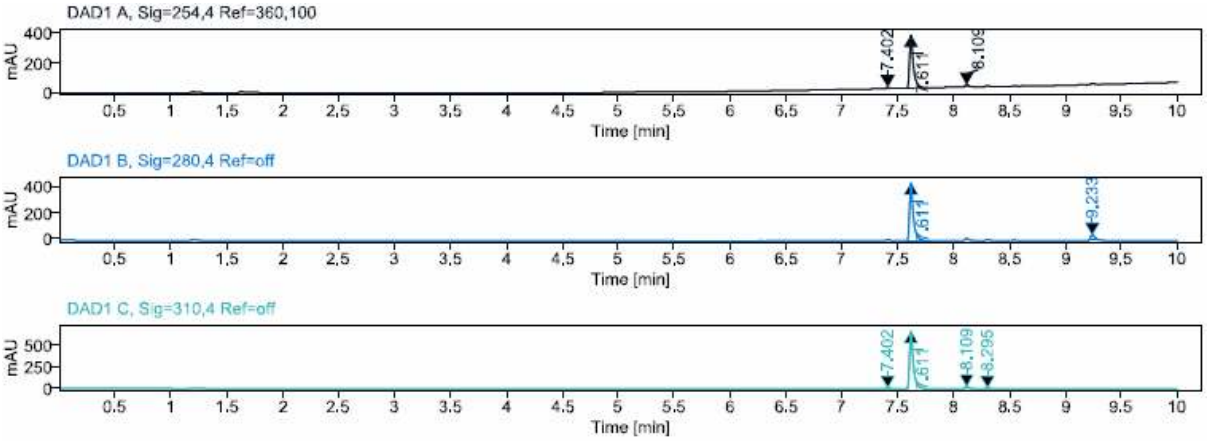

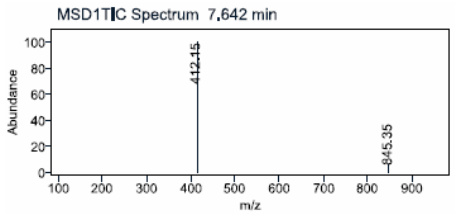

Compound **153**

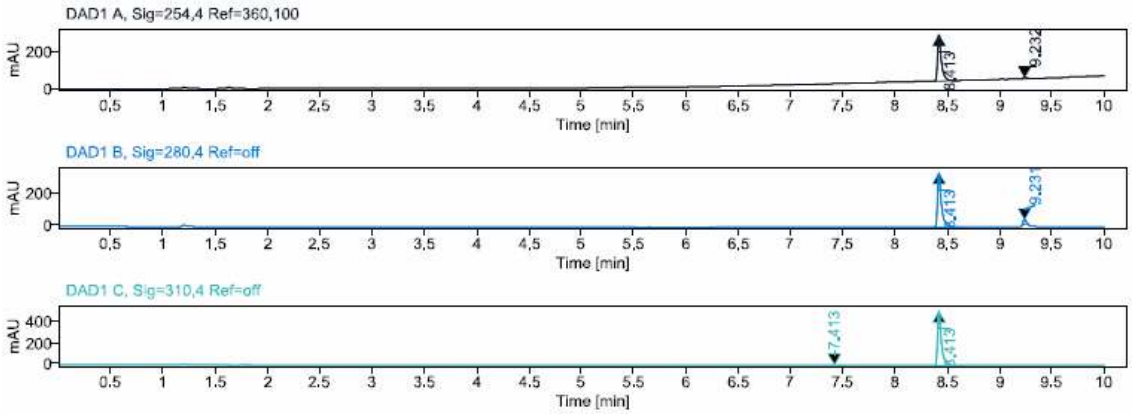

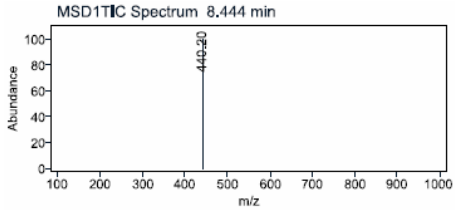

Compound **154**

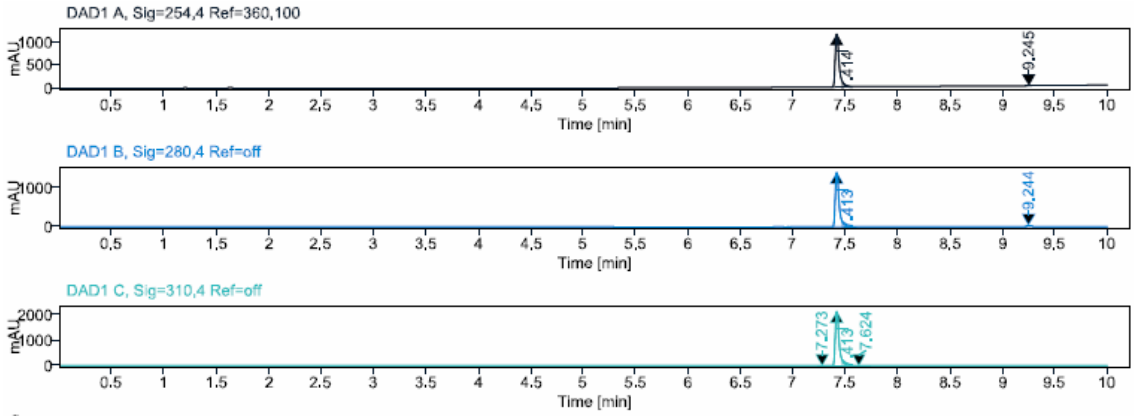

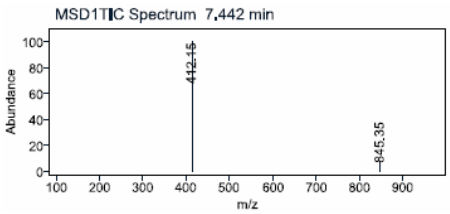

Compound **155**

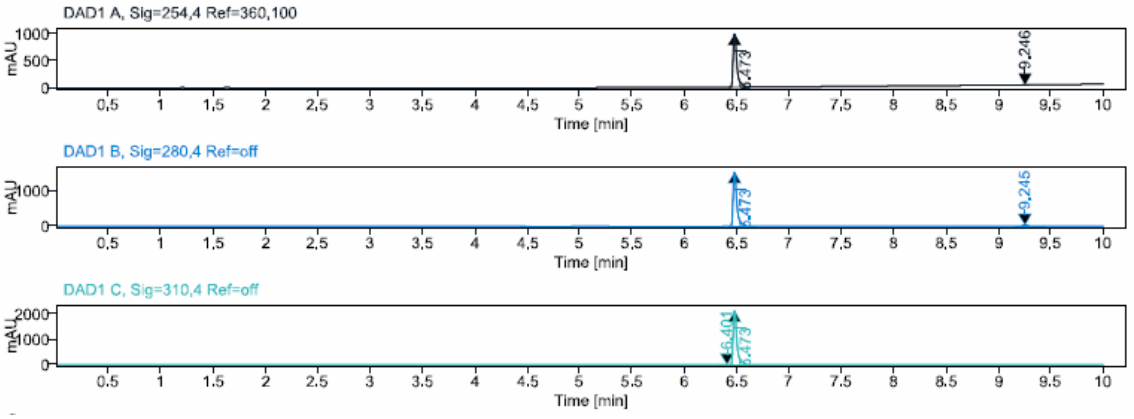

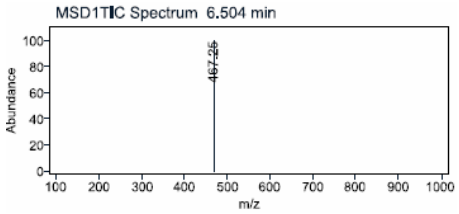

Compound **156**

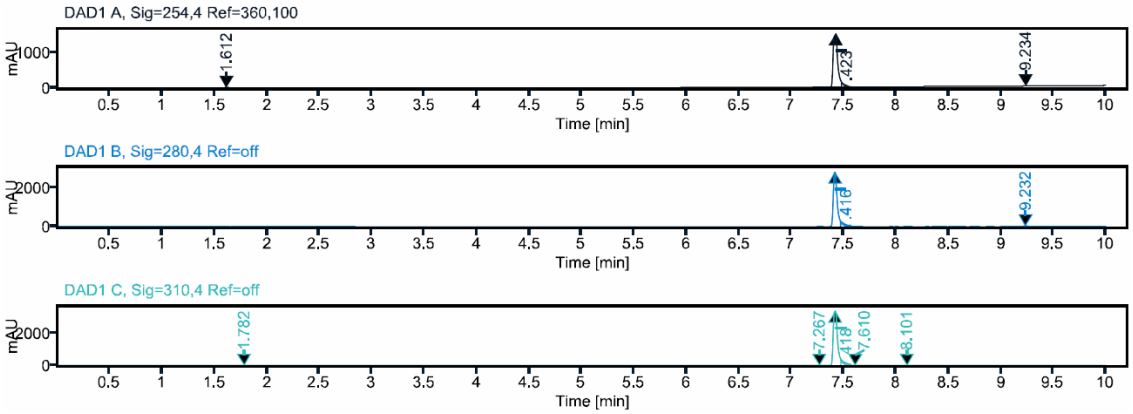

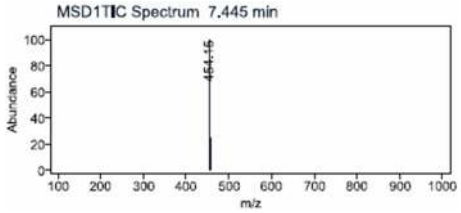

Compound **165**

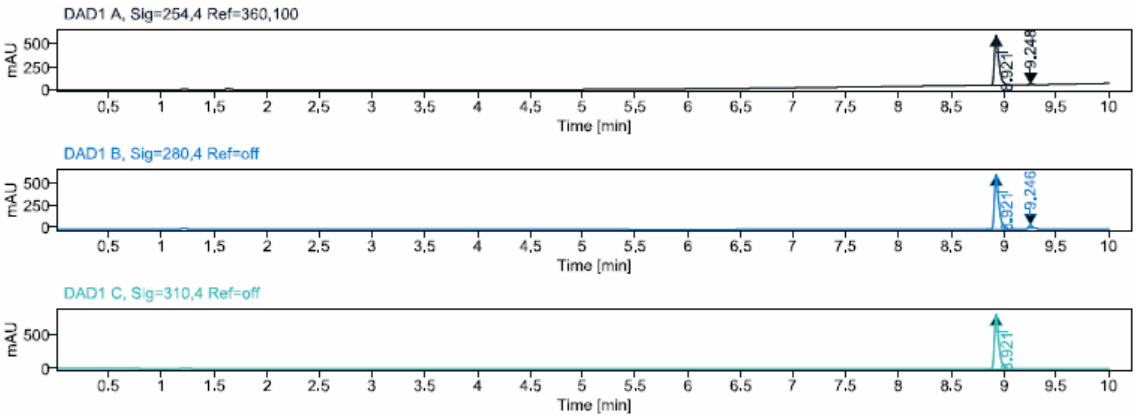

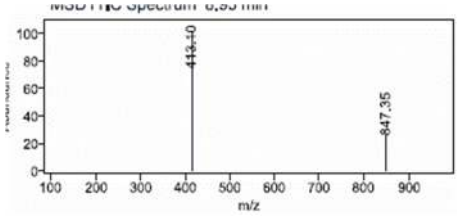

Compound **166**

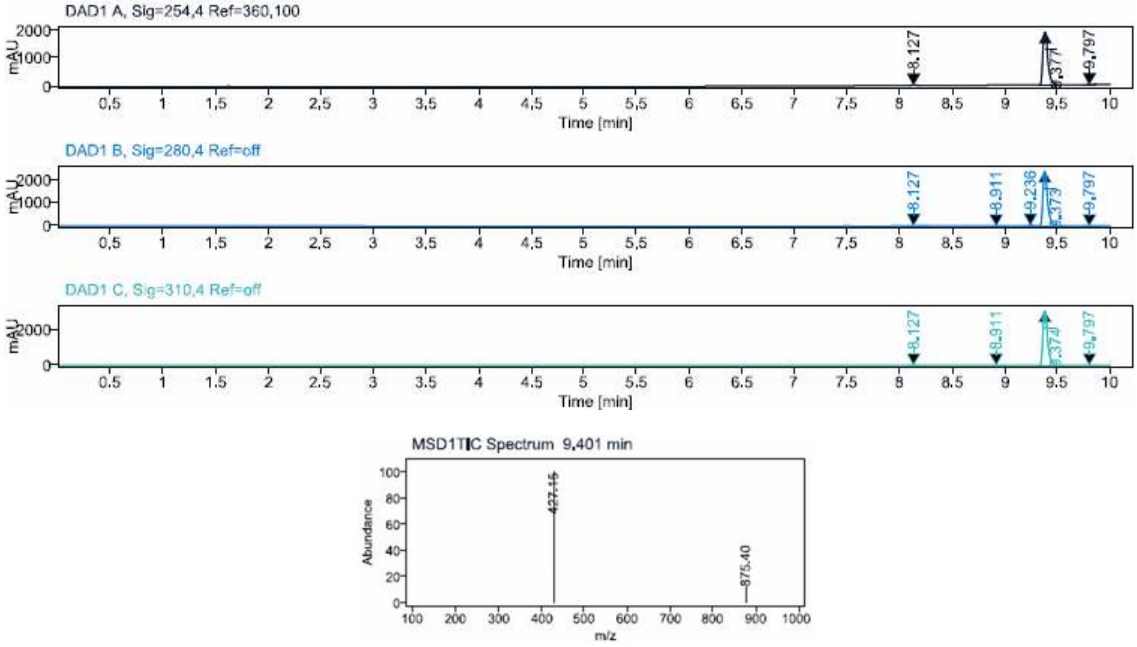

Compound **167**

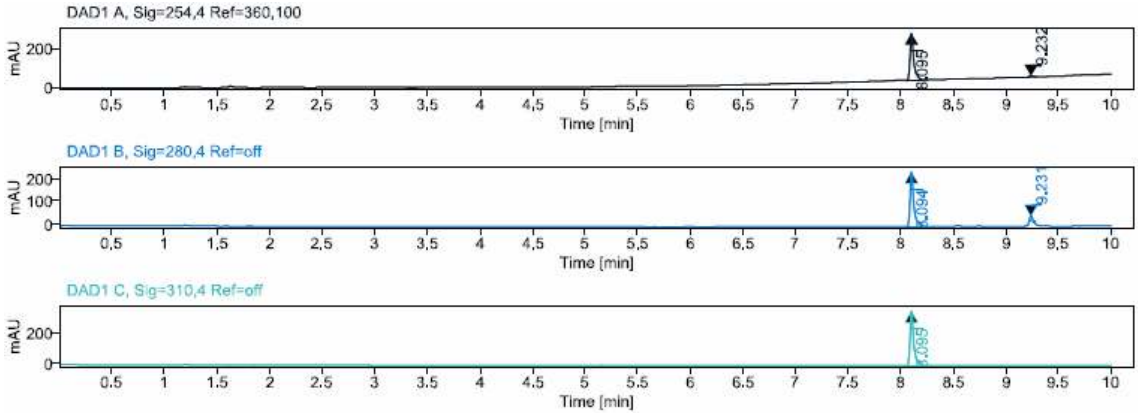

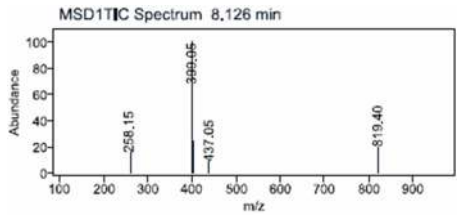

Compound **168**